USGS
science for a changing world

Crustal Thickness and the V_P/V_S Ratio within the Arabia Plate from P-wave Receiver Functions at 154 Broadband Seismic Stations

Open-File Report 2023–1042

U.S. Department of the Interior
U.S. Geological Survey

Crustal Thickness and the V_P/V_S Ratio within the Arabia Plate from P-wave Receiver Functions at 154 Broadband Seismic Stations

By Alexander R. Blanchette, Simon L. Klemperer, and Walter D. Mooney

Open-File Report 2023–1042

U.S. Department of the Interior
U.S. Geological Survey

U.S. Geological Survey, Reston, Virginia: 2023

Suggested citation:
Blanchette, A.R., Klemperer, S.L., and Mooney, W.D., 2023, Crustal thickness and the V_P/V_S ratio within the Arabia Plate from P-wave receiver functions at 154 broadband seismic stations: U.S. Geological Survey Open-File Report 2023–1042, 325 p., https://doi.org/10.3133/ofr20231042.

ISSN 2331-1258 (online)

Contents

Figures

Tables

Conversion Factors

International System of Units to U.S. customary units

Multiply	By	To obtain
kilometer (km)	0.6214	mile (mi)

Datum

Vertical and horizontal coordinate information is referenced to the World Geodetic System of 1984 (WGS84).

Altitude, as used in this report, refers to distance above the vertical datum.

Abbreviations

1D	one dimensional
A.H.	in the year of the Hijra
CCP	common conversion point
C.E.	Common Era
Hz	hertz
IRIS	Incorporated Research Institutions for Seismology
Ma	mega-annum
MMN	Makkah-Madīnah-Nafud volcanic line
Moho	Mohorovičić discontinuity
M_w	moment magnitude
NEZ	north-east-vertical coordinate system
PASSCAL	Portable Array Seismic Studies of the Continental Lithosphere
PRF	P-wave receiver function
PWS	phase-weighted stacking
RTZ	radial-transverse-vertical coordinate system
SGS	Saudi Geological Survey
s	second
s/km	second per kilometer
USGS	U.S. Geological Survey
V_P	P-wave (pressure) velocity
V_S	S-wave (shear) velocity

Crustal Thickness and the V_P/V_S Ratio within the Arabia Plate from P-wave Receiver Functions at 154 Broadband Seismic Stations

By Alexander R. Blanchette,[1] Simon L. Klemperer,[1] and Walter D. Mooney[2]

Abstract

As part of a joint Saudi Geological Survey (SGS) and United States Geological Survey project, we analyzed P-wave receiver functions from seismic stations covering most of the Kingdom of Saudi Arabia to map the thickness of the crust across the Arabia Plate. We present an update of crustal-thickness estimates and fill in gaps for the western Arabian Shield and the rifted margin at the Red Sea (the coastal plain), as well as the eastern Arabian Platform. We applied a conventional *H-k* stacking algorithm and included careful attention to stacking weights, two forms of sedimentary corrections for stations located on the Arabian Platform, and additional processing for noisy stations. We obtained useful results at 154 stations from 898 teleseismic events over a 2-year period from 1995–1997 (for non-SGS stations) and a 6-year period from 2008–2014 (for SGS stations). Average crustal thickness (that is, depth to the Mohorovičić discontinuity [Moho] below the surface) beneath the Red Sea coastal plain (the rift margin) is 29 kilometers (km), beneath the volcanic fields (known in Arabic as harra [plural] or harrat [singular]) is 35 km, beneath the Arabian Shield (excluding harrats) is 37 km, and beneath the Arabian Platform is 38 km. Crustal thinning appears not to extend east of the rift escarpment, suggesting uniform extension that is no broader at depth than at the surface. In contrast to some previous interpretations that the Arabian Platform crust is thicker than that of the Arabian Shield, we find no statistically significant difference between their whole crustal thicknesses. However, the average sub-sedimentary crustal thickness (that is, the crystalline crust) for stations on the Arabian Platform is 34 km, 3 km thinner than the crust of the Arabian Shield. Individual station P-wave (pressure) velocity and S-wave (shear) velocity ratios (V_P/V_S) are highly variable for the Arabia Plate, ranging from 1.60 to 1.97 and averaging 1.75, with a standard deviation of 0.07. There are no statistically significant differences between V_P/V_S ratios of the different geologic regions of Saudi Arabia. Similar V_P/V_S ratios, coupled with similar crustal thicknesses for harrats and the Arabian Shield, indicate that Cenozoic magmatism has contributed negligibly to crustal growth.

[1] Stanford University

[2] U.S. Geological Survey

Introduction

The present-day thickness and composition of the Earth's crust and its lateral variability are products of its evolution from initial formation and through the process of multiple tectonic episodes. As part of a joint Saudi Geological Survey (SGS) and United States Geological Survey (USGS) project, we sought to estimate the crustal thickness of the continental portion of the present-day Arabia Plate with minimal assumptions. We computed P-wave receiver functions (PRFs) and measured the traveltime differences between teleseismic compressional waves (P-waves) and the converted shear-wave (S-wave) phases (Ps, 3p1s, 2p2s) generated at the boundary between the crust and mantle (that is, the Mohorovičić discontinuity [Moho]). Compared to previous PRF studies of crustal thickness of the Kingdom of Saudi Arabia (Sandvol and others, 1998; Julià and others, 2003; Al-Damegh and others, 2005; Tkalčić and others, 2006; Tang and others, 2016, 2019), we: (1) use more stations that recorded data for longer time periods, (2) more thoroughly explore methodological parameters to obtain estimates of uncertainties, and (3) account for sedimentary cover where known.

The Arabian Shield constitutes the eastern part of the formerly continuous Arabian-Nubian Shield and is now separated from the Nubian Shield by the Red Sea rift, a divergent plate boundary that intersects the Dead Sea Transform boundary near its north end (fig. 1*B*). The Arabian-Nubian Shield formed by the accretion of multiple terranes, primarily around 800–550 million years ago (Ma) (summarized by Stern and Johnson, 2010). The Arabian craton began to subside at 725 Ma and its eastern and northern parts gradually accumulated as much as 15 kilometers (km) of Paleozoic through Cenozoic sediments along the margin of the Neotethys Ocean (Konert and others, 2001, summarized by Stern and Johnson, 2010). The arrival of the Afar plume at ~30 Ma triggered extension in East Africa, the Gulf of Aden, and the Red Sea region (Bosworth and others, 2005; Bosworth, 2015). Voluminous flood basalts in Ethiopia, southern Sudan, and western Yemen were succeeded in Syria, Saudi Arabia, Jordan, and Yemen by expansive but generally thin alkali-basalt fields, known in Arabic as harra (plural) or harrat (singular) (Coleman, 1993; Bosworth and others, 2005; Bosworth, 2015). Recent magmatism was recorded in the 2009 intrusion event at

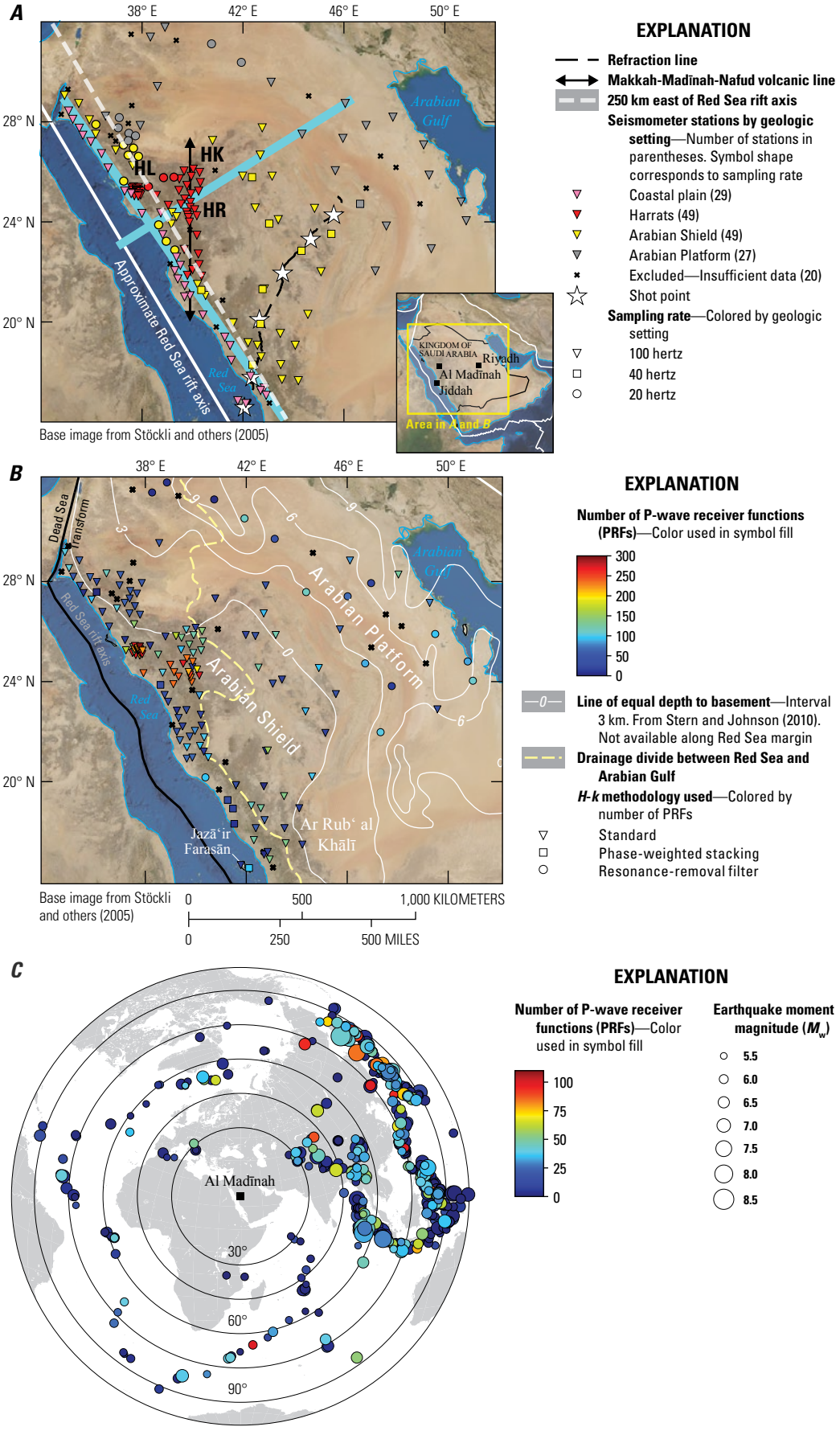

Figure 1. Maps of the study area in the Kingdom of Saudi Arabia and earthquakes analyzed in this study. Inset map shows plate boundaries in white. *A*, True-color image map showing the locations of Saudi Geological Survey (SGS) and Incorporated Research Institutions for Seismology (IRIS) Portable Array Seismic Studies of the Continental Lithosphere (PASSCAL) seismometers. Harrats are named following Camp and others (1991): HL, Harrat Lunayyir; HK, Harrat Khaybar; HR, Harrat Rahat. Common-conversion-point (CCP) profiles parallel and orthogonal to the Red Sea rift shown by thick aqua lines (drawn to be 50 kilometers [km] wide) were drawn to maximize station density rather than to be truly parallel or orthogonal to the straight-line approximation of the Red Sea rift axis (white line). Refraction line and shot points from Healy and others (1983). *B*, Map showing the 154 seismic stations for which we report crustal thickness. The drainage divide between the Red Sea and the Arabian Gulf (dashed yellow line) corresponds to the Great Escarpment south of Jiddah, and in that region is close to the dashed white line in *A*, 250 km from the Red Sea rift. *C*, Polar plot of earthquakes used in this analysis.

Harrat Lunayyir and by historical eruptions at Harrat Rahat in 1256 C.E. (654 in the year of the Hijra [A.H.]) and probably at Harrat Khaybar in 641 C.E. (20 A.H.), which are located along the Makkah-Madīnah-Nafud (MMN) volcanic line (fig. 1*A*) (Camp and Roobol, 1992; Pallister and others, 2010; Champion and others, in press; Stelten and others, in press).

In this report we introduce the newly expanded seismic dataset and then discuss calculation of our receiver functions, including data quality control. We describe the standard *H-k* stacking approach that measures crustal thickness and crustal P-wave (V_P) to S-wave (V_S) seismic velocity ratio (V_P/V_S ratio) based on conversions between P- and S-waves. In addition, we introduce four key improvements over previously reported seismological studies of the crustal structure of Saudi Arabia: (1) a more complete analysis of the effects of the chosen stacking weights; (2) use of a resonance-removal filter (Yu and others, 2015) followed by a sedimentary *H-k* stack for stations where sedimentary reverberations make it difficult to analyze data; (3) application of phase-weighted stacking (PWS; Crotwell, 2007) to noisy data; and, most importantly, (4) accounting for the thickness and velocity of sedimentary cover using the well-measured thicknesses of the Arabian Platform sedimentary section (Konert and others, 2001 [reproduced by Stern and Johnson, 2010]). The main purpose of this report is to provide the detailed *H-k* stacking results at each station across Saudi Arabia. These results are further analyzed in a separate report (Blanchette and others, in press).

Data and Methods

Data and Resources

The seismograms used in this study were recorded by the Saudi National Seismic Network, operated by the Saudi Geological Survey (SGS). The seismic data used may be requested from the SGS (https://sgs.gov.sa/en/e-services).

Preprocessing and Quality Control

We examined data from 165 broadband seismic stations of the Saudi Geological Survey (SGS) National Seismic Network (Endo and others, 2007) that are now deployed in most regions of Saudi Arabia except for Ar Rub‘ al Khālī (“Empty Quarter”; fig. 1), the vast sand desert in the southern part of the Arabian Peninsula. In addition to the SGS seismic stations, we also incorporated nine seismic stations from an Incorporated Research Institutions for Seismology (IRIS) Portable Array Seismic Studies of the Continental Lithosphere (PASSCAL) array deployed from 1995–1997 (Vernon, 1995). The recorders used by both SGS and IRIS are Trillium T40 and T120 and Streckeisen STS2 seismometers. We obtained useful results at 154 stations (fig. 1*A*, *B*; table 1.1) that recorded 898 teleseismic events (fig. 1*C*) over a 2-year period from 1995–1997 (for the IRIS-PASSCAL stations) and a six-year period from 2008–2014 (for the SGS stations). Each three-component recording was used to construct a P-wave receiver function (PRF; Langston, 1979). The PRF method is a well-established technique to image seismic boundaries within the lithosphere, including the Moho and the base of sedimentary rocks that overlie the crystalline crust.

Our data processing involved several steps. We rotated event recordings from their north-east-vertical (NEZ) coordinate system to the radial-transverse-vertical (RTZ) coordinate system, based on the theoretical back azimuth of each recorded teleseismic earthquake. The purpose was to isolate the first arrival (P-wave) on the vertical component and the converted S-wave on the radial component. We picked arrival times for every station-event pair using a short-term average (STA) over long-term average (LTA) algorithm (Earle and Shearer, 1994), and manually refined these arrival times to correct for slight errors in the picking algorithm by visually inspecting the data.

We band-pass filtered the raw data from 0.2 to 1.5 hertz (Hz) and trimmed the filtered traces such that each trace begins 20 seconds (s) before the first P-wave arrival and extends to 80 seconds after, for a total duration of 100 seconds. PRFs were calculated by deconvolving the vertical (Z) signal from the radial (R) signal using an iterative-time domain approach (Ligorria and Ammon, 1999). Some previous workers simply visually inspected the calculated PRFs for quality assurance (for example, Sandvol and others, 1998; Thurner and others, 2015; Miller and others, 2018); Tang and others (2016) used a minimum-fit criterion. In this study, we quantitively used both a minimum-fit criterion and a cross-correlation filter.

The minimum-fit criterion required that we be able to reproduce the radial and transverse components of motion with a fit that is equal to or better than 70 percent when we convolve the respective components of the PRF with the vertical component. The 70-percent minimum-fit criterion is chosen to enforce a decent match between the original signal and the PRF that does not discard an excessive amount of data. The initial dataset comprised 22,716 receiver functions, of which 18,242 (~80 percent) met our 70-percent minimum-fit requirement. The cross-correlation filter constructs a template PRF by stacking all PRFs for a given station and calculates the maximum cross-correlation coefficient of each event with the template. To minimize assumptions about the structure beneath each station, no moveout correction was applied to the PRFs, and we required a low minimum-threshold cross-correlation coefficient of 0.6 on the radial component of the PRFs only. Of the 18,242 receiver functions that passed the minimum-fit criteria, 15,519 (~68 percent of the raw dataset) passed the cross-correlation filter requirement. The final number of receiver functions that passed both the minimum-fit and the cross-correlation filter requirements is far lower on the Arabian Platform (~11 percent of the final usable PRFs) than on the Arabian Shield (~24 percent) or in the harrats (~51 percent; fig. 1*B*). Moment magnitude (M_w) 6 or greater subduction zone earthquakes northeast of the recording array generated a greater percentage of the useable receiver functions than the fewer and smaller midocean ridge events at most other back azimuths (fig. 1*C*).

Standard *H-k* Stacking

PRFs utilize teleseismic P-wave energy from earthquakes that are 30–90° away from the receiver. Some of the P-wave energy is converted to transmitted S-wave motion at first-order (abrupt) impedance boundaries in the lithosphere. This S-wave is denoted Ps (capital letters denote waves that are initially down-going and lowercase letters indicate purely up-going waves). Three other arrivals (also called multiples) are also commonly detected on higher quality P-wave receiver functions: the PpPs (or 3p1s) arrival, and two phases that arrive together (for a one dimensional [1D] Earth model) with the same sense of motion (PsPs and PpSs) and are collectively referred to as 2p2s (fig. 2). The piercing point at the Moho varies between phases and with the earthquake distance but is farthest away from the seismic station (about 50 km; fig. 2*C*) for the 3p1s multiple at th e shortest teleseismic offset used, here 30°. For clarity, we denote the depth of the interface at which the waves are refracting and converting with a subscript (for example, $P_{35}s$ is a P-to-S conversion at 35 km depth). The traveltimes (t, in seconds) of each phase are given by equations 1–3 as functions of depth to a strong impedance contrast (commonly the base of the crust), P-wave velocity, V_P/V_S ratio, and ray parameter:

$$t_{Ps}\left(H,\ k,\ V_P,\ p\right) = H\left[\sqrt{\frac{k^2}{V_P^2} - p^2} - \sqrt{\frac{1}{V_P^2} - p^2}\right] \quad (1)$$

$$t_{3p1s}\left(H,\ k,\ V_P,\ p\right) = H\left[\sqrt{\frac{k^2}{V_P^2} - p^2} + \sqrt{\frac{1}{V_P^2} - p^2}\right] \quad (2)$$

$$t_{2p2s}\left(H,\ k,\ V_P,\ p\right) = 2H\sqrt{\frac{k^2}{V_P^2} - p^2} \quad (3)$$

where

t is traveltime in seconds;
t_{Ps} is the traveltime in seconds of phase Ps;
t_{3p1s} is the traveltime in seconds of phase 3p1s;
t_{2p2s} is the traveltime in seconds of phase 2p2s;
H is the depth in kilometers to the impedance contrast, commonly the base of the crust;
V_P is the P-wave velocity in kilometers per second (km·s^{-1});
k is the V_P/V_S ratio (unitless); and
p is the ray parameter in seconds per kilometer (s/km).

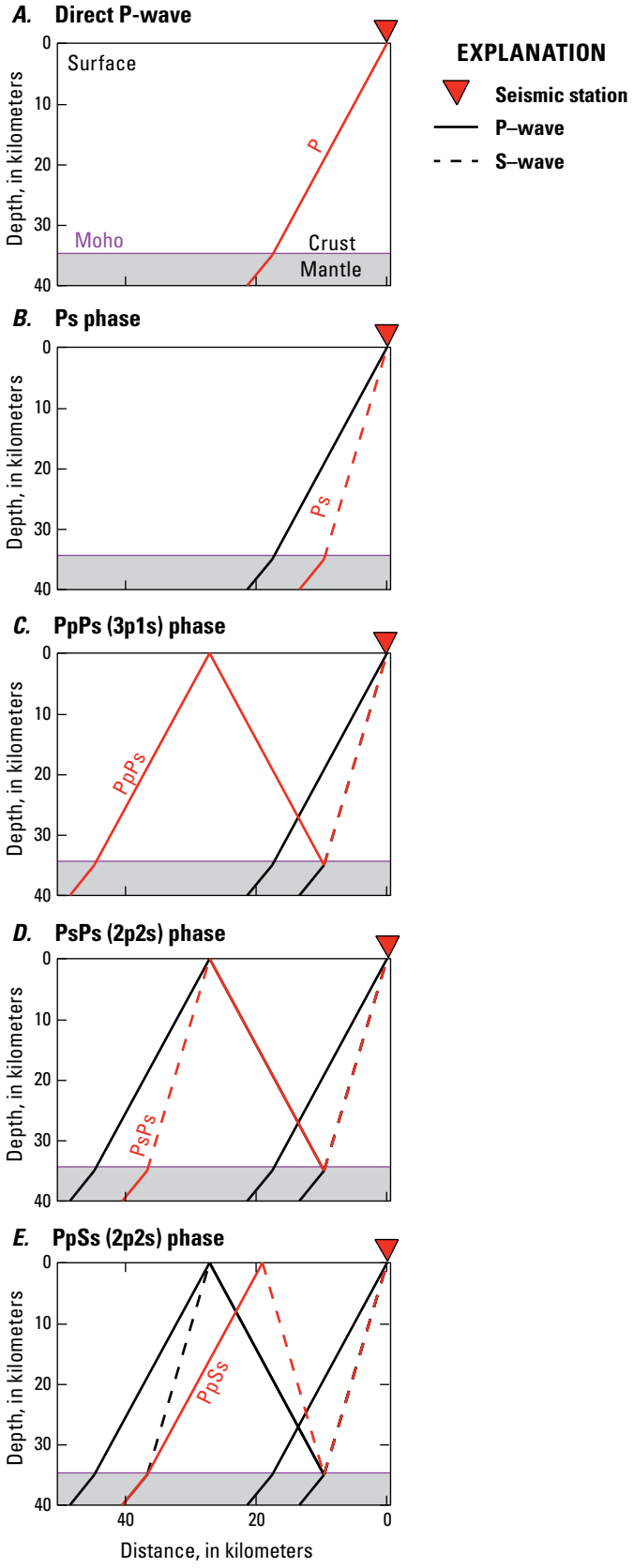

Figure 2. Schematic diagrams of ray paths of P-wave receiver function phases from a shallow earthquake at 30° distance for a 35-kilometer (km)-deep Mohorovičić discontinuity (Moho) separating crust (V_P = 6.1 km/s, k = 1.73) and upper mantle (V_P = 8.04 km/s, k = 1.80). *A*, Direct P-wave. *B*, Ps phase. *C*, PpPs (or 3p1s) phase. *D*, PsPs (or 2p2s) phase. *E*, PpSs phase (also a 2p2s phase). Red lines are the labelled phase; black lines are the phase(s) in the previous panels. $k = V_P/V_S$ ratio, where V_P is P-wave velocity and V_S is S-wave velocity.

H-k stacking (Zhu and Kanamori, 2000) is a standard approach to analyze PRFs for *H* and *k* beneath a given seismic station, normally assuming a homogenous isotropic layer over a half-space beneath the seismic station. Standard *H-k* stacking employs a grid search across *H-k* space for the stacking amplitude at a single station:

$$s(H,\ k) = \frac{1}{N}\sum_{n=1}^{N}\left[w_1 r_n\left(t_{Ps}\right) + w_2 r_n\left(t_{3p1s}\right) - w_3 r_n\left(t_{2p2s}\right)\right] \quad (4)$$

where

s is the stack amplitude sum,

r_n is the amplitude of the nth radial receiver function for the station at the predicted phase arrival time for the appropriate H, k, V_p, and p values,

w_i is the stacking weight for each phase i, and

N is the number of receiver functions.

The normalization condition applied to the stacking weights is $w_1 + w_2 + w_3 = 1$, and we describe *H-k* stacks and their results as "$w_1/w_2/w_3$" to emphasize the weights used. The third term of equation 4 represents the 2p2s phases and is subtracted because it has the opposite polarity with respect to the other phases. The sum, *s*, reaches its maximum value for any seismic station at the average crustal thickness and velocity ratio beneath that station.

We searched over a grid spanning $20 \le H \le 80$ km and $1.60 \le k \le 2.10$ to sample all plausible crustal thicknesses and compositions, using an assumed average crustal wavespeed (V_{Pavg} = 6.5 km/s; Mooney and others, 1985). *H-k* estimates vary only weakly with V_{Pavg}, increasing *H* by less than ~10 km per km/s and *k* by less than ~0.05 per km/s (Karplus and others, 2019). Conventionally, the uncertainty in *H* and *k* values is computed by:

$$\sigma_H^2 = 2\sigma_s\left(\frac{\partial^2 s}{\partial H^2}\right)^{-1} \quad (5)$$

$$\sigma_k^2 = 2\sigma_s\left(\frac{\partial^2 s}{\partial k^2}\right)^{-1} \quad (6)$$

where σ_H,σ_k, and σ_s are the standard deviations of *H*, *k*, and the stack amplitude (*s*) evaluated at the *H* and *k* values that maximize the stack (Zhu and Kanamori, 2000).

We cite uncertainties of two standard deviations (±2σ) throughout this report for individual stations, and in appendix 1 (table 1.1), we cite uncertainties of ±1 for ensemble means.

It is common to use a default set of stacking weights, regardless of the signal-to-noise ratios of the different phases at different stations (see for example, Al-Damegh and others, 2005; Karplus and others, 2019). Instead, we examined the individual contribution of each converted phase at each station to determine the final weights, selecting from among three options (0.4/0.3/0.3, 0.33/0.33/0.33, and 0.5/0.5/0.0) to give the sharpest peak in *H-k* space for the Moho conversions, after Ogden and others (2019). Additional combinations were used to stack shallower conversions, within or at the base of the sedimentary cover, as discussed below. A discussion of our visual inspection and weight choice criteria is presented in Blanchette and others (in press).

Multiple Removal to Improve *H-k* Stacking

Standard *H-k* stacking works well at recovering the thickness of the crust, provided that the Moho is the only layer with a sharp enough impedance contrast to generate strong P-wave to S-wave conversions (Langston, 2011; Yu and others, 2015) and that the crust can be reasonably well-characterized with a single average wavespeed. However, some stations on the Arabian Platform are underlain by as much as 10 km of low-wavespeed sedimentary rocks (fig. 1*B*) (Konert and others, 2001 [reproduced by Stern and Johnson, 2010]), producing interbed conversions and multiples (reverberations) that can interfere with the Moho Ps arrival and its subsequent multiples. A significant number (15 out of 154) of the seismic stations successfully analyzed here were affected by sedimentary multiples and required additional analysis.

We attempted direct removal of the sedimentary reverberations from these PRFs using a resonance-removal filter calculated from the autocorrelations of the PRFs (Yu and others, 2015). This method estimates the apparent thickness and V_P/V_S ratio of the sedimentary layer, as well as a thickness and V_P/V_S ratio for the sub-sedimentary crystalline crust. This approach works best for sedimentary layers thicker than ~0.25 km for which the reverberations have frequencies and traveltimes that interfere with the Moho conversions. However, this method may be inapplicable for layers thicker than ~8 km for which the wave speed contrast at the sediment-basement contact is sufficiently small or gradational that the reverberations do not have a high amplitude. We successfully filtered 15 stations with 2.6–10.7 km of sedimentary rock (Konert and others, 2001 [reproduced by Stern and Johnson, 2010]). We then determined the crustal thicknesses using the *H-k* method on the filtered PRFs.

As in conventional *H-k* stacking, to get sedimentary thickness h_s, we assumed a sedimentary P-wave velocity of 4.0 km/s based on refraction-profiling results showing $2.0 \le V_P \le 5.7$ km/s in the northern Arabian Platform (Seber and others, 1993; Brew and others, 1997) and 3–5 km/s within the western Arabian Platform (Mooney, 1984), and carried out a grid search across *H-k* space. The sedimentary thickness, h_s, is determined reasonably well by the Ps conversion from the sediment-basement interface, but determining the sedimentary V_P/V_S ratio, k_s, requires good constraints on the corresponding 3p1s and 2p2s multiples that tend to have low amplitudes.

Phase Weighted *H-k* Stacking

At five stations (QNF01, QNF02, AMGES, FRSS, and DESA) on the Red Sea rift's eastern subaerial margin (that is, the coastal plain) for which neither the standard *H-k* stacking nor the resonance-removal filter proved useful, we successfully applied phase-weighted stacking (PWS; Crotwell,

2007; Ogden and others, 2019) to remove incoherent noise. In this method, the coherency between the converted (Ps) and multiple (3p1s, 2p2s) arrivals is used to modulate the stacking amplitude $s(H, k)$:

$$s(H,\ k) = \frac{1}{3N}\left|\sum_{n=1}^{N}\left[e^{i\phi_n(t_{Ps})} + e^{i\phi_n(t_{3p1s})} - e^{i\phi_n(t_{2p2s})}\right]\right|^{v}$$

$$\sum_{n=1}^{N}\left[w_1 r_n\left(t_{Ps}\right) + w_2 r_n\left(t_{3p1s}\right) - w_3 r_n\left(t_{2p2s}\right)\right] \tag{7}$$

where ϕ_n are the instantaneous phases of the PRF (derived from the Hilbert transform of the PRF) at the predicted Ps, 3p1s, and 2p2s arrival times for the appropriate H and k values, and v is an arbitrary exponent. Using $v = 0$ corresponds to regular H-k stacking, with $v = 1$ (Crotwell, 2007, and this study) and $v = 2$ (Ogden and others, 2019) representing progressively more aggressive PWS.

PWS uses the relative coherence of the arrivals to determine their contribution to the H-k stack. If the instantaneous phase ϕ of the PRFs at the three predicted arrival times is equal (as expected for noise-free signals), the weighted sum of the PRFs at these three times is given full weight in the H-k stack, whereas if ϕ at the three arrival times is contradictory (as one would expect from random noise), the weighted sum of the PRFs is given much lower, or zero, weight. In the application of PWS, we did not try to select optimum weights, w, for Ps, 3p1s, and 2p2s, but rather assigned each phase a value of ⅓. We attempted PWS H-k stacking only for stations for which we could not otherwise obtain reliable results. We obtained reliable results from an additional five stations. The remaining 20 stations (table 1) defied our efforts to obtain a reliable crustal thickness, either because they have very low signal-to-noise ratios and (or) there are very few PRFs at these stations.

Accounting for Sediment in Crustal Thickness Estimates

Single-layer interpretations of the H-k stacks (whether conventional or using PWS) assume that the entire crustal thickness is adequately approximated with a single constant wavespeed. However, the traveltime of the Ps phase per kilometer of sedimentary rock (in a low-V_p, high-k basin) is larger than in the high-V_p, low-k crystalline crust. Hence, the presence of appreciably thick, low-velocity sedimentary cover leads to overestimates of crustal thickness if calculated solely from H-k stacking (H_{raw}) in amounts that increase in proportion to the thickness of the sedimentary section. For a sedimentary layer thickness, h_s above a crystalline crust thickness h_b (such that true crustal thickness $H_{true} = h_s + h_b$), the traveltime of the converted Ps phase with respect to a direct P phase is given by:

$$t_{Ps} = h_b\left(\sqrt{\frac{k_b^2}{V_{Pb}^2} - p^2} - \sqrt{\frac{1}{V_{Pb}^2} - p^2}\right) + h_s\left(\sqrt{\frac{k_s^2}{V_{Ps}^2} - p^2} - \sqrt{\frac{1}{V_{Ps}^2} - p^2}\right) \tag{8}$$

where subscripts b and s denote crystalline basement and sedimentary values. Therefore, H_{raw} is given by:

$$H_{raw} = \frac{t_{Ps} - h_s\left(\sqrt{\frac{k_s^2}{V_{Ps}^2} - p^2} - \sqrt{\frac{k_b^2}{V_{Pb}^2} - p^2} + \sqrt{\frac{1}{V_{Pb}^2} - p^2} - \sqrt{\frac{1}{V_{Ps}^2} - p^2}\right)}{\sqrt{\frac{k_c^2}{V_{Pc}^2} - p^2} - \sqrt{\frac{1}{V_{Pc}^2} - p^2}} \tag{9}$$

where subscript c denotes the assumed whole crustal values for P-wave velocity and the V_p/V_s ratio used in the H-k stacking (Zhu and Kanamori, 2000).

To correct H_{raw} to the true Moho depth H_{true}, we use the sedimentary thickness h_s (equivalent to the basement depth) that is well known across the Arabian Platform from extensive hydrocarbon exploration (Konert and others, 2001 [reproduced by Stern and Johnson, 2010]) (fig. 1*B*). We define the difference between the true crustal thickness and the raw thickness as the error: $\varepsilon = H_{true} - H_{raw}$. For PRFs, the ray parameter p ranges from 0.04 to 0.08 s/km, and in figure 3*A* we show the variation of ε with sedimentary thickness h_s (that is, $\frac{\partial \varepsilon}{\partial h_s}$) as a function of sedimentary V_P and V_P/V_S ratios for constant p = 0.06 s/km. For a sedimentary layer thickness of h_s, with V_P = 4.0 km/s and k_s = 1.75 (Brocher, 2005; fig. 3*A*), H_{raw} must be reduced by ~$0.6h_s$. Figure 3*B* shows the variation of ε with slowness p (that is, $\frac{\partial \varepsilon}{\partial p}$) is irrelevant for the range of p used here. In the following sections, we present the full crustal thickness H (Moho depth below the surface), after reduction by $0.6h_s$ using sedimentary thicknesses of Konert and others, 2001 (reproduced by Stern and Johnson, 2010), and we discuss crystalline crustal thickness $h_b = H - h_s$ (fig. 4). At stations for which we carried out the resonance-removal and sedimentary-stacking method (Yu and others, 2015), we applied the $0.6h_s$ reduction to the difference between the *H-k* sedimentary thicknesses and the known sedimentary thicknesses (fig. 5). This correction was applied because, in general, the *H-k* sedimentary thicknesses are less than the known sedimentary thicknesses, meaning we are still overestimating the total crustal thickness. There are exactly two stations for which we obtained sedimentary *H-k* values greater than the thicknesses we expected, therefore, at those two stations, the correction is in the opposite direction.

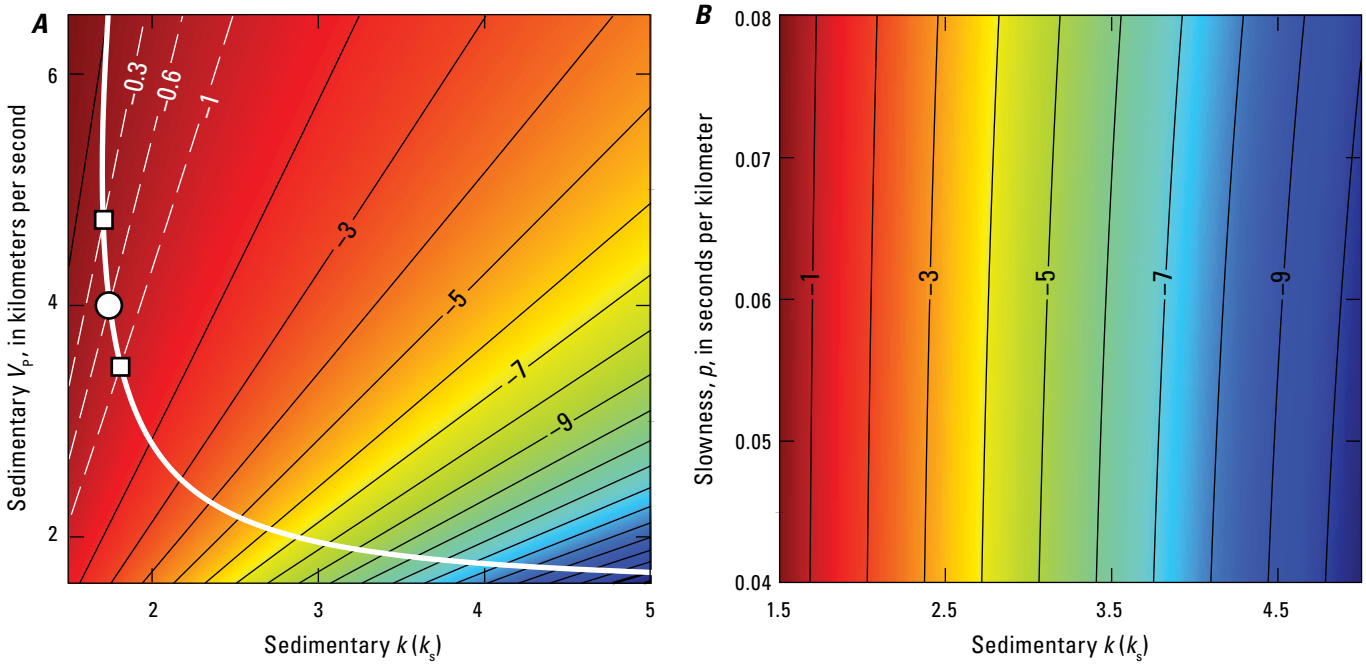

Figure 3. Plots of sedimentary correction factor for varying sedimentary P-wave velocities (V_P), P-wave receiver function ray parameter (p; also called slowness), and V_P/V_S ratios (k_s). *A*, Sedimentary correction factor variation with V_P and k for a crystalline crust that has V_P = 6.5 kilometers per second (km/s) and k = 1.73. Solid white line shows an empirical relation between sedimentary V_P and k from Brocher (2005). Dashed white lines show the range of corrections tested. The white circle (preferred correction, 0.6) and white squares (extreme corrections tested, 0.3 and 1.0) mark the intersections of dashed white lines with Brocher's (2005) empirical relations. *B*, Sedimentary correction factor variation with source-earthquake slowness p and sedimentary k_s. ε, error; h_s, sedimentary rock thickness; $k = V_P/V_S$ ratio, where V_P is P-wave velocity and V_S is S-wave velocity.

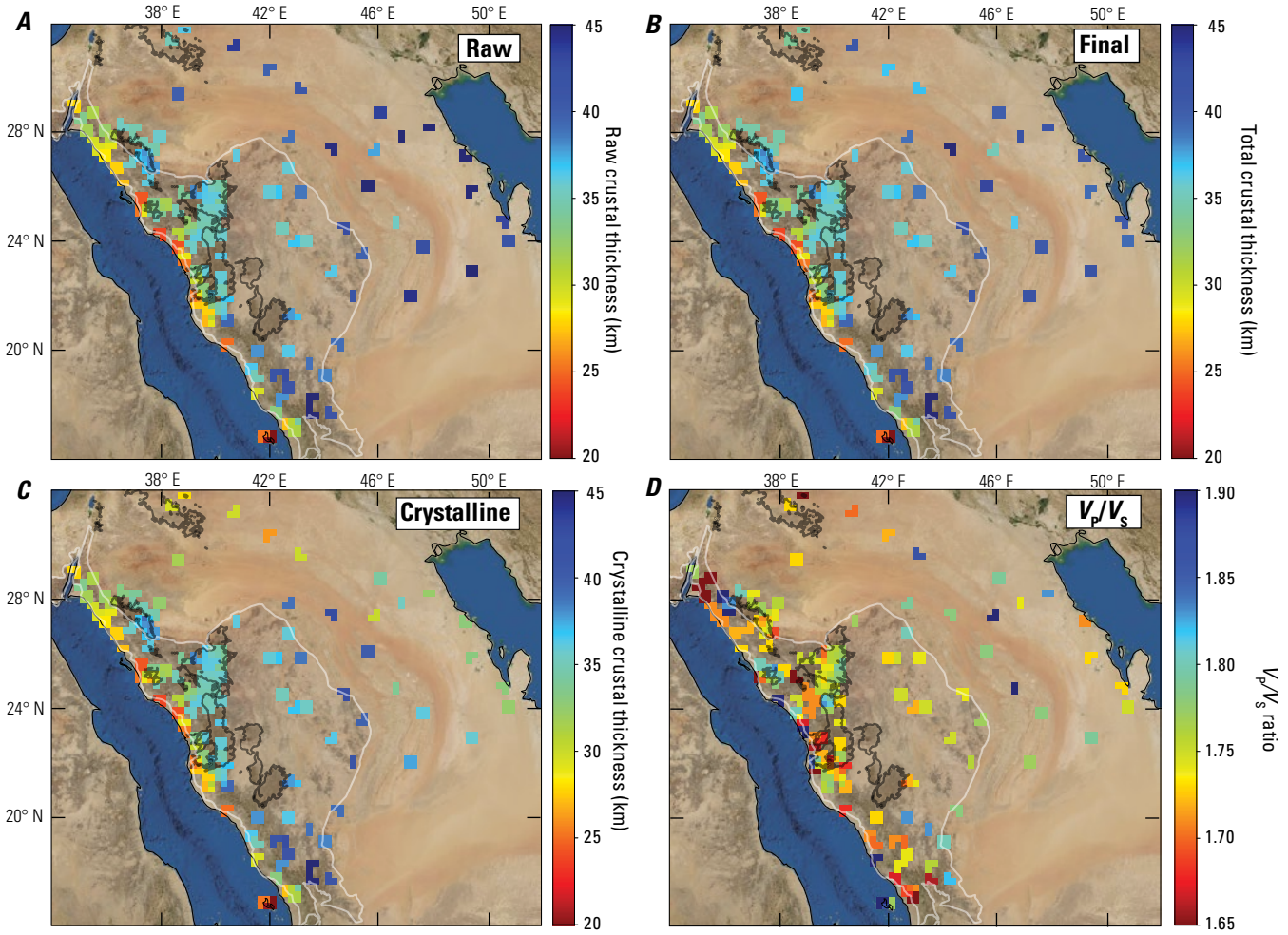

Figure 4. Maps of Saudi Arabia showing crustal thicknesses based on our *H-k* stacking results. Values are averaged within bins with radii of 25 kilometers. Shield boundary shown as thin white line. *A*, "Raw" crustal thickness from *H-k* stacks before sedimentary correction. *B*, "Final" crustal thickness from *H-k* stacks after our preferred sedimentary correction factor of 0.6. *C*, Thickness of the crystalline crust (that is, final thickness minus sedimentary thickness) estimated by Stern and Johnson (2010). *D*, Crustal P-wave to S-wave seismic velocity ratio (V_P/V_S ratio; no sedimentary correction). Harrat boundaries from Pollastro (1998a) and Arabian Shield boundary from Pollastro (1998b). km, kilometers.

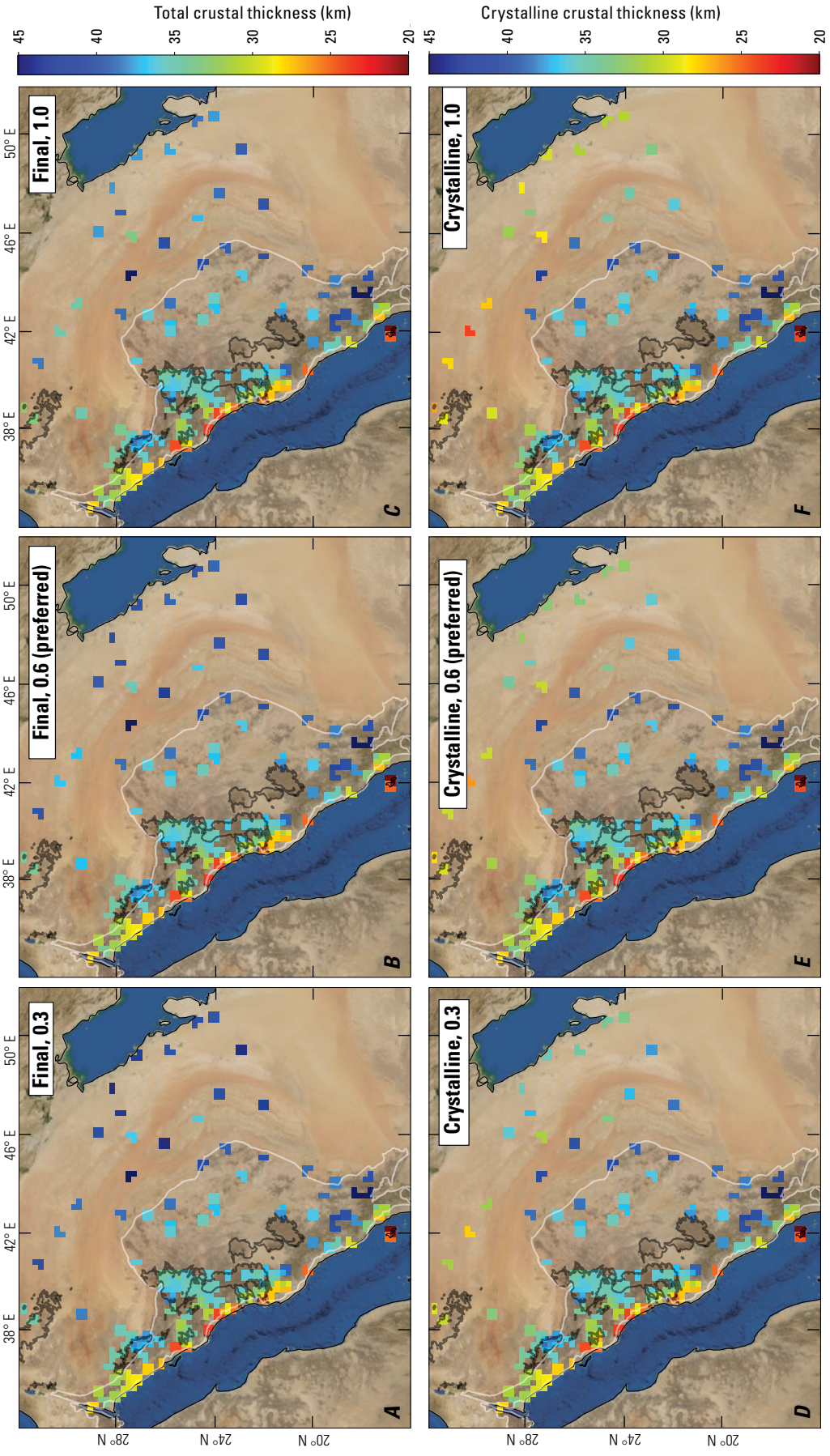

Figure 5. Maps showing comparison of our *H-k* stacking results for total and crystalline crustal thicknesses of Saudi Arabia after applying various sedimentary correction factor values (see fig. 3). *A*, Total crustal thickness from *H-k* stacks after applying a sedimentary correction factor of 0.3. *B*, Total crustal thickness from *H-k* stacks after applying our preferred sedimentary correction factor of 0.6 (as in fig. 4*B*). *C*, Total crustal thickness from *H-k* stacks after applying a sedimentary correction factor of 1.0. *D*, Thickness of the crystalline crust after applying a sedimentary correction factor of 0.3. *E*, Thickness of the crystalline crust after applying our preferred sedimentary correction factor of 0.6 (as in fig. 4*C*). *F*, Thickness of the crystalline crust after applying a sedimentary correction factor of 1.0. km, kilometers.

Station-by-Station Seismic Array Results

Table 1 explains the terminology used in all the figures in this section.

Table 1. Explanation of terminology used in receiver-function plots.

[s/km, seconds per kilometer.]

Term	Meaning and usage
Radial	Receiver function component derived by deconvolving the vertical seismogram from the radial seismogram.
Transverse	Receiver function component derived by deconvolving the vertical seismogram from the transverse seismogram.
Filtered	Radial component of receiver function generated at a station atop a layer of sediments that has had the resonance-removal filter of Yu and others (2015) applied to reduce reverberations.
Raw	Radial component of receiver function generated at a station atop a layer of sediments that has not had the resonance-removal filter of Yu and others (2015) applied. This term could also be applied to stations that are not atop sediments but has been omitted in such cases for the sake of brevity.
Sediment	H-k stack for a sedimentary layer atop the crystalline crust.
Sub-Sediment	H-k stack for the crystalline crust beneath sediments.
PWS	H-k stacking results using phase-weighted stacking.
mo	Shorthand for "moveout." Appears within labels of the form "[station identifier]-mo-[number]" (for example, "WELA-mo-001"). Used to indicate that the plot is against ray parameter and that the arrival-time curves have a moveout correction applied to them based on the changing ray parameter.
baz	Shorthand for "back azimuth." Appears within labels of the form "[station identifier]-baz-[number]" (for example, "WELA-baz-001"). Used to indicate that the plot is against back azimuth and that the arrival-time curves do not have a moveout correction applied but instead assume a constant ray parameter of 0.06 s/km.

H-k Stacking Results

In this section, we first show our *H-k* stacking results across the entire array and the impact of the three different sedimentary correction values (fig. 3) we tested. We then plot the *H-k* stacking results and the receiver functions binned by ray parameter and back azimuth for every single station (figs. 6–313) following the order in table 1.1, wherein seismic stations are sorted from north to south and then from west to east.

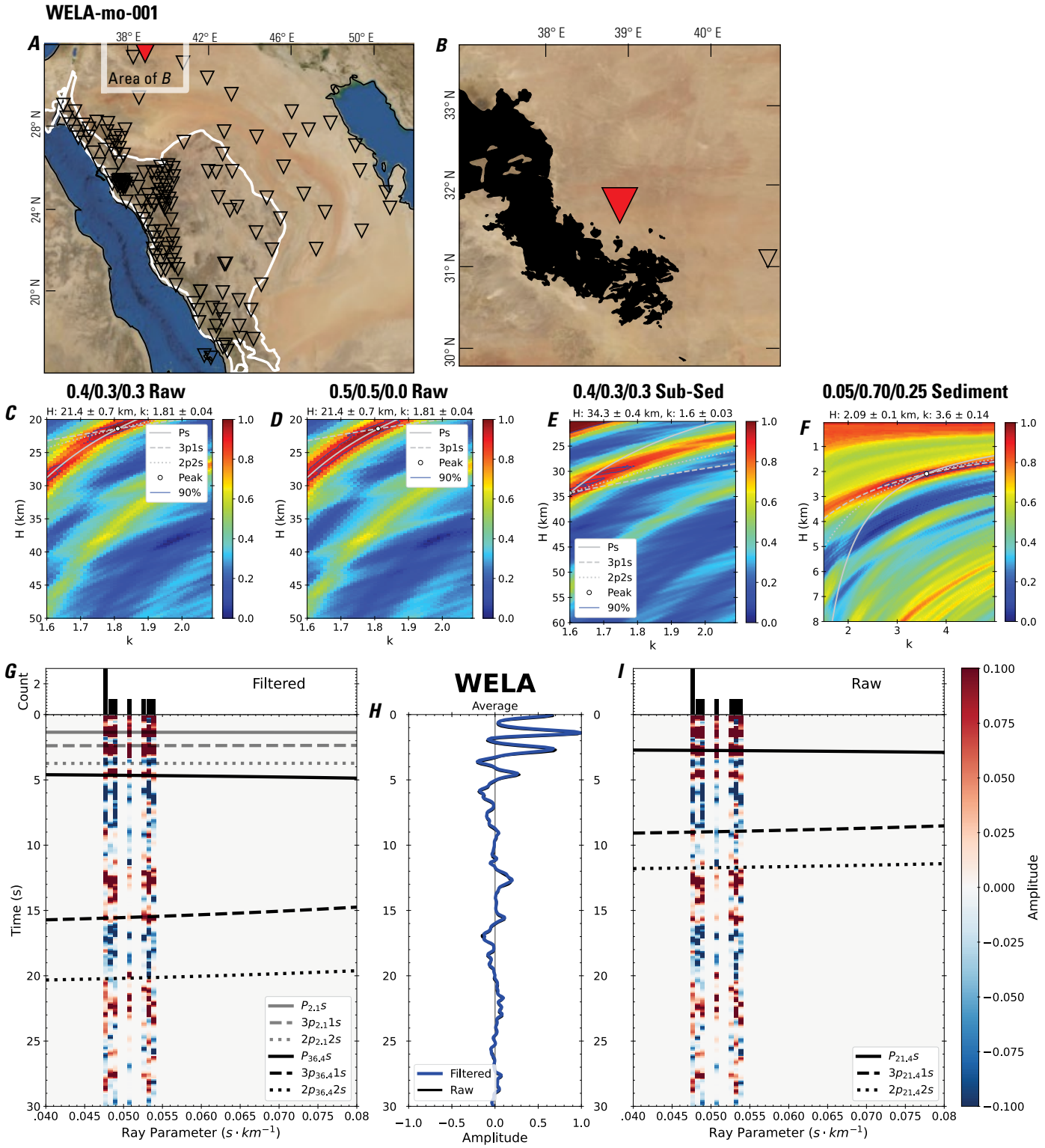
WELA-mo-001
A
38° E
42° E
46° E
50° E
Area of B
28° N
24° N
20° N
B
38° E
39° E
40° E
33° N
32° N
31° N
30° N
C
0.4/0.3/0.3 Raw
H: 21.4 ± 0.7 km, k: 1.81 ± 0.04
D
0.5/0.5/0.0 Raw
H: 21.4 ± 0.7 km, k: 1.81 ± 0.04
E
0.4/0.3/0.3 Sub-Sed
H: 34.3 ± 0.4 km, k: 1.6 ± 0.03
F
0.05/0.70/0.25 Sediment
H: 2.09 ± 0.1 km, k: 3.6 ± 0.14
Ps
3p1s
2p2s
Peak
90%
H (km)
k
G
Filtered
Count
Time (s)
$P_{2.1}s$
$3p_{2.1}1s$
$2p_{2.1}2s$
$P_{36.4}s$
$3p_{36.4}1s$
$2p_{36.4}2s$
Ray Parameter ($s \cdot km^{-1}$)
H
WELA
Average
Filtered
Raw
Amplitude
I
Raw
$P_{21.4}s$
$3p_{21.4}1s$
$2p_{21.4}2s$
Amplitude

Figure 6 (page 12). Receiver-function analysis for station WELA. *A*, Regional map of Saudi Arabia showing the entire array (as inverted triangles), the location of station WELA (red inverted triangle), the shield-platform boundary (white line), and the bounds of the map in *B* (white box). *B*, Local map of station WELA. Harrats are shown in black. *C*, Standard, single-layer *H-k* stack with stacking weights 0.4/0.3/0.3. This *H-k* stack ignores sedimentary effects on the receiver functions. *D*, Standard, single-layer *H-k* stack with stacking weights 0.5/0.5/0.0. This *H-k* stack also ignores sedimentary effects on the receiver functions. *E*, Optimized sub-sedimentary *H-k* stack with stacking weights 0.4/0.3/0.3, following the method of Yu and others (2015). *F*, Optimized sedimentary *H-k* stack with stacking weights 0.05/0.70/0.25, following the method of Yu and others (2015). *G*, Radial component P-wave receiver functions (PRFs) plotted against ray parameter. Individual PRFs have had the resonance-removal filter of Yu and others (2015) applied to them and are normalized to the maximum amplitude within the time window shown, binned, and normalized by the number of traces per bin. *H*, Average of every individual normalized radial receiver function with the application of the resonance-removal filter (blue) and average of every individual normalized raw radial receiver function (red). *I*, Radial component of raw PRFs (that is, PRFs with no resonance-removal filter applied) plotted against ray parameter, normalized as in *G*.

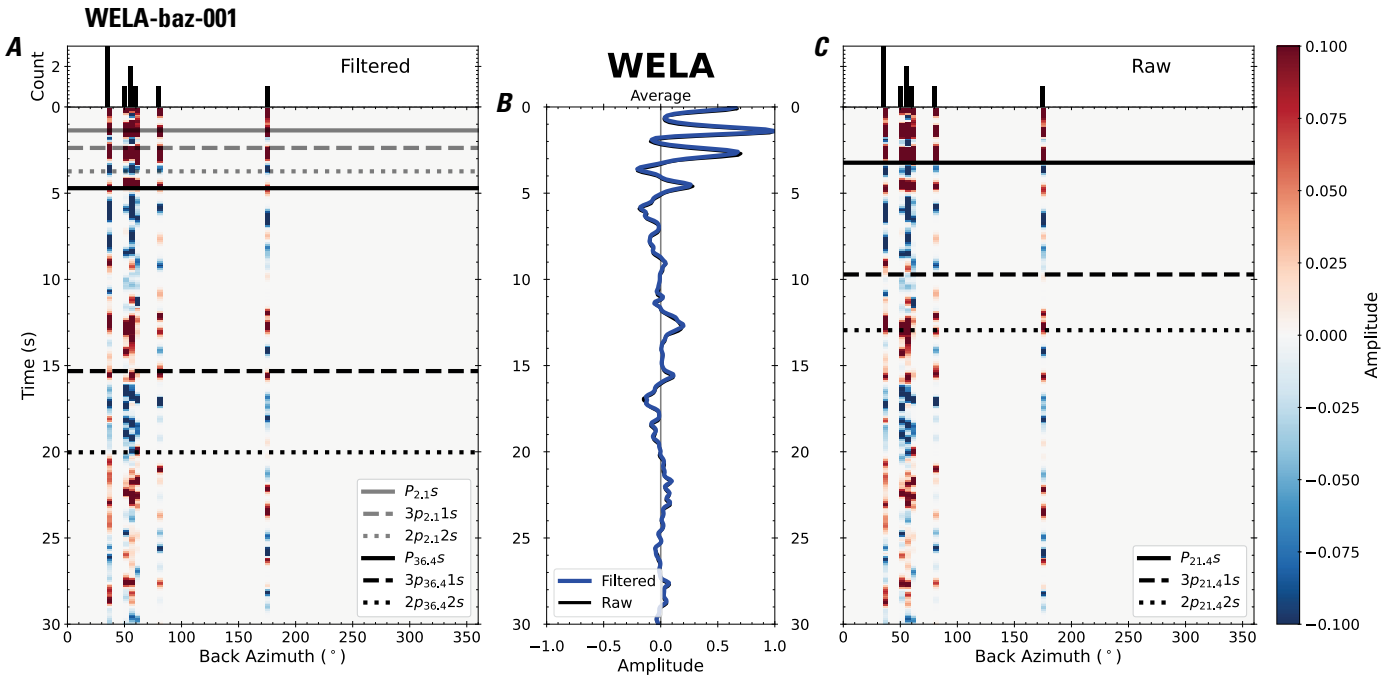

Figure 7. Receiver functions plotted against back azimuth for station WELA. *A*, Radial component of P-wave receiver functions (PRFs) plotted against back azimuth. Individual PRFs have had the resonance-removal filter of Yu and others (2015) applied to them, are normalized to the maximum amplitude within the time window shown, binned, and normalized by the number of traces per bin. *B*, Average of every individual normalized radial receiver function with the application of the resonance-removal filter (blue) and average of every individual normalized raw radial receiver function (red). *C*, Radial component of raw PRFs, plotted against back azimuth, normalized as in *A*. Ps, 3p1s, and 2p2s arrival times predicted for the preferred Moho depth are shown, assuming a ray parameter of 0.06 s/km.

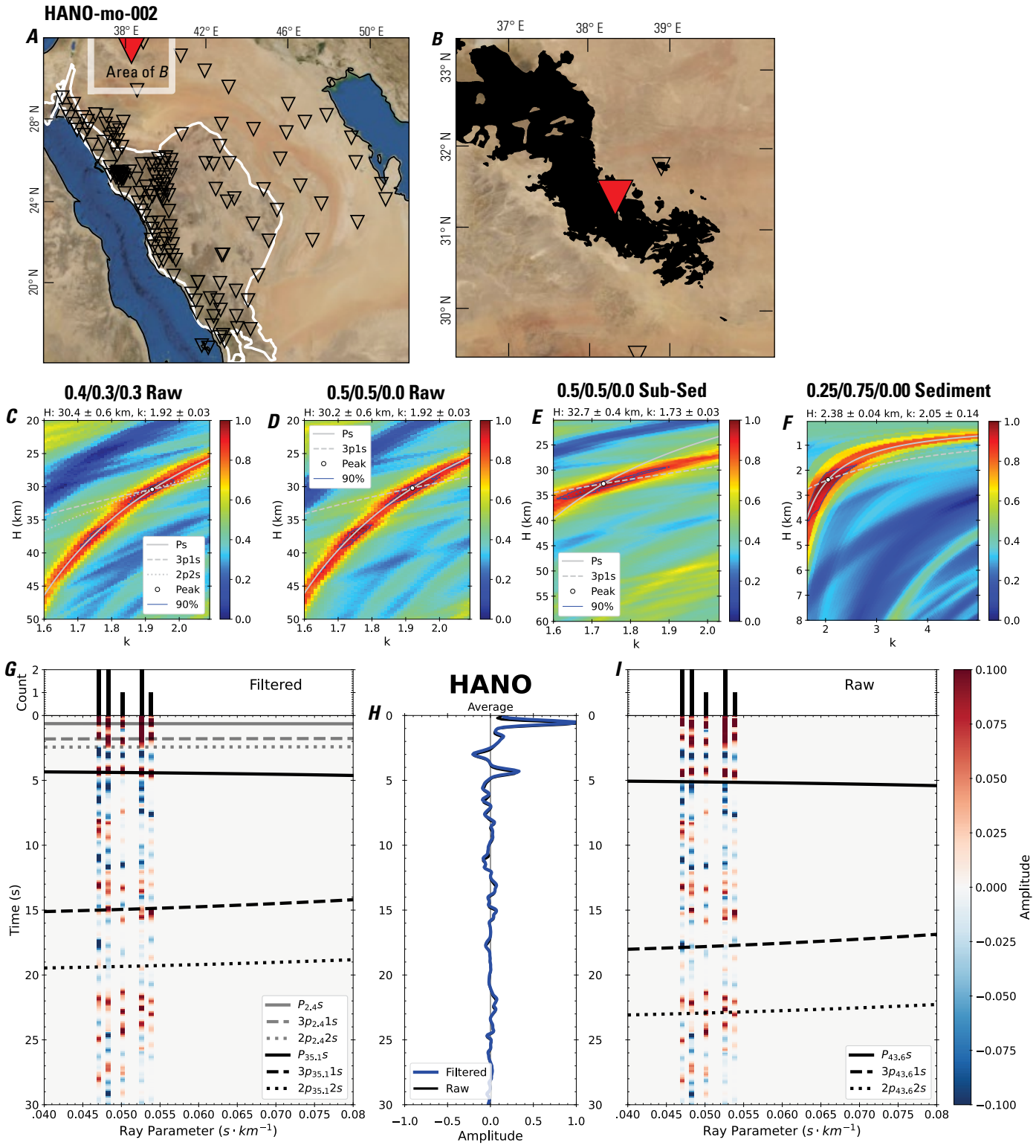
HANO-mo-002
A
38° E
42° E
46° E
50° E
Area of B
28° N
24° N
20° N
B
37° E
38° E
39° E
33° N
32° N
31° N
30° N
0.4/0.3/0.3 Raw
C
H: 30.4 ± 0.6 km, k: 1.92 ± 0.03
0.5/0.5/0.0 Raw
D
H: 30.2 ± 0.6 km, k: 1.92 ± 0.03
0.5/0.5/0.0 Sub-Sed
E
H: 32.7 ± 0.4 km, k: 1.73 ± 0.03
0.25/0.75/0.00 Sediment
F
H: 2.38 ± 0.04 km, k: 2.05 ± 0.14
H (km)
k
Ps
3p1s
2p2s
Peak
90%
G
Filtered
Count
Time (s)
Ray Parameter (s · km⁻¹)
$P_{2.4}s$
$3p_{2.4}1s$
$2p_{2.4}2s$
$P_{35.1}s$
$3p_{35.1}1s$
$2p_{35.1}2s$
HANO
Average
H
Filtered
Raw
Amplitude
I
Raw
$P_{43.6}s$
$3p_{43.6}1s$
$2p_{43.6}2s$
Amplitude

Figure 8 (page 14). Receiver-function analysis for station HANO. *A*, Regional map of Saudi Arabia showing the entire array (as inverted triangles), the location of station HANO (red inverted triangle), the shield-platform boundary (white line), and the bounds of the map in *B* (white box). *B*, Local map of station HANO. Harrats are shown in black. *C*, Standard, single-layer *H-k* stack with stacking weights 0.4/0.3/0.3. This *H-k* stack ignores sedimentary effects on the receiver functions. *D*, Standard, single-layer *H-k* stack with stacking weights 0.5/0.5/0.0. This *H-k* stack also ignores sedimentary effects on the receiver functions. *E*, Optimized sub-sedimentary *H-k* stack with stacking weights 0.4/0.3/0.3, following the method of Yu and others (2015). *F*, Optimized sedimentary *H-k* stack with stacking weights 0.05/0.70/0.25, following the method of Yu and others (2015). *G*, Radial component P-wave receiver functions (PRFs) plotted against ray parameter. Individual PRFs have had the resonance-removal filter of Yu and others (2015) applied to them and are normalized to the maximum amplitude within the time window shown, binned, and normalized by the number of traces per bin. *H*, Average of every individual normalized radial receiver function with the application of the resonance-removal filter (blue) and average of every individual normalized raw radial receiver function (red). *I*, Radial component of raw PRFs (that is, PRFs with no resonance-removal filter applied) plotted against ray parameter, normalized as in *G*.

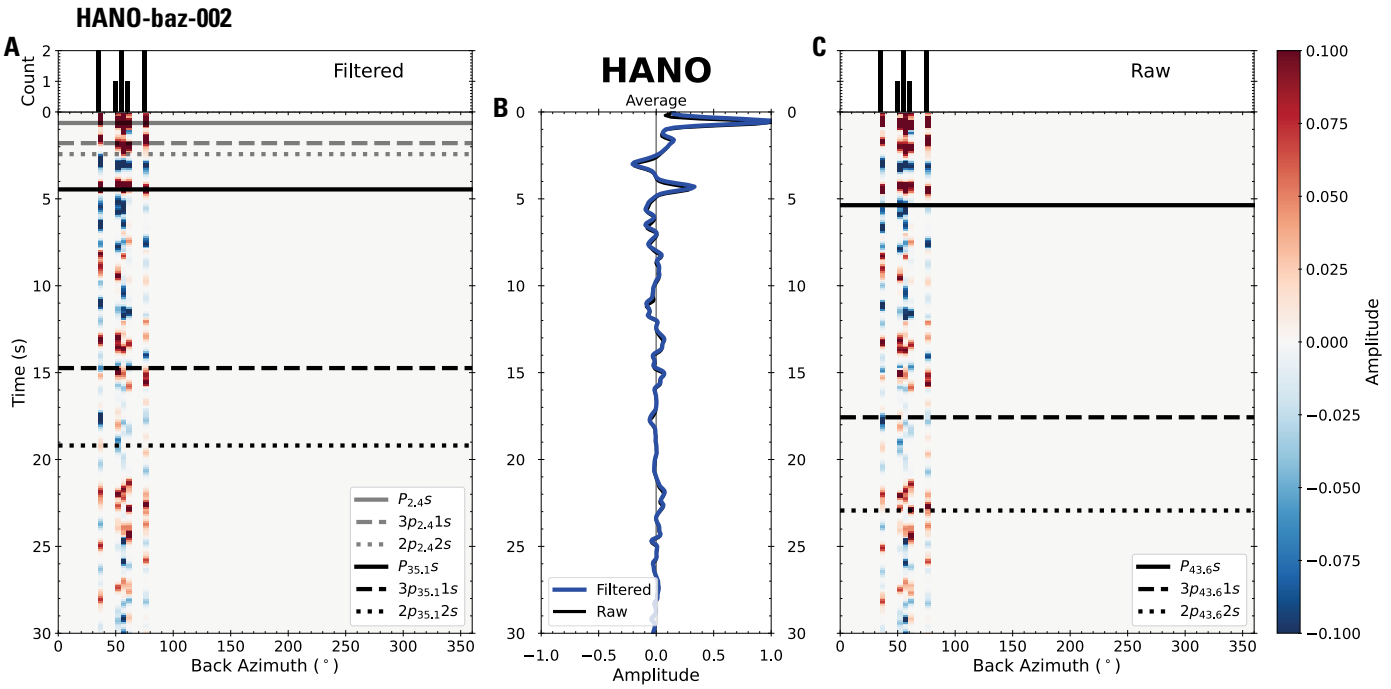

Figure 9. Receiver functions plotted against back azimuth for station HANO. *A*, Radial component of P-wave receiver functions (PRFs) plotted against back azimuth. Individual PRFs have had the resonance-removal filter of Yu and others (2015) applied to them, are normalized to the maximum amplitude within the time window shown, binned, and normalized by the number of traces per bin. *B*, Average of every individual normalized radial receiver function with the application of the resonance-removal filter (blue) and average of every individual normalized raw radial receiver function (red). *C*, Radial component of raw PRFs, plotted against back azimuth, normalized as in *A*. Ps, 3p1s, and 2p2s arrival times predicted for the preferred Moho depth are shown, assuming a ray parameter of 0.06 s/km.

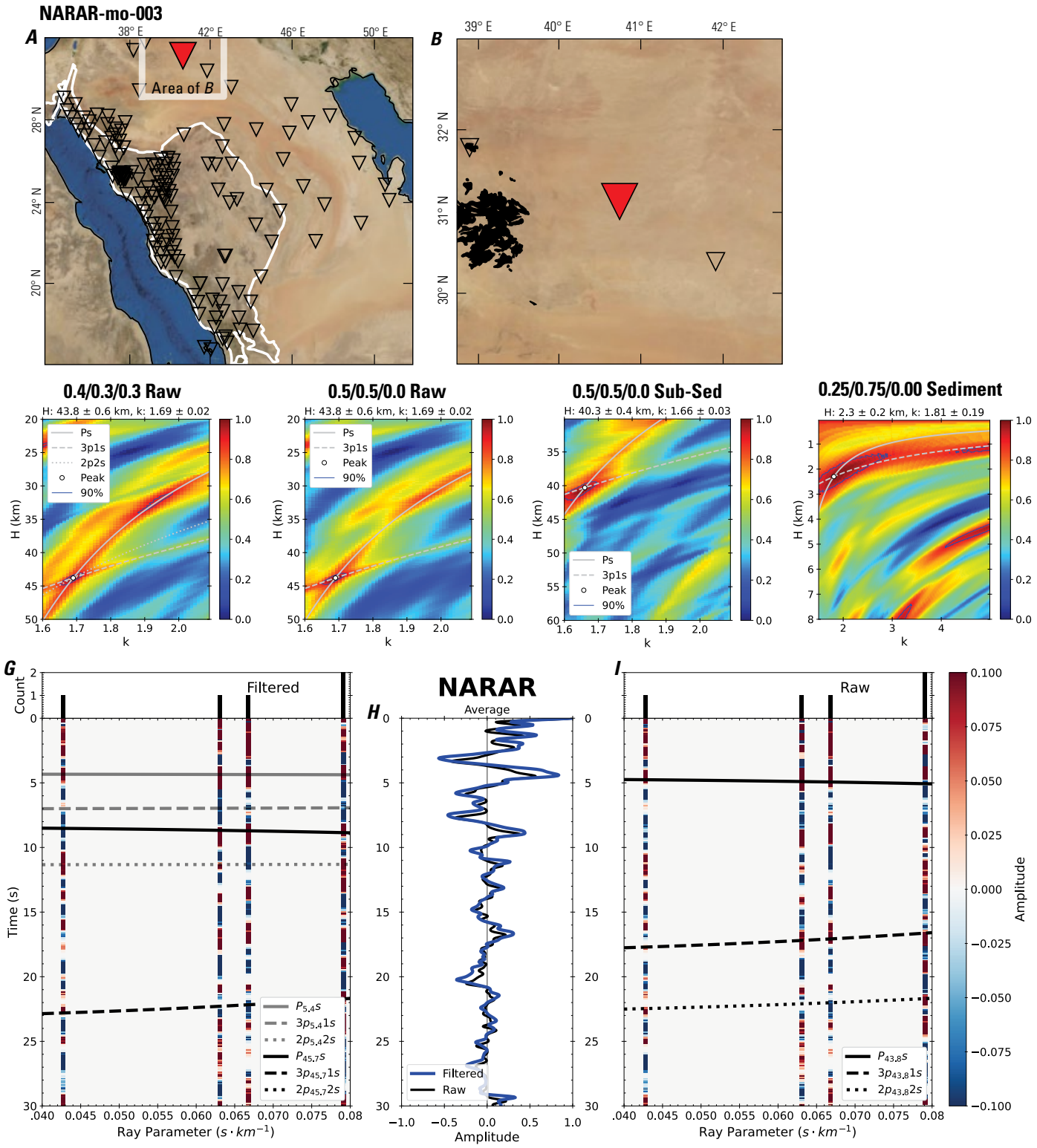
NARAR-mo-003
A
38° E
42° E
46° E
50° E
28° N
24° N
20° N
Area of B
B
39° E
40° E
41° E
42° E
32° N
31° N
30° N
0.4/0.3/0.3 Raw
H: 43.8 ± 0.6 km, k: 1.69 ± 0.02
0.5/0.5/0.0 Raw
H: 43.8 ± 0.6 km, k: 1.69 ± 0.02
0.5/0.5/0.0 Sub-Sed
H: 40.3 ± 0.4 km, k: 1.66 ± 0.03
0.25/0.75/0.00 Sediment
H: 2.3 ± 0.2 km, k: 1.81 ± 0.19
Ps
3p1s
2p2s
Peak
90%
H (km)
k
G
Filtered
Count
Time (s)
$P_{5.4}s$
$3p_{5.4}1s$
$2p_{5.4}2s$
$P_{45.7}s$
$3p_{45.7}1s$
$2p_{45.7}2s$
Ray Parameter ($s \cdot km^{-1}$)
NARAR
Average
H
Filtered
Raw
Amplitude
I
Raw
$P_{43.8}s$
$3p_{43.8}1s$
$2p_{43.8}2s$
Ray Parameter ($s \cdot km^{-1}$)
Amplitude

Figure 10 (page 16). Receiver-function analysis for station NARAR. *A*, Regional map of Saudi Arabia showing the entire array (as inverted triangles), the location of station NARAR (red inverted triangle), the shield-platform boundary (white line), and the bounds of the map in *B* (white box). *B*, Local map of station NARAR. Harrats are shown in black. *C*, Standard, single-layer *H-k* stack with stacking weights 0.4/0.3/0.3. This *H-k* stack ignores sedimentary effects on the receiver functions. *D*, Standard, single-layer *H-k* stack with stacking weights 0.5/0.5/0.0. This *H-k* stack also ignores sedimentary effects on the receiver functions. *E*, Optimized sub-sedimentary *H-k* stack with stacking weights 0.4/0.3/0.3, following the method of Yu and others (2015). *F*, Optimized sedimentary *H-k* stack with stacking weights 0.05/0.70/0.25, following the method of Yu and others (2015). *G*, Radial component P-wave receiver functions (PRFs) plotted against ray parameter. Individual PRFs have had the resonance-removal filter of Yu and others (2015) applied to them and are normalized to the maximum amplitude within the time window shown, binned, and normalized by the number of traces per bin. *H*, Average of every individual normalized radial receiver function with the application of the resonance-removal filter (blue) and average of every individual normalized raw radial receiver function (red). *I*, Radial component of raw PRFs (that is, PRFs with no resonance-removal filter applied) plotted against ray parameter, normalized as in *G*.

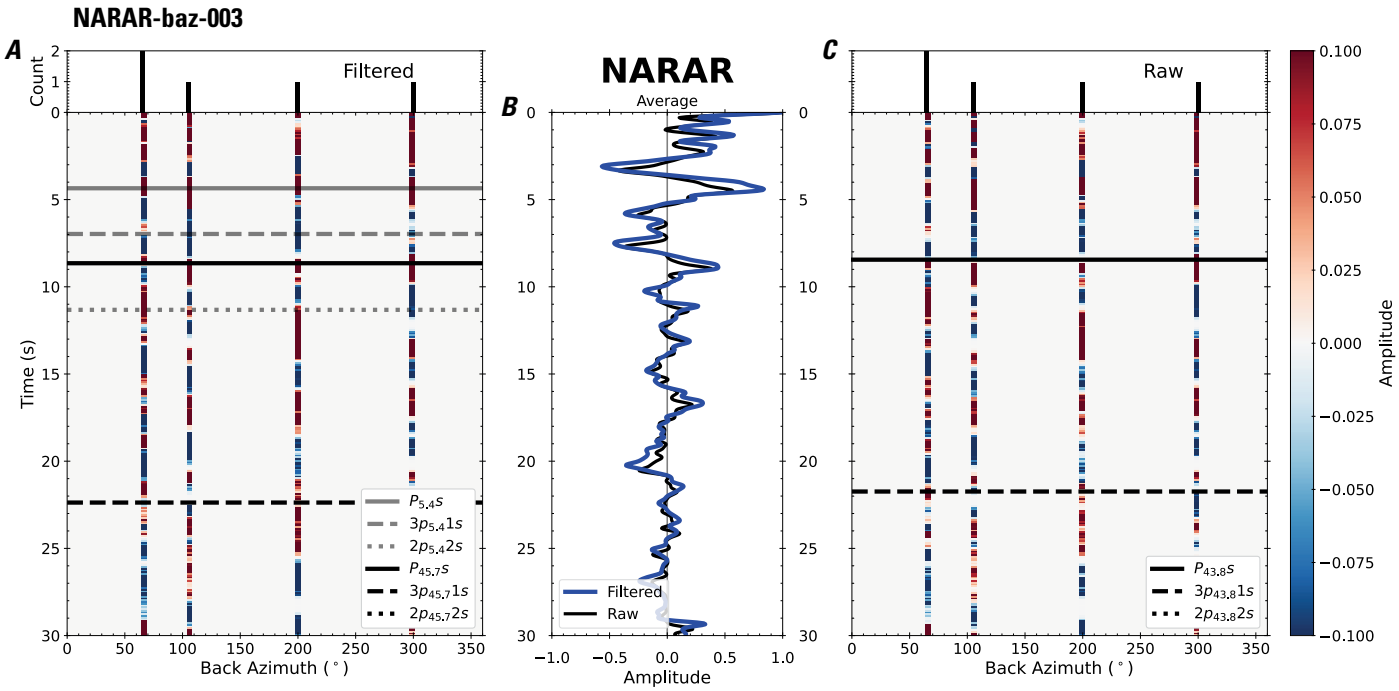

Figure 11. Receiver functions plotted against back azimuth for station NARAR. *A*, Radial component of P-wave receiver functions (PRFs) plotted against back azimuth. Individual PRFs have had the resonance-removal filter of Yu and others (2015) applied to them, are normalized to the maximum amplitude within the time window shown, binned, and normalized by the number of traces per bin. *B*, Average of every individual normalized radial receiver function with the application of the resonance-removal filter (blue) and average of every individual normalized raw radial receiver function (red). *C*, Radial component of raw PRFs, plotted against back azimuth, normalized as in *A*. Ps, 3p1s, and 2p2s arrival times predicted for the preferred Moho depth are shown, assuming a ray parameter of 0.06 s/km.

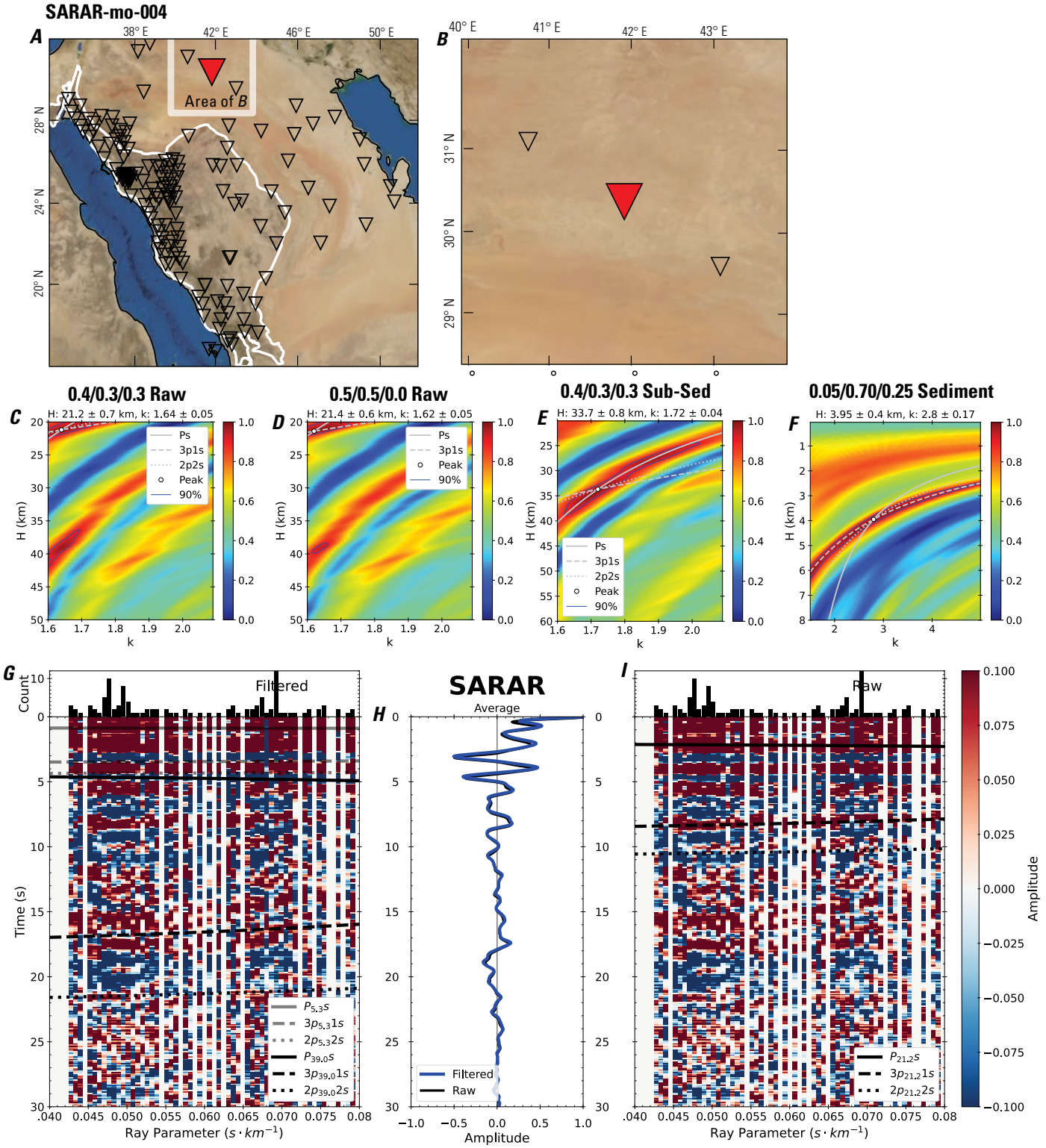
SARAR-mo-004
A
38° E
42° E
46° E
50° E
28° N
24° N
20° N
Area of B
B
40° E
41° E
42° E
43° E
31° N
30° N
29° N
0.4/0.3/0.3 Raw
C
H: 21.2 ± 0.7 km, k: 1.64 ± 0.05
0.5/0.5/0.0 Raw
D
H: 21.4 ± 0.6 km, k: 1.62 ± 0.05
0.4/0.3/0.3 Sub-Sed
E
H: 33.7 ± 0.8 km, k: 1.72 ± 0.04
0.05/0.70/0.25 Sediment
F
H: 3.95 ± 0.4 km, k: 2.8 ± 0.17
Ps
3p1s
2p2s
Peak
90%
H (km)
k
G
Filtered
Count
Time (s)
$P_{5.3}s$
$3p_{5.3}1s$
$2p_{5.3}2s$
$P_{39.0}s$
$3p_{39.0}1s$
$2p_{39.0}2s$
Ray Parameter ($s \cdot km^{-1}$)
SARAR
Average
H
Filtered
Raw
Amplitude
I
Raw
$P_{21.2}s$
$3p_{21.2}1s$
$2p_{21.2}2s$
Amplitude

Figure 12 (page 18). Receiver-function analysis for station SARAR. *A*, Regional map of Saudi Arabia showing the entire array (as inverted triangles), the location of station SARAR (red inverted triangle), the shield-platform boundary (white line), and the bounds of the map in *B* (white box). *B*, Local map of station SARAR. Harrats are shown in black. *C*, Standard, single-layer *H-k* stack with stacking weights 0.4/0.3/0.3. This *H-k* stack ignores sedimentary effects on the receiver functions. *D*, Standard, single-layer *H-k* stack with stacking weights 0.5/0.5/0.0. This *H-k* stack also ignores sedimentary effects on the receiver functions. *E*, Optimized sub-sedimentary *H-k* stack with stacking weights 0.4/0.3/0.3, following the method of Yu and others (2015). *F*, Optimized sedimentary *H-k* stack with stacking weights 0.05/0.70/0.25, following the method of Yu and others (2015). *G*, Radial component P-wave receiver functions (PRFs) plotted against ray parameter. Individual PRFs have had the resonance-removal filter of Yu and others (2015) applied to them and are normalized to the maximum amplitude within the time window shown, binned, and normalized by the number of traces per bin. *H*, Average of every individual normalized radial receiver function with the application of the resonance-removal filter (blue) and average of every individual normalized raw radial receiver function (red). *I*, Radial component of raw PRFs (that is, PRFs with no resonance-removal filter applied) plotted against ray parameter, normalized as in *G*.

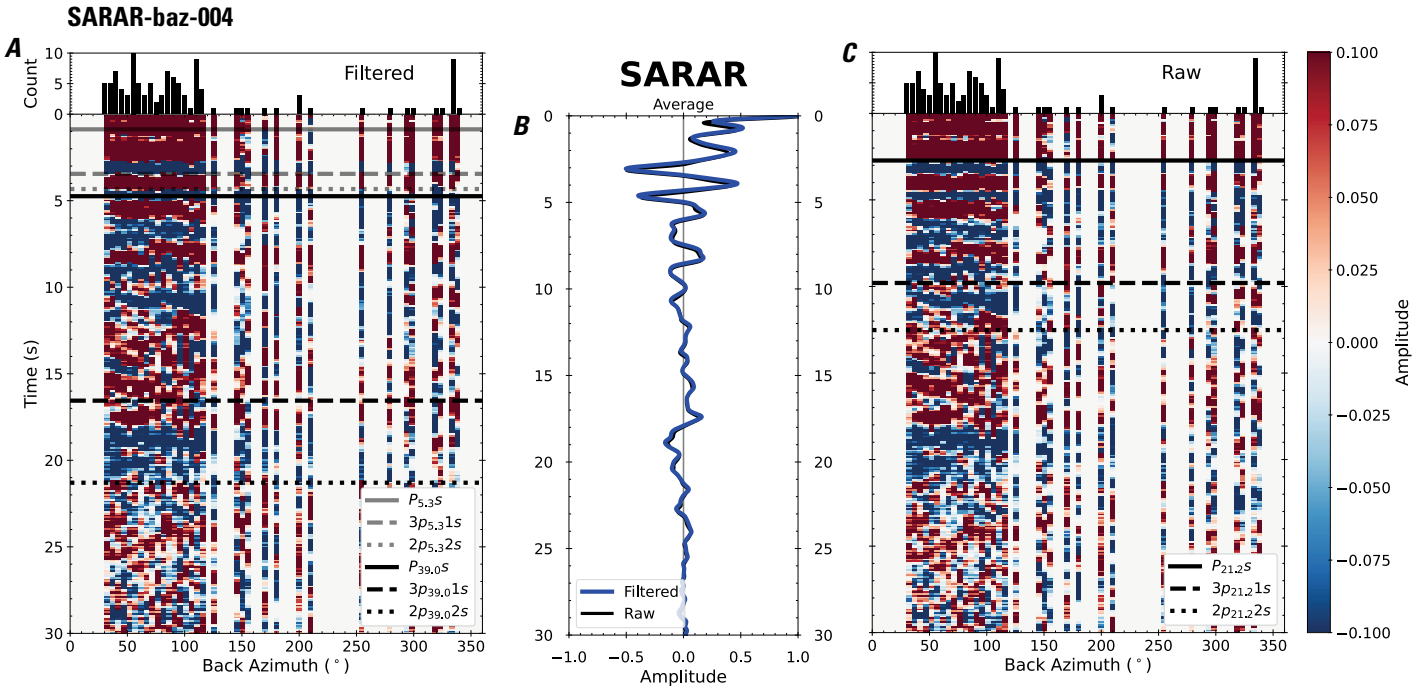

Figure 13. Receiver functions plotted against back azimuth for station SARAR. *A*, Radial component of P-wave receiver functions (PRFs) plotted against back azimuth. Individual PRFs have had the resonance-removal filter of Yu and others (2015) applied to them, are normalized to the maximum amplitude within the time window shown, binned, and normalized by the number of traces per bin. *B*, Average of every individual normalized radial receiver function with the application of the resonance-removal filter (blue) and average of every individual normalized raw radial receiver function (red). *C*, Radial component of raw PRFs, plotted against back azimuth, normalized as in *A*. Ps, 3p1s, and 2p2s arrival times predicted for the preferred Moho depth are shown, assuming a ray parameter of 0.06 s/km.

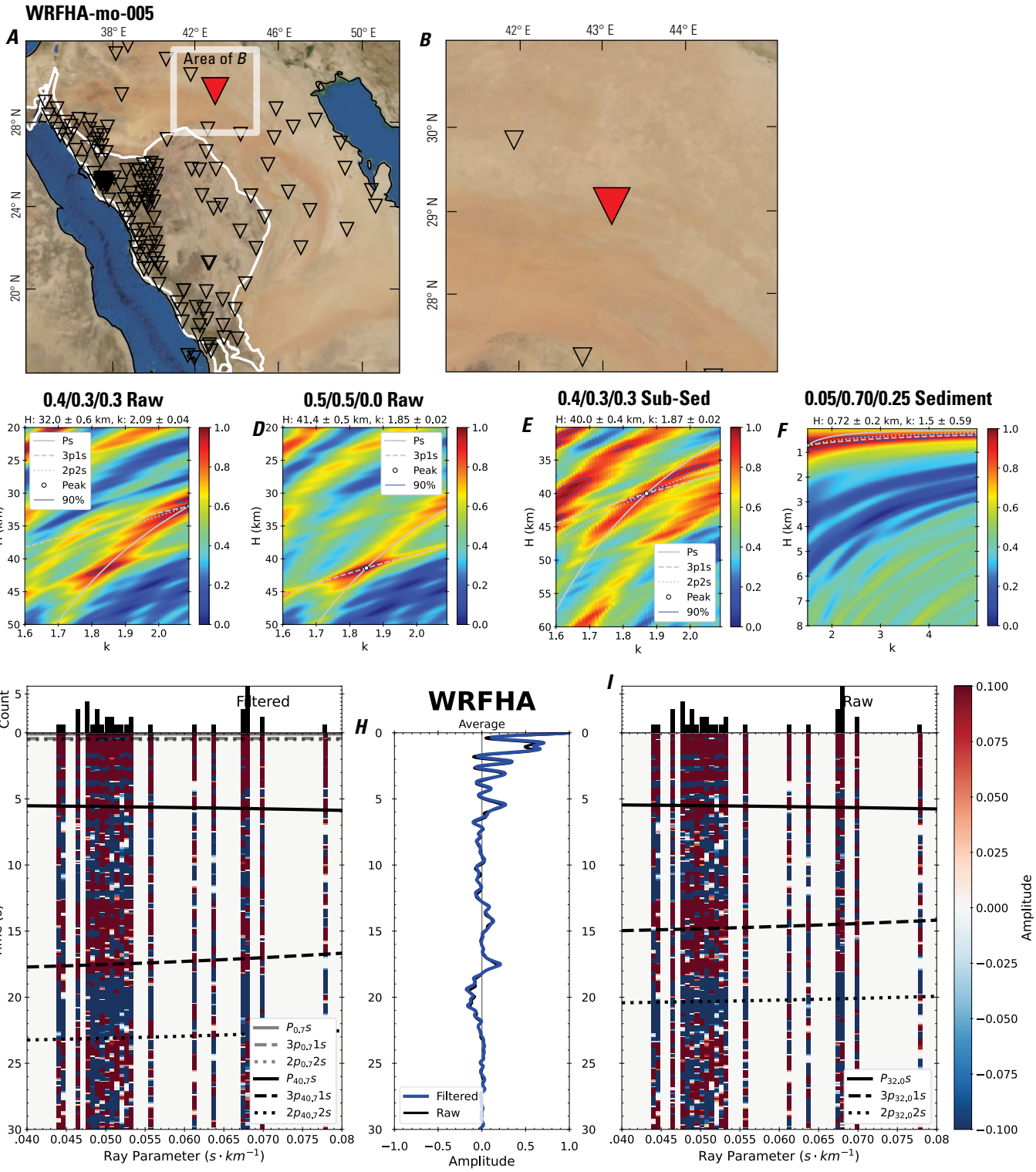
WRFHA-mo-005
A
38° E
42° E
46° E
50° E
28° N
24° N
20° N
Area of B
B
42° E
43° E
44° E
30° N
29° N
28° N
0.4/0.3/0.3 Raw
H: 32.0 ± 0.6 km, k: 2.09 ± 0.04
C
0.5/0.5/0.0 Raw
H: 41.4 ± 0.5 km, k: 1.85 ± 0.02
D
0.4/0.3/0.3 Sub-Sed
H: 40.0 ± 0.4 km, k: 1.87 ± 0.02
E
0.05/0.70/0.25 Sediment
H: 0.72 ± 0.2 km, k: 1.5 ± 0.59
F
Ps
3p1s
2p2s
Peak
90%
H (km)
k
G
Filtered
Count
Time (s)
$P_{0.7}s$
$3p_{0.7}1s$
$2p_{0.7}2s$
$P_{40.7}s$
$3p_{40.7}1s$
$2p_{40.7}2s$
Ray Parameter ($s \cdot km^{-1}$)
H
WRFHA
Average
Filtered
Raw
Amplitude
I
Raw
$P_{32.0}s$
$3p_{32.0}1s$
$2p_{32.0}2s$
Amplitude

Figure 14 (page 20). Receiver-function analysis for station WRFHA. *A*, Regional map of Saudi Arabia showing the entire array (as inverted triangles), the location of station WRFHA (red inverted triangle), the shield-platform boundary (white line), and the bounds of the map in *B* (white box). *B*, Local map of station WRFHA. Harrats are shown in black. *C*, Standard, single-layer *H-k* stack with stacking weights 0.4/0.3/0.3. This *H-k* stack ignores sedimentary effects on the receiver functions. *D*, Standard, single-layer *H-k* stack with stacking weights 0.5/0.5/0.0. This *H-k* stack also ignores sedimentary effects on the receiver functions. *E*, Optimized sub-sedimentary *H-k* stack with stacking weights 0.4/0.3/0.3, following the method of Yu and others (2015). *F*, Optimized sedimentary *H-k* stack with stacking weights 0.05/0.70/0.25, following the method of Yu and others (2015). *G*, Radial component P-wave receiver functions (PRFs) plotted against ray parameter. Individual PRFs have had the resonance-removal filter of Yu and others (2015) applied to them and are normalized to the maximum amplitude within the time window shown, binned, and normalized by the number of traces per bin. *H*, Average of every individual normalized radial receiver function with the application of the resonance-removal filter (blue) and average of every individual normalized raw radial receiver function (red). *I*, Radial component of raw PRFs (that is, PRFs with no resonance-removal filter applied) plotted against ray parameter, normalized as in *G*.

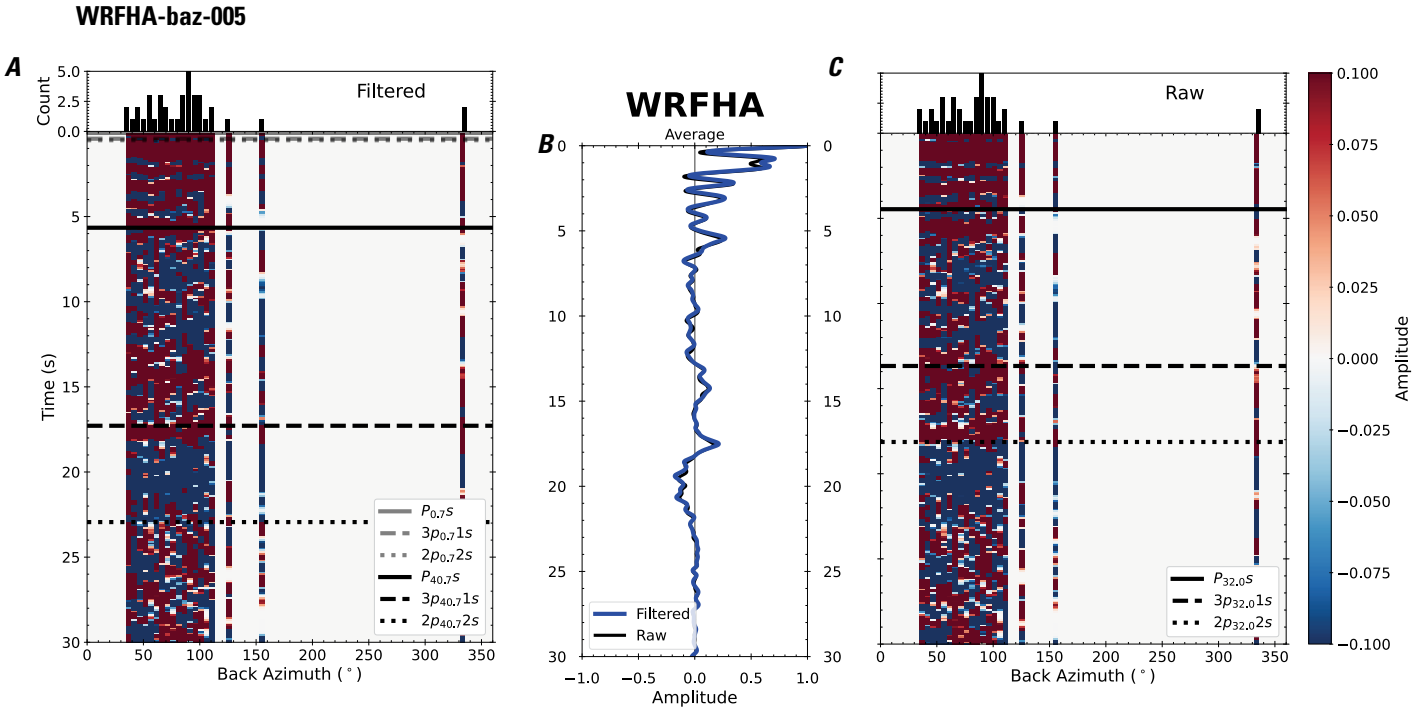

Figure 15. Receiver functions plotted against back azimuth for station WRFHA. *A*, Radial component of P-wave receiver functions (PRFs) plotted against back azimuth. Individual PRFs have had the resonance-removal filter of Yu and others (2015) applied to them, are normalized to the maximum amplitude within the time window shown, binned, and normalized by the number of traces per bin. *B*, Average of every individual normalized radial receiver function with the application of the resonance-removal filter (blue) and average of every individual normalized raw radial receiver function (red). *C*, Radial component of raw PRFs, plotted against back azimuth, normalized as in *A*. Ps, 3p1s, and 2p2s arrival times predicted for the preferred Moho depth are shown, assuming a ray parameter of 0.06 s/km.

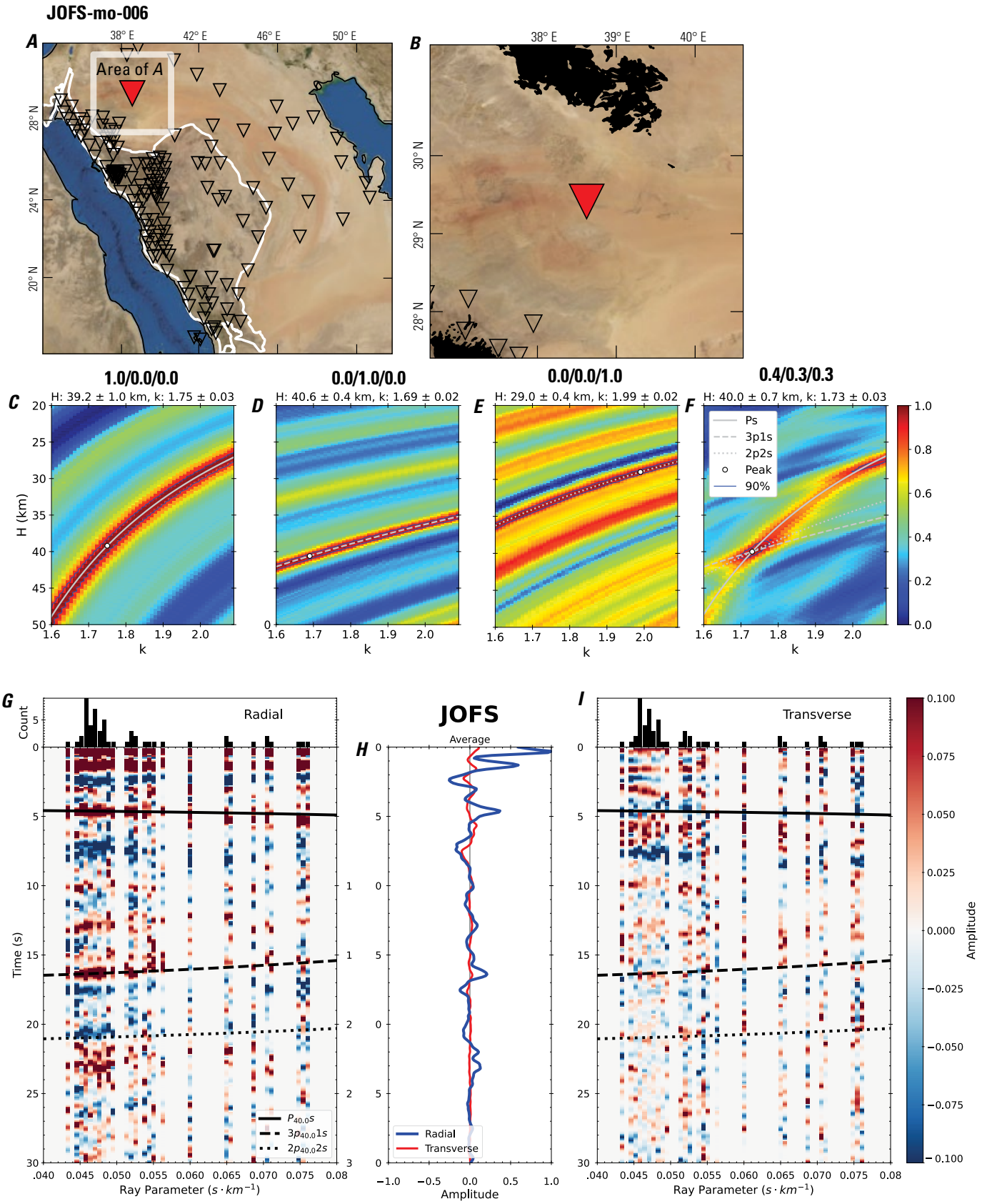
JOFS-mo-006
A
B
Area of A
38° E
42° E
46° E
50° E
28° N
24° N
20° N
39° E
40° E
30° N
29° N
1.0/0.0/0.0
H: 39.2 ± 1.0 km, k: 1.75 ± 0.03
0.0/1.0/0.0
H: 40.6 ± 0.4 km, k: 1.69 ± 0.02
0.0/0.0/1.0
H: 29.0 ± 0.4 km, k: 1.99 ± 0.02
0.4/0.3/0.3
H: 40.0 ± 0.7 km, k: 1.73 ± 0.03
C
D
E
F
H (km)
k
Ps
3p1s
2p2s
Peak
90%
Amplitude
G
Radial
Count
Time (s)
$P_{40.0}s$
$3p_{40.0}1s$
$2p_{40.0}2s$
Ray Parameter ($s \cdot km^{-1}$)
JOFS
Average
H
Radial
Transverse
Amplitude
I
Transverse

Figure 16 (page 22). Receiver-function analysis for station JOFS. *A*, Regional map of Saudi Arabia showing the entire array (as inverted triangles), the location of station JOFS (red inverted triangle), the shield-platform boundary (white line), and the bounds of the map in *B* (white box). *B*, Local map of station JOFS. Harrats are shown in black. *C*, Standard, single-layer *H-k* stack with stacking weights 0.4/0.3/0.3. This *H-k* stack ignores sedimentary effects on the receiver functions. *D*, Standard, single-layer *H-k* stack with stacking weights 0.5/0.5/0.0. This *H-k* stack also ignores sedimentary effects on the receiver functions. *E*, Optimized sub-sedimentary *H-k* stack with stacking weights 0.4/0.3/0.3, following the method of Yu and others (2015). *F*, Optimized sedimentary *H-k* stack with stacking weights 0.05/0.70/0.25, following the method of Yu and others (2015). *G*, Radial component P-wave receiver functions (PRFs) plotted against ray parameter. Individual PRFs have had the resonance-removal filter of Yu and others (2015) applied to them and are normalized to the maximum amplitude within the time window shown, binned, and normalized by the number of traces per bin. *H*, Average of every individual normalized radial receiver function with the application of the resonance-removal filter (blue) and average of every individual normalized raw radial receiver function (red). *I*, Radial component of raw PRFs (that is, PRFs with no resonance-removal filter applied) plotted against ray parameter, normalized as in *G*.

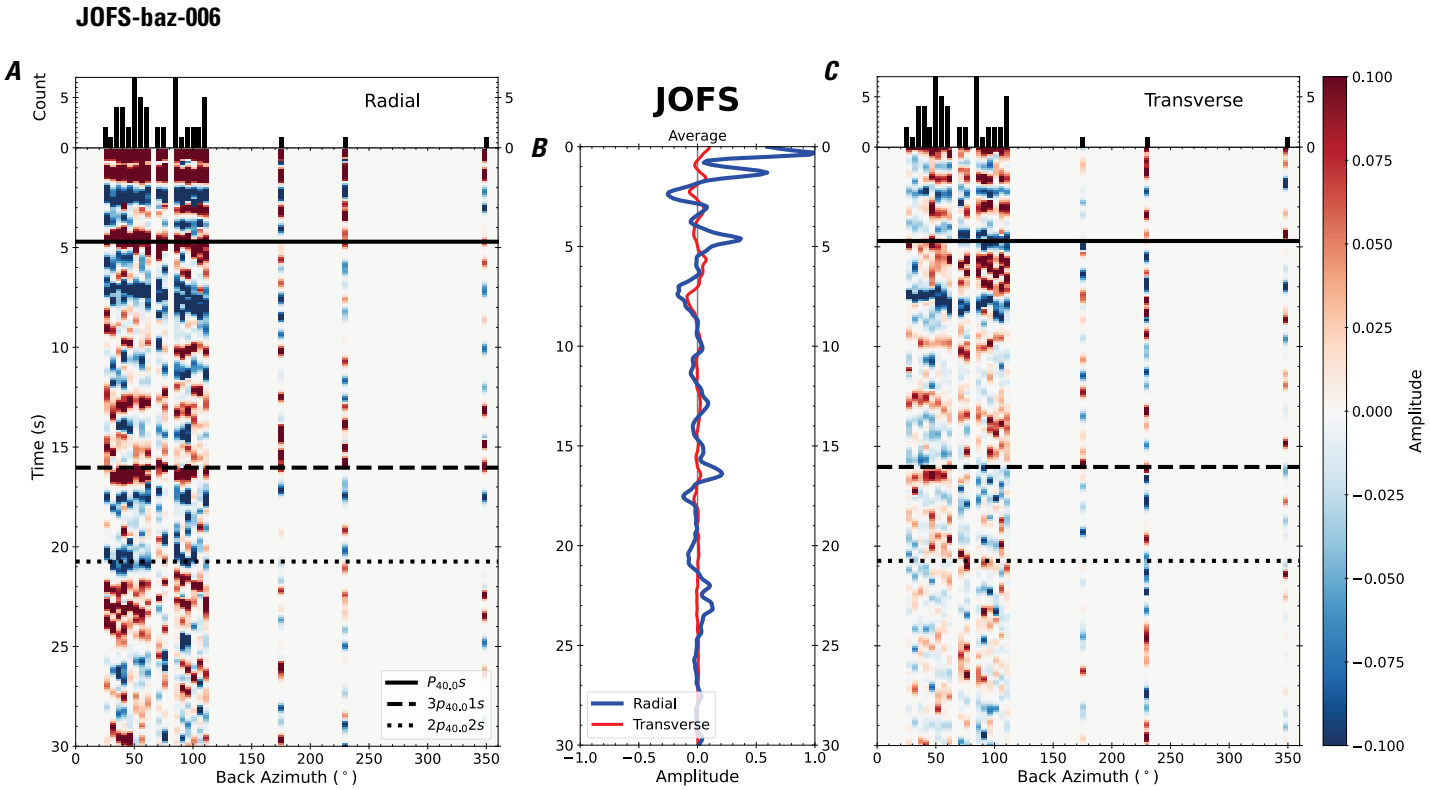

Figure 17. Receiver functions plotted against back azimuth for station JOFS. *A*, Radial component of P-wave receiver functions (PRFs) plotted against back azimuth. Individual PRFs have had the resonance-removal filter of Yu and others (2015) applied to them, are normalized to the maximum amplitude within the time window shown, binned, and normalized by the number of traces per bin. *B*, Average of every individual normalized radial receiver function with the application of the resonance-removal filter (blue) and average of every individual normalized raw radial receiver function (red). *C*, Radial component of raw PRFs, plotted against back azimuth, normalized as in *A*. Ps, 3p1s, and 2p2s arrival times predicted for the preferred Moho depth are shown, assuming a ray parameter of 0.06 s/km.

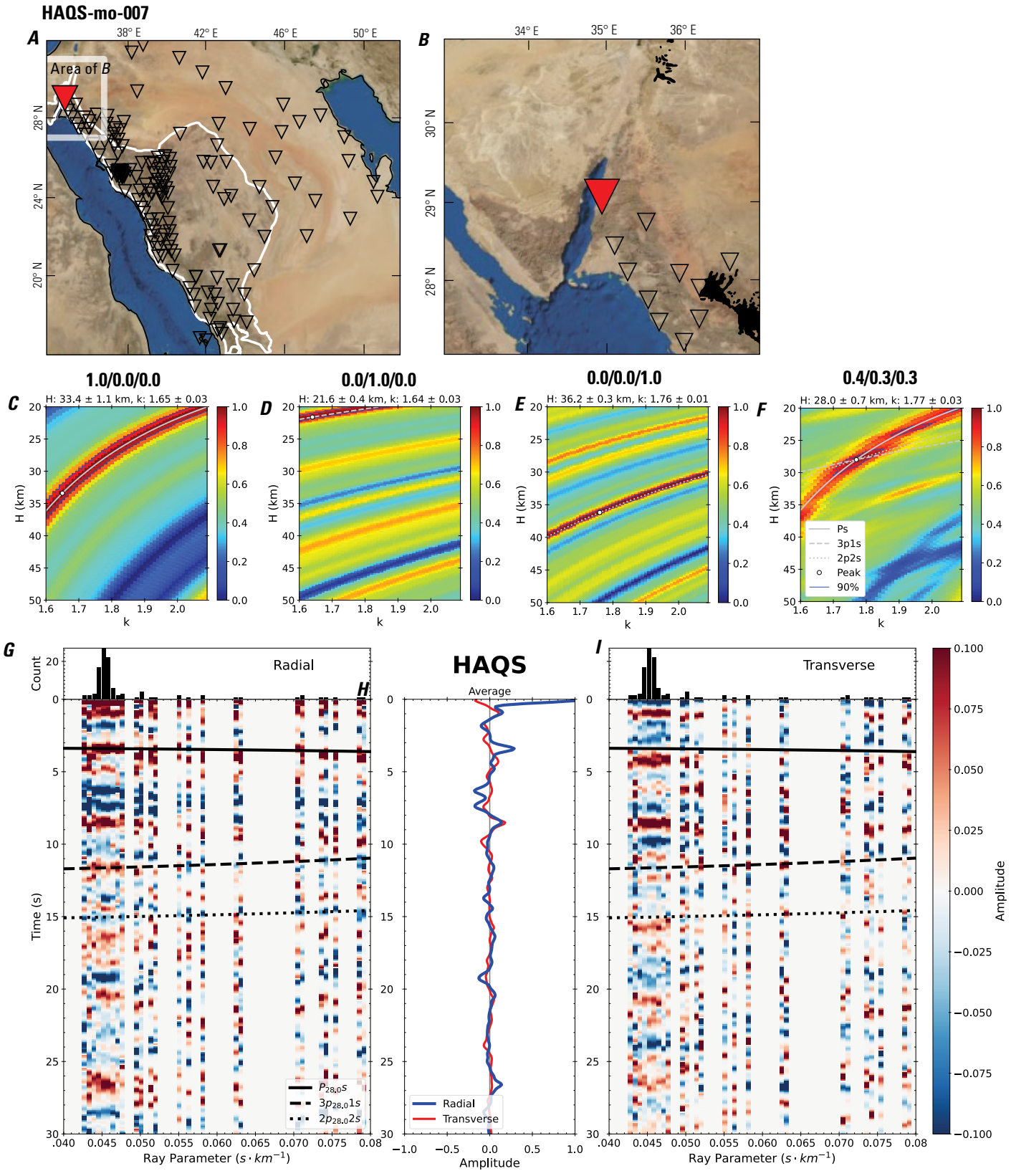
HAQS-mo-007
A
Area of B
38° E
42° E
46° E
50° E
28° N
24° N
20° N
B
34° E
35° E
36° E
30° N
29° N
28° N
1.0/0.0/0.0
0.0/1.0/0.0
0.0/0.0/1.0
0.4/0.3/0.3
C
H: 33.4 ± 1.1 km, k: 1.65 ± 0.03
D
H: 21.6 ± 0.4 km, k: 1.64 ± 0.03
E
H: 36.2 ± 0.3 km, k: 1.76 ± 0.01
F
H: 28.0 ± 0.7 km, k: 1.77 ± 0.03
H (km)
k
Ps
3p1s
2p2s
Peak
90%
G
Radial
H
HAQS
Average
I
Transverse
Count
Time (s)
Ray Parameter ($s \cdot km^{-1}$)
$P_{28.0}s$
$3p_{28.0}1s$
$2p_{28.0}2s$
Radial
Transverse
Amplitude

Figure 18 (page 24). Receiver-function analysis for station HAQS. *A*, Regional map of Saudi Arabia showing the entire array (as inverted triangles), the location of station HAQS (red inverted triangle), the shield-platform boundary (white line), and the bounds of the map in *B* (white box). *B*, Local map of station HAQS. Harrats are shown in black. *C*, Standard, single-layer *H-k* stack with stacking weights 0.4/0.3/0.3. This *H-k* stack ignores sedimentary effects on the receiver functions. *D*, Standard, single-layer *H-k* stack with stacking weights 0.5/0.5/0.0. This *H-k* stack also ignores sedimentary effects on the receiver functions. *E*, Optimized sub-sedimentary *H-k* stack with stacking weights 0.4/0.3/0.3, following the method of Yu and others (2015). *F*, Optimized sedimentary *H-k* stack with stacking weights 0.05/0.70/0.25, following the method of Yu and others (2015). *G*, Radial component P-wave receiver functions (PRFs) plotted against ray parameter. Individual PRFs have had the resonance-removal filter of Yu and others (2015) applied to them and are normalized to the maximum amplitude within the time window shown, binned, and normalized by the number of traces per bin. *H*, Average of every individual normalized radial receiver function with the application of the resonance-removal filter (blue) and average of every individual normalized raw radial receiver function (red). *I*, Radial component of raw PRFs (that is, PRFs with no resonance-removal filter applied) plotted against ray parameter, normalized as in *G*.

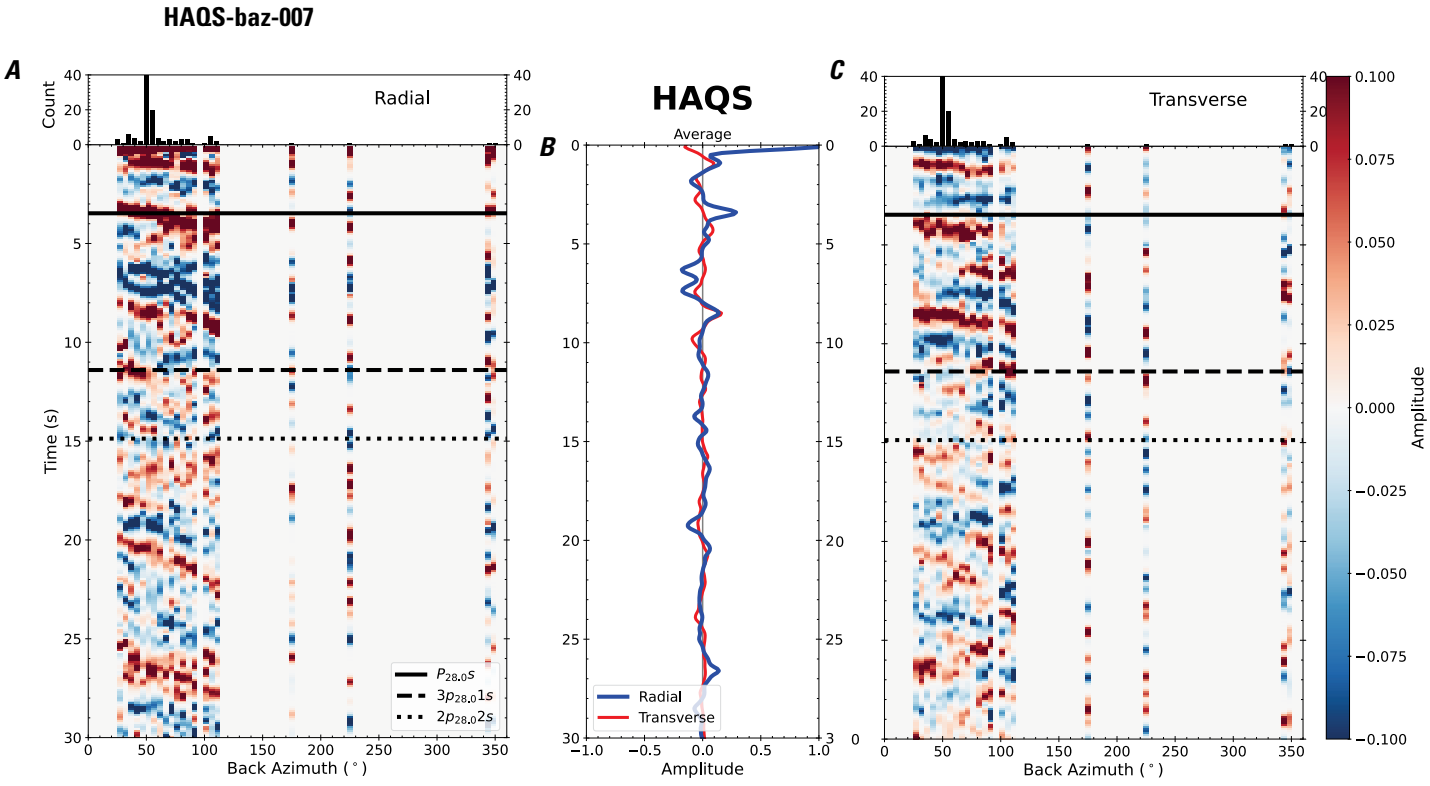

Figure 19. Receiver functions plotted against back azimuth for station HAQS. *A*, Radial component of P-wave receiver functions (PRFs) plotted against back azimuth. Individual PRFs have had the resonance-removal filter of Yu and others (2015) applied to them, are normalized to the maximum amplitude within the time window shown, binned, and normalized by the number of traces per bin. *B*, Average of every individual normalized radial receiver function with the application of the resonance-removal filter (blue) and average of every individual normalized raw radial receiver function (red). *C*, Radial component of raw PRFs, plotted against back azimuth, normalized as in *A*. Ps, 3p1s, and 2p2s arrival times predicted for the preferred Moho depth are shown, assuming a ray parameter of 0.06 s/km.

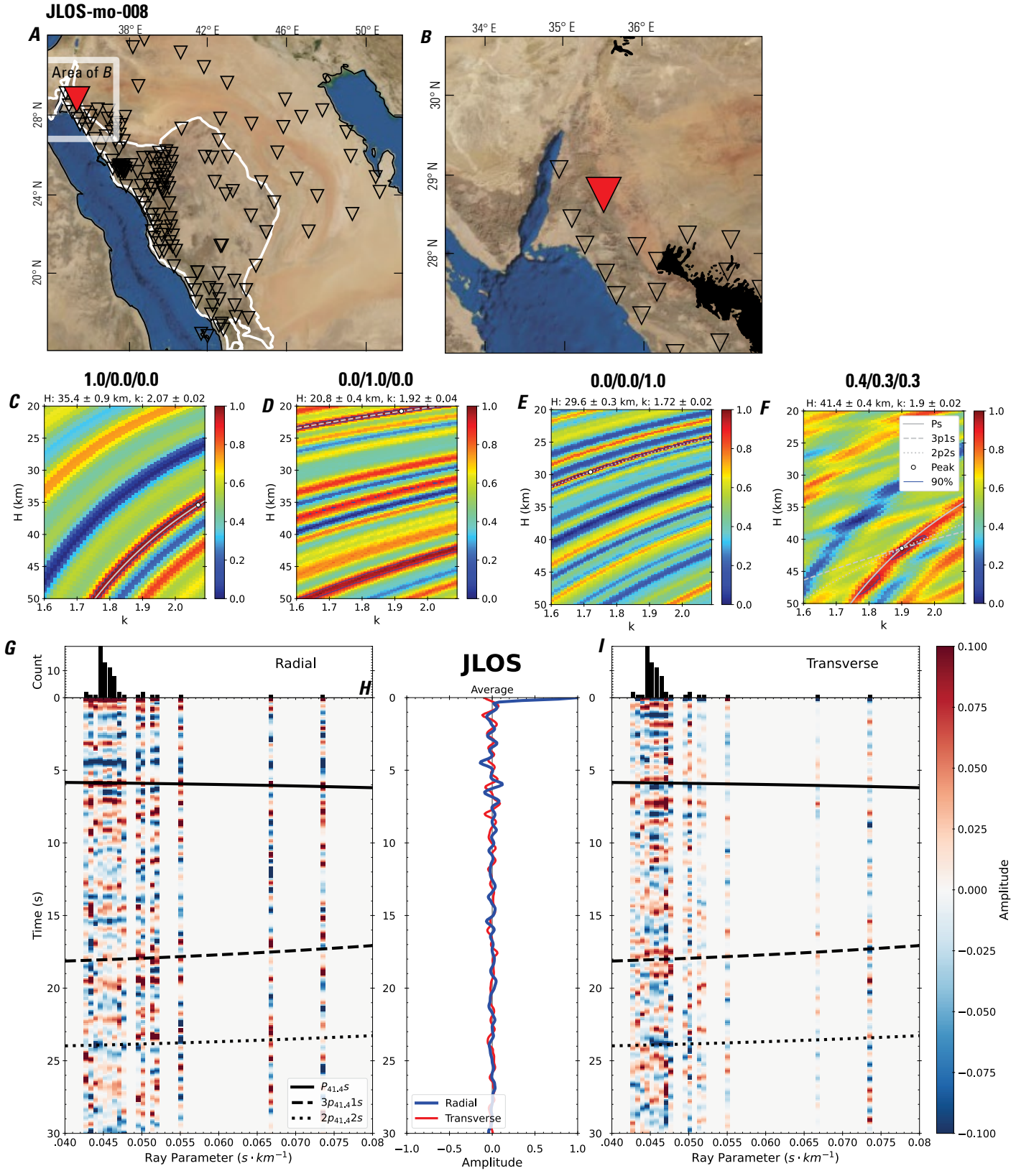
JLOS-mo-008
A
B
Area of B
1.0/0.0/0.0
0.0/1.0/0.0
0.0/0.0/1.0
0.4/0.3/0.3
C
D
E
F
H: 35.4 ± 0.9 km, k: 2.07 ± 0.02
H: 20.8 ± 0.4 km, k: 1.92 ± 0.04
H: 29.6 ± 0.3 km, k: 1.72 ± 0.02
H: 41.4 ± 0.4 km, k: 1.9 ± 0.02
H (km)
k
Ps
3p1s
2p2s
Peak
90%
G
H
I
Radial
Transverse
JLOS
Average
Count
Time (s)
Ray Parameter (s · km⁻¹)
Amplitude
$P_{41.4}s$
$3p_{41.4}1s$
$2p_{41.4}2s$
Radial
Transverse

Figure 20 (page 26). Receiver-function analysis for station JLOS. *A*, Regional map of Saudi Arabia showing the entire array (as inverted triangles), the location of station JLOS (red inverted triangle), the shield-platform boundary (white line), and the bounds of the map in *B* (white box). *B*, Local map of station JLOS. Harrats are shown in black. *C*, Standard, single-layer *H-k* stack with stacking weights 0.4/0.3/0.3. This *H-k* stack ignores sedimentary effects on the receiver functions. *D*, Standard, single-layer *H-k* stack with stacking weights 0.5/0.5/0.0. This *H-k* stack also ignores sedimentary effects on the receiver functions. *E*, Optimized sub-sedimentary *H-k* stack with stacking weights 0.4/0.3/0.3, following the method of Yu and others (2015). *F*, Optimized sedimentary *H-k* stack with stacking weights 0.05/0.70/0.25, following the method of Yu and others (2015). *G*, Radial component P-wave receiver functions (PRFs) plotted against ray parameter. Individual PRFs have had the resonance-removal filter of Yu and others (2015) applied to them and are normalized to the maximum amplitude within the time window shown, binned, and normalized by the number of traces per bin. *H*, Average of every individual normalized radial receiver function with the application of the resonance-removal filter (blue) and average of every individual normalized raw radial receiver function (red). *I*, Radial component of raw PRFs (that is, PRFs with no resonance-removal filter applied) plotted against ray parameter, normalized as in *G*.

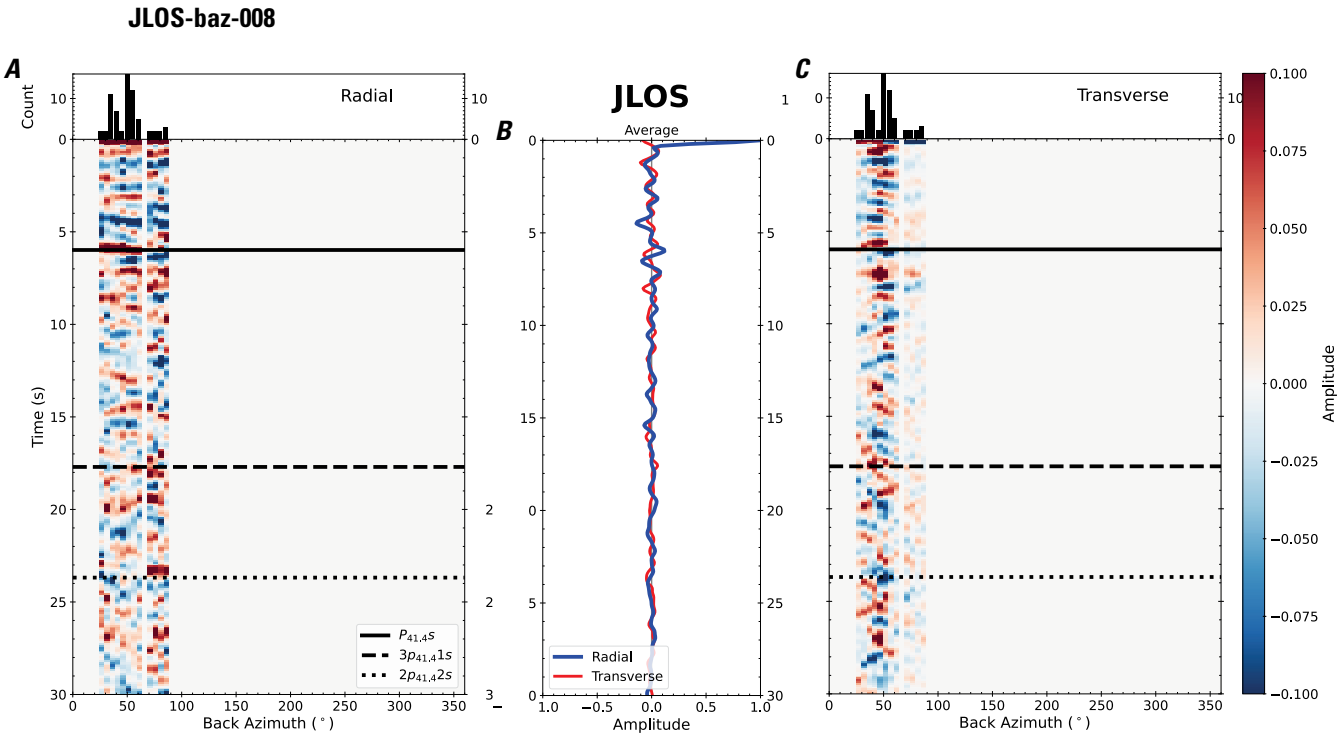

Figure 21. Receiver functions plotted against back azimuth for station JLOS. *A*, Radial component of P-wave receiver functions (PRFs) plotted against back azimuth. Individual PRFs have had the resonance-removal filter of Yu and others (2015) applied to them, are normalized to the maximum amplitude within the time window shown, binned, and normalized by the number of traces per bin. *B*, Average of every individual normalized radial receiver function with the application of the resonance-removal filter (blue) and average of every individual normalized raw radial receiver function (red). *C*, Radial component of raw PRFs, plotted against back azimuth, normalized as in *A*. Ps, 3p1s, and 2p2s arrival times predicted for the preferred Moho depth are shown, assuming a ray parameter of 0.06 s/km.

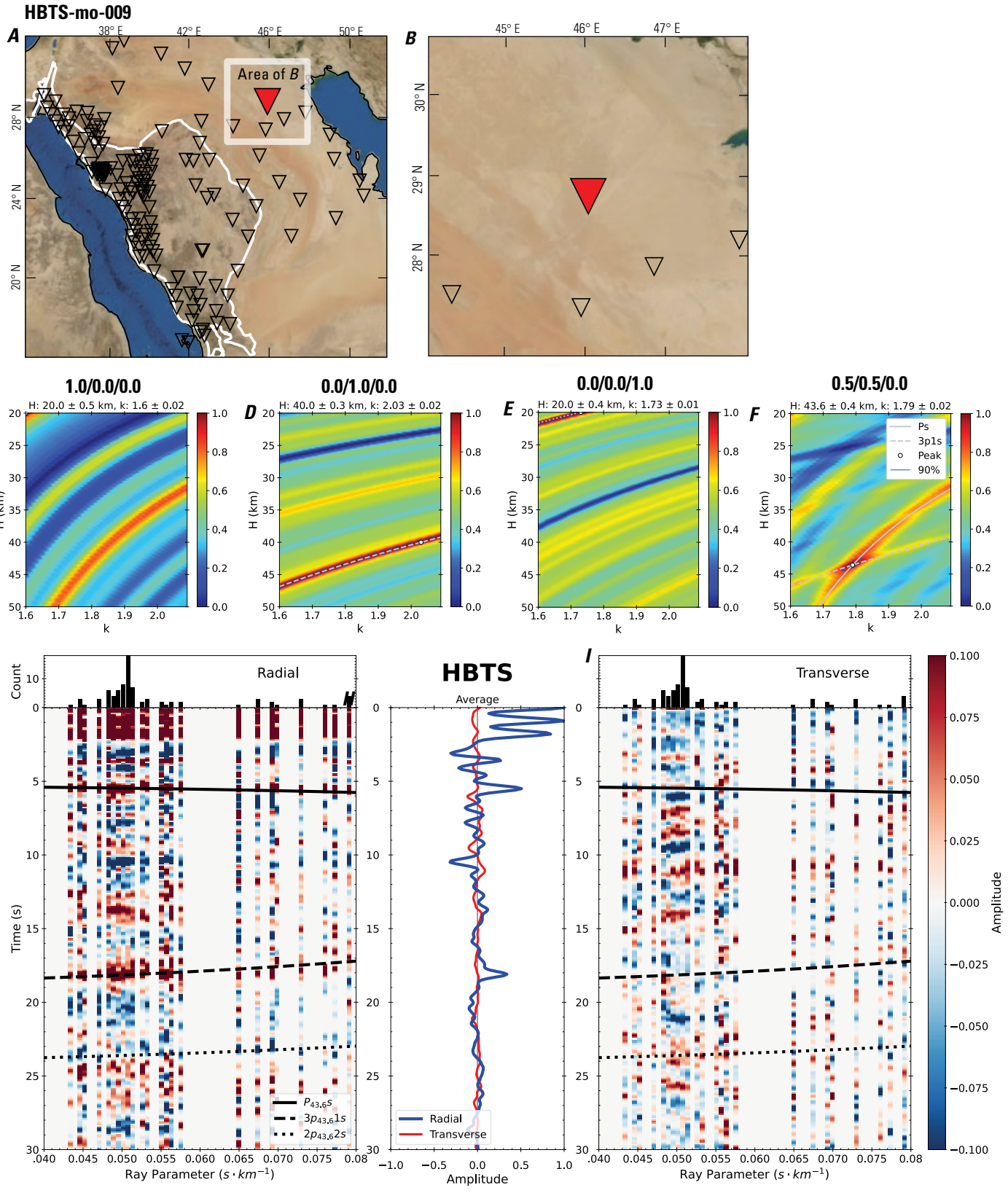
HBTS-mo-009
A
B
Area of B
38° E
42° E
46° E
50° E
28° N
24° N
20° N
45° E
46° E
47° E
30° N
29° N
28° N
1.0/0.0/0.0
0.0/1.0/0.0
0.0/0.0/1.0
0.5/0.5/0.0
C
D
E
F
H: 20.0 ± 0.5 km, k: 1.6 ± 0.02
H: 40.0 ± 0.3 km, k: 2.03 ± 0.02
H: 20.0 ± 0.4 km, k: 1.73 ± 0.01
H: 43.6 ± 0.4 km, k: 1.79 ± 0.02
H (km)
k
Ps
3p1s
Peak
90%
G
H
I
Radial
Transverse
HBTS
Average
Count
Time (s)
Ray Parameter ($s \cdot km^{-1}$)
Amplitude
$P_{43.6}s$
$3p_{43.6}1s$
$2p_{43.6}2s$

Figure 22 (page 28). Receiver-function analysis for station HBTS. *A*, Regional map of Saudi Arabia showing the entire array (as inverted triangles), the location of station HBTS (red inverted triangle), the shield-platform boundary (white line), and the bounds of the map in *B* (white box). *B*, Local map of station HBTS. Harrats are shown in black. *C*, Standard, single-layer *H-k* stack with stacking weights 0.4/0.3/0.3. This *H-k* stack ignores sedimentary effects on the receiver functions. *D*, Standard, single-layer *H-k* stack with stacking weights 0.5/0.5/0.0. This *H-k* stack also ignores sedimentary effects on the receiver functions. *E*, Optimized sub-sedimentary *H-k* stack with stacking weights 0.4/0.3/0.3, following the method of Yu and others (2015). *F*, Optimized sedimentary *H-k* stack with stacking weights 0.05/0.70/0.25, following the method of Yu and others (2015). *G*, Radial component P-wave receiver functions (PRFs) plotted against ray parameter. Individual PRFs have had the resonance-removal filter of Yu and others (2015) applied to them and are normalized to the maximum amplitude within the time window shown, binned, and normalized by the number of traces per bin. *H*, Average of every individual normalized radial receiver function with the application of the resonance-removal filter (blue) and average of every individual normalized raw radial receiver function (red). *I*, Radial component of raw PRFs (that is, PRFs with no resonance-removal filter applied) plotted against ray parameter, normalized as in *G*.

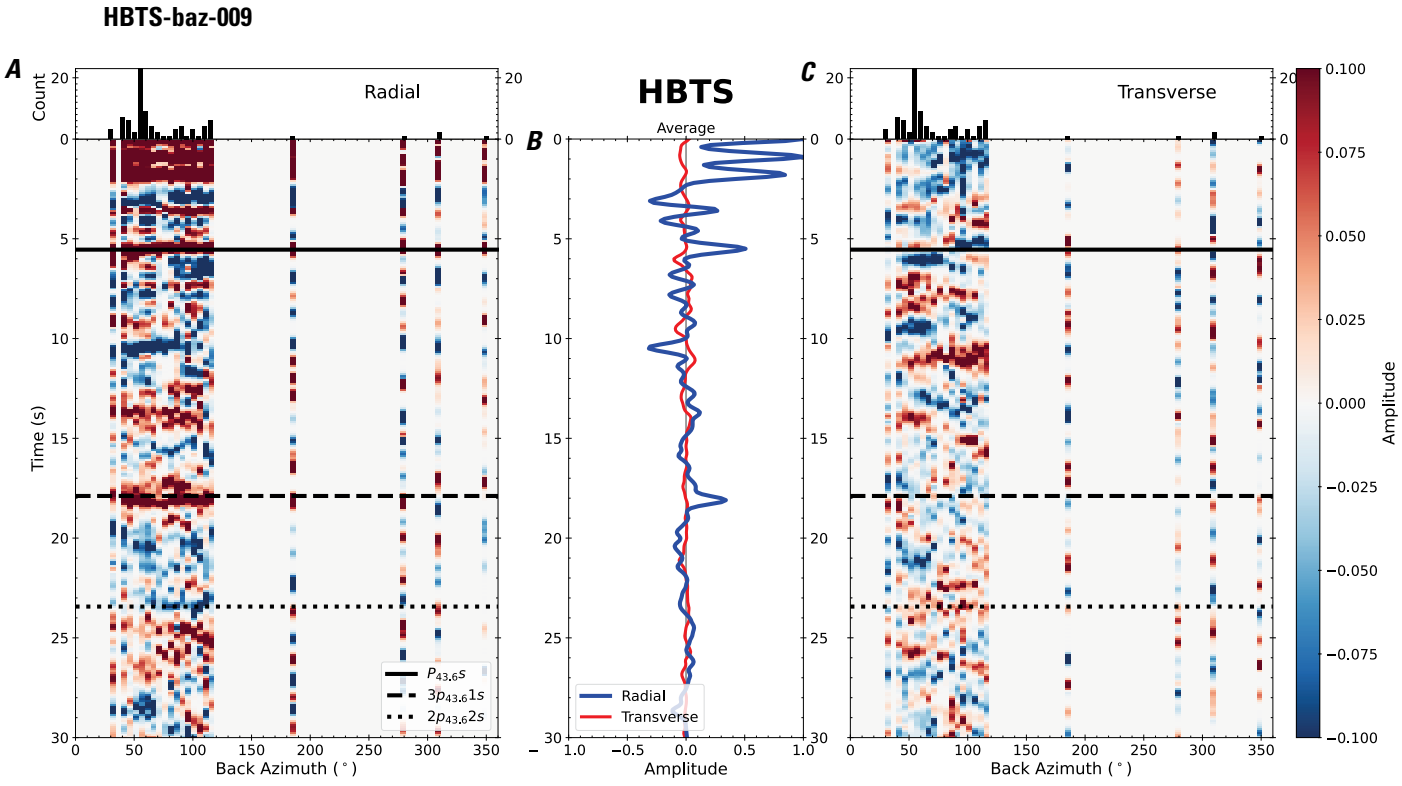

Figure 23. Receiver functions plotted against back azimuth for station HBTS. *A*, Radial component of P-wave receiver functions (PRFs) plotted against back azimuth. Individual PRFs have had the resonance-removal filter of Yu and others (2015) applied to them, are normalized to the maximum amplitude within the time window shown, binned, and normalized by the number of traces per bin. *B*, Average of every individual normalized radial receiver function with the application of the resonance-removal filter (blue) and average of every individual normalized raw radial receiver function (red). *C*, Radial component of raw PRFs, plotted against back azimuth, normalized as in *A*. Ps, 3p1s, and 2p2s arrival times predicted for the preferred Moho depth are shown, assuming a ray parameter of 0.06 s/km.

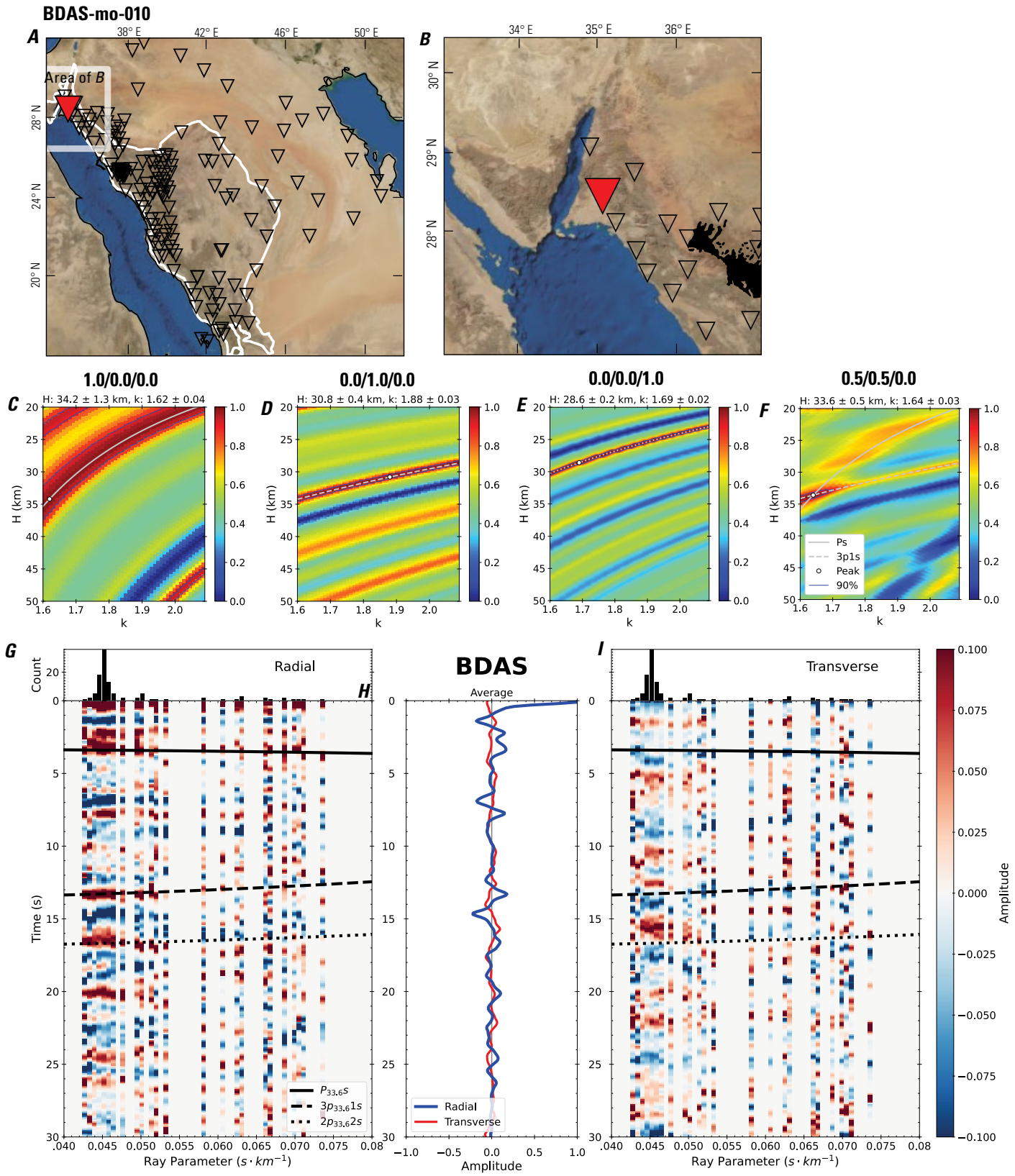
BDAS-mo-010
A
B
Area of B
38° E
42° E
46° E
50° E
28° N
24° N
20° N
34° E
35° E
36° E
30° N
29° N
28° N
1.0/0.0/0.0
0.0/1.0/0.0
0.0/0.0/1.0
0.5/0.5/0.0
C
D
E
F
H: 34.2 ± 1.3 km, k: 1.62 ± 0.04
H: 30.8 ± 0.4 km, k: 1.88 ± 0.03
H: 28.6 ± 0.2 km, k: 1.69 ± 0.02
H: 33.6 ± 0.5 km, k: 1.64 ± 0.03
H (km)
k
Ps
3p1s
Peak
90%
G
I
Radial
Transverse
BDAS
Average
Count
Time (s)
Ray Parameter (s · km⁻¹)
Amplitude
$P_{33.6}s$
$3p_{33.6}1s$
$2p_{33.6}2s$

Figure 24 (page 30). Receiver-function analysis for station BDAS. *A*, Regional map of Saudi Arabia showing the entire array (as inverted triangles), the location of station BDAS (red inverted triangle), the shield-platform boundary (white line), and the bounds of the map in *B* (white box). *B*, Local map of station BDAS. Harrats are shown in black. *C*, Standard, single-layer *H-k* stack with stacking weights 0.4/0.3/0.3. This *H-k* stack ignores sedimentary effects on the receiver functions. *D*, Standard, single-layer *H-k* stack with stacking weights 0.5/0.5/0.0. This *H-k* stack also ignores sedimentary effects on the receiver functions. *E*, Optimized sub-sedimentary *H-k* stack with stacking weights 0.4/0.3/0.3, following the method of Yu and others (2015). *F*, Optimized sedimentary *H-k* stack with stacking weights 0.05/0.70/0.25, following the method of Yu and others (2015). *G*, Radial component P-wave receiver functions (PRFs) plotted against ray parameter. Individual PRFs have had the resonance-removal filter of Yu and others (2015) applied to them and are normalized to the maximum amplitude within the time window shown, binned, and normalized by the number of traces per bin. *H*, Average of every individual normalized radial receiver function with the application of the resonance-removal filter (blue) and average of every individual normalized raw radial receiver function (red). *I*, Radial component of raw PRFs (that is, PRFs with no resonance-removal filter applied) plotted against ray parameter, normalized as in *G*.

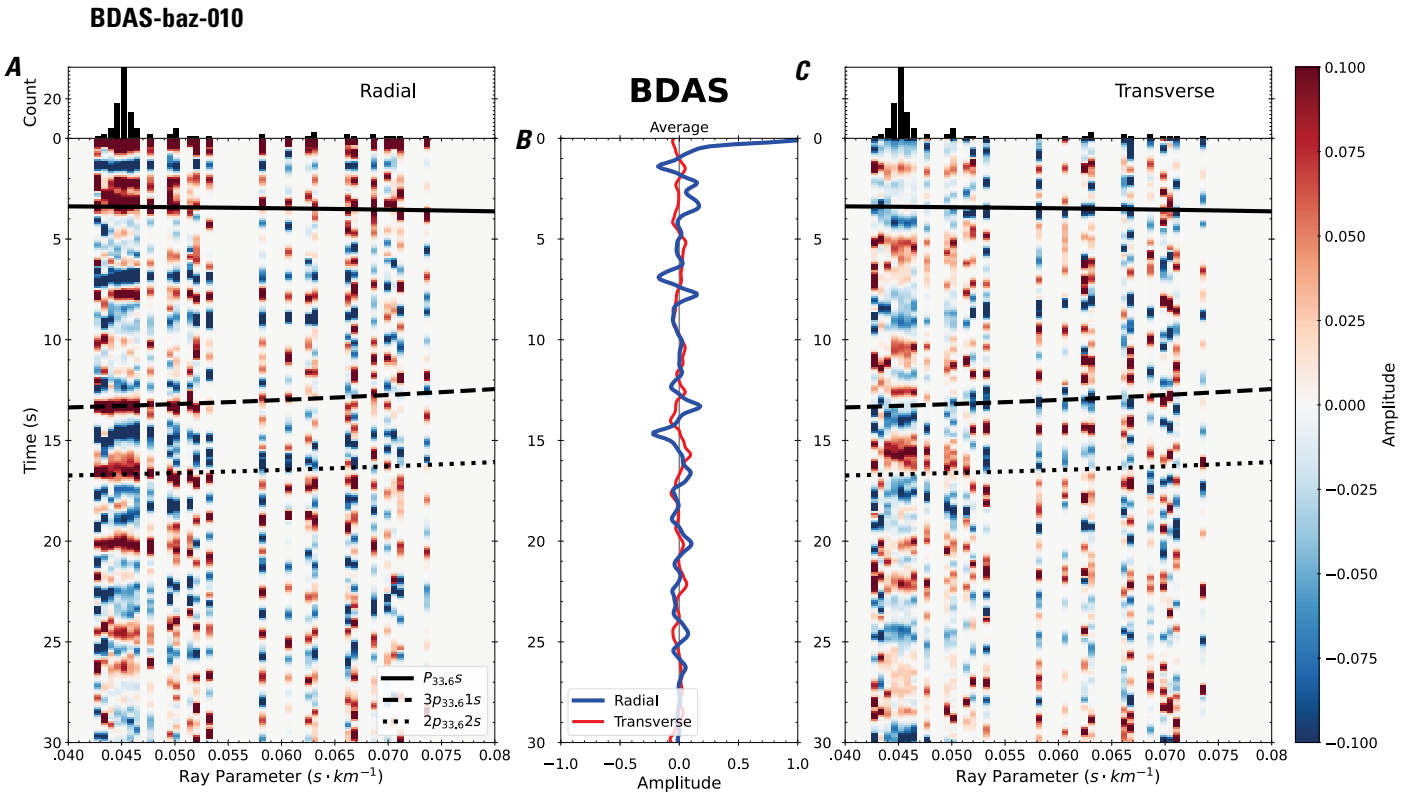

Figure 25. Receiver functions plotted against back azimuth for station BDAS. *A*, Radial component of P-wave receiver functions (PRFs) plotted against back azimuth. Individual PRFs have had the resonance-removal filter of Yu and others (2015) applied to them, are normalized to the maximum amplitude within the time window shown, binned, and normalized by the number of traces per bin. *B*, Average of every individual normalized radial receiver function with the application of the resonance-removal filter (blue) and average of every individual normalized raw radial receiver function (red). *C*, Radial component of raw PRFs, plotted against back azimuth, normalized as in *A*. Ps, 3p1s, and 2p2s arrival times predicted for the preferred Moho depth are shown, assuming a ray parameter of 0.06 s/km.

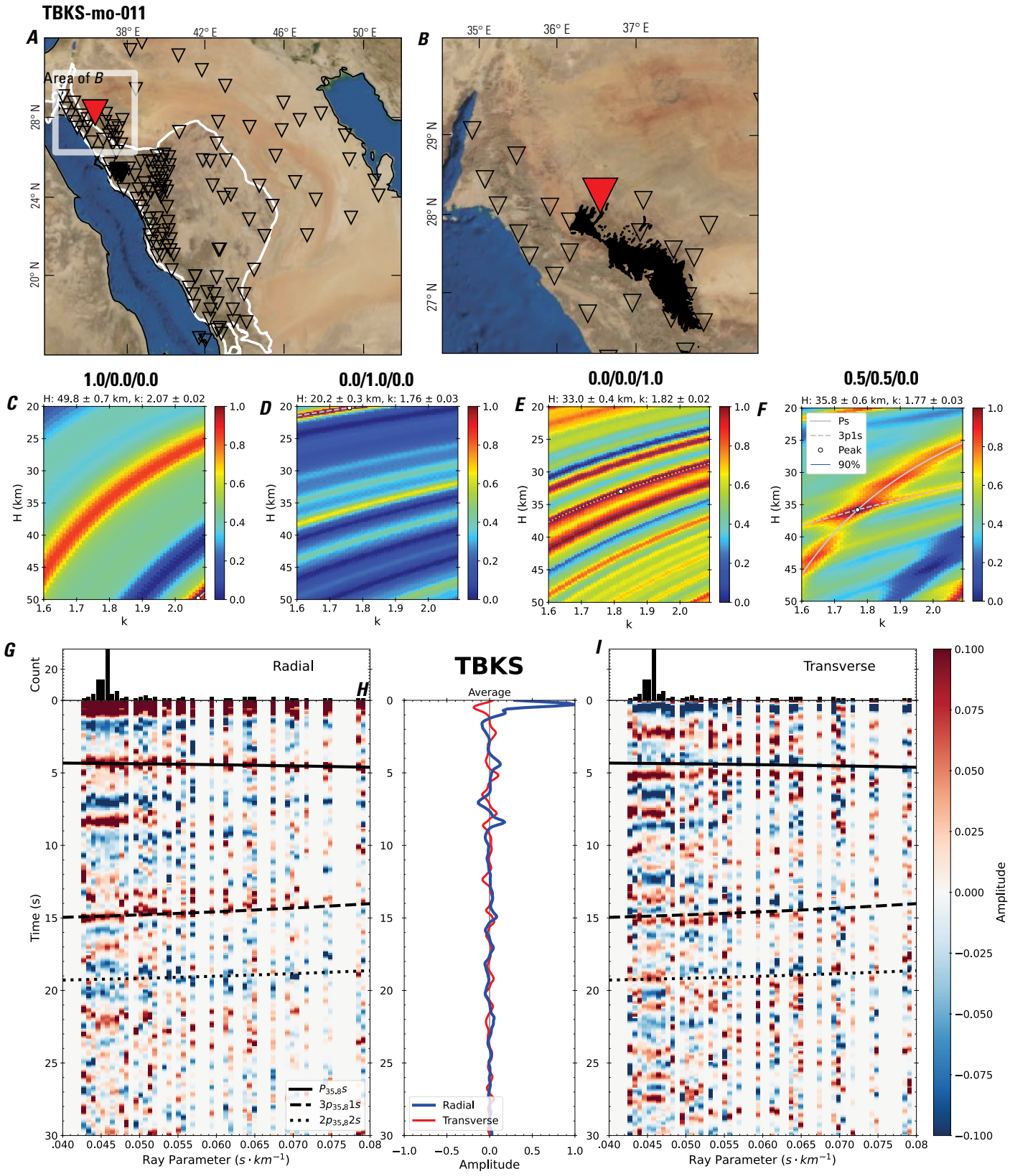
TBKS-mo-011
A
B
Area of B
38° E
42° E
46° E
50° E
28° N
24° N
20° N
35° E
36° E
37° E
29° N
28° N
27° N
1.0/0.0/0.0
0.0/1.0/0.0
0.0/0.0/1.0
0.5/0.5/0.0
C
D
E
F
H: 49.8 ± 0.7 km, k: 2.07 ± 0.02
H: 20.2 ± 0.3 km, k: 1.76 ± 0.03
H: 33.0 ± 0.4 km, k: 1.82 ± 0.02
H: 35.8 ± 0.6 km, k: 1.77 ± 0.03
H (km)
k
Ps
3p1s
Peak
90%
G
I
TBKS
Radial
Transverse
Average
Count
Time (s)
Ray Parameter (s · km⁻¹)
Amplitude
$P_{35.8}s$
$3p_{35.8}1s$
$2p_{35.8}2s$

Figure 26 (page 32). Receiver-function analysis for station TBKS. *A*, Regional map of Saudi Arabia showing the entire array (as inverted triangles), the location of station TBKS (red inverted triangle), the shield-platform boundary (white line), and the bounds of the map in *B* (white box). *B*, Local map of station TBKS. Harrats are shown in black. *C*, Standard, single-layer *H-k* stack with stacking weights 0.4/0.3/0.3. This *H-k* stack ignores sedimentary effects on the receiver functions. *D*, Standard, single-layer *H-k* stack with stacking weights 0.5/0.5/0.0. This *H-k* stack also ignores sedimentary effects on the receiver functions. *E*, Optimized sub-sedimentary *H-k* stack with stacking weights 0.4/0.3/0.3, following the method of Yu and others (2015). *F*, Optimized sedimentary *H-k* stack with stacking weights 0.05/0.70/0.25, following the method of Yu and others (2015). *G*, Radial component P-wave receiver functions (PRFs) plotted against ray parameter. Individual PRFs have had the resonance-removal filter of Yu and others (2015) applied to them and are normalized to the maximum amplitude within the time window shown, binned, and normalized by the number of traces per bin. *H*, Average of every individual normalized radial receiver function with the application of the resonance-removal filter (blue) and average of every individual normalized raw radial receiver function (red). *I*, Radial component of raw PRFs (that is, PRFs with no resonance-removal filter applied) plotted against ray parameter, normalized as in *G*.

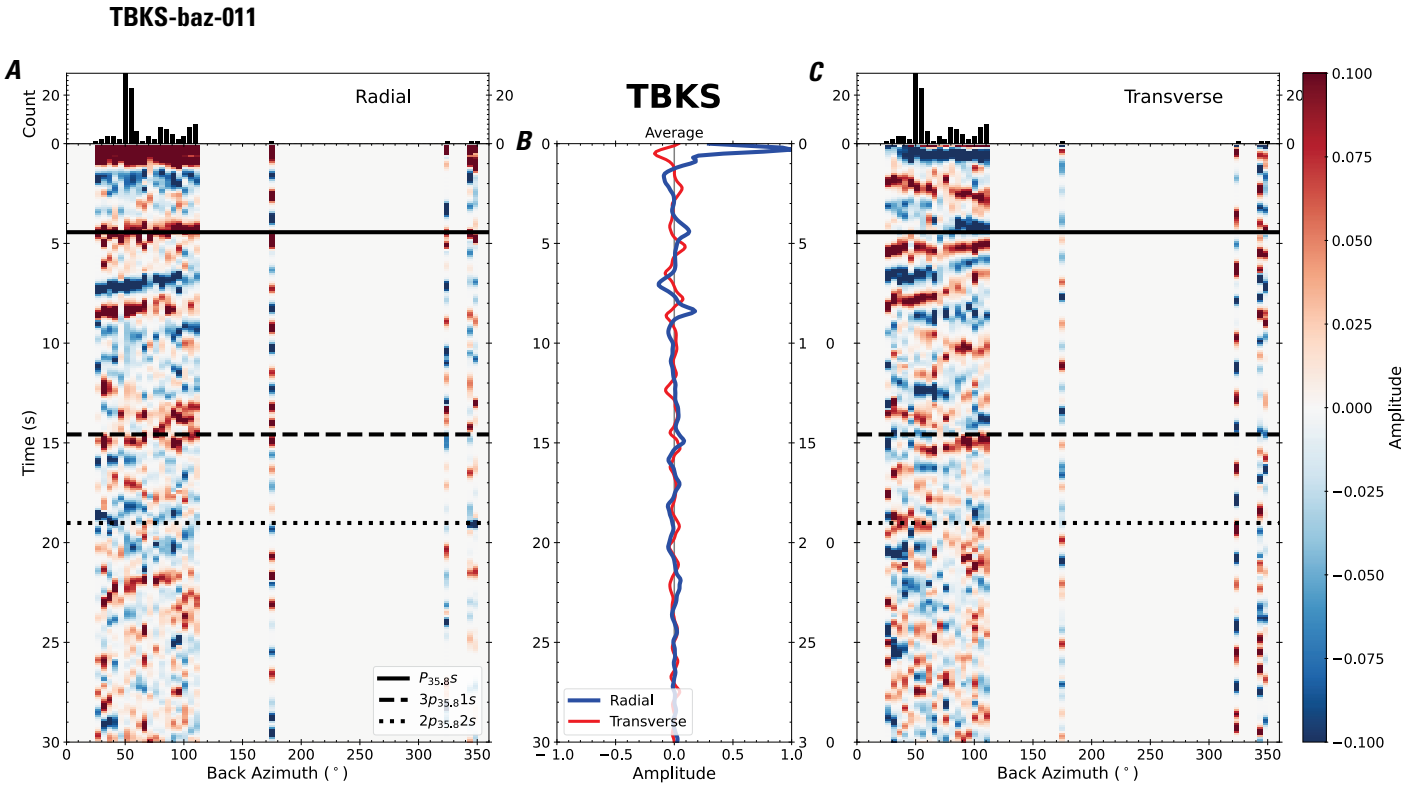

Figure 27. Receiver functions plotted against back azimuth for station TBKS. *A*, Radial component of P-wave receiver functions (PRFs) plotted against back azimuth. Individual PRFs have had the resonance-removal filter of Yu and others (2015) applied to them, are normalized to the maximum amplitude within the time window shown, binned, and normalized by the number of traces per bin. *B*, Average of every individual normalized radial receiver function with the application of the resonance-removal filter (blue) and average of every individual normalized raw radial receiver function (red). *C*, Radial component of raw PRFs, plotted against back azimuth, normalized as in *A*. Ps, 3p1s, and 2p2s arrival times predicted for the preferred Moho depth are shown, assuming a ray parameter of 0.06 s/km.

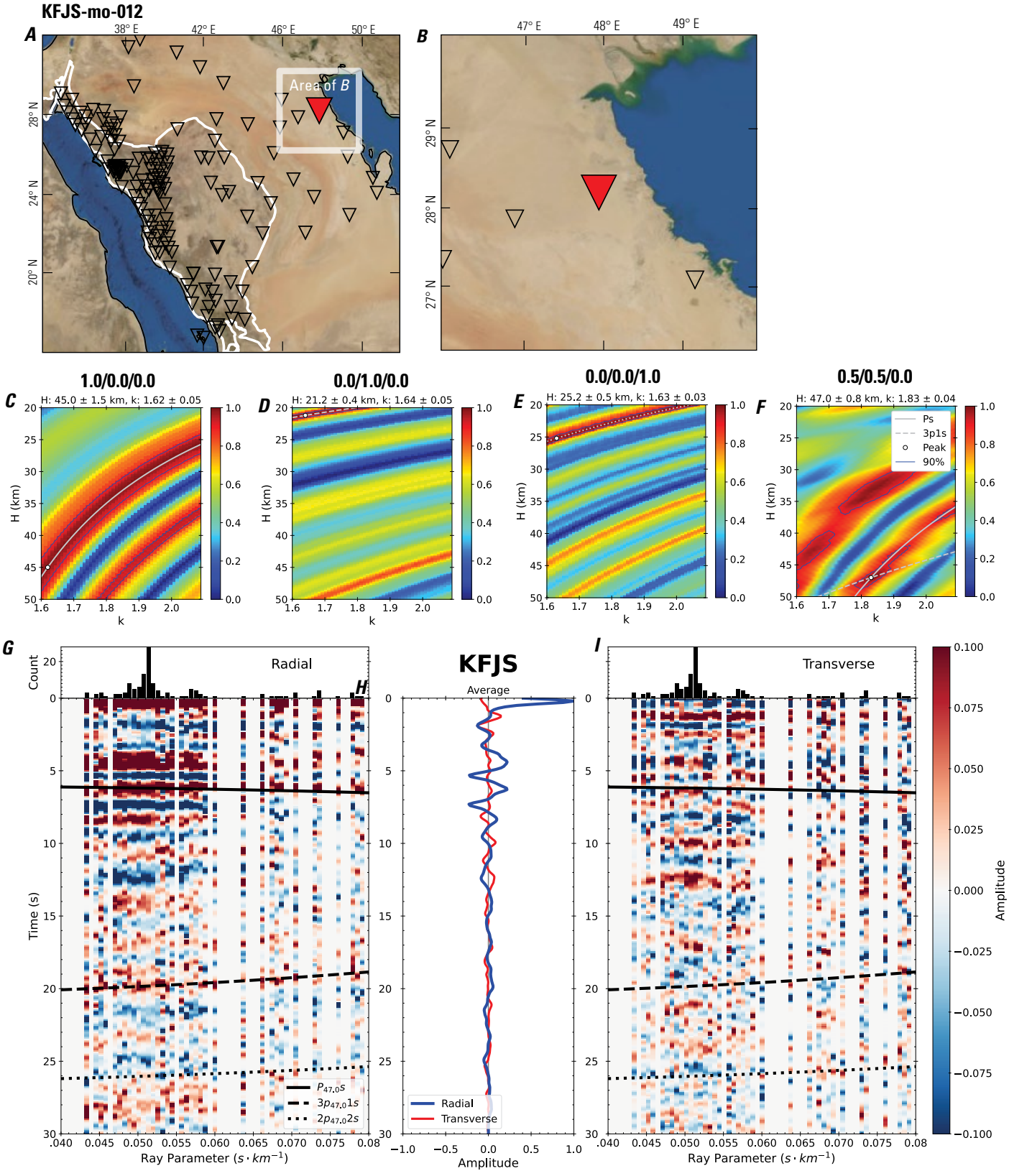
KFJS-mo-012
A
38° E
42° E
46° E
50° E
28° N
24° N
20° N
Area of B
B
47° E
48° E
49° E
29° N
28° N
27° N
1.0/0.0/0.0
0.0/1.0/0.0
0.0/0.0/1.0
0.5/0.5/0.0
C
H: 45.0 ± 1.5 km, k: 1.62 ± 0.05
D
H: 21.2 ± 0.4 km, k: 1.64 ± 0.05
E
H: 25.2 ± 0.5 km, k: 1.63 ± 0.03
F
H: 47.0 ± 0.8 km, k: 1.83 ± 0.04
H (km)
k
Ps
3p1s
Peak
90%
G
Radial
H
Count
Time (s)
Ray Parameter (s · km⁻¹)
P47.0s
3p47.01s
2p47.02s
KFJS
Average
Radial
Transverse
Amplitude
I
Transverse
Amplitude

Figure 28 (page 34). Receiver-function analysis for station KFJS. *A*, Regional map of Saudi Arabia showing the entire array (as inverted triangles), the location of station KFJS (red inverted triangle), the shield-platform boundary (white line), and the bounds of the map in *B* (white box). *B*, Local map of station KFJS. Harrats are shown in black. *C*, Standard, single-layer *H-k* stack with stacking weights 0.4/0.3/0.3. This *H-k* stack ignores sedimentary effects on the receiver functions. *D*, Standard, single-layer *H-k* stack with stacking weights 0.5/0.5/0.0. This *H-k* stack also ignores sedimentary effects on the receiver functions. *E*, Optimized sub-sedimentary *H-k* stack with stacking weights 0.4/0.3/0.3, following the method of Yu and others (2015). *F*, Optimized sedimentary *H-k* stack with stacking weights 0.05/0.70/0.25, following the method of Yu and others (2015). *G*, Radial component P-wave receiver functions (PRFs) plotted against ray parameter. Individual PRFs have had the resonance-removal filter of Yu and others (2015) applied to them and are normalized to the maximum amplitude within the time window shown, binned, and normalized by the number of traces per bin. *H*, Average of every individual normalized radial receiver function with the application of the resonance-removal filter (blue) and average of every individual normalized raw radial receiver function (red). *I*, Radial component of raw PRFs (that is, PRFs with no resonance-removal filter applied) plotted against ray parameter, normalized as in *G*.

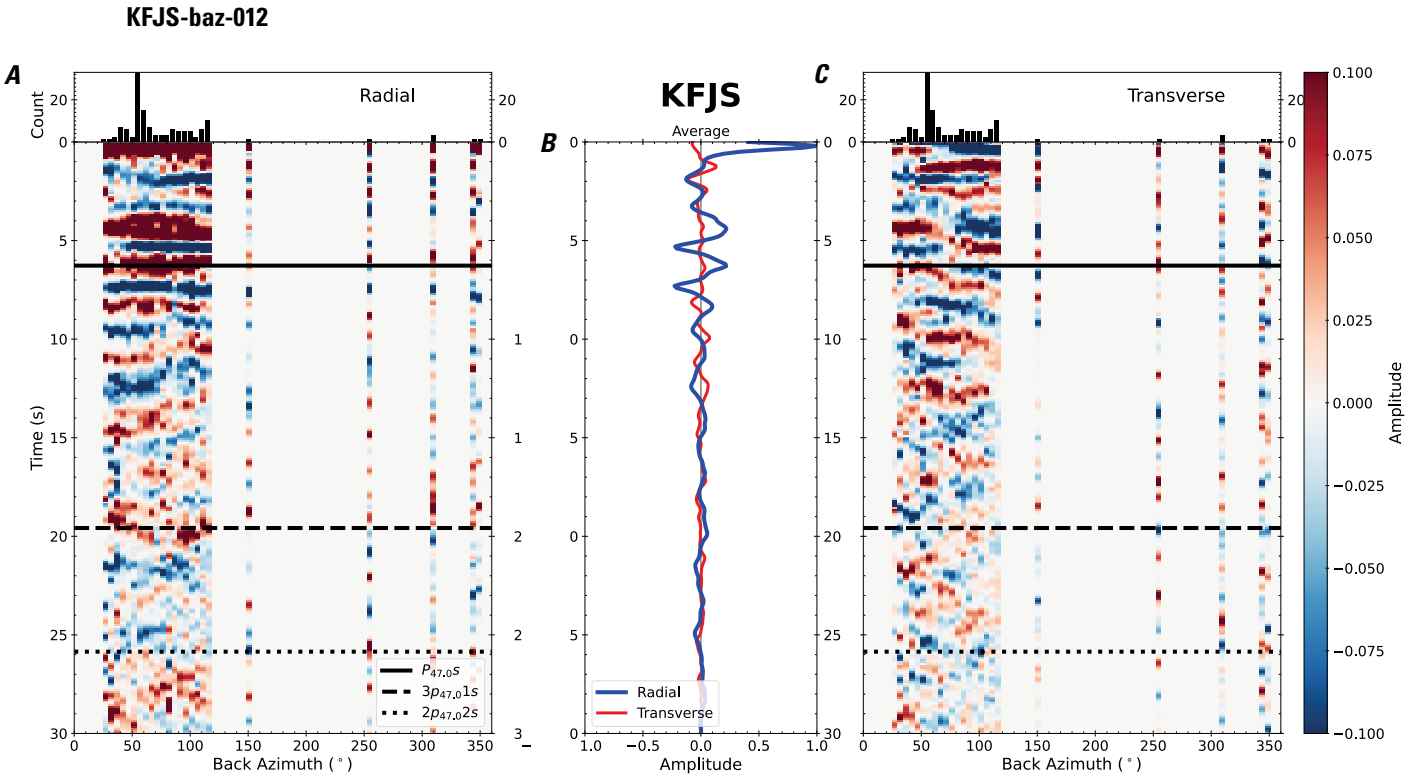

Figure 29. Receiver functions plotted against back azimuth for station KFJS. *A*, Radial component of P-wave receiver functions (PRFs) plotted against back azimuth. Individual PRFs have had the resonance-removal filter of Yu and others (2015) applied to them, are normalized to the maximum amplitude within the time window shown, binned, and normalized by the number of traces per bin. *B*, Average of every individual normalized radial receiver function with the application of the resonance-removal filter (blue) and average of every individual normalized raw radial receiver function (red). *C*, Radial component of raw PRFs, plotted against back azimuth, normalized as in *A*. Ps, 3p1s, and 2p2s arrival times predicted for the preferred Moho depth are shown, assuming a ray parameter of 0.06 s/km.

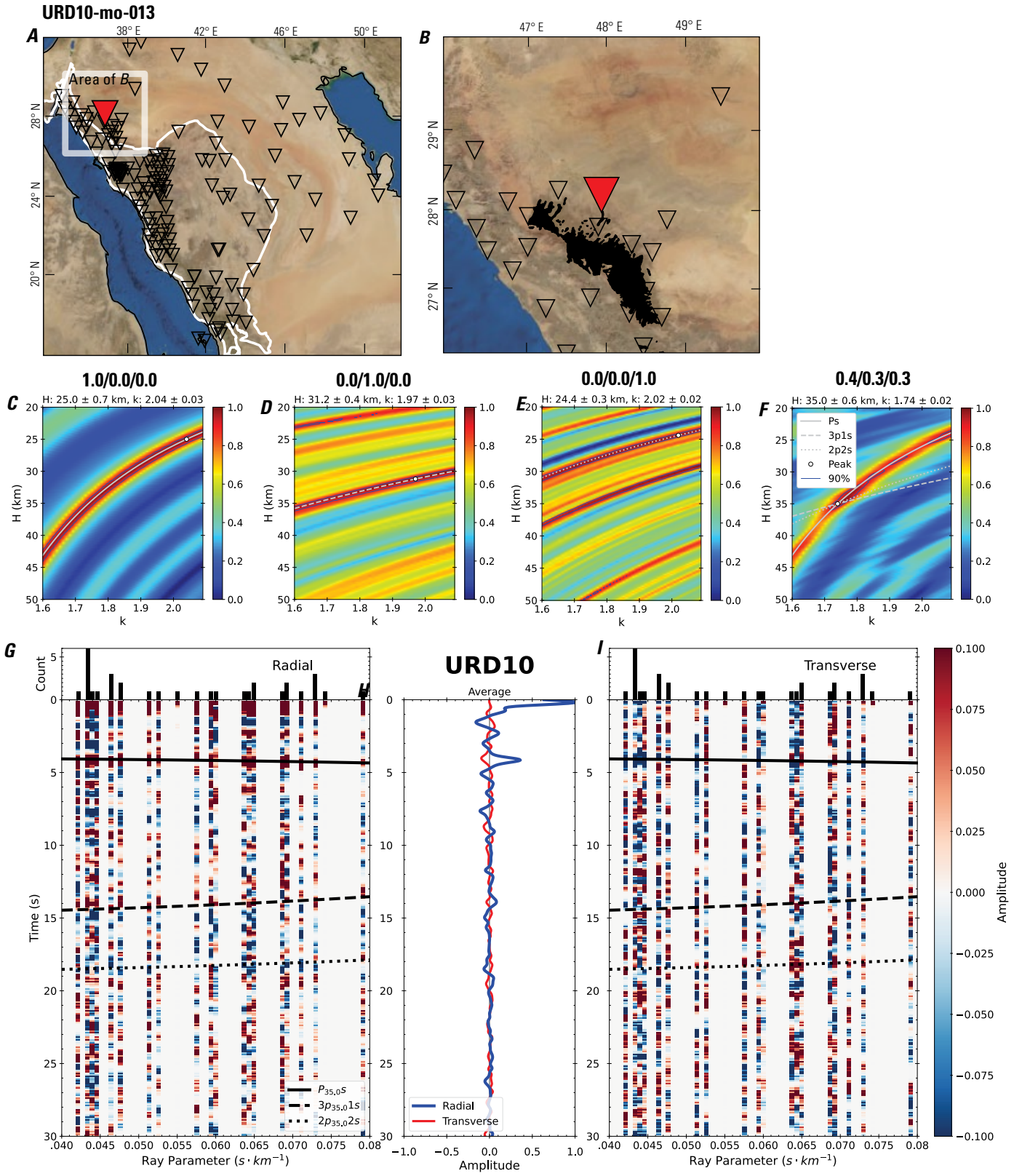
URD10-mo-013
A
38° E
42° E
46° E
50° E
Area of B
28° N
24° N
20° N
B
47° E
48° E
49° E
29° N
28° N
27° N
1.0/0.0/0.0
C
H: 25.0 ± 0.7 km, k: 2.04 ± 0.03
0.0/1.0/0.0
D
H: 31.2 ± 0.4 km, k: 1.97 ± 0.03
0.0/0.0/1.0
E
H: 24.4 ± 0.3 km, k: 2.02 ± 0.02
0.4/0.3/0.3
F
H: 35.0 ± 0.6 km, k: 1.74 ± 0.02
Ps
3p1s
2p2s
Peak
90%
H (km)
k
G
Radial
Count
Time (s)
$P_{35.0}s$
$3p_{35.0}1s$
$2p_{35.0}2s$
Ray Parameter ($s \cdot km^{-1}$)
URD10
Average
Radial
Transverse
Amplitude
I
Transverse
Amplitude

Figure 30 (page 36). Receiver-function analysis for station URD10. *A*, Regional map of Saudi Arabia showing the entire array (as inverted triangles), the location of station URD10 (red inverted triangle), the shield-platform boundary (white line), and the bounds of the map in *B* (white box). *B*, Local map of station URD10. Harrats are shown in black. *C*, Standard, single-layer *H-k* stack with stacking weights 0.4/0.3/0.3. This *H-k* stack ignores sedimentary effects on the receiver functions. *D*, Standard, single-layer *H-k* stack with stacking weights 0.5/0.5/0.0. This *H-k* stack also ignores sedimentary effects on the receiver functions. *E*, Optimized sub-sedimentary *H-k* stack with stacking weights 0.4/0.3/0.3, following the method of Yu and others (2015). *F*, Optimized sedimentary *H-k* stack with stacking weights 0.05/0.70/0.25, following the method of Yu and others (2015). *G*, Radial component P-wave receiver functions (PRFs) plotted against ray parameter. Individual PRFs have had the resonance-removal filter of Yu and others (2015) applied to them and are normalized to the maximum amplitude within the time window shown, binned, and normalized by the number of traces per bin. *H*, Average of every individual normalized radial receiver function with the application of the resonance-removal filter (blue) and average of every individual normalized raw radial receiver function (red). *I*, Radial component of raw PRFs (that is, PRFs with no resonance-removal filter applied) plotted against ray parameter, normalized as in *G*.

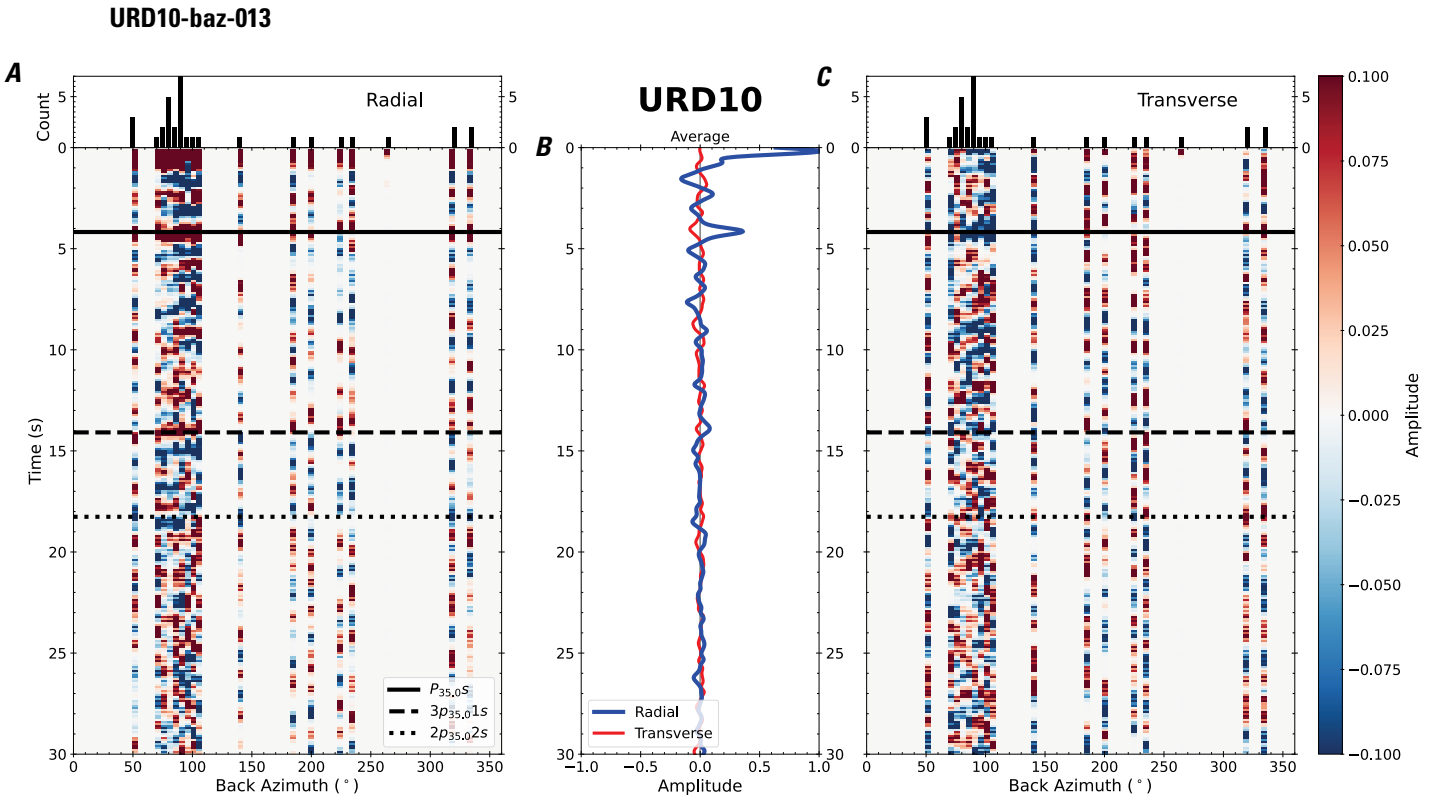

Figure 31. Receiver functions plotted against back azimuth for station URD10. *A*, Radial component of P-wave receiver functions (PRFs) plotted against back azimuth. Individual PRFs have had the resonance-removal filter of Yu and others (2015) applied to them, are normalized to the maximum amplitude within the time window shown, binned, and normalized by the number of traces per bin. *B*, Average of every individual normalized radial receiver function with the application of the resonance-removal filter (blue) and average of every individual normalized raw radial receiver function (red). *C*, Radial component of raw PRFs, plotted against back azimuth, normalized as in *A*. Ps, 3p1s, and 2p2s arrival times predicted for the preferred Moho depth are shown, assuming a ray parameter of 0.06 s/km.

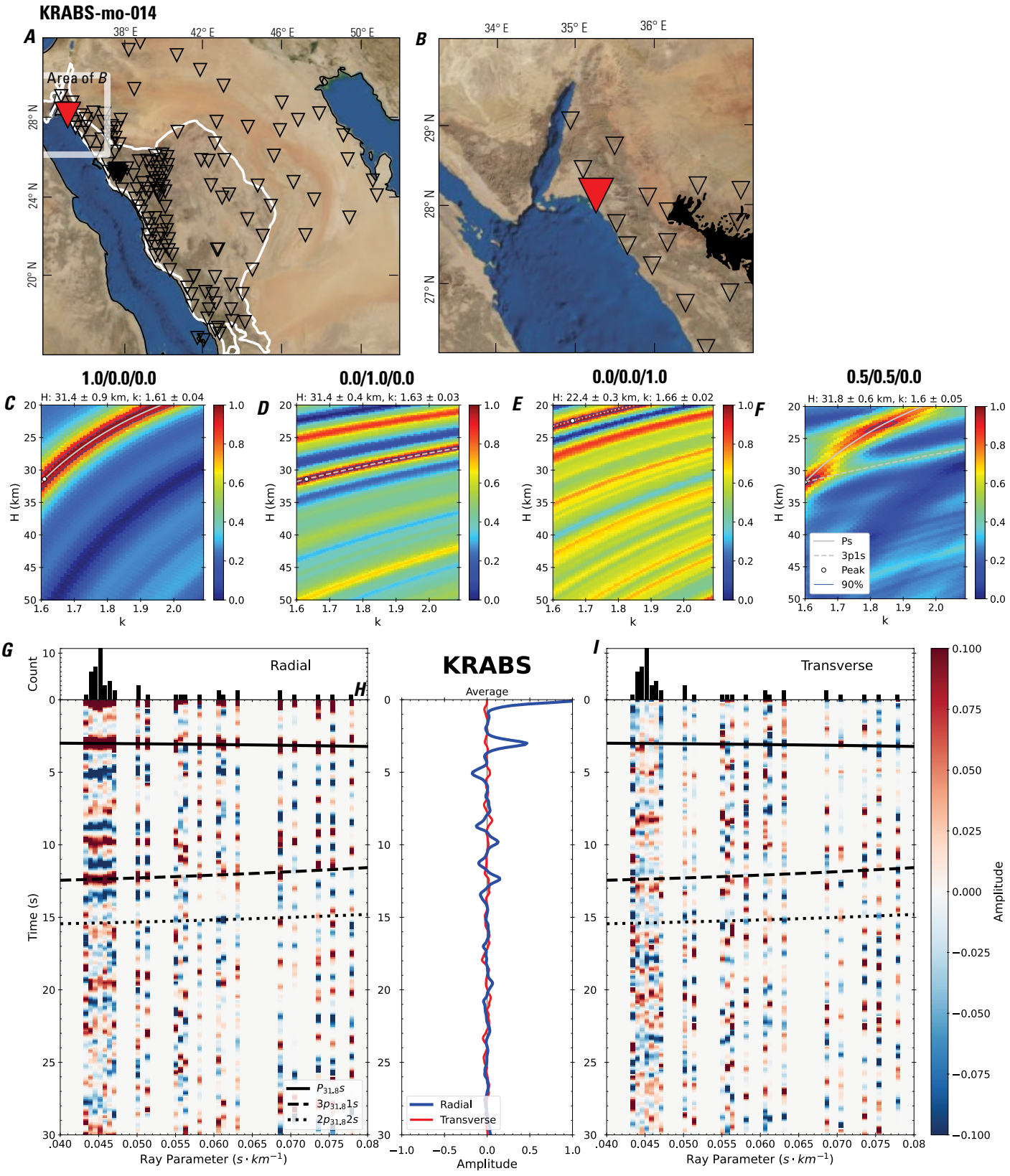
KRABS-mo-014
A
B
Area of B
38° E
42° E
46° E
50° E
28° N
24° N
20° N
34° E
35° E
36° E
29° N
28° N
27° N
1.0/0.0/0.0
0.0/1.0/0.0
0.0/0.0/1.0
0.5/0.5/0.0
C
D
E
F
H: 31.4 ± 0.9 km, k: 1.61 ± 0.04
H: 31.4 ± 0.4 km, k: 1.63 ± 0.03
H: 22.4 ± 0.3 km, k: 1.66 ± 0.02
H: 31.8 ± 0.6 km, k: 1.6 ± 0.05
H (km)
k
Ps
3p1s
Peak
90%
G
H
I
Radial
Transverse
KRABS
Average
Count
Time (s)
Ray Parameter (s · km⁻¹)
Amplitude
$P_{31.8}s$
$3p_{31.8}1s$
$2p_{31.8}2s$

Figure 32 (page 38). Receiver-function analysis for station KRABS. *A*, Regional map of Saudi Arabia showing the entire array (as inverted triangles), the location of station KRABS (red inverted triangle), the shield-platform boundary (white line), and the bounds of the map in *B* (white box). *B*, Local map of station KRABS. Harrats are shown in black. *C*, Standard, single-layer *H-k* stack with stacking weights 0.4/0.3/0.3. This *H-k* stack ignores sedimentary effects on the receiver functions. *D*, Standard, single-layer *H-k* stack with stacking weights 0.5/0.5/0.0. This *H-k* stack also ignores sedimentary effects on the receiver functions. *E*, Optimized sub-sedimentary *H-k* stack with stacking weights 0.4/0.3/0.3, following the method of Yu and others (2015). *F*, Optimized sedimentary *H-k* stack with stacking weights 0.05/0.70/0.25, following the method of Yu and others (2015). *G*, Radial component P-wave receiver functions (PRFs) plotted against ray parameter. Individual PRFs have had the resonance-removal filter of Yu and others (2015) applied to them and are normalized to the maximum amplitude within the time window shown, binned, and normalized by the number of traces per bin. *H*, Average of every individual normalized radial receiver function with the application of the resonance-removal filter (blue) and average of every individual normalized raw radial receiver function (red). *I*, Radial component of raw PRFs (that is, PRFs with no resonance-removal filter applied) plotted against ray parameter, normalized as in *G*.

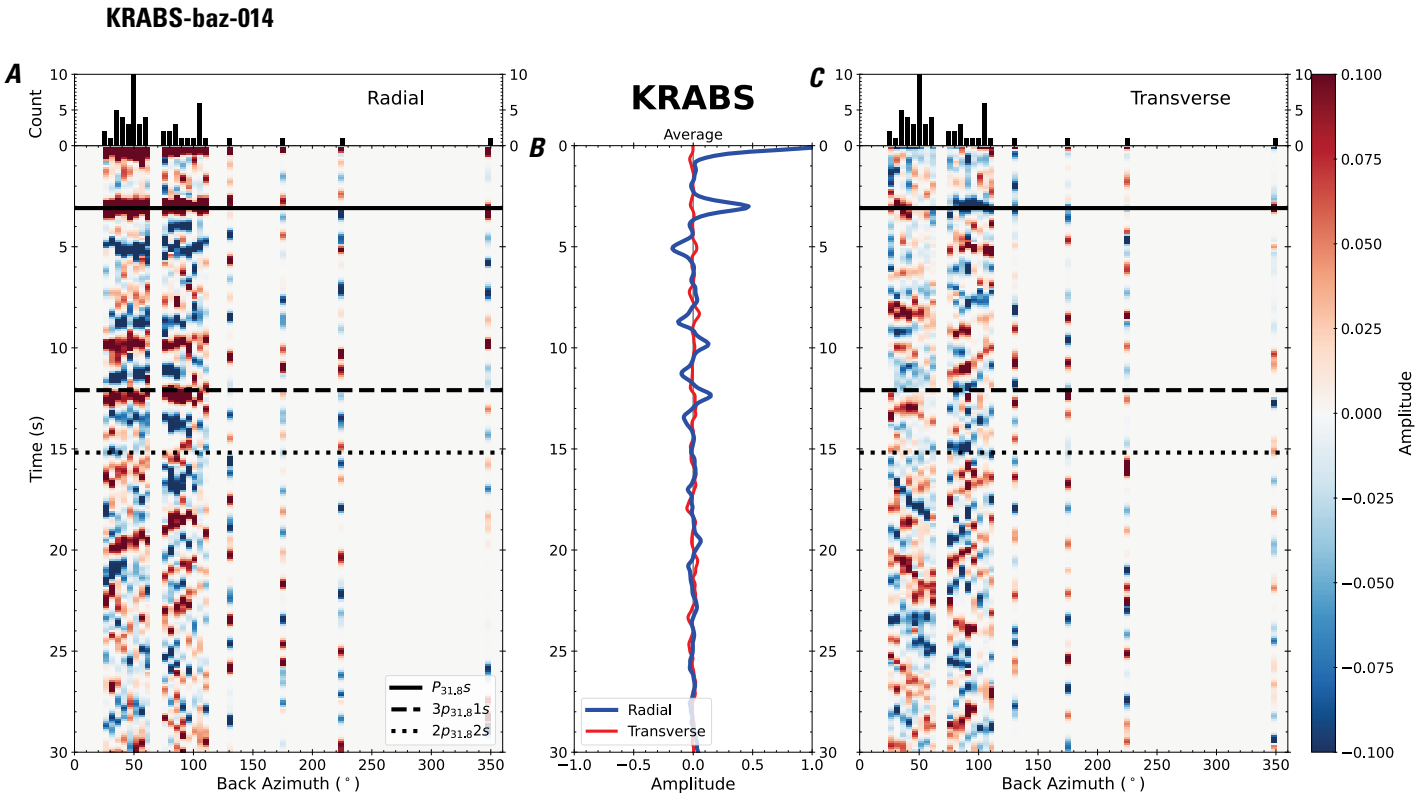

Figure 33. Receiver functions plotted against back azimuth for station KRABS. *A*, Radial component of P-wave receiver functions (PRFs) plotted against back azimuth. Individual PRFs have had the resonance-removal filter of Yu and others (2015) applied to them, are normalized to the maximum amplitude within the time window shown, binned, and normalized by the number of traces per bin. *B*, Average of every individual normalized radial receiver function with the application of the resonance-removal filter (blue) and average of every individual normalized raw radial receiver function (red). *C*, Radial component of raw PRFs, plotted against back azimuth, normalized as in *A*. Ps, 3p1s, and 2p2s arrival times predicted for the preferred Moho depth are shown, assuming a ray parameter of 0.06 s/km.

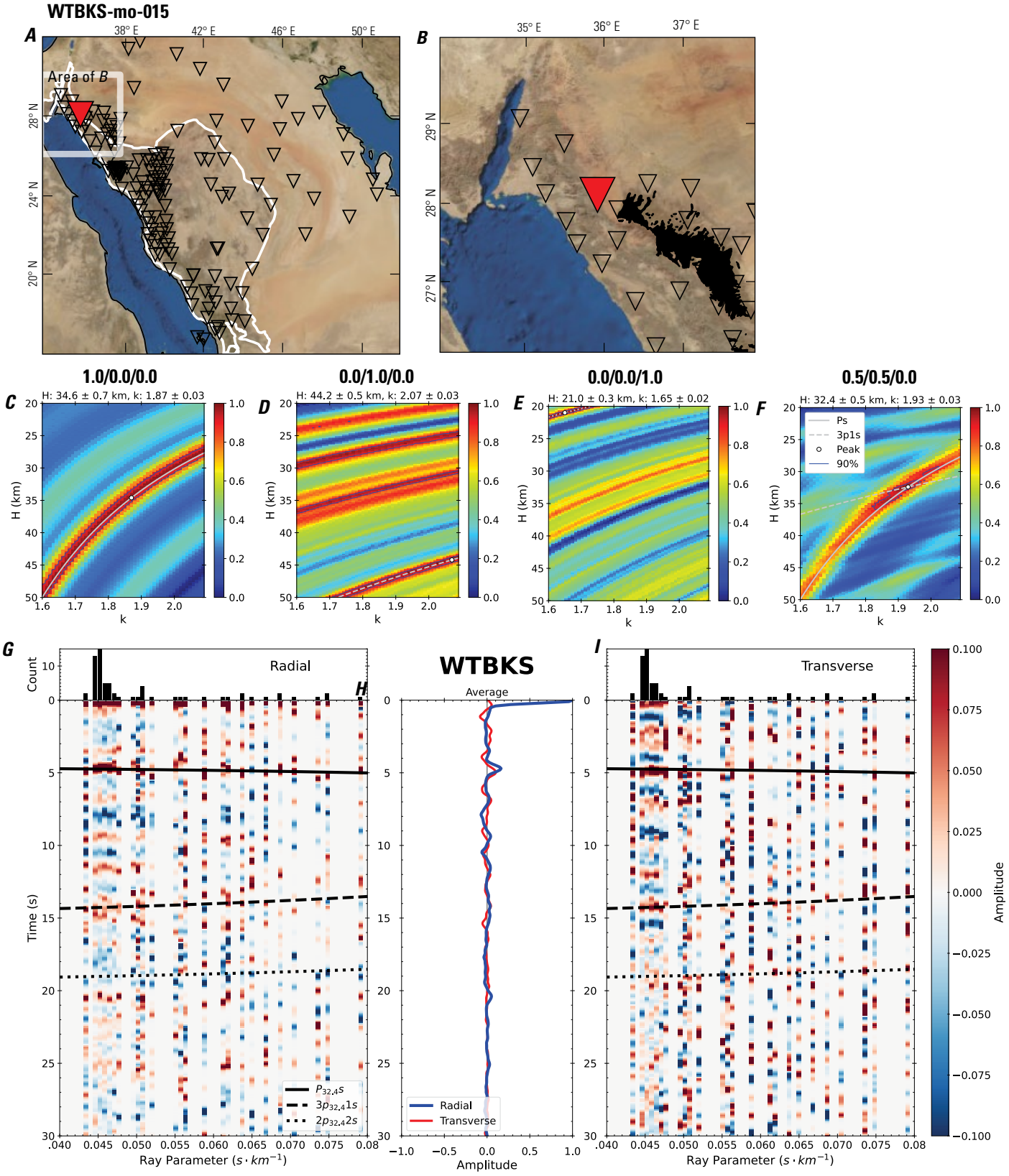
WTBKS-mo-015
A
B
Area of B
38° E
42° E
46° E
50° E
28° N
24° N
20° N
35° E
36° E
37° E
29° N
28° N
27° N
1.0/0.0/0.0
0.0/1.0/0.0
0.0/0.0/1.0
0.5/0.5/0.0
C
D
E
F
H: 34.6 ± 0.7 km, k: 1.87 ± 0.03
H: 44.2 ± 0.5 km, k: 2.07 ± 0.03
H: 21.0 ± 0.3 km, k: 1.65 ± 0.02
H: 32.4 ± 0.5 km, k: 1.93 ± 0.03
H (km)
k
Ps
3p1s
Peak
90%
G
H
I
WTBKS
Radial
Transverse
Average
Count
Time (s)
Ray Parameter (s · km⁻¹)
Amplitude
$P_{32.4}s$
$3p_{32.4}1s$
$2p_{32.4}2s$
Radial
Transverse

Figure 34 (page 40). Receiver-function analysis for station WTBKS. *A*, Regional map of Saudi Arabia showing the entire array (as inverted triangles), the location of station WTBKS (red inverted triangle), the shield-platform boundary (white line), and the bounds of the map in *B* (white box). *B*, Local map of station WTBKS. Harrats are shown in black. *C*, Standard, single-layer *H-k* stack with stacking weights 0.4/0.3/0.3. This *H-k* stack ignores sedimentary effects on the receiver functions. *D*, Standard, single-layer *H-k* stack with stacking weights 0.5/0.5/0.0. This *H-k* stack also ignores sedimentary effects on the receiver functions. *E*, Optimized sub-sedimentary *H-k* stack with stacking weights 0.4/0.3/0.3, following the method of Yu and others (2015). *F*, Optimized sedimentary *H-k* stack with stacking weights 0.05/0.70/0.25, following the method of Yu and others (2015). *G*, Radial component P-wave receiver functions (PRFs) plotted against ray parameter. Individual PRFs have had the resonance-removal filter of Yu and others (2015) applied to them and are normalized to the maximum amplitude within the time window shown, binned, and normalized by the number of traces per bin. *H*, Average of every individual normalized radial receiver function with the application of the resonance-removal filter (blue) and average of every individual normalized raw radial receiver function (red). *I*, Radial component of raw PRFs (that is, PRFs with no resonance-removal filter applied) plotted against ray parameter, normalized as in *G*.

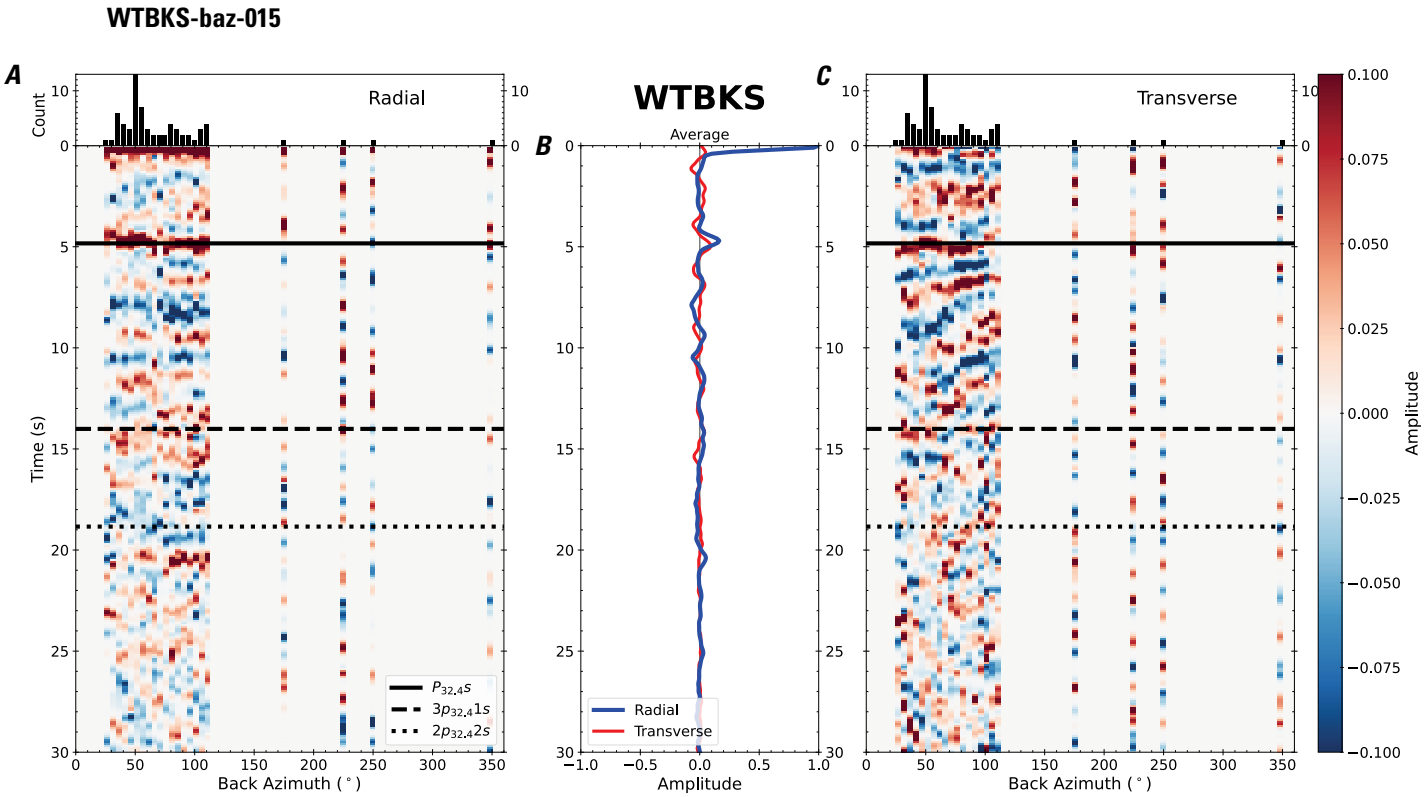

Figure 35. Receiver functions plotted against back azimuth for station WTBKS. *A*, Radial component of P-wave receiver functions (PRFs) plotted against back azimuth. Individual PRFs have had the resonance-removal filter of Yu and others (2015) applied to them, are normalized to the maximum amplitude within the time window shown, binned, and normalized by the number of traces per bin. *B*, Average of every individual normalized radial receiver function with the application of the resonance-removal filter (blue) and average of every individual normalized raw radial receiver function (red). *C*, Radial component of raw PRFs, plotted against back azimuth, normalized as in *A*. Ps, 3p1s, and 2p2s arrival times predicted for the preferred Moho depth are shown, assuming a ray parameter of 0.06 s/km.

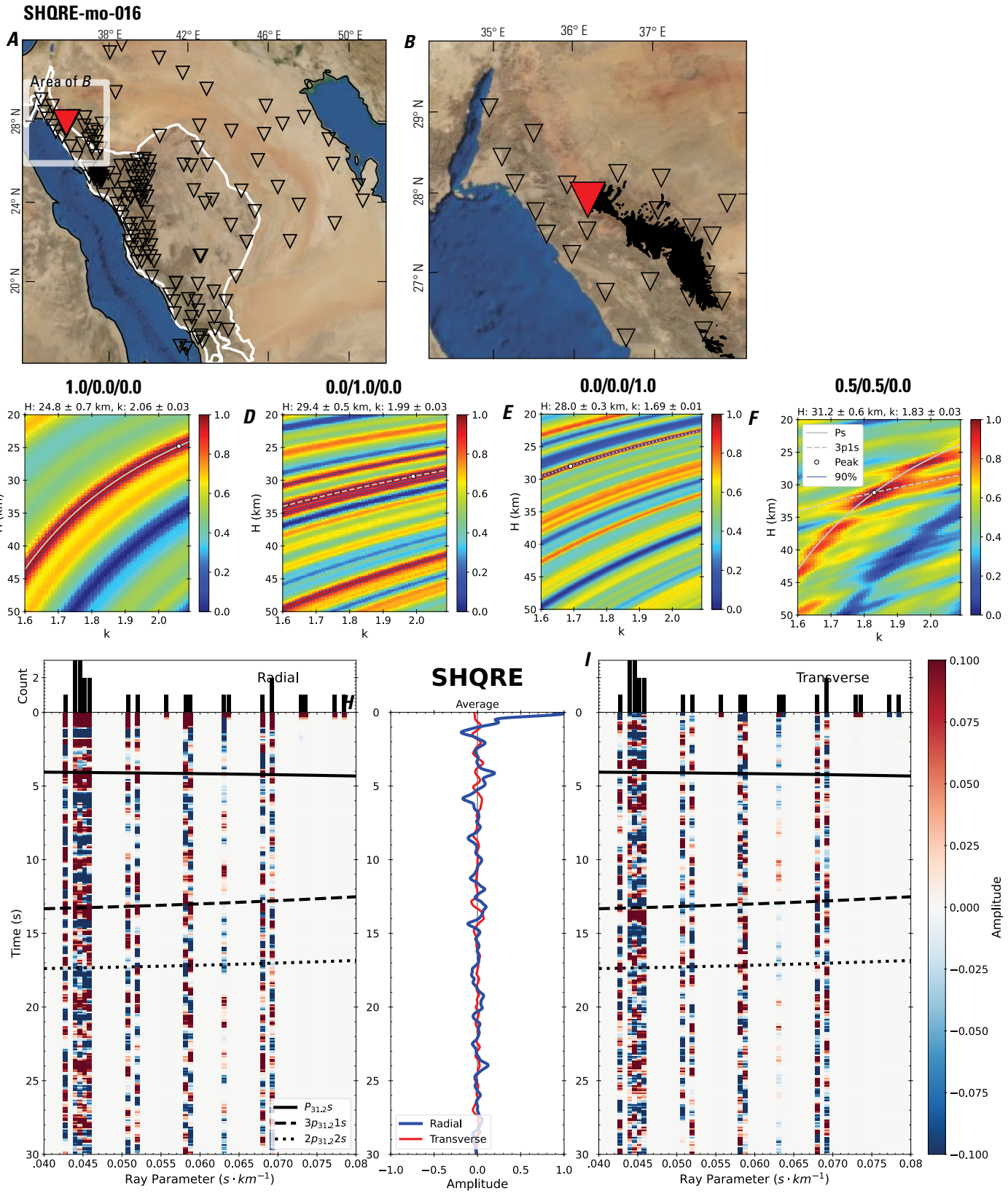
SHQRE-mo-016
A
B
Area of B
38° E
42° E
46° E
50° E
20° N
24° N
28° N
35° E
36° E
37° E
27° N
28° N
29° N
1.0/0.0/0.0
0.0/1.0/0.0
0.0/0.0/1.0
0.5/0.5/0.0
C
D
E
F
H: 24.8 ± 0.7 km, k: 2.06 ± 0.03
H: 29.4 ± 0.5 km, k: 1.99 ± 0.03
H: 28.0 ± 0.3 km, k: 1.69 ± 0.01
H: 31.2 ± 0.6 km, k: 1.83 ± 0.03
H (km)
k
Ps
3p1s
Peak
90%
G
H
I
SHQRE
Radial
Transverse
Average
Count
Time (s)
Ray Parameter (s · km⁻¹)
Amplitude
$P_{31,2}s$
$3p_{31,2}1s$
$2p_{31,2}2s$

Figure 36 (page 42). Receiver-function analysis for station SHQRE. *A*, Regional map of Saudi Arabia showing the entire array (as inverted triangles), the location of station SHQRE (red inverted triangle), the shield-platform boundary (white line), and the bounds of the map in *B* (white box). *B*, Local map of station SHQRE. Harrats are shown in black. *C*, Standard, single-layer *H-k* stack with stacking weights 0.4/0.3/0.3. This *H-k* stack ignores sedimentary effects on the receiver functions. *D*, Standard, single-layer *H-k* stack with stacking weights 0.5/0.5/0.0. This *H-k* stack also ignores sedimentary effects on the receiver functions. *E*, Optimized sub-sedimentary *H-k* stack with stacking weights 0.4/0.3/0.3, following the method of Yu and others (2015). *F*, Optimized sedimentary *H-k* stack with stacking weights 0.05/0.70/0.25, following the method of Yu and others (2015). *G*, Radial component P-wave receiver functions (PRFs) plotted against ray parameter. Individual PRFs have had the resonance-removal filter of Yu and others (2015) applied to them and are normalized to the maximum amplitude within the time window shown, binned, and normalized by the number of traces per bin. *H*, Average of every individual normalized radial receiver function with the application of the resonance-removal filter (blue) and average of every individual normalized raw radial receiver function (red). *I*, Radial component of raw PRFs (that is, PRFs with no resonance-removal filter applied) plotted against ray parameter, normalized as in *G*.

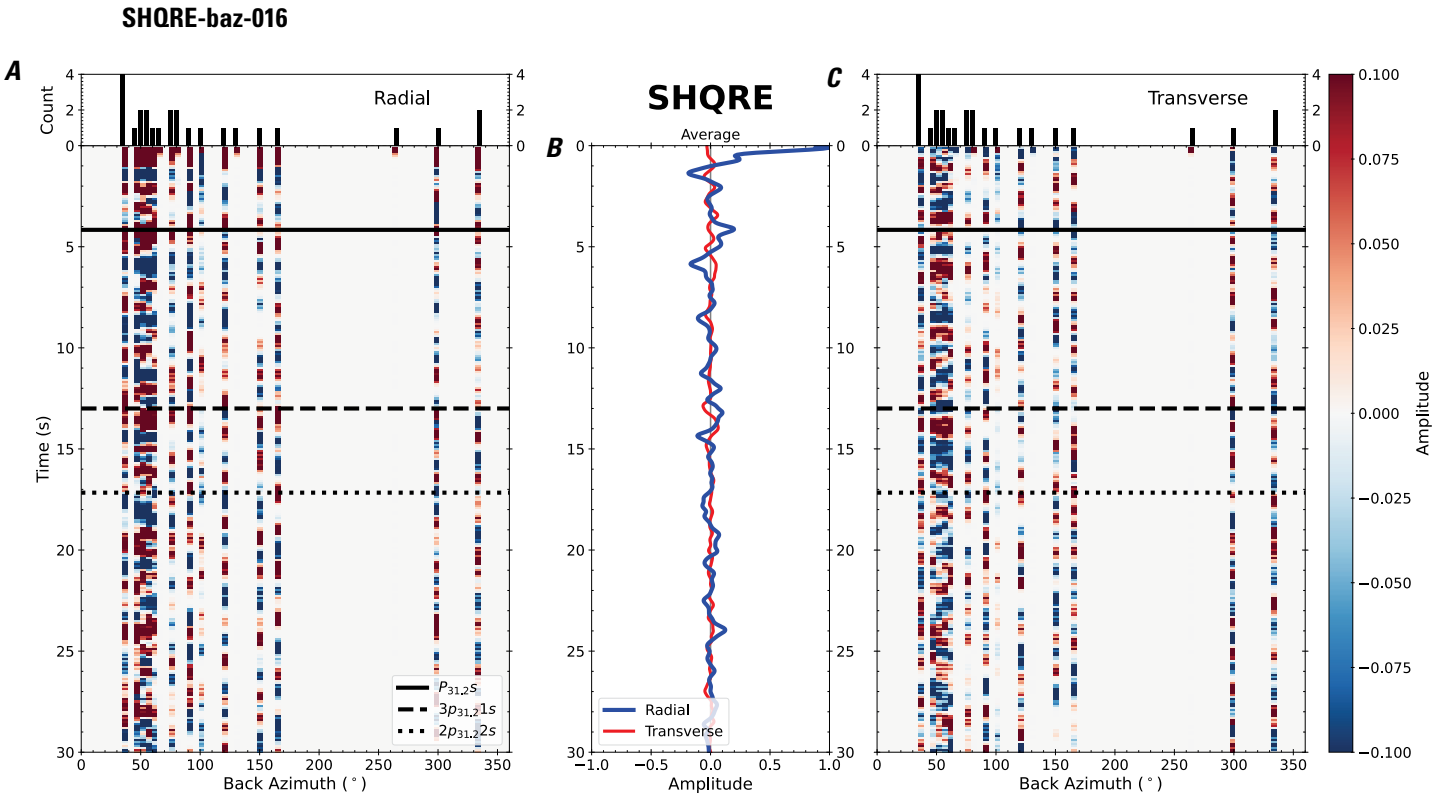

Figure 37. Receiver functions plotted against back azimuth for station SHQRE. *A*, Radial component of P-wave receiver functions (PRFs) plotted against back azimuth. Individual PRFs have had the resonance-removal filter of Yu and others (2015) applied to them, are normalized to the maximum amplitude within the time window shown, binned, and normalized by the number of traces per bin. *B*, Average of every individual normalized radial receiver function with the application of the resonance-removal filter (blue) and average of every individual normalized raw radial receiver function (red). *C*, Radial component of raw PRFs, plotted against back azimuth, normalized as in *A*. Ps, 3p1s, and 2p2s arrival times predicted for the preferred Moho depth are shown, assuming a ray parameter of 0.06 s/km.

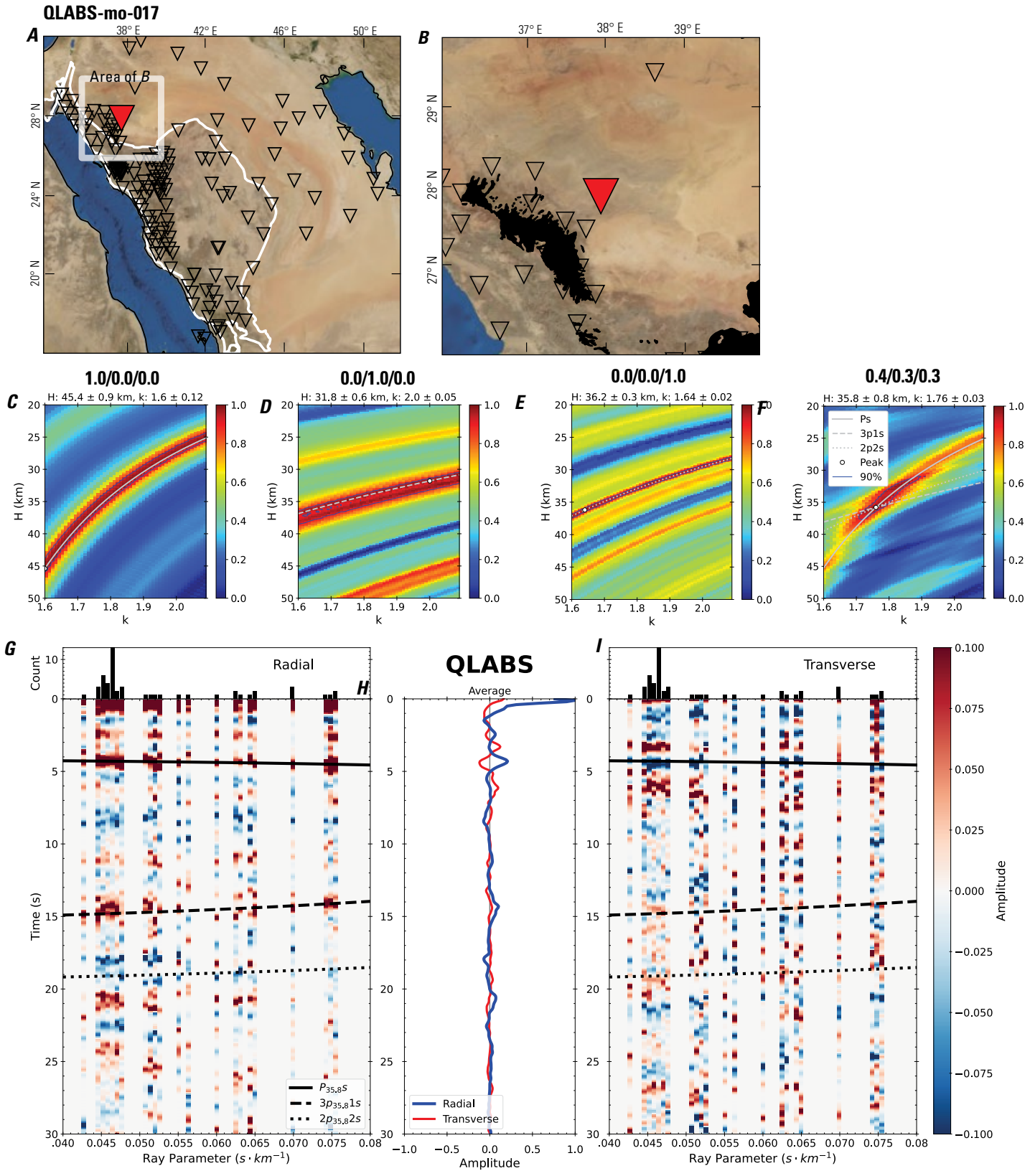
QLABS-mo-017
A
B
Area of B
38° E
42° E
46° E
50° E
37° E
38° E
39° E
28° N
24° N
20° N
29° N
28° N
27° N
1.0/0.0/0.0
0.0/1.0/0.0
0.0/0.0/1.0
0.4/0.3/0.3
C
D
E
F
H: 45.4 ± 0.9 km, k: 1.6 ± 0.12
H: 31.8 ± 0.6 km, k: 2.0 ± 0.05
H: 36.2 ± 0.3 km, k: 1.64 ± 0.02
H: 35.8 ± 0.8 km, k: 1.76 ± 0.03
H (km)
k
Ps
3p1s
2p2s
Peak
90%
G
H
I
Radial
Transverse
QLABS
Average
Count
Time (s)
Ray Parameter (s · km⁻¹)
Amplitude
P35.8s
3p35.81s
2p35.82s
Radial
Transverse

Figure 38 (page 44). Receiver-function analysis for station QLABS. *A*, Regional map of Saudi Arabia showing the entire array (as inverted triangles), the location of station QLABS (red inverted triangle), the shield-platform boundary (white line), and the bounds of the map in *B* (white box). *B*, Local map of station QLABS. Harrats are shown in black. *C*, Standard, single-layer *H-k* stack with stacking weights 0.4/0.3/0.3. This *H-k* stack ignores sedimentary effects on the receiver functions. *D*, Standard, single-layer *H-k* stack with stacking weights 0.5/0.5/0.0. This *H-k* stack also ignores sedimentary effects on the receiver functions. *E*, Optimized sub-sedimentary *H-k* stack with stacking weights 0.4/0.3/0.3, following the method of Yu and others (2015). *F*, Optimized sedimentary *H-k* stack with stacking weights 0.05/0.70/0.25, following the method of Yu and others (2015). *G*, Radial component P-wave receiver functions (PRFs) plotted against ray parameter. Individual PRFs have had the resonance-removal filter of Yu and others (2015) applied to them and are normalized to the maximum amplitude within the time window shown, binned, and normalized by the number of traces per bin. *H*, Average of every individual normalized radial receiver function with the application of the resonance-removal filter (blue) and average of every individual normalized raw radial receiver function (red). *I*, Radial component of raw PRFs (that is, PRFs with no resonance-removal filter applied) plotted against ray parameter, normalized as in *G*.

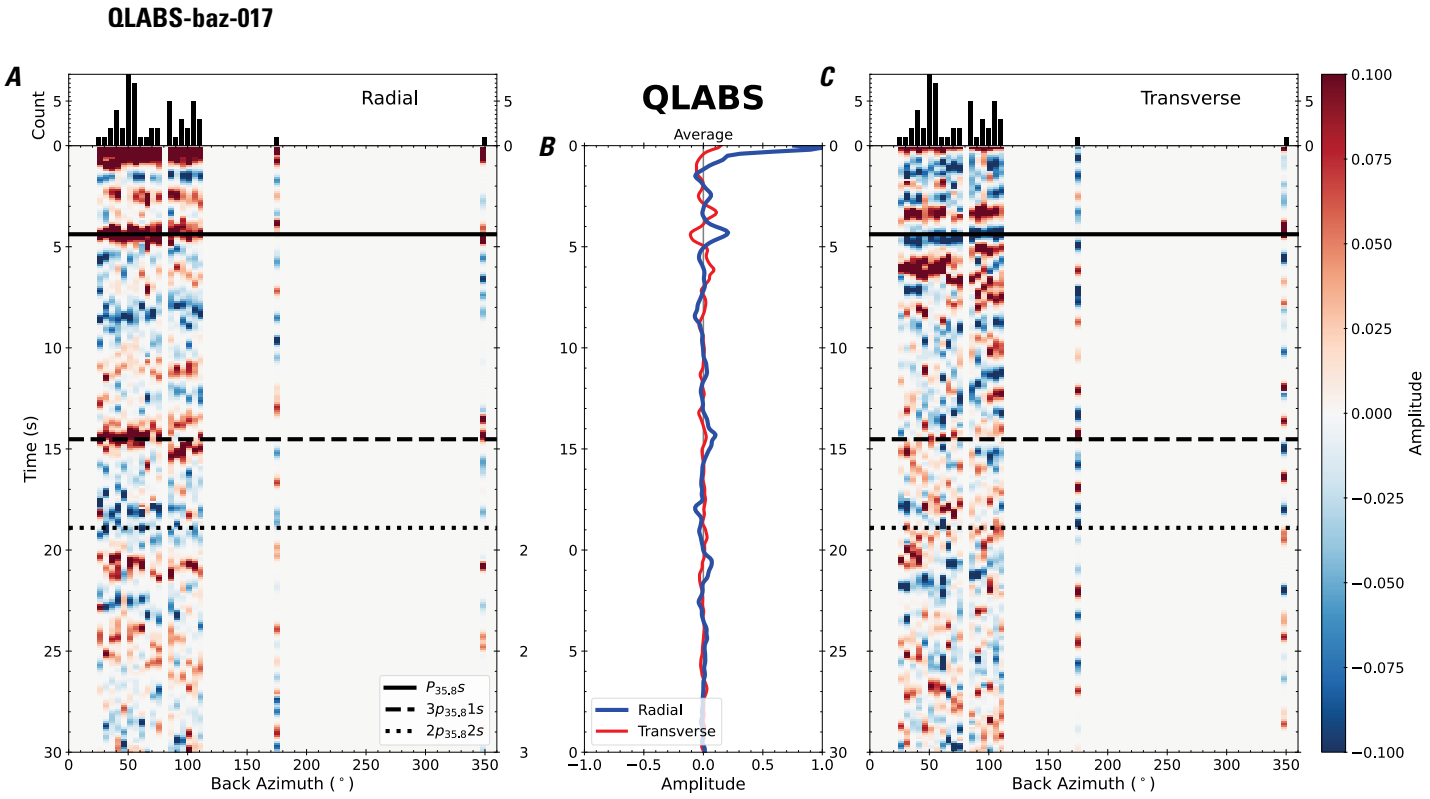

Figure 39. Receiver functions plotted against back azimuth for station QLABS. *A*, Radial component of P-wave receiver functions (PRFs) plotted against back azimuth. Individual PRFs have had the resonance-removal filter of Yu and others (2015) applied to them, are normalized to the maximum amplitude within the time window shown, binned, and normalized by the number of traces per bin. *B*, Average of every individual normalized radial receiver function with the application of the resonance-removal filter (blue) and average of every individual normalized raw radial receiver function (red). *C*, Radial component of raw PRFs, plotted against back azimuth, normalized as in *A*. Ps, 3p1s, and 2p2s arrival times predicted for the preferred Moho depth are shown, assuming a ray parameter of 0.06 s/km.

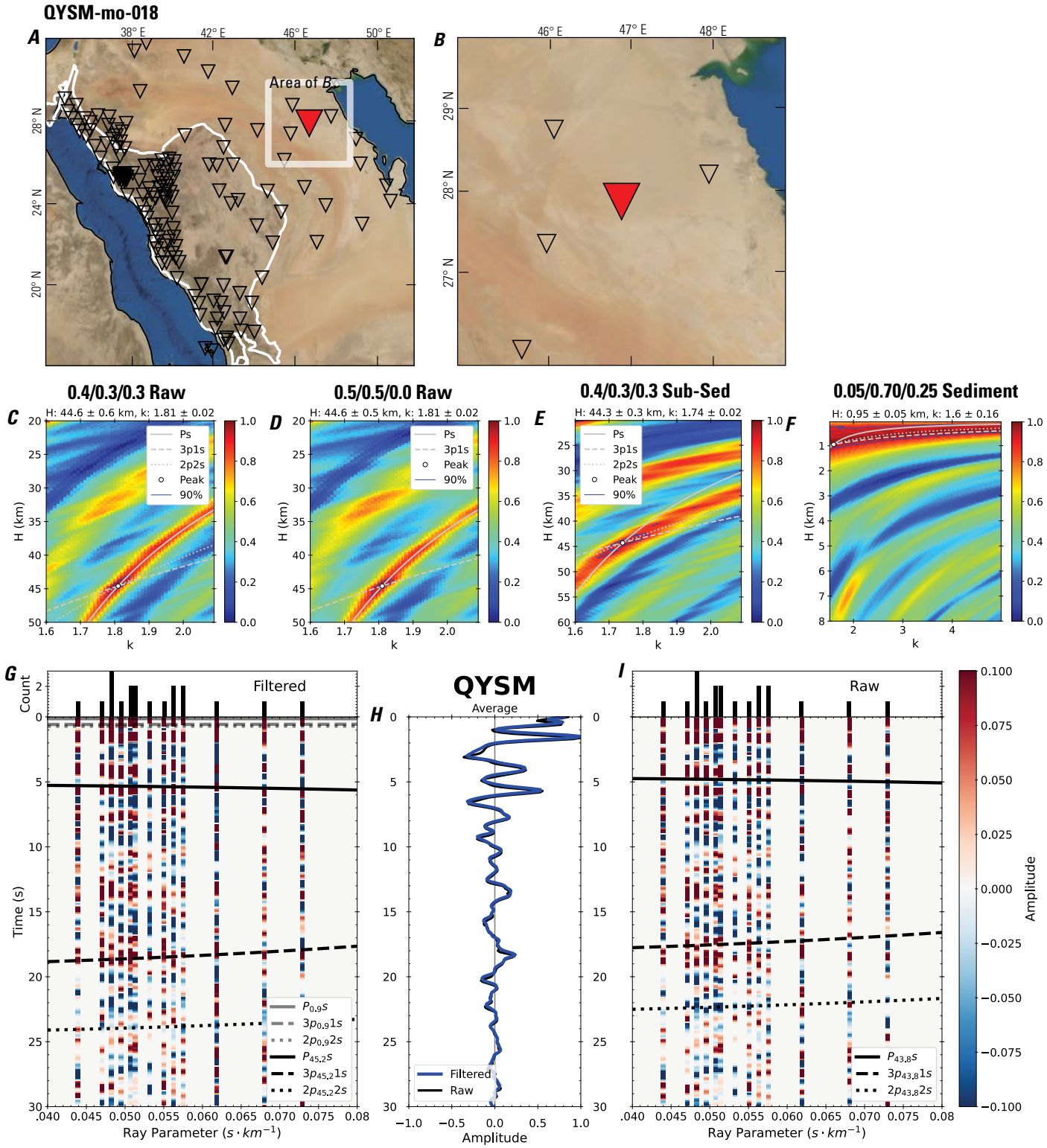
QYSM-mo-018
A
B
Area of B
C
0.4/0.3/0.3 Raw
H: 44.6 ± 0.6 km, k: 1.81 ± 0.02
D
0.5/0.5/0.0 Raw
H: 44.6 ± 0.5 km, k: 1.81 ± 0.02
E
0.4/0.3/0.3 Sub-Sed
H: 44.3 ± 0.3 km, k: 1.74 ± 0.02
F
0.05/0.70/0.25 Sediment
H: 0.95 ± 0.05 km, k: 1.6 ± 0.16
Ps
3p1s
2p2s
Peak
90%
H (km)
k
G
Filtered
Count
Time (s)
Ray Parameter (s · km⁻¹)
H
QYSM
Average
Filtered
Raw
Amplitude
I
Raw
Amplitude

Figure 40 (page 46). Receiver-function analysis for station QYSM. *A*, Regional map of Saudi Arabia showing the entire array (as inverted triangles), the location of station QYSM (red inverted triangle), the shield-platform boundary (white line), and the bounds of the map in *B* (white box). *B*, Local map of station QYSM. Harrats are shown in black. *C*, Standard, single-layer *H-k* stack with stacking weights 0.4/0.3/0.3. This *H-k* stack ignores sedimentary effects on the receiver functions. *D*, Standard, single-layer *H-k* stack with stacking weights 0.5/0.5/0.0. This *H-k* stack also ignores sedimentary effects on the receiver functions. *E*, Optimized sub-sedimentary *H-k* stack with stacking weights 0.4/0.3/0.3, following the method of Yu and others (2015). *F*, Optimized sedimentary *H-k* stack with stacking weights 0.05/0.70/0.25, following the method of Yu and others (2015). *G*, Radial component P-wave receiver functions (PRFs) plotted against ray parameter. Individual PRFs have had the resonance-removal filter of Yu and others (2015) applied to them and are normalized to the maximum amplitude within the time window shown, binned, and normalized by the number of traces per bin. *H*, Average of every individual normalized radial receiver function with the application of the resonance-removal filter (blue) and average of every individual normalized raw radial receiver function (red). *I*, Radial component of raw PRFs (that is, PRFs with no resonance-removal filter applied) plotted against ray parameter, normalized as in *G*.

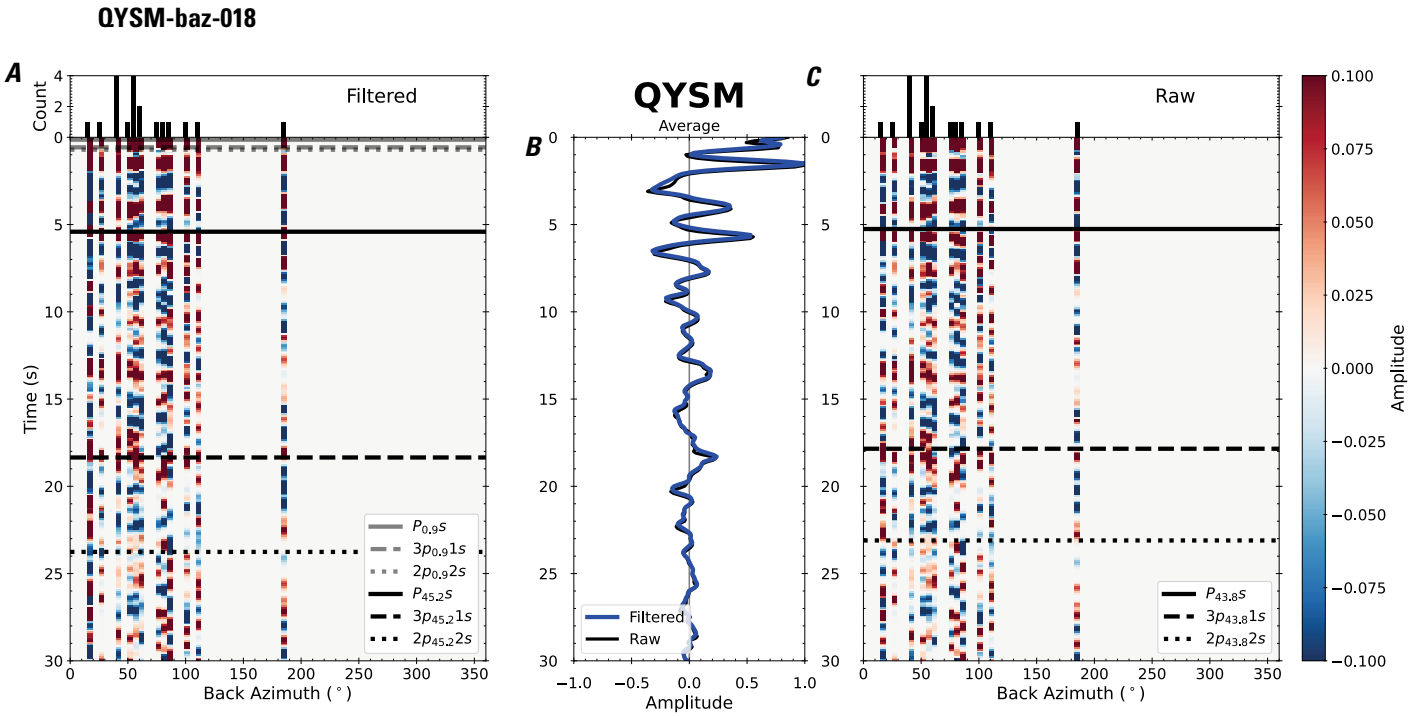

Figure 41. Receiver functions plotted against back azimuth for station QYSM. *A*, Radial component of P-wave receiver functions (PRFs) plotted against back azimuth. Individual PRFs have had the resonance-removal filter of Yu and others (2015) applied to them, are normalized to the maximum amplitude within the time window shown, binned, and normalized by the number of traces per bin. *B*, Average of every individual normalized radial receiver function with the application of the resonance-removal filter (blue) and average of every individual normalized raw radial receiver function (red). *C*, Radial component of raw PRFs, plotted against back azimuth, normalized as in *A*. Ps, 3p1s, and 2p2s arrival times predicted for the preferred Moho depth are shown, assuming a ray parameter of 0.06 s/km.

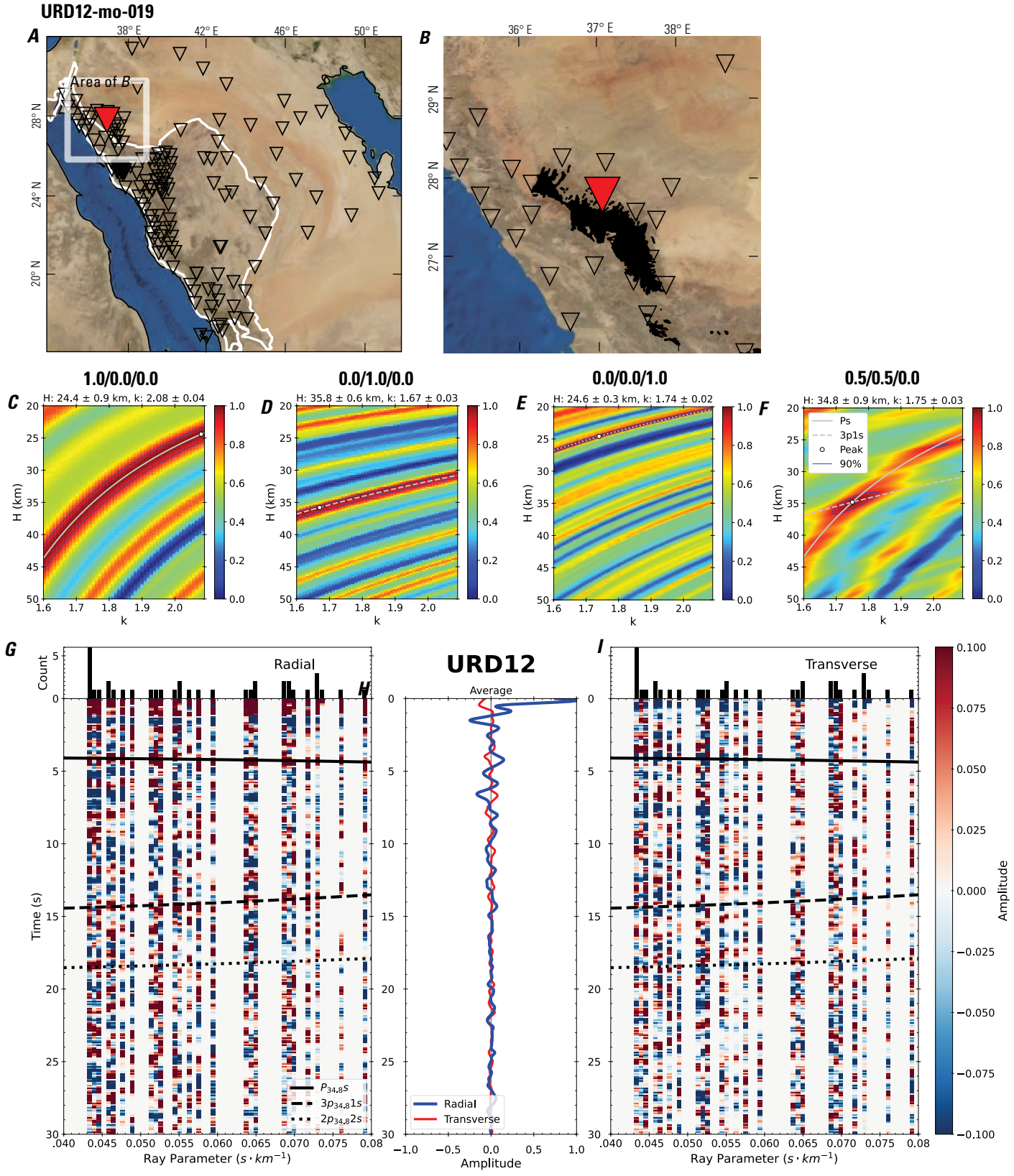
URD12-mo-019
A
B
Area of B
38° E
42° E
46° E
50° E
36° E
37° E
38° E
28° N
24° N
20° N
29° N
27° N
1.0/0.0/0.0
0.0/1.0/0.0
0.0/0.0/1.0
0.5/0.5/0.0
C
D
E
F
H: 24.4 ± 0.9 km, k: 2.08 ± 0.04
H: 35.8 ± 0.6 km, k: 1.67 ± 0.03
H: 24.6 ± 0.3 km, k: 1.74 ± 0.02
H: 34.8 ± 0.9 km, k: 1.75 ± 0.03
H (km)
k
Ps
3p1s
Peak
90%
G
I
URD12
Radial
Transverse
Average
Count
Time (s)
Ray Parameter (s · km⁻¹)
Amplitude
$P_{34.8}s$
$3p_{34.8}1s$
$2p_{34.8}2s$

Figure 42 (page 48). Receiver-function analysis for station URD12. *A*, Regional map of Saudi Arabia showing the entire array (as inverted triangles), the location of station URD12 (red inverted triangle), the shield-platform boundary (white line), and the bounds of the map in *B* (white box). *B*, Local map of station URD12. Harrats are shown in black. *C*, Standard, single-layer *H-k* stack with stacking weights 0.4/0.3/0.3. This *H-k* stack ignores sedimentary effects on the receiver functions. *D*, Standard, single-layer *H-k* stack with stacking weights 0.5/0.5/0.0. This *H-k* stack also ignores sedimentary effects on the receiver functions. *E*, Optimized sub-sedimentary *H-k* stack with stacking weights 0.4/0.3/0.3, following the method of Yu and others (2015). *F*, Optimized sedimentary *H-k* stack with stacking weights 0.05/0.70/0.25, following the method of Yu and others (2015). *G*, Radial component P-wave receiver functions (PRFs) plotted against ray parameter. Individual PRFs have had the resonance-removal filter of Yu and others (2015) applied to them and are normalized to the maximum amplitude within the time window shown, binned, and normalized by the number of traces per bin. *H*, Average of every individual normalized radial receiver function with the application of the resonance-removal filter (blue) and average of every individual normalized raw radial receiver function (red). *I*, Radial component of raw PRFs (that is, PRFs with no resonance-removal filter applied) plotted against ray parameter, normalized as in *G*.

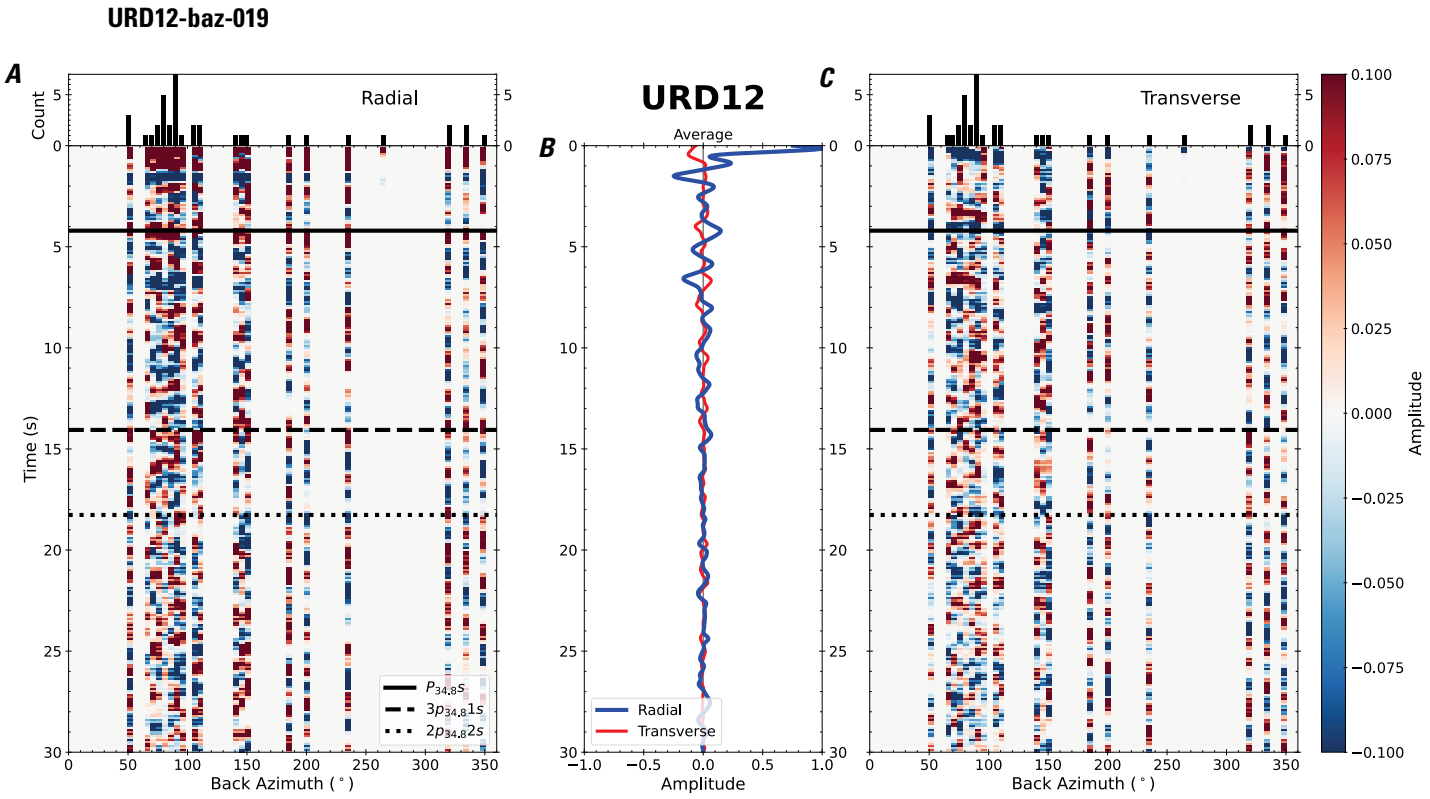

Figure 43. Receiver functions plotted against back azimuth for station URD12. *A*, Radial component of P-wave receiver functions (PRFs) plotted against back azimuth. Individual PRFs have had the resonance-removal filter of Yu and others (2015) applied to them, are normalized to the maximum amplitude within the time window shown, binned, and normalized by the number of traces per bin. *B*, Average of every individual normalized radial receiver function with the application of the resonance-removal filter (blue) and average of every individual normalized raw radial receiver function (red). *C*, Radial component of raw PRFs, plotted against back azimuth, normalized as in *A*. Ps, 3p1s, and 2p2s arrival times predicted for the preferred Moho depth are shown, assuming a ray parameter of 0.06 s/km.

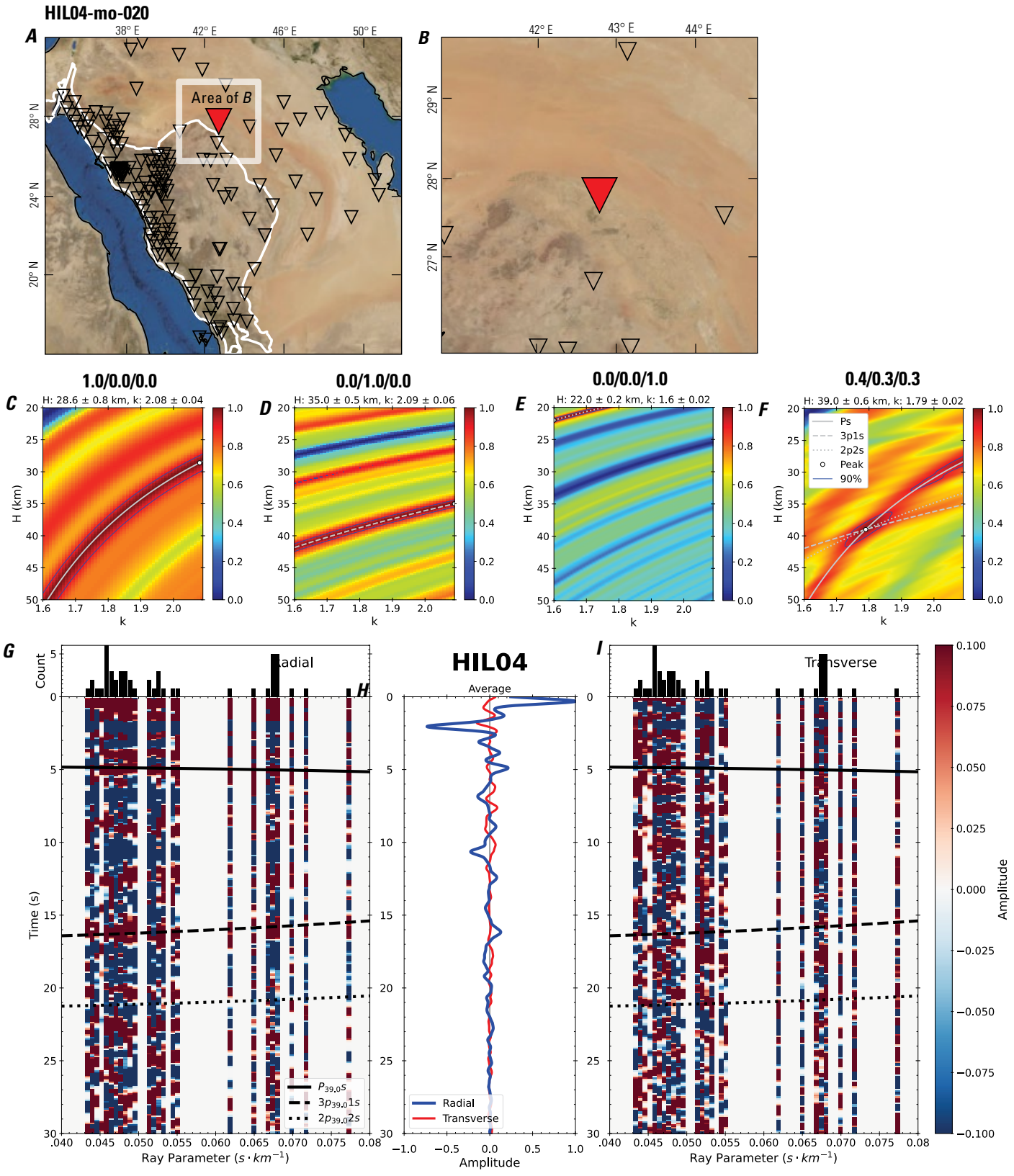
HIL04-mo-020
A
B
Area of B
1.0/0.0/0.0
0.0/1.0/0.0
0.0/0.0/1.0
0.4/0.3/0.3
C
D
E
F
H: 28.6 ± 0.8 km, k: 2.08 ± 0.04
H: 35.0 ± 0.5 km, k: 2.09 ± 0.06
H: 22.0 ± 0.2 km, k: 1.6 ± 0.02
H: 39.0 ± 0.6 km, k: 1.79 ± 0.02
H (km)
k
Ps
3p1s
2p2s
Peak
90%
G
I
HIL04
Average
Radial
Transverse
Count
Time (s)
Ray Parameter (s · km⁻¹)
Amplitude
$P_{39.0}s$
$3p_{39.0}1s$
$2p_{39.0}2s$

Figure 44 (page 50). Receiver-function analysis for station HIL04. *A*, Regional map of Saudi Arabia showing the entire array (as inverted triangles), the location of station HIL04 (red inverted triangle), the shield-platform boundary (white line), and the bounds of the map in *B* (white box). *B*, Local map of station HIL04. Harrats are shown in black. *C*, Standard, single-layer *H-k* stack with stacking weights 0.4/0.3/0.3. This *H-k* stack ignores sedimentary effects on the receiver functions. *D*, Standard, single-layer *H-k* stack with stacking weights 0.5/0.5/0.0. This *H-k* stack also ignores sedimentary effects on the receiver functions. *E*, Optimized sub-sedimentary *H-k* stack with stacking weights 0.4/0.3/0.3, following the method of Yu and others (2015). *F*, Optimized sedimentary *H-k* stack with stacking weights 0.05/0.70/0.25, following the method of Yu and others (2015). *G*, Radial component P-wave receiver functions (PRFs) plotted against ray parameter. Individual PRFs have had the resonance-removal filter of Yu and others (2015) applied to them and are normalized to the maximum amplitude within the time window shown, binned, and normalized by the number of traces per bin. *H*, Average of every individual normalized radial receiver function with the application of the resonance-removal filter (blue) and average of every individual normalized raw radial receiver function (red). *I*, Radial component of raw PRFs (that is, PRFs with no resonance-removal filter applied) plotted against ray parameter, normalized as in *G*.

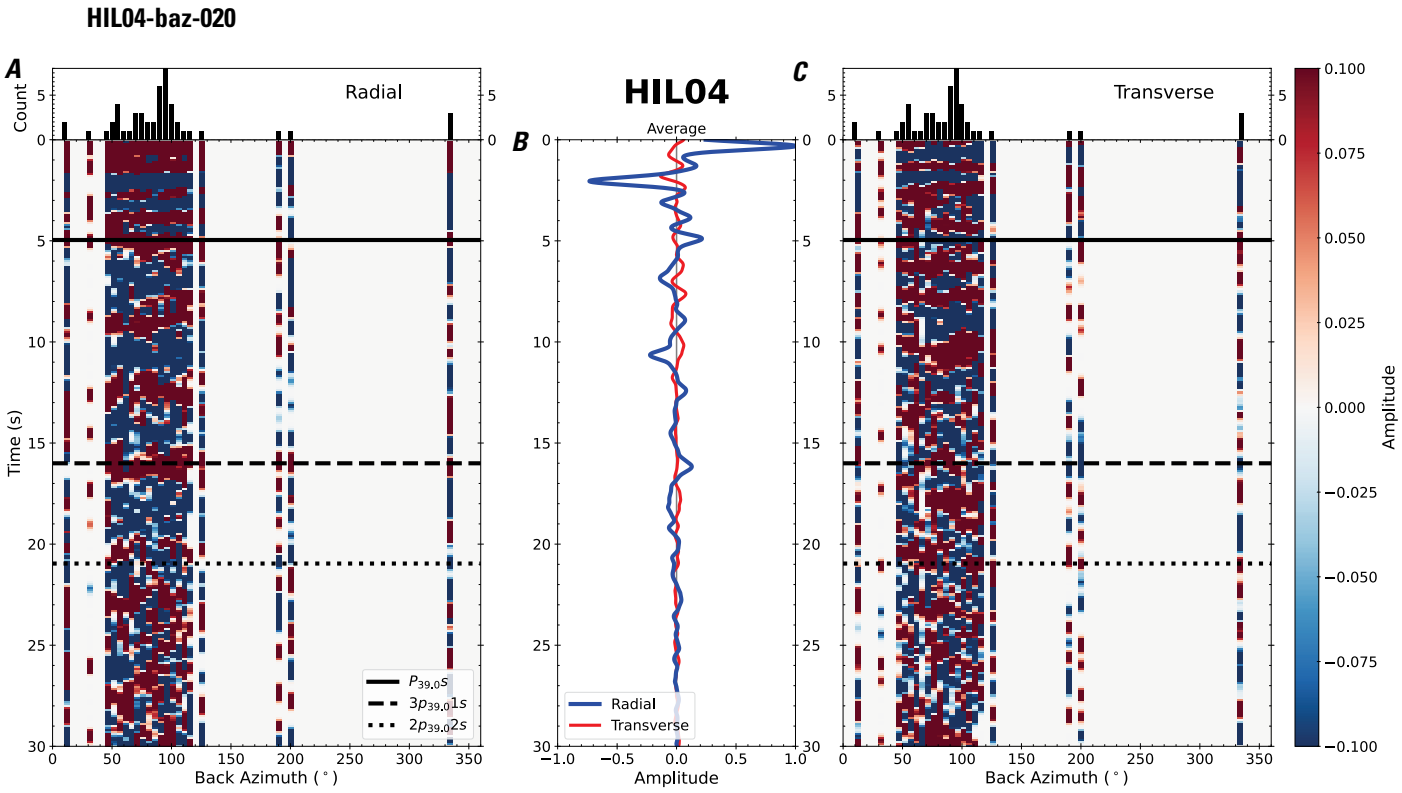

Figure 45. Receiver functions plotted against back azimuth for station HIL04. *A*, Radial component of P-wave receiver functions (PRFs) plotted against back azimuth. Individual PRFs have had the resonance-removal filter of Yu and others (2015) applied to them, are normalized to the maximum amplitude within the time window shown, binned, and normalized by the number of traces per bin. *B*, Average of every individual normalized radial receiver function with the application of the resonance-removal filter (blue) and average of every individual normalized raw radial receiver function (red). *C*, Radial component of raw PRFs, plotted against back azimuth, normalized as in *A*. Ps, 3p1s, and 2p2s arrival times predicted for the preferred Moho depth are shown, assuming a ray parameter of 0.06 s/km.

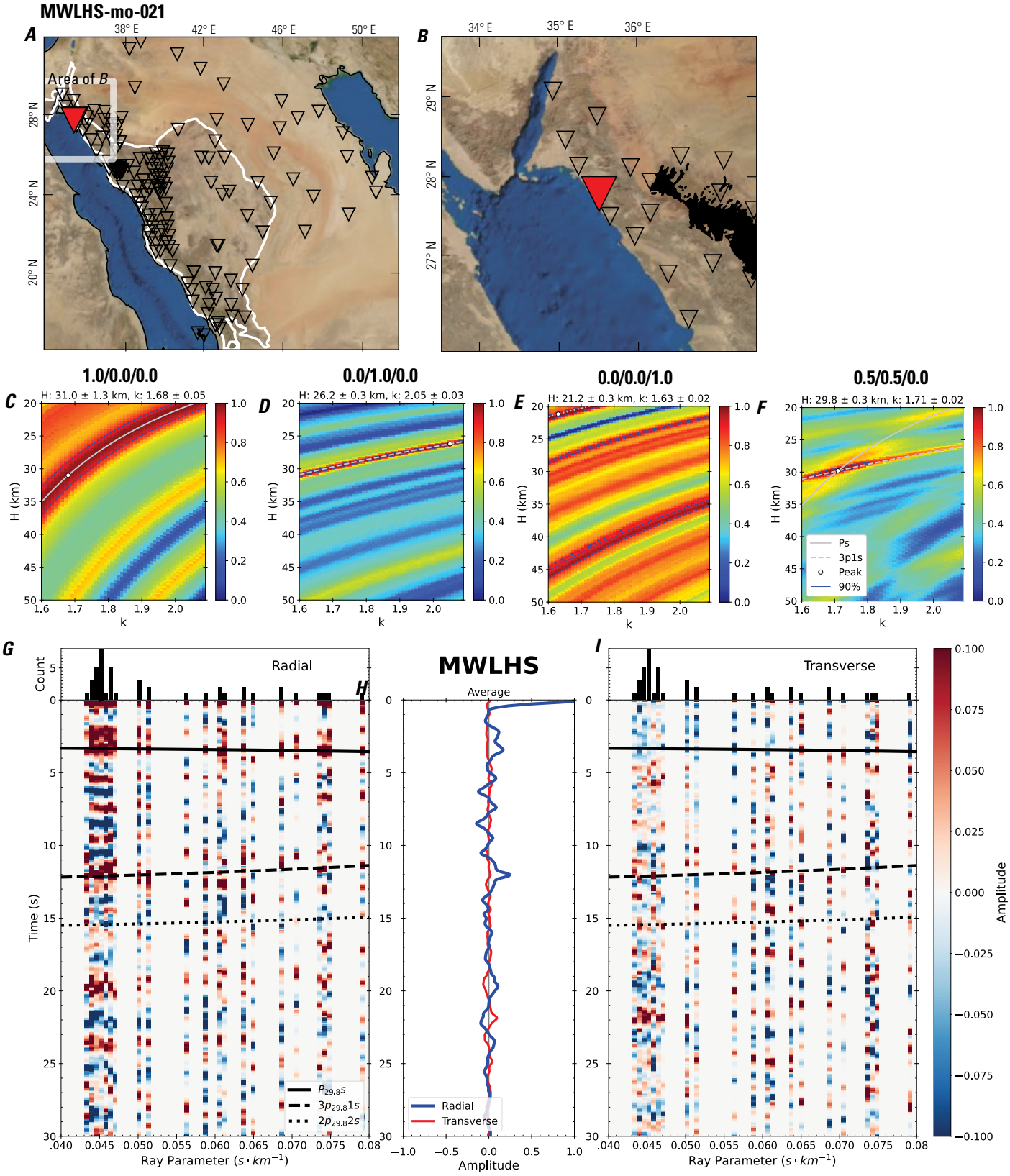
MWLHS-mo-021
A
38° E
42° E
46° E
50° E
Area of B
28° N
24° N
20° N
B
34° E
35° E
36° E
29° N
28° N
27° N
1.0/0.0/0.0
0.0/1.0/0.0
0.0/0.0/1.0
0.5/0.5/0.0
C
H: 31.0 ± 1.3 km, k: 1.68 ± 0.05
D
H: 26.2 ± 0.3 km, k: 2.05 ± 0.03
E
H: 21.2 ± 0.3 km, k: 1.63 ± 0.02
F
H: 29.8 ± 0.3 km, k: 1.71 ± 0.02
H (km)
k
Ps
3p1s
Peak
90%
G
Radial
H
I
Transverse
MWLHS
Average
Count
Time (s)
Ray Parameter (s · km⁻¹)
Amplitude
$P_{29.8}s$
$3p_{29.8}1s$
$2p_{29.8}2s$
Radial
Transverse

Figure 46 (page 52). Receiver-function analysis for station MWLHS. *A*, Regional map of Saudi Arabia showing the entire array (as inverted triangles), the location of station MWLHS (red inverted triangle), the shield-platform boundary (white line), and the bounds of the map in *B* (white box). *B*, Local map of station MWLHS. Harrats are shown in black. *C*, Standard, single-layer *H-k* stack with stacking weights 0.4/0.3/0.3. This *H-k* stack ignores sedimentary effects on the receiver functions. *D*, Standard, single-layer *H-k* stack with stacking weights 0.5/0.5/0.0. This *H-k* stack also ignores sedimentary effects on the receiver functions. *E*, Optimized sub-sedimentary *H-k* stack with stacking weights 0.4/0.3/0.3, following the method of Yu and others (2015). *F*, Optimized sedimentary *H-k* stack with stacking weights 0.05/0.70/0.25, following the method of Yu and others (2015). *G*, Radial component P-wave receiver functions (PRFs) plotted against ray parameter. Individual PRFs have had the resonance-removal filter of Yu and others (2015) applied to them and are normalized to the maximum amplitude within the time window shown, binned, and normalized by the number of traces per bin. *H*, Average of every individual normalized radial receiver function with the application of the resonance-removal filter (blue) and average of every individual normalized raw radial receiver function (red). *I*, Radial component of raw PRFs (that is, PRFs with no resonance-removal filter applied) plotted against ray parameter, normalized as in *G*.

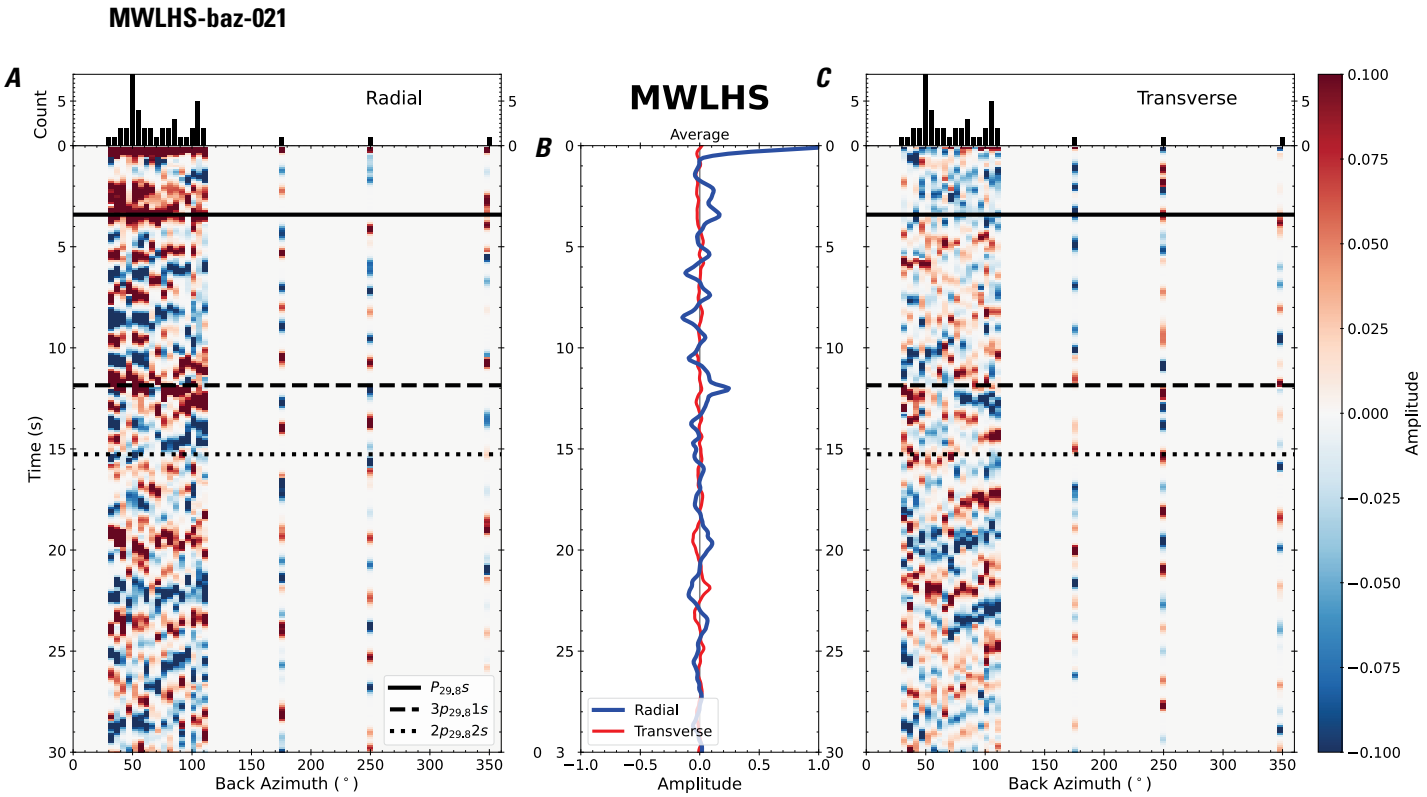

Figure 47. Receiver functions plotted against back azimuth for station MWLHS. *A*, Radial component of P-wave receiver functions (PRFs) plotted against back azimuth. Individual PRFs have had the resonance-removal filter of Yu and others (2015) applied to them, are normalized to the maximum amplitude within the time window shown, binned, and normalized by the number of traces per bin. *B*, Average of every individual normalized radial receiver function with the application of the resonance-removal filter (blue) and average of every individual normalized raw radial receiver function (red). *C*, Radial component of raw PRFs, plotted against back azimuth, normalized as in *A*. Ps, 3p1s, and 2p2s arrival times predicted for the preferred Moho depth are shown, assuming a ray parameter of 0.06 s/km.

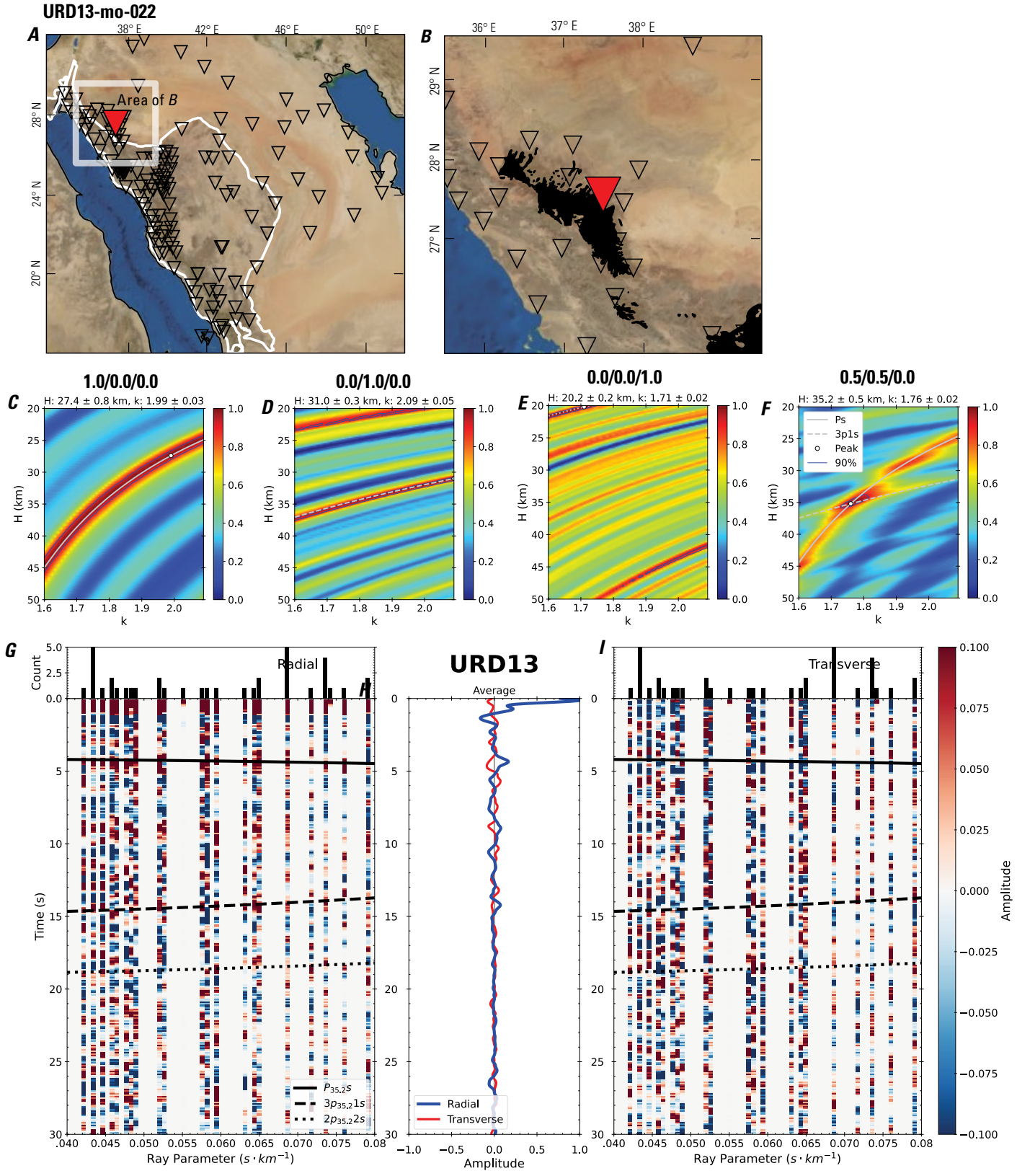
URD13-mo-022
A
B
Area of B
C
D
E
F
1.0/0.0/0.0
0.0/1.0/0.0
0.0/0.0/1.0
0.5/0.5/0.0
H: 27.4 ± 0.8 km, k: 1.99 ± 0.03
H: 31.0 ± 0.3 km, k: 2.09 ± 0.05
H: 20.2 ± 0.2 km, k: 1.71 ± 0.02
H: 35.2 ± 0.5 km, k: 1.76 ± 0.02
Ps
3p1s
Peak
90%
H (km)
k
G
H
I
URD13
Radial
Transverse
Average
Count
Time (s)
Ray Parameter (s · km⁻¹)
Amplitude
$P_{35.2}s$
$3p_{35.2}1s$
$2p_{35.2}2s$

Figure 48 (page 54). Receiver-function analysis for station URD13. *A*, Regional map of Saudi Arabia showing the entire array (as inverted triangles), the location of station URD13 (red inverted triangle), the shield-platform boundary (white line), and the bounds of the map in *B* (white box). *B*, Local map of station URD13. Harrats are shown in black. *C*, Standard, single-layer *H-k* stack with stacking weights 0.4/0.3/0.3. This *H-k* stack ignores sedimentary effects on the receiver functions. *D*, Standard, single-layer *H-k* stack with stacking weights 0.5/0.5/0.0. This *H-k* stack also ignores sedimentary effects on the receiver functions. *E*, Optimized sub-sedimentary *H-k* stack with stacking weights 0.4/0.3/0.3, following the method of Yu and others (2015). *F*, Optimized sedimentary *H-k* stack with stacking weights 0.05/0.70/0.25, following the method of Yu and others (2015). *G*, Radial component P-wave receiver functions (PRFs) plotted against ray parameter. Individual PRFs have had the resonance-removal filter of Yu and others (2015) applied to them and are normalized to the maximum amplitude within the time window shown, binned, and normalized by the number of traces per bin. *H*, Average of every individual normalized radial receiver function with the application of the resonance-removal filter (blue) and average of every individual normalized raw radial receiver function (red). *I*, Radial component of raw PRFs (that is, PRFs with no resonance-removal filter applied) plotted against ray parameter, normalized as in *G*.

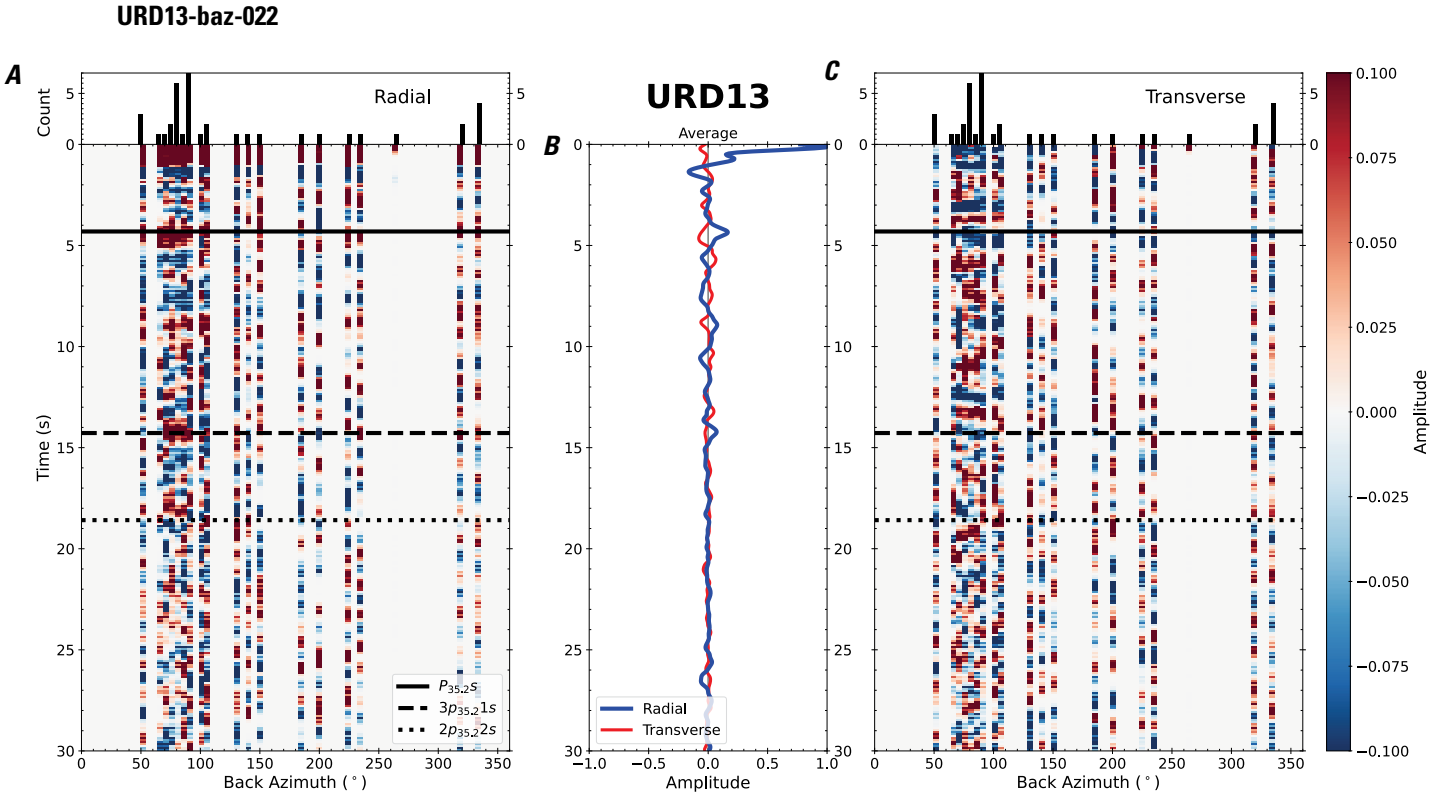

Figure 49. Receiver functions plotted against back azimuth for station URD13. *A*, Radial component of P-wave receiver functions (PRFs) plotted against back azimuth. Individual PRFs have had the resonance-removal filter of Yu and others (2015) applied to them, are normalized to the maximum amplitude within the time window shown, binned, and normalized by the number of traces per bin. *B*, Average of every individual normalized radial receiver function with the application of the resonance-removal filter (blue) and average of every individual normalized raw radial receiver function (red). *C*, Radial component of raw PRFs, plotted against back azimuth, normalized as in *A*. Ps, 3p1s, and 2p2s arrival times predicted for the preferred Moho depth are shown, assuming a ray parameter of 0.06 s/km.

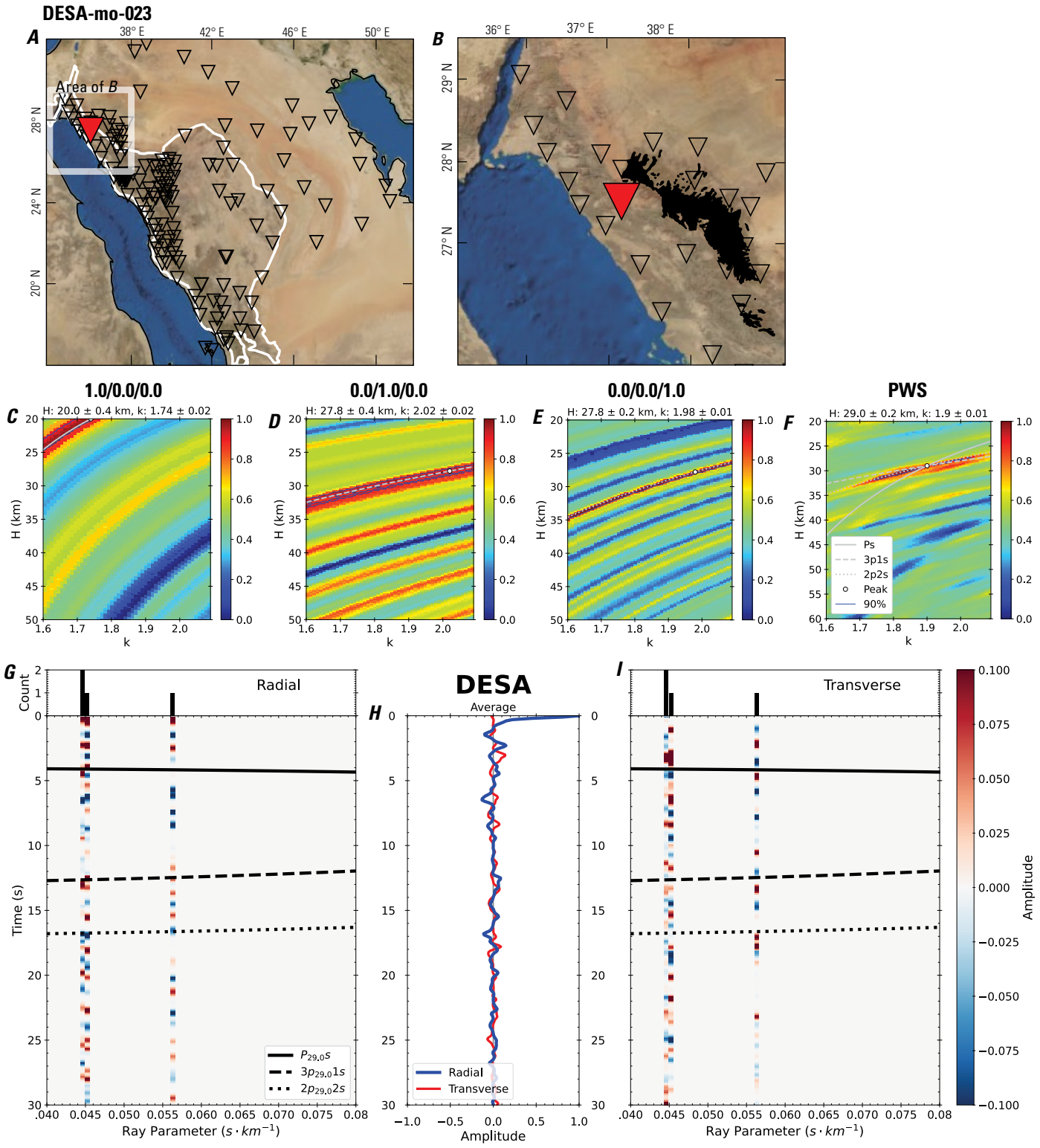
DESA-mo-023
A
B
Area of B
1.0/0.0/0.0
0.0/1.0/0.0
0.0/0.0/1.0
PWS
C
D
E
F
H: 20.0 ± 0.4 km, k: 1.74 ± 0.02
H: 27.8 ± 0.4 km, k: 2.02 ± 0.02
H: 27.8 ± 0.2 km, k: 1.98 ± 0.01
H: 29.0 ± 0.2 km, k: 1.9 ± 0.01
H (km)
k
Ps
3p1s
2p2s
Peak
90%
G
H
I
Radial
Transverse
DESA
Average
Count
Time (s)
Ray Parameter (s · km⁻¹)
Amplitude
$P_{29,0}s$
$3p_{29,0}1s$
$2p_{29,0}2s$

Figure 50 (page 56). Receiver-function analysis for station DESA. *A*, Regional map of Saudi Arabia showing the entire array (as inverted triangles), the location of station DESA (red inverted triangle), the shield-platform boundary (white line), and the bounds of the map in *B* (white box). *B*, Local map of station DESA. Harrats are shown in black. *C*, Standard, single-layer *H-k* stack with stacking weights 0.4/0.3/0.3. This *H-k* stack ignores sedimentary effects on the receiver functions. *D*, Standard, single-layer *H-k* stack with stacking weights 0.5/0.5/0.0. This *H-k* stack also ignores sedimentary effects on the receiver functions. *E*, Optimized sub-sedimentary *H-k* stack with stacking weights 0.4/0.3/0.3, following the method of Yu and others (2015). *F*, Optimized sedimentary *H-k* stack with stacking weights 0.05/0.70/0.25, following the method of Yu and others (2015). *G*, Radial component P-wave receiver functions (PRFs) plotted against ray parameter. Individual PRFs have had the resonance-removal filter of Yu and others (2015) applied to them and are normalized to the maximum amplitude within the time window shown, binned, and normalized by the number of traces per bin. *H*, Average of every individual normalized radial receiver function with the application of the resonance-removal filter (blue) and average of every individual normalized raw radial receiver function (red). *I*, Radial component of raw PRFs (that is, PRFs with no resonance-removal filter applied) plotted against ray parameter, normalized as in *G*.

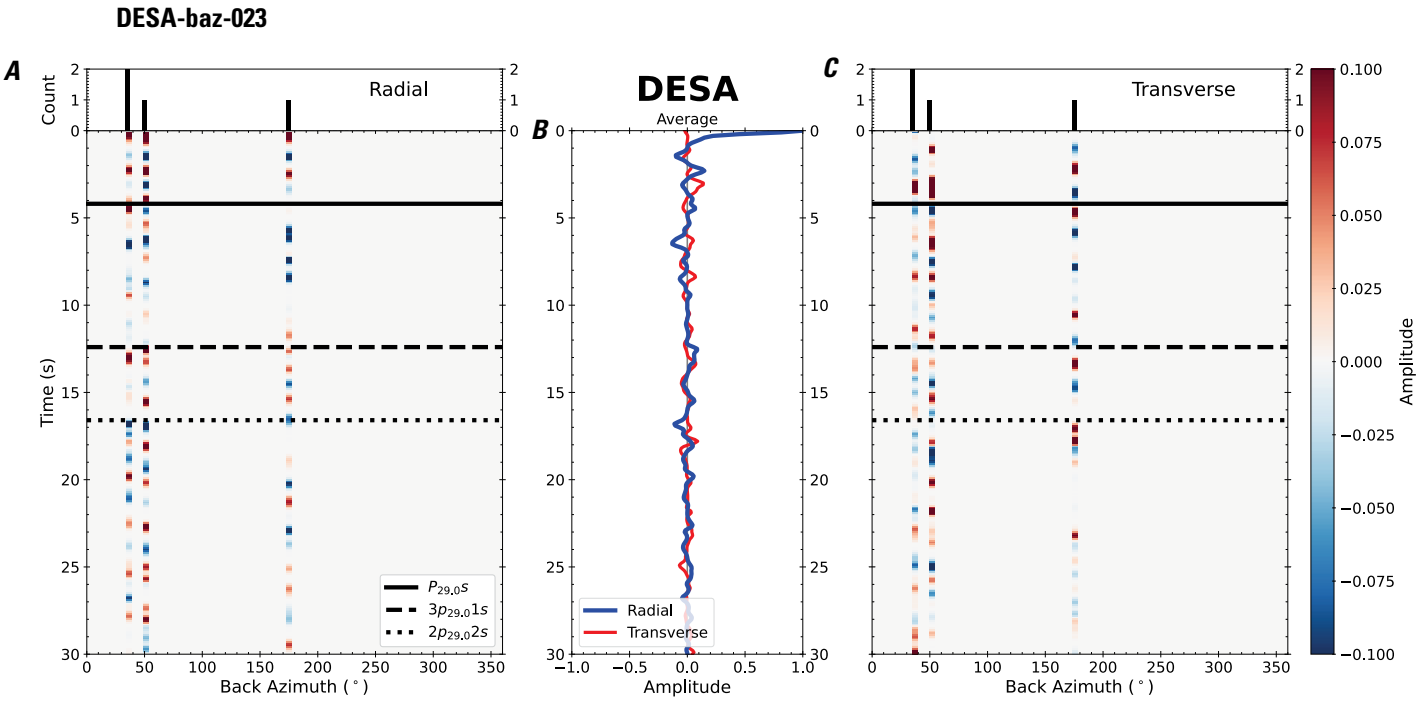

Figure 51. Receiver functions plotted against back azimuth for station DESA. *A*, Radial component of P-wave receiver functions (PRFs) plotted against back azimuth. Individual PRFs have had the resonance-removal filter of Yu and others (2015) applied to them, are normalized to the maximum amplitude within the time window shown, binned, and normalized by the number of traces per bin. *B*, Average of every individual normalized radial receiver function with the application of the resonance-removal filter (blue) and average of every individual normalized raw radial receiver function (red). *C*, Radial component of raw PRFs, plotted against back azimuth, normalized as in *A*. Ps, 3p1s, and 2p2s arrival times predicted for the preferred Moho depth are shown, assuming a ray parameter of 0.06 s/km.

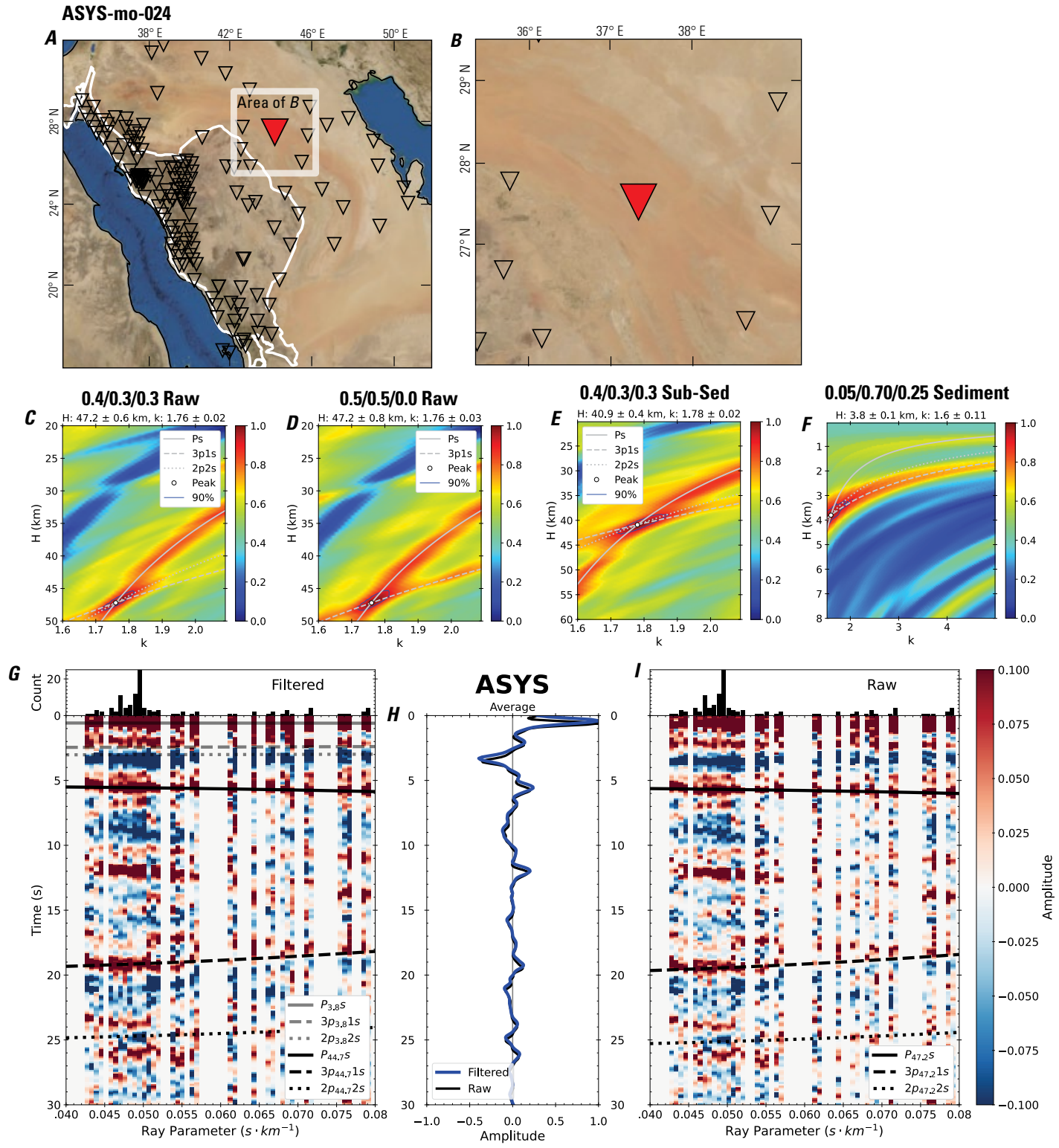
ASYS-mo-024
A
38° E
42° E
46° E
50° E
28° N
24° N
20° N
Area of B
B
36° E
37° E
38° E
29° N
28° N
27° N
0.4/0.3/0.3 Raw
C
H: 47.2 ± 0.6 km, k: 1.76 ± 0.02
0.5/0.5/0.0 Raw
D
H: 47.2 ± 0.8 km, k: 1.76 ± 0.03
0.4/0.3/0.3 Sub-Sed
E
H: 40.9 ± 0.4 km, k: 1.78 ± 0.02
0.05/0.70/0.25 Sediment
F
H: 3.8 ± 0.1 km, k: 1.6 ± 0.11
Ps
3p1s
2p2s
Peak
90%
H (km)
k
G
Filtered
Count
Time (s)
$P_{3.8}s$
$3p_{3.8}1s$
$2p_{3.8}2s$
$P_{44.7}s$
$3p_{44.7}1s$
$2p_{44.7}2s$
Ray Parameter ($s \cdot km^{-1}$)
ASYS
Average
H
Filtered
Raw
Amplitude
I
Raw
$P_{47.2}s$
$3p_{47.2}1s$
$2p_{47.2}2s$
Amplitude

Figure 52 (page 58). Receiver-function analysis for station ASYS. *A*, Regional map of Saudi Arabia showing the entire array (as inverted triangles), the location of station ASYS (red inverted triangle), the shield-platform boundary (white line), and the bounds of the map in *B* (white box). *B*, Local map of station ASYS. Harrats are shown in black. *C*, Standard, single-layer *H-k* stack with stacking weights 0.4/0.3/0.3. This *H-k* stack ignores sedimentary effects on the receiver functions. *D*, Standard, single-layer *H-k* stack with stacking weights 0.5/0.5/0.0. This *H-k* stack also ignores sedimentary effects on the receiver functions. *E*, Optimized sub-sedimentary *H-k* stack with stacking weights 0.4/0.3/0.3, following the method of Yu and others (2015). *F*, Optimized sedimentary *H-k* stack with stacking weights 0.05/0.70/0.25, following the method of Yu and others (2015). *G*, Radial component P-wave receiver functions (PRFs) plotted against ray parameter. Individual PRFs have had the resonance-removal filter of Yu and others (2015) applied to them and are normalized to the maximum amplitude within the time window shown, binned, and normalized by the number of traces per bin. *H*, Average of every individual normalized radial receiver function with the application of the resonance-removal filter (blue) and average of every individual normalized raw radial receiver function (red). *I*, Radial component of raw PRFs (that is, PRFs with no resonance-removal filter applied) plotted against ray parameter, normalized as in *G*.

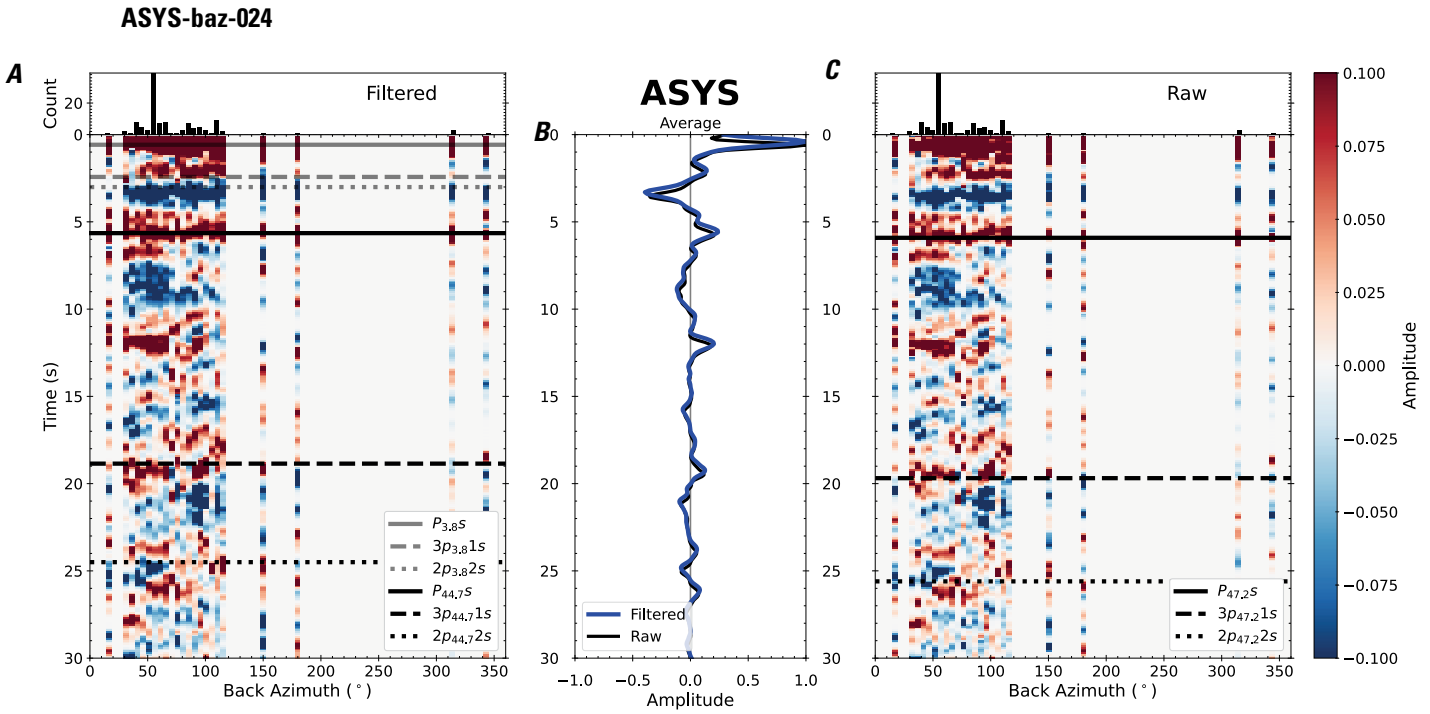

Figure 53. Receiver functions plotted against back azimuth for station ASYS. *A*, Radial component of P-wave receiver functions (PRFs) plotted against back azimuth. Individual PRFs have had the resonance-removal filter of Yu and others (2015) applied to them, are normalized to the maximum amplitude within the time window shown, binned, and normalized by the number of traces per bin. *B*, Average of every individual normalized radial receiver function with the application of the resonance-removal filter (blue) and average of every individual normalized raw radial receiver function (red). *C*, Radial component of raw PRFs, plotted against back azimuth, normalized as in *A*. Ps, 3p1s, and 2p2s arrival times predicted for the preferred Moho depth are shown, assuming a ray parameter of 0.06 s/km.

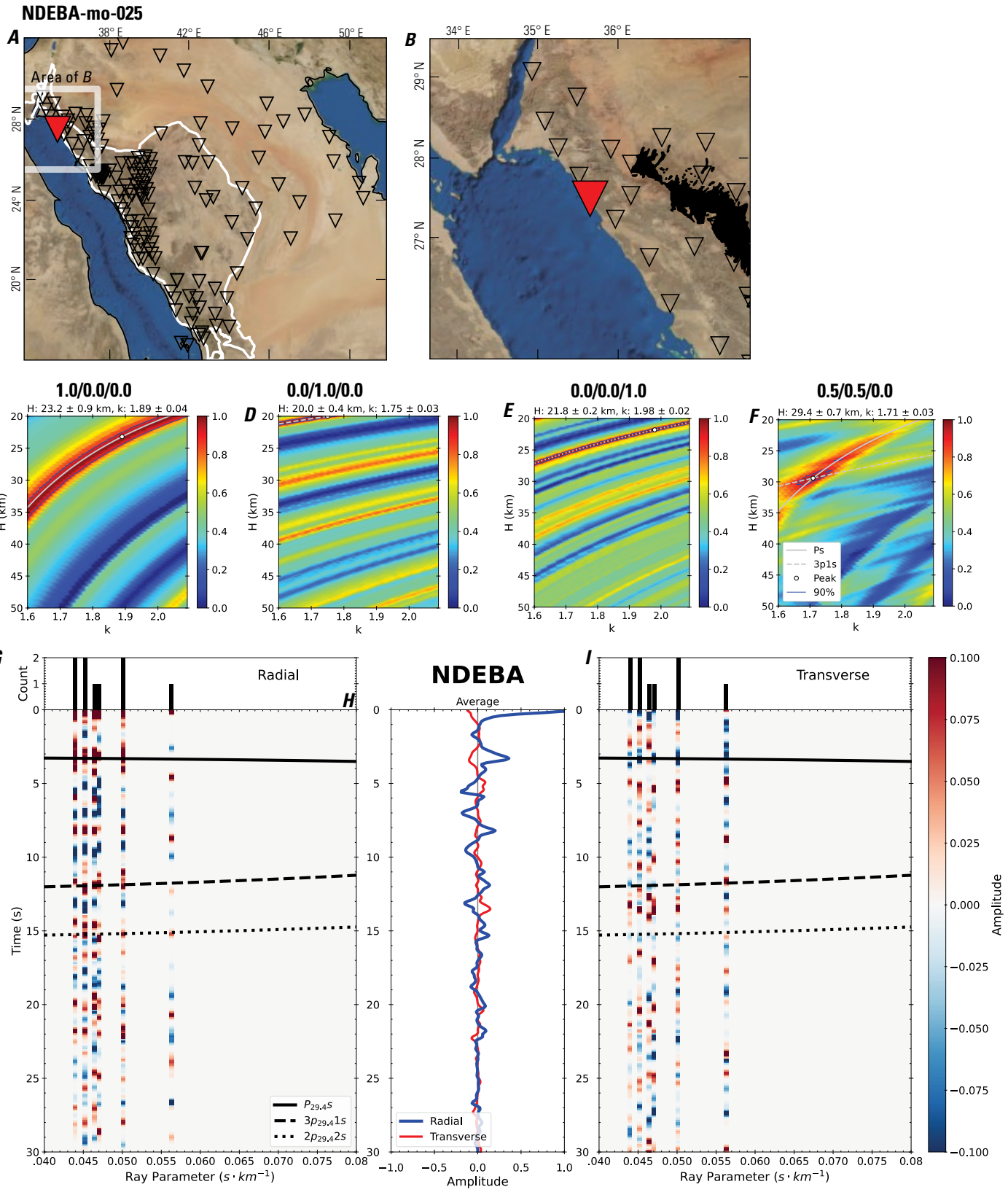
NDEBA-mo-025
A
B
Area of B
38° E
42° E
46° E
50° E
34° E
35° E
36° E
28° N
24° N
20° N
29° N
27° N
1.0/0.0/0.0
0.0/1.0/0.0
0.0/0.0/1.0
0.5/0.5/0.0
C
D
E
F
H: 23.2 ± 0.9 km, k: 1.89 ± 0.04
H: 20.0 ± 0.4 km, k: 1.75 ± 0.03
H: 21.8 ± 0.2 km, k: 1.98 ± 0.02
H: 29.4 ± 0.7 km, k: 1.71 ± 0.03
H (km)
k
Ps
3p1s
Peak
90%
G
H
I
NDEBA
Radial
Transverse
Average
Count
Time (s)
Ray Parameter (s · km⁻¹)
Amplitude
$P_{29.4}s$
$3p_{29.4}1s$
$2p_{29.4}2s$

Figure 54 (page 60). Receiver-function analysis for station NDEBA. *A*, Regional map of Saudi Arabia showing the entire array (as inverted triangles), the location of station NDEBA (red inverted triangle), the shield-platform boundary (white line), and the bounds of the map in *B* (white box). *B*, Local map of station NDEBA. Harrats are shown in black. *C*, Standard, single-layer *H-k* stack with stacking weights 0.4/0.3/0.3. This *H-k* stack ignores sedimentary effects on the receiver functions. *D*, Standard, single-layer *H-k* stack with stacking weights 0.5/0.5/0.0. This *H-k* stack also ignores sedimentary effects on the receiver functions. *E*, Optimized sub-sedimentary *H-k* stack with stacking weights 0.4/0.3/0.3, following the method of Yu and others (2015). *F*, Optimized sedimentary *H-k* stack with stacking weights 0.05/0.70/0.25, following the method of Yu and others (2015). *G*, Radial component P-wave receiver functions (PRFs) plotted against ray parameter. Individual PRFs have had the resonance-removal filter of Yu and others (2015) applied to them and are normalized to the maximum amplitude within the time window shown, binned, and normalized by the number of traces per bin. *H*, Average of every individual normalized radial receiver function with the application of the resonance-removal filter (blue) and average of every individual normalized raw radial receiver function (red). *I*, Radial component of raw PRFs (that is, PRFs with no resonance-removal filter applied) plotted against ray parameter, normalized as in *G*.

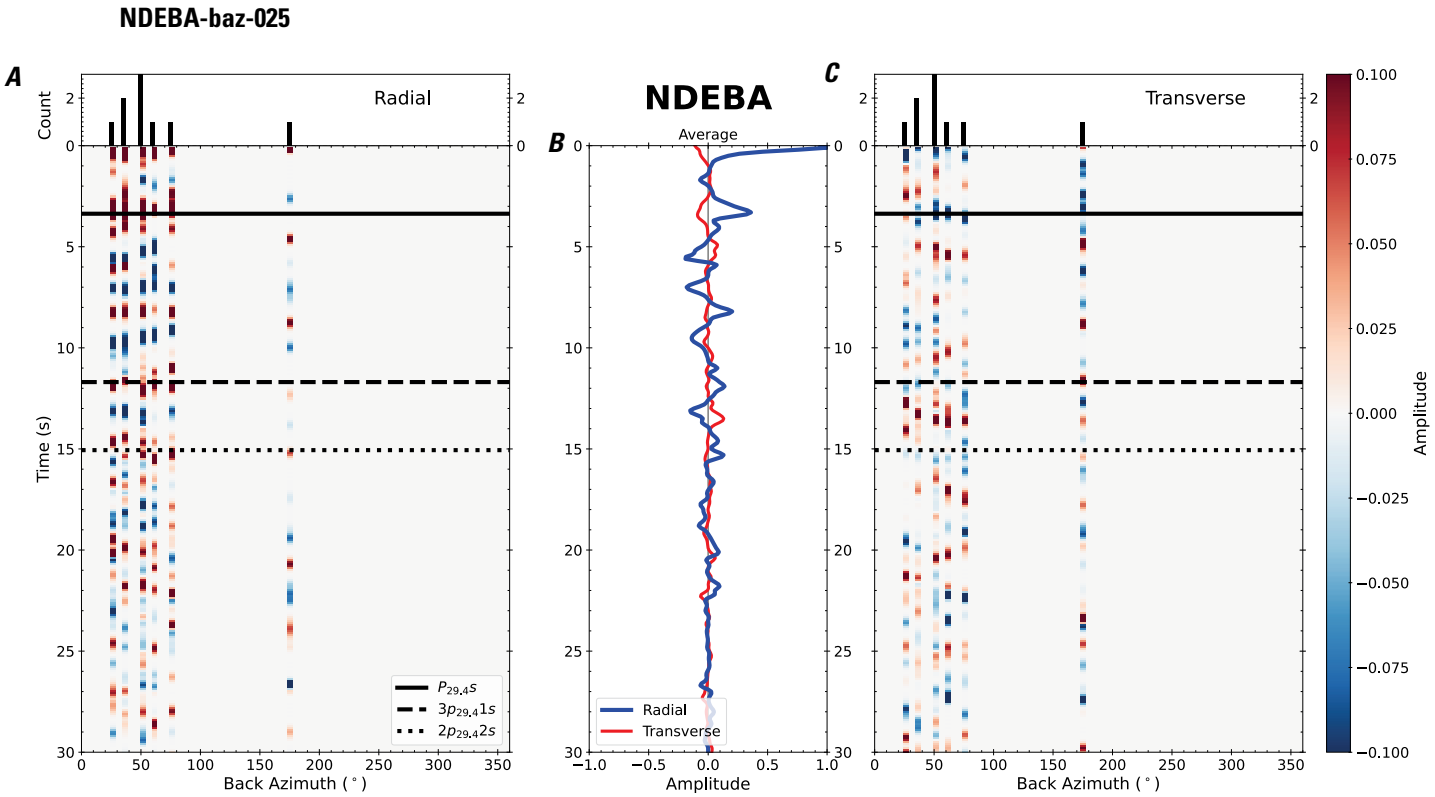

Figure 55. Receiver functions plotted against back azimuth for station NDEBA. *A*, Radial component of P-wave receiver functions (PRFs) plotted against back azimuth. Individual PRFs have had the resonance-removal filter of Yu and others (2015) applied to them, are normalized to the maximum amplitude within the time window shown, binned, and normalized by the number of traces per bin. *B*, Average of every individual normalized radial receiver function with the application of the resonance-removal filter (blue) and average of every individual normalized raw radial receiver function (red). *C*, Radial component of raw PRFs, plotted against back azimuth, normalized as in *A*. Ps, 3p1s, and 2p2s arrival times predicted for the preferred Moho depth are shown, assuming a ray parameter of 0.06 s/km.

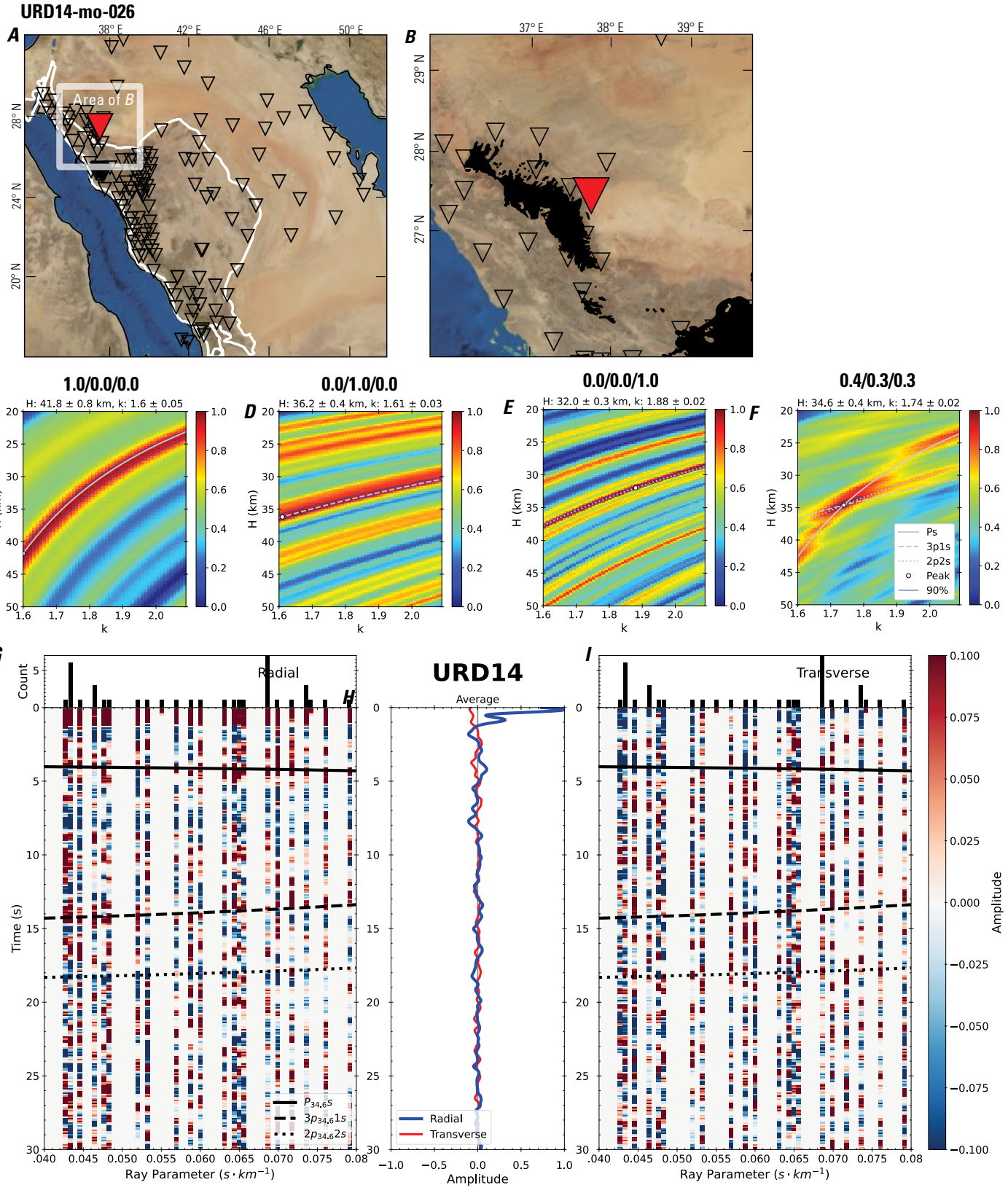
URD14-mo-026
A
B
Area of B
1.0/0.0/0.0
0.0/1.0/0.0
0.0/0.0/1.0
0.4/0.3/0.3
C
D
E
F
H: 41.8 ± 0.8 km, k: 1.6 ± 0.05
H: 36.2 ± 0.4 km, k: 1.61 ± 0.03
H: 32.0 ± 0.3 km, k: 1.88 ± 0.02
H: 34.6 ± 0.4 km, k: 1.74 ± 0.02
H (km)
k
Ps
3p1s
2p2s
Peak
90%
G
H
I
URD14
Radial
Transverse
Average
Count
Time (s)
Ray Parameter (s · km⁻¹)
Amplitude
$P_{34.6}s$
$3p_{34.6}1s$
$2p_{34.6}2s$

Figure 56 (page 62). Receiver-function analysis for station URD14. *A*, Regional map of Saudi Arabia showing the entire array (as inverted triangles), the location of station URD14 (red inverted triangle), the shield-platform boundary (white line), and the bounds of the map in *B* (white box). *B*, Local map of station URD14. Harrats are shown in black. *C*, Standard, single-layer *H-k* stack with stacking weights 0.4/0.3/0.3. This *H-k* stack ignores sedimentary effects on the receiver functions. *D*, Standard, single-layer *H-k* stack with stacking weights 0.5/0.5/0.0. This *H-k* stack also ignores sedimentary effects on the receiver functions. *E*, Optimized sub-sedimentary *H-k* stack with stacking weights 0.4/0.3/0.3, following the method of Yu and others (2015). *F*, Optimized sedimentary *H-k* stack with stacking weights 0.05/0.70/0.25, following the method of Yu and others (2015). *G*, Radial component P-wave receiver functions (PRFs) plotted against ray parameter. Individual PRFs have had the resonance-removal filter of Yu and others (2015) applied to them and are normalized to the maximum amplitude within the time window shown, binned, and normalized by the number of traces per bin. *H*, Average of every individual normalized radial receiver function with the application of the resonance-removal filter (blue) and average of every individual normalized raw radial receiver function (red). *I*, Radial component of raw PRFs (that is, PRFs with no resonance-removal filter applied) plotted against ray parameter, normalized as in *G*.

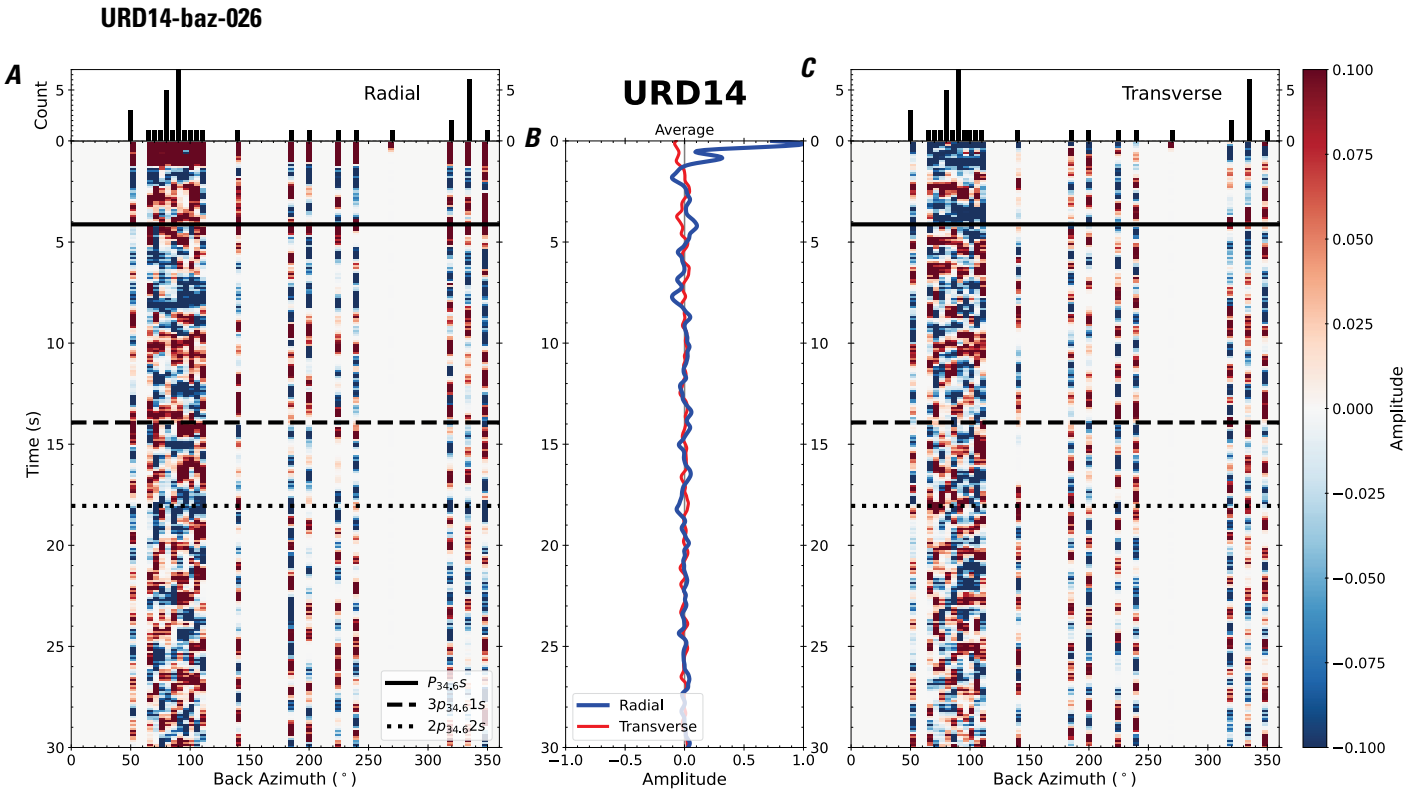

Figure 57. Receiver functions plotted against back azimuth for station URD14. *A*, Radial component of P-wave receiver functions (PRFs) plotted against back azimuth. Individual PRFs have had the resonance-removal filter of Yu and others (2015) applied to them, are normalized to the maximum amplitude within the time window shown, binned, and normalized by the number of traces per bin. *B*, Average of every individual normalized radial receiver function with the application of the resonance-removal filter (blue) and average of every individual normalized raw radial receiver function (red). *C*, Radial component of raw PRFs, plotted against back azimuth, normalized as in *A*. Ps, 3p1s, and 2p2s arrival times predicted for the preferred Moho depth are shown, assuming a ray parameter of 0.06 s/km.

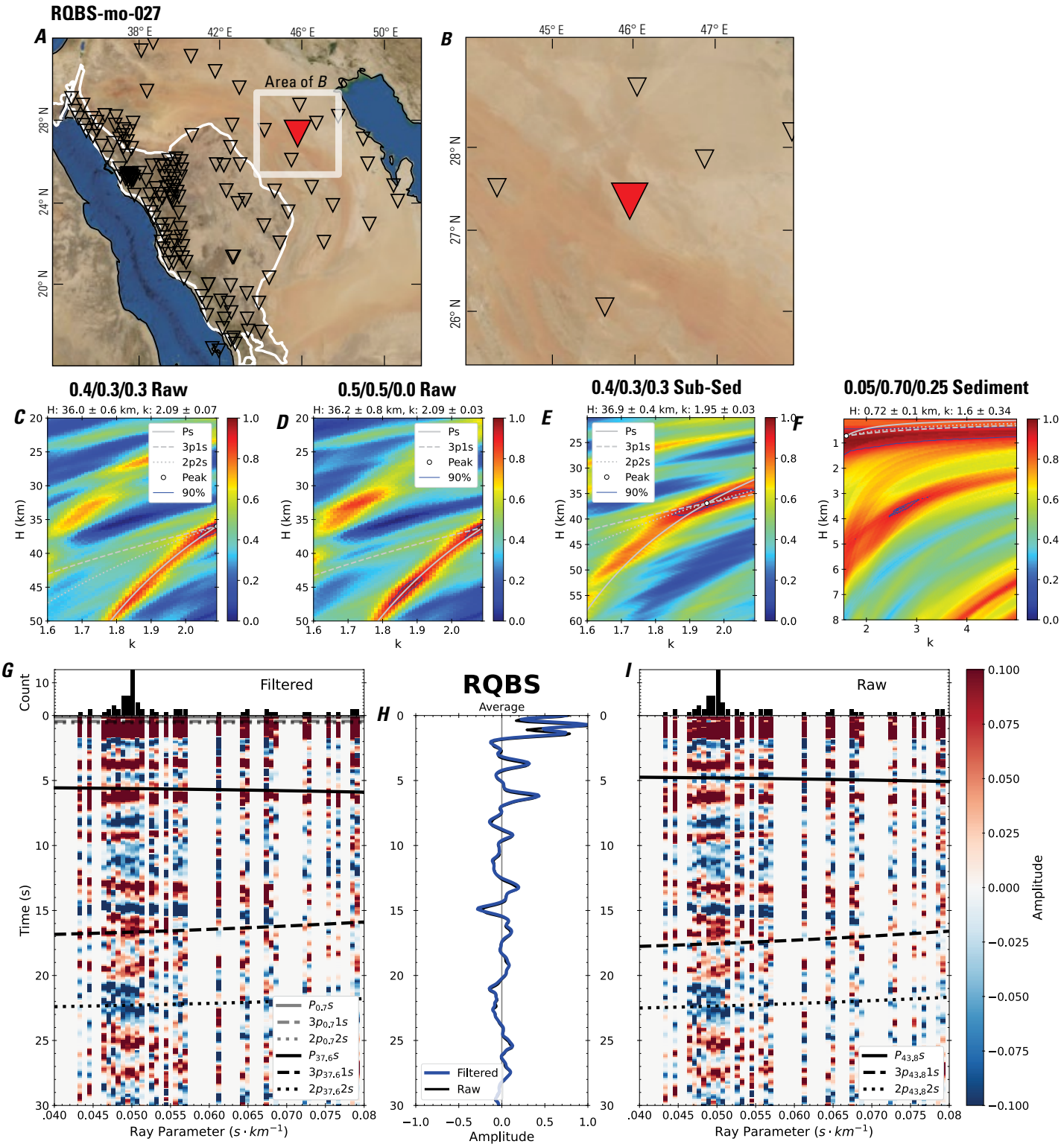
RQBS-mo-027
A
B
Area of B
38° E
42° E
46° E
50° E
28° N
24° N
20° N
45° E
46° E
47° E
27° N
26° N
0.4/0.3/0.3 Raw
0.5/0.5/0.0 Raw
0.4/0.3/0.3 Sub-Sed
0.05/0.70/0.25 Sediment
H: 36.0 ± 0.6 km, k: 2.09 ± 0.07
H: 36.2 ± 0.8 km, k: 2.09 ± 0.03
H: 36.9 ± 0.4 km, k: 1.95 ± 0.03
H: 0.72 ± 0.1 km, k: 1.6 ± 0.34
Ps
3p1s
2p2s
Peak
90%
H (km)
k
G
H
I
Filtered
Raw
Count
Time (s)
RQBS
Average
Amplitude
Ray Parameter (s · km⁻¹)
$P_{0.7}s$
$3p_{0.7}1s$
$2p_{0.7}2s$
$P_{37.6}s$
$3p_{37.6}1s$
$2p_{37.6}2s$
$P_{43.8}s$
$3p_{43.8}1s$
$2p_{43.8}2s$

Figure 58 (page 64). Receiver-function analysis for station RQBS. *A*, Regional map of Saudi Arabia showing the entire array (as inverted triangles), the location of station RQBS (red inverted triangle), the shield-platform boundary (white line), and the bounds of the map in *B* (white box). *B*, Local map of station RQBS. Harrats are shown in black. *C*, Standard, single-layer *H-k* stack with stacking weights 0.4/0.3/0.3. This *H-k* stack ignores sedimentary effects on the receiver functions. *D*, Standard, single-layer *H-k* stack with stacking weights 0.5/0.5/0.0. This *H-k* stack also ignores sedimentary effects on the receiver functions. *E*, Optimized sub-sedimentary *H-k* stack with stacking weights 0.4/0.3/0.3, following the method of Yu and others (2015). *F*, Optimized sedimentary *H-k* stack with stacking weights 0.05/0.70/0.25, following the method of Yu and others (2015). *G*, Radial component P-wave receiver functions (PRFs) plotted against ray parameter. Individual PRFs have had the resonance-removal filter of Yu and others (2015) applied to them and are normalized to the maximum amplitude within the time window shown, binned, and normalized by the number of traces per bin. *H*, Average of every individual normalized radial receiver function with the application of the resonance-removal filter (blue) and average of every individual normalized raw radial receiver function (red). *I*, Radial component of raw PRFs (that is, PRFs with no resonance-removal filter applied) plotted against ray parameter, normalized as in *G*.

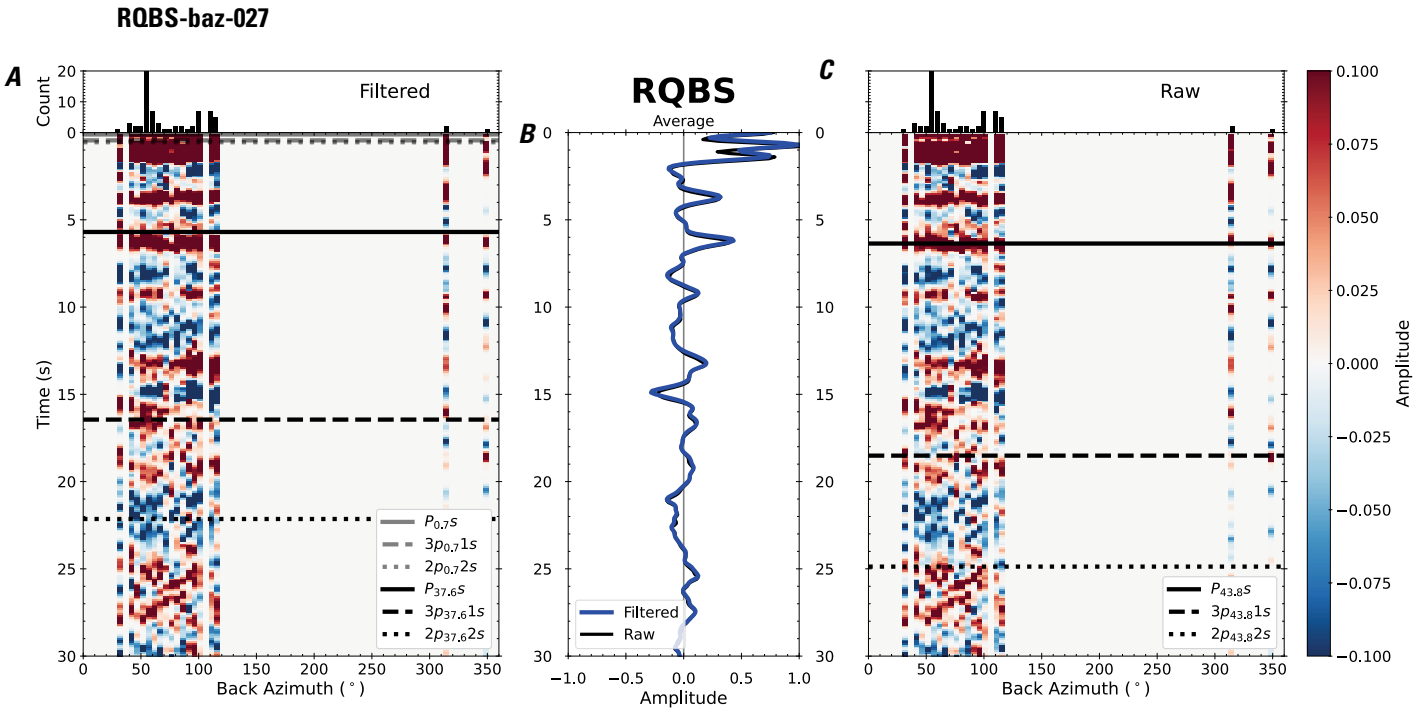

Figure 59. Receiver functions plotted against back azimuth for station RQBS. *A*, Radial component of P-wave receiver functions (PRFs) plotted against back azimuth. Individual PRFs have had the resonance-removal filter of Yu and others (2015) applied to them, are normalized to the maximum amplitude within the time window shown, binned, and normalized by the number of traces per bin. *B*, Average of every individual normalized radial receiver function with the application of the resonance-removal filter (blue) and average of every individual normalized raw radial receiver function (red). *C*, Radial component of raw PRFs, plotted against back azimuth, normalized as in *A*. Ps, 3p1s, and 2p2s arrival times predicted for the preferred Moho depth are shown, assuming a ray parameter of 0.06 s/km.

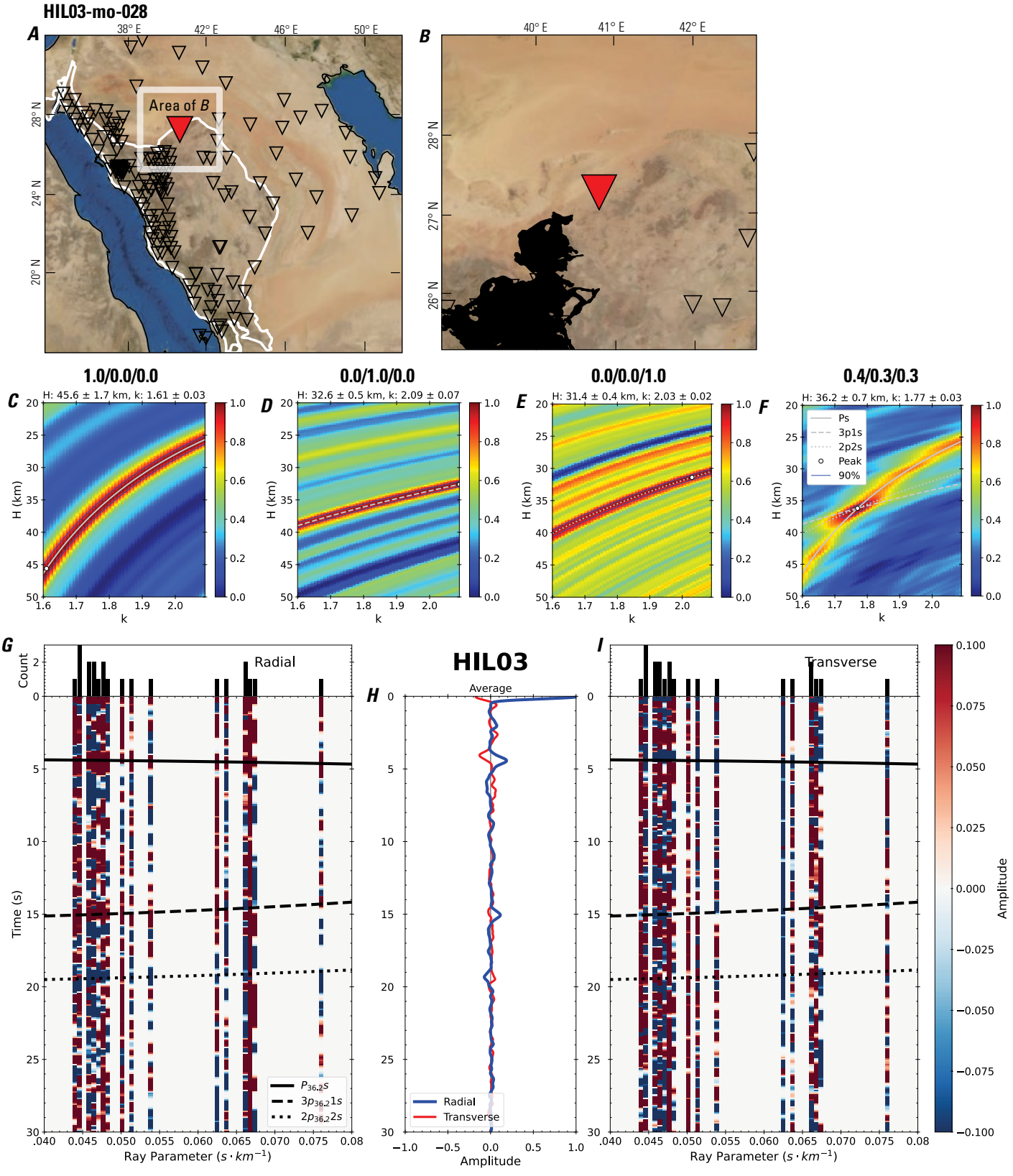
HIL03-mo-028
A
B
Area of B
1.0/0.0/0.0
0.0/1.0/0.0
0.0/0.0/1.0
0.4/0.3/0.3
C
D
E
F
H: 45.6 ± 1.7 km, k: 1.61 ± 0.03
H: 32.6 ± 0.5 km, k: 2.09 ± 0.07
H: 31.4 ± 0.4 km, k: 2.03 ± 0.02
H: 36.2 ± 0.7 km, k: 1.77 ± 0.03
H (km)
k
Ps
3p1s
2p2s
Peak
90%
G
H
I
HIL03
Radial
Transverse
Average
Count
Time (s)
Ray Parameter (s · km⁻¹)
Amplitude
P36.2s
3p36.2 1s
2p36.2 2s

Figure 60 (page 66). Receiver-function analysis for station HIL03. *A*, Regional map of Saudi Arabia showing the entire array (as inverted triangles), the location of station HIL03 (red inverted triangle), the shield-platform boundary (white line), and the bounds of the map in *B* (white box). *B*, Local map of station HIL03. Harrats are shown in black. *C*, Standard, single-layer *H-k* stack with stacking weights 0.4/0.3/0.3. This *H-k* stack ignores sedimentary effects on the receiver functions. *D*, Standard, single-layer *H-k* stack with stacking weights 0.5/0.5/0.0. This *H-k* stack also ignores sedimentary effects on the receiver functions. *E*, Optimized sub-sedimentary *H-k* stack with stacking weights 0.4/0.3/0.3, following the method of Yu and others (2015). *F*, Optimized sedimentary *H-k* stack with stacking weights 0.05/0.70/0.25, following the method of Yu and others (2015). *G*, Radial component P-wave receiver functions (PRFs) plotted against ray parameter. Individual PRFs have had the resonance-removal filter of Yu and others (2015) applied to them and are normalized to the maximum amplitude within the time window shown, binned, and normalized by the number of traces per bin. *H*, Average of every individual normalized radial receiver function with the application of the resonance-removal filter (blue) and average of every individual normalized raw radial receiver function (red). *I*, Radial component of raw PRFs (that is, PRFs with no resonance-removal filter applied) plotted against ray parameter, normalized as in *G*.

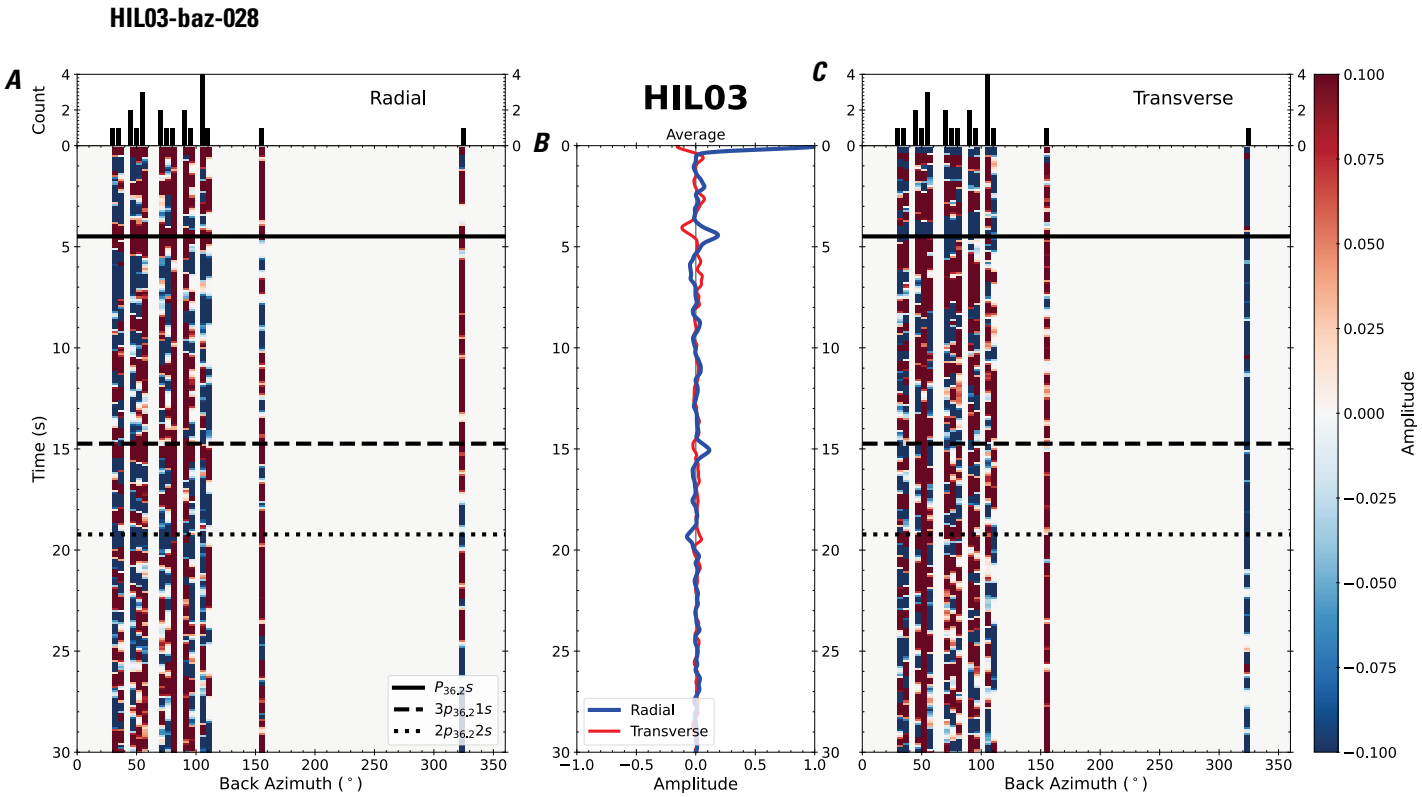

Figure 61. Receiver functions plotted against back azimuth for station HIL03. *A*, Radial component of P-wave receiver functions (PRFs) plotted against back azimuth. Individual PRFs have had the resonance-removal filter of Yu and others (2015) applied to them, are normalized to the maximum amplitude within the time window shown, binned, and normalized by the number of traces per bin. *B*, Average of every individual normalized radial receiver function with the application of the resonance-removal filter (blue) and average of every individual normalized raw radial receiver function (red). *C*, Radial component of raw PRFs, plotted against back azimuth, normalized as in *A*. Ps, 3p1s, and 2p2s arrival times predicted for the preferred Moho depth are shown, assuming a ray parameter of 0.06 s/km.

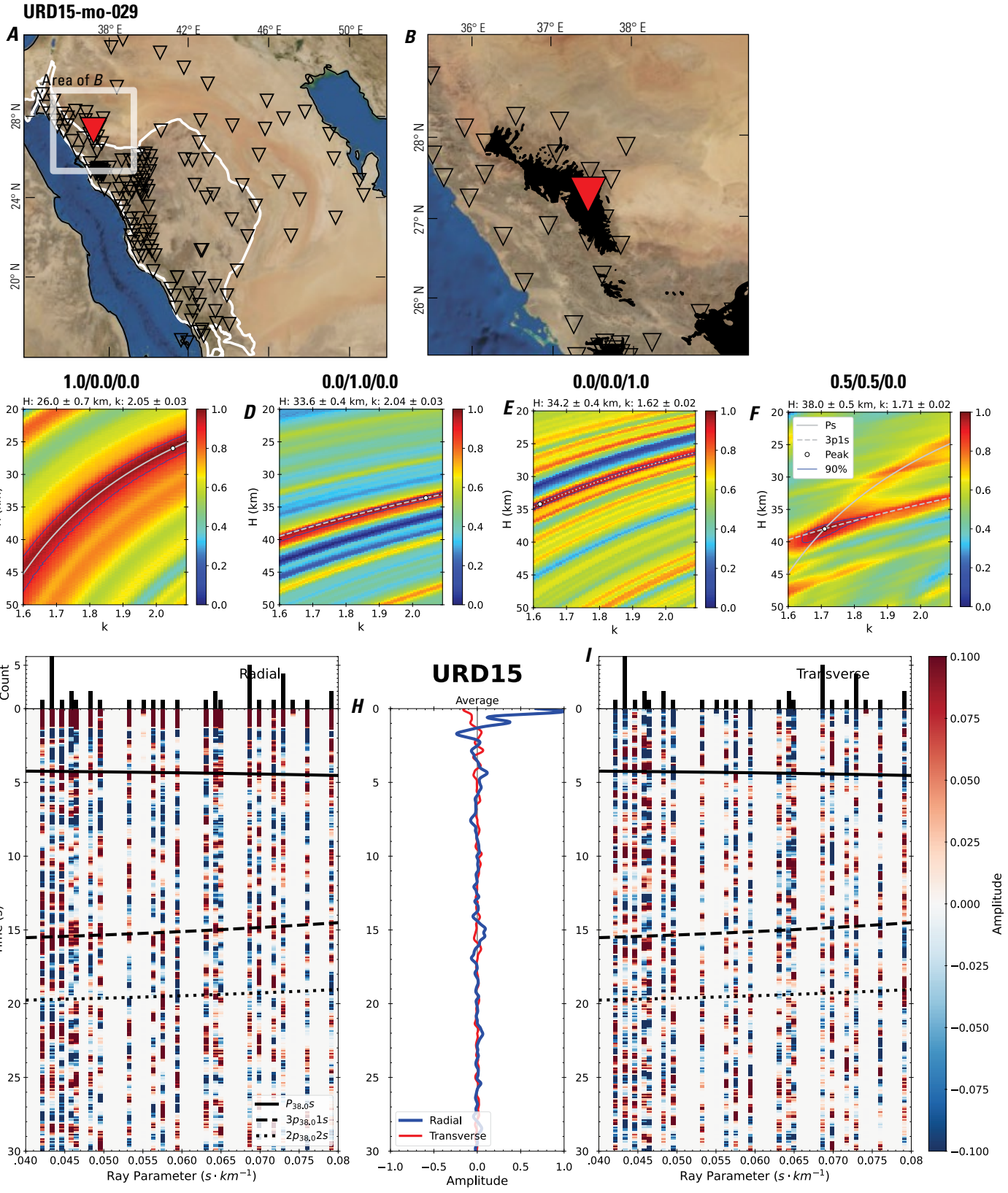
URD15-mo-029
A
B
Area of B
1.0/0.0/0.0
0.0/1.0/0.0
0.0/0.0/1.0
0.5/0.5/0.0
C
D
E
F
H: 26.0 ± 0.7 km, k: 2.05 ± 0.03
H: 33.6 ± 0.4 km, k: 2.04 ± 0.03
H: 34.2 ± 0.4 km, k: 1.62 ± 0.02
H: 38.0 ± 0.5 km, k: 1.71 ± 0.02
H (km)
k
Ps
3p1s
Peak
90%
G
H
I
URD15
Radial
Transverse
Average
Count
Time (s)
Ray Parameter (s · km⁻¹)
Amplitude
P38.0s
3p38.01s
2p38.02s

Figure 62 (page 68). Receiver-function analysis for station URD15. *A*, Regional map of Saudi Arabia showing the entire array (as inverted triangles), the location of station URD15 (red inverted triangle), the shield-platform boundary (white line), and the bounds of the map in *B* (white box). *B*, Local map of station URD15. Harrats are shown in black. *C*, Standard, single-layer *H-k* stack with stacking weights 0.4/0.3/0.3. This *H-k* stack ignores sedimentary effects on the receiver functions. *D*, Standard, single-layer *H-k* stack with stacking weights 0.5/0.5/0.0. This *H-k* stack also ignores sedimentary effects on the receiver functions. *E*, Optimized sub-sedimentary *H-k* stack with stacking weights 0.4/0.3/0.3, following the method of Yu and others (2015). *F*, Optimized sedimentary *H-k* stack with stacking weights 0.05/0.70/0.25, following the method of Yu and others (2015). *G*, Radial component P-wave receiver functions (PRFs) plotted against ray parameter. Individual PRFs have had the resonance-removal filter of Yu and others (2015) applied to them and are normalized to the maximum amplitude within the time window shown, binned, and normalized by the number of traces per bin. *H*, Average of every individual normalized radial receiver function with the application of the resonance-removal filter (blue) and average of every individual normalized raw radial receiver function (red). *I*, Radial component of raw PRFs (that is, PRFs with no resonance-removal filter applied) plotted against ray parameter, normalized as in *G*.

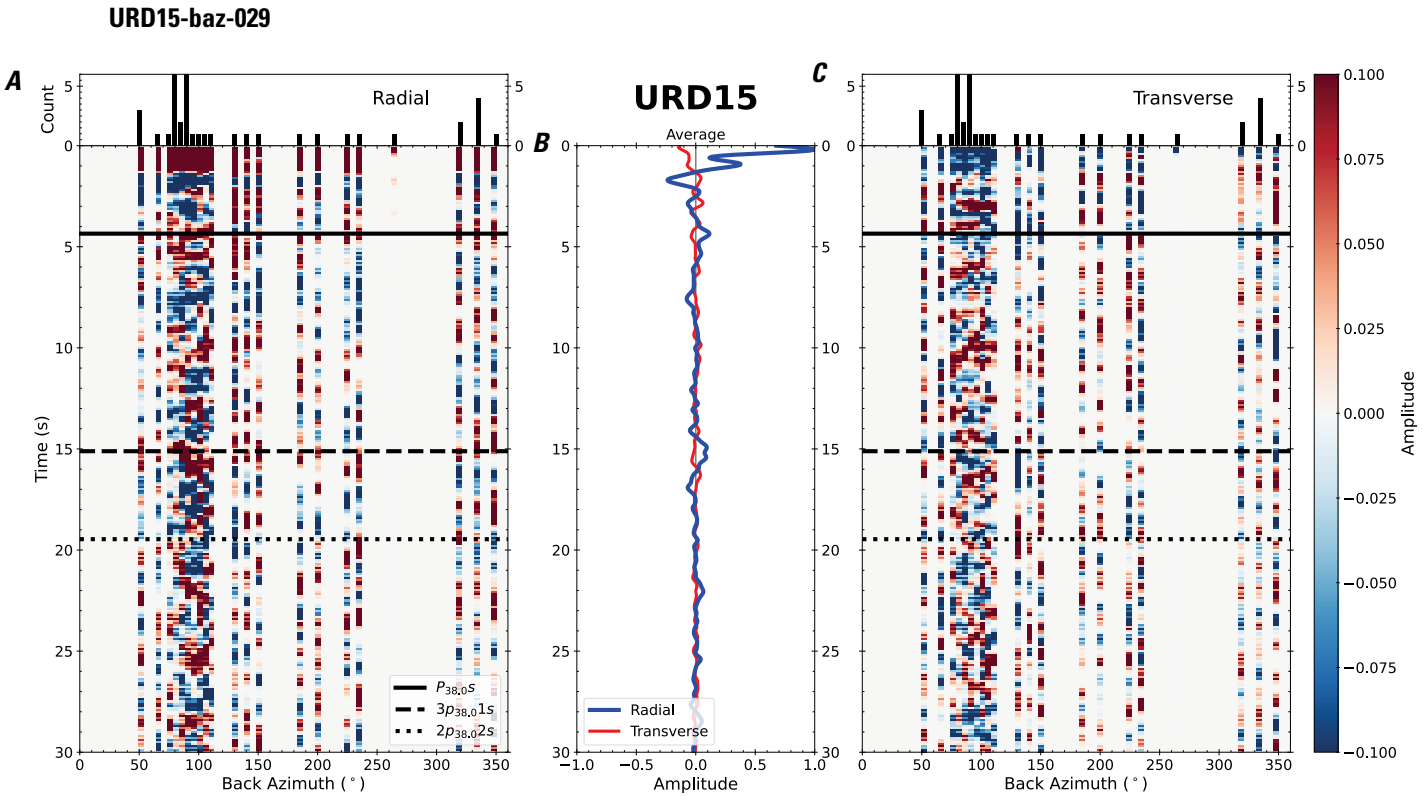

Figure 63. Receiver functions plotted against back azimuth for station URD15. *A*, Radial component of P-wave receiver functions (PRFs) plotted against back azimuth. Individual PRFs have had the resonance-removal filter of Yu and others (2015) applied to them, are normalized to the maximum amplitude within the time window shown, binned, and normalized by the number of traces per bin. *B*, Average of every individual normalized radial receiver function with the application of the resonance-removal filter (blue) and average of every individual normalized raw radial receiver function (red). *C*, Radial component of raw PRFs, plotted against back azimuth, normalized as in *A*. Ps, 3p1s, and 2p2s arrival times predicted for the preferred Moho depth are shown, assuming a ray parameter of 0.06 s/km.

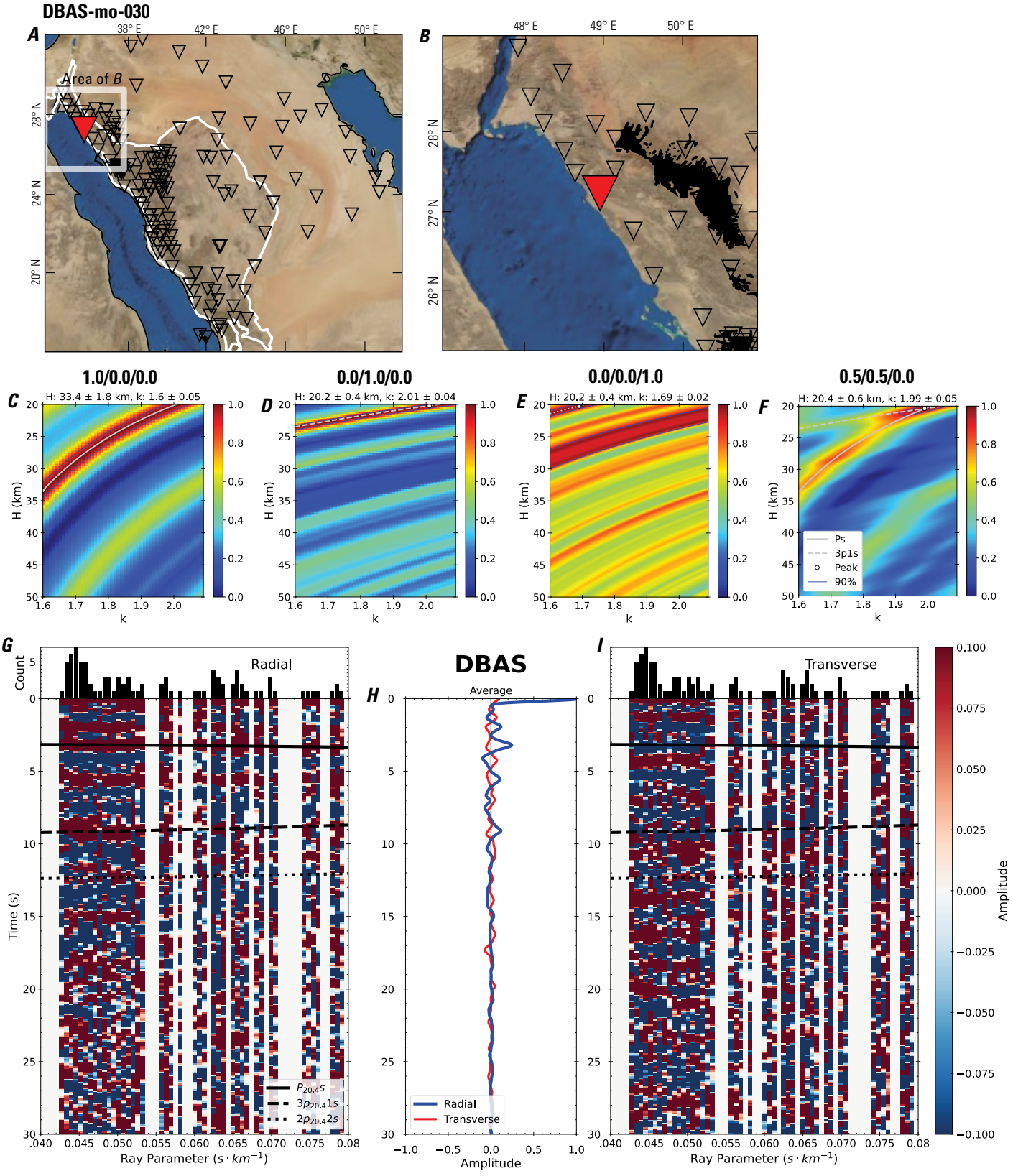
DBAS-mo-030
A
B
Area of B
38° E
42° E
46° E
50° E
48° E
49° E
50° E
28° N
24° N
20° N
27° N
26° N
1.0/0.0/0.0
0.0/1.0/0.0
0.0/0.0/1.0
0.5/0.5/0.0
C
D
E
F
H: 33.4 ± 1.8 km, k: 1.6 ± 0.05
H: 20.2 ± 0.4 km, k: 2.01 ± 0.04
H: 20.2 ± 0.4 km, k: 1.69 ± 0.02
H: 20.4 ± 0.6 km, k: 1.99 ± 0.05
H (km)
k
Ps
3p1s
Peak
90%
G
H
I
DBAS
Radial
Transverse
Average
Count
Time (s)
Ray Parameter (s · km⁻¹)
Amplitude
$P_{20.4}s$
$3p_{20.4}1s$
$2p_{20.4}2s$
Radial
Transverse

Figure 64 (page 70). Receiver-function analysis for station DBAS. *A*, Regional map of Saudi Arabia showing the entire array (as inverted triangles), the location of station DBAS (red inverted triangle), the shield-platform boundary (white line), and the bounds of the map in *B* (white box). *B*, Local map of station DBAS. Harrats are shown in black. *C*, Standard, single-layer *H-k* stack with stacking weights 0.4/0.3/0.3. This *H-k* stack ignores sedimentary effects on the receiver functions. *D*, Standard, single-layer *H-k* stack with stacking weights 0.5/0.5/0.0. This *H-k* stack also ignores sedimentary effects on the receiver functions. *E*, Optimized sub-sedimentary *H-k* stack with stacking weights 0.4/0.3/0.3, following the method of Yu and others (2015). *F*, Optimized sedimentary *H-k* stack with stacking weights 0.05/0.70/0.25, following the method of Yu and others (2015). *G*, Radial component P-wave receiver functions (PRFs) plotted against ray parameter. Individual PRFs have had the resonance-removal filter of Yu and others (2015) applied to them and are normalized to the maximum amplitude within the time window shown, binned, and normalized by the number of traces per bin. *H*, Average of every individual normalized radial receiver function with the application of the resonance-removal filter (blue) and average of every individual normalized raw radial receiver function (red). *I*, Radial component of raw PRFs (that is, PRFs with no resonance-removal filter applied) plotted against ray parameter, normalized as in *G*.

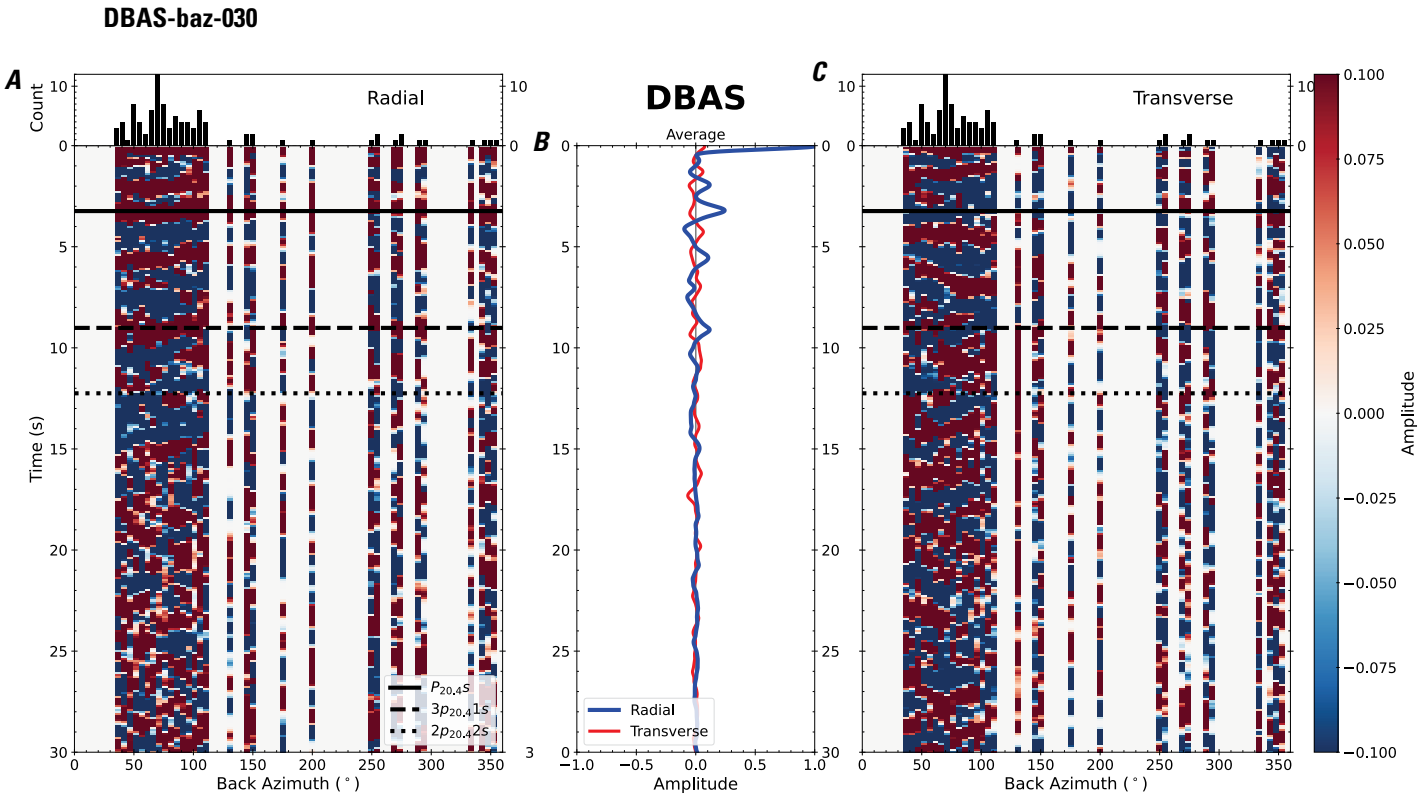

Figure 65. Receiver functions plotted against back azimuth for station DBAS. *A*, Radial component of P-wave receiver functions (PRFs) plotted against back azimuth. Individual PRFs have had the resonance-removal filter of Yu and others (2015) applied to them, are normalized to the maximum amplitude within the time window shown, binned, and normalized by the number of traces per bin. *B*, Average of every individual normalized radial receiver function with the application of the resonance-removal filter (blue) and average of every individual normalized raw radial receiver function (red). *C*, Radial component of raw PRFs, plotted against back azimuth, normalized as in *A*. Ps, 3p1s, and 2p2s arrival times predicted for the preferred Moho depth are shown, assuming a ray parameter of 0.06 s/km.

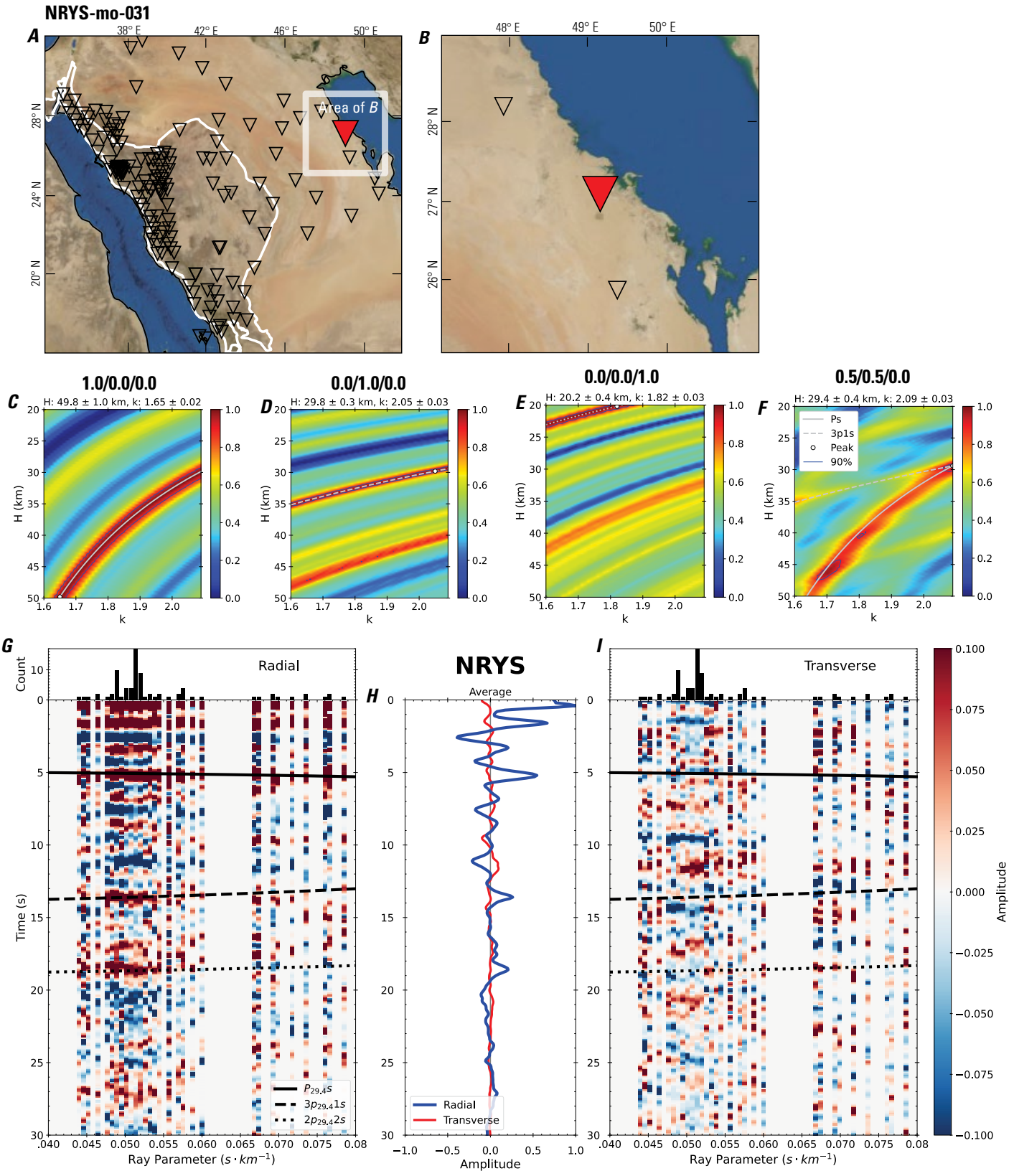
NRYS-mo-031
A
38° E
42° E
46° E
50° E
28° N
24° N
20° N
Area of B
B
48° E
49° E
50° E
28° N
27° N
26° N
1.0/0.0/0.0
C
H: 49.8 ± 1.0 km, k: 1.65 ± 0.02
0.0/1.0/0.0
D
H: 29.8 ± 0.3 km, k: 2.05 ± 0.03
0.0/0.0/1.0
E
H: 20.2 ± 0.4 km, k: 1.82 ± 0.03
0.5/0.5/0.0
F
H: 29.4 ± 0.4 km, k: 2.09 ± 0.03
Ps
3p1s
Peak
90%
H (km)
k
G
Radial
Count
Time (s)
$P_{29.4}s$
$3p_{29.4}1s$
$2p_{29.4}2s$
Ray Parameter ($s \cdot km^{-1}$)
NRYS
Average
H
Radial
Transverse
Amplitude
I
Transverse
Ray Parameter ($s \cdot km^{-1}$)
Amplitude

Figure 66 (page 72). Receiver-function analysis for station NRYS. *A*, Regional map of Saudi Arabia showing the entire array (as inverted triangles), the location of station NRYS (red inverted triangle), the shield-platform boundary (white line), and the bounds of the map in *B* (white box). *B*, Local map of station NRYS. Harrats are shown in black. *C*, Standard, single-layer *H-k* stack with stacking weights 0.4/0.3/0.3. This *H-k* stack ignores sedimentary effects on the receiver functions. *D*, Standard, single-layer *H-k* stack with stacking weights 0.5/0.5/0.0. This *H-k* stack also ignores sedimentary effects on the receiver functions. *E*, Optimized sub-sedimentary *H-k* stack with stacking weights 0.4/0.3/0.3, following the method of Yu and others (2015). *F*, Optimized sedimentary *H-k* stack with stacking weights 0.05/0.70/0.25, following the method of Yu and others (2015). *G*, Radial component P-wave receiver functions (PRFs) plotted against ray parameter. Individual PRFs have had the resonance-removal filter of Yu and others (2015) applied to them and are normalized to the maximum amplitude within the time window shown, binned, and normalized by the number of traces per bin. *H*, Average of every individual normalized radial receiver function with the application of the resonance-removal filter (blue) and average of every individual normalized raw radial receiver function (red). *I*, Radial component of raw PRFs (that is, PRFs with no resonance-removal filter applied) plotted against ray parameter, normalized as in *G*.

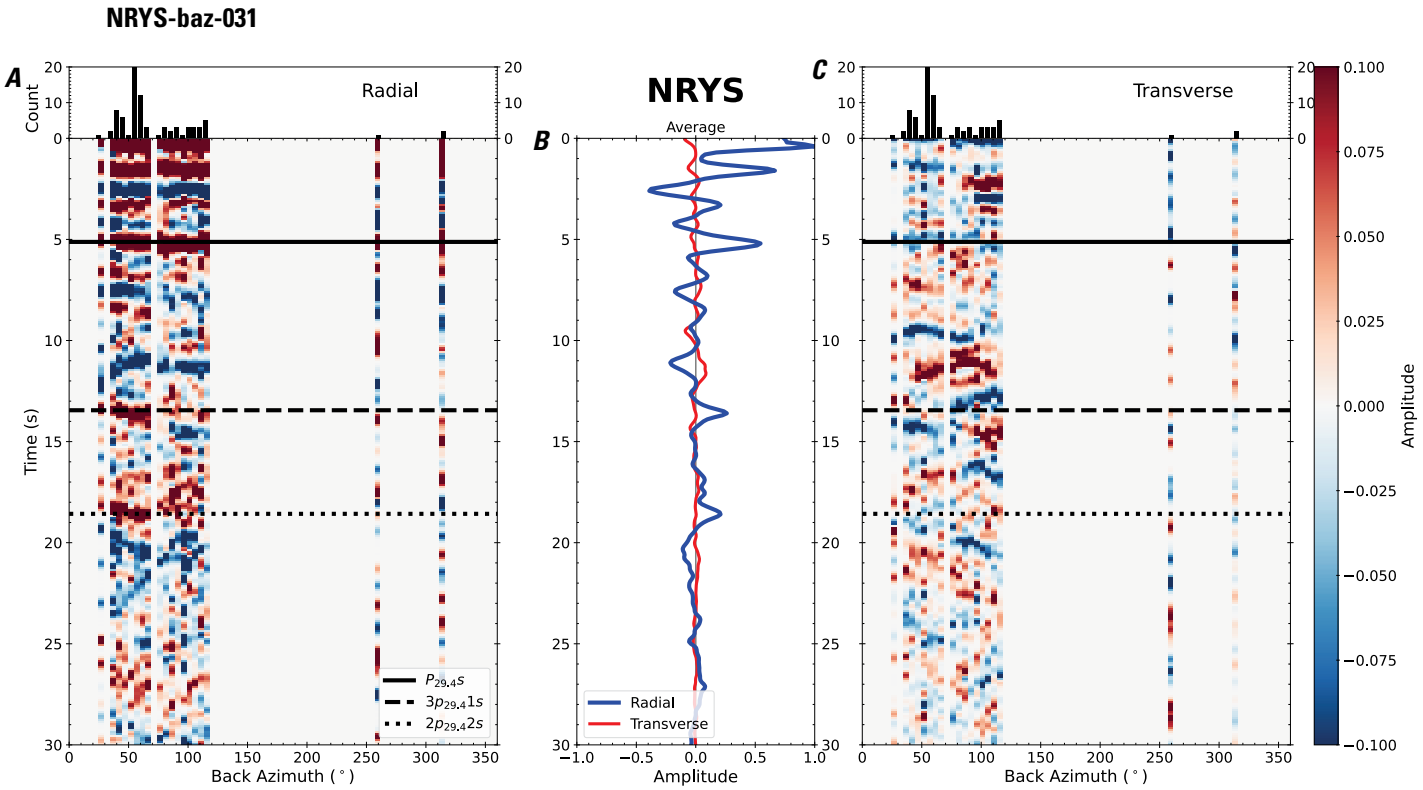

Figure 67. Receiver functions plotted against back azimuth for station NRYS. *A*, Radial component of P-wave receiver functions (PRFs) plotted against back azimuth. Individual PRFs have had the resonance-removal filter of Yu and others (2015) applied to them, are normalized to the maximum amplitude within the time window shown, binned, and normalized by the number of traces per bin. *B*, Average of every individual normalized radial receiver function with the application of the resonance-removal filter (blue) and average of every individual normalized raw radial receiver function (red). *C*, Radial component of raw PRFs, plotted against back azimuth, normalized as in *A*. Ps, 3p1s, and 2p2s arrival times predicted for the preferred Moho depth are shown, assuming a ray parameter of 0.06 s/km.

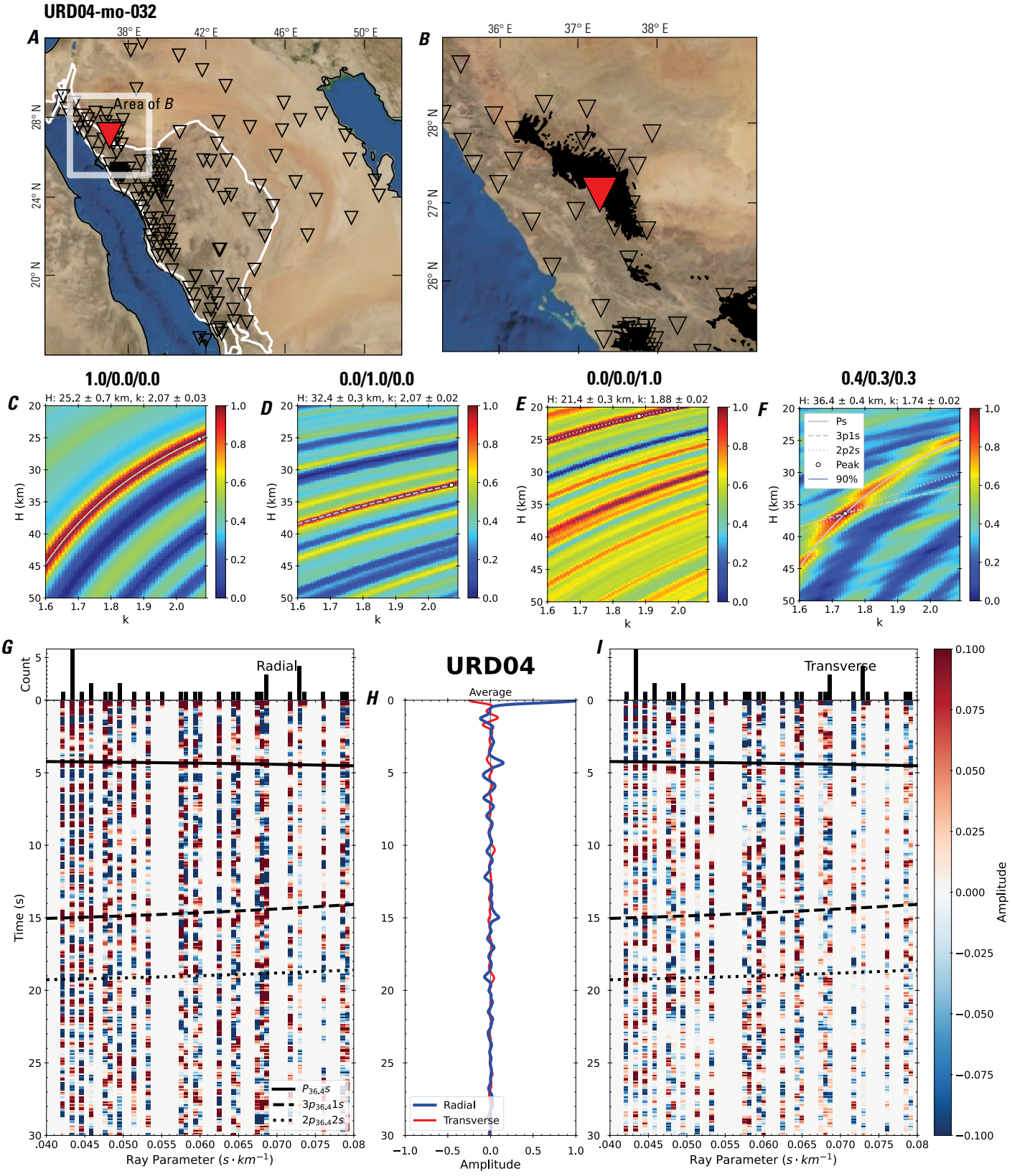
URD04-mo-032
A
38° E
42° E
46° E
50° E
28° N
24° N
20° N
Area of B
B
36° E
37° E
38° E
28° N
27° N
26° N
1.0/0.0/0.0
0.0/1.0/0.0
0.0/0.0/1.0
0.4/0.3/0.3
C
H: 25.2 ± 0.7 km, k: 2.07 ± 0.03
D
H: 32.4 ± 0.3 km, k: 2.07 ± 0.02
E
H: 21.4 ± 0.3 km, k: 1.88 ± 0.02
F
H: 36.4 ± 0.4 km, k: 1.74 ± 0.02
Ps
3p1s
2p2s
Peak
90%
H (km)
k
G
Radial
Count
Time (s)
$P_{36.4}s$
$3p_{36.4}1s$
$2p_{36.4}2s$
Ray Parameter ($s \cdot km^{-1}$)
URD04
H
Average
Radial
Transverse
Amplitude
I
Transverse
Amplitude

Figure 68 (page 74). Receiver-function analysis for station URD04. *A*, Regional map of Saudi Arabia showing the entire array (as inverted triangles), the location of station URD04 (red inverted triangle), the shield-platform boundary (white line), and the bounds of the map in *B* (white box). *B*, Local map of station URD04. Harrats are shown in black. *C*, Standard, single-layer *H-k* stack with stacking weights 0.4/0.3/0.3. This *H-k* stack ignores sedimentary effects on the receiver functions. *D*, Standard, single-layer *H-k* stack with stacking weights 0.5/0.5/0.0. This *H-k* stack also ignores sedimentary effects on the receiver functions. *E*, Optimized sub-sedimentary *H-k* stack with stacking weights 0.4/0.3/0.3, following the method of Yu and others (2015). *F*, Optimized sedimentary *H-k* stack with stacking weights 0.05/0.70/0.25, following the method of Yu and others (2015). *G*, Radial component P-wave receiver functions (PRFs) plotted against ray parameter. Individual PRFs have had the resonance-removal filter of Yu and others (2015) applied to them and are normalized to the maximum amplitude within the time window shown, binned, and normalized by the number of traces per bin. *H*, Average of every individual normalized radial receiver function with the application of the resonance-removal filter (blue) and average of every individual normalized raw radial receiver function (red). *I*, Radial component of raw PRFs (that is, PRFs with no resonance-removal filter applied) plotted against ray parameter, normalized as in *G*.

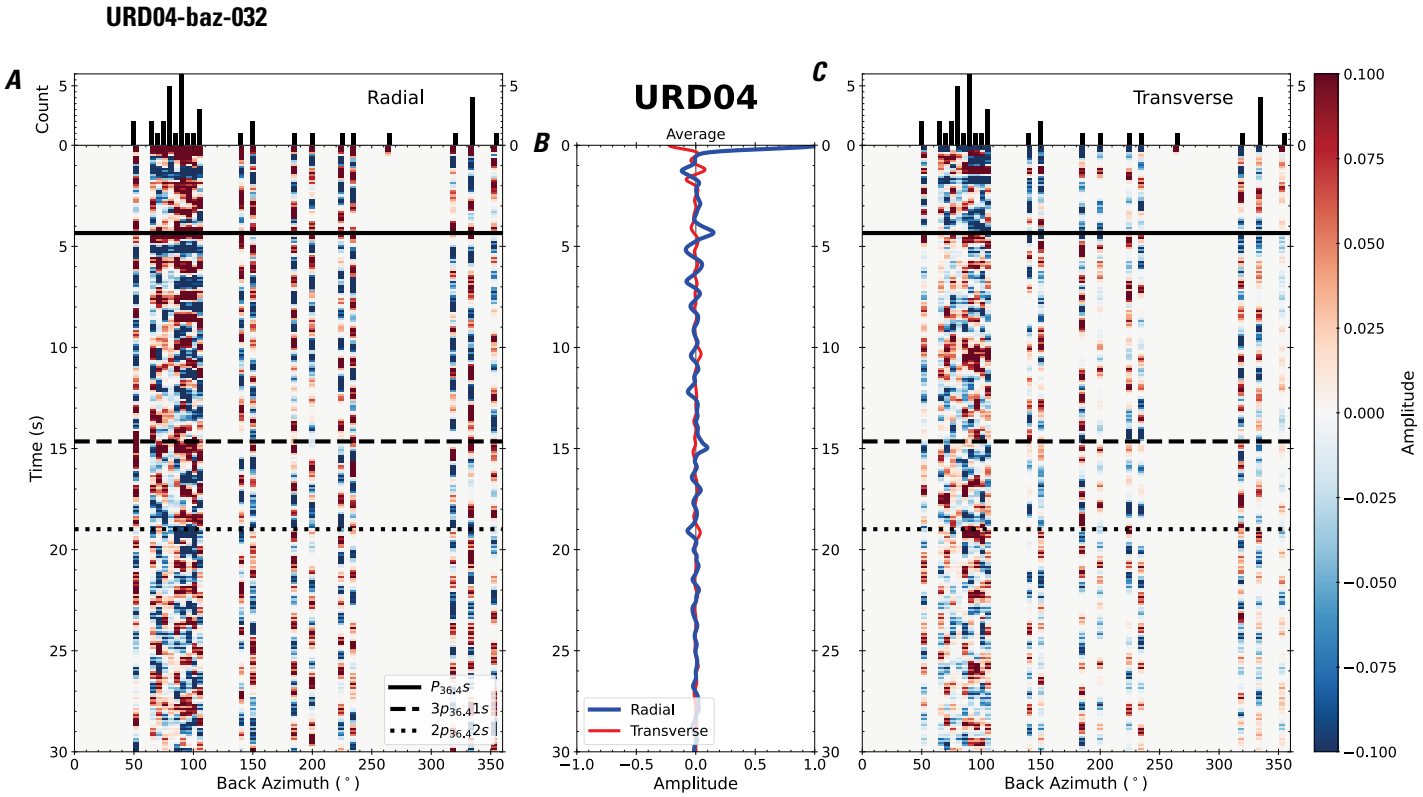

Figure 69. Receiver functions plotted against back azimuth for station URD04. *A*, Radial component of P-wave receiver functions (PRFs) plotted against back azimuth. Individual PRFs have had the resonance-removal filter of Yu and others (2015) applied to them, are normalized to the maximum amplitude within the time window shown, binned, and normalized by the number of traces per bin. *B*, Average of every individual normalized radial receiver function with the application of the resonance-removal filter (blue) and average of every individual normalized raw radial receiver function (red). *C*, Radial component of raw PRFs, plotted against back azimuth, normalized as in *A*. Ps, 3p1s, and 2p2s arrival times predicted for the preferred Moho depth are shown, assuming a ray parameter of 0.06 s/km.

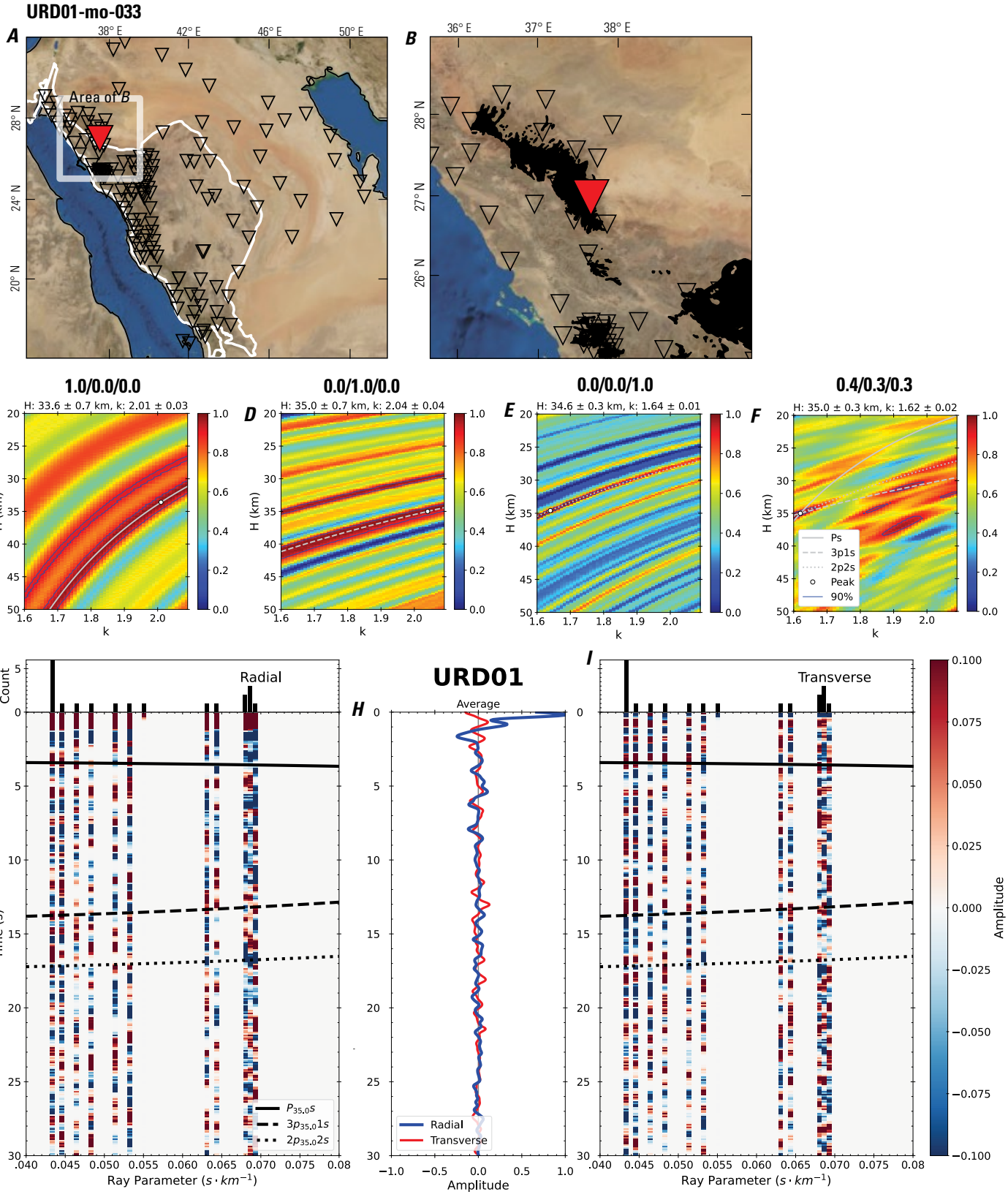
URD01-mo-033
A
B
Area of B
1.0/0.0/0.0
0.0/1.0/0.0
0.0/0.0/1.0
0.4/0.3/0.3
C
D
E
F
H: 33.6 ± 0.7 km, k: 2.01 ± 0.03
H: 35.0 ± 0.7 km, k: 2.04 ± 0.04
H: 34.6 ± 0.3 km, k: 1.64 ± 0.01
H: 35.0 ± 0.3 km, k: 1.62 ± 0.02
H (km)
k
Ps
3p1s
2p2s
Peak
90%
G
H
I
URD01
Radial
Transverse
Average
Count
Time (s)
Ray Parameter (s · km⁻¹)
Amplitude
$P_{35.0}s$
$3p_{35.0}1s$
$2p_{35.0}2s$

Figure 70 (page 76). Receiver-function analysis for station URD01. *A*, Regional map of Saudi Arabia showing the entire array (as inverted triangles), the location of station URD01 (red inverted triangle), the shield-platform boundary (white line), and the bounds of the map in *B* (white box). *B*, Local map of station URD01. Harrats are shown in black. *C*, Standard, single-layer *H-k* stack with stacking weights 0.4/0.3/0.3. This *H-k* stack ignores sedimentary effects on the receiver functions. *D*, Standard, single-layer *H-k* stack with stacking weights 0.5/0.5/0.0. This *H-k* stack also ignores sedimentary effects on the receiver functions. *E*, Optimized sub-sedimentary *H-k* stack with stacking weights 0.4/0.3/0.3, following the method of Yu and others (2015). *F*, Optimized sedimentary *H-k* stack with stacking weights 0.05/0.70/0.25, following the method of Yu and others (2015). *G*, Radial component P-wave receiver functions (PRFs) plotted against ray parameter. Individual PRFs have had the resonance-removal filter of Yu and others (2015) applied to them and are normalized to the maximum amplitude within the time window shown, binned, and normalized by the number of traces per bin. *H*, Average of every individual normalized radial receiver function with the application of the resonance-removal filter (blue) and average of every individual normalized raw radial receiver function (red). *I*, Radial component of raw PRFs (that is, PRFs with no resonance-removal filter applied) plotted against ray parameter, normalized as in *G*.

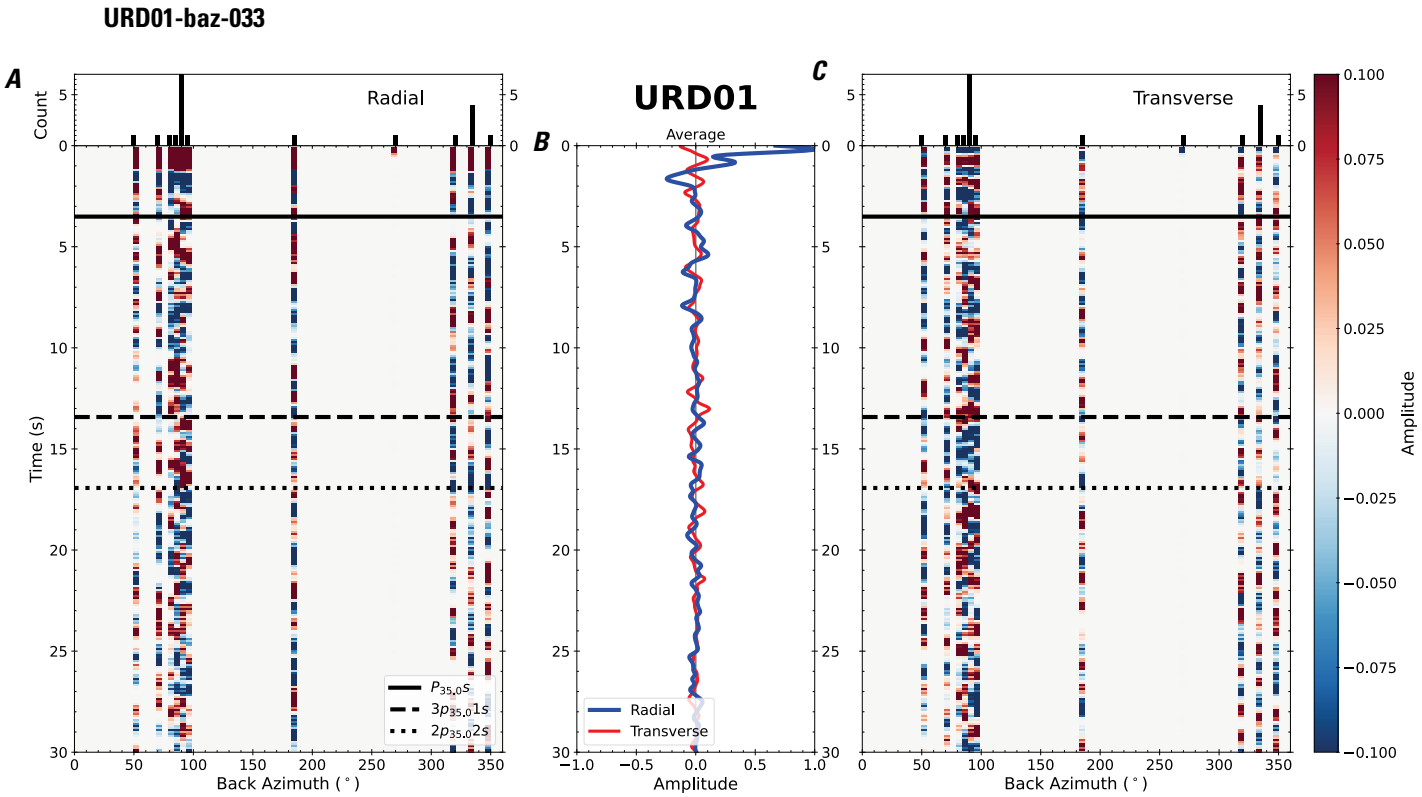

Figure 71. Receiver functions plotted against back azimuth for station URD01. *A*, Radial component of P-wave receiver functions (PRFs) plotted against back azimuth. Individual PRFs have had the resonance-removal filter of Yu and others (2015) applied to them, are normalized to the maximum amplitude within the time window shown, binned, and normalized by the number of traces per bin. *B*, Average of every individual normalized radial receiver function with the application of the resonance-removal filter (blue) and average of every individual normalized raw radial receiver function (red). *C*, Radial component of raw PRFs, plotted against back azimuth, normalized as in *A*. Ps, 3p1s, and 2p2s arrival times predicted for the preferred Moho depth are shown, assuming a ray parameter of 0.06 s/km.

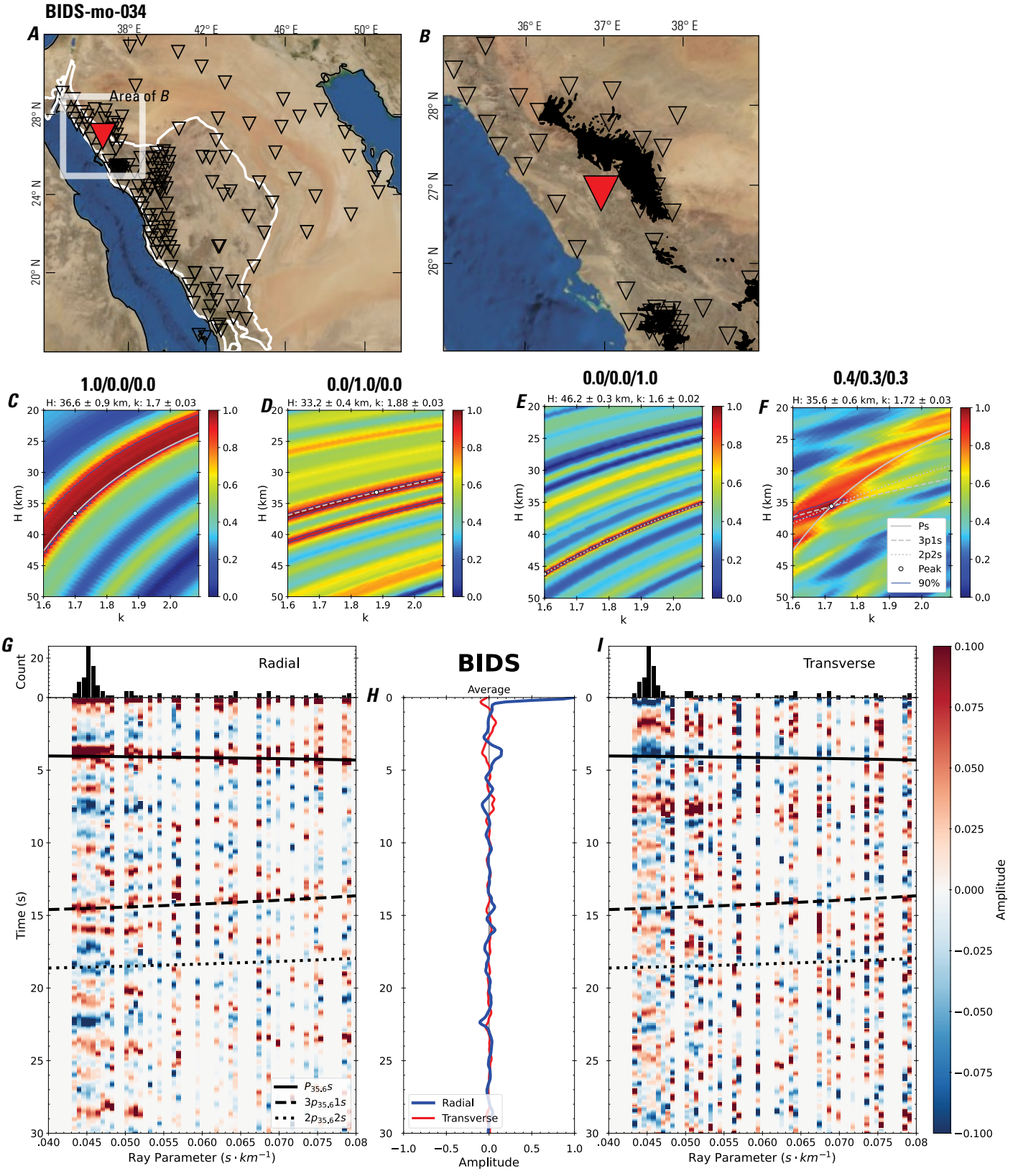
BIDS-mo-034
A
B
Area of B
1.0/0.0/0.0
0.0/1.0/0.0
0.0/0.0/1.0
0.4/0.3/0.3
C
D
E
F
H: 36.6 ± 0.9 km, k: 1.7 ± 0.03
H: 33.2 ± 0.4 km, k: 1.88 ± 0.03
H: 46.2 ± 0.3 km, k: 1.6 ± 0.02
H: 35.6 ± 0.6 km, k: 1.72 ± 0.03
H (km)
k
Ps
3p1s
2p2s
Peak
90%
G
H
I
BIDS
Radial
Transverse
Average
Count
Time (s)
Ray Parameter (s · km⁻¹)
Amplitude
$P_{35.6}s$
$3p_{35.6}1s$
$2p_{35.6}2s$

Figure 72 (page 78). Receiver-function analysis for station BIDS. *A*, Regional map of Saudi Arabia showing the entire array (as inverted triangles), the location of station BIDS (red inverted triangle), the shield-platform boundary (white line), and the bounds of the map in *B* (white box). *B*, Local map of station BIDS. Harrats are shown in black. *C*, Standard, single-layer *H-k* stack with stacking weights 0.4/0.3/0.3. This *H-k* stack ignores sedimentary effects on the receiver functions. *D*, Standard, single-layer *H-k* stack with stacking weights 0.5/0.5/0.0. This *H-k* stack also ignores sedimentary effects on the receiver functions. *E*, Optimized sub-sedimentary *H-k* stack with stacking weights 0.4/0.3/0.3, following the method of Yu and others (2015). *F*, Optimized sedimentary *H-k* stack with stacking weights 0.05/0.70/0.25, following the method of Yu and others (2015). *G*, Radial component P-wave receiver functions (PRFs) plotted against ray parameter. Individual PRFs have had the resonance-removal filter of Yu and others (2015) applied to them and are normalized to the maximum amplitude within the time window shown, binned, and normalized by the number of traces per bin. *H*, Average of every individual normalized radial receiver function with the application of the resonance-removal filter (blue) and average of every individual normalized raw radial receiver function (red). *I*, Radial component of raw PRFs (that is, PRFs with no resonance-removal filter applied) plotted against ray parameter, normalized as in *G*.

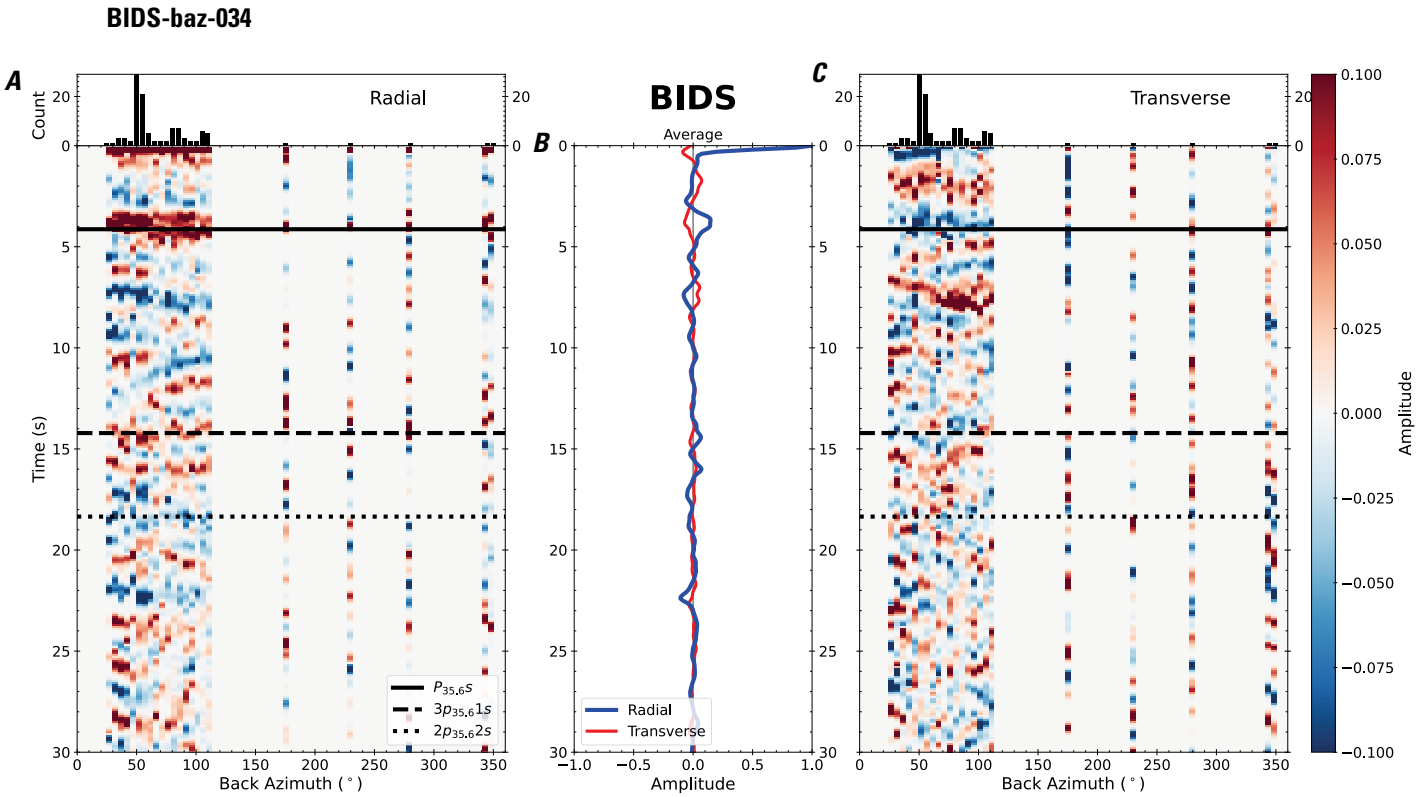

Figure 73. Receiver functions plotted against back azimuth for station BIDS. *A*, Radial component of P-wave receiver functions (PRFs) plotted against back azimuth. Individual PRFs have had the resonance-removal filter of Yu and others (2015) applied to them, are normalized to the maximum amplitude within the time window shown, binned, and normalized by the number of traces per bin. *B*, Average of every individual normalized radial receiver function with the application of the resonance-removal filter (blue) and average of every individual normalized raw radial receiver function (red). *C*, Radial component of raw PRFs, plotted against back azimuth, normalized as in *A*. Ps, 3p1s, and 2p2s arrival times predicted for the preferred Moho depth are shown, assuming a ray parameter of 0.06 s/km.

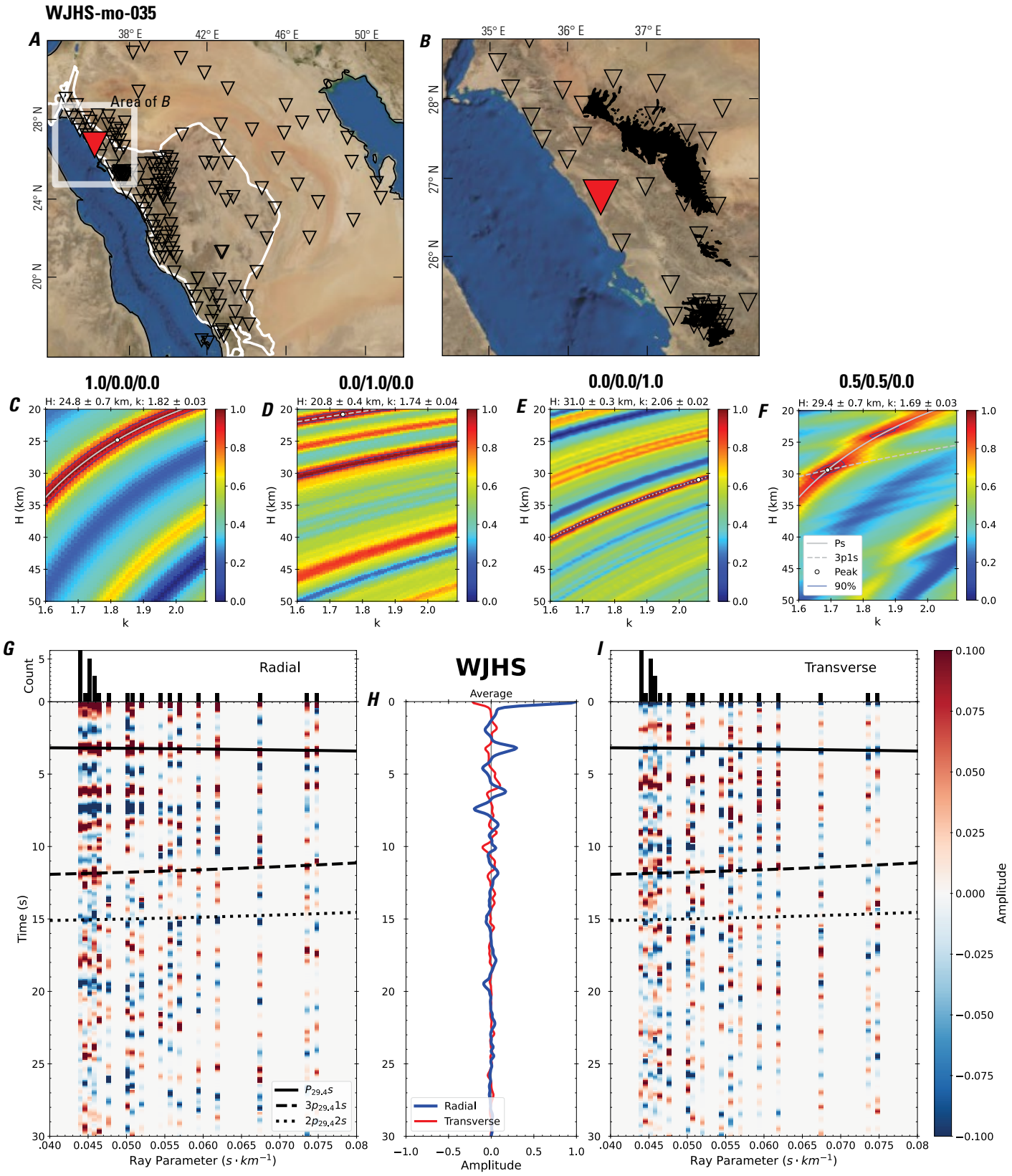
WJHS-mo-035
A
B
Area of B
38° E
42° E
46° E
50° E
35° E
36° E
37° E
28° N
24° N
20° N
27° N
26° N
1.0/0.0/0.0
0.0/1.0/0.0
0.0/0.0/1.0
0.5/0.5/0.0
C
D
E
F
H: 24.8 ± 0.7 km, k: 1.82 ± 0.03
H: 20.8 ± 0.4 km, k: 1.74 ± 0.04
H: 31.0 ± 0.3 km, k: 2.06 ± 0.02
H: 29.4 ± 0.7 km, k: 1.69 ± 0.03
H (km)
k
Ps
3p1s
Peak
90%
G
H
I
WJHS
Radial
Transverse
Average
Count
Time (s)
Ray Parameter (s · km⁻¹)
Amplitude
$P_{29.4}s$
$3p_{29.4}1s$
$2p_{29.4}2s$

Figure 74 (page 80). Receiver-function analysis for station WJHS. *A*, Regional map of Saudi Arabia showing the entire array (as inverted triangles), the location of station WJHS (red inverted triangle), the shield-platform boundary (white line), and the bounds of the map in *B* (white box). *B*, Local map of station WJHS. Harrats are shown in black. *C*, Standard, single-layer *H-k* stack with stacking weights 0.4/0.3/0.3. This *H-k* stack ignores sedimentary effects on the receiver functions. *D*, Standard, single-layer *H-k* stack with stacking weights 0.5/0.5/0.0. This *H-k* stack also ignores sedimentary effects on the receiver functions. *E*, Optimized sub-sedimentary *H-k* stack with stacking weights 0.4/0.3/0.3, following the method of Yu and others (2015). *F*, Optimized sedimentary *H-k* stack with stacking weights 0.05/0.70/0.25, following the method of Yu and others (2015). *G*, Radial component P-wave receiver functions (PRFs) plotted against ray parameter. Individual PRFs have had the resonance-removal filter of Yu and others (2015) applied to them and are normalized to the maximum amplitude within the time window shown, binned, and normalized by the number of traces per bin. *H*, Average of every individual normalized radial receiver function with the application of the resonance-removal filter (blue) and average of every individual normalized raw radial receiver function (red). *I*, Radial component of raw PRFs (that is, PRFs with no resonance-removal filter applied) plotted against ray parameter, normalized as in *G*.

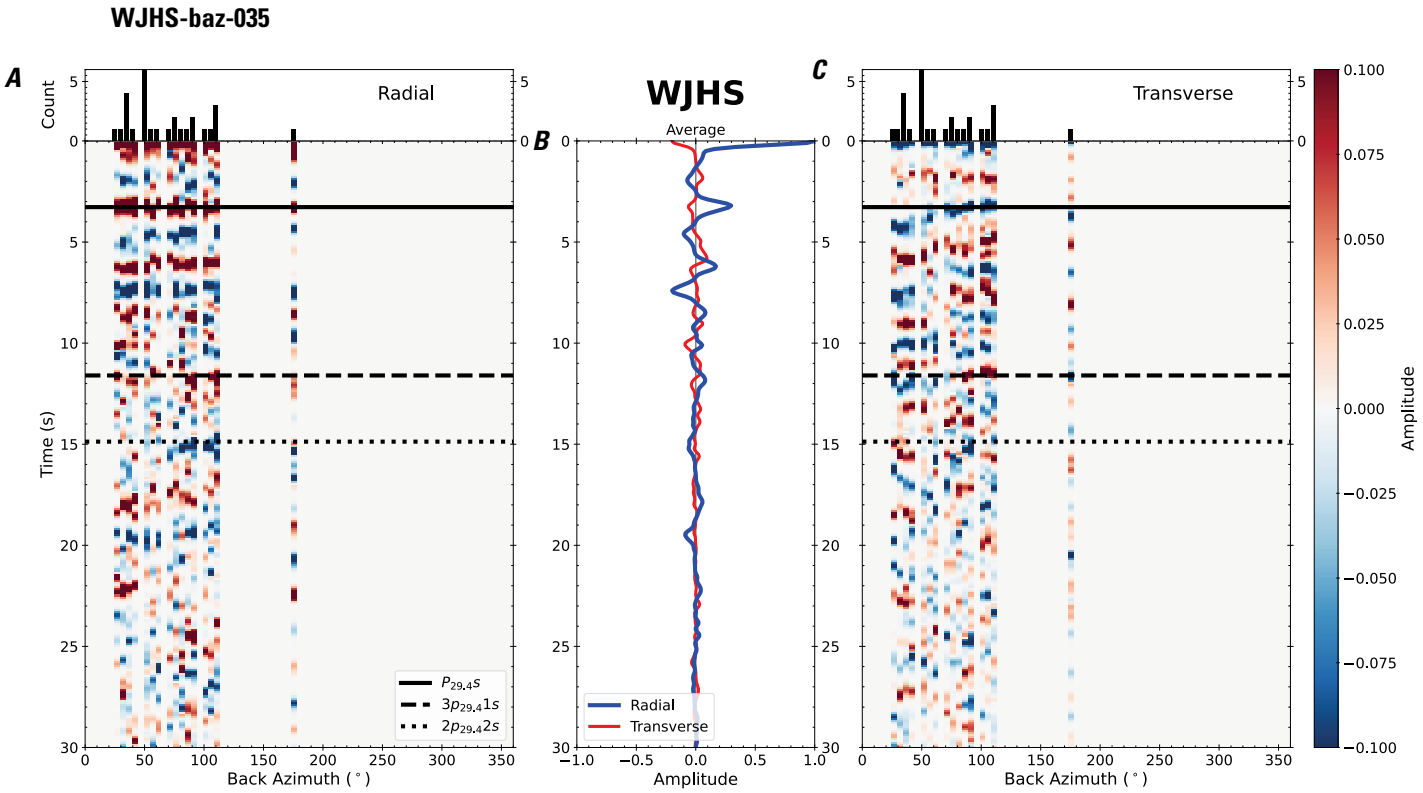

Figure 75. Receiver functions plotted against back azimuth for station WJHS. *A*, Radial component of P-wave receiver functions (PRFs) plotted against back azimuth. Individual PRFs have had the resonance-removal filter of Yu and others (2015) applied to them, are normalized to the maximum amplitude within the time window shown, binned, and normalized by the number of traces per bin. *B*, Average of every individual normalized radial receiver function with the application of the resonance-removal filter (blue) and average of every individual normalized raw radial receiver function (red). *C*, Radial component of raw PRFs, plotted against back azimuth, normalized as in *A*. Ps, 3p1s, and 2p2s arrival times predicted for the preferred Moho depth are shown, assuming a ray parameter of 0.06 s/km.

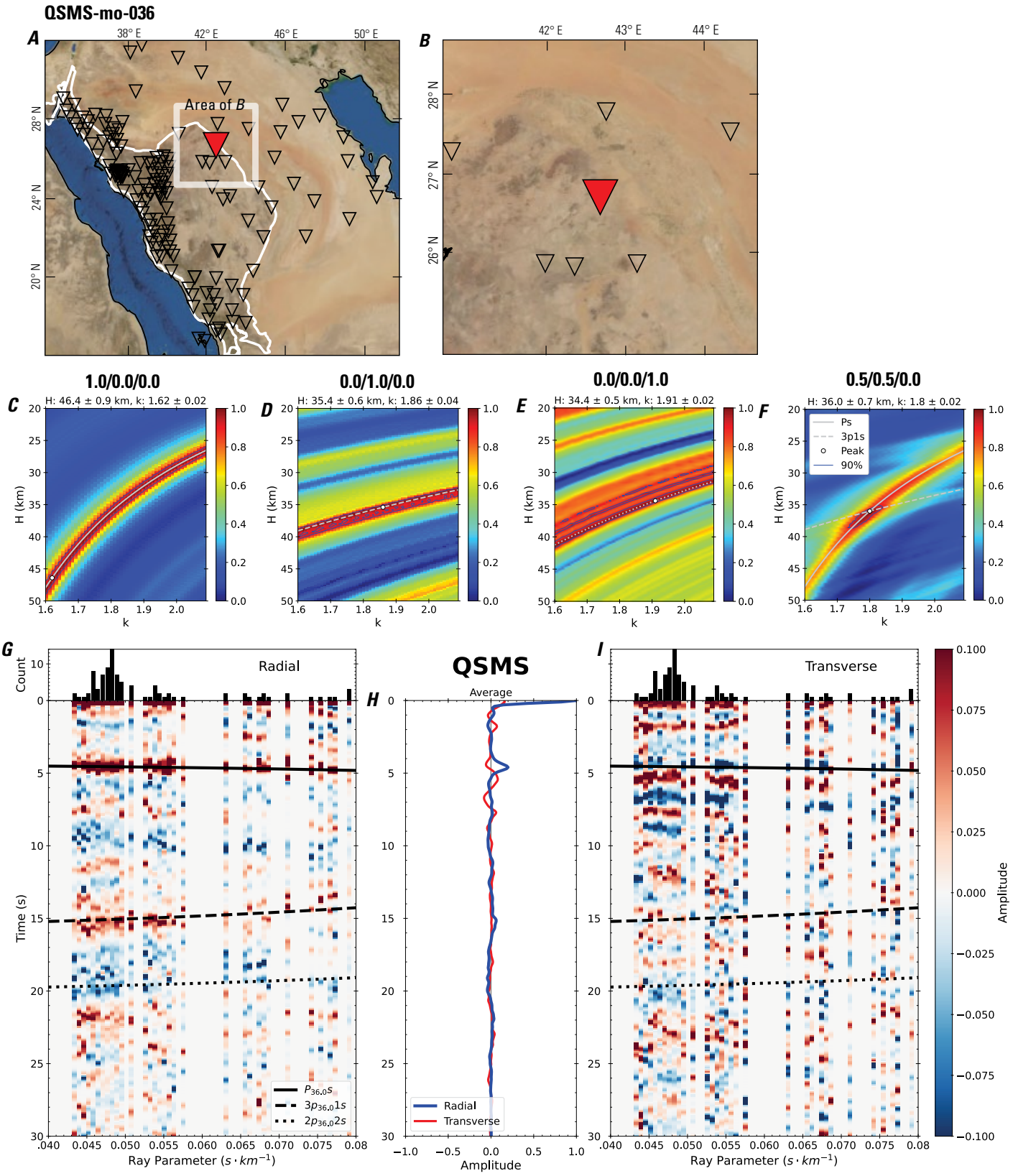
QSMS-mo-036
A
B
Area of B
1.0/0.0/0.0
0.0/1.0/0.0
0.0/0.0/1.0
0.5/0.5/0.0
C
D
E
F
H: 46.4 ± 0.9 km, k: 1.62 ± 0.02
H: 35.4 ± 0.6 km, k: 1.86 ± 0.04
H: 34.4 ± 0.5 km, k: 1.91 ± 0.02
H: 36.0 ± 0.7 km, k: 1.8 ± 0.02
H (km)
k
Ps
3p1s
Peak
90%
G
H
I
QSMS
Radial
Transverse
Average
Count
Time (s)
Ray Parameter (s · km⁻¹)
Amplitude
$P_{36.0}s$
$3p_{36.0}1s$
$2p_{36.0}2s$

Figure 76 (page 82). Receiver-function analysis for station QSMS. *A*, Regional map of Saudi Arabia showing the entire array (as inverted triangles), the location of station QSMS (red inverted triangle), the shield-platform boundary (white line), and the bounds of the map in *B* (white box). *B*, Local map of station QSMS. Harrats are shown in black. *C*, Standard, single-layer *H-k* stack with stacking weights 0.4/0.3/0.3. This *H-k* stack ignores sedimentary effects on the receiver functions. *D*, Standard, single-layer *H-k* stack with stacking weights 0.5/0.5/0.0. This *H-k* stack also ignores sedimentary effects on the receiver functions. *E*, Optimized sub-sedimentary *H-k* stack with stacking weights 0.4/0.3/0.3, following the method of Yu and others (2015). *F*, Optimized sedimentary *H-k* stack with stacking weights 0.05/0.70/0.25, following the method of Yu and others (2015). *G*, Radial component P-wave receiver functions (PRFs) plotted against ray parameter. Individual PRFs have had the resonance-removal filter of Yu and others (2015) applied to them and are normalized to the maximum amplitude within the time window shown, binned, and normalized by the number of traces per bin. *H*, Average of every individual normalized radial receiver function with the application of the resonance-removal filter (blue) and average of every individual normalized raw radial receiver function (red). *I*, Radial component of raw PRFs (that is, PRFs with no resonance-removal filter applied) plotted against ray parameter, normalized as in *G*.

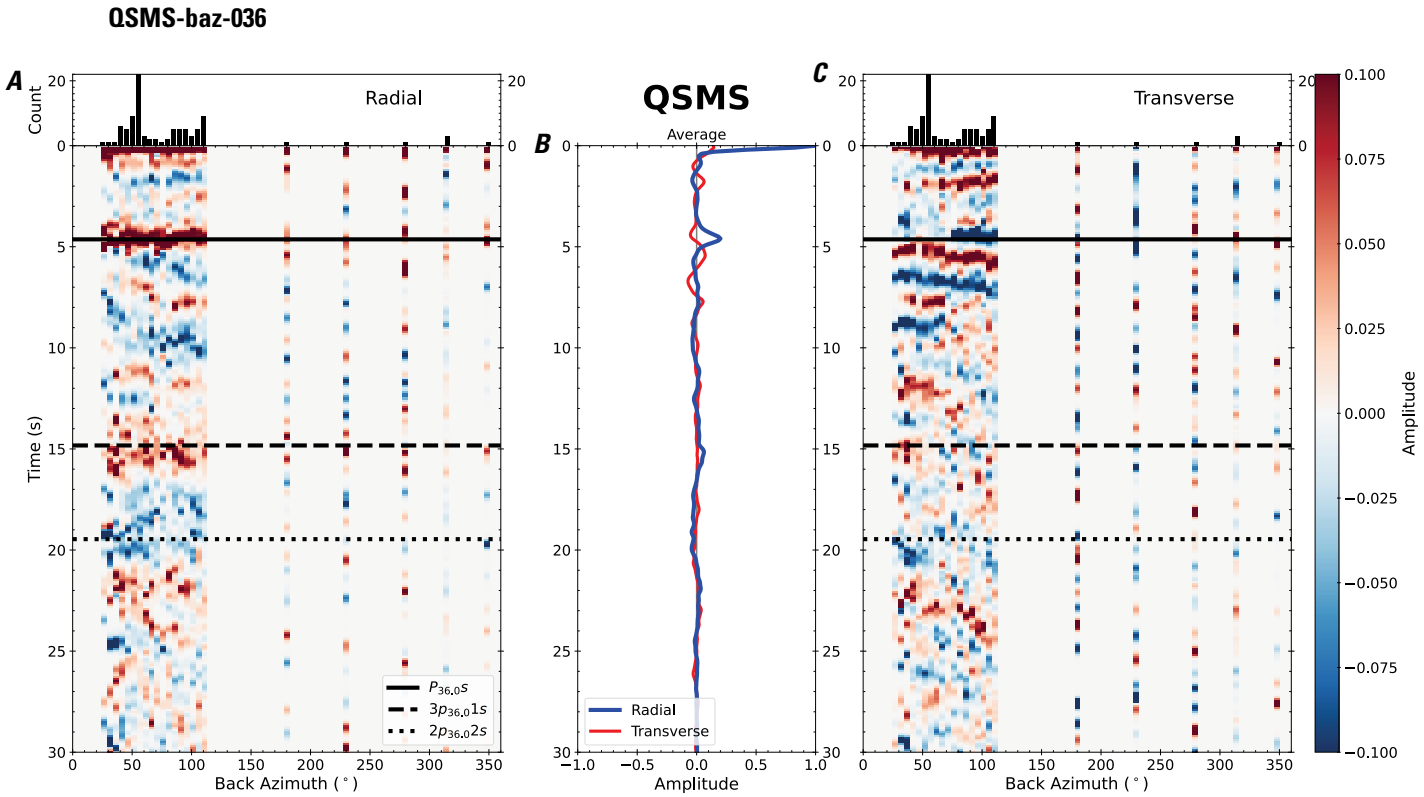

Figure 77. Receiver functions plotted against back azimuth for station QSMS. *A*, Radial component of P-wave receiver functions (PRFs) plotted against back azimuth. Individual PRFs have had the resonance-removal filter of Yu and others (2015) applied to them, are normalized to the maximum amplitude within the time window shown, binned, and normalized by the number of traces per bin. *B*, Average of every individual normalized radial receiver function with the application of the resonance-removal filter (blue) and average of every individual normalized raw radial receiver function (red). *C*, Radial component of raw PRFs, plotted against back azimuth, normalized as in *A*. Ps, 3p1s, and 2p2s arrival times predicted for the preferred Moho depth are shown, assuming a ray parameter of 0.06 s/km.

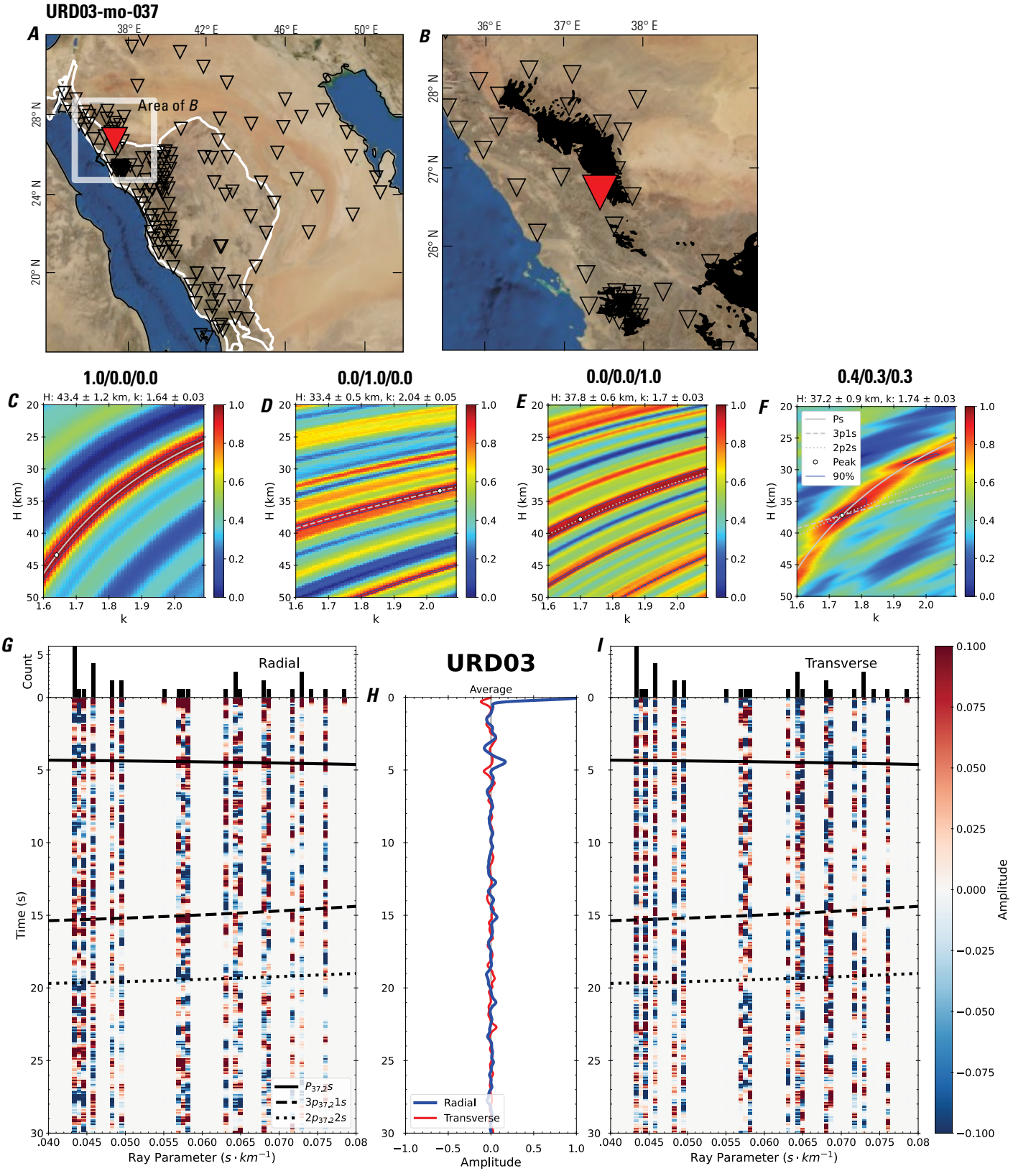
URD03-mo-037
A
B
Area of B
1.0/0.0/0.0
0.0/1.0/0.0
0.0/0.0/1.0
0.4/0.3/0.3
C
D
E
F
H: 43.4 ± 1.2 km, k: 1.64 ± 0.03
H: 33.4 ± 0.5 km, k: 2.04 ± 0.05
H: 37.8 ± 0.6 km, k: 1.7 ± 0.03
H: 37.2 ± 0.9 km, k: 1.74 ± 0.03
H (km)
k
Ps
3p1s
2p2s
Peak
90%
G
H
I
URD03
Radial
Transverse
Average
Count
Time (s)
Ray Parameter (s · km⁻¹)
Amplitude
$P_{37.2}s$
$3p_{37.2}1s$
$2p_{37.2}2s$

Figure 78 (page 84). Receiver-function analysis for station URD03. *A*, Regional map of Saudi Arabia showing the entire array (as inverted triangles), the location of station URD03 (red inverted triangle), the shield-platform boundary (white line), and the bounds of the map in *B* (white box). *B*, Local map of station URD03. Harrats are shown in black. *C*, Standard, single-layer *H-k* stack with stacking weights 0.4/0.3/0.3. This *H-k* stack ignores sedimentary effects on the receiver functions. *D*, Standard, single-layer *H-k* stack with stacking weights 0.5/0.5/0.0. This *H-k* stack also ignores sedimentary effects on the receiver functions. *E*, Optimized sub-sedimentary *H-k* stack with stacking weights 0.4/0.3/0.3, following the method of Yu and others (2015). *F*, Optimized sedimentary *H-k* stack with stacking weights 0.05/0.70/0.25, following the method of Yu and others (2015). *G*, Radial component P-wave receiver functions (PRFs) plotted against ray parameter. Individual PRFs have had the resonance-removal filter of Yu and others (2015) applied to them and are normalized to the maximum amplitude within the time window shown, binned, and normalized by the number of traces per bin. *H*, Average of every individual normalized radial receiver function with the application of the resonance-removal filter (blue) and average of every individual normalized raw radial receiver function (red). *I*, Radial component of raw PRFs (that is, PRFs with no resonance-removal filter applied) plotted against ray parameter, normalized as in *G*.

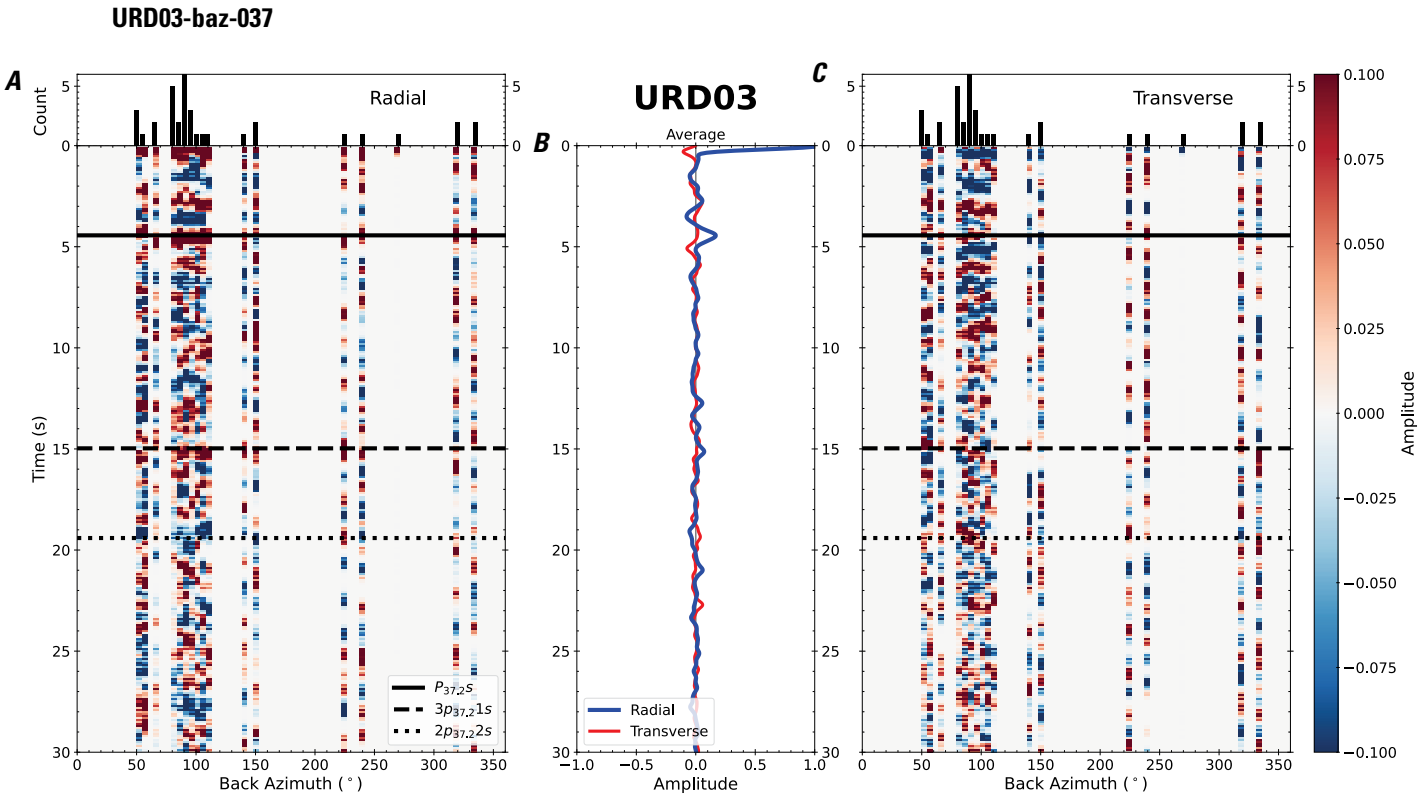

Figure 79. Receiver functions plotted against back azimuth for station URD03. *A*, Radial component of P-wave receiver functions (PRFs) plotted against back azimuth. Individual PRFs have had the resonance-removal filter of Yu and others (2015) applied to them, are normalized to the maximum amplitude within the time window shown, binned, and normalized by the number of traces per bin. *B*, Average of every individual normalized radial receiver function with the application of the resonance-removal filter (blue) and average of every individual normalized raw radial receiver function (red). *C*, Radial component of raw PRFs, plotted against back azimuth, normalized as in *A*. Ps, 3p1s, and 2p2s arrival times predicted for the preferred Moho depth are shown, assuming a ray parameter of 0.06 s/km.

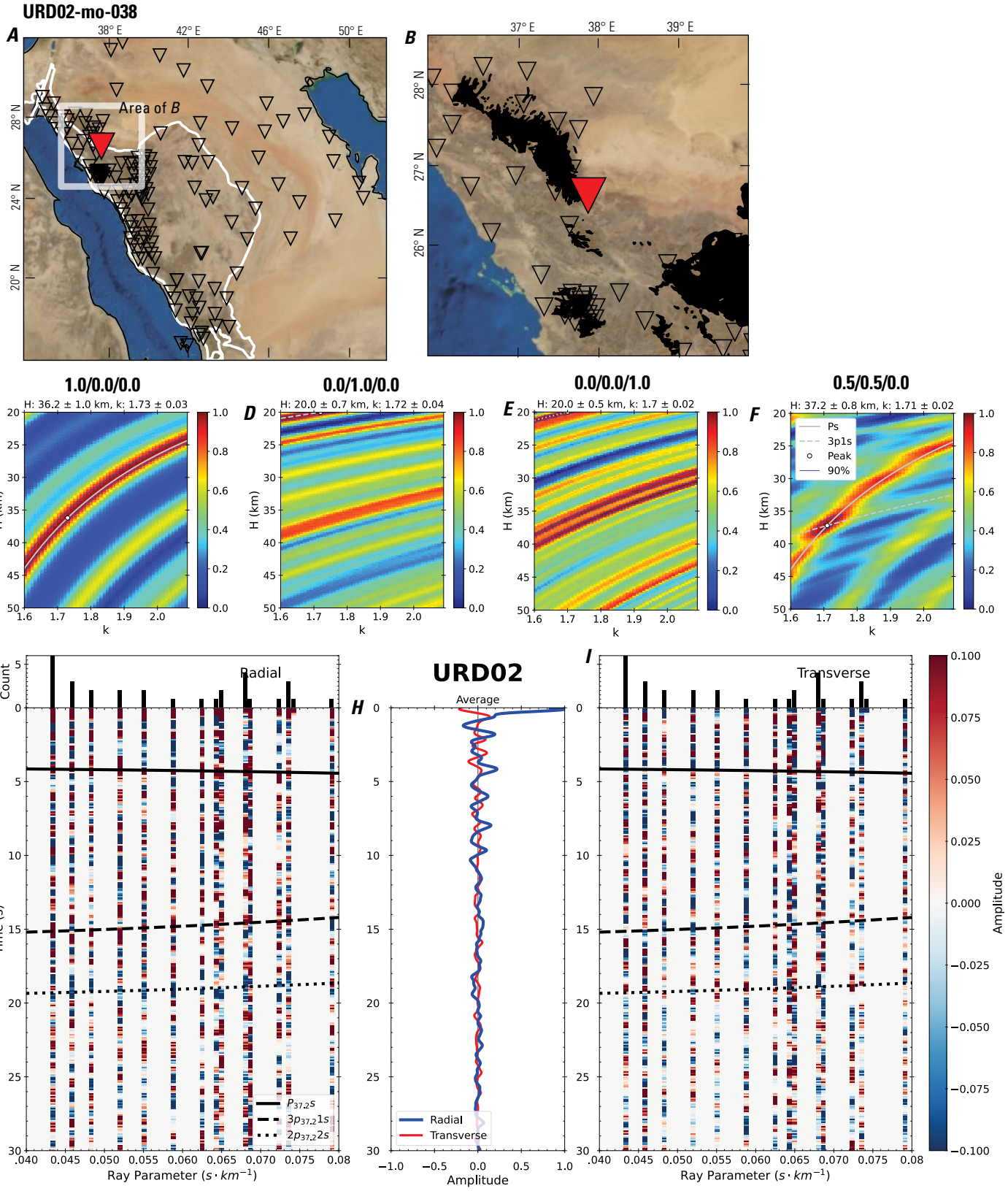
URD02-mo-038
A
38° E
42° E
46° E
50° E
28° N
24° N
20° N
Area of B
B
37° E
38° E
39° E
28° N
27° N
26° N
1.0/0.0/0.0
0.0/1.0/0.0
0.0/0.0/1.0
0.5/0.5/0.0
C
H: 36.2 ± 1.0 km, k: 1.73 ± 0.03
D
H: 20.0 ± 0.7 km, k: 1.72 ± 0.04
E
H: 20.0 ± 0.5 km, k: 1.7 ± 0.02
F
H: 37.2 ± 0.8 km, k: 1.71 ± 0.02
Ps
3p1s
Peak
90%
H (km)
k
G
Radial
Count
Time (s)
$P_{37.2}s$
$3p_{37.2}1s$
$2p_{37.2}2s$
Ray Parameter ($s \cdot km^{-1}$)
URD02
H
Average
Radial
Transverse
Amplitude
I
Transverse
Amplitude

Figure 80 (page 86). Receiver-function analysis for station URD02. *A*, Regional map of Saudi Arabia showing the entire array (as inverted triangles), the location of station URD02 (red inverted triangle), the shield-platform boundary (white line), and the bounds of the map in *B* (white box). *B*, Local map of station URD02. Harrats are shown in black. *C*, Standard, single-layer *H-k* stack with stacking weights 0.4/0.3/0.3. This *H-k* stack ignores sedimentary effects on the receiver functions. *D*, Standard, single-layer *H-k* stack with stacking weights 0.5/0.5/0.0. This *H-k* stack also ignores sedimentary effects on the receiver functions. *E*, Optimized sub-sedimentary *H-k* stack with stacking weights 0.4/0.3/0.3, following the method of Yu and others (2015). *F*, Optimized sedimentary *H-k* stack with stacking weights 0.05/0.70/0.25, following the method of Yu and others (2015). *G*, Radial component P-wave receiver functions (PRFs) plotted against ray parameter. Individual PRFs have had the resonance-removal filter of Yu and others (2015) applied to them and are normalized to the maximum amplitude within the time window shown, binned, and normalized by the number of traces per bin. *H*, Average of every individual normalized radial receiver function with the application of the resonance-removal filter (blue) and average of every individual normalized raw radial receiver function (red). *I*, Radial component of raw PRFs (that is, PRFs with no resonance-removal filter applied) plotted against ray parameter, normalized as in *G*.

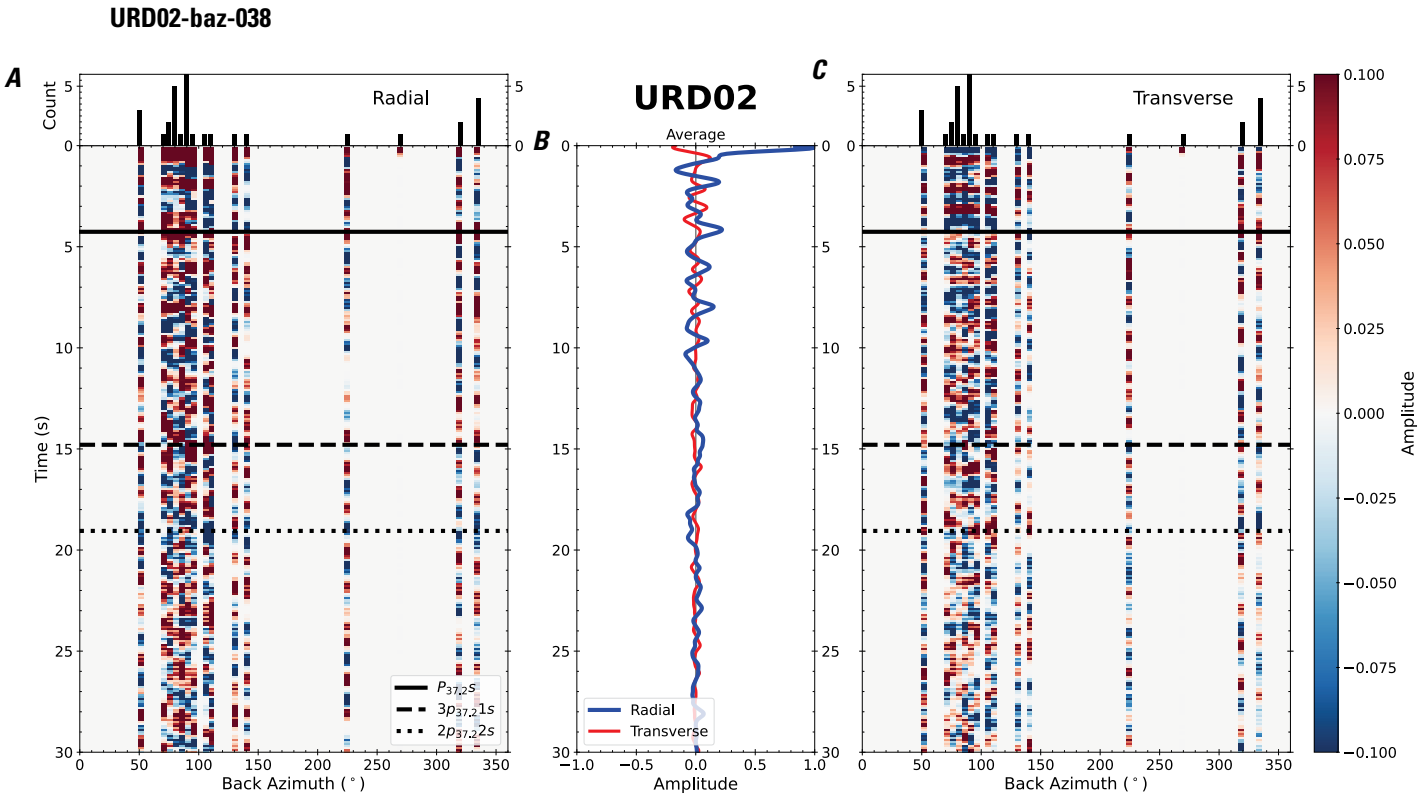

Figure 81. Receiver functions plotted against back azimuth for station URD02. *A*, Radial component of P-wave receiver functions (PRFs) plotted against back azimuth. Individual PRFs have had the resonance-removal filter of Yu and others (2015) applied to them, are normalized to the maximum amplitude within the time window shown, binned, and normalized by the number of traces per bin. *B*, Average of every individual normalized radial receiver function with the application of the resonance-removal filter (blue) and average of every individual normalized raw radial receiver function (red). *C*, Radial component of raw PRFs, plotted against back azimuth, normalized as in *A*. Ps, 3p1s, and 2p2s arrival times predicted for the preferred Moho depth are shown, assuming a ray parameter of 0.06 s/km.

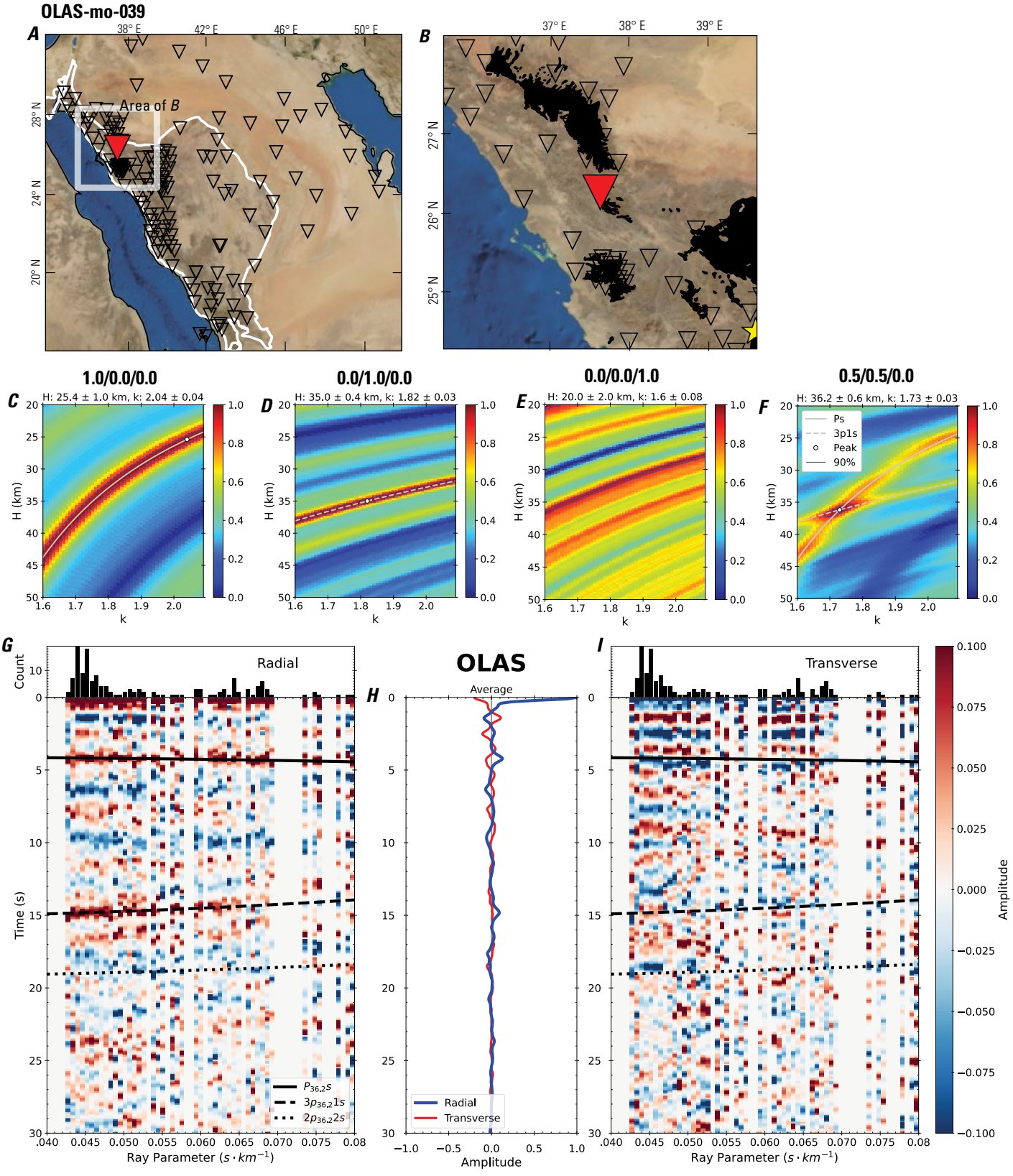
OLAS-mo-039
A
B
Area of B
1.0/0.0/0.0
0.0/1.0/0.0
0.0/0.0/1.0
0.5/0.5/0.0
C
D
E
F
H: 25.4 ± 1.0 km, k: 2.04 ± 0.04
H: 35.0 ± 0.4 km, k: 1.82 ± 0.03
H: 20.0 ± 2.0 km, k: 1.6 ± 0.08
H: 36.2 ± 0.6 km, k: 1.73 ± 0.03
H (km)
k
Ps
3p1s
Peak
90%
G
H
I
Radial
Transverse
OLAS
Average
Count
Time (s)
Ray Parameter (s · km⁻¹)
Amplitude
$P_{36.2}s$
$3p_{36.2}1s$
$2p_{36.2}2s$

Figure 82 (page 88). Receiver-function analysis for station OLAS. *A*, Regional map of Saudi Arabia showing the entire array (as inverted triangles), the location of station OLAS (red inverted triangle), the shield-platform boundary (white line), and the bounds of the map in *B* (white box). *B*, Local map of station OLAS. Harrats are shown in black. *C*, Standard, single-layer *H-k* stack with stacking weights 0.4/0.3/0.3. This *H-k* stack ignores sedimentary effects on the receiver functions. *D*, Standard, single-layer *H-k* stack with stacking weights 0.5/0.5/0.0. This *H-k* stack also ignores sedimentary effects on the receiver functions. *E*, Optimized sub-sedimentary *H-k* stack with stacking weights 0.4/0.3/0.3, following the method of Yu and others (2015). *F*, Optimized sedimentary *H-k* stack with stacking weights 0.05/0.70/0.25, following the method of Yu and others (2015). *G*, Radial component P-wave receiver functions (PRFs) plotted against ray parameter. Individual PRFs have had the resonance-removal filter of Yu and others (2015) applied to them and are normalized to the maximum amplitude within the time window shown, binned, and normalized by the number of traces per bin. *H*, Average of every individual normalized radial receiver function with the application of the resonance-removal filter (blue) and average of every individual normalized raw radial receiver function (red). *I*, Radial component of raw PRFs (that is, PRFs with no resonance-removal filter applied) plotted against ray parameter, normalized as in *G*.

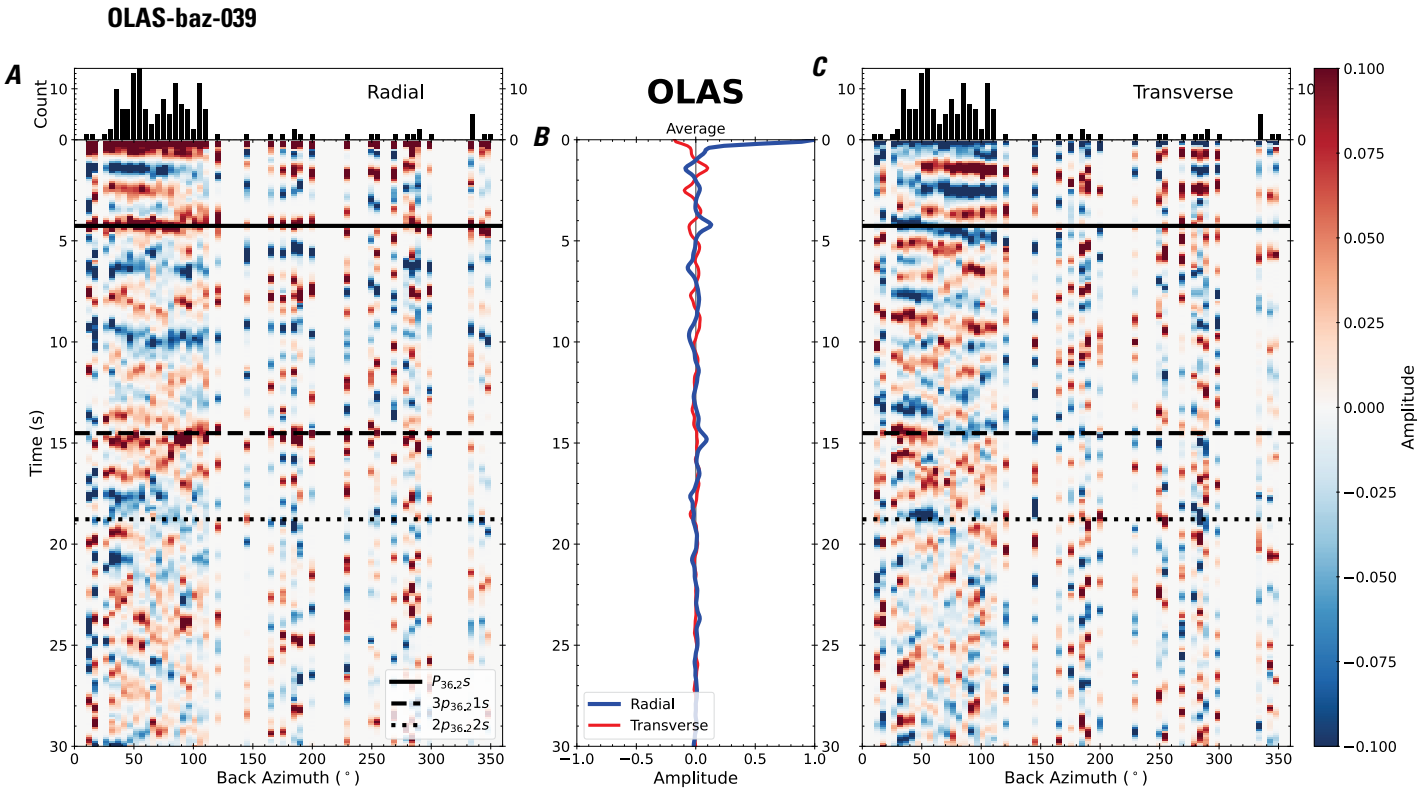

Figure 83. Receiver functions plotted against back azimuth for station OLAS. *A*, Radial component of P-wave receiver functions (PRFs) plotted against back azimuth. Individual PRFs have had the resonance-removal filter of Yu and others (2015) applied to them, are normalized to the maximum amplitude within the time window shown, binned, and normalized by the number of traces per bin. *B*, Average of every individual normalized radial receiver function with the application of the resonance-removal filter (blue) and average of every individual normalized raw radial receiver function (red). *C*, Radial component of raw PRFs, plotted against back azimuth, normalized as in *A*. Ps, 3p1s, and 2p2s arrival times predicted for the preferred Moho depth are shown, assuming a ray parameter of 0.06 s/km.

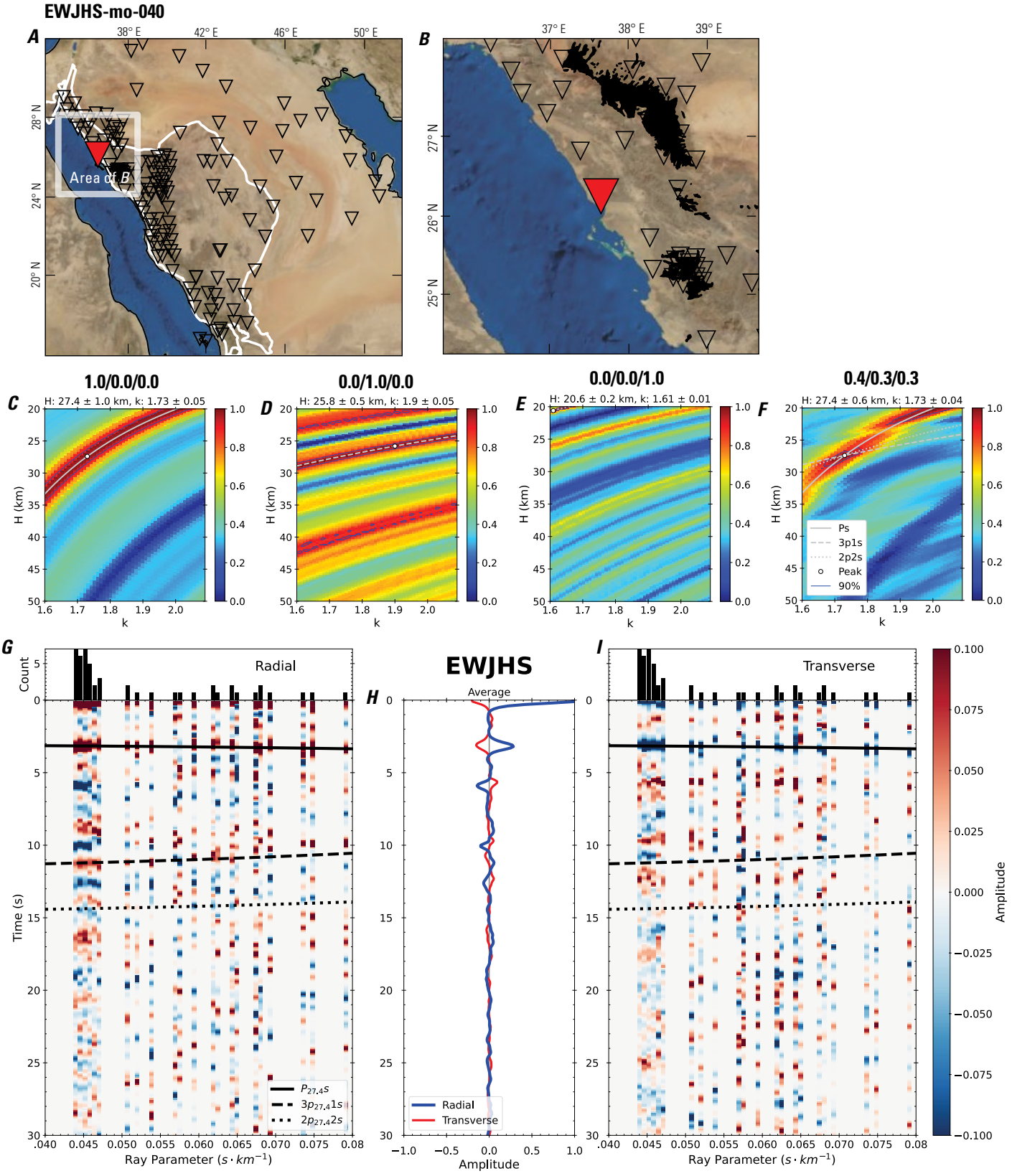
EWJHS-mo-040
A
38° E
42° E
46° E
50° E
28° N
24° N
20° N
Area of B
B
37° E
38° E
39° E
27° N
26° N
25° N
1.0/0.0/0.0
0.0/1.0/0.0
0.0/0.0/1.0
0.4/0.3/0.3
C
H: 27.4 ± 1.0 km, k: 1.73 ± 0.05
D
H: 25.8 ± 0.5 km, k: 1.9 ± 0.05
E
H: 20.6 ± 0.2 km, k: 1.61 ± 0.01
F
H: 27.4 ± 0.6 km, k: 1.73 ± 0.04
H (km)
k
Ps
3p1s
2p2s
Peak
90%
G
Radial
Count
Time (s)
Ray Parameter (s · km⁻¹)
$P_{27.4}s$
$3p_{27.4}1s$
$2p_{27.4}2s$
EWJHS
H
Average
Radial
Transverse
Amplitude
I
Transverse
Amplitude

Figure 84 (page 90). Receiver-function analysis for station EWJHS. *A*, Regional map of Saudi Arabia showing the entire array (as inverted triangles), the location of station EWJHS (red inverted triangle), the shield-platform boundary (white line), and the bounds of the map in *B* (white box). *B*, Local map of station EWJHS. Harrats are shown in black. *C*, Standard, single-layer *H-k* stack with stacking weights 0.4/0.3/0.3. This *H-k* stack ignores sedimentary effects on the receiver functions. *D*, Standard, single-layer *H-k* stack with stacking weights 0.5/0.5/0.0. This *H-k* stack also ignores sedimentary effects on the receiver functions. *E*, Optimized sub-sedimentary *H-k* stack with stacking weights 0.4/0.3/0.3, following the method of Yu and others (2015). *F*, Optimized sedimentary *H-k* stack with stacking weights 0.05/0.70/0.25, following the method of Yu and others (2015). *G*, Radial component P-wave receiver functions (PRFs) plotted against ray parameter. Individual PRFs have had the resonance-removal filter of Yu and others (2015) applied to them and are normalized to the maximum amplitude within the time window shown, binned, and normalized by the number of traces per bin. *H*, Average of every individual normalized radial receiver function with the application of the resonance-removal filter (blue) and average of every individual normalized raw radial receiver function (red). *I*, Radial component of raw PRFs (that is, PRFs with no resonance-removal filter applied) plotted against ray parameter, normalized as in *G*.

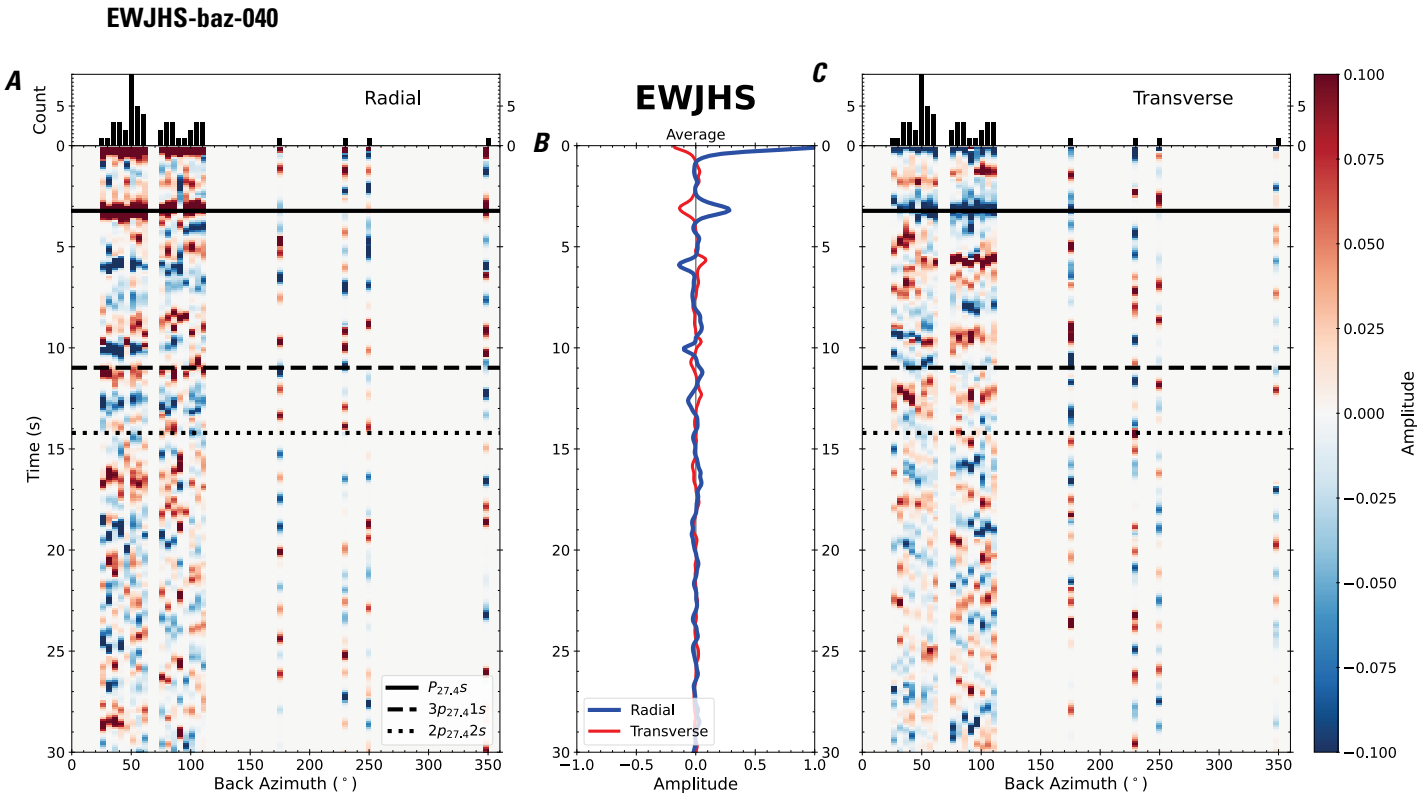

Figure 85. Receiver functions plotted against back azimuth for station EWJHS. *A*, Radial component of P-wave receiver functions (PRFs) plotted against back azimuth. Individual PRFs have had the resonance-removal filter of Yu and others (2015) applied to them, are normalized to the maximum amplitude within the time window shown, binned, and normalized by the number of traces per bin. *B*, Average of every individual normalized radial receiver function with the application of the resonance-removal filter (blue) and average of every individual normalized raw radial receiver function (red). *C*, Radial component of raw PRFs, plotted against back azimuth, normalized as in *A*. Ps, 3p1s, and 2p2s arrival times predicted for the preferred Moho depth are shown, assuming a ray parameter of 0.06 s/km.

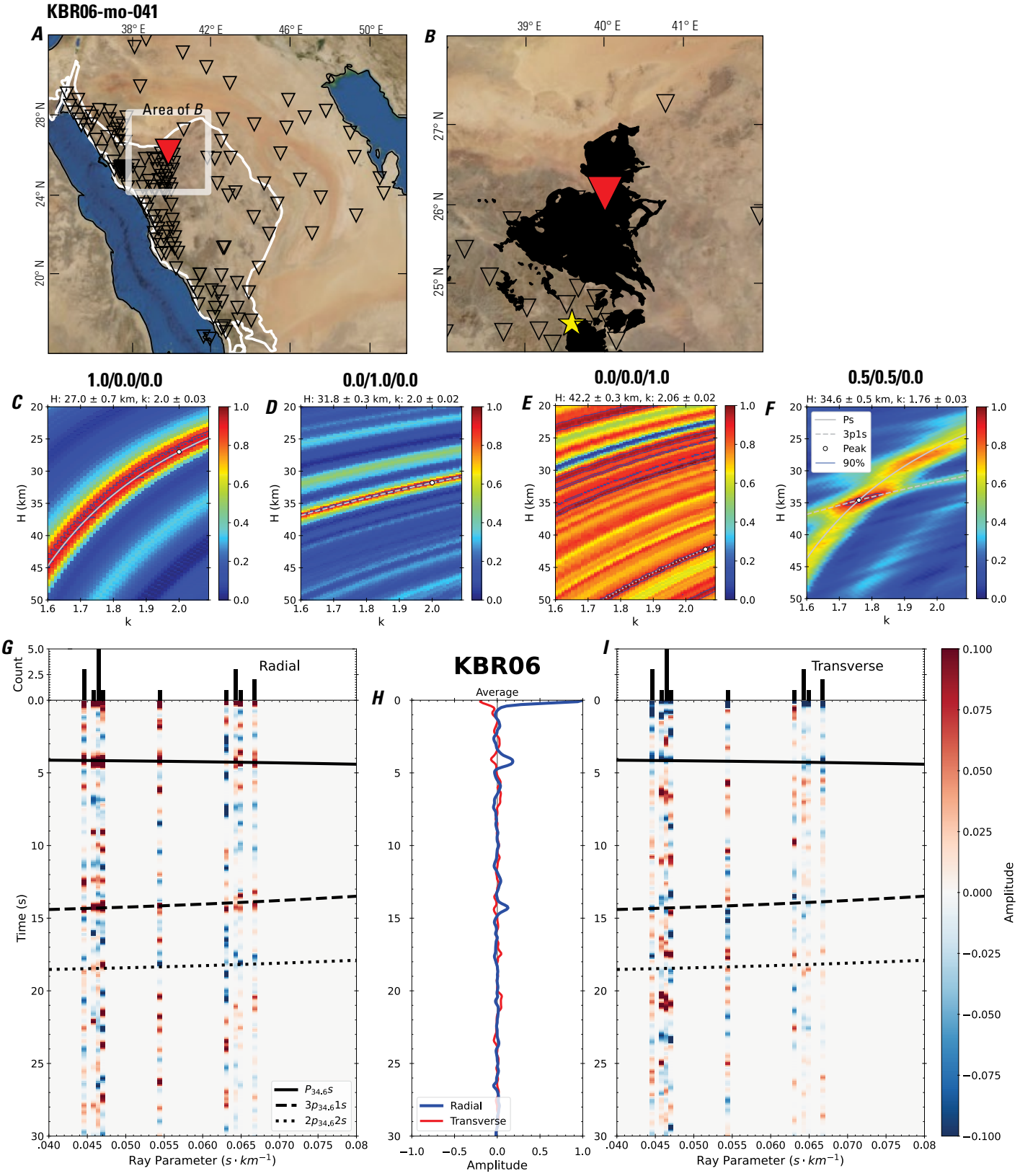
KBR06-mo-041
A
38° E
42° E
46° E
50° E
28° N
24° N
20° N
Area of B
B
39° E
40° E
41° E
27° N
26° N
25° N
1.0/0.0/0.0
C
H: 27.0 ± 0.7 km, k: 2.0 ± 0.03
0.0/1.0/0.0
D
H: 31.8 ± 0.3 km, k: 2.0 ± 0.02
0.0/0.0/1.0
E
H: 42.2 ± 0.3 km, k: 2.06 ± 0.02
0.5/0.5/0.0
F
H: 34.6 ± 0.5 km, k: 1.76 ± 0.03
Ps
3p1s
Peak
90%
H (km)
k
G
Radial
Count
Time (s)
$P_{34.6}s$
$3p_{34.6}1s$
$2p_{34.6}2s$
Ray Parameter ($s \cdot km^{-1}$)
KBR06
H
Average
Radial
Transverse
Amplitude
I
Transverse
Amplitude

Figure 86 (page 92). Receiver-function analysis for station KBR06. *A*, Regional map of Saudi Arabia showing the entire array (as inverted triangles), the location of station KBR06 (red inverted triangle), the shield-platform boundary (white line), and the bounds of the map in *B* (white box). *B*, Local map of station KBR06. Harrats are shown in black. *C*, Standard, single-layer *H-k* stack with stacking weights 0.4/0.3/0.3. This *H-k* stack ignores sedimentary effects on the receiver functions. *D*, Standard, single-layer *H-k* stack with stacking weights 0.5/0.5/0.0. This *H-k* stack also ignores sedimentary effects on the receiver functions. *E*, Optimized sub-sedimentary *H-k* stack with stacking weights 0.4/0.3/0.3, following the method of Yu and others (2015). *F*, Optimized sedimentary *H-k* stack with stacking weights 0.05/0.70/0.25, following the method of Yu and others (2015). *G*, Radial component P-wave receiver functions (PRFs) plotted against ray parameter. Individual PRFs have had the resonance-removal filter of Yu and others (2015) applied to them and are normalized to the maximum amplitude within the time window shown, binned, and normalized by the number of traces per bin. *H*, Average of every individual normalized radial receiver function with the application of the resonance-removal filter (blue) and average of every individual normalized raw radial receiver function (red). *I*, Radial component of raw PRFs (that is, PRFs with no resonance-removal filter applied) plotted against ray parameter, normalized as in *G*.

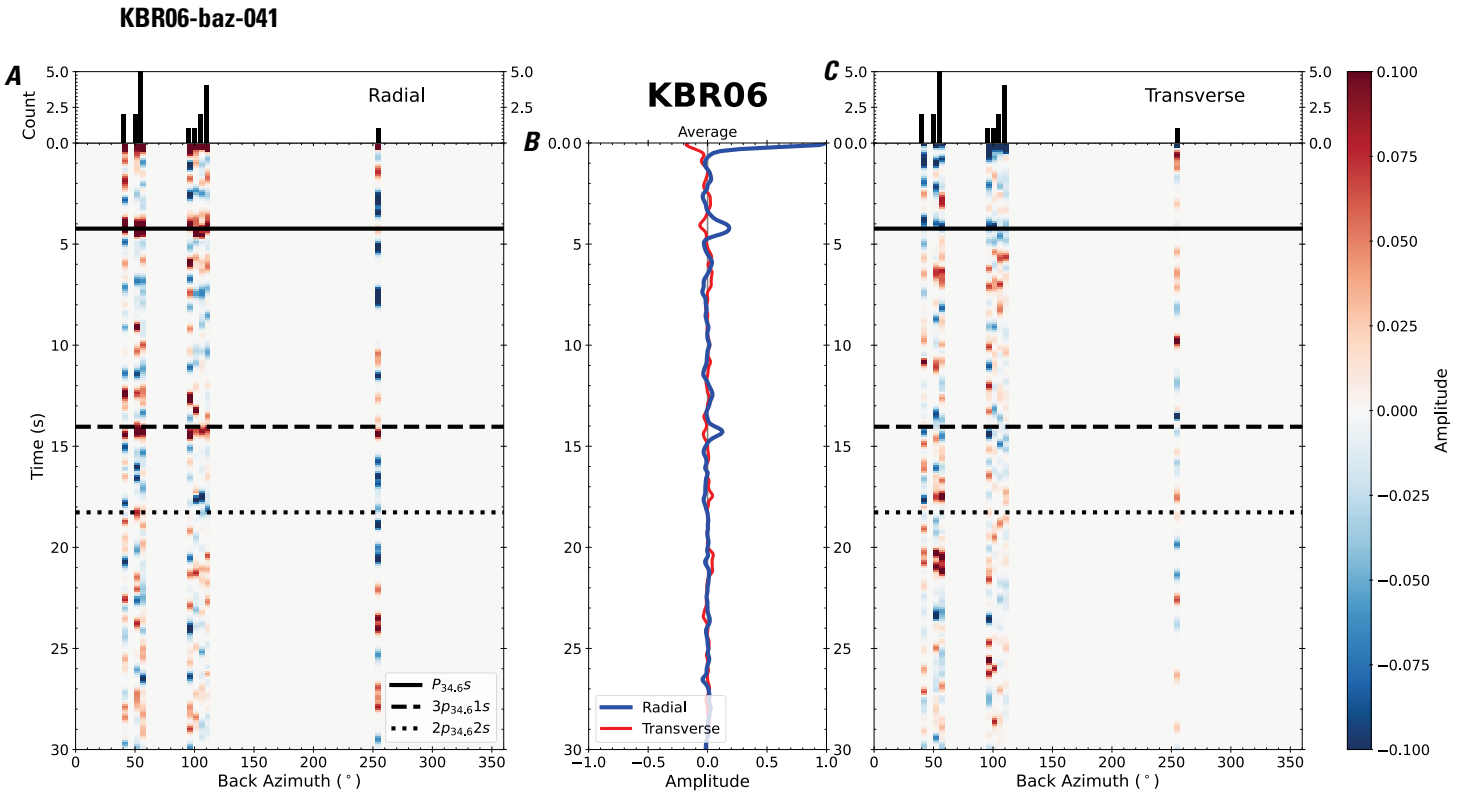

Figure 87. Receiver functions plotted against back azimuth for station KBR06. *A*, Radial component of P-wave receiver functions (PRFs) plotted against back azimuth. Individual PRFs have had the resonance-removal filter of Yu and others (2015) applied to them, are normalized to the maximum amplitude within the time window shown, binned, and normalized by the number of traces per bin. *B*, Average of every individual normalized radial receiver function with the application of the resonance-removal filter (blue) and average of every individual normalized raw radial receiver function (red). *C*, Radial component of raw PRFs, plotted against back azimuth, normalized as in *A*. Ps, 3p1s, and 2p2s arrival times predicted for the preferred Moho depth are shown, assuming a ray parameter of 0.06 s/km.

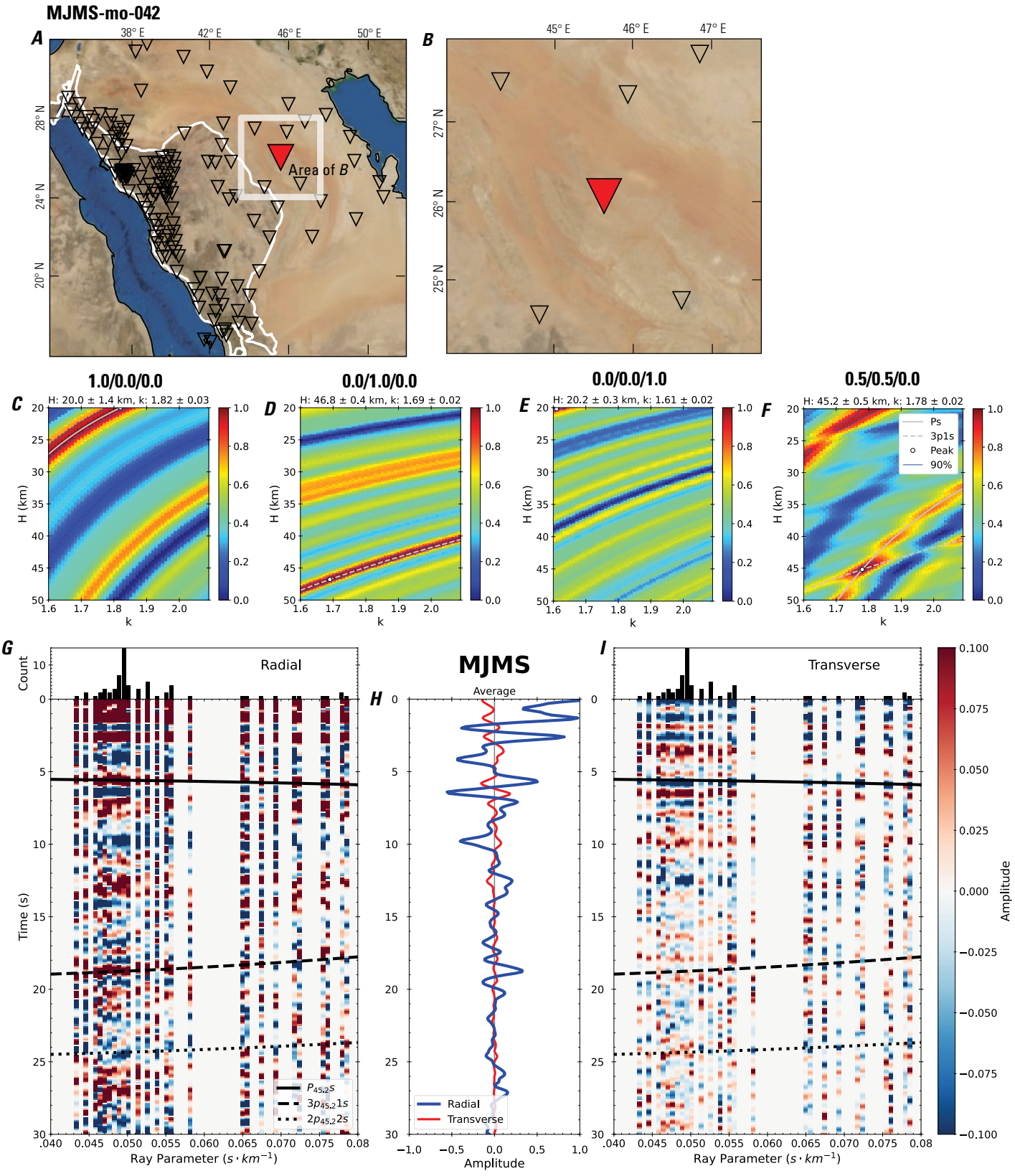
MJMS-mo-042
A
38° E
42° E
46° E
50° E
28° N
24° N
20° N
Area of B
B
45° E
46° E
47° E
27° N
26° N
25° N
1.0/0.0/0.0
0.0/1.0/0.0
0.0/0.0/1.0
0.5/0.5/0.0
C
D
E
F
H: 20.0 ± 1.4 km, k: 1.82 ± 0.03
H: 46.8 ± 0.4 km, k: 1.69 ± 0.02
H: 20.2 ± 0.3 km, k: 1.61 ± 0.02
H: 45.2 ± 0.5 km, k: 1.78 ± 0.02
H (km)
k
Ps
3p1s
Peak
90%
G
Radial
Count
Time (s)
Ray Parameter (s · km⁻¹)
P45.2s
3p45.21s
2p45.22s
MJMS
H
Average
Radial
Transverse
Amplitude
I
Transverse
Amplitude

Figure 88 (page 94). Receiver-function analysis for station MJMS. *A*, Regional map of Saudi Arabia showing the entire array (as inverted triangles), the location of station MJMS (red inverted triangle), the shield-platform boundary (white line), and the bounds of the map in *B* (white box). *B*, Local map of station MJMS. Harrats are shown in black. *C*, Standard, single-layer *H-k* stack with stacking weights 0.4/0.3/0.3. This *H-k* stack ignores sedimentary effects on the receiver functions. *D*, Standard, single-layer *H-k* stack with stacking weights 0.5/0.5/0.0. This *H-k* stack also ignores sedimentary effects on the receiver functions. *E*, Optimized sub-sedimentary *H-k* stack with stacking weights 0.4/0.3/0.3, following the method of Yu and others (2015). *F*, Optimized sedimentary *H-k* stack with stacking weights 0.05/0.70/0.25, following the method of Yu and others (2015). *G*, Radial component P-wave receiver functions (PRFs) plotted against ray parameter. Individual PRFs have had the resonance-removal filter of Yu and others (2015) applied to them and are normalized to the maximum amplitude within the time window shown, binned, and normalized by the number of traces per bin. *H*, Average of every individual normalized radial receiver function with the application of the resonance-removal filter (blue) and average of every individual normalized raw radial receiver function (red). *I*, Radial component of raw PRFs (that is, PRFs with no resonance-removal filter applied) plotted against ray parameter, normalized as in *G*.

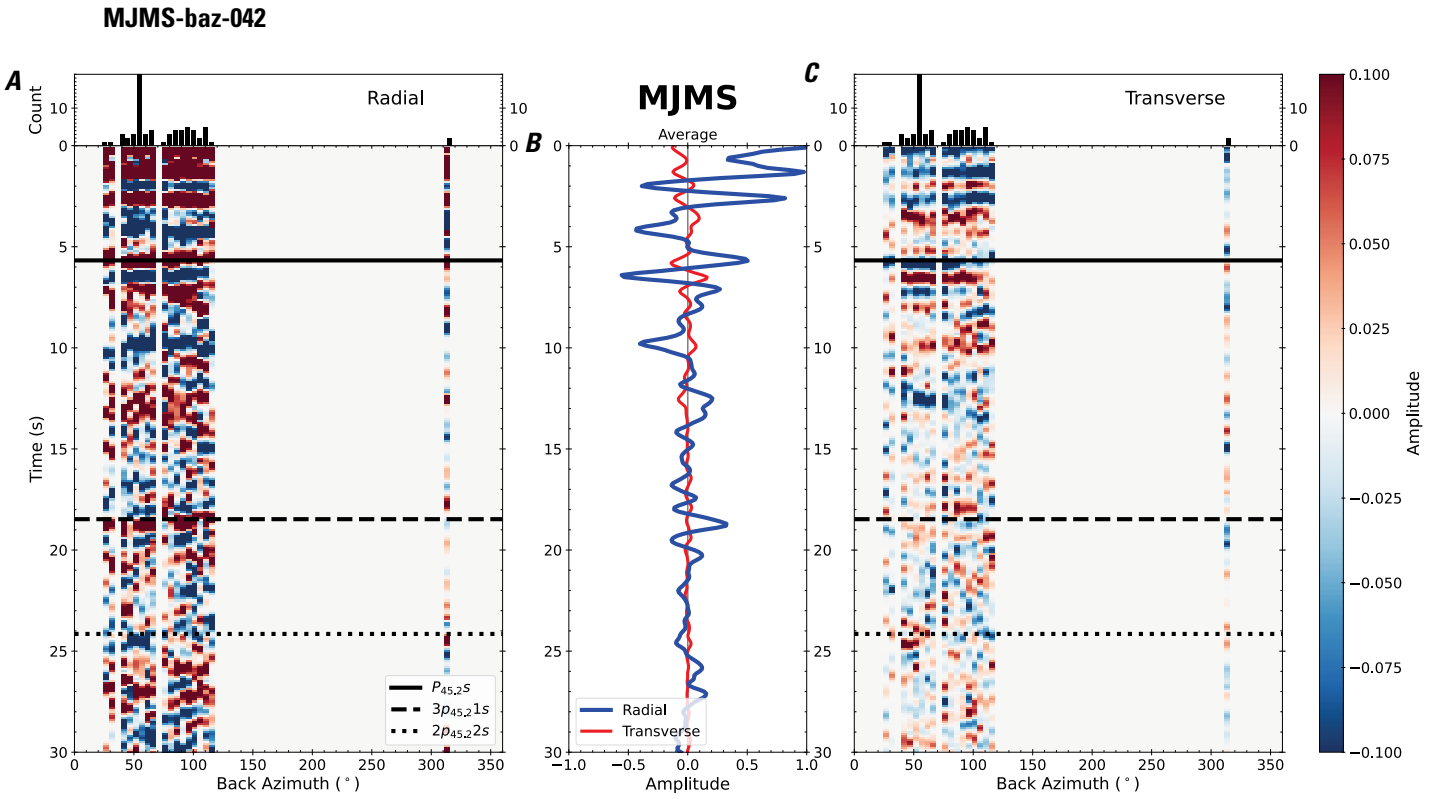

Figure 89. Receiver functions plotted against back azimuth for station MJMS. *A*, Radial component of P-wave receiver functions (PRFs) plotted against back azimuth. Individual PRFs have had the resonance-removal filter of Yu and others (2015) applied to them, are normalized to the maximum amplitude within the time window shown, binned, and normalized by the number of traces per bin. *B*, Average of every individual normalized radial receiver function with the application of the resonance-removal filter (blue) and average of every individual normalized raw radial receiver function (red). *C*, Radial component of raw PRFs, plotted against back azimuth, normalized as in *A*. Ps, 3p1s, and 2p2s arrival times predicted for the preferred Moho depth are shown, assuming a ray parameter of 0.06 s/km.

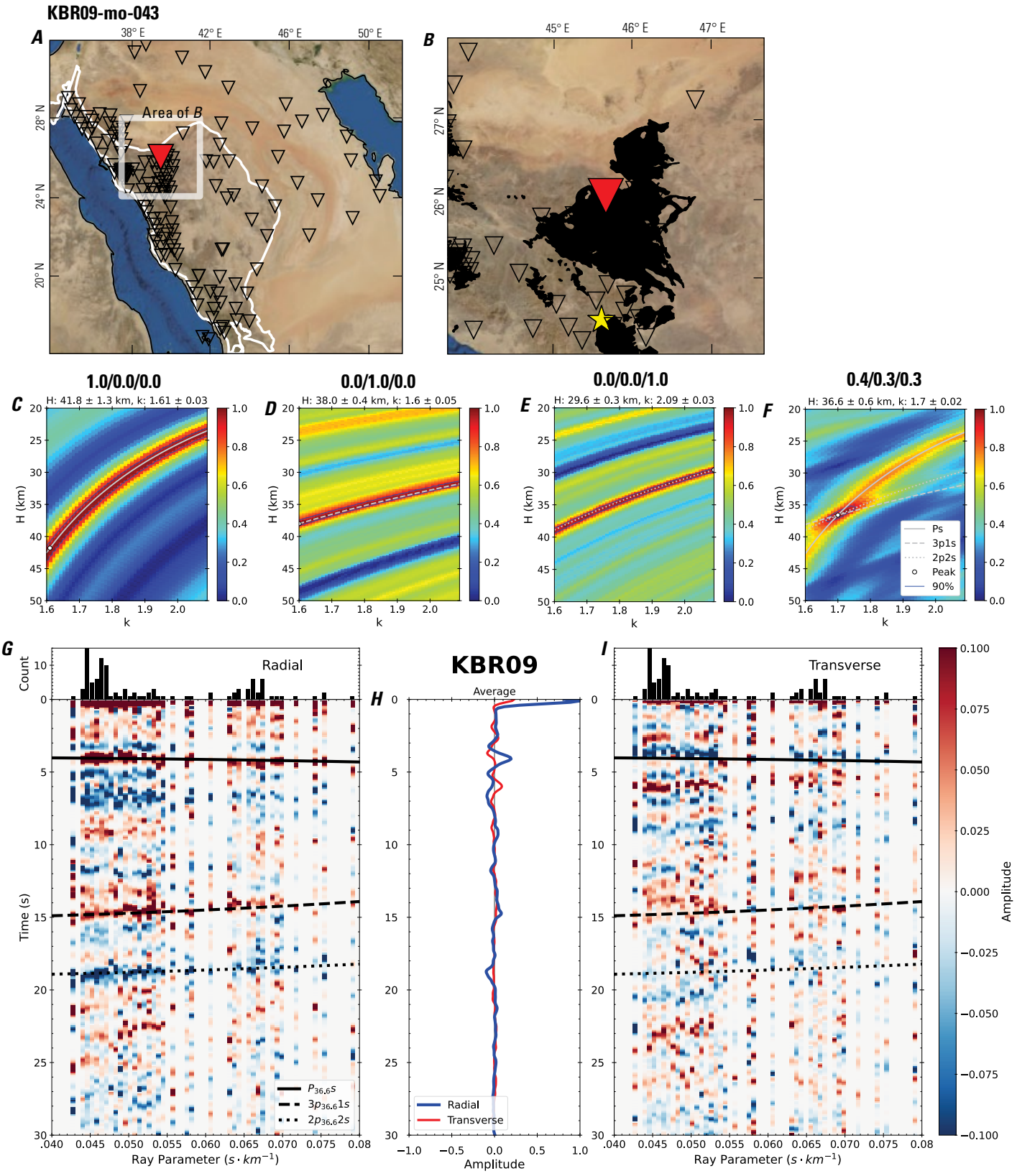
KBR09-mo-043
A
38° E
42° E
46° E
50° E
28° N
24° N
20° N
Area of B
B
45° E
46° E
47° E
27° N
26° N
25° N
1.0/0.0/0.0
0.0/1.0/0.0
0.0/0.0/1.0
0.4/0.3/0.3
C
H: 41.8 ± 1.3 km, k: 1.61 ± 0.03
D
H: 38.0 ± 0.4 km, k: 1.6 ± 0.05
E
H: 29.6 ± 0.3 km, k: 2.09 ± 0.03
F
H: 36.6 ± 0.6 km, k: 1.7 ± 0.02
H (km)
k
Ps
3p1s
2p2s
Peak
90%
G
Radial
Count
Time (s)
Ray Parameter (s · km⁻¹)
P36.6s
3p36.61s
2p36.62s
H
KBR09
Average
Radial
Transverse
Amplitude
I
Transverse
Amplitude

Figure 90 (page 96). Receiver-function analysis for station KBR09. *A*, Regional map of Saudi Arabia showing the entire array (as inverted triangles), the location of station KBR09 (red inverted triangle), the shield-platform boundary (white line), and the bounds of the map in *B* (white box). *B*, Local map of station KBR09. Harrats are shown in black. *C*, Standard, single-layer *H-k* stack with stacking weights 0.4/0.3/0.3. This *H-k* stack ignores sedimentary effects on the receiver functions. *D*, Standard, single-layer *H-k* stack with stacking weights 0.5/0.5/0.0. This *H-k* stack also ignores sedimentary effects on the receiver functions. *E*, Optimized sub-sedimentary *H-k* stack with stacking weights 0.4/0.3/0.3, following the method of Yu and others (2015). *F*, Optimized sedimentary *H-k* stack with stacking weights 0.05/0.70/0.25, following the method of Yu and others (2015). *G*, Radial component P-wave receiver functions (PRFs) plotted against ray parameter. Individual PRFs have had the resonance-removal filter of Yu and others (2015) applied to them and are normalized to the maximum amplitude within the time window shown, binned, and normalized by the number of traces per bin. *H*, Average of every individual normalized radial receiver function with the application of the resonance-removal filter (blue) and average of every individual normalized raw radial receiver function (red). *I*, Radial component of raw PRFs (that is, PRFs with no resonance-removal filter applied) plotted against ray parameter, normalized as in *G*.

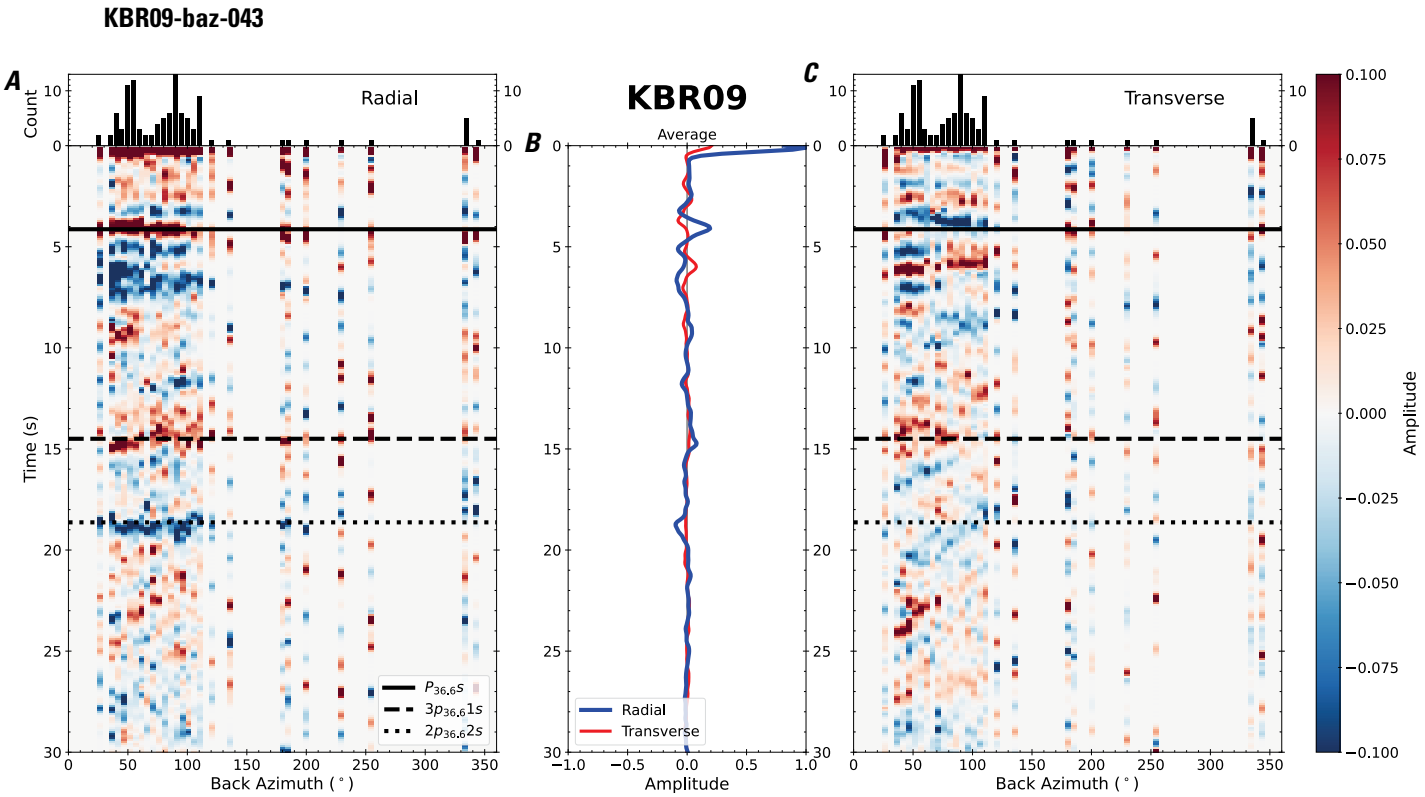

Figure 91. Receiver functions plotted against back azimuth for station KBR09. *A*, Radial component of P-wave receiver functions (PRFs) plotted against back azimuth. Individual PRFs have had the resonance-removal filter of Yu and others (2015) applied to them, are normalized to the maximum amplitude within the time window shown, binned, and normalized by the number of traces per bin. *B*, Average of every individual normalized radial receiver function with the application of the resonance-removal filter (blue) and average of every individual normalized raw radial receiver function (red). *C*, Radial component of raw PRFs, plotted against back azimuth, normalized as in *A*. Ps, 3p1s, and 2p2s arrival times predicted for the preferred Moho depth are shown, assuming a ray parameter of 0.06 s/km.

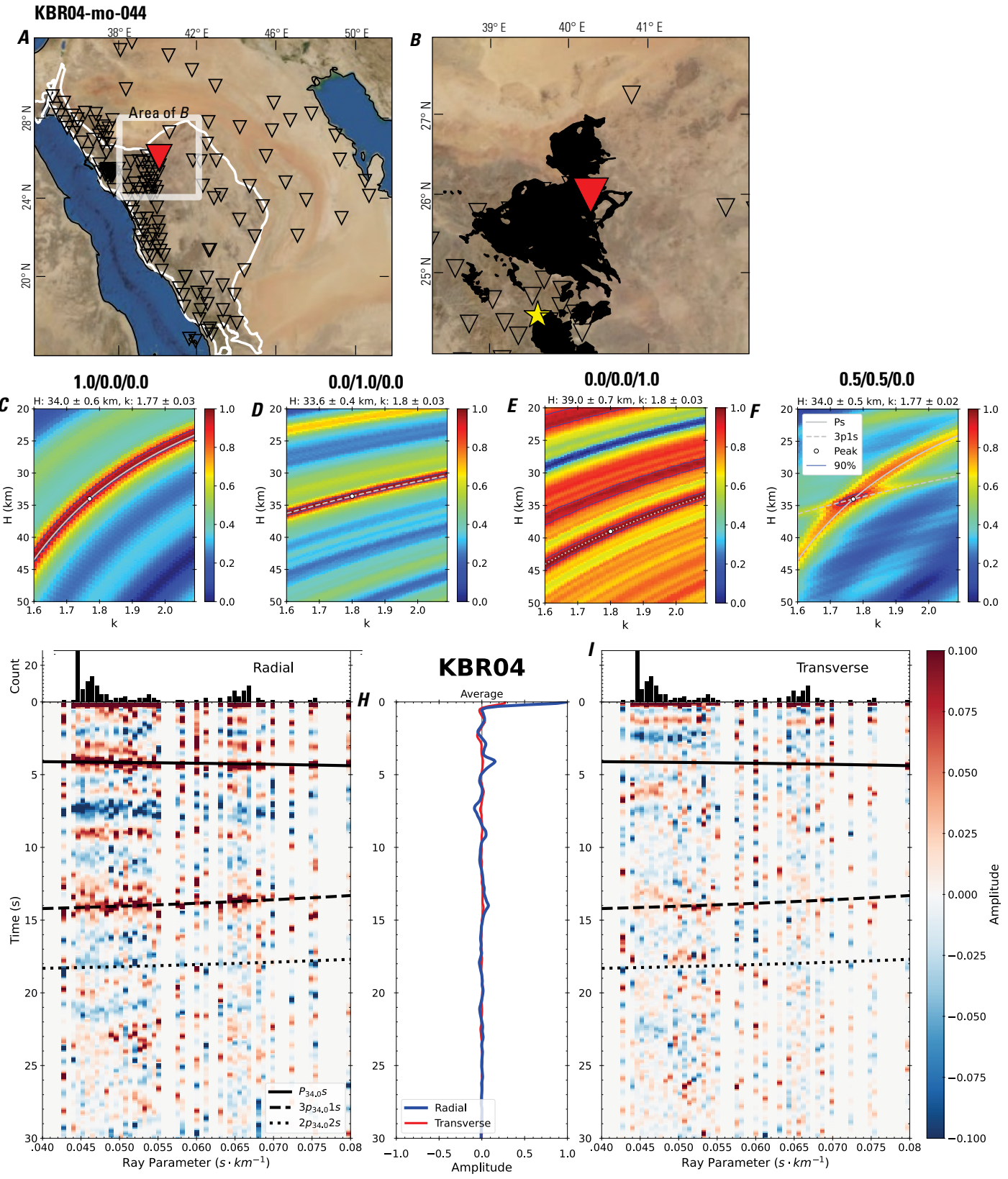
KBR04-mo-044
A
B
Area of B
1.0/0.0/0.0
0.0/1.0/0.0
0.0/0.0/1.0
0.5/0.5/0.0
C
D
E
F
H: 34.0 ± 0.6 km, k: 1.77 ± 0.03
H: 33.6 ± 0.4 km, k: 1.8 ± 0.03
H: 39.0 ± 0.7 km, k: 1.8 ± 0.03
H: 34.0 ± 0.5 km, k: 1.77 ± 0.02
Ps
3p1s
Peak
90%
H (km)
k
G
H
I
KBR04
Radial
Transverse
Average
Count
Time (s)
Ray Parameter (s · km⁻¹)
Amplitude
$P_{34.0}s$
$3p_{34.0}1s$
$2p_{34.0}2s$

Figure 92 (page 98). Receiver-function analysis for station KBR04. *A*, Regional map of Saudi Arabia showing the entire array (as inverted triangles), the location of station KBR04 (red inverted triangle), the shield-platform boundary (white line), and the bounds of the map in *B* (white box). *B*, Local map of station KBR04. Harrats are shown in black. *C*, Standard, single-layer *H-k* stack with stacking weights 0.4/0.3/0.3. This *H-k* stack ignores sedimentary effects on the receiver functions. *D*, Standard, single-layer *H-k* stack with stacking weights 0.5/0.5/0.0. This *H-k* stack also ignores sedimentary effects on the receiver functions. *E*, Optimized sub-sedimentary *H-k* stack with stacking weights 0.4/0.3/0.3, following the method of Yu and others (2015). *F*, Optimized sedimentary *H-k* stack with stacking weights 0.05/0.70/0.25, following the method of Yu and others (2015). *G*, Radial component P-wave receiver functions (PRFs) plotted against ray parameter. Individual PRFs have had the resonance-removal filter of Yu and others (2015) applied to them and are normalized to the maximum amplitude within the time window shown, binned, and normalized by the number of traces per bin. *H*, Average of every individual normalized radial receiver function with the application of the resonance-removal filter (blue) and average of every individual normalized raw radial receiver function (red). *I*, Radial component of raw PRFs (that is, PRFs with no resonance-removal filter applied) plotted against ray parameter, normalized as in *G*.

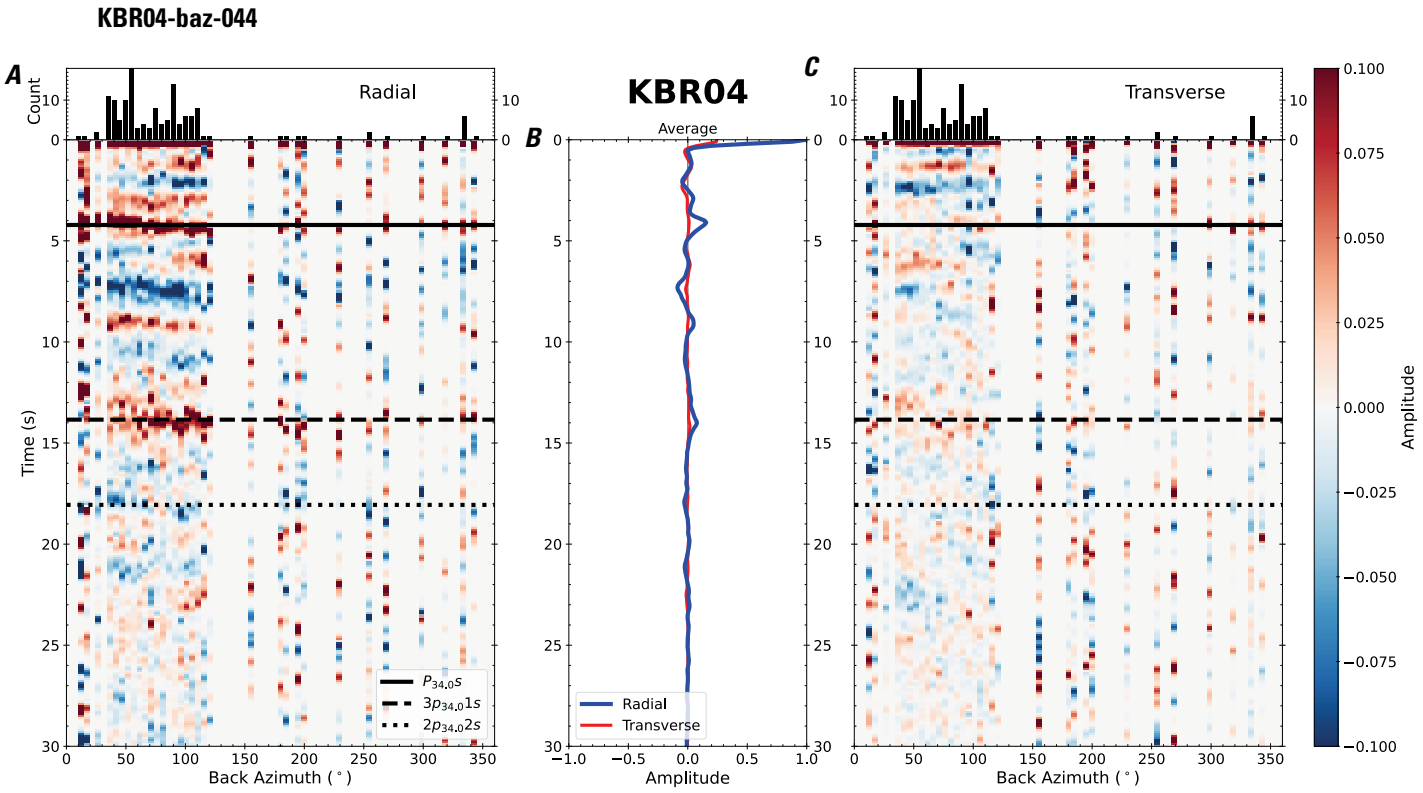

Figure 93. Receiver functions plotted against back azimuth for station KBR04. *A*, Radial component of P-wave receiver functions (PRFs) plotted against back azimuth. Individual PRFs have had the resonance-removal filter of Yu and others (2015) applied to them, are normalized to the maximum amplitude within the time window shown, binned, and normalized by the number of traces per bin. *B*, Average of every individual normalized radial receiver function with the application of the resonance-removal filter (blue) and average of every individual normalized raw radial receiver function (red). *C*, Radial component of raw PRFs, plotted against back azimuth, normalized as in *A*. Ps, 3p1s, and 2p2s arrival times predicted for the preferred Moho depth are shown, assuming a ray parameter of 0.06 s/km.

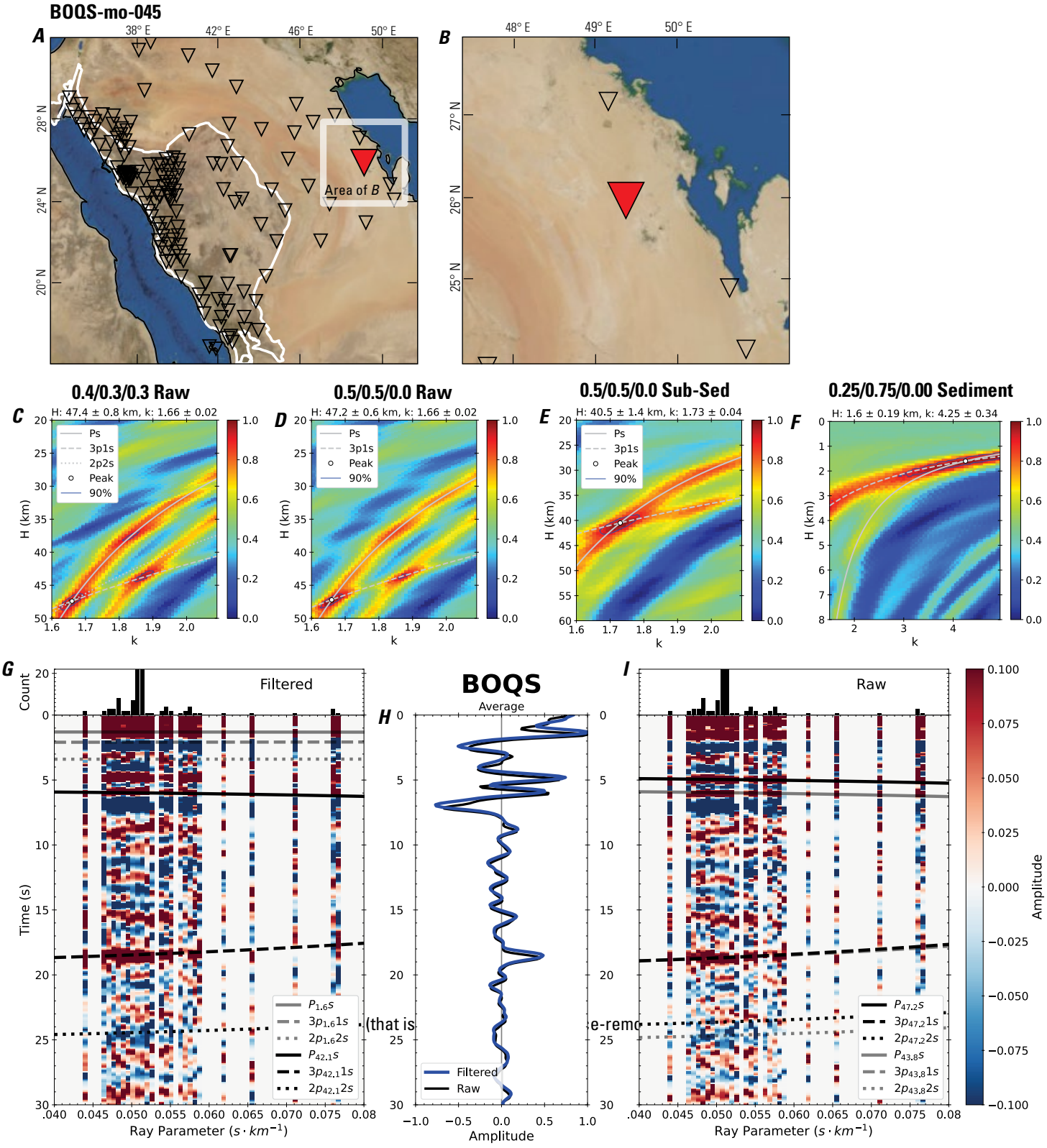
BOQS-mo-045
A
38° E
42° E
46° E
50° E
28° N
24° N
20° N
Area of B
B
48° E
49° E
50° E
27° N
26° N
25° N
0.4/0.3/0.3 Raw
0.5/0.5/0.0 Raw
0.5/0.5/0.0 Sub-Sed
0.25/0.75/0.00 Sediment
C
H: 47.4 ± 0.8 km, k: 1.66 ± 0.02
D
H: 47.2 ± 0.6 km, k: 1.66 ± 0.02
E
H: 40.5 ± 1.4 km, k: 1.73 ± 0.04
F
H: 1.6 ± 0.19 km, k: 4.25 ± 0.34
Ps
3p1s
2p2s
Peak
90%
H (km)
k
G
Filtered
Count
Time (s)
$P_{1.6}s$
$3p_{1.6}1s$
$2p_{1.6}2s$
$P_{42.1}s$
$3p_{42.1}1s$
$2p_{42.1}2s$
Ray Parameter ($s \cdot km^{-1}$)
H
BOQS
Average
Filtered
Raw
Amplitude
I
Raw
$P_{47.2}s$
$3p_{47.2}1s$
$2p_{47.2}2s$
$P_{43.8}s$
$3p_{43.8}1s$
$2p_{43.8}2s$
Amplitude

Figure 94 (page 100). Receiver-function analysis for station BOQS. *A*, Regional map of Saudi Arabia showing the entire array (as inverted triangles), the location of station BOQS (red inverted triangle), the shield-platform boundary (white line), and the bounds of the map in *B* (white box). *B*, Local map of station BOQS. Harrats are shown in black. *C*, Standard, single-layer *H-k* stack with stacking weights 0.4/0.3/0.3. This *H-k* stack ignores sedimentary effects on the receiver functions. *D*, Standard, single-layer *H-k* stack with stacking weights 0.5/0.5/0.0. This *H-k* stack also ignores sedimentary effects on the receiver functions. *E*, Optimized sub-sedimentary *H-k* stack with stacking weights 0.4/0.3/0.3, following the method of Yu and others (2015). *F*, Optimized sedimentary *H-k* stack with stacking weights 0.05/0.70/0.25, following the method of Yu and others (2015). *G*, Radial component P-wave receiver functions (PRFs) plotted against ray parameter. Individual PRFs have had the resonance-removal filter of Yu and others (2015) applied to them and are normalized to the maximum amplitude within the time window shown, binned, and normalized by the number of traces per bin. *H*, Average of every individual normalized radial receiver function with the application of the resonance-removal filter (blue) and average of every individual normalized raw radial receiver function (red). *I*, Radial component of raw PRFs (that is, PRFs with no resonance-removal filter applied) plotted against ray parameter, normalized as in *G*.

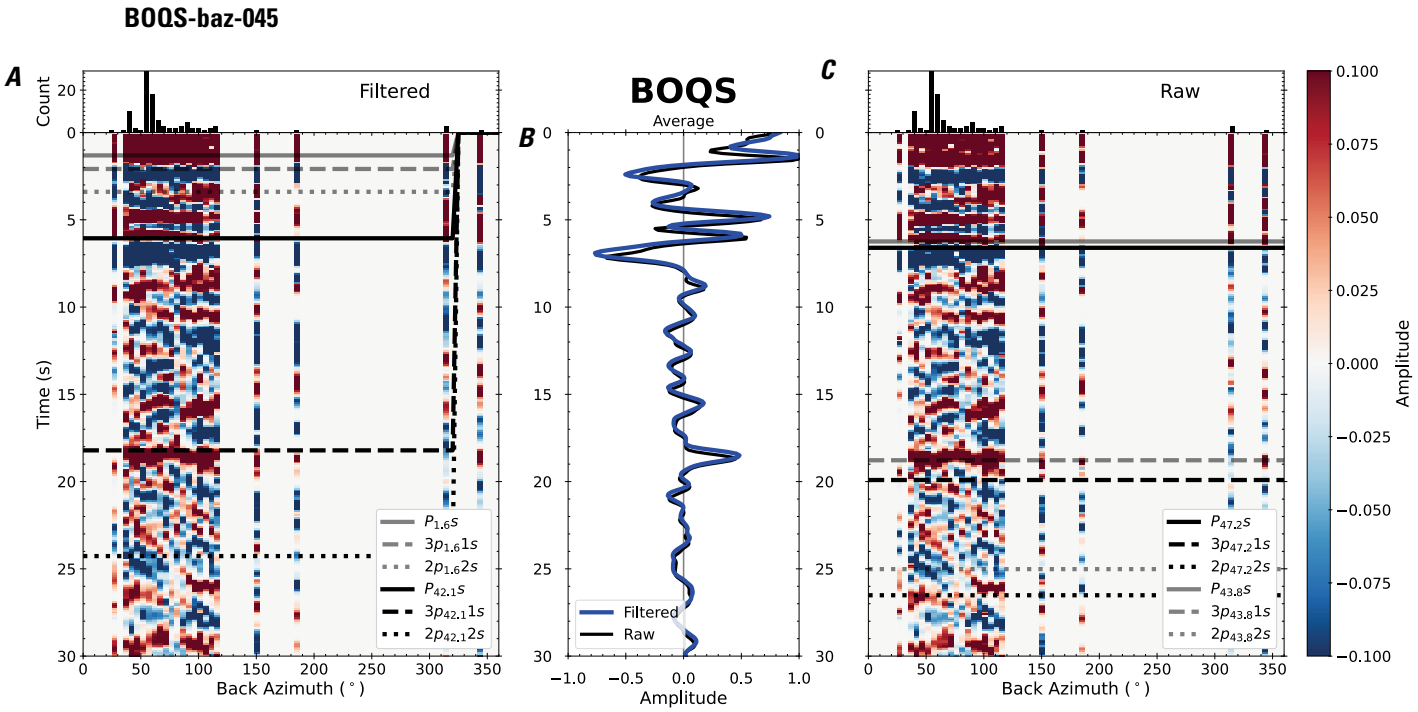

Figure 95. Receiver functions plotted against back azimuth for station BOQS. *A*, Radial component of P-wave receiver functions (PRFs) plotted against back azimuth. Individual PRFs have had the resonance-removal filter of Yu and others (2015) applied to them, are normalized to the maximum amplitude within the time window shown, binned, and normalized by the number of traces per bin. *B*, Average of every individual normalized radial receiver function with the application of the resonance-removal filter (blue) and average of every individual normalized raw radial receiver function (red). *C*, Radial component of raw PRFs, plotted against back azimuth, normalized as in *A*. Ps, 3p1s, and 2p2s arrival times predicted for the preferred Moho depth are shown, assuming a ray parameter of 0.06 s/km.

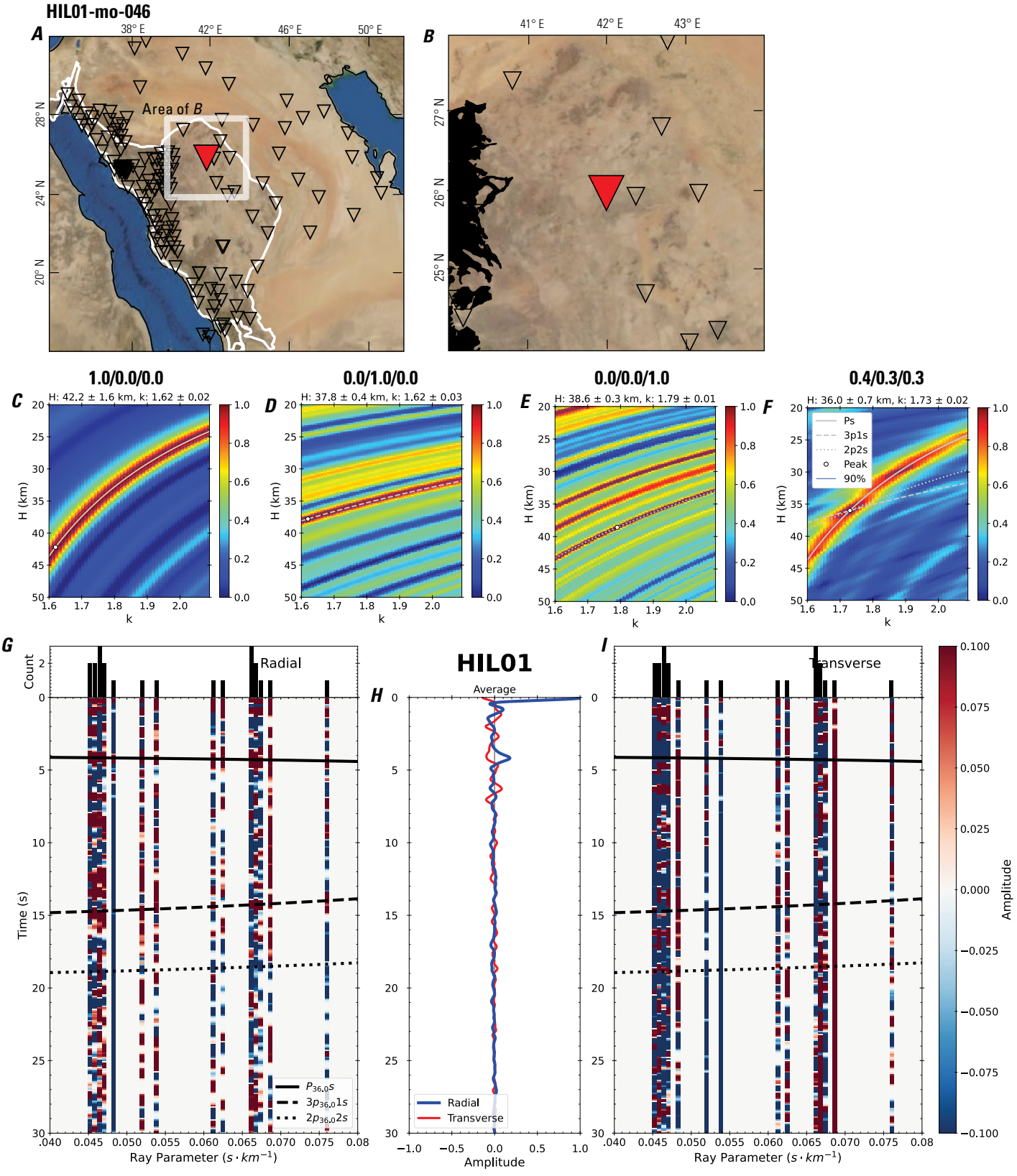
HIL01-mo-046
A
38° E
42° E
46° E
50° E
28° N
24° N
20° N
Area of B
B
41° E
42° E
43° E
27° N
26° N
25° N
1.0/0.0/0.0
C
H: 42.2 ± 1.6 km, k: 1.62 ± 0.02
0.0/1.0/0.0
D
H: 37.8 ± 0.4 km, k: 1.62 ± 0.03
0.0/0.0/1.0
E
H: 38.6 ± 0.3 km, k: 1.79 ± 0.01
0.4/0.3/0.3
F
H: 36.0 ± 0.7 km, k: 1.73 ± 0.02
Ps
3p1s
2p2s
Peak
90%
H (km)
k
G
Radial
Count
Time (s)
$P_{36.0}s$
$3p_{36.0}1s$
$2p_{36.0}2s$
Ray Parameter ($s \cdot km^{-1}$)
HIL01
H
Average
Radial
Transverse
Amplitude
I
Transverse
Amplitude

Figure 96 (page 102). Receiver-function analysis for station HIL01. *A*, Regional map of Saudi Arabia showing the entire array (as inverted triangles), the location of station HIL01 (red inverted triangle), the shield-platform boundary (white line), and the bounds of the map in *B* (white box). *B*, Local map of station HIL01. Harrats are shown in black. *C*, Standard, single-layer *H-k* stack with stacking weights 0.4/0.3/0.3. This *H-k* stack ignores sedimentary effects on the receiver functions. *D*, Standard, single-layer *H-k* stack with stacking weights 0.5/0.5/0.0. This *H-k* stack also ignores sedimentary effects on the receiver functions. *E*, Optimized sub-sedimentary *H-k* stack with stacking weights 0.4/0.3/0.3, following the method of Yu and others (2015). *F*, Optimized sedimentary *H-k* stack with stacking weights 0.05/0.70/0.25, following the method of Yu and others (2015). *G*, Radial component P-wave receiver functions (PRFs) plotted against ray parameter. Individual PRFs have had the resonance-removal filter of Yu and others (2015) applied to them and are normalized to the maximum amplitude within the time window shown, binned, and normalized by the number of traces per bin. *H*, Average of every individual normalized radial receiver function with the application of the resonance-removal filter (blue) and average of every individual normalized raw radial receiver function (red). *I*, Radial component of raw PRFs (that is, PRFs with no resonance-removal filter applied) plotted against ray parameter, normalized as in *G*.

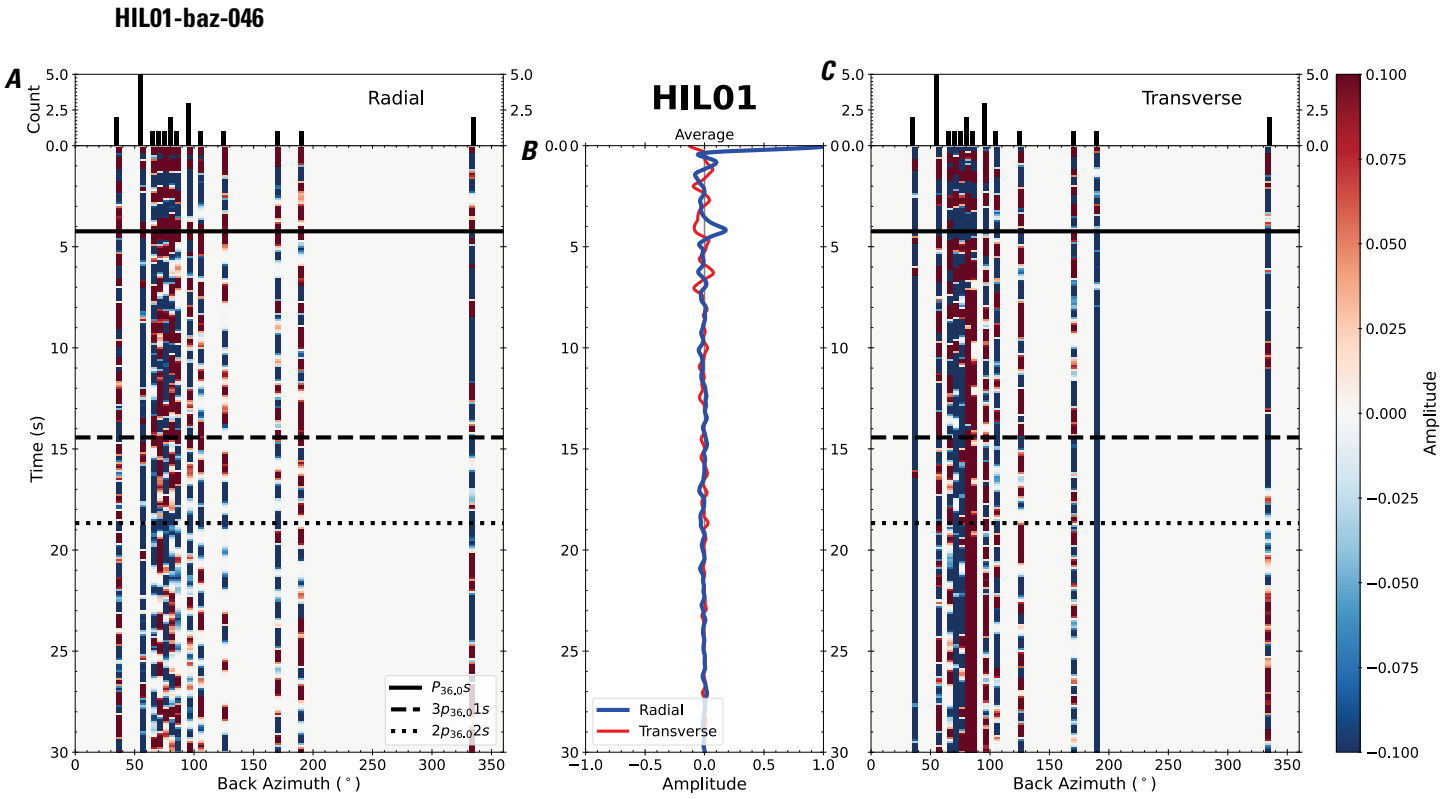

Figure 97. Receiver functions plotted against back azimuth for station HIL01. *A*, Radial component of P-wave receiver functions (PRFs) plotted against back azimuth. Individual PRFs have had the resonance-removal filter of Yu and others (2015) applied to them, are normalized to the maximum amplitude within the time window shown, binned, and normalized by the number of traces per bin. *B*, Average of every individual normalized radial receiver function with the application of the resonance-removal filter (blue) and average of every individual normalized raw radial receiver function (red). *C*, Radial component of raw PRFs, plotted against back azimuth, normalized as in *A*. Ps, 3p1s, and 2p2s arrival times predicted for the preferred Moho depth are shown, assuming a ray parameter of 0.06 s/km.

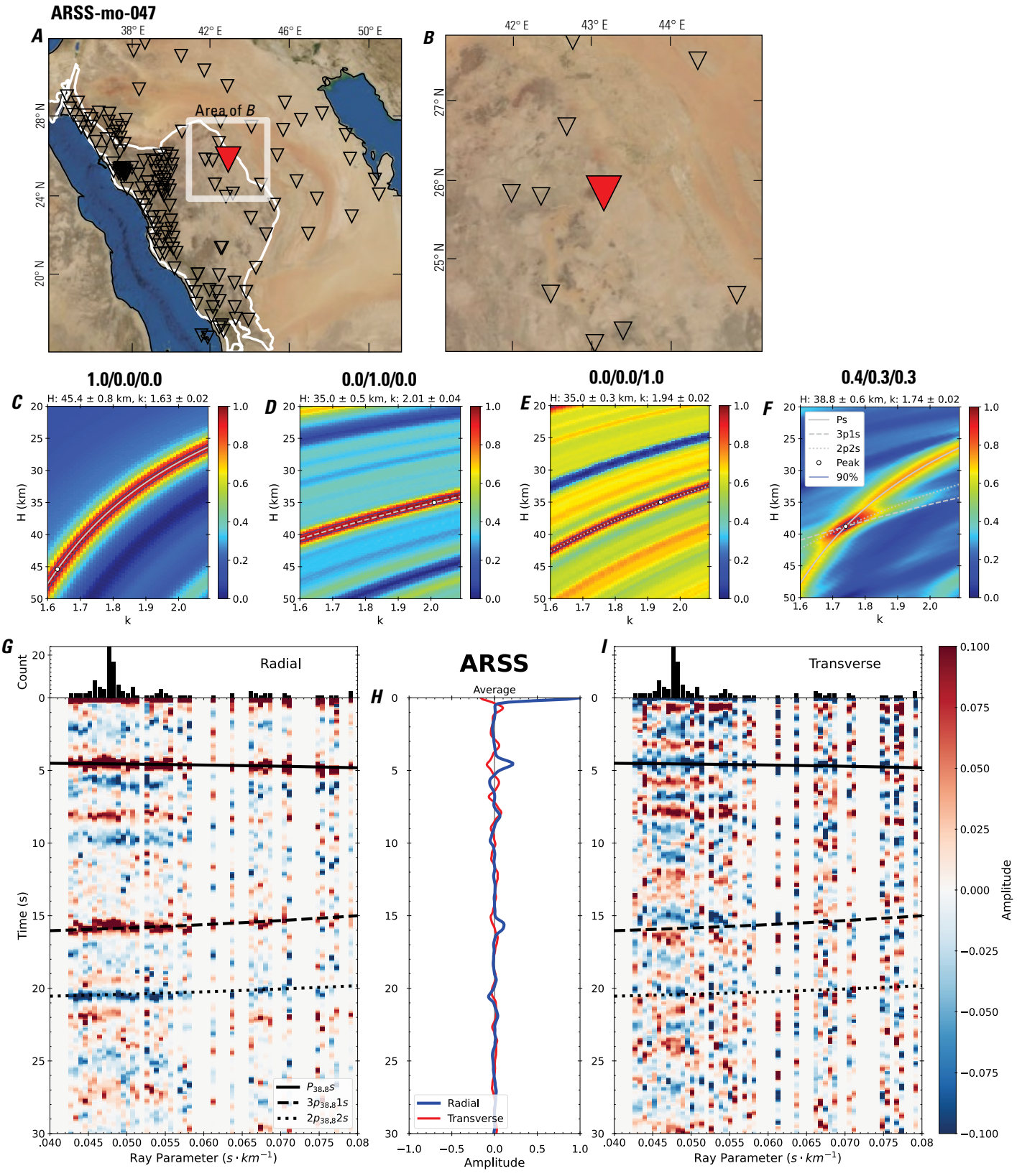
ARSS-mo-047
A
38° E
42° E
46° E
50° E
28° N
24° N
20° N
Area of B
B
42° E
43° E
44° E
27° N
26° N
25° N
1.0/0.0/0.0
0.0/1.0/0.0
0.0/0.0/1.0
0.4/0.3/0.3
C
H: 45.4 ± 0.8 km, k: 1.63 ± 0.02
D
H: 35.0 ± 0.5 km, k: 2.01 ± 0.04
E
H: 35.0 ± 0.3 km, k: 1.94 ± 0.02
F
H: 38.8 ± 0.6 km, k: 1.74 ± 0.02
Ps
3p1s
2p2s
Peak
90%
H (km)
k
G
Radial
Count
Time (s)
$P_{38.8}s$
$3p_{38.8}1s$
$2p_{38.8}2s$
Ray Parameter ($s \cdot km^{-1}$)
H
ARSS
Average
Radial
Transverse
Amplitude
I
Transverse
Amplitude

Figure 98 (page 104). Receiver-function analysis for station ARSS. *A*, Regional map of Saudi Arabia showing the entire array (as inverted triangles), the location of station ARSS (red inverted triangle), the shield-platform boundary (white line), and the bounds of the map in *B* (white box). *B*, Local map of station ARSS. Harrats are shown in black. *C*, Standard, single-layer *H-k* stack with stacking weights 0.4/0.3/0.3. This *H-k* stack ignores sedimentary effects on the receiver functions. *D*, Standard, single-layer *H-k* stack with stacking weights 0.5/0.5/0.0. This *H-k* stack also ignores sedimentary effects on the receiver functions. *E*, Optimized sub-sedimentary *H-k* stack with stacking weights 0.4/0.3/0.3, following the method of Yu and others (2015). *F*, Optimized sedimentary *H-k* stack with stacking weights 0.05/0.70/0.25, following the method of Yu and others (2015). *G*, Radial component P-wave receiver functions (PRFs) plotted against ray parameter. Individual PRFs have had the resonance-removal filter of Yu and others (2015) applied to them and are normalized to the maximum amplitude within the time window shown, binned, and normalized by the number of traces per bin. *H*, Average of every individual normalized radial receiver function with the application of the resonance-removal filter (blue) and average of every individual normalized raw radial receiver function (red). *I*, Radial component of raw PRFs (that is, PRFs with no resonance-removal filter applied) plotted against ray parameter, normalized as in *G*.

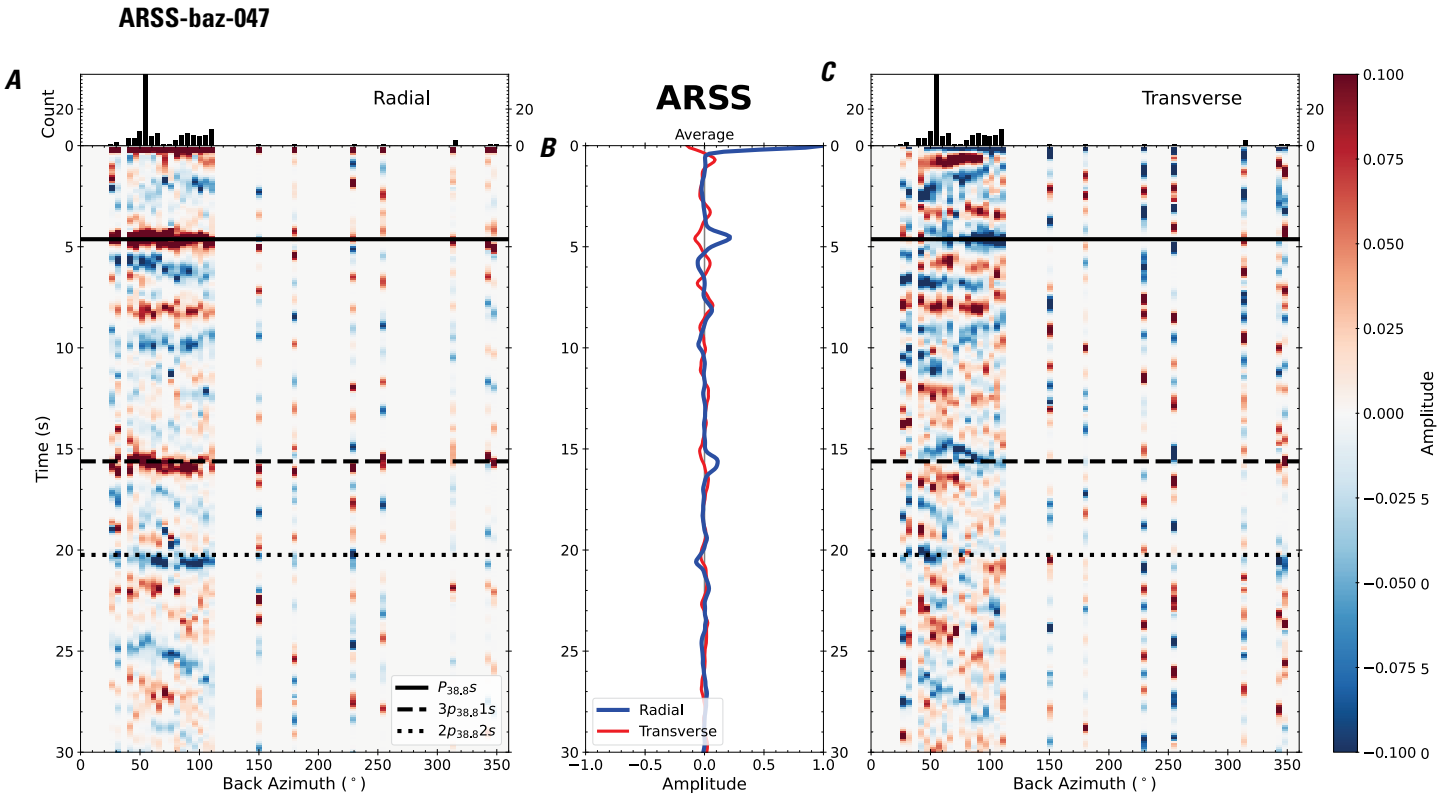

Figure 99. Receiver functions plotted against back azimuth for station ARSS. *A*, Radial component of P-wave receiver functions (PRFs) plotted against back azimuth. Individual PRFs have had the resonance-removal filter of Yu and others (2015) applied to them, are normalized to the maximum amplitude within the time window shown, binned, and normalized by the number of traces per bin. *B*, Average of every individual normalized radial receiver function with the application of the resonance-removal filter (blue) and average of every individual normalized raw radial receiver function (red). *C*, Radial component of raw PRFs, plotted against back azimuth, normalized as in *A*. Ps, 3p1s, and 2p2s arrival times predicted for the preferred Moho depth are shown, assuming a ray parameter of 0.06 s/km.

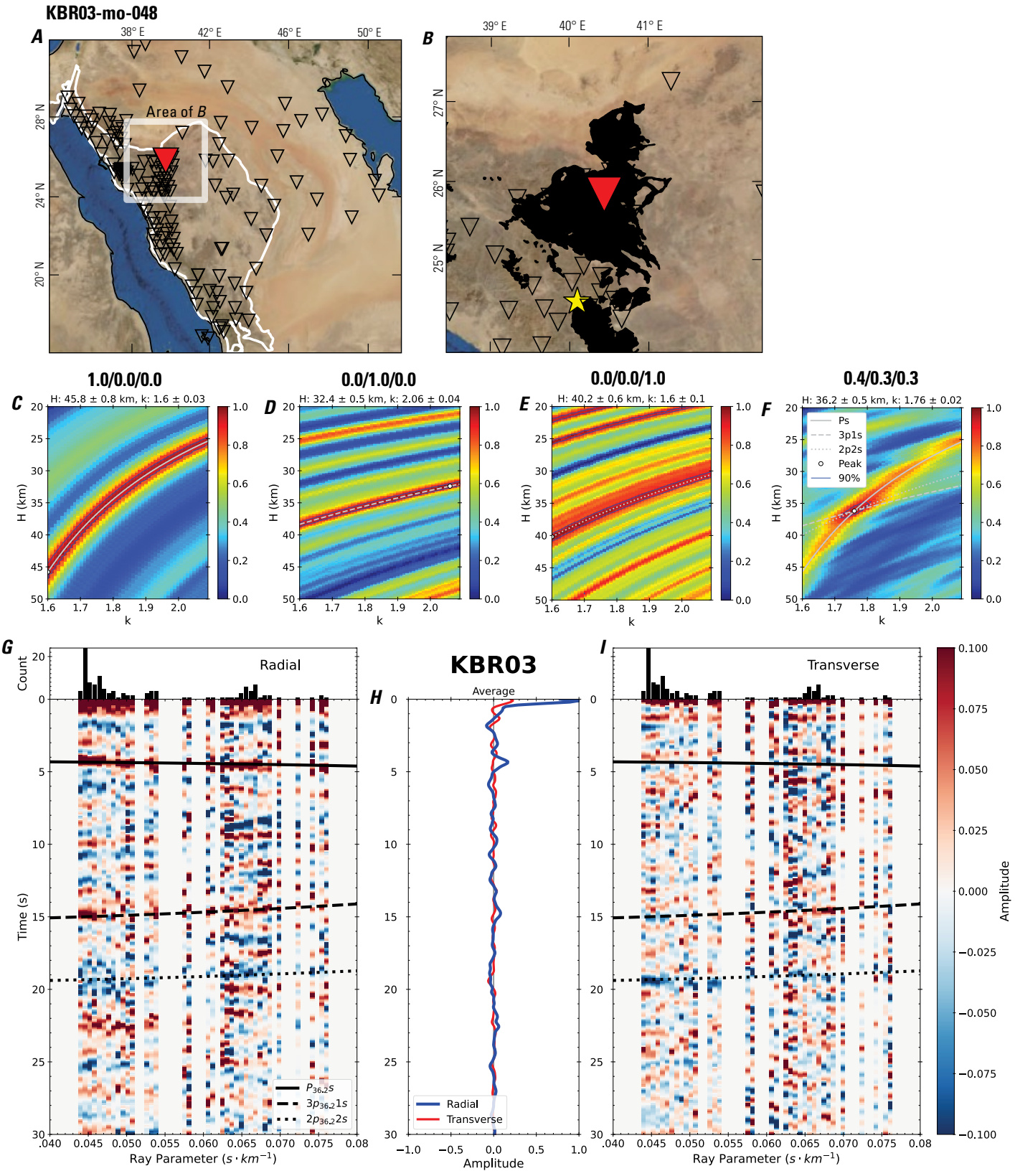
KBR03-mo-048
A
38° E
42° E
46° E
50° E
28° N
24° N
20° N
Area of B
B
39° E
40° E
41° E
27° N
26° N
25° N
1.0/0.0/0.0
0.0/1.0/0.0
0.0/0.0/1.0
0.4/0.3/0.3
C
H: 45.8 ± 0.8 km, k: 1.6 ± 0.03
D
H: 32.4 ± 0.5 km, k: 2.06 ± 0.04
E
H: 40.2 ± 0.6 km, k: 1.6 ± 0.1
F
H: 36.2 ± 0.5 km, k: 1.76 ± 0.02
H (km)
k
Ps
3p1s
2p2s
Peak
90%
G
Radial
Count
Time (s)
Ray Parameter (s · km⁻¹)
P36.2s
3p36.21s
2p36.22s
KBR03
Average
H
Radial
Transverse
Amplitude
I
Transverse
Amplitude

Figure 100 (page 106). Receiver-function analysis for station KBR03. *A*, Regional map of Saudi Arabia showing the entire array (as inverted triangles), the location of station KBR03 (red inverted triangle), the shield-platform boundary (white line), and the bounds of the map in *B* (white box). *B*, Local map of station KBR03. Harrats are shown in black. *C*, Standard, single-layer *H-k* stack with stacking weights 0.4/0.3/0.3. This *H-k* stack ignores sedimentary effects on the receiver functions. *D*, Standard, single-layer *H-k* stack with stacking weights 0.5/0.5/0.0. This *H-k* stack also ignores sedimentary effects on the receiver functions. *E*, Optimized sub-sedimentary *H-k* stack with stacking weights 0.4/0.3/0.3, following the method of Yu and others (2015). *F*, Optimized sedimentary *H-k* stack with stacking weights 0.05/0.70/0.25, following the method of Yu and others (2015). *G*, Radial component P-wave receiver functions (PRFs) plotted against ray parameter. Individual PRFs have had the resonance-removal filter of Yu and others (2015) applied to them and are normalized to the maximum amplitude within the time window shown, binned, and normalized by the number of traces per bin. *H*, Average of every individual normalized radial receiver function with the application of the resonance-removal filter (blue) and average of every individual normalized raw radial receiver function (red). *I*, Radial component of raw PRFs (that is, PRFs with no resonance-removal filter applied) plotted against ray parameter, normalized as in *G*.

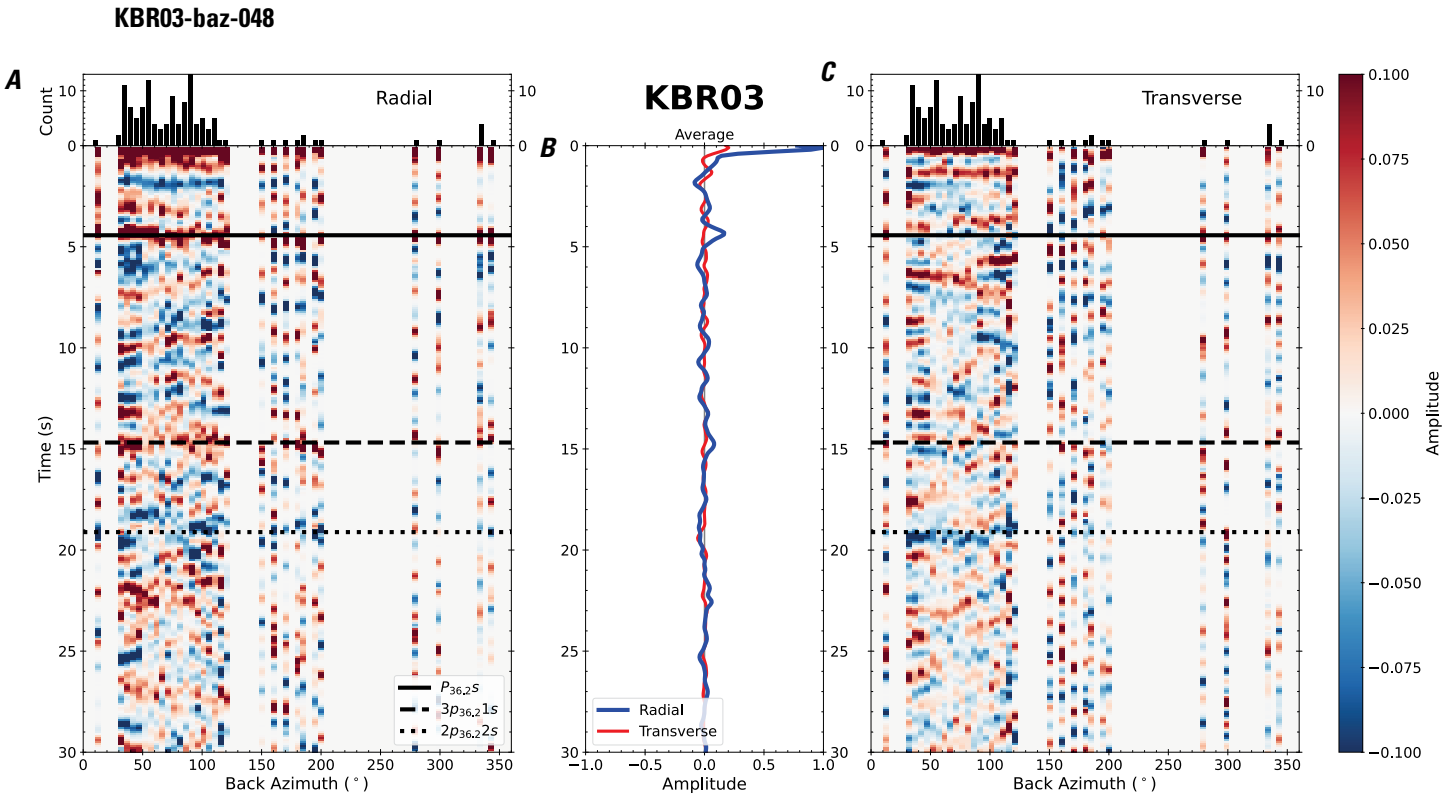

Figure 101. Receiver functions plotted against back azimuth for station KBR03. *A*, Radial component of P-wave receiver functions (PRFs) plotted against back azimuth. Individual PRFs have had the resonance-removal filter of Yu and others (2015) applied to them, are normalized to the maximum amplitude within the time window shown, binned, and normalized by the number of traces per bin. *B*, Average of every individual normalized radial receiver function with the application of the resonance-removal filter (blue) and average of every individual normalized raw radial receiver function (red). *C*, Radial component of raw PRFs, plotted against back azimuth, normalized as in *A*. Ps, 3p1s, and 2p2s arrival times predicted for the preferred Moho depth are shown, assuming a ray parameter of 0.06 s/km.

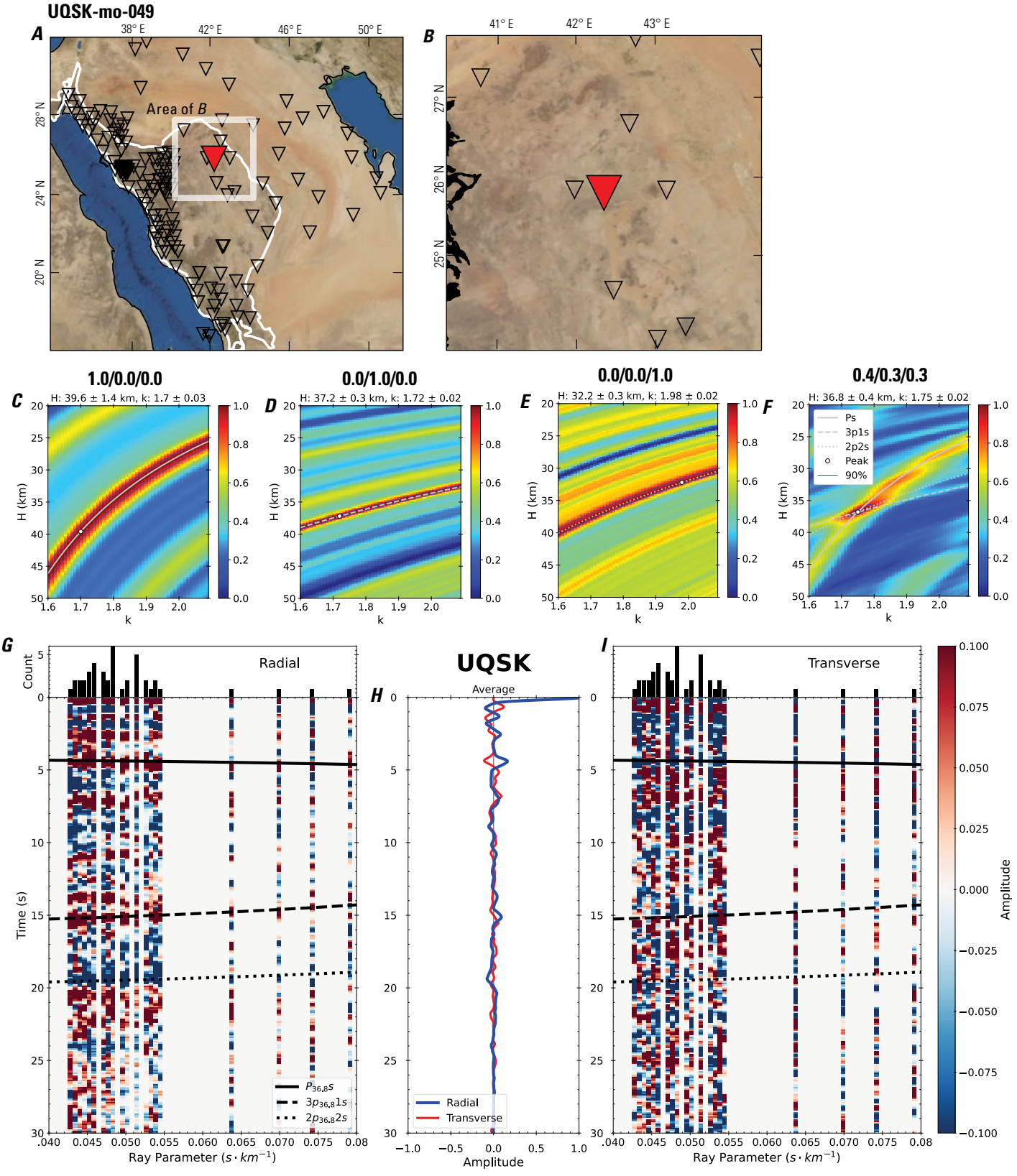
UQSK-mo-049
A
38° E
42° E
46° E
50° E
28° N
24° N
20° N
Area of B
B
41° E
42° E
43° E
27° N
26° N
25° N
C
1.0/0.0/0.0
H: 39.6 ± 1.4 km, k: 1.7 ± 0.03
D
0.0/1.0/0.0
H: 37.2 ± 0.3 km, k: 1.72 ± 0.02
E
0.0/0.0/1.0
H: 32.2 ± 0.3 km, k: 1.98 ± 0.02
F
0.4/0.3/0.3
H: 36.8 ± 0.4 km, k: 1.75 ± 0.02
Ps
3p1s
2p2s
Peak
90%
H (km)
k
G
Radial
Count
Time (s)
$P_{36.8}s$
$3p_{36.8}1s$
$2p_{36.8}2s$
Ray Parameter ($s \cdot km^{-1}$)
UQSK
H
Average
Radial
Transverse
Amplitude
I
Transverse
Amplitude

Figure 102 (page 108). Receiver-function analysis for station UQSK. *A*, Regional map of Saudi Arabia showing the entire array (as inverted triangles), the location of station UQSK (red inverted triangle), the shield-platform boundary (white line), and the bounds of the map in *B* (white box). *B*, Local map of station UQSK. Harrats are shown in black. *C*, Standard, single-layer *H-k* stack with stacking weights 0.4/0.3/0.3. This *H-k* stack ignores sedimentary effects on the receiver functions. *D*, Standard, single-layer *H-k* stack with stacking weights 0.5/0.5/0.0. This *H-k* stack also ignores sedimentary effects on the receiver functions. *E*, Optimized sub-sedimentary *H-k* stack with stacking weights 0.4/0.3/0.3, following the method of Yu and others (2015). *F*, Optimized sedimentary *H-k* stack with stacking weights 0.05/0.70/0.25, following the method of Yu and others (2015). *G*, Radial component P-wave receiver functions (PRFs) plotted against ray parameter. Individual PRFs have had the resonance-removal filter of Yu and others (2015) applied to them and are normalized to the maximum amplitude within the time window shown, binned, and normalized by the number of traces per bin. *H*, Average of every individual normalized radial receiver function with the application of the resonance-removal filter (blue) and average of every individual normalized raw radial receiver function (red). *I*, Radial component of raw PRFs (that is, PRFs with no resonance-removal filter applied) plotted against ray parameter, normalized as in *G*.

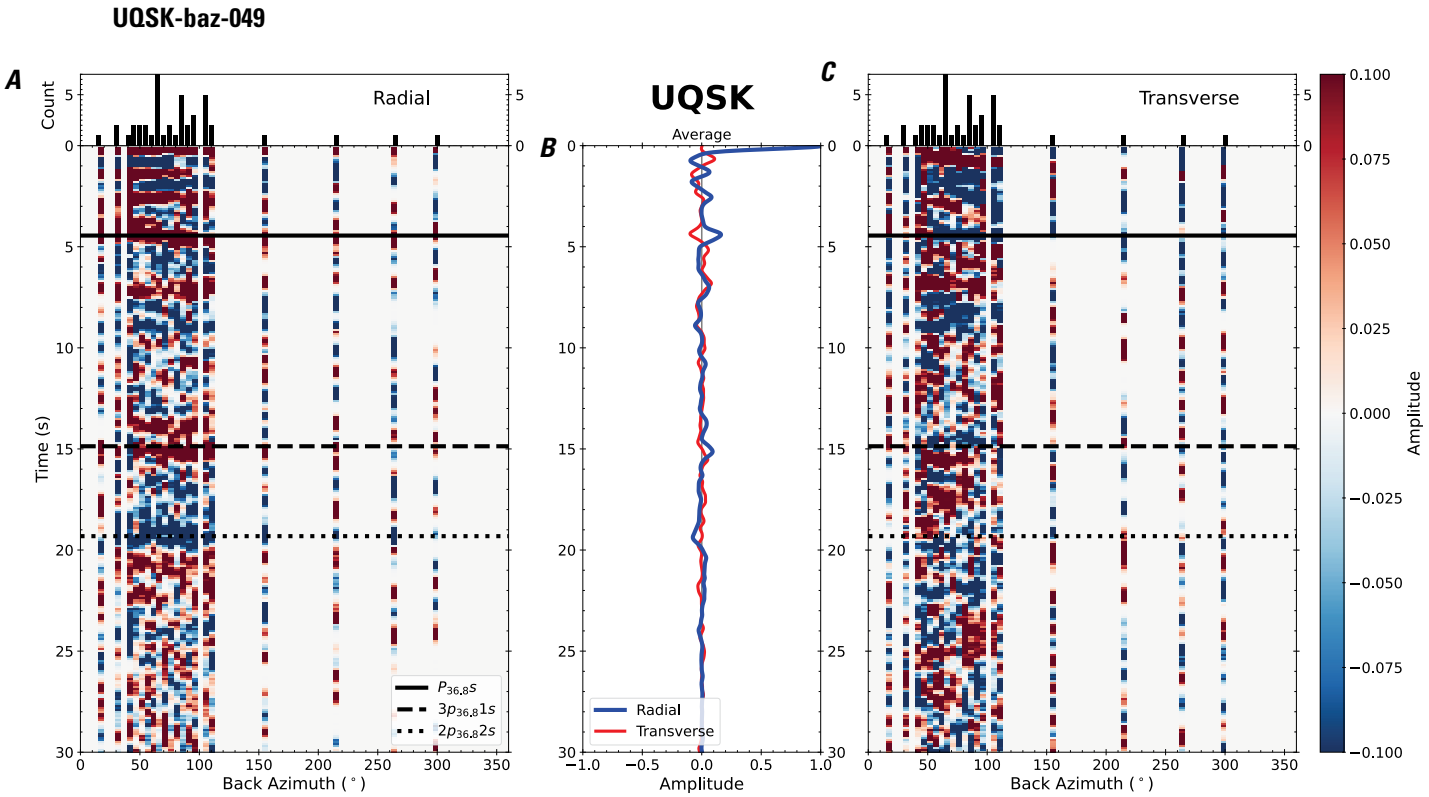

Figure 103. Receiver functions plotted against back azimuth for station UQSK. *A*, Radial component of P-wave receiver functions (PRFs) plotted against back azimuth. Individual PRFs have had the resonance-removal filter of Yu and others (2015) applied to them, are normalized to the maximum amplitude within the time window shown, binned, and normalized by the number of traces per bin. *B*, Average of every individual normalized radial receiver function with the application of the resonance-removal filter (blue) and average of every individual normalized raw radial receiver function (red). *C*, Radial component of raw PRFs, plotted against back azimuth, normalized as in *A*. Ps, 3p1s, and 2p2s arrival times predicted for the preferred Moho depth are shown, assuming a ray parameter of 0.06 s/km.

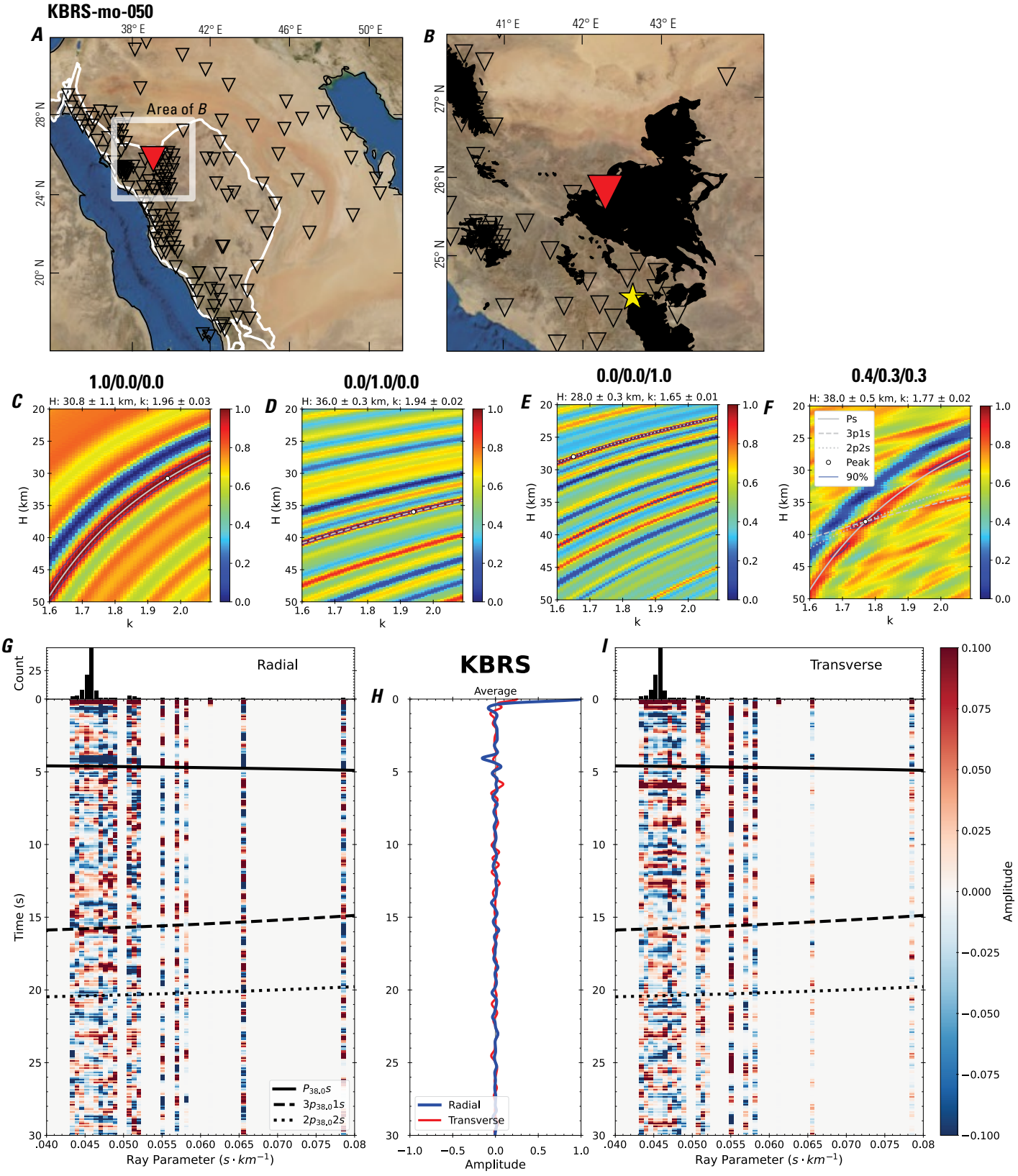
KBRS-mo-050
A
38° E
42° E
46° E
50° E
28° N
24° N
20° N
Area of B
B
41° E
42° E
43° E
27° N
26° N
25° N
C
1.0/0.0/0.0
H: 30.8 ± 1.1 km, k: 1.96 ± 0.03
D
0.0/1.0/0.0
H: 36.0 ± 0.3 km, k: 1.94 ± 0.02
E
0.0/0.0/1.0
H: 28.0 ± 0.3 km, k: 1.65 ± 0.01
F
0.4/0.3/0.3
H: 38.0 ± 0.5 km, k: 1.77 ± 0.02
Ps
3p1s
2p2s
Peak
90%
H (km)
k
G
Radial
Count
Time (s)
Ray Parameter (s · km⁻¹)
$P_{38.0}s$
$3p_{38.0}1s$
$2p_{38.0}2s$
H
KBRS
Average
Radial
Transverse
Amplitude
I
Transverse
Amplitude

Figure 104 (page 110). Receiver-function analysis for station KBRS. *A*, Regional map of Saudi Arabia showing the entire array (as inverted triangles), the location of station KBRS (red inverted triangle), the shield-platform boundary (white line), and the bounds of the map in *B* (white box). *B*, Local map of station KBRS. Harrats are shown in black. *C*, Standard, single-layer *H-k* stack with stacking weights 0.4/0.3/0.3. This *H-k* stack ignores sedimentary effects on the receiver functions. *D*, Standard, single-layer *H-k* stack with stacking weights 0.5/0.5/0.0. This *H-k* stack also ignores sedimentary effects on the receiver functions. *E*, Optimized sub-sedimentary *H-k* stack with stacking weights 0.4/0.3/0.3, following the method of Yu and others (2015). *F*, Optimized sedimentary *H-k* stack with stacking weights 0.05/0.70/0.25, following the method of Yu and others (2015). *G*, Radial component P-wave receiver functions (PRFs) plotted against ray parameter. Individual PRFs have had the resonance-removal filter of Yu and others (2015) applied to them and are normalized to the maximum amplitude within the time window shown, binned, and normalized by the number of traces per bin. *H*, Average of every individual normalized radial receiver function with the application of the resonance-removal filter (blue) and average of every individual normalized raw radial receiver function (red). *I*, Radial component of raw PRFs (that is, PRFs with no resonance-removal filter applied) plotted against ray parameter, normalized as in *G*.

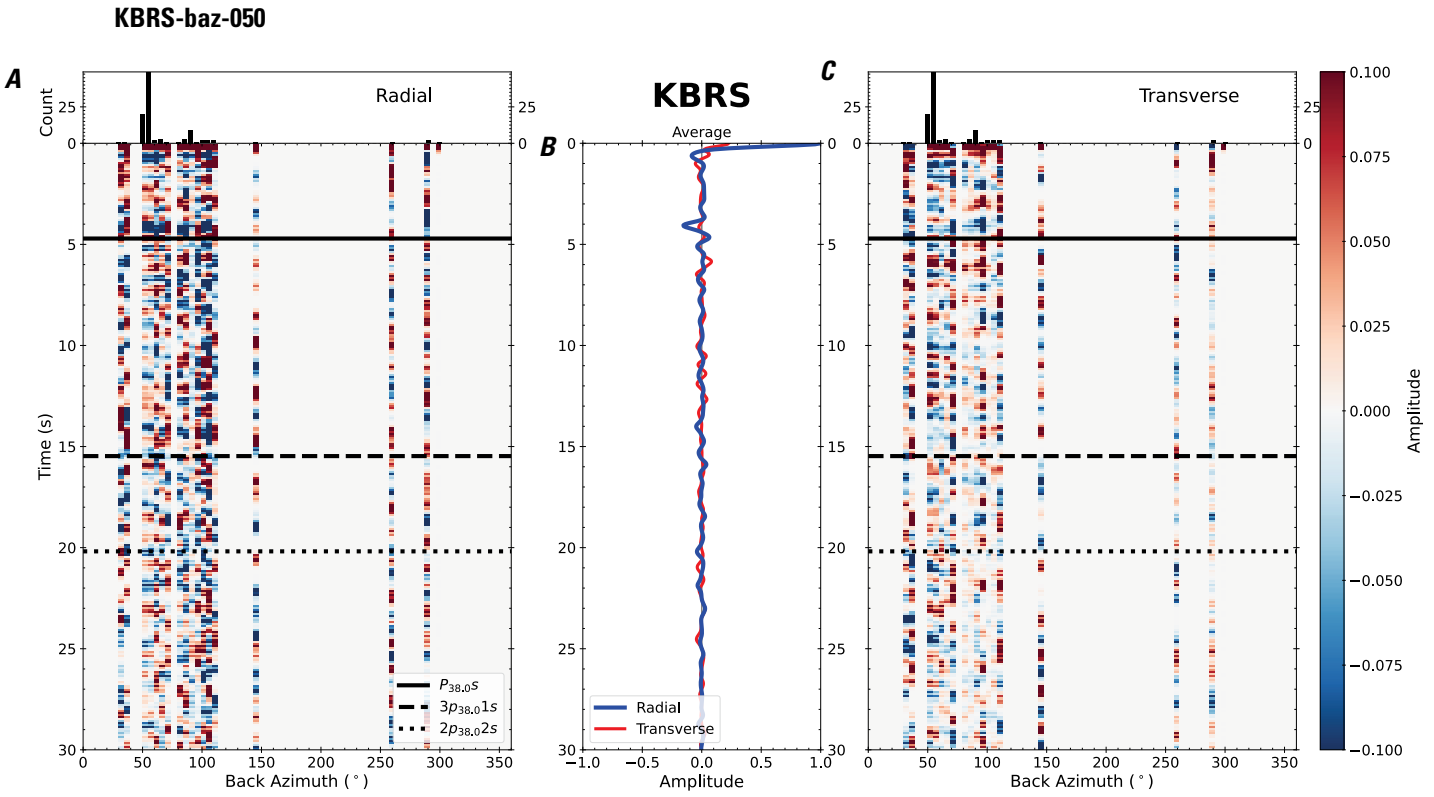

Figure 105. Receiver functions plotted against back azimuth for station KBRS. *A*, Radial component of P-wave receiver functions (PRFs) plotted against back azimuth. Individual PRFs have had the resonance-removal filter of Yu and others (2015) applied to them, are normalized to the maximum amplitude within the time window shown, binned, and normalized by the number of traces per bin. *B*, Average of every individual normalized radial receiver function with the application of the resonance-removal filter (blue) and average of every individual normalized raw radial receiver function (red). *C*, Radial component of raw PRFs, plotted against back azimuth, normalized as in *A*. Ps, 3p1s, and 2p2s arrival times predicted for the preferred Moho depth are shown, assuming a ray parameter of 0.06 s/km.

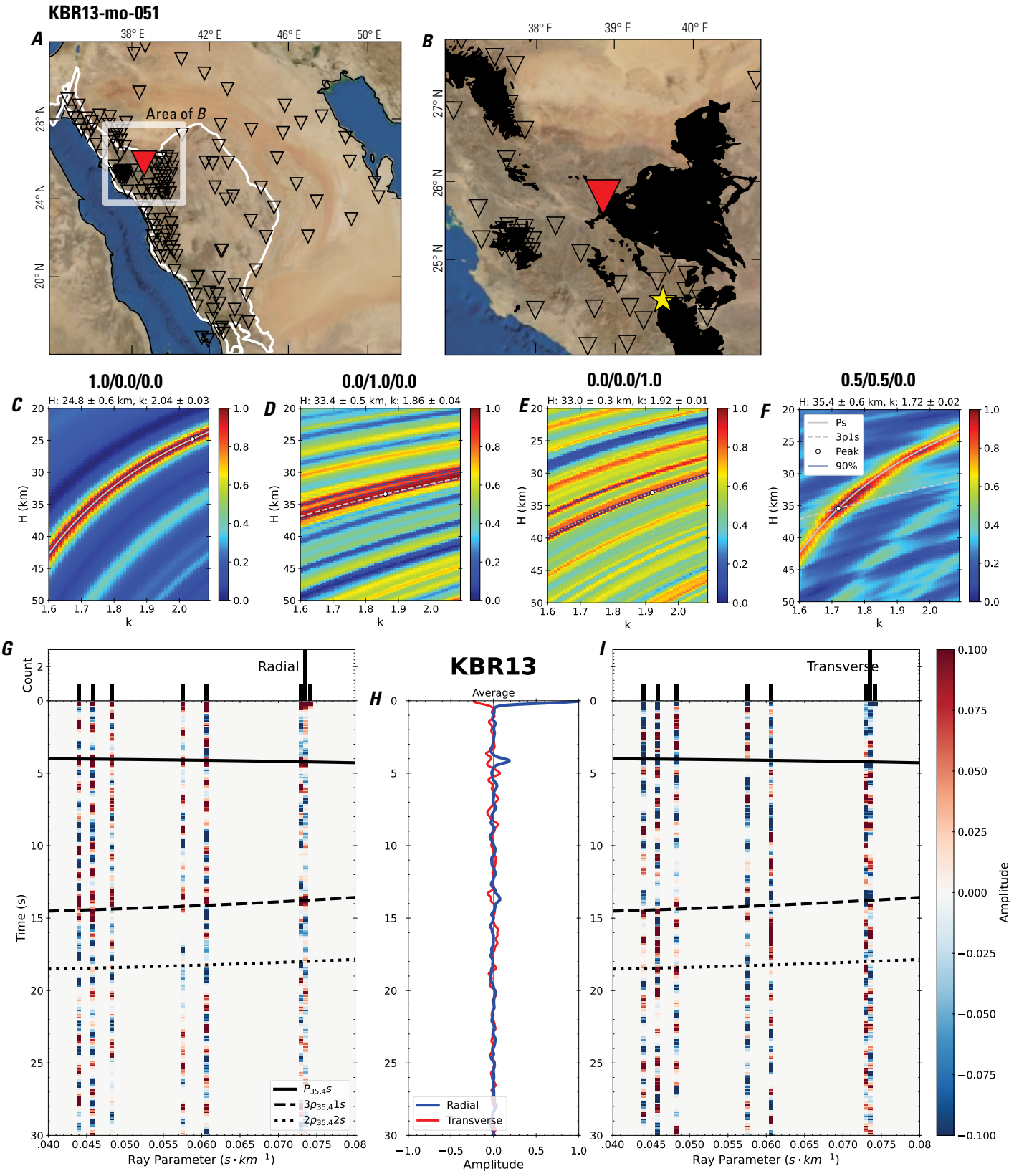
KBR13-mo-051
A
38° E
42° E
46° E
50° E
28° N
24° N
20° N
Area of B
B
38° E
39° E
40° E
27° N
26° N
25° N
1.0/0.0/0.0
0.0/1.0/0.0
0.0/0.0/1.0
0.5/0.5/0.0
C
H: 24.8 ± 0.6 km, k: 2.04 ± 0.03
D
H: 33.4 ± 0.5 km, k: 1.86 ± 0.04
E
H: 33.0 ± 0.3 km, k: 1.92 ± 0.01
F
H: 35.4 ± 0.6 km, k: 1.72 ± 0.02
Ps
3p1s
Peak
90%
H (km)
k
G
Radial
Count
Time (s)
$P_{35,4}s$
$3p_{35,4}1s$
$2p_{35,4}2s$
Ray Parameter ($s \cdot km^{-1}$)
H
KBR13
Average
Radial
Transverse
Amplitude
I
Transverse
Amplitude

Figure 106 (page 112). Receiver-function analysis for station KBR13. *A*, Regional map of Saudi Arabia showing the entire array (as inverted triangles), the location of station KBR13 (red inverted triangle), the shield-platform boundary (white line), and the bounds of the map in *B* (white box). *B*, Local map of station KBR13. Harrats are shown in black. *C*, Standard, single-layer *H-k* stack with stacking weights 0.4/0.3/0.3. This *H-k* stack ignores sedimentary effects on the receiver functions. *D*, Standard, single-layer *H-k* stack with stacking weights 0.5/0.5/0.0. This *H-k* stack also ignores sedimentary effects on the receiver functions. *E*, Optimized sub-sedimentary *H-k* stack with stacking weights 0.4/0.3/0.3, following the method of Yu and others (2015). *F*, Optimized sedimentary *H-k* stack with stacking weights 0.05/0.70/0.25, following the method of Yu and others (2015). *G*, Radial component P-wave receiver functions (PRFs) plotted against ray parameter. Individual PRFs have had the resonance-removal filter of Yu and others (2015) applied to them and are normalized to the maximum amplitude within the time window shown, binned, and normalized by the number of traces per bin. *H*, Average of every individual normalized radial receiver function with the application of the resonance-removal filter (blue) and average of every individual normalized raw radial receiver function (red). *I*, Radial component of raw PRFs (that is, PRFs with no resonance-removal filter applied) plotted against ray parameter, normalized as in *G*.

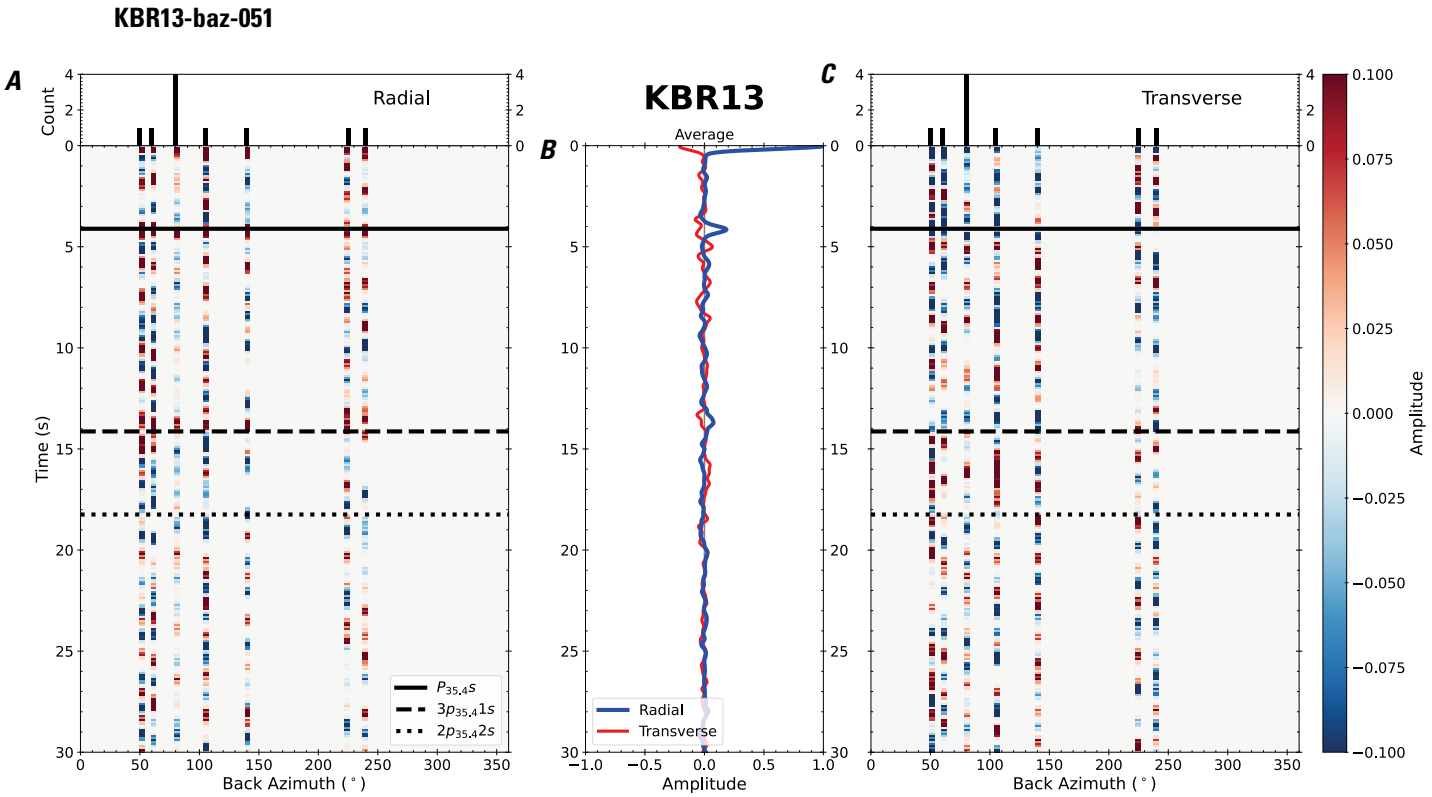

Figure 107. Receiver functions plotted against back azimuth for station KBR13. *A*, Radial component of P-wave receiver functions (PRFs) plotted against back azimuth. Individual PRFs have had the resonance-removal filter of Yu and others (2015) applied to them, are normalized to the maximum amplitude within the time window shown, binned, and normalized by the number of traces per bin. *B*, Average of every individual normalized radial receiver function with the application of the resonance-removal filter (blue) and average of every individual normalized raw radial receiver function (red). *C*, Radial component of raw PRFs, plotted against back azimuth, normalized as in *A*. Ps, 3p1s, and 2p2s arrival times predicted for the preferred Moho depth are shown, assuming a ray parameter of 0.06 s/km.

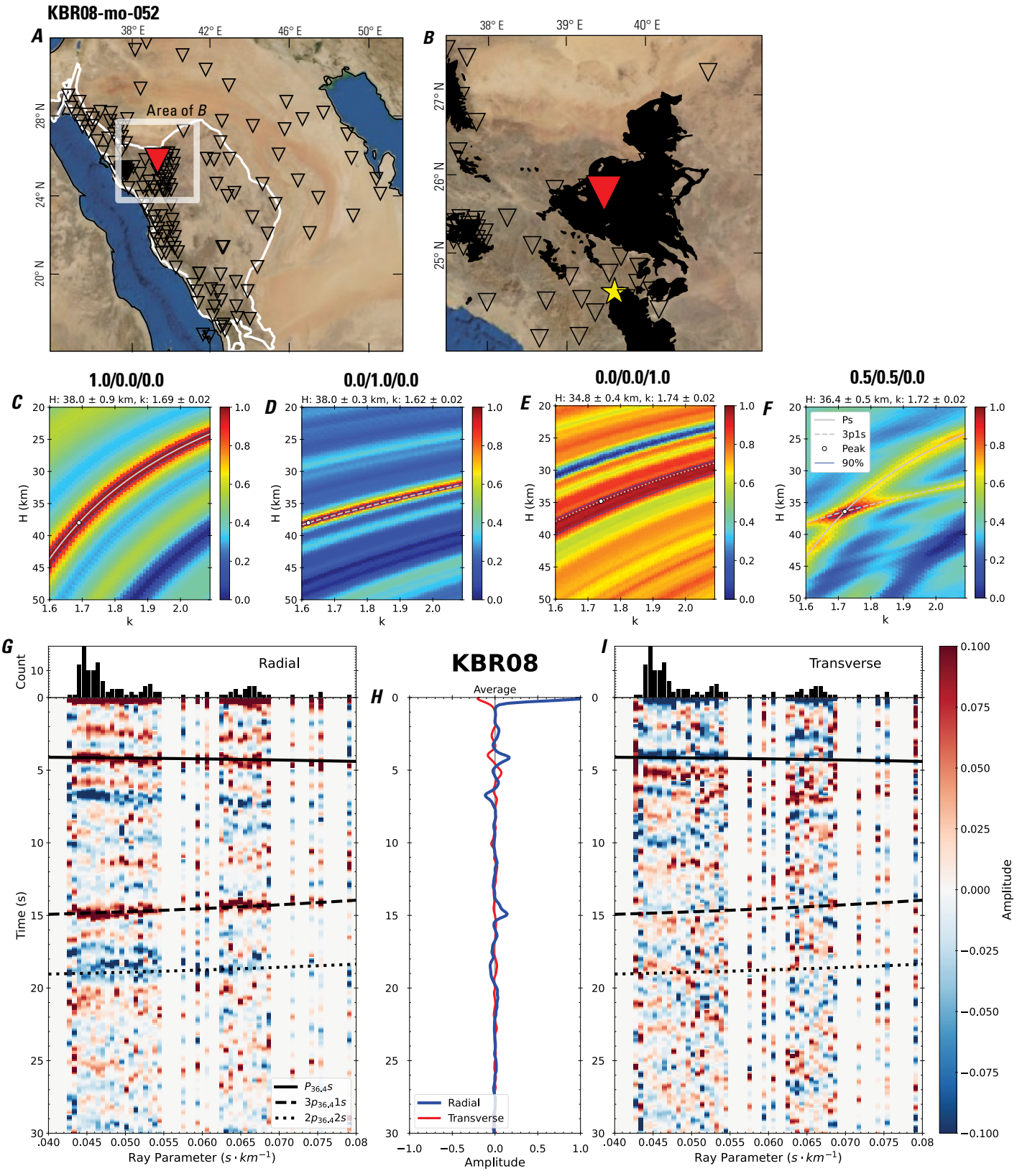
KBR08-mo-052
A
B
Area of B
1.0/0.0/0.0
0.0/1.0/0.0
0.0/0.0/1.0
0.5/0.5/0.0
C
D
E
F
H: 38.0 ± 0.9 km, k: 1.69 ± 0.02
H: 38.0 ± 0.3 km, k: 1.62 ± 0.02
H: 34.8 ± 0.4 km, k: 1.74 ± 0.02
H: 36.4 ± 0.5 km, k: 1.72 ± 0.02
H (km)
k
Ps
3p1s
Peak
90%
G
H
I
KBR08
Radial
Transverse
Average
Count
Time (s)
Ray Parameter (s · km⁻¹)
Amplitude
$P_{36.4}s$
$3p_{36.4}1s$
$2p_{36.4}2s$

Figure 108 (page 114). Receiver-function analysis for station KBR08. *A*, Regional map of Saudi Arabia showing the entire array (as inverted triangles), the location of station KBR08 (red inverted triangle), the shield-platform boundary (white line), and the bounds of the map in *B* (white box). *B*, Local map of station KBR08. Harrats are shown in black. *C*, Standard, single-layer *H-k* stack with stacking weights 0.4/0.3/0.3. This *H-k* stack ignores sedimentary effects on the receiver functions. *D*, Standard, single-layer *H-k* stack with stacking weights 0.5/0.5/0.0. This *H-k* stack also ignores sedimentary effects on the receiver functions. *E*, Optimized sub-sedimentary *H-k* stack with stacking weights 0.4/0.3/0.3, following the method of Yu and others (2015). *F*, Optimized sedimentary *H-k* stack with stacking weights 0.05/0.70/0.25, following the method of Yu and others (2015). *G*, Radial component P-wave receiver functions (PRFs) plotted against ray parameter. Individual PRFs have had the resonance-removal filter of Yu and others (2015) applied to them and are normalized to the maximum amplitude within the time window shown, binned, and normalized by the number of traces per bin. *H*, Average of every individual normalized radial receiver function with the application of the resonance-removal filter (blue) and average of every individual normalized raw radial receiver function (red). *I*, Radial component of raw PRFs (that is, PRFs with no resonance-removal filter applied) plotted against ray parameter, normalized as in *G*.

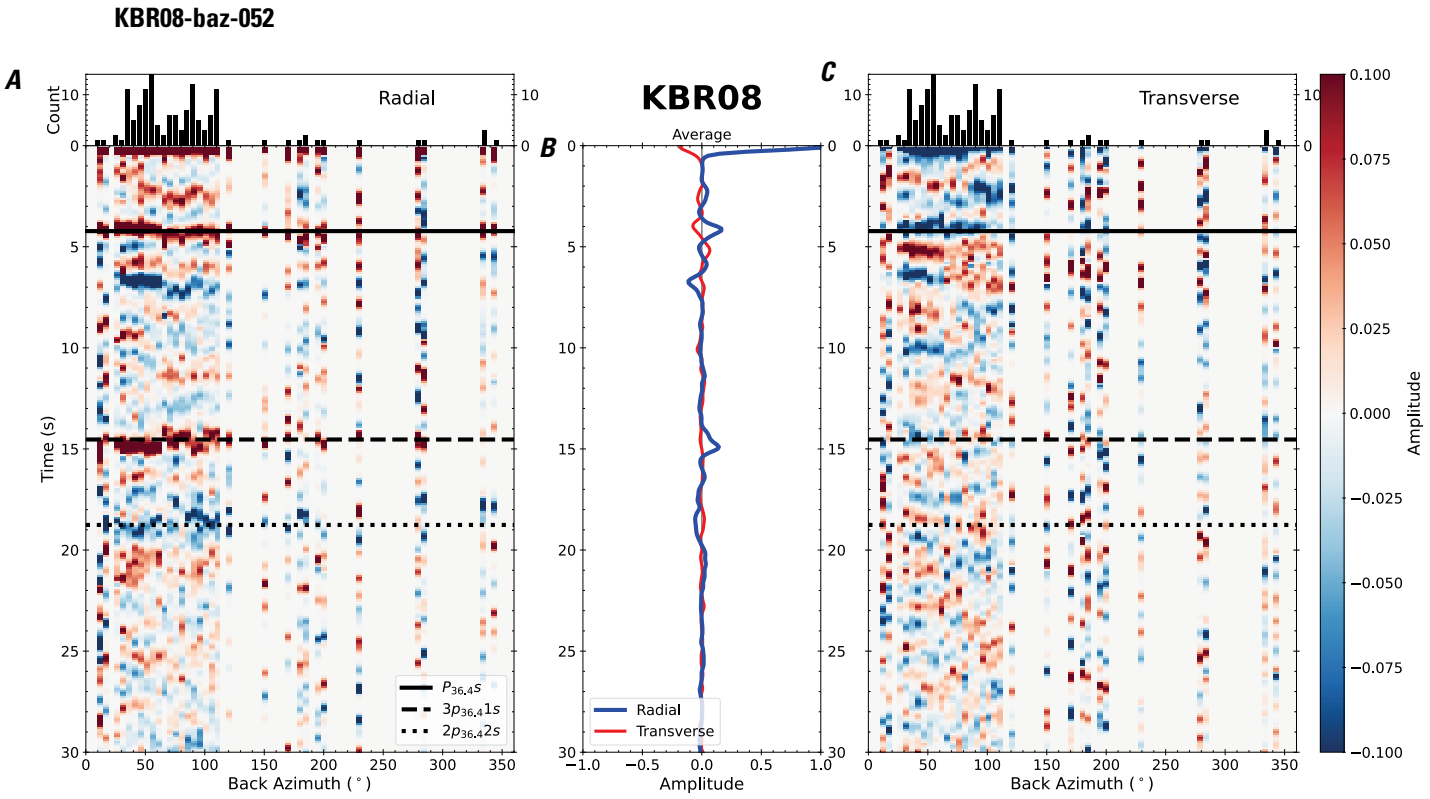

Figure 109. Receiver functions plotted against back azimuth for station KBR08. *A*, Radial component of P-wave receiver functions (PRFs) plotted against back azimuth. Individual PRFs have had the resonance-removal filter of Yu and others (2015) applied to them, are normalized to the maximum amplitude within the time window shown, binned, and normalized by the number of traces per bin. *B*, Average of every individual normalized radial receiver function with the application of the resonance-removal filter (blue) and average of every individual normalized raw radial receiver function (red). *C*, Radial component of raw PRFs, plotted against back azimuth, normalized as in *A*. Ps, 3p1s, and 2p2s arrival times predicted for the preferred Moho depth are shown, assuming a ray parameter of 0.06 s/km.

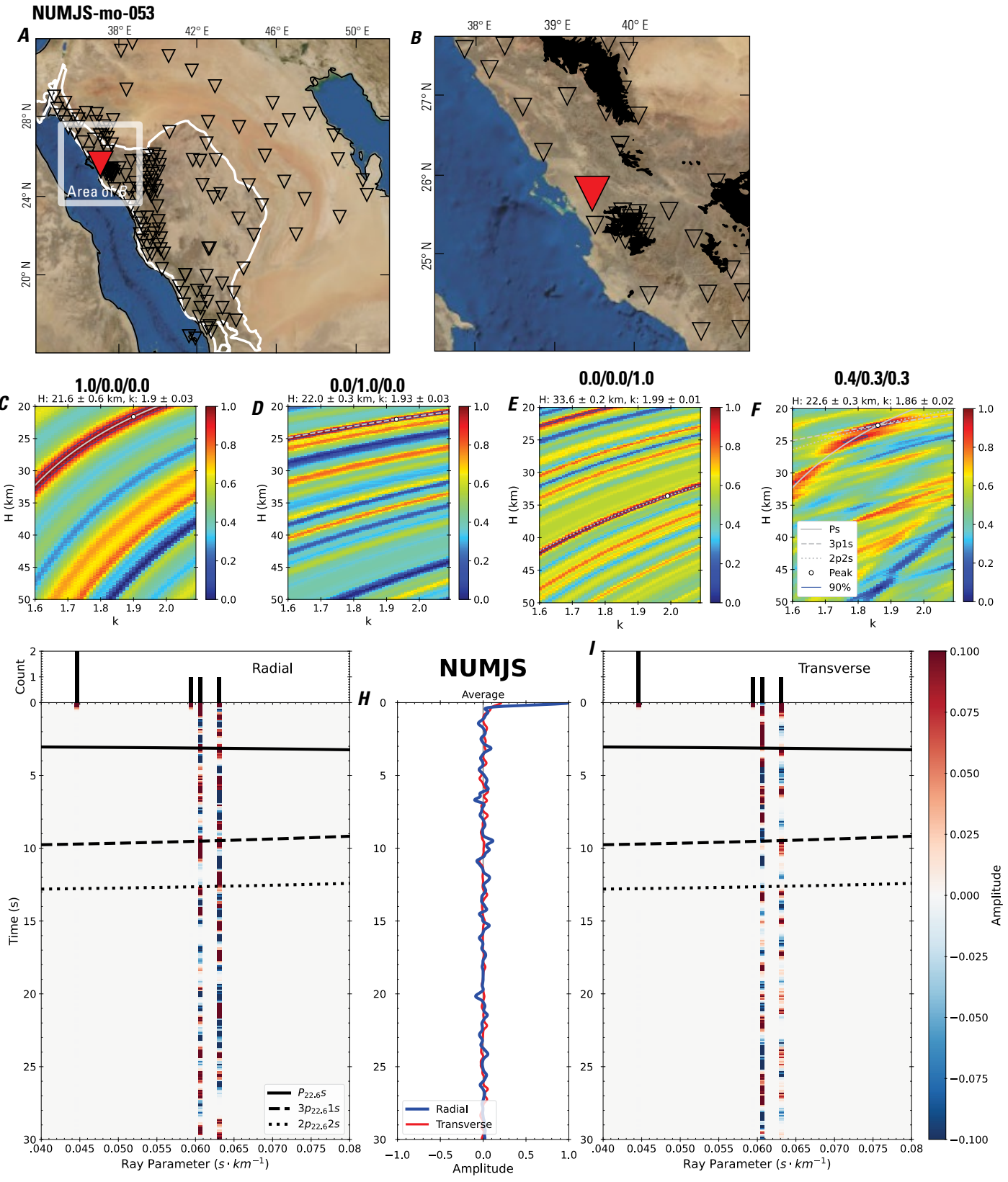
NUMJS-mo-053
A
38° E
42° E
46° E
50° E
28° N
24° N
20° N
Area of B
B
38° E
39° E
40° E
27° N
26° N
25° N
C
1.0/0.0/0.0
H: 21.6 ± 0.6 km, k: 1.9 ± 0.03
D
0.0/1.0/0.0
H: 22.0 ± 0.3 km, k: 1.93 ± 0.03
E
0.0/0.0/1.0
H: 33.6 ± 0.2 km, k: 1.99 ± 0.01
F
0.4/0.3/0.3
H: 22.6 ± 0.3 km, k: 1.86 ± 0.02
H (km)
k
Ps
3p1s
2p2s
Peak
90%
G
Radial
Count
Time (s)
Ray Parameter (s · km⁻¹)
$P_{22.6}s$
$3p_{22.6}1s$
$2p_{22.6}2s$
H
NUMJS
Average
Radial
Transverse
Amplitude
I
Transverse
Amplitude

Figure 110 (page 116). Receiver-function analysis for station NUMJS. *A*, Regional map of Saudi Arabia showing the entire array (as inverted triangles), the location of station NUMJS (red inverted triangle), the shield-platform boundary (white line), and the bounds of the map in *B* (white box). *B*, Local map of station NUMJS. Harrats are shown in black. *C*, Standard, single-layer *H-k* stack with stacking weights 0.4/0.3/0.3. This *H-k* stack ignores sedimentary effects on the receiver functions. *D*, Standard, single-layer *H-k* stack with stacking weights 0.5/0.5/0.0. This *H-k* stack also ignores sedimentary effects on the receiver functions. *E*, Optimized sub-sedimentary *H-k* stack with stacking weights 0.4/0.3/0.3, following the method of Yu and others (2015). *F*, Optimized sedimentary *H-k* stack with stacking weights 0.05/0.70/0.25, following the method of Yu and others (2015). *G*, Radial component P-wave receiver functions (PRFs) plotted against ray parameter. Individual PRFs have had the resonance-removal filter of Yu and others (2015) applied to them and are normalized to the maximum amplitude within the time window shown, binned, and normalized by the number of traces per bin. *H*, Average of every individual normalized radial receiver function with the application of the resonance-removal filter (blue) and average of every individual normalized raw radial receiver function (red). *I*, Radial component of raw PRFs (that is, PRFs with no resonance-removal filter applied) plotted against ray parameter, normalized as in *G*.

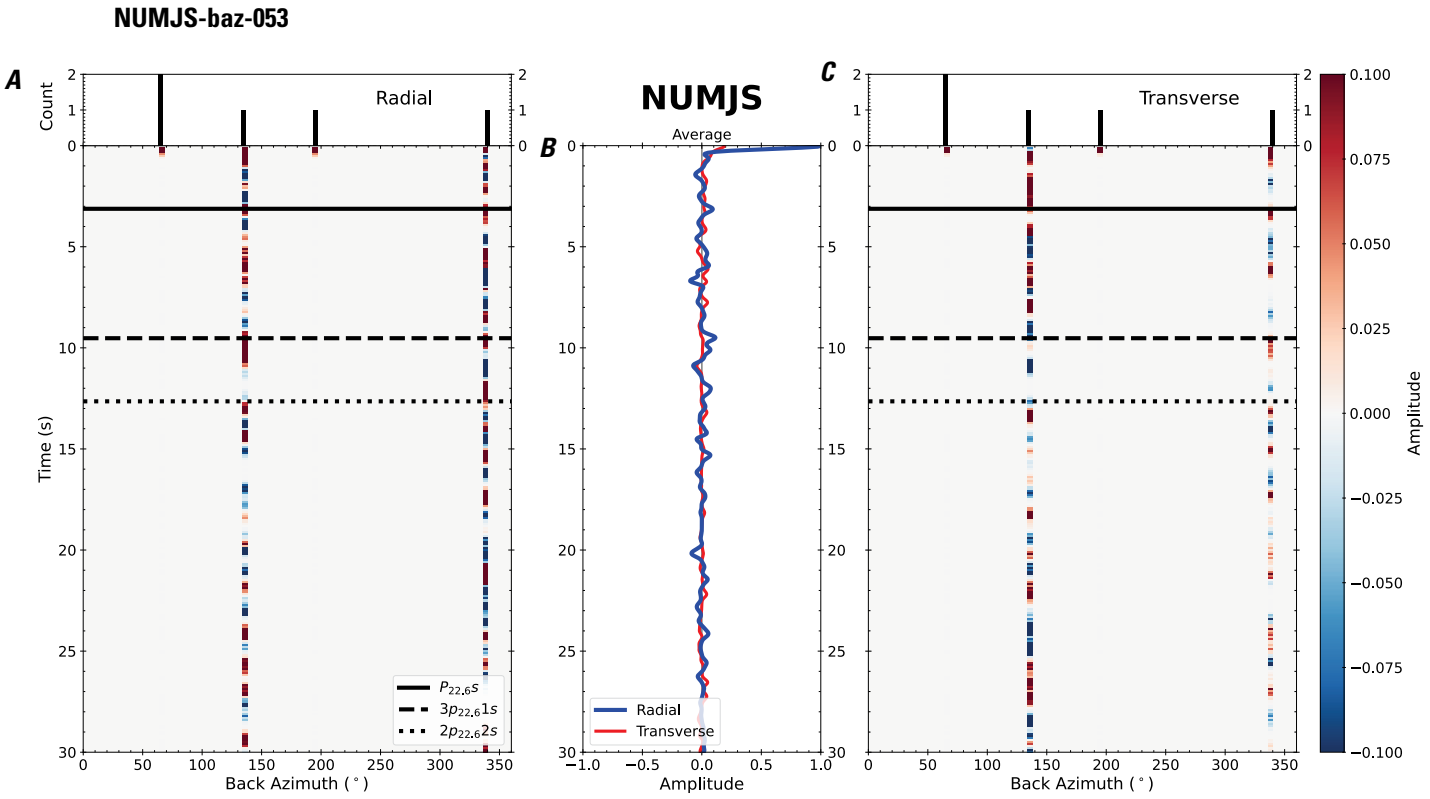

Figure 111. Receiver functions plotted against back azimuth for station NUMJS. *A*, Radial component of P-wave receiver functions (PRFs) plotted against back azimuth. Individual PRFs have had the resonance-removal filter of Yu and others (2015) applied to them, are normalized to the maximum amplitude within the time window shown, binned, and normalized by the number of traces per bin. *B*, Average of every individual normalized radial receiver function with the application of the resonance-removal filter (blue) and average of every individual normalized raw radial receiver function (red). *C*, Radial component of raw PRFs, plotted against back azimuth, normalized as in *A*. Ps, 3p1s, and 2p2s arrival times predicted for the preferred Moho depth are shown, assuming a ray parameter of 0.06 s/km.

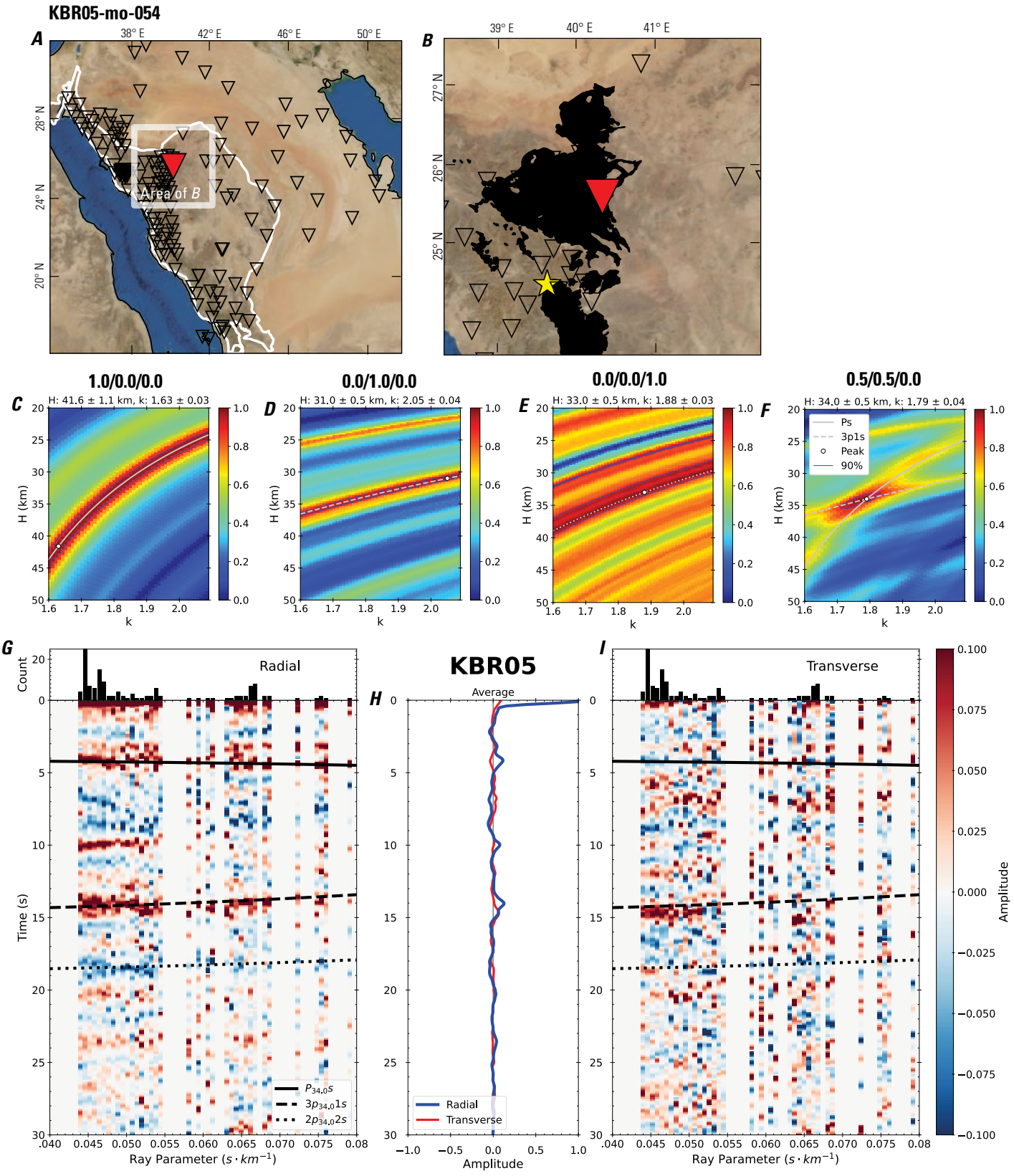
KBR05-mo-054
A
B
Area of B
1.0/0.0/0.0
0.0/1.0/0.0
0.0/0.0/1.0
0.5/0.5/0.0
C
D
E
F
H: 41.6 ± 1.1 km, k: 1.63 ± 0.03
H: 31.0 ± 0.5 km, k: 2.05 ± 0.04
H: 33.0 ± 0.5 km, k: 1.88 ± 0.03
H: 34.0 ± 0.5 km, k: 1.79 ± 0.04
H (km)
k
Ps
3p1s
Peak
90%
G
H
I
KBR05
Radial
Transverse
Average
Count
Time (s)
Ray Parameter (s · km⁻¹)
Amplitude
$P_{34.0}s$
$3p_{34.0}1s$
$2p_{34.0}2s$

Figure 112 (page 118). Receiver-function analysis for station KBR05. *A*, Regional map of Saudi Arabia showing the entire array (as inverted triangles), the location of station KBR05 (red inverted triangle), the shield-platform boundary (white line), and the bounds of the map in *B* (white box). *B*, Local map of station KBR05. Harrats are shown in black. *C*, Standard, single-layer *H-k* stack with stacking weights 0.4/0.3/0.3. This *H-k* stack ignores sedimentary effects on the receiver functions. *D*, Standard, single-layer *H-k* stack with stacking weights 0.5/0.5/0.0. This *H-k* stack also ignores sedimentary effects on the receiver functions. *E*, Optimized sub-sedimentary *H-k* stack with stacking weights 0.4/0.3/0.3, following the method of Yu and others (2015). *F*, Optimized sedimentary *H-k* stack with stacking weights 0.05/0.70/0.25, following the method of Yu and others (2015). *G*, Radial component P-wave receiver functions (PRFs) plotted against ray parameter. Individual PRFs have had the resonance-removal filter of Yu and others (2015) applied to them and are normalized to the maximum amplitude within the time window shown, binned, and normalized by the number of traces per bin. *H*, Average of every individual normalized radial receiver function with the application of the resonance-removal filter (blue) and average of every individual normalized raw radial receiver function (red). *I*, Radial component of raw PRFs (that is, PRFs with no resonance-removal filter applied) plotted against ray parameter, normalized as in *G*.

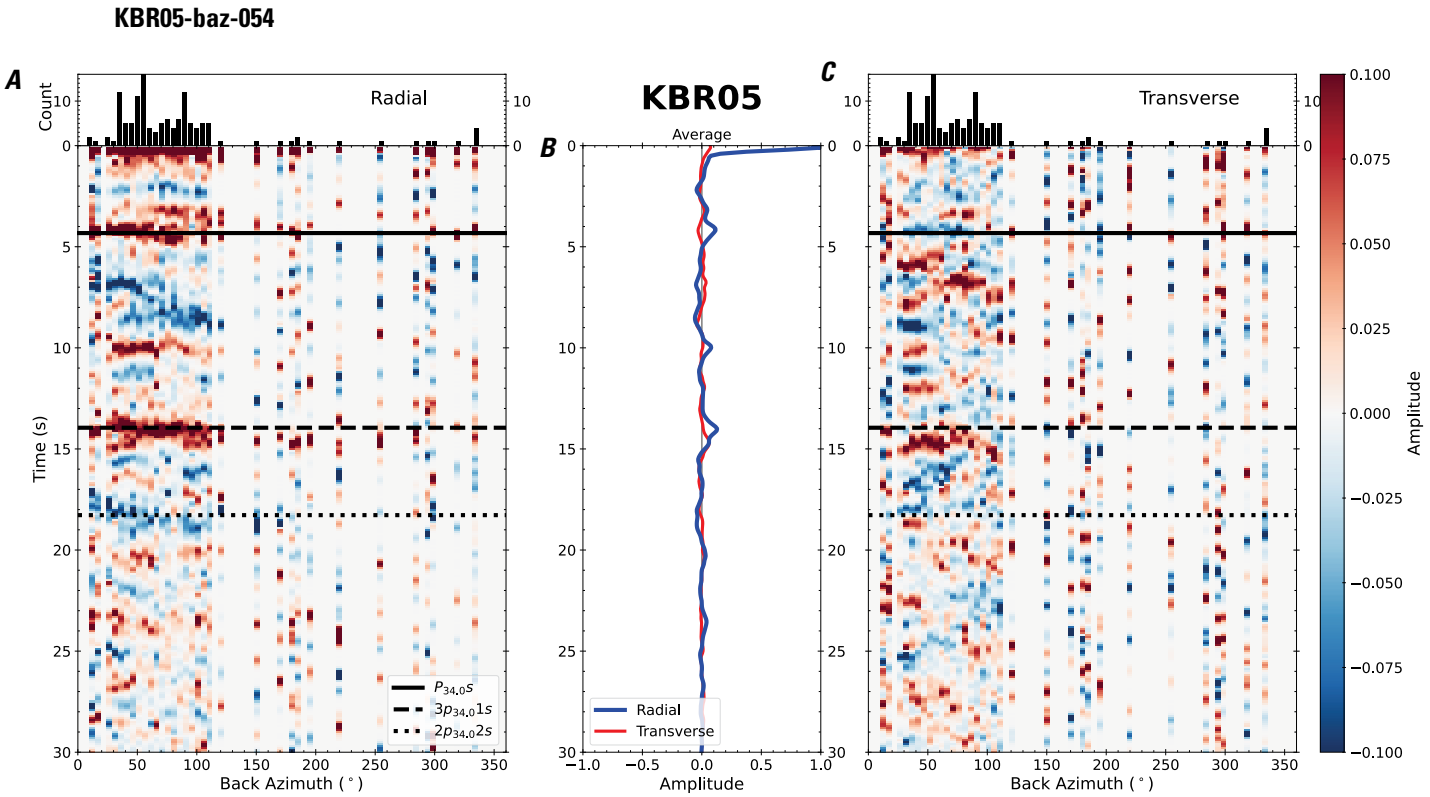

Figure 113. Receiver functions plotted against back azimuth for station KBR05. *A*, Radial component of P-wave receiver functions (PRFs) plotted against back azimuth. Individual PRFs have had the resonance-removal filter of Yu and others (2015) applied to them, are normalized to the maximum amplitude within the time window shown, binned, and normalized by the number of traces per bin. *B*, Average of every individual normalized radial receiver function with the application of the resonance-removal filter (blue) and average of every individual normalized raw radial receiver function (red). *C*, Radial component of raw PRFs, plotted against back azimuth, normalized as in *A*. Ps, 3p1s, and 2p2s arrival times predicted for the preferred Moho depth are shown, assuming a ray parameter of 0.06 s/km.

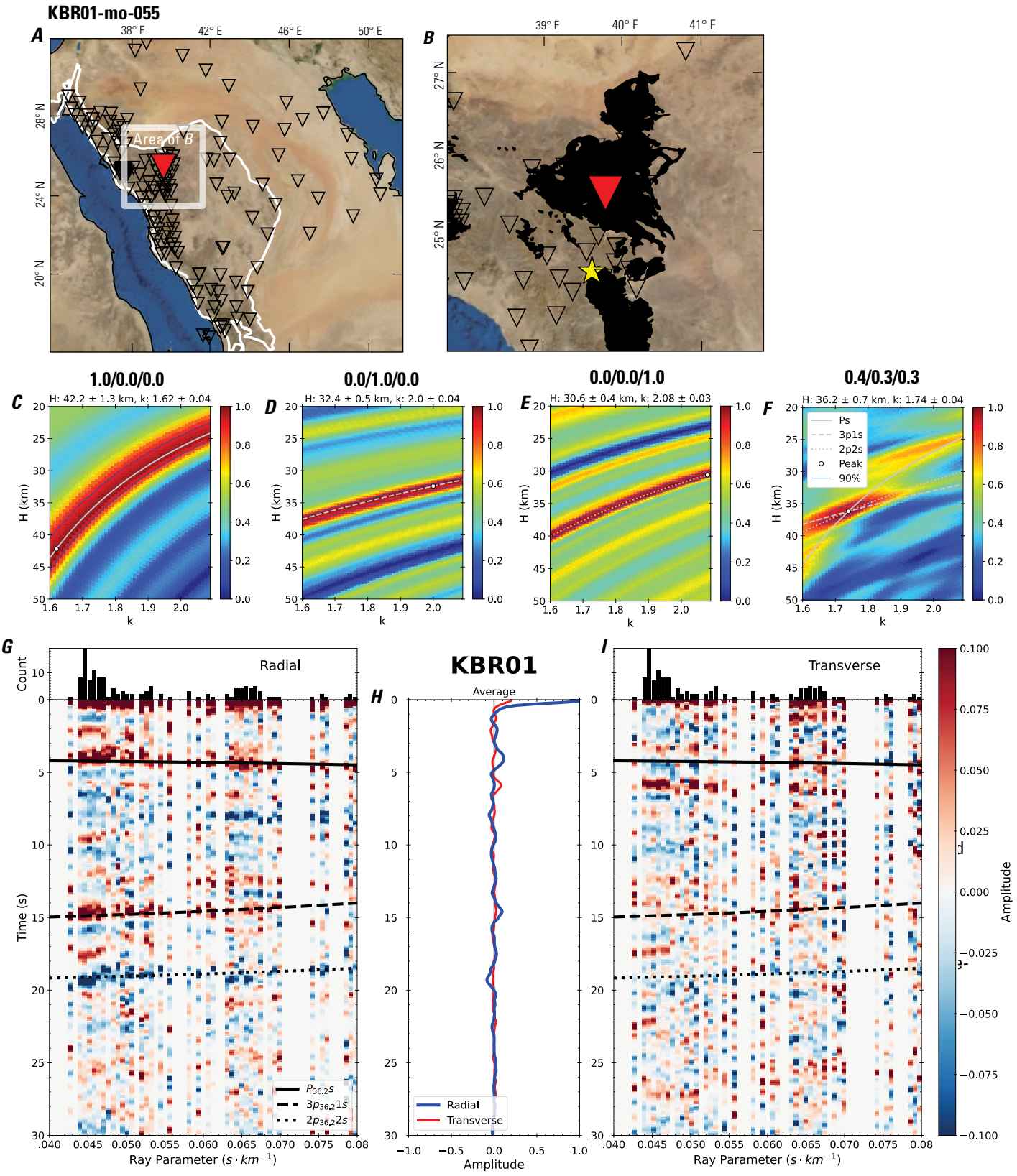
KBR01-mo-055
A
38° E
42° E
46° E
50° E
28° N
24° N
20° N
Area of B
B
39° E
40° E
41° E
27° N
26° N
25° N
1.0/0.0/0.0
0.0/1.0/0.0
0.0/0.0/1.0
0.4/0.3/0.3
C
H: 42.2 ± 1.3 km, k: 1.62 ± 0.04
D
H: 32.4 ± 0.5 km, k: 2.0 ± 0.04
E
H: 30.6 ± 0.4 km, k: 2.08 ± 0.03
F
H: 36.2 ± 0.7 km, k: 1.74 ± 0.04
Ps
3p1s
2p2s
Peak
90%
H (km)
k
G
Radial
Count
Time (s)
$P_{36.2}s$
$3p_{36.2}1s$
$2p_{36.2}2s$
Ray Parameter ($s \cdot km^{-1}$)
KBR01
Average
H
Radial
Transverse
Amplitude
I
Transverse
Amplitude

Figure 114 (page 120). Receiver-function analysis for station KBR01. *A*, Regional map of Saudi Arabia showing the entire array (as inverted triangles), the location of station KBR01 (red inverted triangle), the shield-platform boundary (white line), and the bounds of the map in *B* (white box). *B*, Local map of station KBR01. Harrats are shown in black. *C*, Standard, single-layer *H-k* stack with stacking weights 0.4/0.3/0.3. This *H-k* stack ignores sedimentary effects on the receiver functions. *D*, Standard, single-layer *H-k* stack with stacking weights 0.5/0.5/0.0. This *H-k* stack also ignores sedimentary effects on the receiver functions. *E*, Optimized sub-sedimentary *H-k* stack with stacking weights 0.4/0.3/0.3, following the method of Yu and others (2015). *F*, Optimized sedimentary *H-k* stack with stacking weights 0.05/0.70/0.25, following the method of Yu and others (2015). *G*, Radial component P-wave receiver functions (PRFs) plotted against ray parameter. Individual PRFs have had the resonance-removal filter of Yu and others (2015) applied to them and are normalized to the maximum amplitude within the time window shown, binned, and normalized by the number of traces per bin. *H*, Average of every individual normalized radial receiver function with the application of the resonance-removal filter (blue) and average of every individual normalized raw radial receiver function (red). *I*, Radial component of raw PRFs (that is, PRFs with no resonance-removal filter applied) plotted against ray parameter, normalized as in *G*.

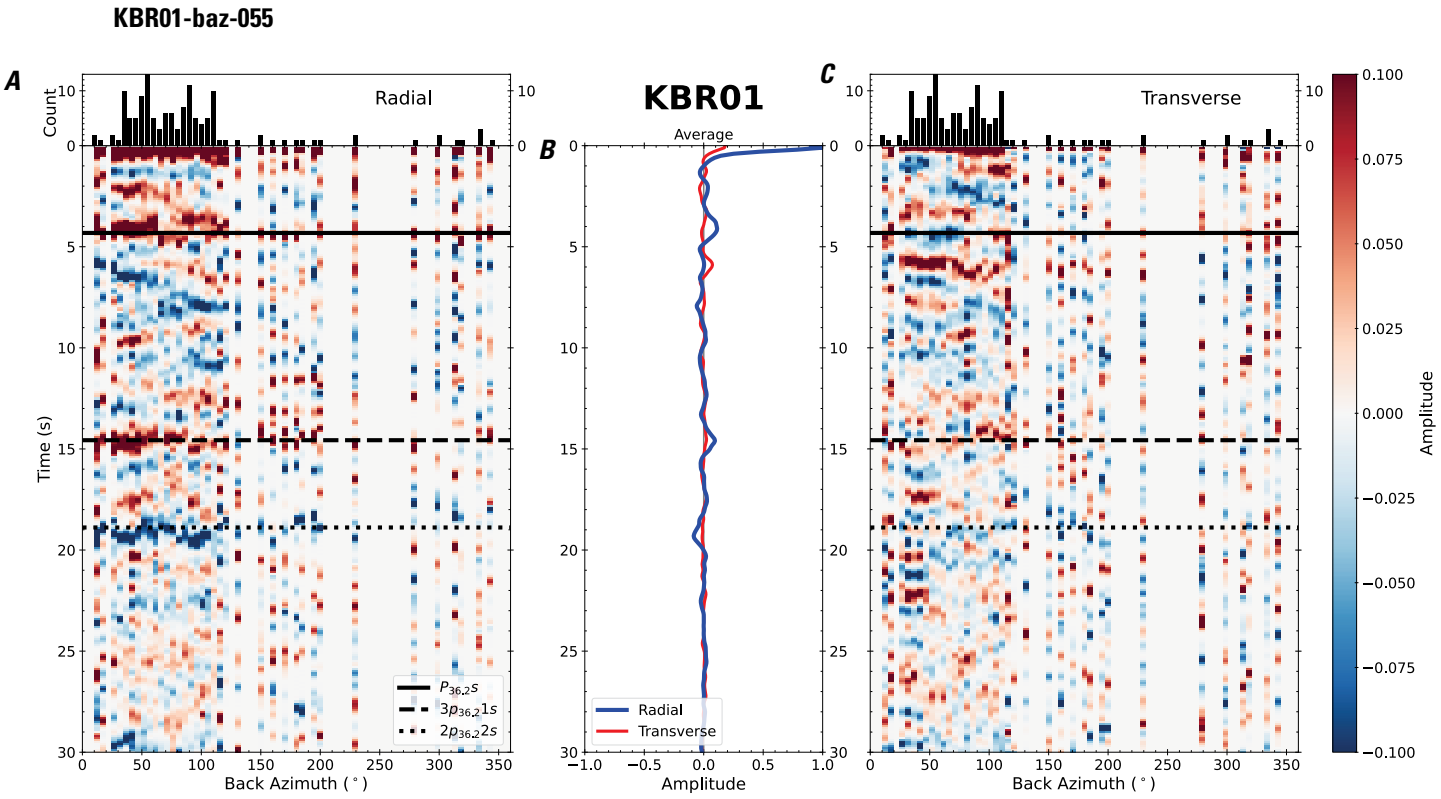

Figure 115. Receiver functions plotted against back azimuth for station KBR01. *A*, Radial component of P-wave receiver functions (PRFs) plotted against back azimuth. Individual PRFs have had the resonance-removal filter of Yu and others (2015) applied to them, are normalized to the maximum amplitude within the time window shown, binned, and normalized by the number of traces per bin. *B*, Average of every individual normalized radial receiver function with the application of the resonance-removal filter (blue) and average of every individual normalized raw radial receiver function (red). *C*, Radial component of raw PRFs, plotted against back azimuth, normalized as in *A*. Ps, 3p1s, and 2p2s arrival times predicted for the preferred Moho depth are shown, assuming a ray parameter of 0.06 s/km.

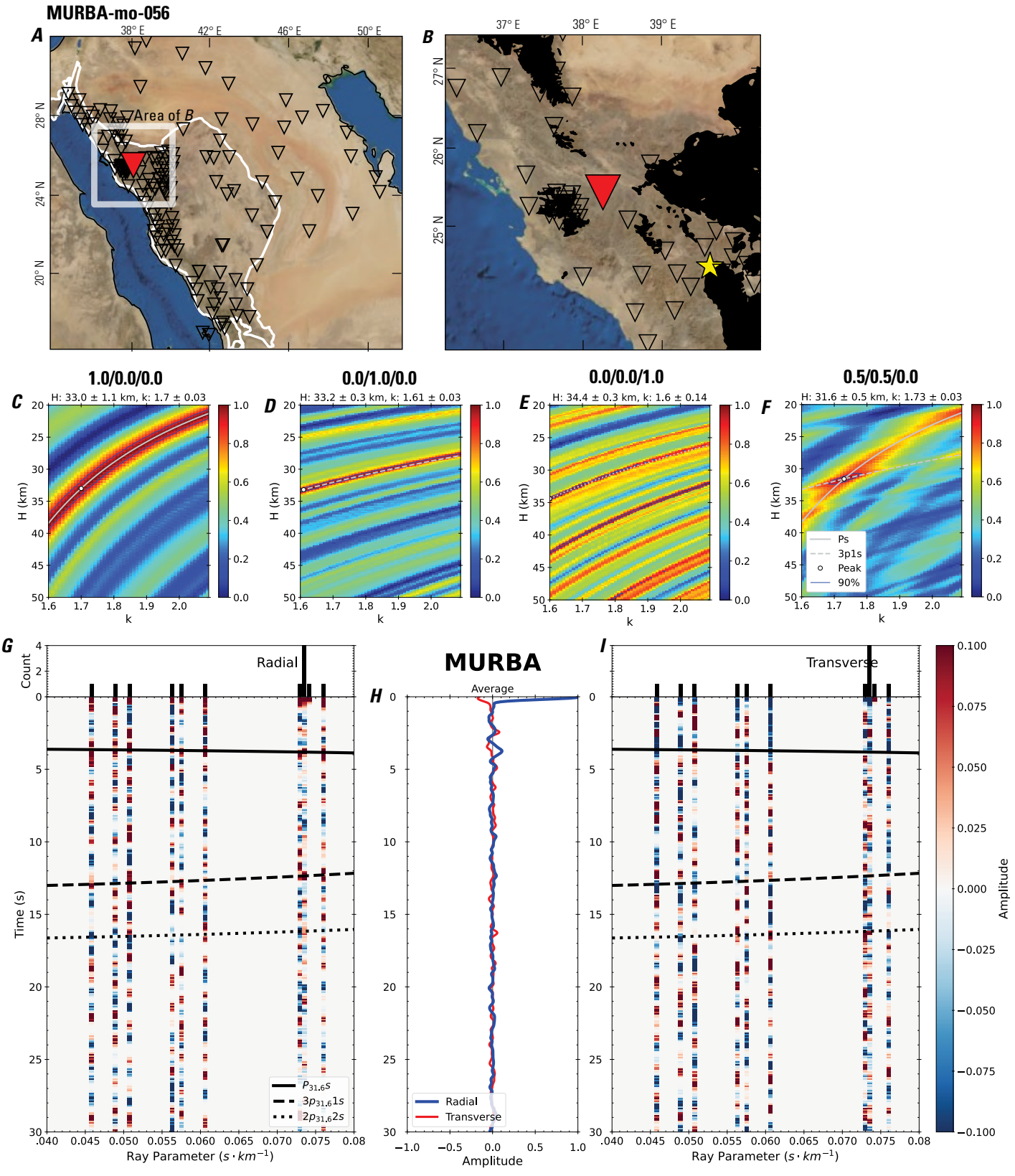
MURBA-mo-056
A
38° E
42° E
46° E
50° E
28° N
24° N
20° N
Area of B
B
37° E
38° E
39° E
27° N
26° N
25° N
1.0/0.0/0.0
C
H: 33.0 ± 1.1 km, k: 1.7 ± 0.03
0.0/1.0/0.0
D
H: 33.2 ± 0.3 km, k: 1.61 ± 0.03
0.0/0.0/1.0
E
H: 34.4 ± 0.3 km, k: 1.6 ± 0.14
0.5/0.5/0.0
F
H: 31.6 ± 0.5 km, k: 1.73 ± 0.03
H (km)
k
Ps
3p1s
Peak
90%
G
Radial
Count
Time (s)
$P_{31.6}s$
$3p_{31.6}1s$
$2p_{31.6}2s$
Ray Parameter ($s \cdot km^{-1}$)
MURBA
H
Average
Radial
Transverse
Amplitude
I
Transverse
Amplitude

Figure 116 (page 121). Receiver-function analysis for station MURBA. *A*, Regional map of Saudi Arabia showing the entire array (as inverted triangles), the location of station MURBA (red inverted triangle), the shield-platform boundary (white line), and the bounds of the map in *B* (white box). *B*, Local map of station MURBA. Harrats are shown in black. *C*, Standard, single-layer *H-k* stack with stacking weights 0.4/0.3/0.3. This *H-k* stack ignores sedimentary effects on the receiver functions. *D*, Standard, single-layer *H-k* stack with stacking weights 0.5/0.5/0.0. This *H-k* stack also ignores sedimentary effects on the receiver functions. *E*, Optimized sub-sedimentary *H-k* stack with stacking weights 0.4/0.3/0.3, following the method of Yu and others (2015). *F*, Optimized sedimentary *H-k* stack with stacking weights 0.05/0.70/0.25, following the method of Yu and others (2015). *G*, Radial component P-wave receiver functions (PRFs) plotted against ray parameter. Individual PRFs have had the resonance-removal filter of Yu and others (2015) applied to them and are normalized to the maximum amplitude within the time window shown, binned, and normalized by the number of traces per bin. *H*, Average of every individual normalized radial receiver function with the application of the resonance-removal filter (blue) and average of every individual normalized raw radial receiver function (red). *I*, Radial component of raw PRFs (that is, PRFs with no resonance-removal filter applied) plotted against ray parameter, normalized as in *G*.

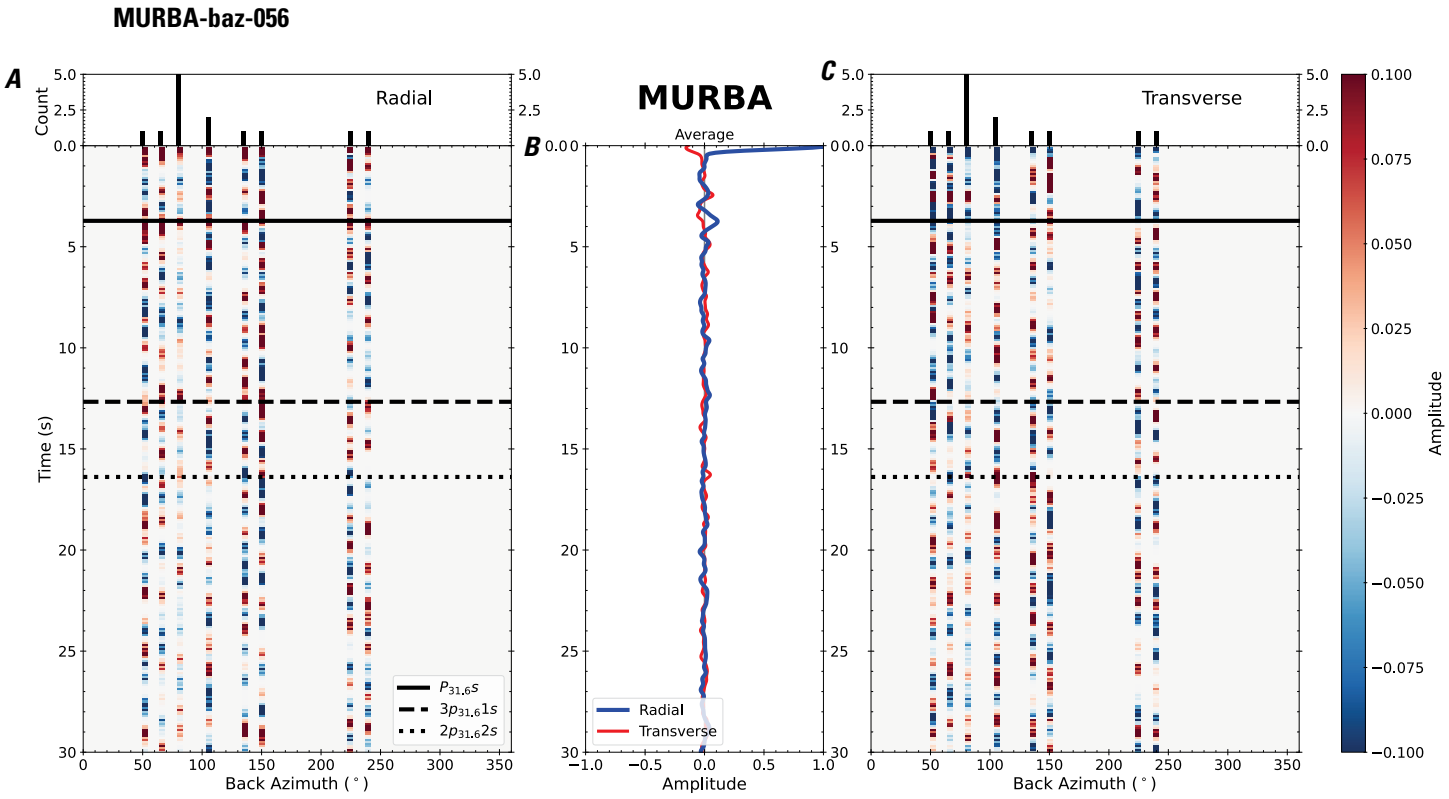

Figure 117. Receiver functions plotted against back azimuth for station MURBA. *A*, Radial component of P-wave receiver functions (PRFs) plotted against back azimuth. Individual PRFs have had the resonance-removal filter of Yu and others (2015) applied to them, are normalized to the maximum amplitude within the time window shown, binned, and normalized by the number of traces per bin. *B*, Average of every individual normalized radial receiver function with the application of the resonance-removal filter (blue) and average of every individual normalized raw radial receiver function (red). *C*, Radial component of raw PRFs, plotted against back azimuth, normalized as in *A*. Ps, 3p1s, and 2p2s arrival times predicted for the preferred Moho depth are shown, assuming a ray parameter of 0.06 s/km.

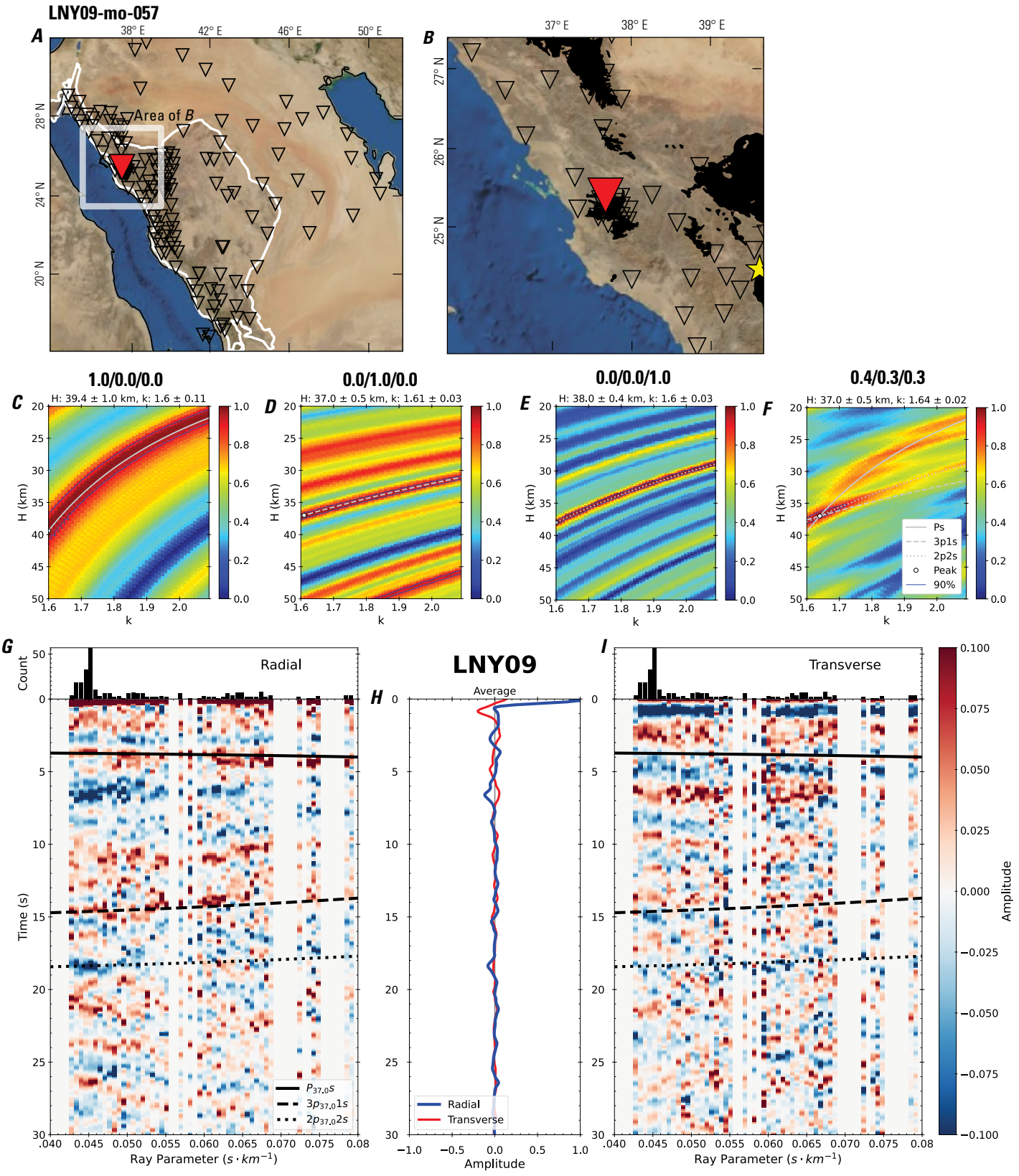
LNY09-mo-057
A
38° E
42° E
46° E
50° E
28° N
24° N
20° N
Area of B
B
37° E
38° E
39° E
27° N
26° N
25° N
1.0/0.0/0.0
C
H: 39.4 ± 1.0 km, k: 1.6 ± 0.11
0.0/1.0/0.0
D
H: 37.0 ± 0.5 km, k: 1.61 ± 0.03
0.0/0.0/1.0
E
H: 38.0 ± 0.4 km, k: 1.6 ± 0.03
0.4/0.3/0.3
F
H: 37.0 ± 0.5 km, k: 1.64 ± 0.02
H (km)
k
Ps
3p1s
2p2s
Peak
90%
G
Radial
Count
Time (s)
Ray Parameter (s · km⁻¹)
$P_{37.0}s$
$3p_{37.0}1s$
$2p_{37.0}2s$
LNY09
H
Average
Radial
Transverse
Amplitude
I
Transverse
Amplitude

Figure 118 (page 124). Receiver-function analysis for station LNY09. *A*, Regional map of Saudi Arabia showing the entire array (as inverted triangles), the location of station LNY09 (red inverted triangle), the shield-platform boundary (white line), and the bounds of the map in *B* (white box). *B*, Local map of station LNY09. Harrats are shown in black. *C*, Standard, single-layer *H-k* stack with stacking weights 0.4/0.3/0.3. This *H-k* stack ignores sedimentary effects on the receiver functions. *D*, Standard, single-layer *H-k* stack with stacking weights 0.5/0.5/0.0. This *H-k* stack also ignores sedimentary effects on the receiver functions. *E*, Optimized sub-sedimentary *H-k* stack with stacking weights 0.4/0.3/0.3, following the method of Yu and others (2015). *F*, Optimized sedimentary *H-k* stack with stacking weights 0.05/0.70/0.25, following the method of Yu and others (2015). *G*, Radial component P-wave receiver functions (PRFs) plotted against ray parameter. Individual PRFs have had the resonance-removal filter of Yu and others (2015) applied to them and are normalized to the maximum amplitude within the time window shown, binned, and normalized by the number of traces per bin. *H*, Average of every individual normalized radial receiver function with the application of the resonance-removal filter (blue) and average of every individual normalized raw radial receiver function (red). *I*, Radial component of raw PRFs (that is, PRFs with no resonance-removal filter applied) plotted against ray parameter, normalized as in *G*.

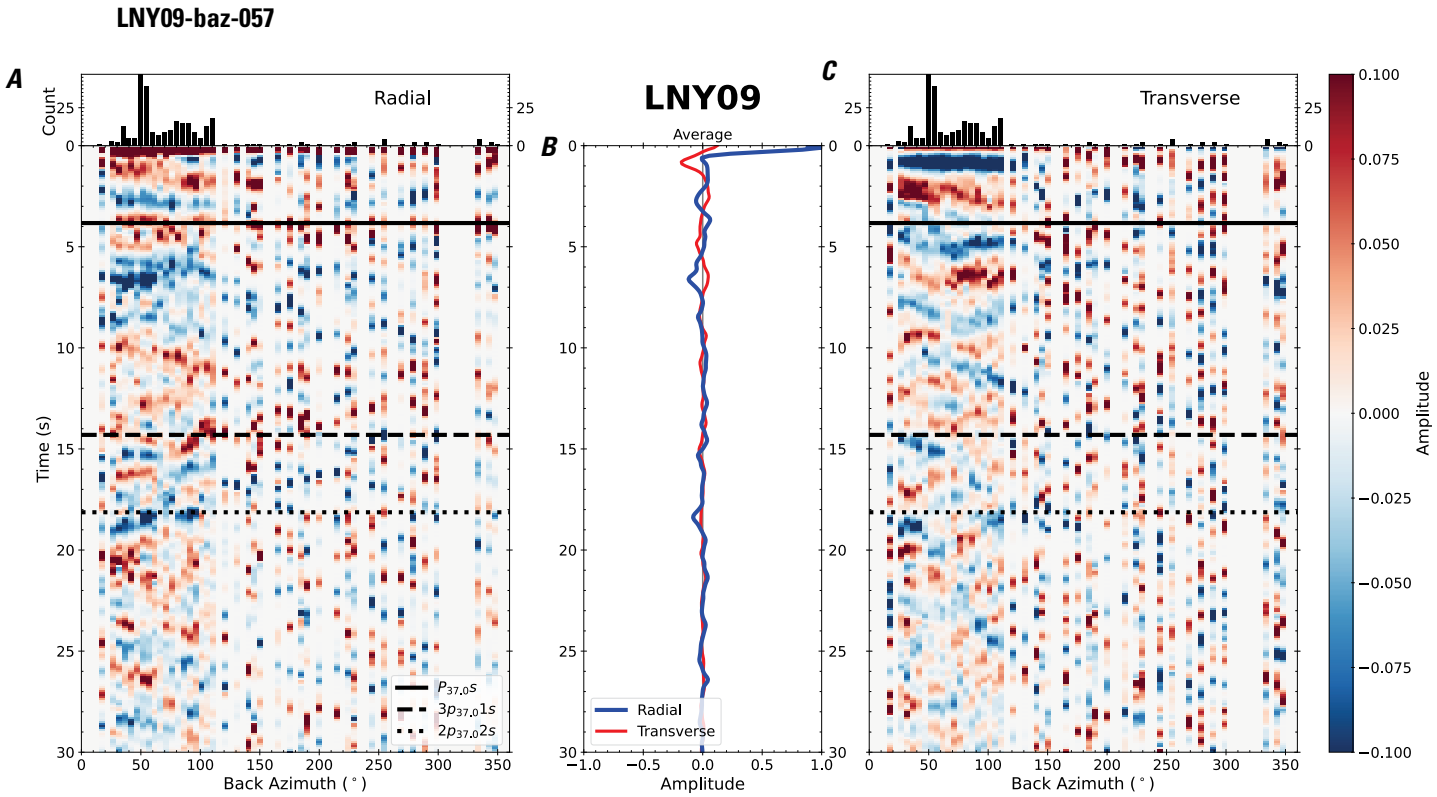

Figure 119. Receiver functions plotted against back azimuth for station LNY09. *A*, Radial component of P-wave receiver functions (PRFs) plotted against back azimuth. Individual PRFs have had the resonance-removal filter of Yu and others (2015) applied to them, are normalized to the maximum amplitude within the time window shown, binned, and normalized by the number of traces per bin. *B*, Average of every individual normalized radial receiver function with the application of the resonance-removal filter (blue) and average of every individual normalized raw radial receiver function (red). *C*, Radial component of raw PRFs, plotted against back azimuth, normalized as in *A*. Ps, 3p1s, and 2p2s arrival times predicted for the preferred Moho depth are shown, assuming a ray parameter of 0.06 s/km.

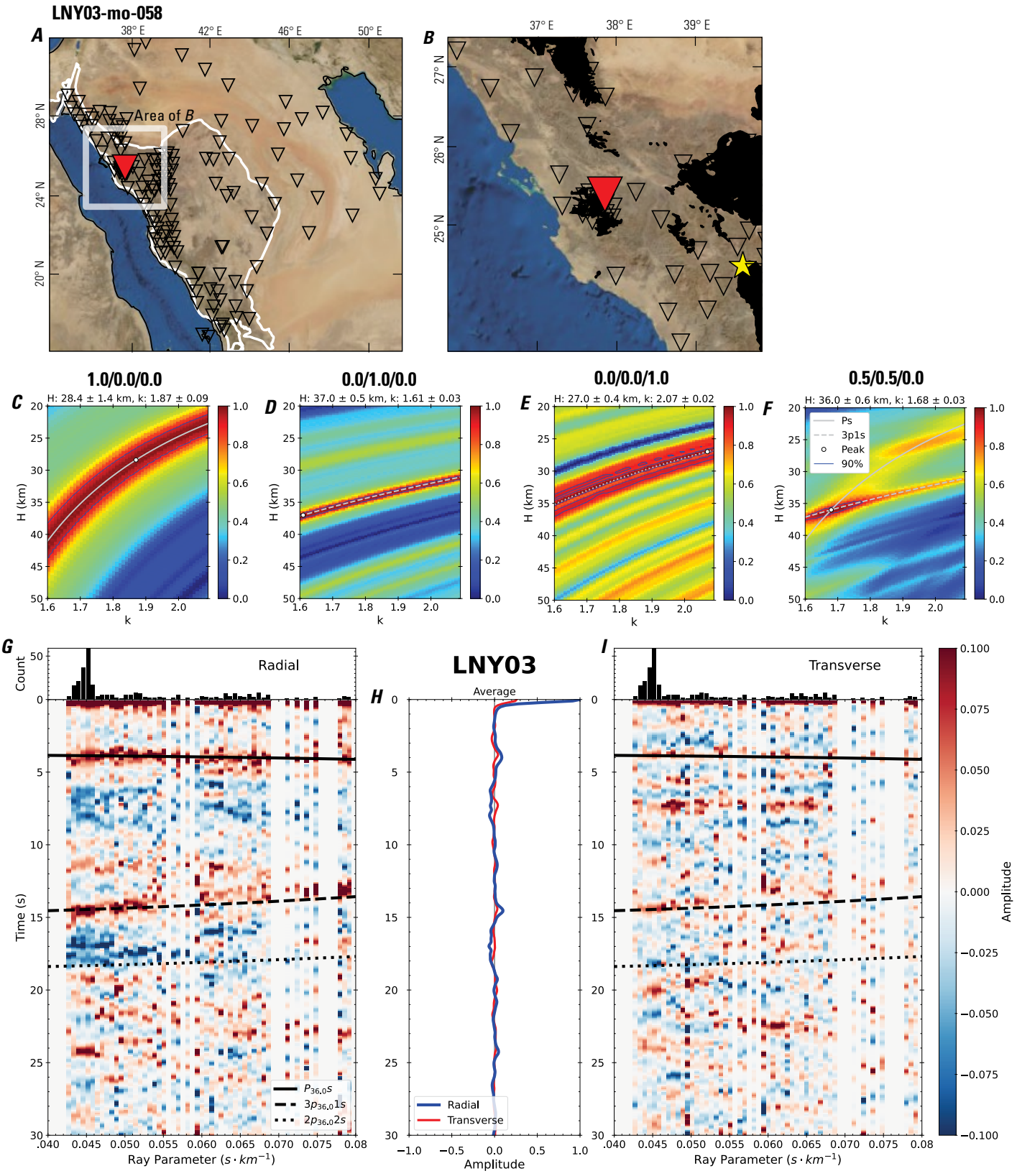
LNY03-mo-058
A
B
Area of B
1.0/0.0/0.0
0.0/1.0/0.0
0.0/0.0/1.0
0.5/0.5/0.0
C
D
E
F
H: 28.4 ± 1.4 km, k: 1.87 ± 0.09
H: 37.0 ± 0.5 km, k: 1.61 ± 0.03
H: 27.0 ± 0.4 km, k: 2.07 ± 0.02
H: 36.0 ± 0.6 km, k: 1.68 ± 0.03
Ps
3p1s
Peak
90%
H (km)
k
G
H
I
LNY03
Radial
Transverse
Average
Count
Time (s)
Ray Parameter (s · km⁻¹)
Amplitude
$P_{36.0}s$
$3p_{36.0}1s$
$2p_{36.0}2s$

Figure 120 (page 126). Receiver-function analysis for station LNY03. *A*, Regional map of Saudi Arabia showing the entire array (as inverted triangles), the location of station LNY03 (red inverted triangle), the shield-platform boundary (white line), and the bounds of the map in *B* (white box). *B*, Local map of station LNY03. Harrats are shown in black. *C*, Standard, single-layer *H-k* stack with stacking weights 0.4/0.3/0.3. This *H-k* stack ignores sedimentary effects on the receiver functions. *D*, Standard, single-layer *H-k* stack with stacking weights 0.5/0.5/0.0. This *H-k* stack also ignores sedimentary effects on the receiver functions. *E*, Optimized sub-sedimentary *H-k* stack with stacking weights 0.4/0.3/0.3, following the method of Yu and others (2015). *F*, Optimized sedimentary *H-k* stack with stacking weights 0.05/0.70/0.25, following the method of Yu and others (2015). *G*, Radial component P-wave receiver functions (PRFs) plotted against ray parameter. Individual PRFs have had the resonance-removal filter of Yu and others (2015) applied to them and are normalized to the maximum amplitude within the time window shown, binned, and normalized by the number of traces per bin. *H*, Average of every individual normalized radial receiver function with the application of the resonance-removal filter (blue) and average of every individual normalized raw radial receiver function (red). *I*, Radial component of raw PRFs (that is, PRFs with no resonance-removal filter applied) plotted against ray parameter, normalized as in *G*.

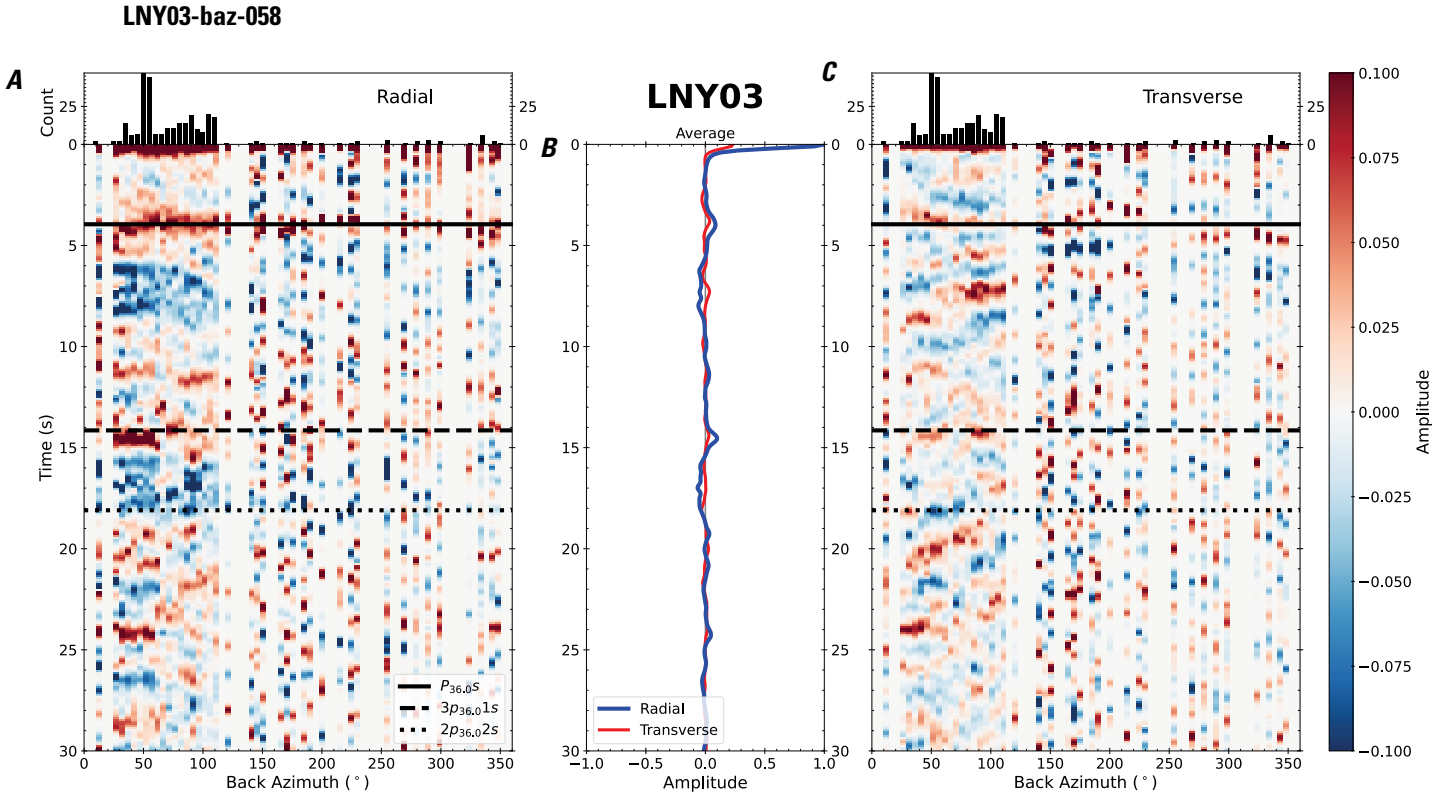

Figure 121. Receiver functions plotted against back azimuth for station LNY03. *A*, Radial component of P-wave receiver functions (PRFs) plotted against back azimuth. Individual PRFs have had the resonance-removal filter of Yu and others (2015) applied to them, are normalized to the maximum amplitude within the time window shown, binned, and normalized by the number of traces per bin. *B*, Average of every individual normalized radial receiver function with the application of the resonance-removal filter (blue) and average of every individual normalized raw radial receiver function (red). *C*, Radial component of raw PRFs, plotted against back azimuth, normalized as in *A*. Ps, 3p1s, and 2p2s arrival times predicted for the preferred Moho depth are shown, assuming a ray parameter of 0.06 s/km.

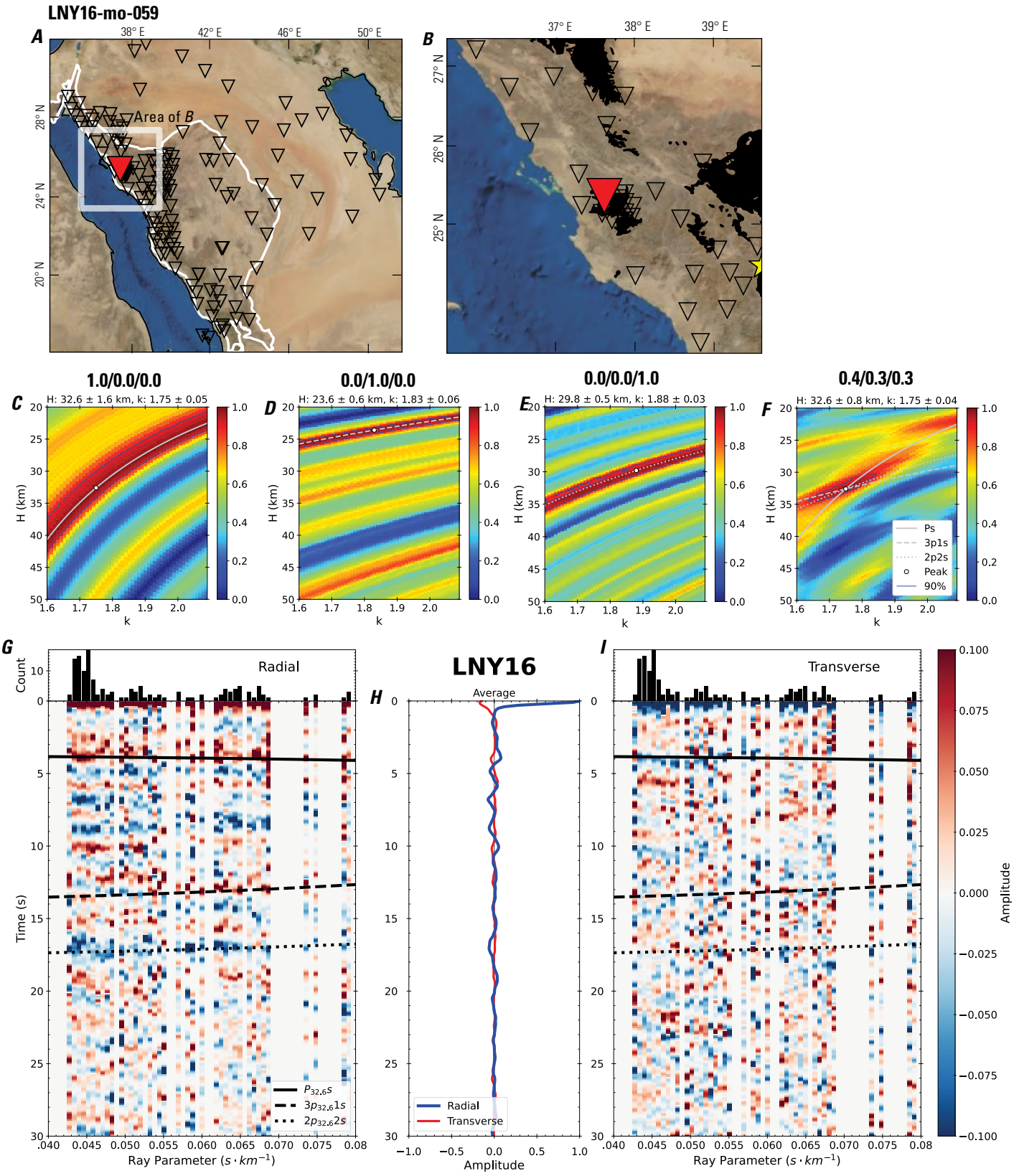
LNY16-mo-059
A
B
Area of B
1.0/0.0/0.0
0.0/1.0/0.0
0.0/0.0/1.0
0.4/0.3/0.3
C
D
E
F
H: 32.6 ± 1.6 km, k: 1.75 ± 0.05
H: 23.6 ± 0.6 km, k: 1.83 ± 0.06
H: 29.8 ± 0.5 km, k: 1.88 ± 0.03
H: 32.6 ± 0.8 km, k: 1.75 ± 0.04
H (km)
k
Ps
3p1s
2p2s
Peak
90%
G
H
I
LNY16
Radial
Transverse
Average
Count
Time (s)
Ray Parameter (s · km⁻¹)
Amplitude
$P_{32.6}s$
$3p_{32.6}1s$
$2p_{32.6}2s$

Figure 122 (page 128). Receiver-function analysis for station LNY16. *A*, Regional map of Saudi Arabia showing the entire array (as inverted triangles), the location of station LNY16 (red inverted triangle), the shield-platform boundary (white line), and the bounds of the map in *B* (white box). *B*, Local map of station LNY16. Harrats are shown in black. *C*, Standard, single-layer *H-k* stack with stacking weights 0.4/0.3/0.3. This *H-k* stack ignores sedimentary effects on the receiver functions. *D*, Standard, single-layer *H-k* stack with stacking weights 0.5/0.5/0.0. This *H-k* stack also ignores sedimentary effects on the receiver functions. *E*, Optimized sub-sedimentary *H-k* stack with stacking weights 0.4/0.3/0.3, following the method of Yu and others (2015). *F*, Optimized sedimentary *H-k* stack with stacking weights 0.05/0.70/0.25, following the method of Yu and others (2015). *G*, Radial component P-wave receiver functions (PRFs) plotted against ray parameter. Individual PRFs have had the resonance-removal filter of Yu and others (2015) applied to them and are normalized to the maximum amplitude within the time window shown, binned, and normalized by the number of traces per bin. *H*, Average of every individual normalized radial receiver function with the application of the resonance-removal filter (blue) and average of every individual normalized raw radial receiver function (red). *I*, Radial component of raw PRFs (that is, PRFs with no resonance-removal filter applied) plotted against ray parameter, normalized as in *G*.

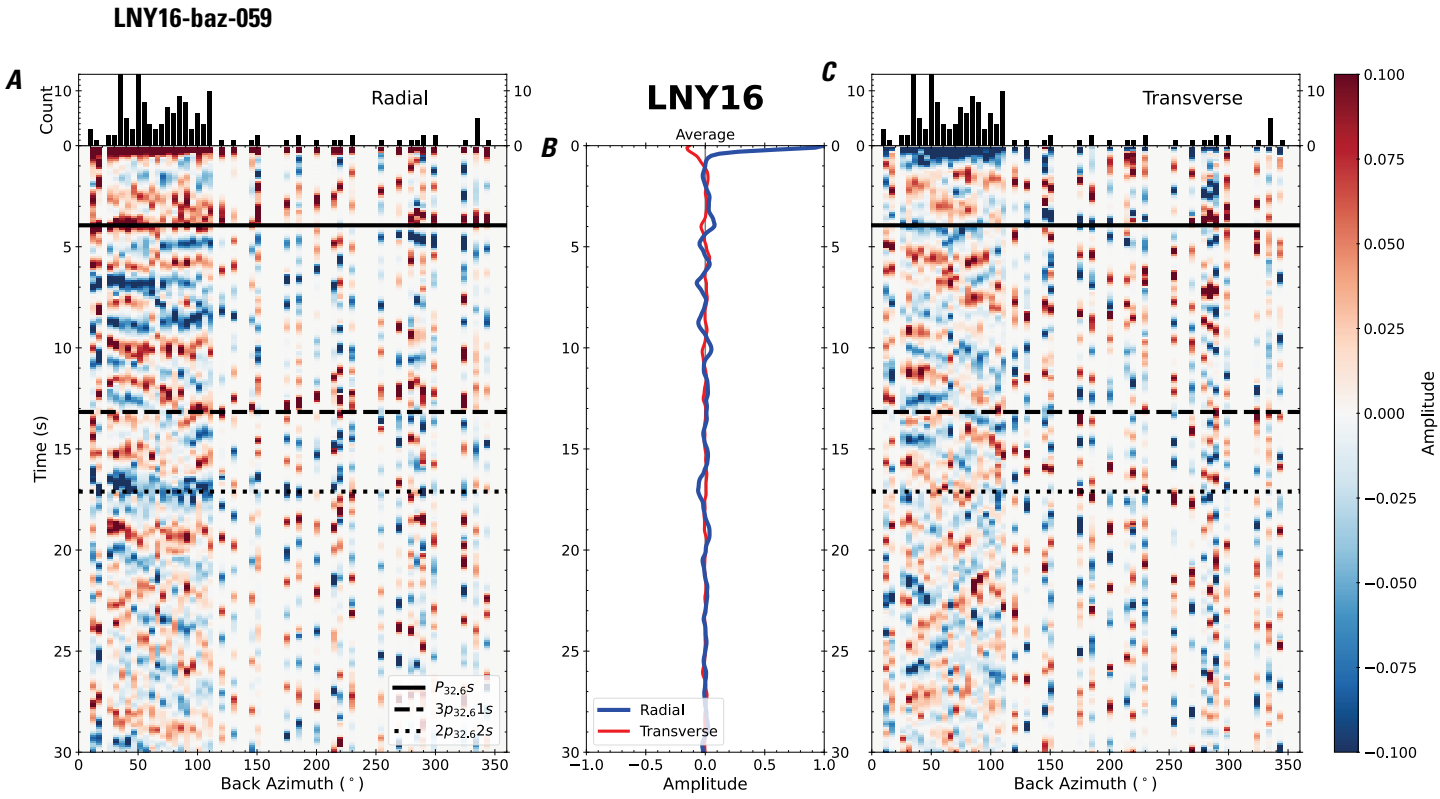

Figure 123. Receiver functions plotted against back azimuth for station LNY16. *A*, Radial component of P-wave receiver functions (PRFs) plotted against back azimuth. Individual PRFs have had the resonance-removal filter of Yu and others (2015) applied to them, are normalized to the maximum amplitude within the time window shown, binned, and normalized by the number of traces per bin. *B*, Average of every individual normalized radial receiver function with the application of the resonance-removal filter (blue) and average of every individual normalized raw radial receiver function (red). *C*, Radial component of raw PRFs, plotted against back azimuth, normalized as in *A*. Ps, 3p1s, and 2p2s arrival times predicted for the preferred Moho depth are shown, assuming a ray parameter of 0.06 s/km.

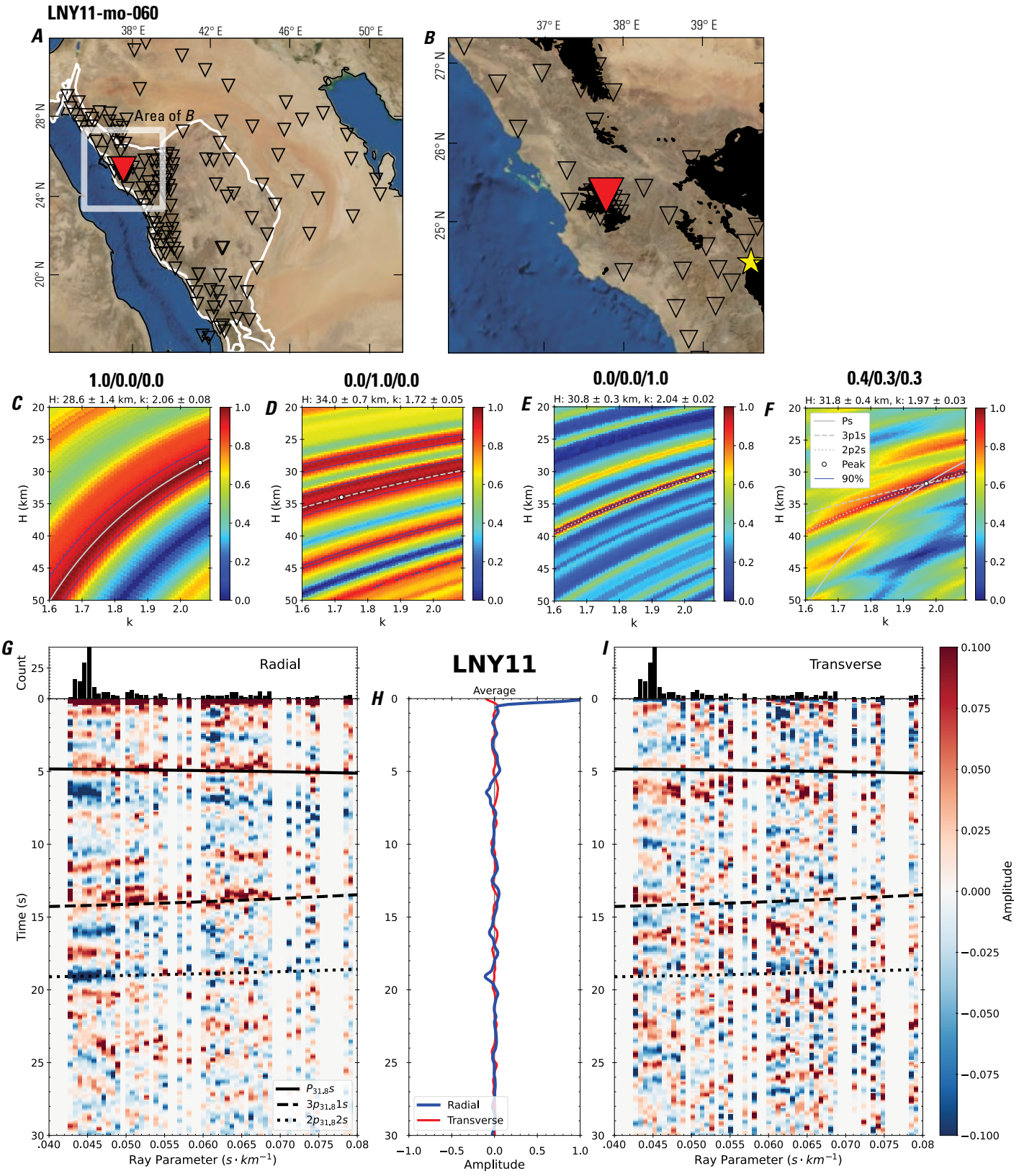
LNY11-mo-060
A
B
Area of B
1.0/0.0/0.0
0.0/1.0/0.0
0.0/0.0/1.0
0.4/0.3/0.3
C
D
E
F
H: 28.6 ± 1.4 km, k: 2.06 ± 0.08
H: 34.0 ± 0.7 km, k: 1.72 ± 0.05
H: 30.8 ± 0.3 km, k: 2.04 ± 0.02
H: 31.8 ± 0.4 km, k: 1.97 ± 0.03
H (km)
k
Ps
3p1s
2p2s
Peak
90%
G
H
I
LNY11
Radial
Transverse
Average
Count
Time (s)
Ray Parameter (s · km⁻¹)
Amplitude
$P_{31.8}s$
$3p_{31.8}1s$
$2p_{31.8}2s$

Figure 124 (page 130). Receiver-function analysis for station LNY11. *A*, Regional map of Saudi Arabia showing the entire array (as inverted triangles), the location of station LNY11 (red inverted triangle), the shield-platform boundary (white line), and the bounds of the map in *B* (white box). *B*, Local map of station LNY11. Harrats are shown in black. *C*, Standard, single-layer *H-k* stack with stacking weights 0.4/0.3/0.3. This *H-k* stack ignores sedimentary effects on the receiver functions. *D*, Standard, single-layer *H-k* stack with stacking weights 0.5/0.5/0.0. This *H-k* stack also ignores sedimentary effects on the receiver functions. *E*, Optimized sub-sedimentary *H-k* stack with stacking weights 0.4/0.3/0.3, following the method of Yu and others (2015). *F*, Optimized sedimentary *H-k* stack with stacking weights 0.05/0.70/0.25, following the method of Yu and others (2015). *G*, Radial component P-wave receiver functions (PRFs) plotted against ray parameter. Individual PRFs have had the resonance-removal filter of Yu and others (2015) applied to them and are normalized to the maximum amplitude within the time window shown, binned, and normalized by the number of traces per bin. *H*, Average of every individual normalized radial receiver function with the application of the resonance-removal filter (blue) and average of every individual normalized raw radial receiver function (red). *I*, Radial component of raw PRFs (that is, PRFs with no resonance-removal filter applied) plotted against ray parameter, normalized as in *G*.

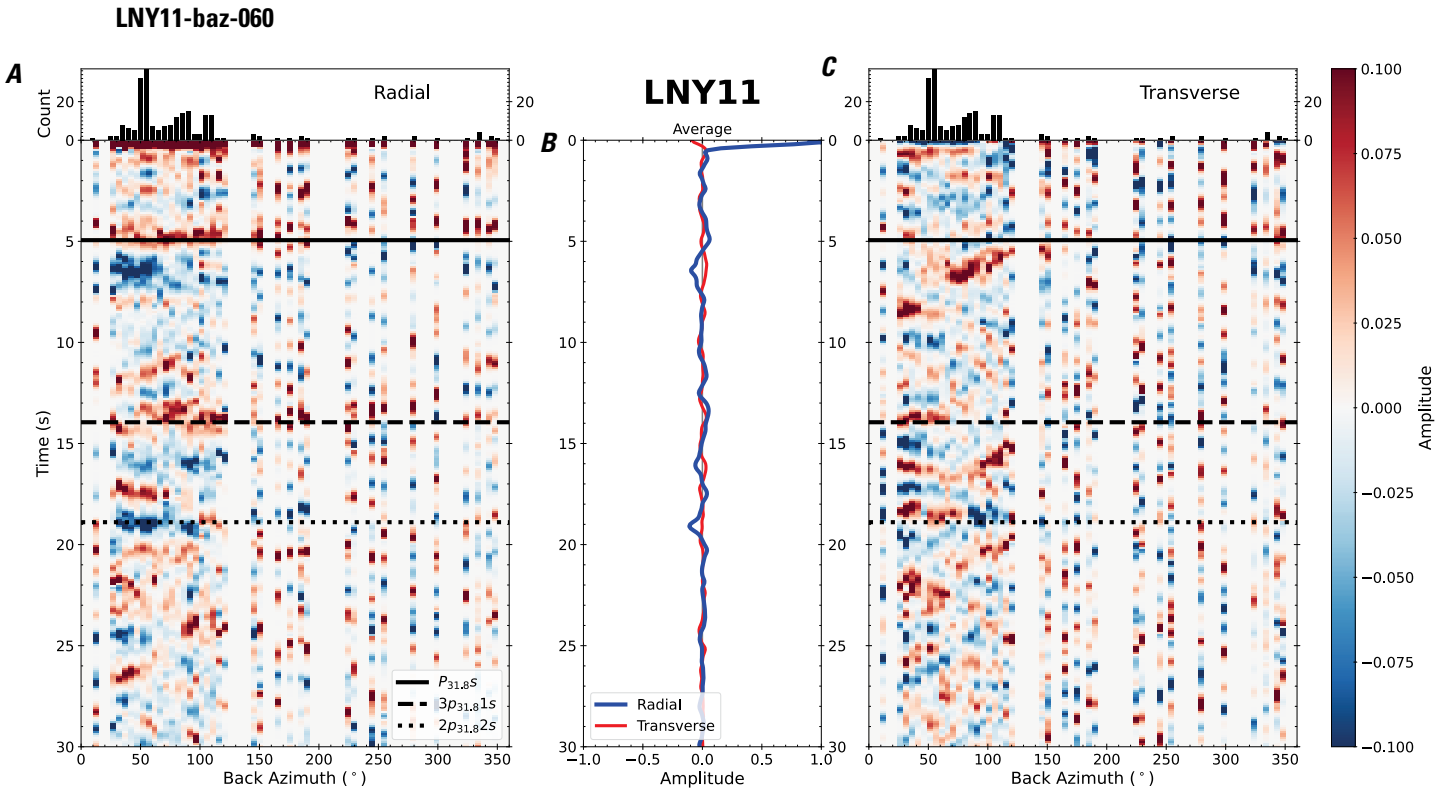

Figure 125. Receiver functions plotted against back azimuth for station LNY11. *A*, Radial component of P-wave receiver functions (PRFs) plotted against back azimuth. Individual PRFs have had the resonance-removal filter of Yu and others (2015) applied to them, are normalized to the maximum amplitude within the time window shown, binned, and normalized by the number of traces per bin. *B*, Average of every individual normalized radial receiver function with the application of the resonance-removal filter (blue) and average of every individual normalized raw radial receiver function (red). *C*, Radial component of raw PRFs, plotted against back azimuth, normalized as in *A*. Ps, 3p1s, and 2p2s arrival times predicted for the preferred Moho depth are shown, assuming a ray parameter of 0.06 s/km.

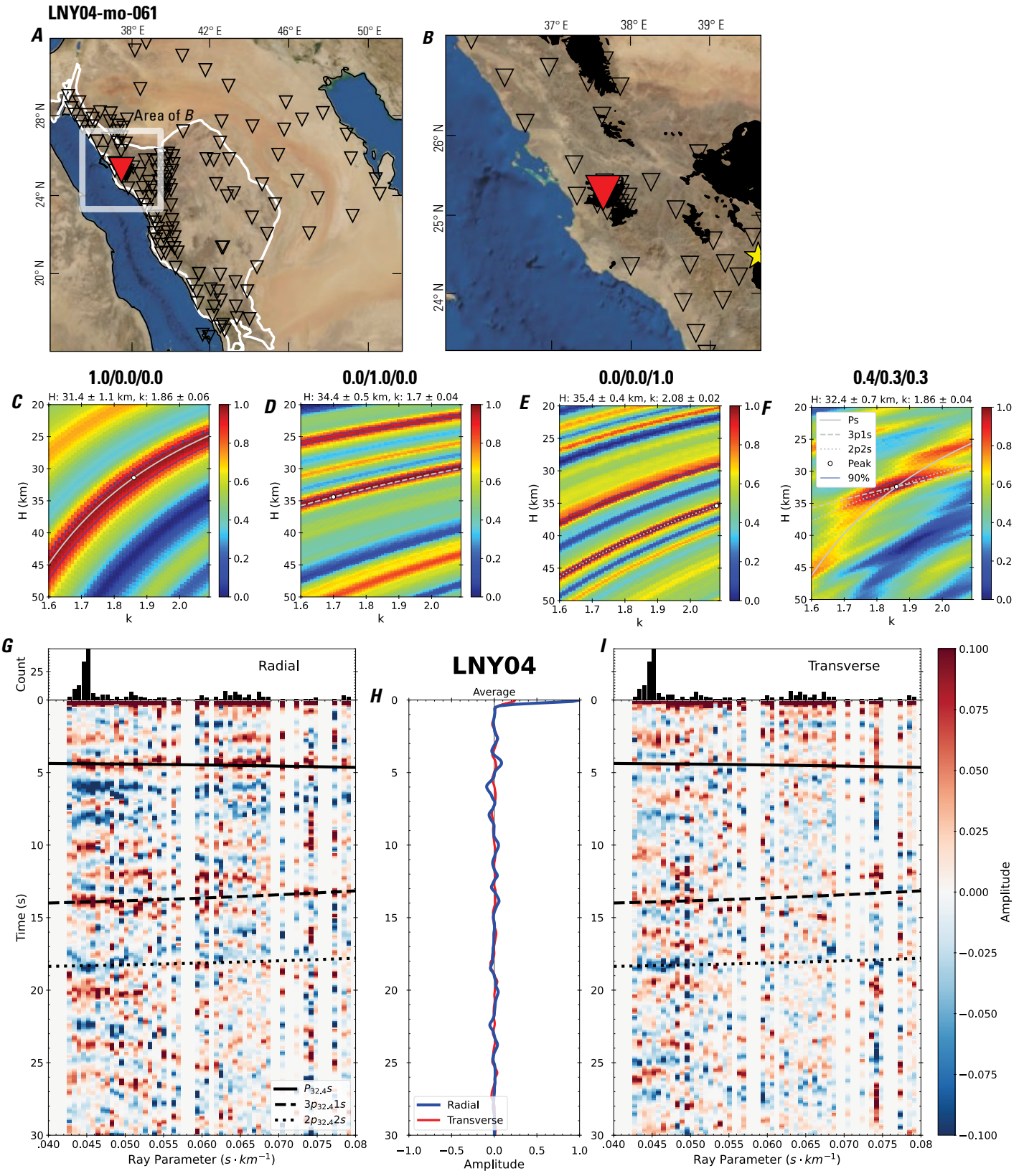
LNY04-mo-061
A
B
Area of B
1.0/0.0/0.0
0.0/1.0/0.0
0.0/0.0/1.0
0.4/0.3/0.3
C
D
E
F
H: 31.4 ± 1.1 km, k: 1.86 ± 0.06
H: 34.4 ± 0.5 km, k: 1.7 ± 0.04
H: 35.4 ± 0.4 km, k: 2.08 ± 0.02
H: 32.4 ± 0.7 km, k: 1.86 ± 0.04
H (km)
k
Ps
3p1s
2p2s
Peak
90%
G
H
I
LNY04
Radial
Transverse
Average
Count
Time (s)
Ray Parameter (s · km⁻¹)
Amplitude
$P_{32.4}s$
$3p_{32.4}1s$
$2p_{32.4}2s$

Figure 126 (page 132). Receiver-function analysis for station LNY04. *A*, Regional map of Saudi Arabia showing the entire array (as inverted triangles), the location of station LNY04 (red inverted triangle), the shield-platform boundary (white line), and the bounds of the map in *B* (white box). *B*, Local map of station LNY04. Harrats are shown in black. *C*, Standard, single-layer *H-k* stack with stacking weights 0.4/0.3/0.3. This *H-k* stack ignores sedimentary effects on the receiver functions. *D*, Standard, single-layer *H-k* stack with stacking weights 0.5/0.5/0.0. This *H-k* stack also ignores sedimentary effects on the receiver functions. *E*, Optimized sub-sedimentary *H-k* stack with stacking weights 0.4/0.3/0.3, following the method of Yu and others (2015). *F*, Optimized sedimentary *H-k* stack with stacking weights 0.05/0.70/0.25, following the method of Yu and others (2015). *G*, Radial component P-wave receiver functions (PRFs) plotted against ray parameter. Individual PRFs have had the resonance-removal filter of Yu and others (2015) applied to them and are normalized to the maximum amplitude within the time window shown, binned, and normalized by the number of traces per bin. *H*, Average of every individual normalized radial receiver function with the application of the resonance-removal filter (blue) and average of every individual normalized raw radial receiver function (red). *I*, Radial component of raw PRFs (that is, PRFs with no resonance-removal filter applied) plotted against ray parameter, normalized as in *G*.

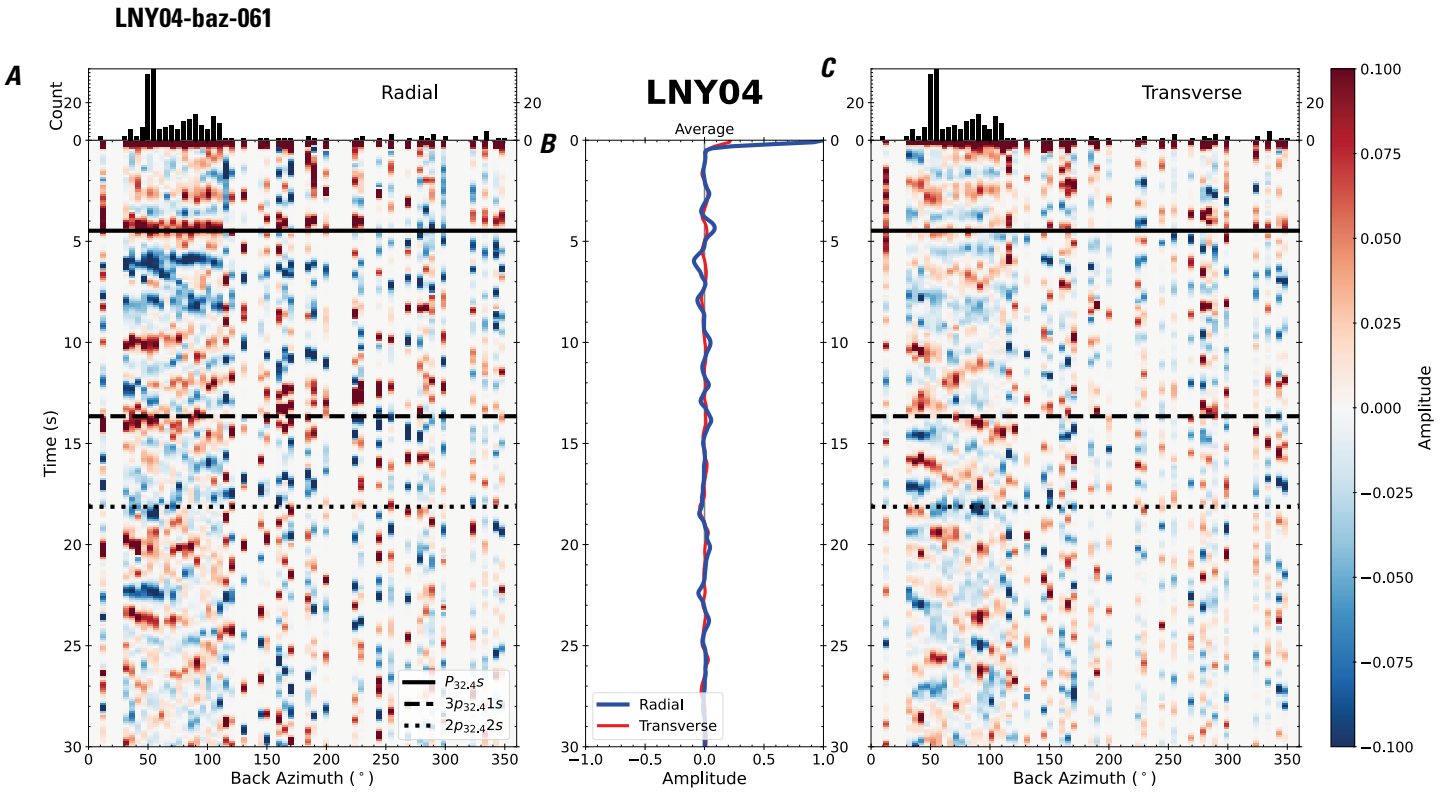

Figure 127. Receiver functions plotted against back azimuth for station LNY04. *A*, Radial component of P-wave receiver functions (PRFs) plotted against back azimuth. Individual PRFs have had the resonance-removal filter of Yu and others (2015) applied to them, are normalized to the maximum amplitude within the time window shown, binned, and normalized by the number of traces per bin. *B*, Average of every individual normalized radial receiver function with the application of the resonance-removal filter (blue) and average of every individual normalized raw radial receiver function (red). *C*, Radial component of raw PRFs, plotted against back azimuth, normalized as in *A*. Ps, 3p1s, and 2p2s arrival times predicted for the preferred Moho depth are shown, assuming a ray parameter of 0.06 s/km.

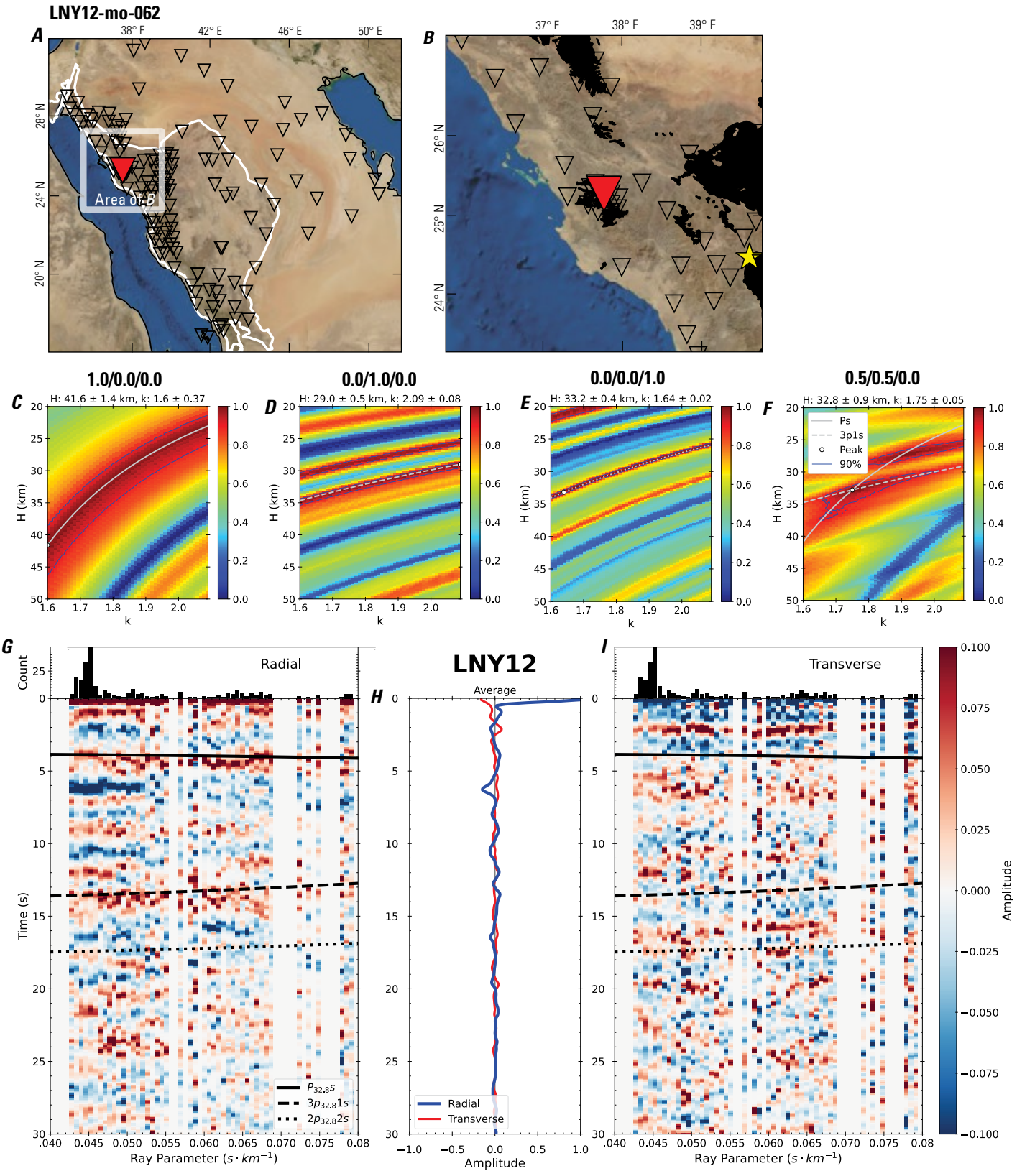
LNY12-mo-062
A
B
Area of B
1.0/0.0/0.0
0.0/1.0/0.0
0.0/0.0/1.0
0.5/0.5/0.0
C
D
E
F
H: 41.6 ± 1.4 km, k: 1.6 ± 0.37
H: 29.0 ± 0.5 km, k: 2.09 ± 0.08
H: 33.2 ± 0.4 km, k: 1.64 ± 0.02
H: 32.8 ± 0.9 km, k: 1.75 ± 0.05
H (km)
k
Ps
3p1s
Peak
90%
G
H
I
LNY12
Radial
Transverse
Average
Count
Time (s)
Ray Parameter (s · km⁻¹)
Amplitude
P32.8s
3p32.81s
2p32.82s
Radial
Transverse

Figure 128 (page 134). Receiver-function analysis for station LNY12. *A*, Regional map of Saudi Arabia showing the entire array (as inverted triangles), the location of station LNY12 (red inverted triangle), the shield-platform boundary (white line), and the bounds of the map in *B* (white box). *B*, Local map of station LNY12. Harrats are shown in black. *C*, Standard, single-layer *H-k* stack with stacking weights 0.4/0.3/0.3. This *H-k* stack ignores sedimentary effects on the receiver functions. *D*, Standard, single-layer *H-k* stack with stacking weights 0.5/0.5/0.0. This *H-k* stack also ignores sedimentary effects on the receiver functions. *E*, Optimized sub-sedimentary *H-k* stack with stacking weights 0.4/0.3/0.3, following the method of Yu and others (2015). *F*, Optimized sedimentary *H-k* stack with stacking weights 0.05/0.70/0.25, following the method of Yu and others (2015). *G*, Radial component P-wave receiver functions (PRFs) plotted against ray parameter. Individual PRFs have had the resonance-removal filter of Yu and others (2015) applied to them and are normalized to the maximum amplitude within the time window shown, binned, and normalized by the number of traces per bin. *H*, Average of every individual normalized radial receiver function with the application of the resonance-removal filter (blue) and average of every individual normalized raw radial receiver function (red). *I*, Radial component of raw PRFs (that is, PRFs with no resonance-removal filter applied) plotted against ray parameter, normalized as in *G*.

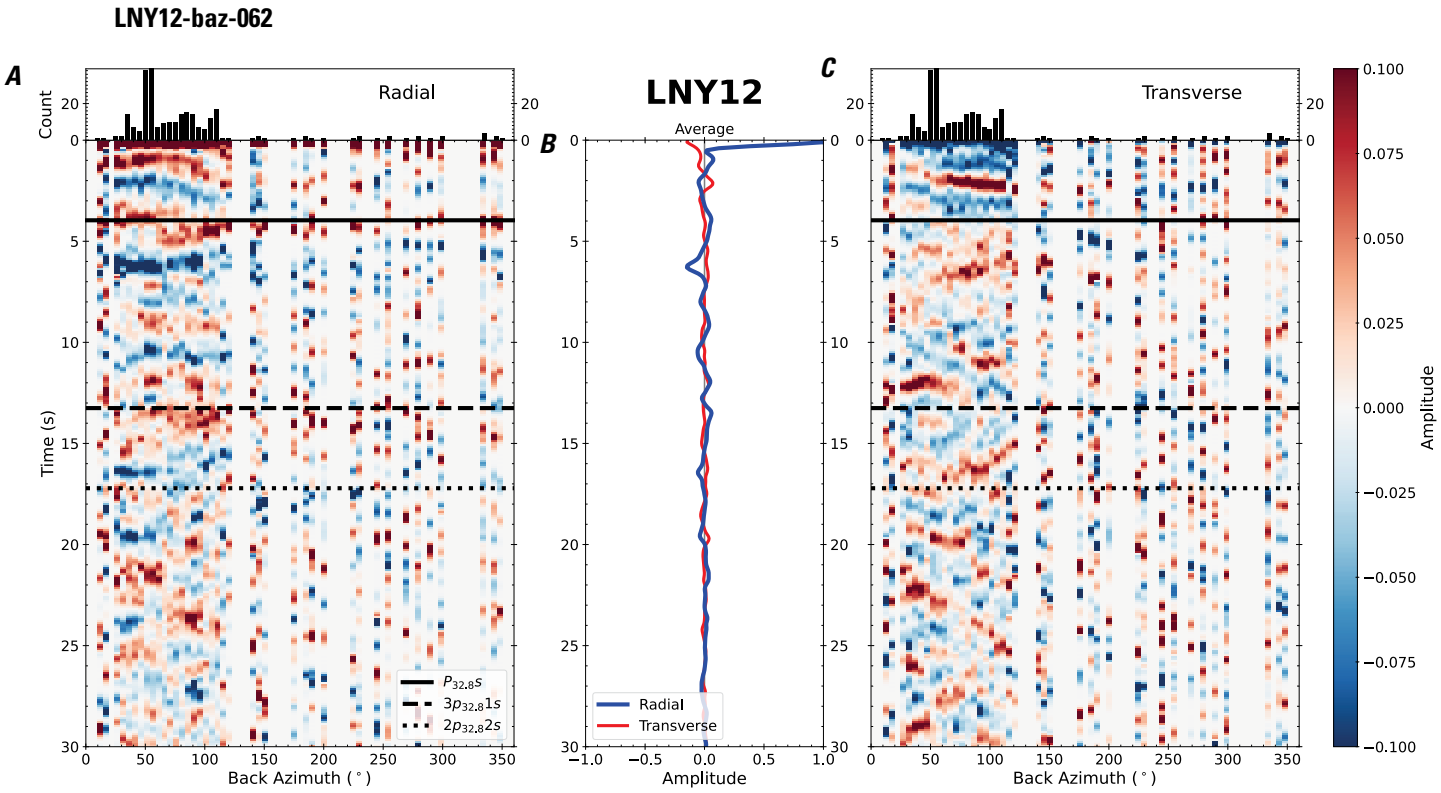

FIgure 129. Receiver functions plotted against back azimuth for station LNY12. *A*, Radial component of P-wave receiver functions (PRFs) plotted against back azimuth. Individual PRFs have had the resonance-removal filter of Yu and others (2015) applied to them, are normalized to the maximum amplitude within the time window shown, binned, and normalized by the number of traces per bin. *B*, Average of every individual normalized radial receiver function with the application of the resonance-removal filter (blue) and average of every individual normalized raw radial receiver function (red). *C*, Radial component of raw PRFs, plotted against back azimuth, normalized as in *A*. Ps, 3p1s, and 2p2s arrival times predicted for the preferred Moho depth are shown, assuming a ray parameter of 0.06 s/km.

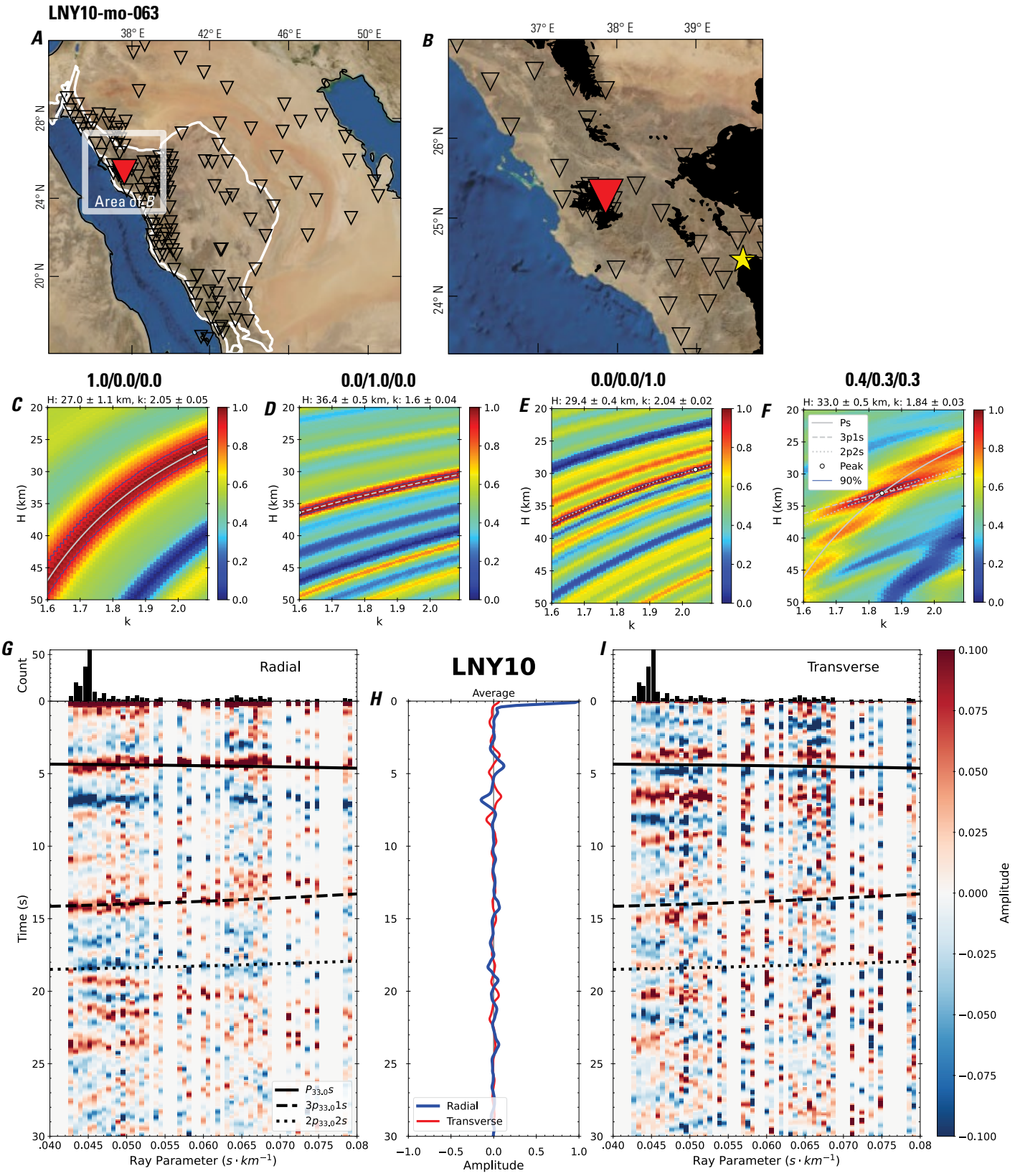
LNY10-mo-063
A
38° E
42° E
46° E
50° E
28° N
24° N
20° N
Area of B
B
37° E
38° E
39° E
26° N
25° N
24° N
1.0/0.0/0.0
0.0/1.0/0.0
0.0/0.0/1.0
0.4/0.3/0.3
C
H: 27.0 ± 1.1 km, k: 2.05 ± 0.05
D
H: 36.4 ± 0.5 km, k: 1.6 ± 0.04
E
H: 29.4 ± 0.4 km, k: 2.04 ± 0.02
F
H: 33.0 ± 0.5 km, k: 1.84 ± 0.03
Ps
3p1s
2p2s
Peak
90%
H (km)
k
G
Radial
Count
Time (s)
$P_{33.0}s$
$3p_{33.0}1s$
$2p_{33.0}2s$
Ray Parameter ($s \cdot km^{-1}$)
LNY10
H
Average
Radial
Transverse
Amplitude
I
Transverse
Amplitude

Figure 130 (page 136). Receiver-function analysis for station LNY10. *A*, Regional map of Saudi Arabia showing the entire array (as inverted triangles), the location of station LNY10 (red inverted triangle), the shield-platform boundary (white line), and the bounds of the map in *B* (white box). *B*, Local map of station LNY10. Harrats are shown in black. *C*, Standard, single-layer *H-k* stack with stacking weights 0.4/0.3/0.3. This *H-k* stack ignores sedimentary effects on the receiver functions. *D*, Standard, single-layer *H-k* stack with stacking weights 0.5/0.5/0.0. This *H-k* stack also ignores sedimentary effects on the receiver functions. *E*, Optimized sub-sedimentary *H-k* stack with stacking weights 0.4/0.3/0.3, following the method of Yu and others (2015). *F*, Optimized sedimentary *H-k* stack with stacking weights 0.05/0.70/0.25, following the method of Yu and others (2015). *G*, Radial component P-wave receiver functions (PRFs) plotted against ray parameter. Individual PRFs have had the resonance-removal filter of Yu and others (2015) applied to them and are normalized to the maximum amplitude within the time window shown, binned, and normalized by the number of traces per bin. *H*, Average of every individual normalized radial receiver function with the application of the resonance-removal filter (blue) and average of every individual normalized raw radial receiver function (red). *I*, Radial component of raw PRFs (that is, PRFs with no resonance-removal filter applied) plotted against ray parameter, normalized as in *G*.

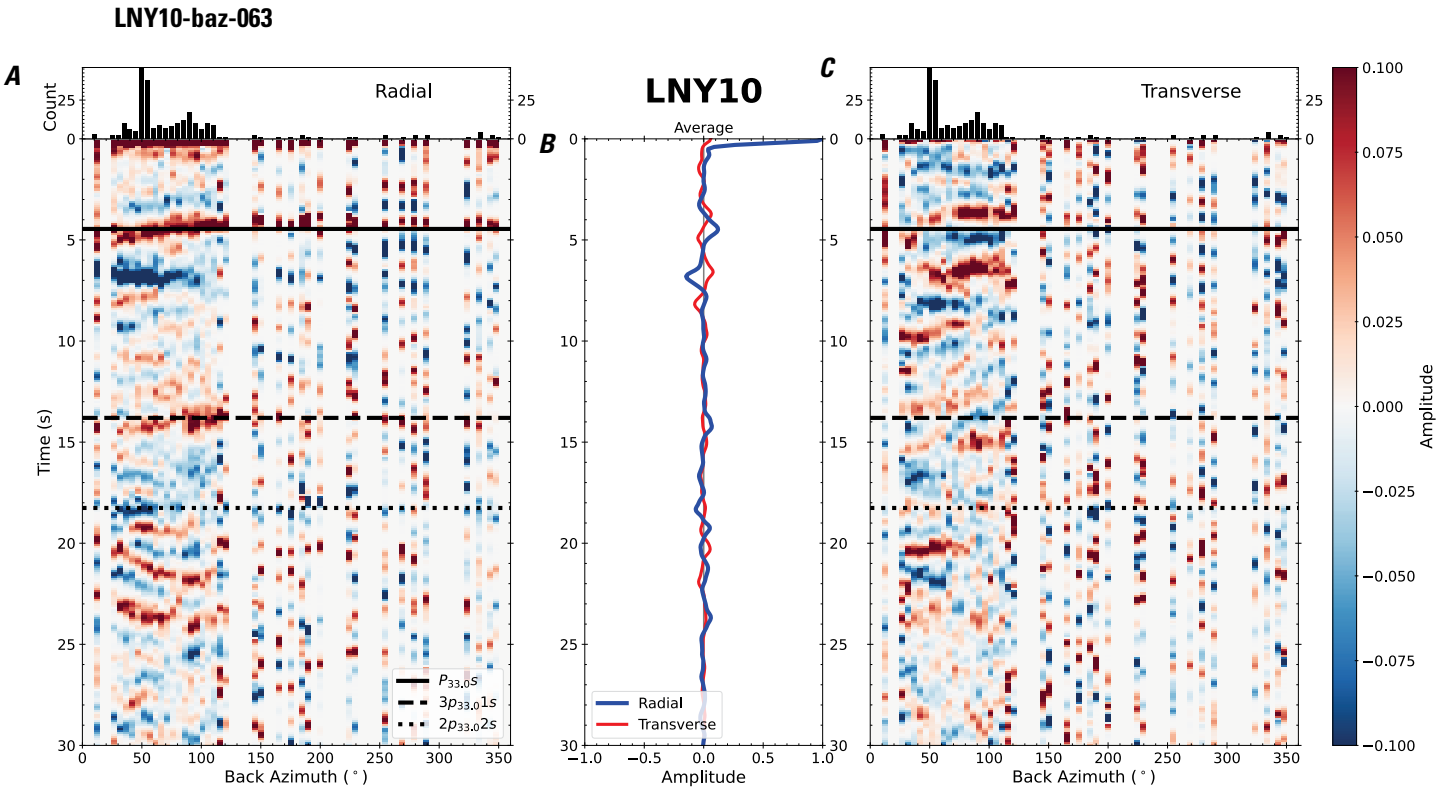

Figure 131. Receiver functions plotted against back azimuth for station LNY10. *A*, Radial component of P-wave receiver functions (PRFs) plotted against back azimuth. Individual PRFs have had the resonance-removal filter of Yu and others (2015) applied to them, are normalized to the maximum amplitude within the time window shown, binned, and normalized by the number of traces per bin. *B*, Average of every individual normalized radial receiver function with the application of the resonance-removal filter (blue) and average of every individual normalized raw radial receiver function (red). *C*, Radial component of raw PRFs, plotted against back azimuth, normalized as in *A*. Ps, 3p1s, and 2p2s arrival times predicted for the preferred Moho depth are shown, assuming a ray parameter of 0.06 s/km.

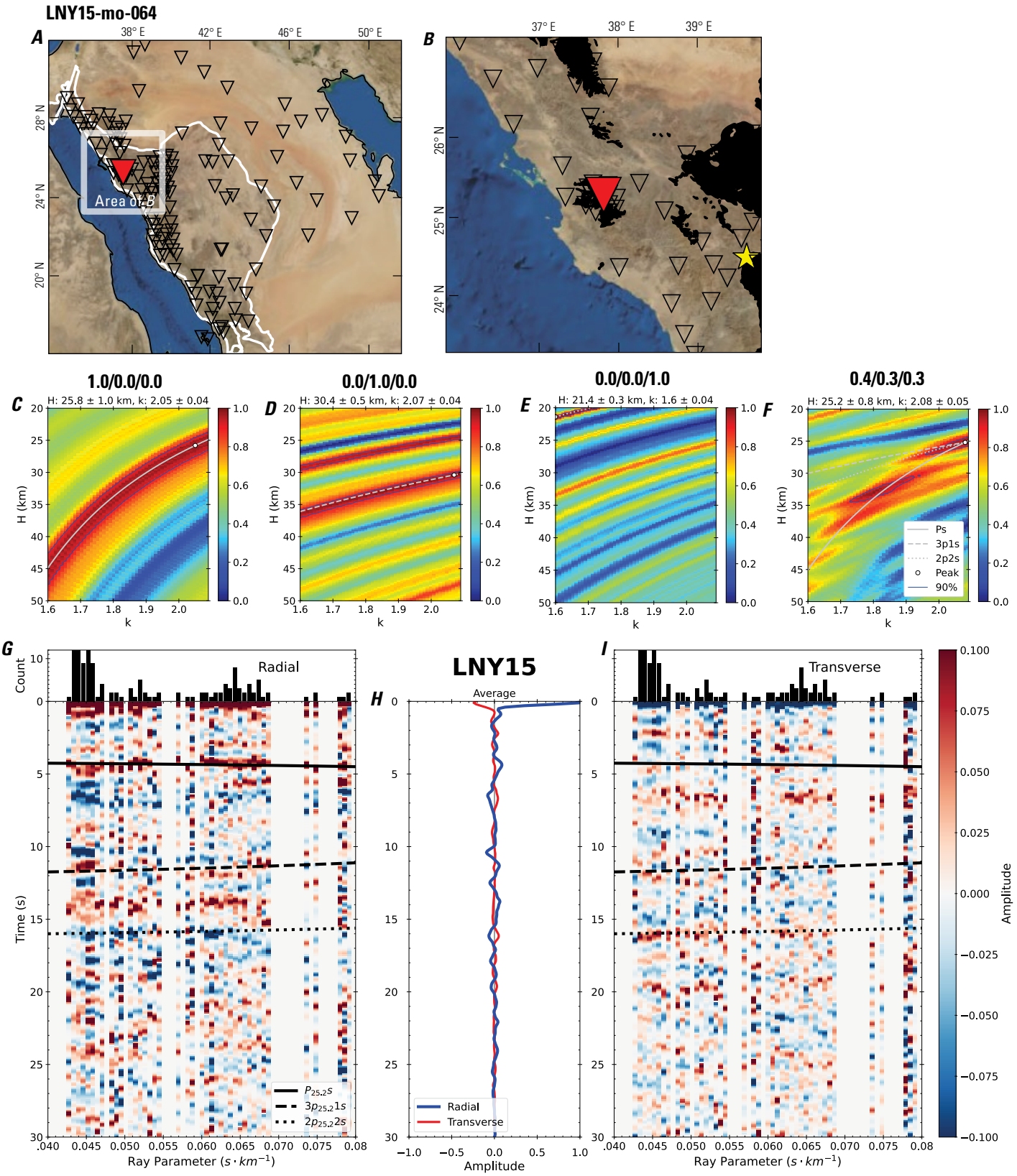
LNY15-mo-064
A
B
Area of B
1.0/0.0/0.0
0.0/1.0/0.0
0.0/0.0/1.0
0.4/0.3/0.3
C
D
E
F
H: 25.8 ± 1.0 km, k: 2.05 ± 0.04
H: 30.4 ± 0.5 km, k: 2.07 ± 0.04
H: 21.4 ± 0.3 km, k: 1.6 ± 0.04
H: 25.2 ± 0.8 km, k: 2.08 ± 0.05
H (km)
k
Ps
3p1s
2p2s
Peak
90%
G
H
I
LNY15
Radial
Transverse
Average
Count
Time (s)
Ray Parameter (s · km⁻¹)
Amplitude
P25,2s
3p25,21s
2p25,22s

Figure 132 (page 138). Receiver-function analysis for station LNY15. *A*, Regional map of Saudi Arabia showing the entire array (as inverted triangles), the location of station LNY15 (red inverted triangle), the shield-platform boundary (white line), and the bounds of the map in *B* (white box). *B*, Local map of station LNY15. Harrats are shown in black. *C*, Standard, single-layer *H-k* stack with stacking weights 0.4/0.3/0.3. This *H-k* stack ignores sedimentary effects on the receiver functions. *D*, Standard, single-layer *H-k* stack with stacking weights 0.5/0.5/0.0. This *H-k* stack also ignores sedimentary effects on the receiver functions. *E*, Optimized sub-sedimentary *H-k* stack with stacking weights 0.4/0.3/0.3, following the method of Yu and others (2015). *F*, Optimized sedimentary *H-k* stack with stacking weights 0.05/0.70/0.25, following the method of Yu and others (2015). *G*, Radial component P-wave receiver functions (PRFs) plotted against ray parameter. Individual PRFs have had the resonance-removal filter of Yu and others (2015) applied to them and are normalized to the maximum amplitude within the time window shown, binned, and normalized by the number of traces per bin. *H*, Average of every individual normalized radial receiver function with the application of the resonance-removal filter (blue) and average of every individual normalized raw radial receiver function (red). *I*, Radial component of raw PRFs (that is, PRFs with no resonance-removal filter applied) plotted against ray parameter, normalized as in *G*.

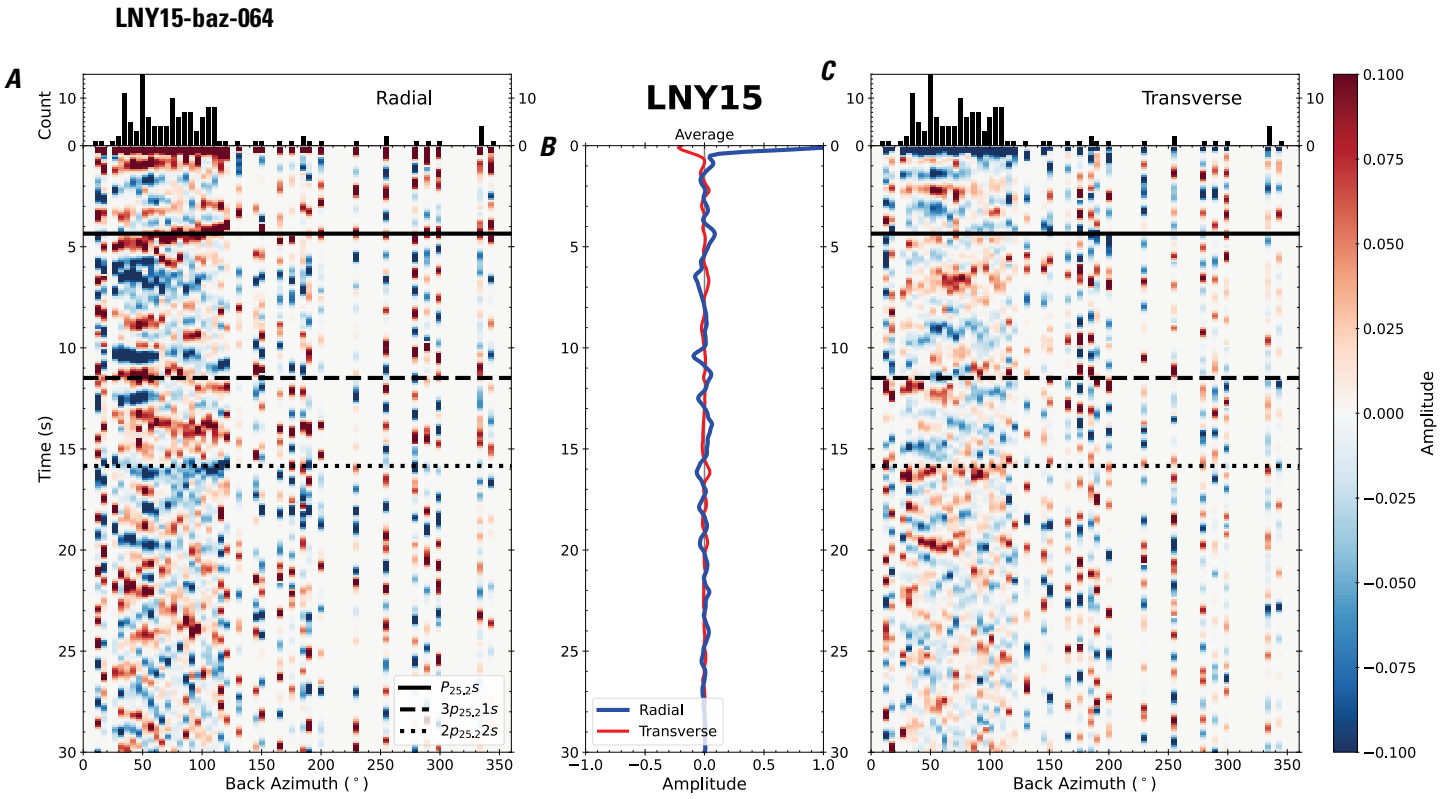

Figure 133. Receiver functions plotted against back azimuth for station LNY15. *A*, Radial component of P-wave receiver functions (PRFs) plotted against back azimuth. Individual PRFs have had the resonance-removal filter of Yu and others (2015) applied to them, are normalized to the maximum amplitude within the time window shown, binned, and normalized by the number of traces per bin. *B*, Average of every individual normalized radial receiver function with the application of the resonance-removal filter (blue) and average of every individual normalized raw radial receiver function (red). *C*, Radial component of raw PRFs, plotted against back azimuth, normalized as in *A*. Ps, 3p1s, and 2p2s arrival times predicted for the preferred Moho depth are shown, assuming a ray parameter of 0.06 s/km.

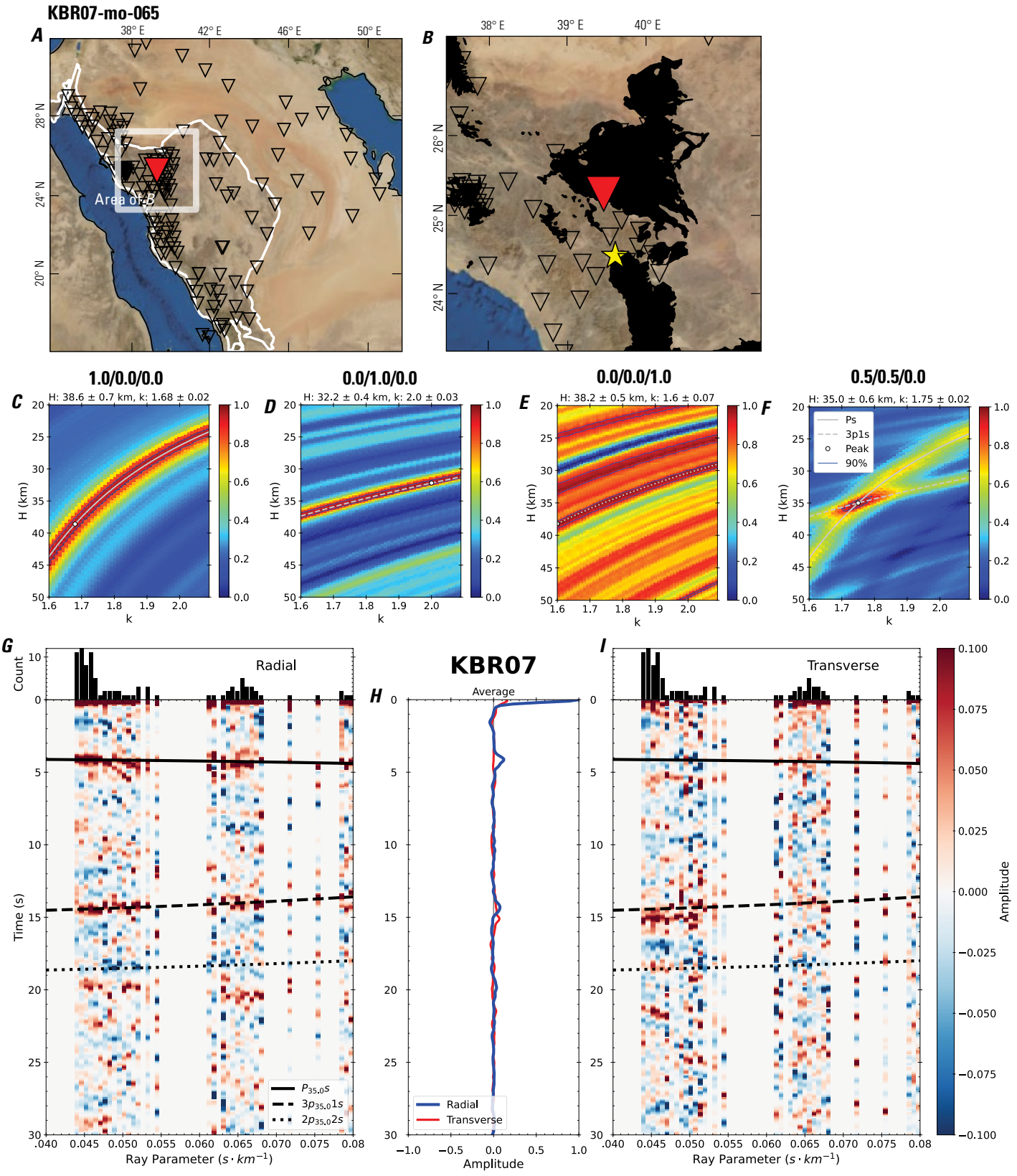
KBR07-mo-065
A
38° E
42° E
46° E
50° E
28° N
24° N
20° N
Area of B
B
38° E
39° E
40° E
26° N
25° N
24° N
1.0/0.0/0.0
0.0/1.0/0.0
0.0/0.0/1.0
0.5/0.5/0.0
C
H: 38.6 ± 0.7 km, k: 1.68 ± 0.02
D
H: 32.2 ± 0.4 km, k: 2.0 ± 0.03
E
H: 38.2 ± 0.5 km, k: 1.6 ± 0.07
F
H: 35.0 ± 0.6 km, k: 1.75 ± 0.02
Ps
3p1s
Peak
90%
H (km)
k
G
Radial
Count
Time (s)
$P_{35.0}s$
$3p_{35.0}1s$
$2p_{35.0}2s$
Ray Parameter ($s \cdot km^{-1}$)
KBR07
H
Average
Radial
Transverse
Amplitude
I
Transverse
Amplitude

Figure 134 (page 140). Receiver-function analysis for station KBR07. *A*, Regional map of Saudi Arabia showing the entire array (as inverted triangles), the location of station KBR07 (red inverted triangle), the shield-platform boundary (white line), and the bounds of the map in *B* (white box). *B*, Local map of station KBR07. Harrats are shown in black. *C*, Standard, single-layer *H-k* stack with stacking weights 0.4/0.3/0.3. This *H-k* stack ignores sedimentary effects on the receiver functions. *D*, Standard, single-layer *H-k* stack with stacking weights 0.5/0.5/0.0. This *H-k* stack also ignores sedimentary effects on the receiver functions. *E*, Optimized sub-sedimentary *H-k* stack with stacking weights 0.4/0.3/0.3, following the method of Yu and others (2015). *F*, Optimized sedimentary *H-k* stack with stacking weights 0.05/0.70/0.25, following the method of Yu and others (2015). *G*, Radial component P-wave receiver functions (PRFs) plotted against ray parameter. Individual PRFs have had the resonance-removal filter of Yu and others (2015) applied to them and are normalized to the maximum amplitude within the time window shown, binned, and normalized by the number of traces per bin. *H*, Average of every individual normalized radial receiver function with the application of the resonance-removal filter (blue) and average of every individual normalized raw radial receiver function (red). *I*, Radial component of raw PRFs (that is, PRFs with no resonance-removal filter applied) plotted against ray parameter, normalized as in *G*.

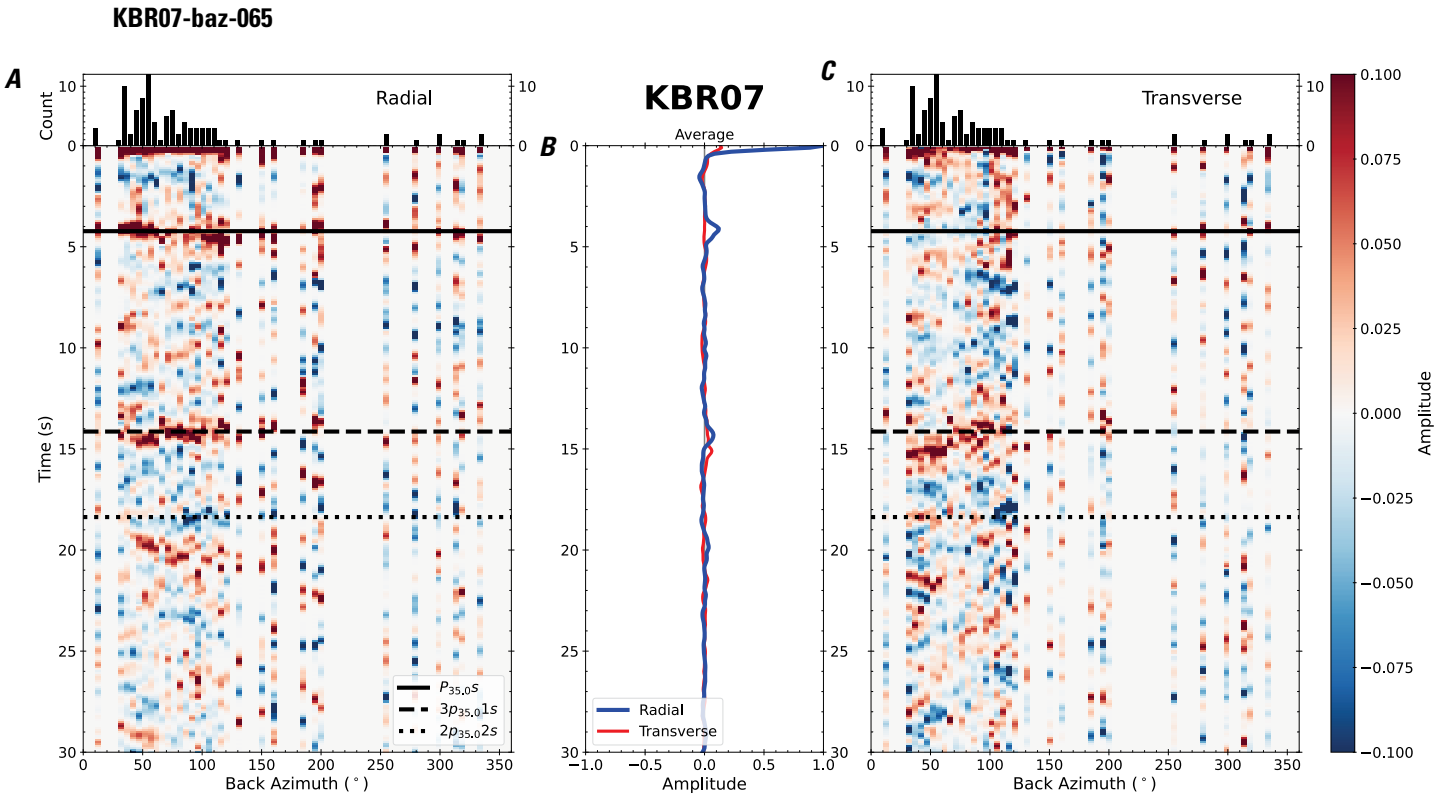

Figure 135. Receiver functions plotted against back azimuth for station KBR07. *A*, Radial component of P-wave receiver functions (PRFs) plotted against back azimuth. Individual PRFs have had the resonance-removal filter of Yu and others (2015) applied to them, are normalized to the maximum amplitude within the time window shown, binned, and normalized by the number of traces per bin. *B*, Average of every individual normalized radial receiver function with the application of the resonance-removal filter (blue) and average of every individual normalized raw radial receiver function (red). *C*, Radial component of raw PRFs, plotted against back azimuth, normalized as in *A*. Ps, 3p1s, and 2p2s arrival times predicted for the preferred Moho depth are shown, assuming a ray parameter of 0.06 s/km.

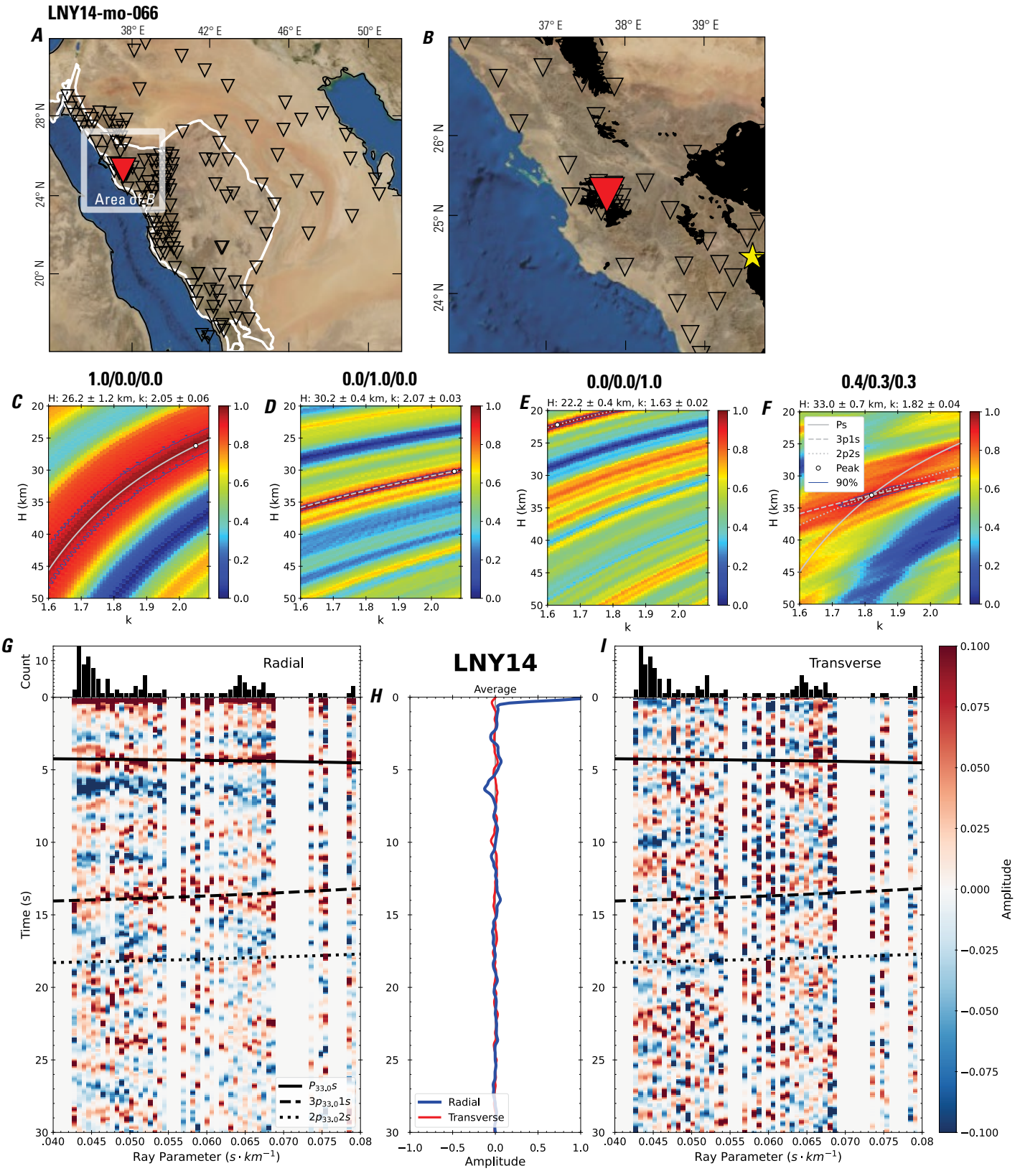
LNY14-mo-066
A
B
Area of B
1.0/0.0/0.0
0.0/1.0/0.0
0.0/0.0/1.0
0.4/0.3/0.3
C
D
E
F
H: 26.2 ± 1.2 km, k: 2.05 ± 0.06
H: 30.2 ± 0.4 km, k: 2.07 ± 0.03
H: 22.2 ± 0.4 km, k: 1.63 ± 0.02
H: 33.0 ± 0.7 km, k: 1.82 ± 0.04
H (km)
k
Ps
3p1s
2p2s
Peak
90%
G
H
I
LNY14
Radial
Transverse
Average
Count
Time (s)
Ray Parameter (s · km⁻¹)
Amplitude
$P_{33.0}s$
$3p_{33.0}1s$
$2p_{33.0}2s$

Figure 136 (page 142). Receiver-function analysis for station LNY14. *A*, Regional map of Saudi Arabia showing the entire array (as inverted triangles), the location of station LNY14 (red inverted triangle), the shield-platform boundary (white line), and the bounds of the map in *B* (white box). *B*, Local map of station LNY14. Harrats are shown in black. *C*, Standard, single-layer *H-k* stack with stacking weights 0.4/0.3/0.3. This *H-k* stack ignores sedimentary effects on the receiver functions. *D*, Standard, single-layer *H-k* stack with stacking weights 0.5/0.5/0.0. This *H-k* stack also ignores sedimentary effects on the receiver functions. *E*, Optimized sub-sedimentary *H-k* stack with stacking weights 0.4/0.3/0.3, following the method of Yu and others (2015). *F*, Optimized sedimentary *H-k* stack with stacking weights 0.05/0.70/0.25, following the method of Yu and others (2015). *G*, Radial component P-wave receiver functions (PRFs) plotted against ray parameter. Individual PRFs have had the resonance-removal filter of Yu and others (2015) applied to them and are normalized to the maximum amplitude within the time window shown, binned, and normalized by the number of traces per bin. *H*, Average of every individual normalized radial receiver function with the application of the resonance-removal filter (blue) and average of every individual normalized raw radial receiver function (red). *I*, Radial component of raw PRFs (that is, PRFs with no resonance-removal filter applied) plotted against ray parameter, normalized as in *G*.

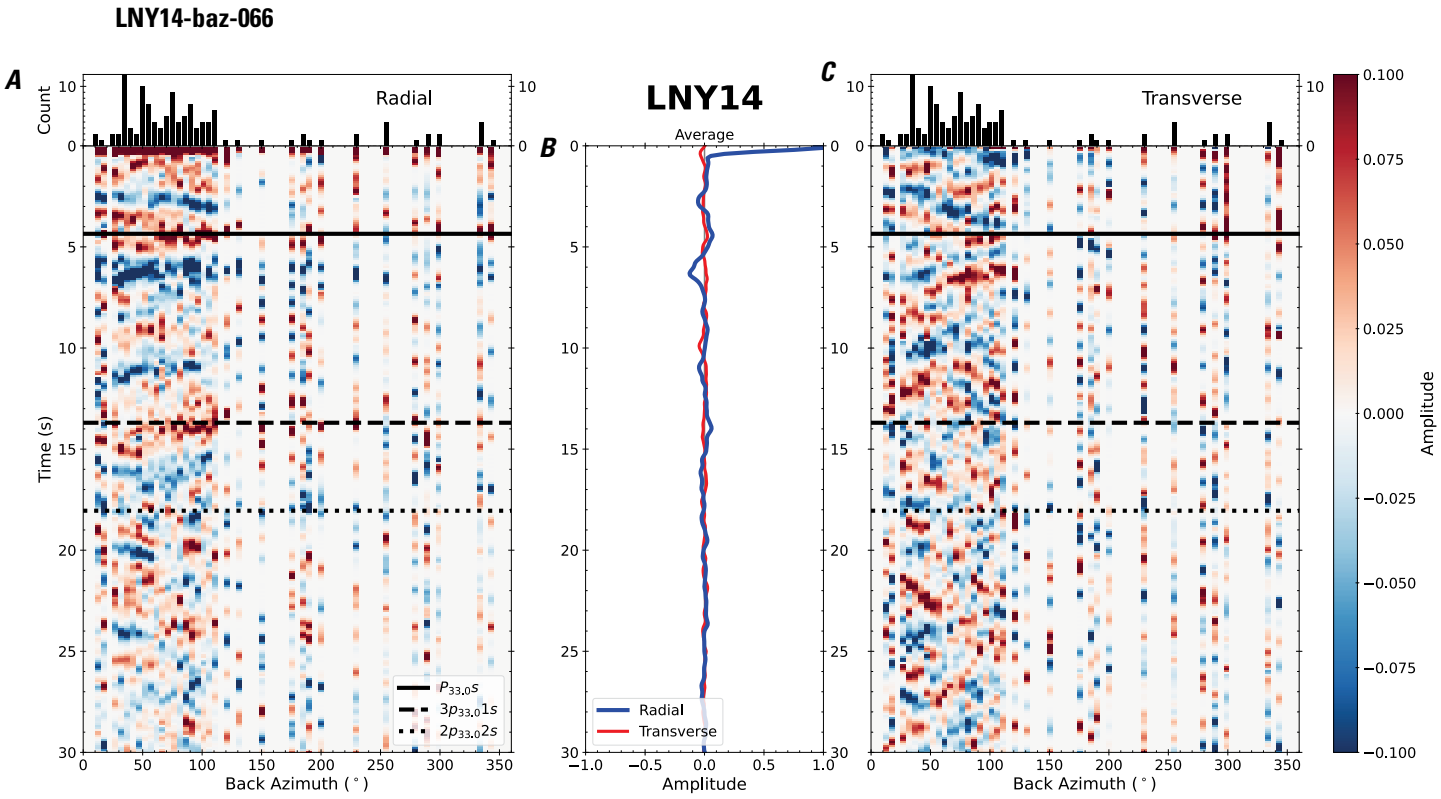

Figure 137. Receiver functions plotted against back azimuth for station LNY14. *A*, Radial component of P-wave receiver functions (PRFs) plotted against back azimuth. Individual PRFs have had the resonance-removal filter of Yu and others (2015) applied to them, are normalized to the maximum amplitude within the time window shown, binned, and normalized by the number of traces per bin. *B*, Average of every individual normalized radial receiver function with the application of the resonance-removal filter (blue) and average of every individual normalized raw radial receiver function (red). *C*, Radial component of raw PRFs, plotted against back azimuth, normalized as in *A*. Ps, 3p1s, and 2p2s arrival times predicted for the preferred Moho depth are shown, assuming a ray parameter of 0.06 s/km.

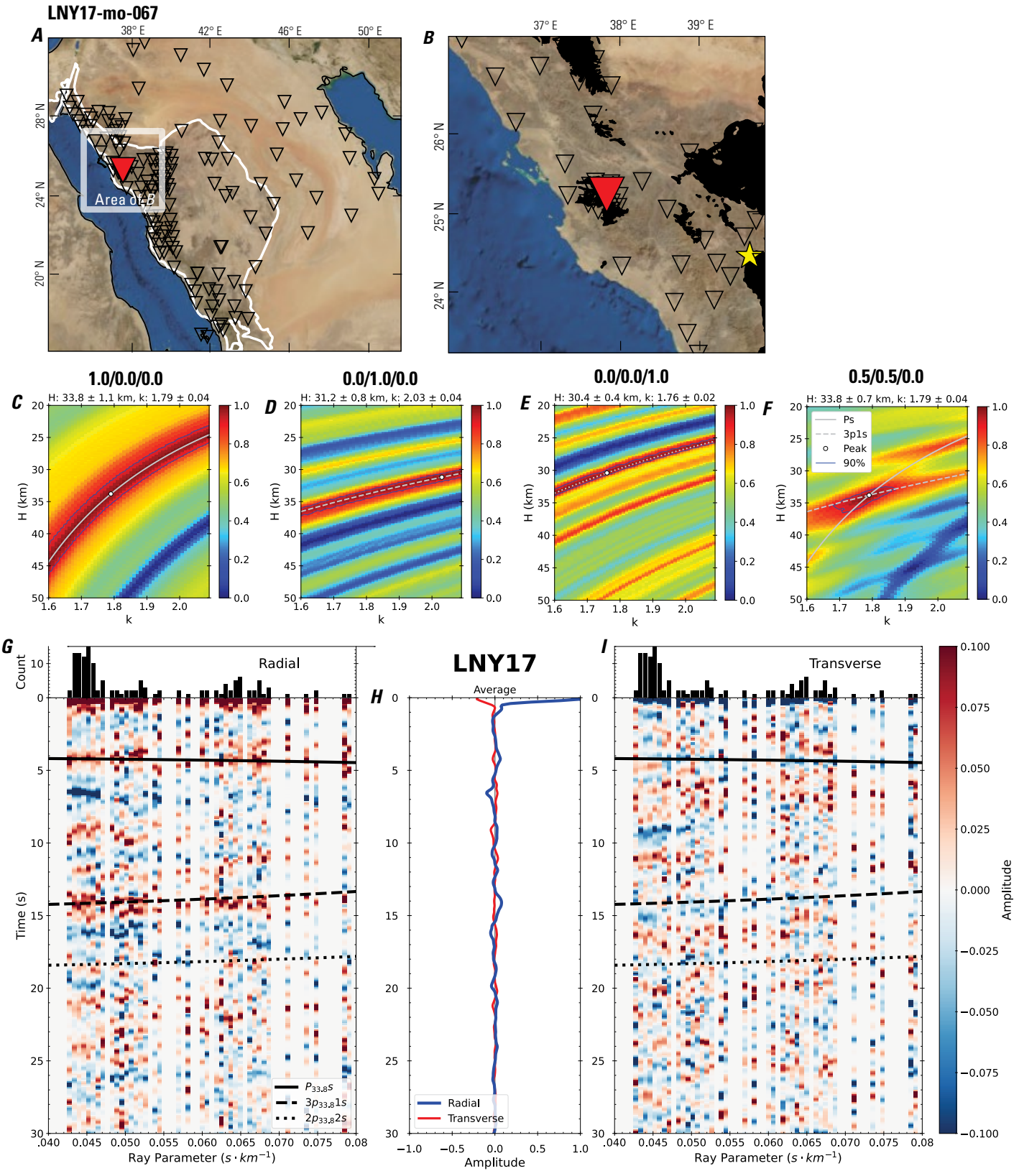
LNY17-mo-067
A
38° E
42° E
46° E
50° E
28° N
24° N
20° N
Area of B
B
37° E
38° E
39° E
26° N
25° N
24° N
1.0/0.0/0.0
0.0/1.0/0.0
0.0/0.0/1.0
0.5/0.5/0.0
C
D
E
F
H: 33.8 ± 1.1 km, k: 1.79 ± 0.04
H: 31.2 ± 0.8 km, k: 2.03 ± 0.04
H: 30.4 ± 0.4 km, k: 1.76 ± 0.02
H: 33.8 ± 0.7 km, k: 1.79 ± 0.04
H (km)
k
Ps
3p1s
Peak
90%
G
Radial
Count
Time (s)
$P_{33.8}s$
$3p_{33.8}1s$
$2p_{33.8}2s$
Ray Parameter ($s \cdot km^{-1}$)
H
LNY17
Average
Radial
Transverse
Amplitude
I
Transverse
Amplitude

Figure 138 (page 144). Receiver-function analysis for station LNY17. *A*, Regional map of Saudi Arabia showing the entire array (as inverted triangles), the location of station LNY17 (red inverted triangle), the shield-platform boundary (white line), and the bounds of the map in *B* (white box). *B*, Local map of station LNY17. Harrats are shown in black. *C*, Standard, single-layer *H-k* stack with stacking weights 0.4/0.3/0.3. This *H-k* stack ignores sedimentary effects on the receiver functions. *D*, Standard, single-layer *H-k* stack with stacking weights 0.5/0.5/0.0. This *H-k* stack also ignores sedimentary effects on the receiver functions. *E*, Optimized sub-sedimentary *H-k* stack with stacking weights 0.4/0.3/0.3, following the method of Yu and others (2015). *F*, Optimized sedimentary *H-k* stack with stacking weights 0.05/0.70/0.25, following the method of Yu and others (2015). *G*, Radial component P-wave receiver functions (PRFs) plotted against ray parameter. Individual PRFs have had the resonance-removal filter of Yu and others (2015) applied to them and are normalized to the maximum amplitude within the time window shown, binned, and normalized by the number of traces per bin. *H*, Average of every individual normalized radial receiver function with the application of the resonance-removal filter (blue) and average of every individual normalized raw radial receiver function (red). *I*, Radial component of raw PRFs (that is, PRFs with no resonance-removal filter applied) plotted against ray parameter, normalized as in *G*.

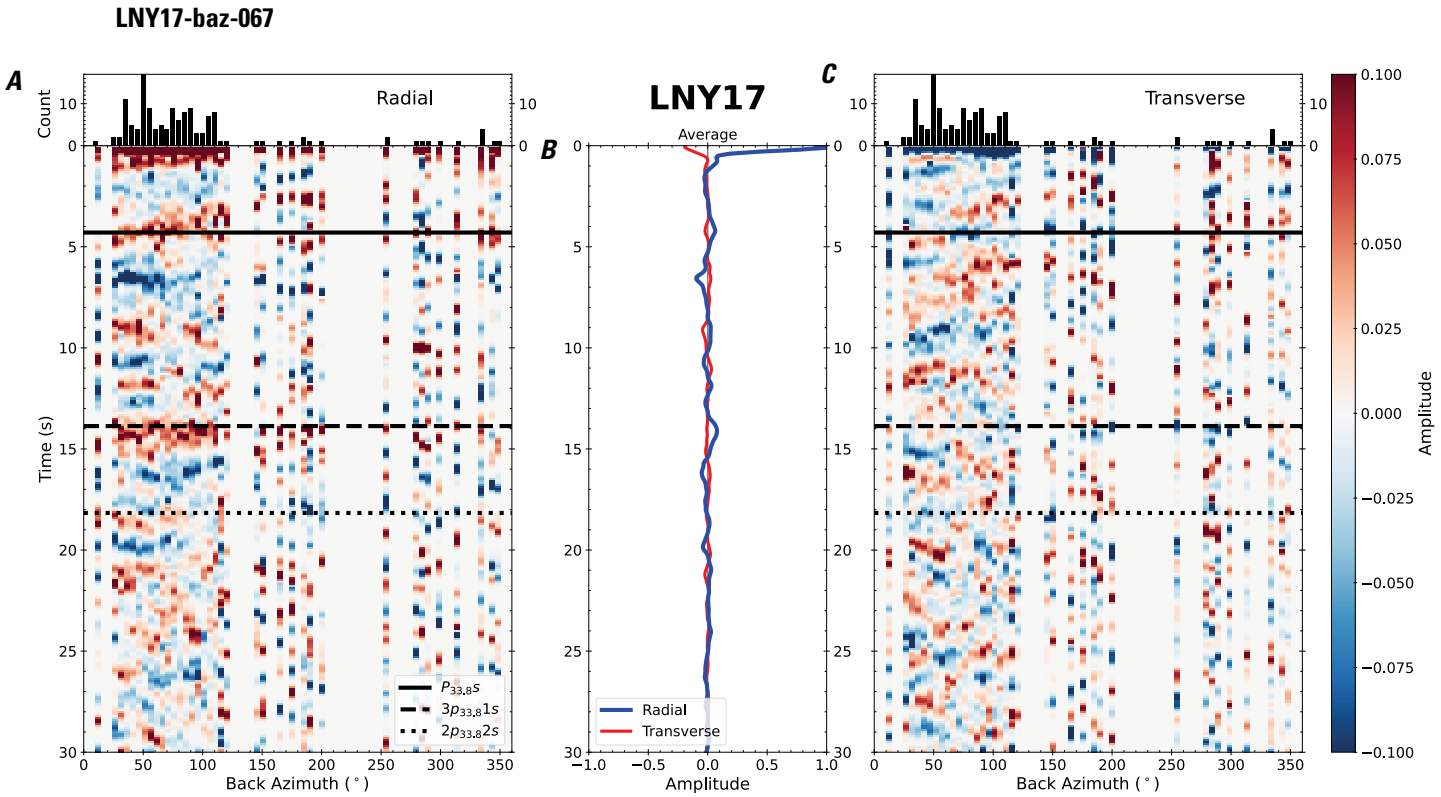

Figure 139. Receiver functions plotted against back azimuth for station LNY17. *A*, Radial component of P-wave receiver functions (PRFs) plotted against back azimuth. Individual PRFs have had the resonance-removal filter of Yu and others (2015) applied to them, are normalized to the maximum amplitude within the time window shown, binned, and normalized by the number of traces per bin. *B*, Average of every individual normalized radial receiver function with the application of the resonance-removal filter (blue) and average of every individual normalized raw radial receiver function (red). *C*, Radial component of raw PRFs, plotted against back azimuth, normalized as in *A*. Ps, 3p1s, and 2p2s arrival times predicted for the preferred Moho depth are shown, assuming a ray parameter of 0.06 s/km.

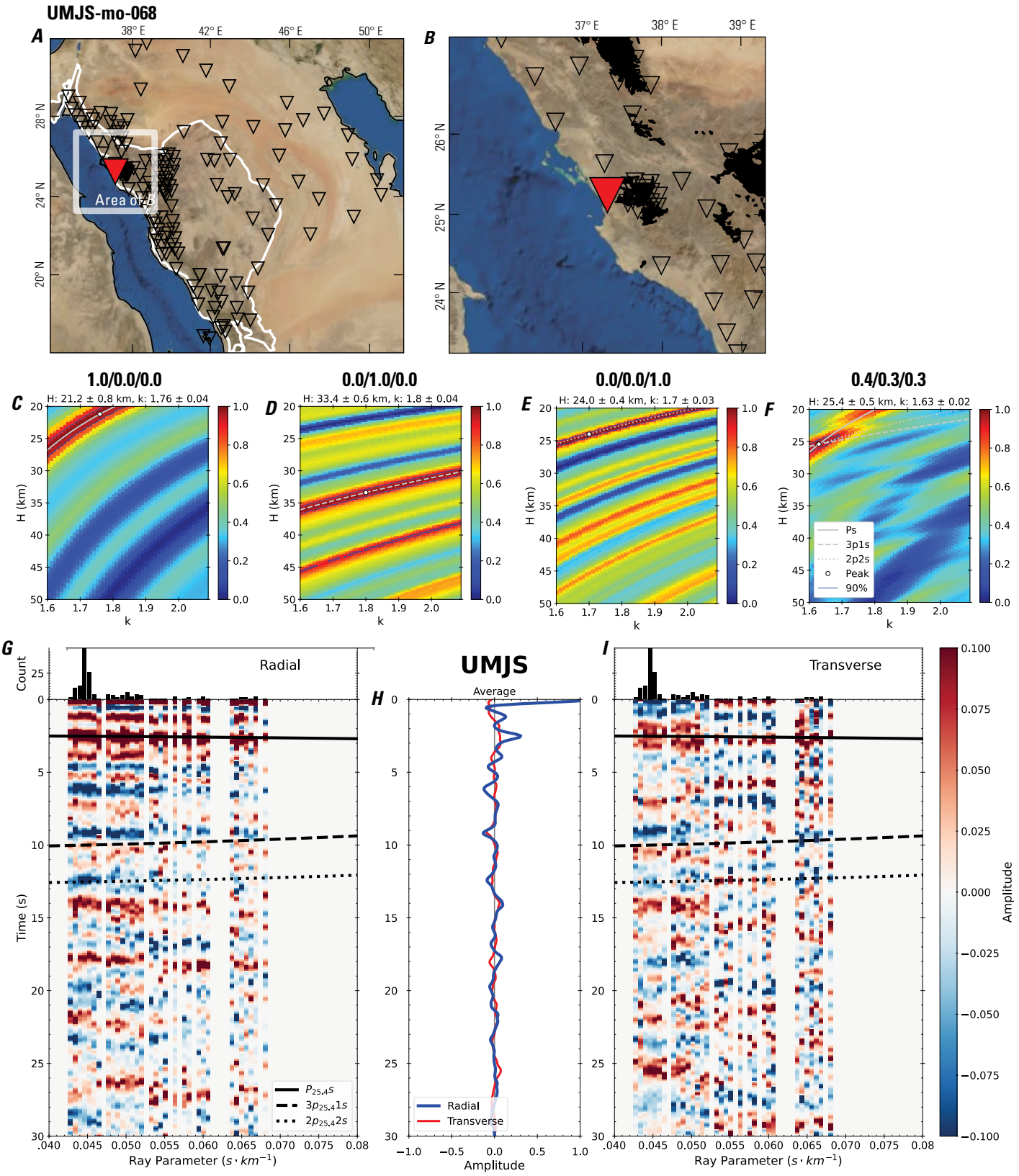
UMJS-mo-068
A
38° E
42° E
46° E
50° E
28° N
24° N
20° N
Area of B
B
37° E
38° E
39° E
26° N
25° N
24° N
1.0/0.0/0.0
0.0/1.0/0.0
0.0/0.0/1.0
0.4/0.3/0.3
C
H: 21.2 ± 0.8 km, k: 1.76 ± 0.04
D
H: 33.4 ± 0.6 km, k: 1.8 ± 0.04
E
H: 24.0 ± 0.4 km, k: 1.7 ± 0.03
F
H: 25.4 ± 0.5 km, k: 1.63 ± 0.02
H (km)
k
Ps
3p1s
2p2s
Peak
90%
G
Radial
Count
Time (s)
$P_{25.4}s$
$3p_{25.4}1s$
$2p_{25.4}2s$
Ray Parameter ($s \cdot km^{-1}$)
UMJS
Average
H
Radial
Transverse
Amplitude
I
Transverse
Amplitude

Figure 140 (page 146). Receiver-function analysis for station UMJS. *A*, Regional map of Saudi Arabia showing the entire array (as inverted triangles), the location of station UMJS (red inverted triangle), the shield-platform boundary (white line), and the bounds of the map in *B* (white box). *B*, Local map of station UMJS. Harrats are shown in black. *C*, Standard, single-layer *H-k* stack with stacking weights 0.4/0.3/0.3. This *H-k* stack ignores sedimentary effects on the receiver functions. *D*, Standard, single-layer *H-k* stack with stacking weights 0.5/0.5/0.0. This *H-k* stack also ignores sedimentary effects on the receiver functions. *E*, Optimized sub-sedimentary *H-k* stack with stacking weights 0.4/0.3/0.3, following the method of Yu and others (2015). *F*, Optimized sedimentary *H-k* stack with stacking weights 0.05/0.70/0.25, following the method of Yu and others (2015). *G*, Radial component P-wave receiver functions (PRFs) plotted against ray parameter. Individual PRFs have had the resonance-removal filter of Yu and others (2015) applied to them and are normalized to the maximum amplitude within the time window shown, binned, and normalized by the number of traces per bin. *H*, Average of every individual normalized radial receiver function with the application of the resonance-removal filter (blue) and average of every individual normalized raw radial receiver function (red). *I*, Radial component of raw PRFs (that is, PRFs with no resonance-removal filter applied) plotted against ray parameter, normalized as in *G*.

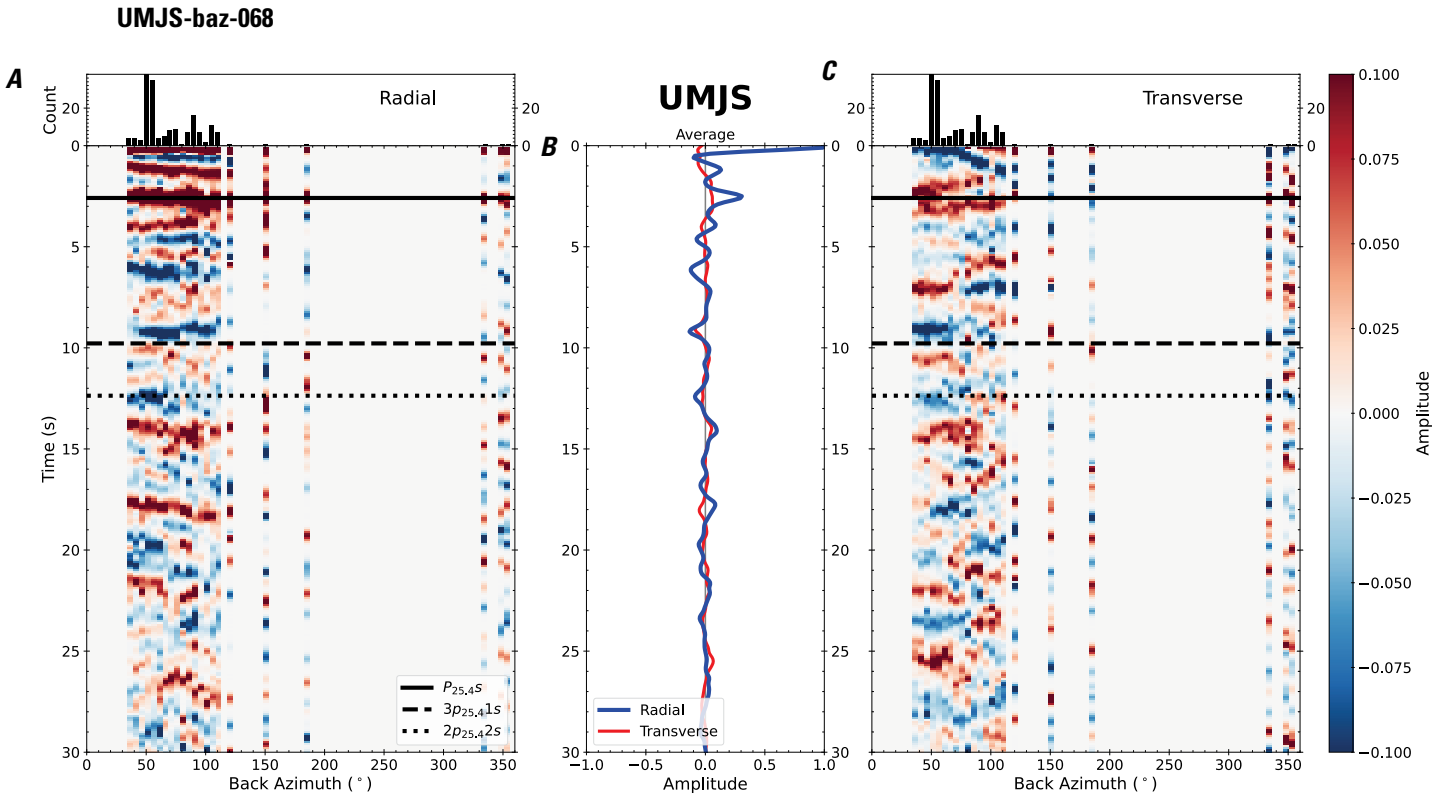

Figure 141. Receiver functions plotted against back azimuth for station UMJS. *A*, Radial component of P-wave receiver functions (PRFs) plotted against back azimuth. Individual PRFs have had the resonance-removal filter of Yu and others (2015) applied to them, are normalized to the maximum amplitude within the time window shown, binned, and normalized by the number of traces per bin. *B*, Average of every individual normalized radial receiver function with the application of the resonance-removal filter (blue) and average of every individual normalized raw radial receiver function (red). *C*, Radial component of raw PRFs, plotted against back azimuth, normalized as in *A*. Ps, 3p1s, and 2p2s arrival times predicted for the preferred Moho depth are shown, assuming a ray parameter of 0.06 s/km.

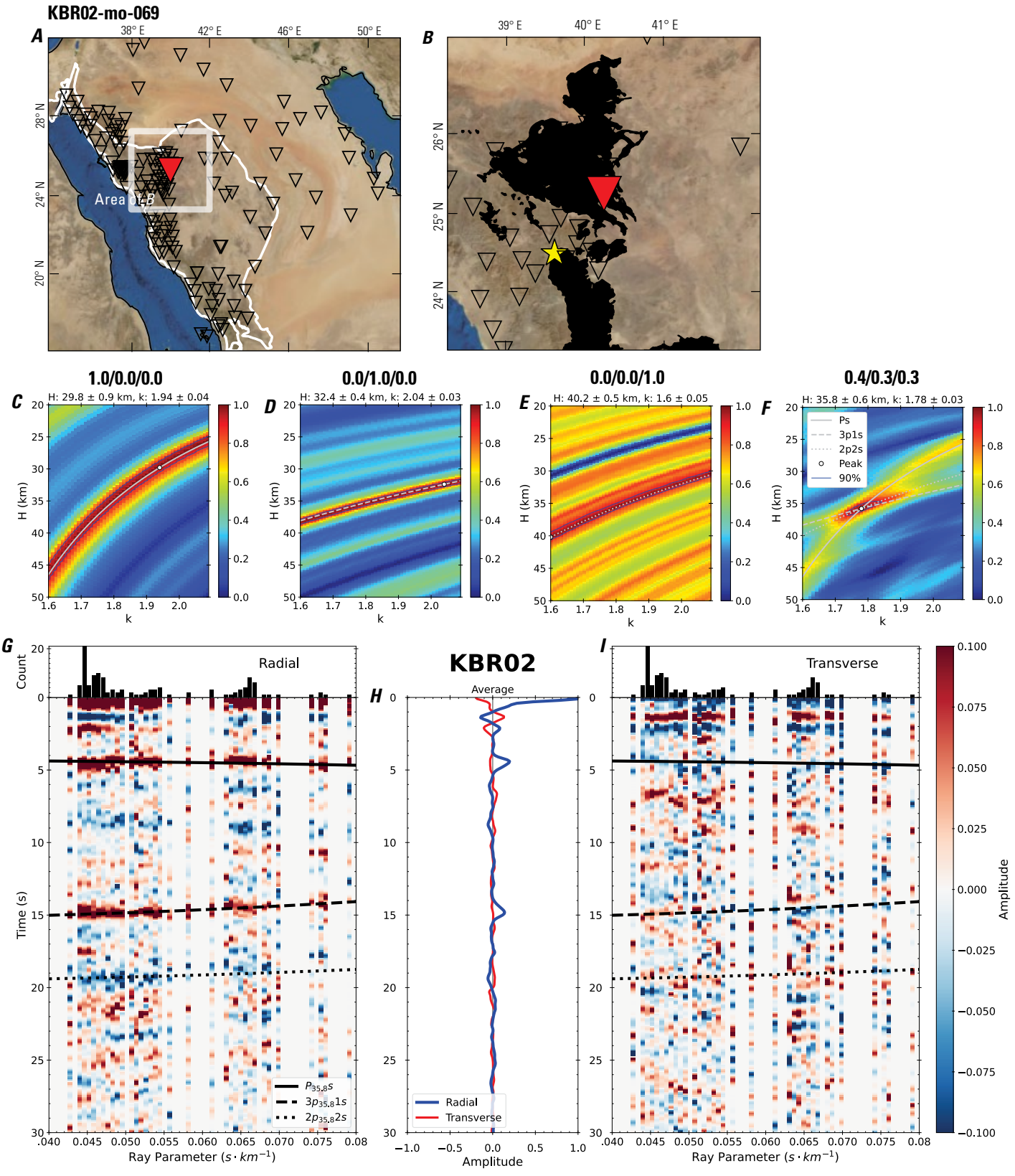
KBR02-mo-069
A
B
Area of B
1.0/0.0/0.0
0.0/1.0/0.0
0.0/0.0/1.0
0.4/0.3/0.3
C
D
E
F
H: 29.8 ± 0.9 km, k: 1.94 ± 0.04
H: 32.4 ± 0.4 km, k: 2.04 ± 0.03
H: 40.2 ± 0.5 km, k: 1.6 ± 0.05
H: 35.8 ± 0.6 km, k: 1.78 ± 0.03
H (km)
k
Ps
3p1s
2p2s
Peak
90%
G
H
I
KBR02
Radial
Transverse
Average
Count
Time (s)
Ray Parameter (s · km⁻¹)
Amplitude
$P_{35.8}s$
$3p_{35.8}1s$
$2p_{35.8}2s$

Figure 142 (page 148). Receiver-function analysis for station KBR02. *A*, Regional map of Saudi Arabia showing the entire array (as inverted triangles), the location of station KBR02 (red inverted triangle), the shield-platform boundary (white line), and the bounds of the map in *B* (white box). *B*, Local map of station KBR02. Harrats are shown in black. *C*, Standard, single-layer *H-k* stack with stacking weights 0.4/0.3/0.3. This *H-k* stack ignores sedimentary effects on the receiver functions. *D*, Standard, single-layer *H-k* stack with stacking weights 0.5/0.5/0.0. This *H-k* stack also ignores sedimentary effects on the receiver functions. *E*, Optimized sub-sedimentary *H-k* stack with stacking weights 0.4/0.3/0.3, following the method of Yu and others (2015). *F*, Optimized sedimentary *H-k* stack with stacking weights 0.05/0.70/0.25, following the method of Yu and others (2015). *G*, Radial component P-wave receiver functions (PRFs) plotted against ray parameter. Individual PRFs have had the resonance-removal filter of Yu and others (2015) applied to them and are normalized to the maximum amplitude within the time window shown, binned, and normalized by the number of traces per bin. *H*, Average of every individual normalized radial receiver function with the application of the resonance-removal filter (blue) and average of every individual normalized raw radial receiver function (red). *I*, Radial component of raw PRFs (that is, PRFs with no resonance-removal filter applied) plotted against ray parameter, normalized as in *G*.

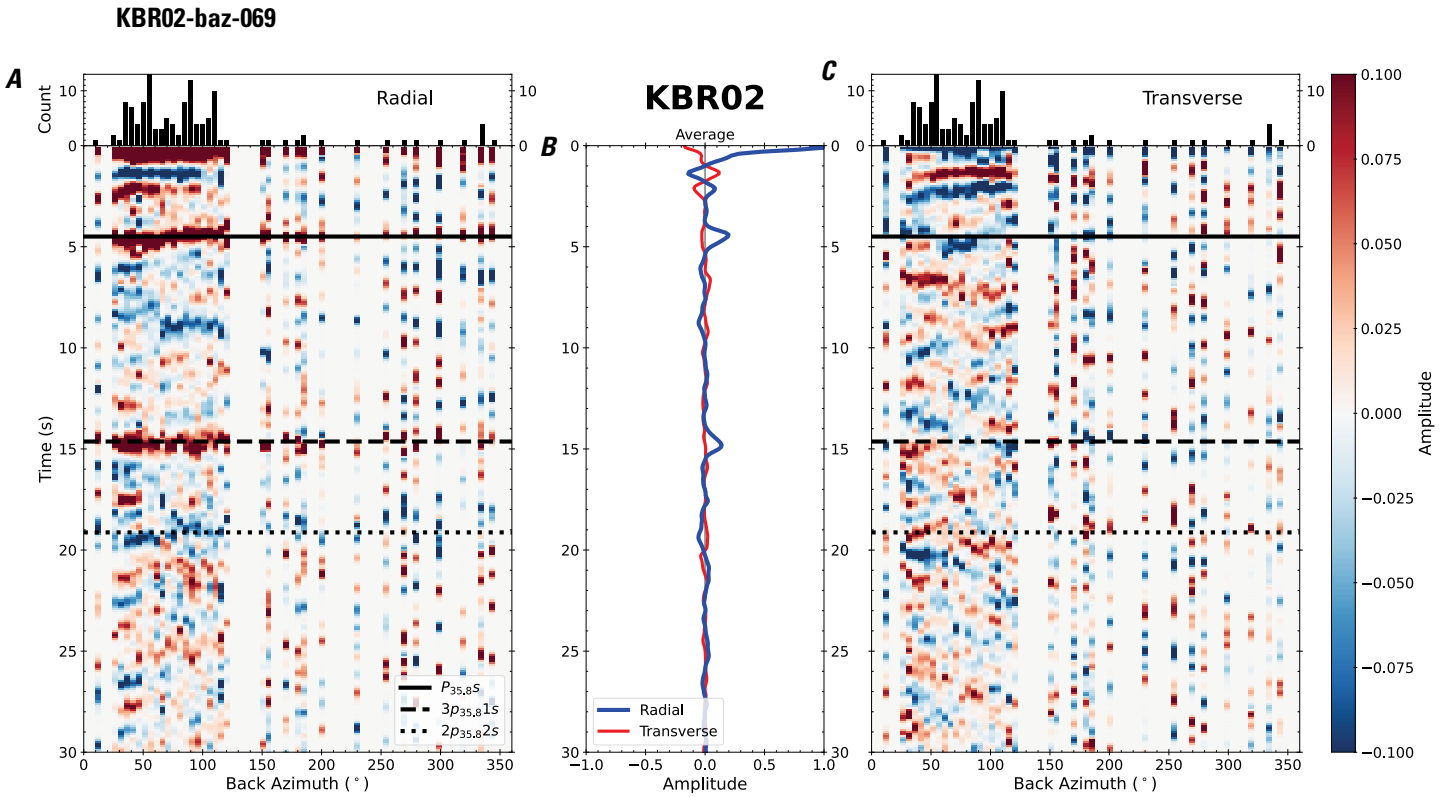

Figure 143. Receiver functions plotted against back azimuth for station KBR02. *A*, Radial component of P-wave receiver functions (PRFs) plotted against back azimuth. Individual PRFs have had the resonance-removal filter of Yu and others (2015) applied to them, are normalized to the maximum amplitude within the time window shown, binned, and normalized by the number of traces per bin. *B*, Average of every individual normalized radial receiver function with the application of the resonance-removal filter (blue) and average of every individual normalized raw radial receiver function (red). *C*, Radial component of raw PRFs, plotted against back azimuth, normalized as in *A*. Ps, 3p1s, and 2p2s arrival times predicted for the preferred Moho depth are shown, assuming a ray parameter of 0.06 s/km.

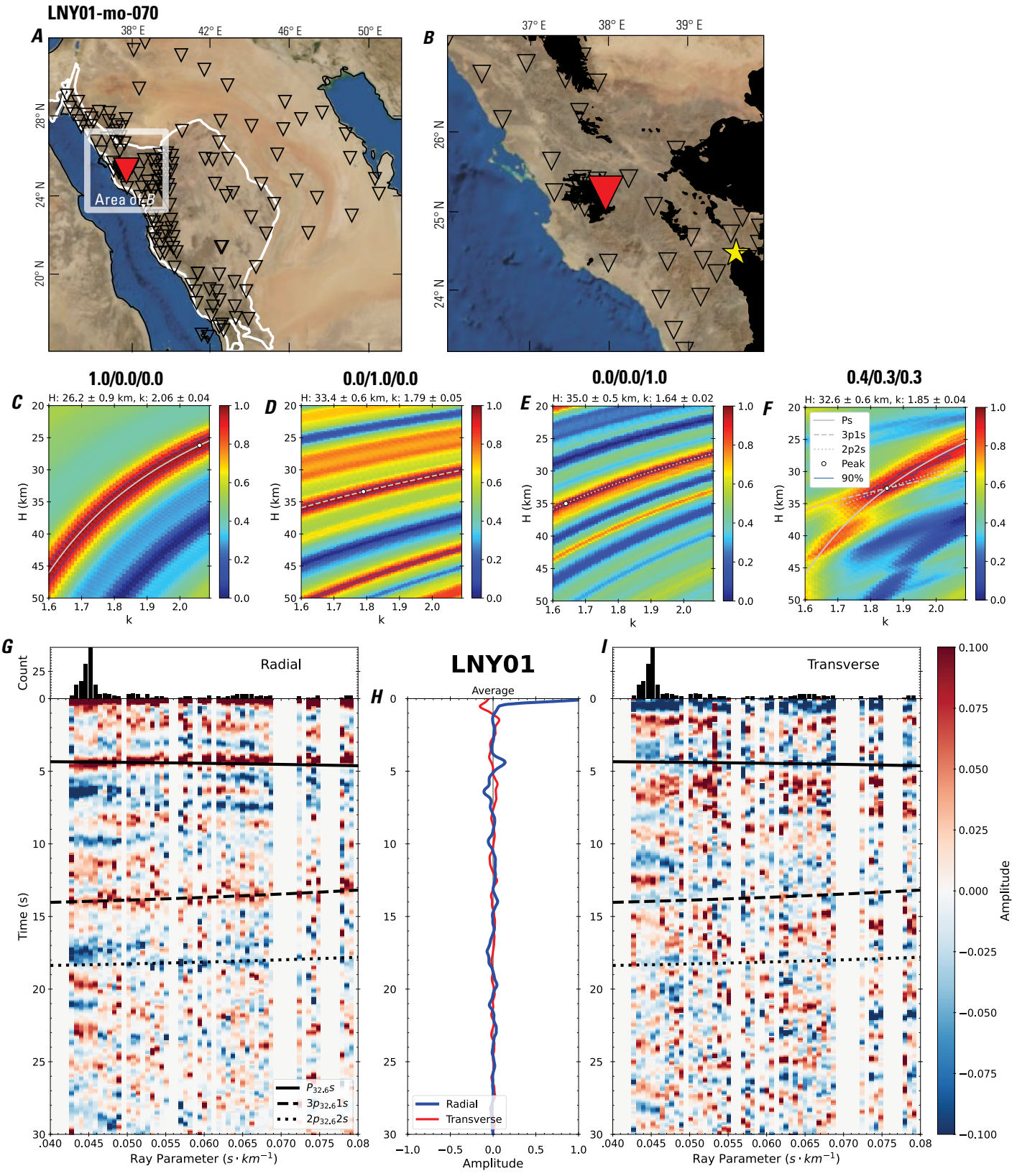
LNY01-mo-070
A
B
Area of B
1.0/0.0/0.0
0.0/1.0/0.0
0.0/0.0/1.0
0.4/0.3/0.3
C
D
E
F
H: 26.2 ± 0.9 km, k: 2.06 ± 0.04
H: 33.4 ± 0.6 km, k: 1.79 ± 0.05
H: 35.0 ± 0.5 km, k: 1.64 ± 0.02
H: 32.6 ± 0.6 km, k: 1.85 ± 0.04
H (km)
k
Ps
3p1s
2p2s
Peak
90%
G
H
I
LNY01
Radial
Transverse
Average
Count
Time (s)
Ray Parameter (s · km⁻¹)
Amplitude
$P_{32.6}s$
$3p_{32.6}1s$
$2p_{32.6}2s$

Figure 144 (page 150). Receiver-function analysis for station LNY01. *A*, Regional map of Saudi Arabia showing the entire array (as inverted triangles), the location of station LNY01 (red inverted triangle), the shield-platform boundary (white line), and the bounds of the map in *B* (white box). *B*, Local map of station LNY01. Harrats are shown in black. *C*, Standard, single-layer *H-k* stack with stacking weights 0.4/0.3/0.3. This *H-k* stack ignores sedimentary effects on the receiver functions. *D*, Standard, single-layer *H-k* stack with stacking weights 0.5/0.5/0.0. This *H-k* stack also ignores sedimentary effects on the receiver functions. *E*, Optimized sub-sedimentary *H-k* stack with stacking weights 0.4/0.3/0.3, following the method of Yu and others (2015). *F*, Optimized sedimentary *H-k* stack with stacking weights 0.05/0.70/0.25, following the method of Yu and others (2015). *G*, Radial component P-wave receiver functions (PRFs) plotted against ray parameter. Individual PRFs have had the resonance-removal filter of Yu and others (2015) applied to them and are normalized to the maximum amplitude within the time window shown, binned, and normalized by the number of traces per bin. *H*, Average of every individual normalized radial receiver function with the application of the resonance-removal filter (blue) and average of every individual normalized raw radial receiver function (red). *I*, Radial component of raw PRFs (that is, PRFs with no resonance-removal filter applied) plotted against ray parameter, normalized as in *G*.

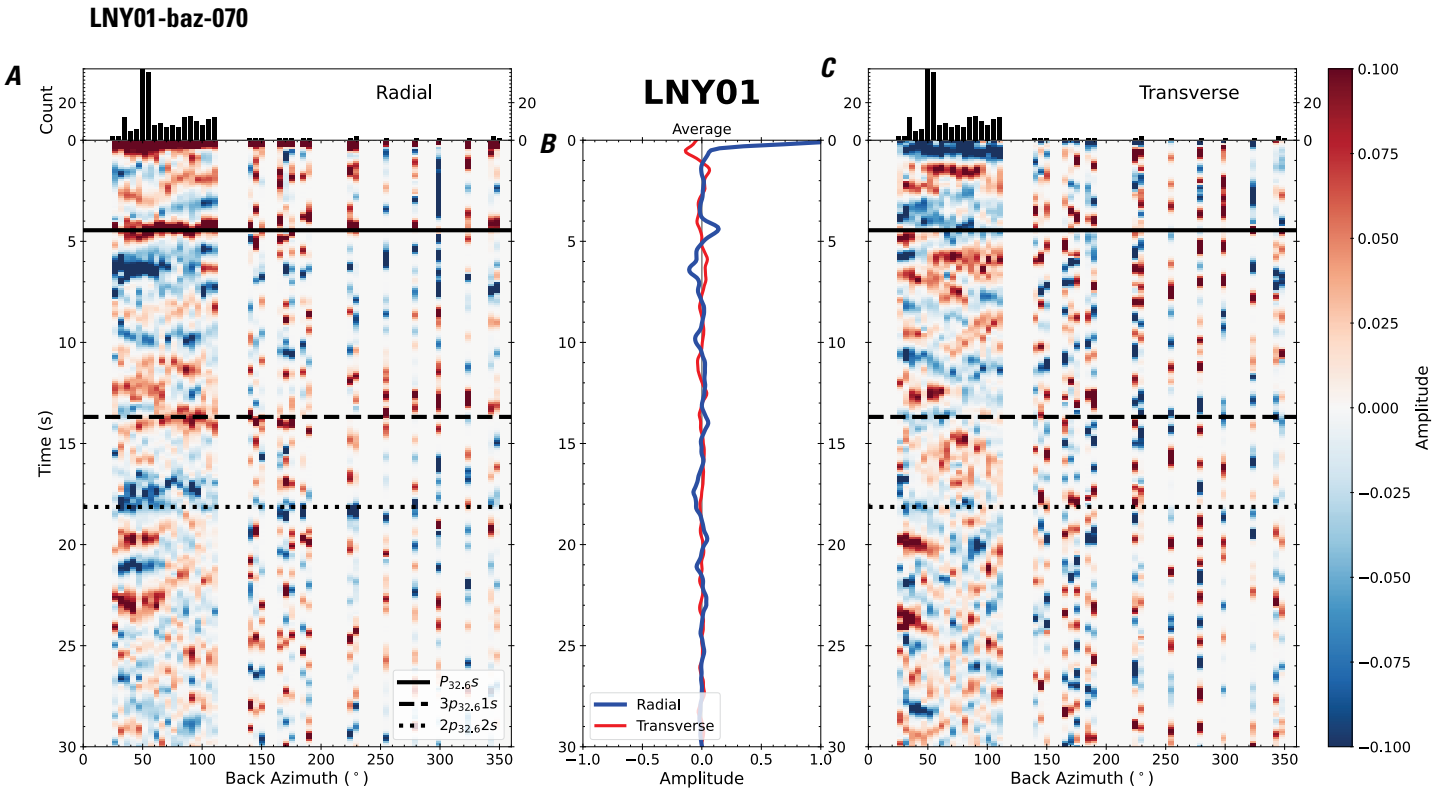

Figure 145. Receiver functions plotted against back azimuth for station LNY01. *A*, Radial component of P-wave receiver functions (PRFs) plotted against back azimuth. Individual PRFs have had the resonance-removal filter of Yu and others (2015) applied to them, are normalized to the maximum amplitude within the time window shown, binned, and normalized by the number of traces per bin. *B*, Average of every individual normalized radial receiver function with the application of the resonance-removal filter (blue) and average of every individual normalized raw radial receiver function (red). *C*, Radial component of raw PRFs, plotted against back azimuth, normalized as in *A*. Ps, 3p1s, and 2p2s arrival times predicted for the preferred Moho depth are shown, assuming a ray parameter of 0.06 s/km.

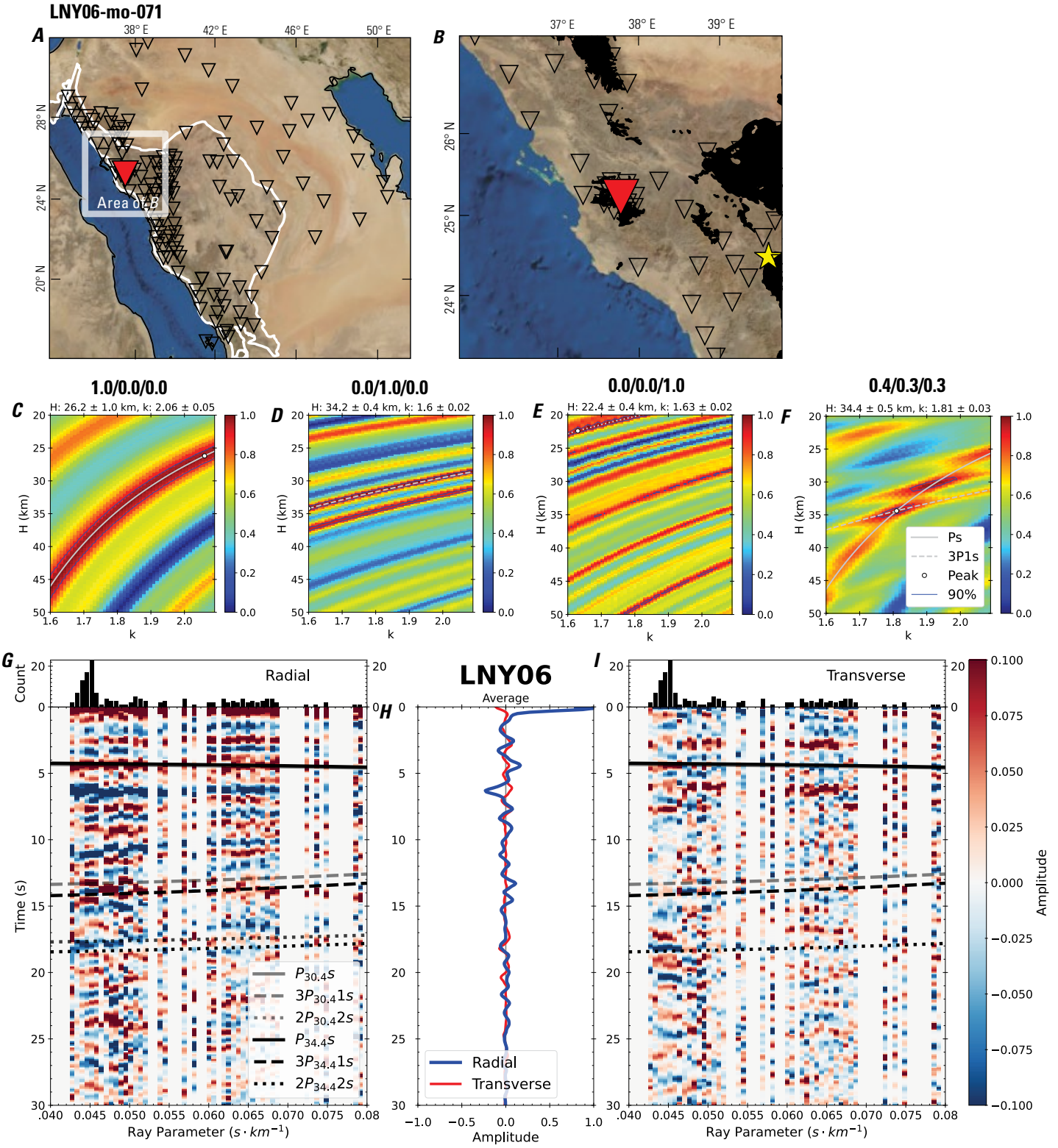
LNY06-mo-071
A
38° E
42° E
46° E
50° E
28° N
24° N
20° N
Area of B
B
37° E
38° E
39° E
26° N
25° N
24° N
1.0/0.0/0.0
0.0/1.0/0.0
0.0/0.0/1.0
0.4/0.3/0.3
C
D
E
F
H: 26.2 ± 1.0 km, k: 2.06 ± 0.05
H: 34.2 ± 0.4 km, k: 1.6 ± 0.02
H: 22.4 ± 0.4 km, k: 1.63 ± 0.02
H: 34.4 ± 0.5 km, k: 1.81 ± 0.03
H (km)
k
Ps
3P1s
Peak
90%
G
H
I
Radial
Transverse
LNY06
Average
Count
Time (s)
Ray Parameter (s · km⁻¹)
Amplitude
$P_{30.4}s$
$3P_{30.4}1s$
$2P_{30.4}2s$
$P_{34.4}s$
$3P_{34.4}1s$
$2P_{34.4}2s$
Radial
Transverse

Figure 146 (page 152). Receiver-function analysis for station LNY06. *A*, Regional map of Saudi Arabia showing the entire array (as inverted triangles), the location of station LNY06 (red inverted triangle), the shield-platform boundary (white line), and the bounds of the map in *B* (white box). *B*, Local map of station LNY06. Harrats are shown in black. *C*, Standard, single-layer *H-k* stack with stacking weights 0.4/0.3/0.3. This *H-k* stack ignores sedimentary effects on the receiver functions. *D*, Standard, single-layer *H-k* stack with stacking weights 0.5/0.5/0.0. This *H-k* stack also ignores sedimentary effects on the receiver functions. *E*, Optimized sub-sedimentary *H-k* stack with stacking weights 0.4/0.3/0.3, following the method of Yu and others (2015). *F*, Optimized sedimentary *H-k* stack with stacking weights 0.05/0.70/0.25, following the method of Yu and others (2015). *G*, Radial component P-wave receiver functions (PRFs) plotted against ray parameter. Individual PRFs have had the resonance-removal filter of Yu and others (2015) applied to them and are normalized to the maximum amplitude within the time window shown, binned, and normalized by the number of traces per bin. *H*, Average of every individual normalized radial receiver function with the application of the resonance-removal filter (blue) and average of every individual normalized raw radial receiver function (red). *I*, Radial component of raw PRFs (that is, PRFs with no resonance-removal filter applied) plotted against ray parameter, normalized as in *G*.

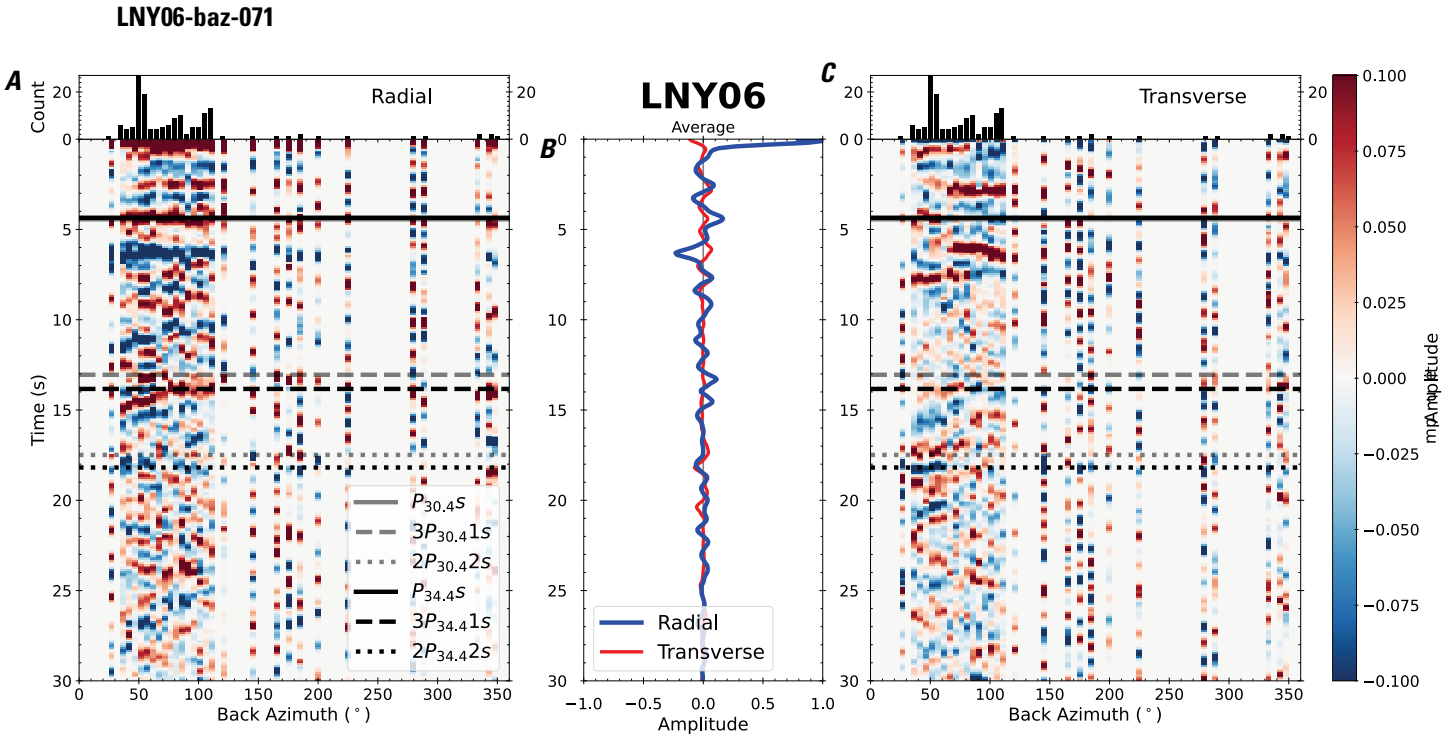

Figure 147. Receiver functions plotted against back azimuth for station LNY06. *A*, Radial component of P-wave receiver functions (PRFs) plotted against back azimuth. Individual PRFs have had the resonance-removal filter of Yu and others (2015) applied to them, are normalized to the maximum amplitude within the time window shown, binned, and normalized by the number of traces per bin. *B*, Average of every individual normalized radial receiver function with the application of the resonance-removal filter (blue) and average of every individual normalized raw radial receiver function (red). *C*, Radial component of raw PRFs, plotted against back azimuth, normalized as in *A*. Ps, 3p1s, and 2p2s arrival times predicted for the preferred Moho depth are shown, assuming a ray parameter of 0.06 s/km.

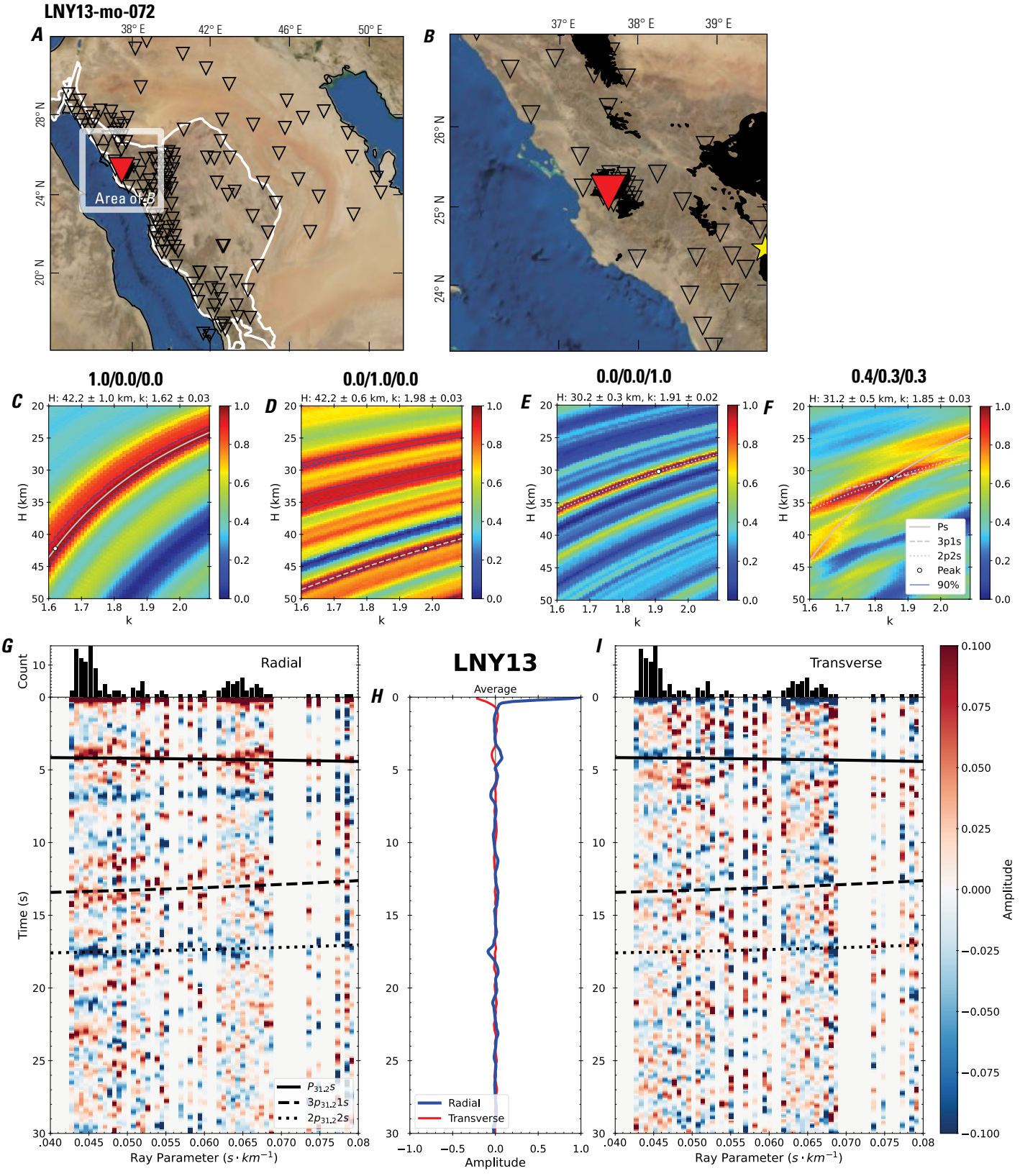
LNY13-mo-072
A
38° E
42° E
46° E
50° E
28° N
24° N
20° N
Area of B
B
37° E
38° E
39° E
26° N
25° N
24° N
1.0/0.0/0.0
0.0/1.0/0.0
0.0/0.0/1.0
0.4/0.3/0.3
C
H: 42.2 ± 1.0 km, k: 1.62 ± 0.03
D
H: 42.2 ± 0.6 km, k: 1.98 ± 0.03
E
H: 30.2 ± 0.3 km, k: 1.91 ± 0.02
F
H: 31.2 ± 0.5 km, k: 1.85 ± 0.03
H (km)
k
Ps
3p1s
2p2s
Peak
90%
G
Radial
Count
Time (s)
Ray Parameter (s · km⁻¹)
$P_{31.2}s$
$3p_{31.2}1s$
$2p_{31.2}2s$
LNY13
H
Average
Radial
Transverse
Amplitude
I
Transverse
Amplitude

Figure 148 (page 154). Receiver-function analysis for station LNY13. *A*, Regional map of Saudi Arabia showing the entire array (as inverted triangles), the location of station LNY13 (red inverted triangle), the shield-platform boundary (white line), and the bounds of the map in *B* (white box). *B*, Local map of station LNY13. Harrats are shown in black. *C*, Standard, single-layer *H-k* stack with stacking weights 0.4/0.3/0.3. This *H-k* stack ignores sedimentary effects on the receiver functions. *D*, Standard, single-layer *H-k* stack with stacking weights 0.5/0.5/0.0. This *H-k* stack also ignores sedimentary effects on the receiver functions. *E*, Optimized sub-sedimentary *H-k* stack with stacking weights 0.4/0.3/0.3, following the method of Yu and others (2015). *F*, Optimized sedimentary *H-k* stack with stacking weights 0.05/0.70/0.25, following the method of Yu and others (2015). *G*, Radial component P-wave receiver functions (PRFs) plotted against ray parameter. Individual PRFs have had the resonance-removal filter of Yu and others (2015) applied to them and are normalized to the maximum amplitude within the time window shown, binned, and normalized by the number of traces per bin. *H*, Average of every individual normalized radial receiver function with the application of the resonance-removal filter (blue) and average of every individual normalized raw radial receiver function (red). *I*, Radial component of raw PRFs (that is, PRFs with no resonance-removal filter applied) plotted against ray parameter, normalized as in *G*.

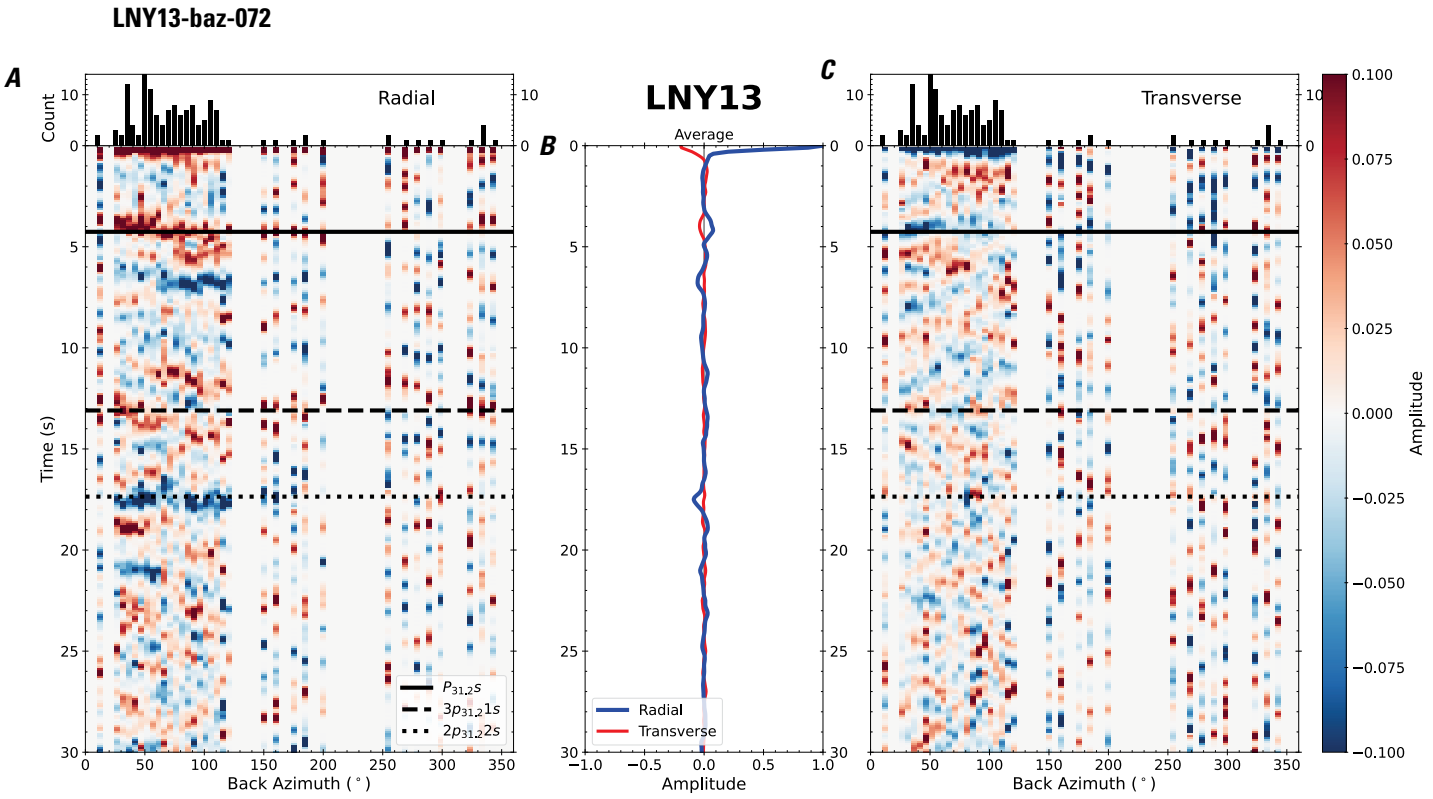

Figure 149. Receiver functions plotted against back azimuth for station LNY13. *A*, Radial component of P-wave receiver functions (PRFs) plotted against back azimuth. Individual PRFs have had the resonance-removal filter of Yu and others (2015) applied to them, are normalized to the maximum amplitude within the time window shown, binned, and normalized by the number of traces per bin. *B*, Average of every individual normalized radial receiver function with the application of the resonance-removal filter (blue) and average of every individual normalized raw radial receiver function (red). *C*, Radial component of raw PRFs, plotted against back azimuth, normalized as in *A*. Ps, 3p1s, and 2p2s arrival times predicted for the preferred Moho depth are shown, assuming a ray parameter of 0.06 s/km.

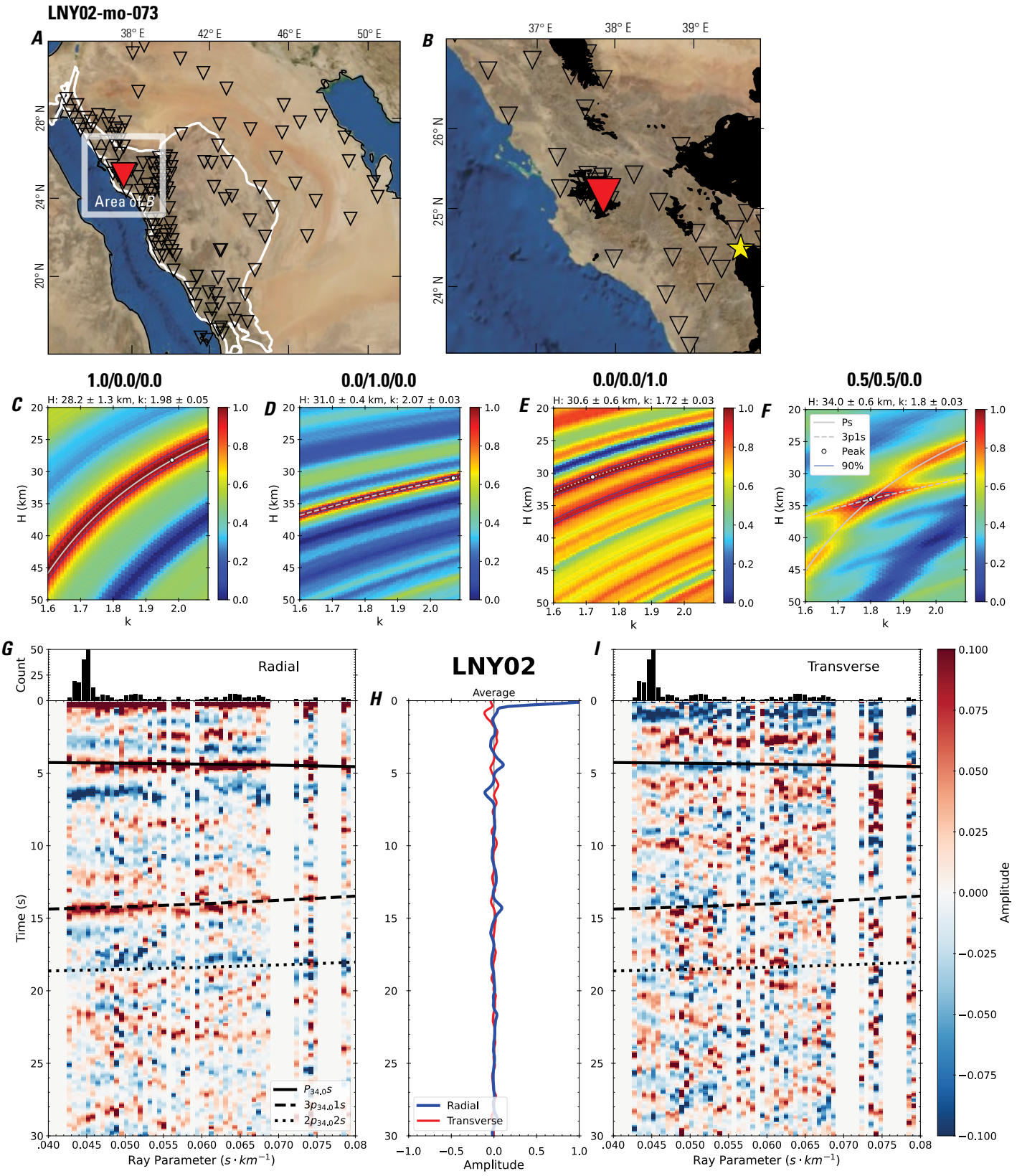
LNY02-mo-073
A
B
Area of B
1.0/0.0/0.0
0.0/1.0/0.0
0.0/0.0/1.0
0.5/0.5/0.0
C
D
E
F
H: 28.2 ± 1.3 km, k: 1.98 ± 0.05
H: 31.0 ± 0.4 km, k: 2.07 ± 0.03
H: 30.6 ± 0.6 km, k: 1.72 ± 0.03
H: 34.0 ± 0.6 km, k: 1.8 ± 0.03
H (km)
k
Ps
3p1s
Peak
90%
G
H
I
LNY02
Radial
Transverse
Average
Count
Time (s)
Ray Parameter (s · km⁻¹)
Amplitude
$P_{34.0}s$
$3p_{34.0}1s$
$2p_{34.0}2s$

Figure 150 (page 156). Receiver-function analysis for station LNY02. *A*, Regional map of Saudi Arabia showing the entire array (as inverted triangles), the location of station LNY02 (red inverted triangle), the shield-platform boundary (white line), and the bounds of the map in *B* (white box). *B*, Local map of station LNY02. Harrats are shown in black. *C*, Standard, single-layer *H-k* stack with stacking weights 0.4/0.3/0.3. This *H-k* stack ignores sedimentary effects on the receiver functions. *D*, Standard, single-layer *H-k* stack with stacking weights 0.5/0.5/0.0. This *H-k* stack also ignores sedimentary effects on the receiver functions. *E*, Optimized sub-sedimentary *H-k* stack with stacking weights 0.4/0.3/0.3, following the method of Yu and others (2015). *F*, Optimized sedimentary *H-k* stack with stacking weights 0.05/0.70/0.25, following the method of Yu and others (2015). *G*, Radial component P-wave receiver functions (PRFs) plotted against ray parameter. Individual PRFs have had the resonance-removal filter of Yu and others (2015) applied to them and are normalized to the maximum amplitude within the time window shown, binned, and normalized by the number of traces per bin. *H*, Average of every individual normalized radial receiver function with the application of the resonance-removal filter (blue) and average of every individual normalized raw radial receiver function (red). *I*, Radial component of raw PRFs (that is, PRFs with no resonance-removal filter applied) plotted against ray parameter, normalized as in *G*.

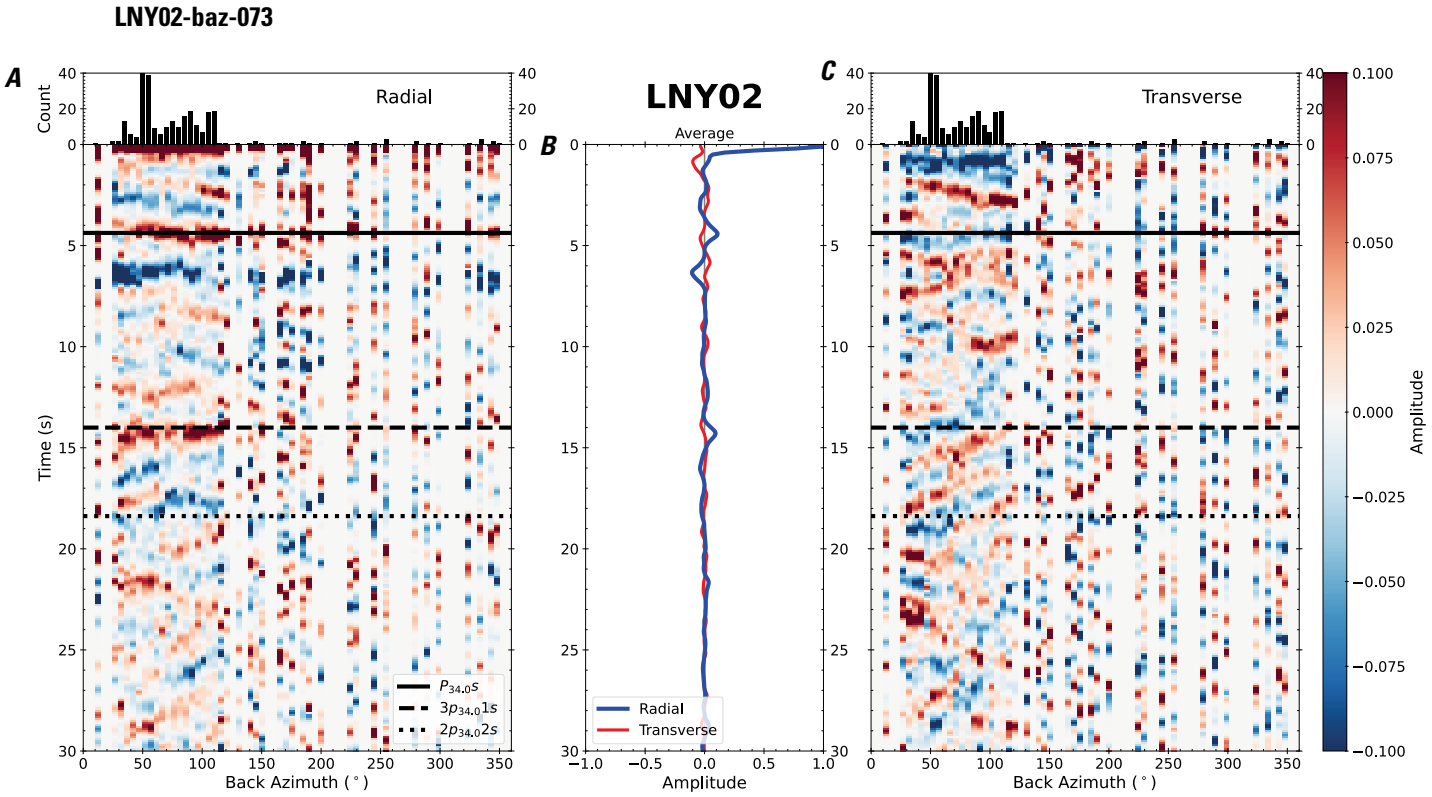

Figure 151. Receiver functions plotted against back azimuth for station LNY02. *A*, Radial component of P-wave receiver functions (PRFs) plotted against back azimuth. Individual PRFs have had the resonance-removal filter of Yu and others (2015) applied to them, are normalized to the maximum amplitude within the time window shown, binned, and normalized by the number of traces per bin. *B*, Average of every individual normalized radial receiver function with the application of the resonance-removal filter (blue) and average of every individual normalized raw radial receiver function (red). *C*, Radial component of raw PRFs, plotted against back azimuth, normalized as in *A*. Ps, 3p1s, and 2p2s arrival times predicted for the preferred Moho depth are shown, assuming a ray parameter of 0.06 s/km.

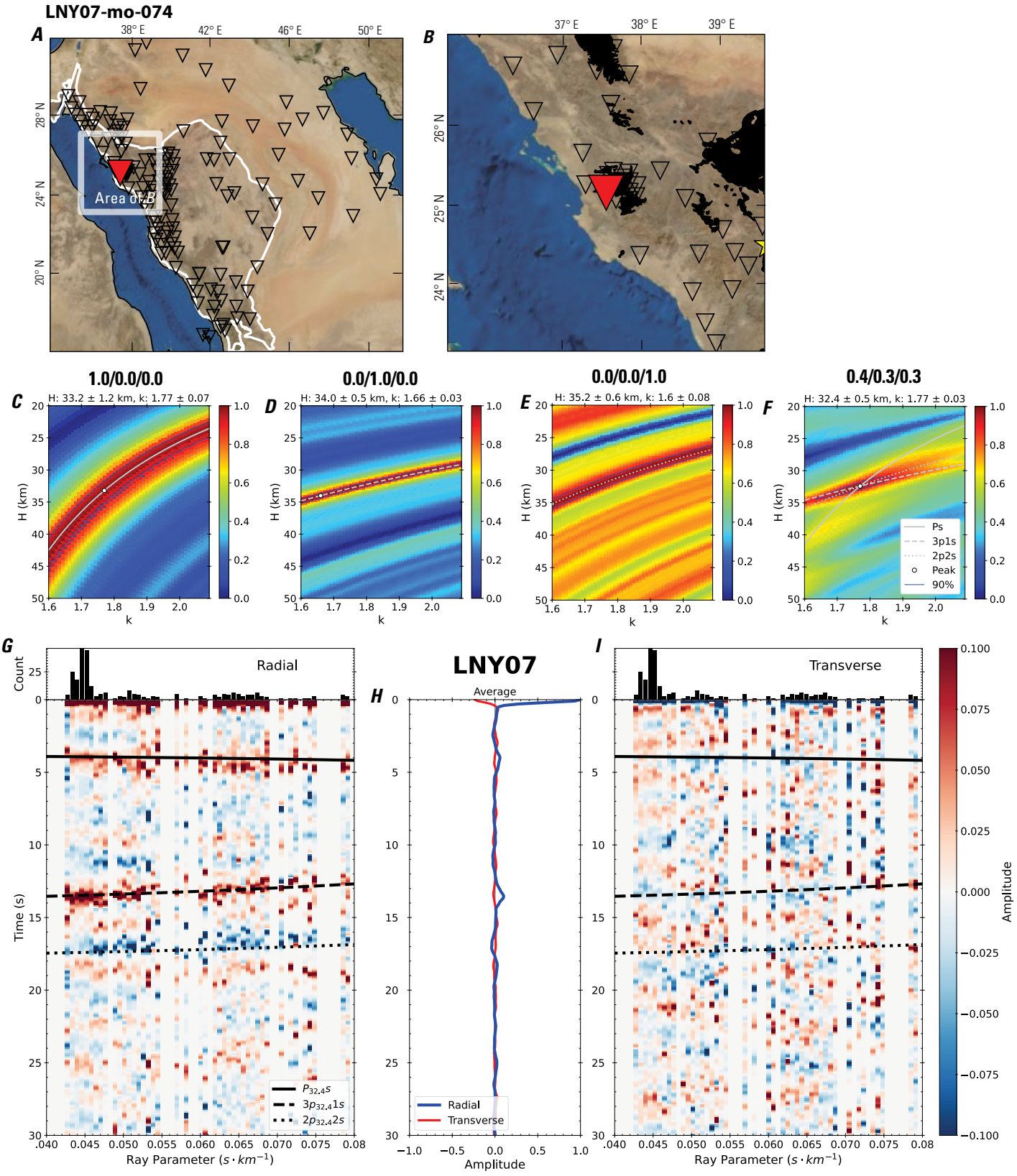
LNY07-mo-074
A
38° E
42° E
46° E
50° E
28° N
24° N
20° N
Area of B
B
37° E
38° E
39° E
26° N
25° N
24° N
1.0/0.0/0.0
0.0/1.0/0.0
0.0/0.0/1.0
0.4/0.3/0.3
C
H: 33.2 ± 1.2 km, k: 1.77 ± 0.07
D
H: 34.0 ± 0.5 km, k: 1.66 ± 0.03
E
H: 35.2 ± 0.6 km, k: 1.6 ± 0.08
F
H: 32.4 ± 0.5 km, k: 1.77 ± 0.03
H (km)
k
Ps
3p1s
2p2s
Peak
90%
G
Radial
Count
Time (s)
$P_{32,4}s$
$3p_{32,4}1s$
$2p_{32,4}2s$
Ray Parameter ($s \cdot km^{-1}$)
LNY07
H
Average
Radial
Transverse
Amplitude
I
Transverse
Amplitude

Figure 152 (page 158). Receiver-function analysis for station LNY07. *A*, Regional map of Saudi Arabia showing the entire array (as inverted triangles), the location of station LNY07 (red inverted triangle), the shield-platform boundary (white line), and the bounds of the map in *B* (white box). *B*, Local map of station LNY07. Harrats are shown in black. *C*, Standard, single-layer *H-k* stack with stacking weights 0.4/0.3/0.3. This *H-k* stack ignores sedimentary effects on the receiver functions. *D*, Standard, single-layer *H-k* stack with stacking weights 0.5/0.5/0.0. This *H-k* stack also ignores sedimentary effects on the receiver functions. *E*, Optimized sub-sedimentary *H-k* stack with stacking weights 0.4/0.3/0.3, following the method of Yu and others (2015). *F*, Optimized sedimentary *H-k* stack with stacking weights 0.05/0.70/0.25, following the method of Yu and others (2015). *G*, Radial component P-wave receiver functions (PRFs) plotted against ray parameter. Individual PRFs have had the resonance-removal filter of Yu and others (2015) applied to them and are normalized to the maximum amplitude within the time window shown, binned, and normalized by the number of traces per bin. *H*, Average of every individual normalized radial receiver function with the application of the resonance-removal filter (blue) and average of every individual normalized raw radial receiver function (red). *I*, Radial component of raw PRFs (that is, PRFs with no resonance-removal filter applied) plotted against ray parameter, normalized as in *G*.

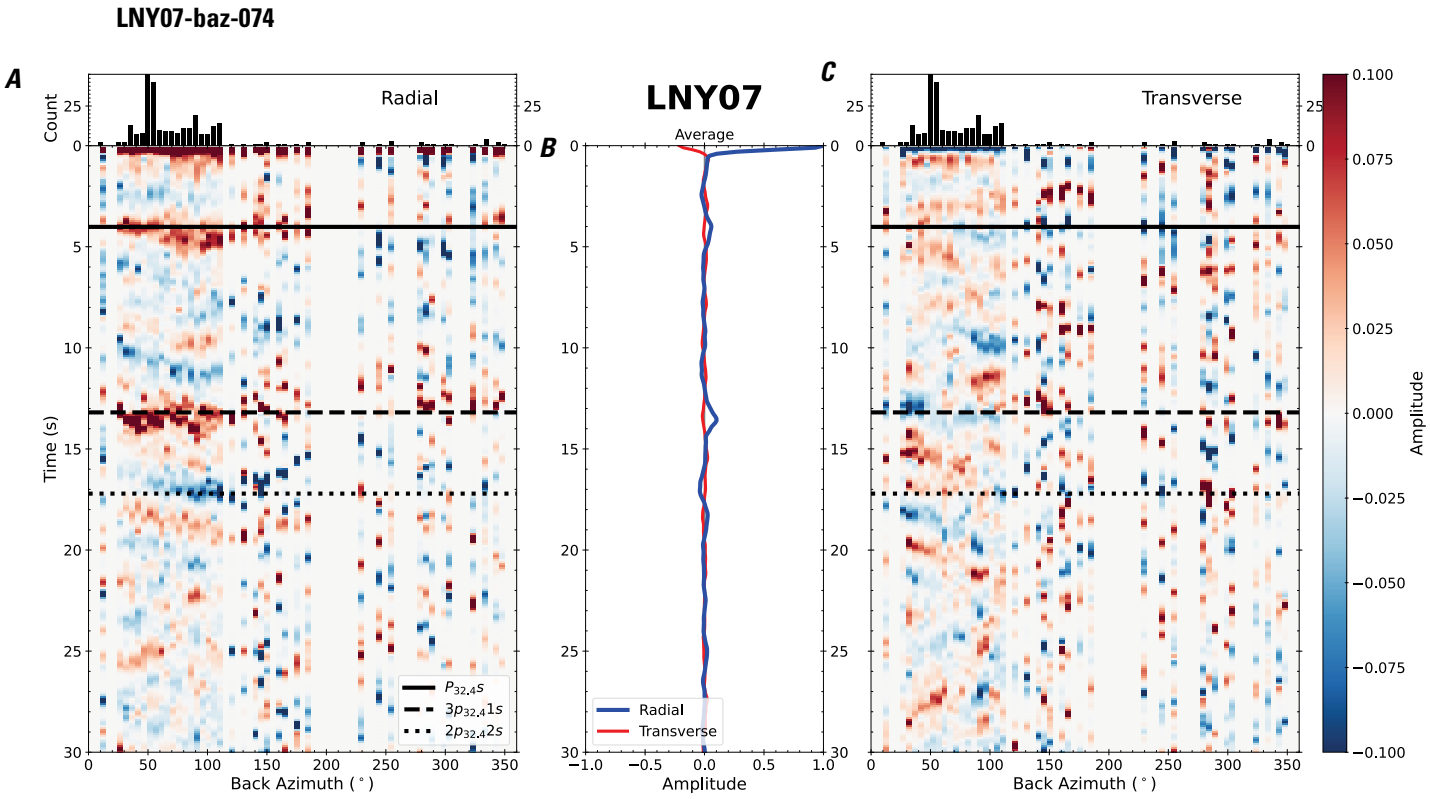

Figure153. Receiver functions plotted against back azimuth for station LNY07. *A*, Radial component of P-wave receiver functions (PRFs) plotted against back azimuth. Individual PRFs have had the resonance-removal filter of Yu and others (2015) applied to them, are normalized to the maximum amplitude within the time window shown, binned, and normalized by the number of traces per bin. *B*, Average of every individual normalized radial receiver function with the application of the resonance-removal filter (blue) and average of every individual normalized raw radial receiver function (red). *C*, Radial component of raw PRFs, plotted against back azimuth, normalized as in *A*. Ps, 3p1s, and 2p2s arrival times predicted for the preferred Moho depth are shown, assuming a ray parameter of 0.06 s/km.

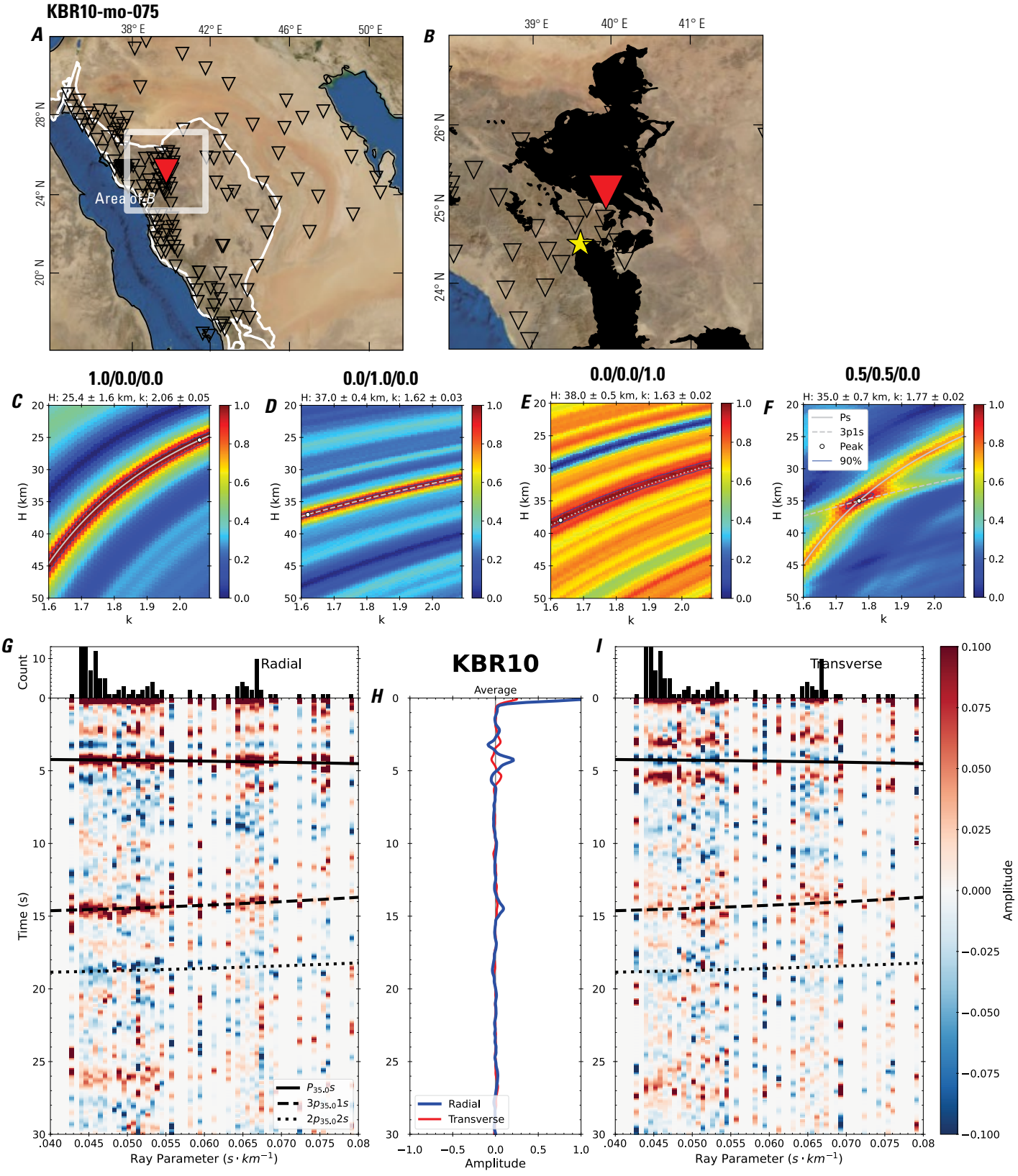
KBR10-mo-075
A
38° E
42° E
46° E
50° E
28° N
24° N
20° N
Area of B
B
39° E
40° E
41° E
26° N
25° N
24° N
1.0/0.0/0.0
C
H: 25.4 ± 1.6 km, k: 2.06 ± 0.05
0.0/1.0/0.0
D
H: 37.0 ± 0.4 km, k: 1.62 ± 0.03
0.0/0.0/1.0
E
H: 38.0 ± 0.5 km, k: 1.63 ± 0.02
0.5/0.5/0.0
F
H: 35.0 ± 0.7 km, k: 1.77 ± 0.02
Ps
3p1s
Peak
90%
H (km)
k
G
Radial
Count
Time (s)
$P_{35.0}s$
$3p_{35.0}1s$
$2p_{35.0}2s$
Ray Parameter ($s \cdot km^{-1}$)
KBR10
H
Average
Radial
Transverse
Amplitude
I
Transverse
Amplitude

Figure 154 (page 160). Receiver-function analysis for station KBR10. *A*, Regional map of Saudi Arabia showing the entire array (as inverted triangles), the location of station KBR10 (red inverted triangle), the shield-platform boundary (white line), and the bounds of the map in *B* (white box). *B*, Local map of station KBR10. Harrats are shown in black. *C*, Standard, single-layer *H-k* stack with stacking weights 0.4/0.3/0.3. This *H-k* stack ignores sedimentary effects on the receiver functions. *D*, Standard, single-layer *H-k* stack with stacking weights 0.5/0.5/0.0. This *H-k* stack also ignores sedimentary effects on the receiver functions. *E*, Optimized sub-sedimentary *H-k* stack with stacking weights 0.4/0.3/0.3, following the method of Yu and others (2015). *F*, Optimized sedimentary *H-k* stack with stacking weights 0.05/0.70/0.25, following the method of Yu and others (2015). *G*, Radial component P-wave receiver functions (PRFs) plotted against ray parameter. Individual PRFs have had the resonance-removal filter of Yu and others (2015) applied to them and are normalized to the maximum amplitude within the time window shown, binned, and normalized by the number of traces per bin. *H*, Average of every individual normalized radial receiver function with the application of the resonance-removal filter (blue) and average of every individual normalized raw radial receiver function (red). *I*, Radial component of raw PRFs (that is, PRFs with no resonance-removal filter applied) plotted against ray parameter, normalized as in *G*.

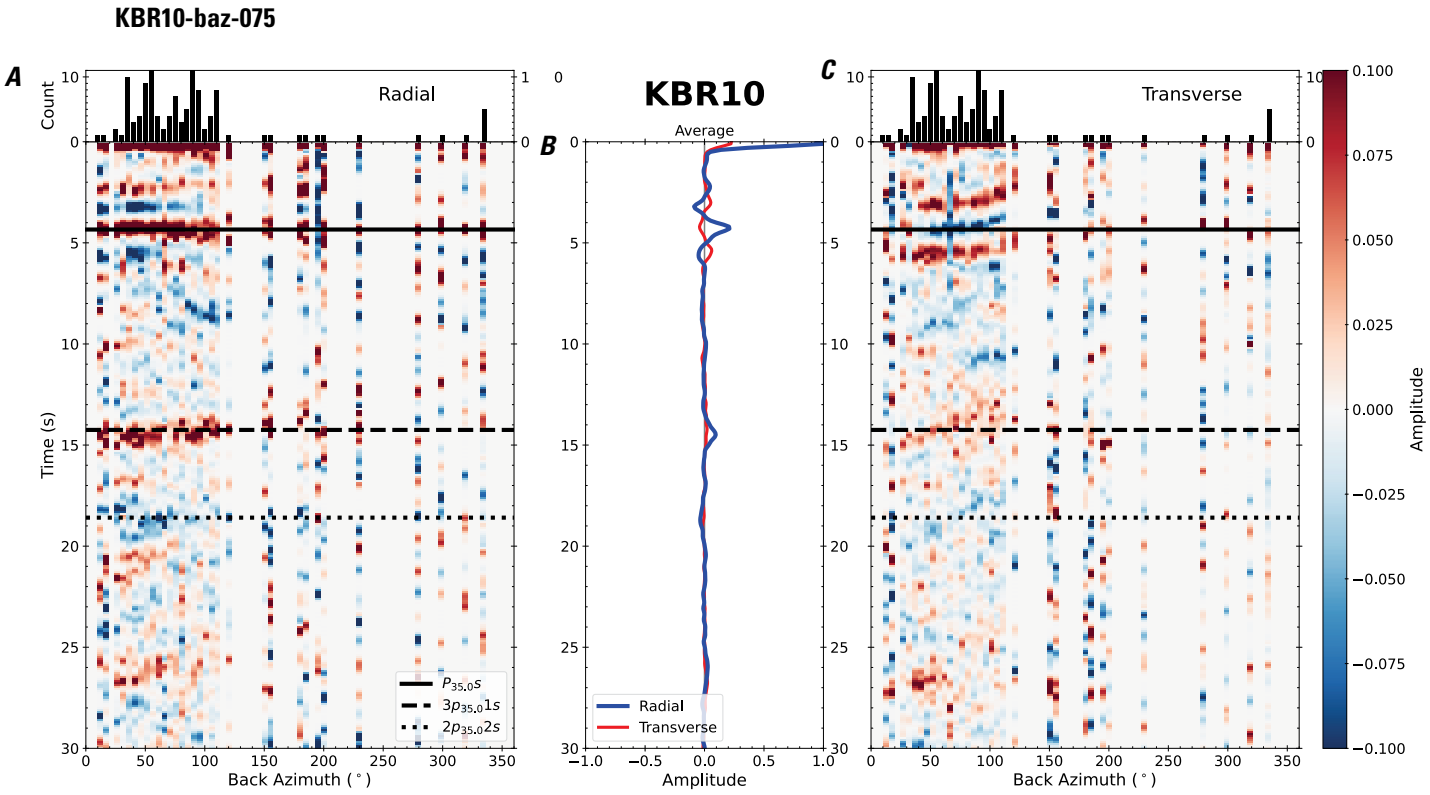

Figure 155. Receiver functions plotted against back azimuth for station KBR10. *A*, Radial component of P-wave receiver functions (PRFs) plotted against back azimuth. Individual PRFs have had the resonance-removal filter of Yu and others (2015) applied to them, are normalized to the maximum amplitude within the time window shown, binned, and normalized by the number of traces per bin. *B*, Average of every individual normalized radial receiver function with the application of the resonance-removal filter (blue) and average of every individual normalized raw radial receiver function (red). *C*, Radial component of raw PRFs, plotted against back azimuth, normalized as in *A*. Ps, 3p1s, and 2p2s arrival times predicted for the preferred Moho depth are shown, assuming a ray parameter of 0.06 s/km.

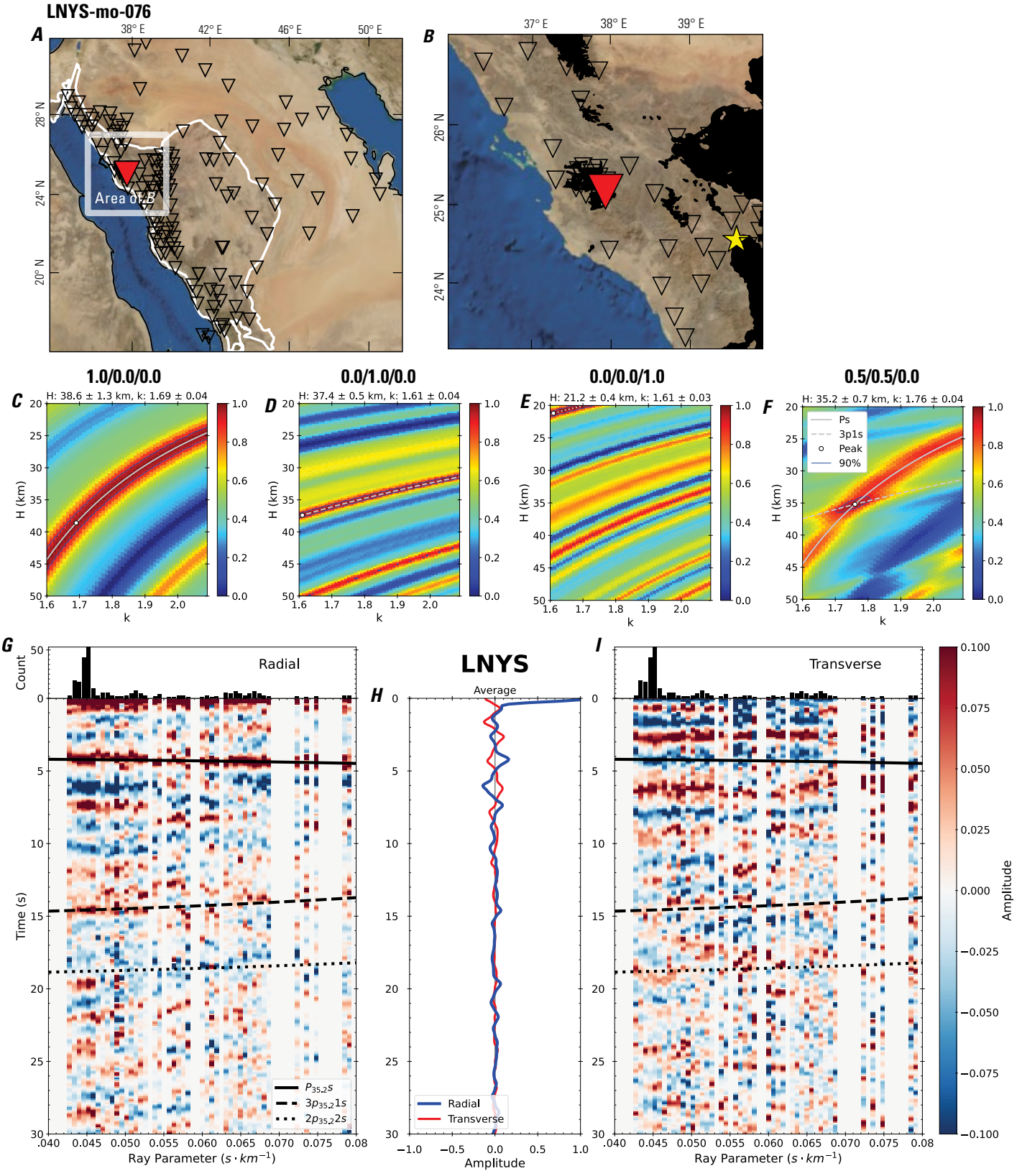
LNYS-mo-076
A
B
Area of B
1.0/0.0/0.0
0.0/1.0/0.0
0.0/0.0/1.0
0.5/0.5/0.0
C
D
E
F
H: 38.6 ± 1.3 km, k: 1.69 ± 0.04
H: 37.4 ± 0.5 km, k: 1.61 ± 0.04
H: 21.2 ± 0.4 km, k: 1.61 ± 0.03
H: 35.2 ± 0.7 km, k: 1.76 ± 0.04
H (km)
k
Ps
3p1s
Peak
90%
G
H
I
LNYS
Radial
Transverse
Average
Count
Time (s)
Ray Parameter (s · km⁻¹)
Amplitude
P35,2s
3p35,21s
2p35,22s

Figure 156 (page 162). Receiver-function analysis for station LNYS. *A*, Regional map of Saudi Arabia showing the entire array (as inverted triangles), the location of station LNYS (red inverted triangle), the shield-platform boundary (white line), and the bounds of the map in *B* (white box). *B*, Local map of station LNYS. Harrats are shown in black. *C*, Standard, single-layer *H-k* stack with stacking weights 0.4/0.3/0.3. This *H-k* stack ignores sedimentary effects on the receiver functions. *D*, Standard, single-layer *H-k* stack with stacking weights 0.5/0.5/0.0. This *H-k* stack also ignores sedimentary effects on the receiver functions. *E*, Optimized sub-sedimentary *H-k* stack with stacking weights 0.4/0.3/0.3, following the method of Yu and others (2015). *F*, Optimized sedimentary *H-k* stack with stacking weights 0.05/0.70/0.25, following the method of Yu and others (2015). *G*, Radial component P-wave receiver functions (PRFs) plotted against ray parameter. Individual PRFs have had the resonance-removal filter of Yu and others (2015) applied to them and are normalized to the maximum amplitude within the time window shown, binned, and normalized by the number of traces per bin. *H*, Average of every individual normalized radial receiver function with the application of the resonance-removal filter (blue) and average of every individual normalized raw radial receiver function (red). *I*, Radial component of raw PRFs (that is, PRFs with no resonance-removal filter applied) plotted against ray parameter, normalized as in *G*.

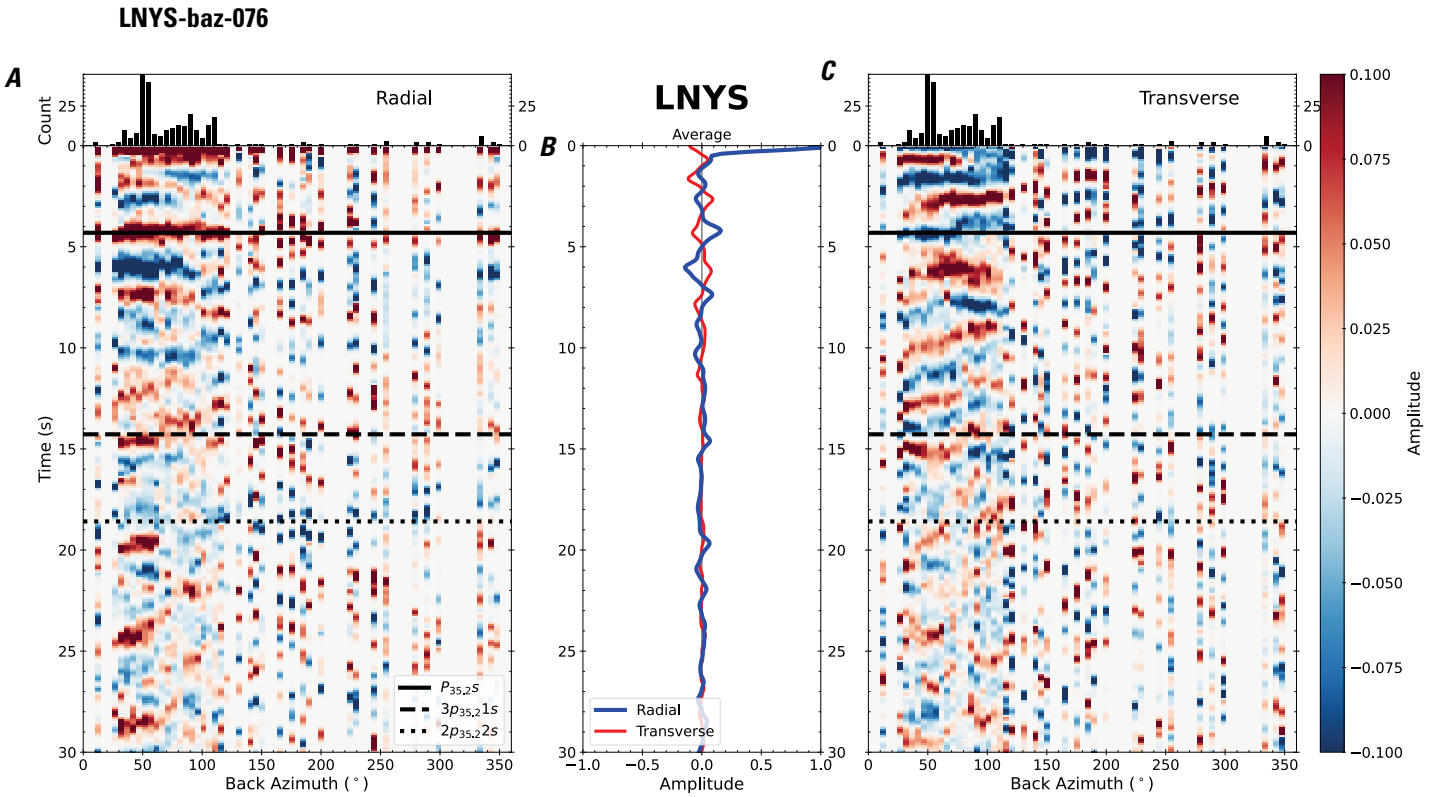

Figure 157. Receiver functions plotted against back azimuth for station LNYS. *A*, Radial component of P-wave receiver functions (PRFs) plotted against back azimuth. Individual PRFs have had the resonance-removal filter of Yu and others (2015) applied to them, are normalized to the maximum amplitude within the time window shown, binned, and normalized by the number of traces per bin. *B*, Average of every individual normalized radial receiver function with the application of the resonance-removal filter (blue) and average of every individual normalized raw radial receiver function (red). *C*, Radial component of raw PRFs, plotted against back azimuth, normalized as in *A*. Ps, 3p1s, and 2p2s arrival times predicted for the preferred Moho depth are shown, assuming a ray parameter of 0.06 s/km.

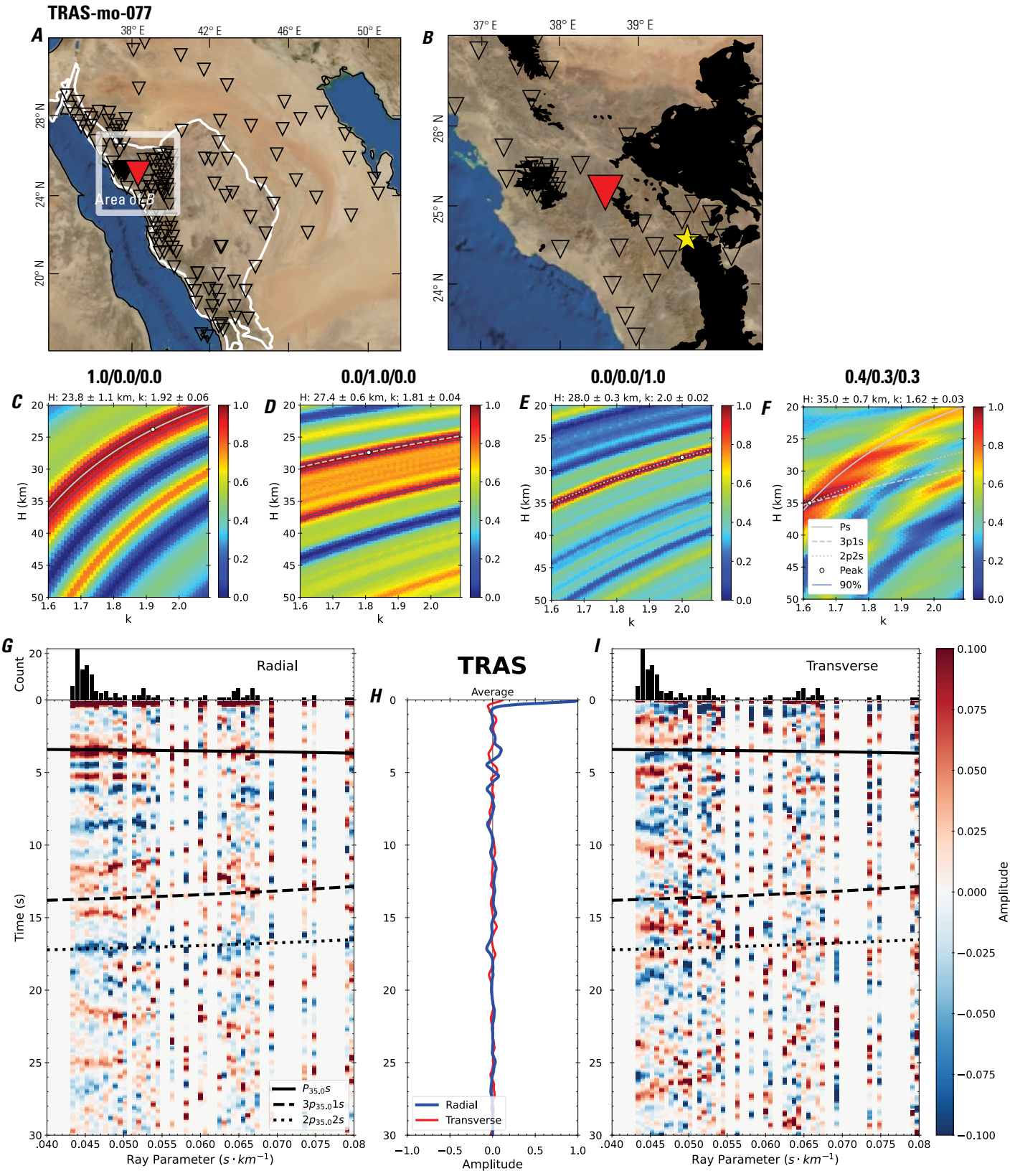
TRAS-mo-077
A
B
Area of B
1.0/0.0/0.0
0.0/1.0/0.0
0.0/0.0/1.0
0.4/0.3/0.3
C
D
E
F
H: 23.8 ± 1.1 km, k: 1.92 ± 0.06
H: 27.4 ± 0.6 km, k: 1.81 ± 0.04
H: 28.0 ± 0.3 km, k: 2.0 ± 0.02
H: 35.0 ± 0.7 km, k: 1.62 ± 0.03
H (km)
k
Ps
3p1s
2p2s
Peak
90%
G
H
I
TRAS
Radial
Transverse
Average
Count
Time (s)
Ray Parameter (s · km⁻¹)
Amplitude
$P_{35.0}s$
$3p_{35.0}1s$
$2p_{35.0}2s$

Figure 158 (page 164). Receiver-function analysis for station TRAS. *A*, Regional map of Saudi Arabia showing the entire array (as inverted triangles), the location of station TRAS (red inverted triangle), the shield-platform boundary (white line), and the bounds of the map in *B* (white box). *B*, Local map of station TRAS. Harrats are shown in black. *C*, Standard, single-layer *H-k* stack with stacking weights 0.4/0.3/0.3. This *H-k* stack ignores sedimentary effects on the receiver functions. *D*, Standard, single-layer *H-k* stack with stacking weights 0.5/0.5/0.0. This *H-k* stack also ignores sedimentary effects on the receiver functions. *E*, Optimized sub-sedimentary *H-k* stack with stacking weights 0.4/0.3/0.3, following the method of Yu and others (2015). *F*, Optimized sedimentary *H-k* stack with stacking weights 0.05/0.70/0.25, following the method of Yu and others (2015). *G*, Radial component P-wave receiver functions (PRFs) plotted against ray parameter. Individual PRFs have had the resonance-removal filter of Yu and others (2015) applied to them and are normalized to the maximum amplitude within the time window shown, binned, and normalized by the number of traces per bin. *H*, Average of every individual normalized radial receiver function with the application of the resonance-removal filter (blue) and average of every individual normalized raw radial receiver function (red). *I*, Radial component of raw PRFs (that is, PRFs with no resonance-removal filter applied) plotted against ray parameter, normalized as in *G*.

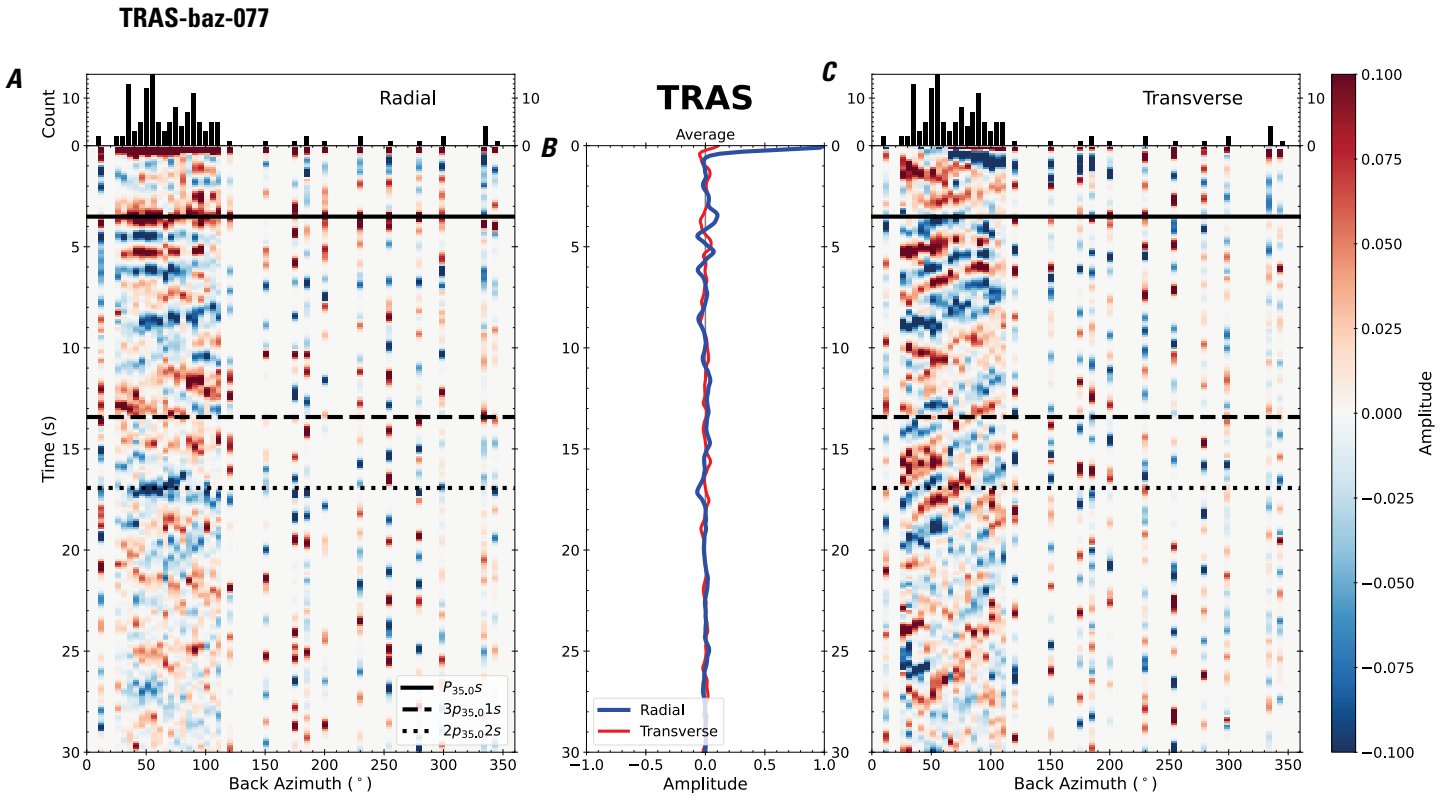

Figure 159. Receiver functions plotted against back azimuth for station TRAS. *A*, Radial component of P-wave receiver functions (PRFs) plotted against back azimuth. Individual PRFs have had the resonance-removal filter of Yu and others (2015) applied to them, are normalized to the maximum amplitude within the time window shown, binned, and normalized by the number of traces per bin. *B*, Average of every individual normalized radial receiver function with the application of the resonance-removal filter (blue) and average of every individual normalized raw radial receiver function (red). *C*, Radial component of raw PRFs, plotted against back azimuth, normalized as in *A*. Ps, 3p1s, and 2p2s arrival times predicted for the preferred Moho depth are shown, assuming a ray parameter of 0.06 s/km.

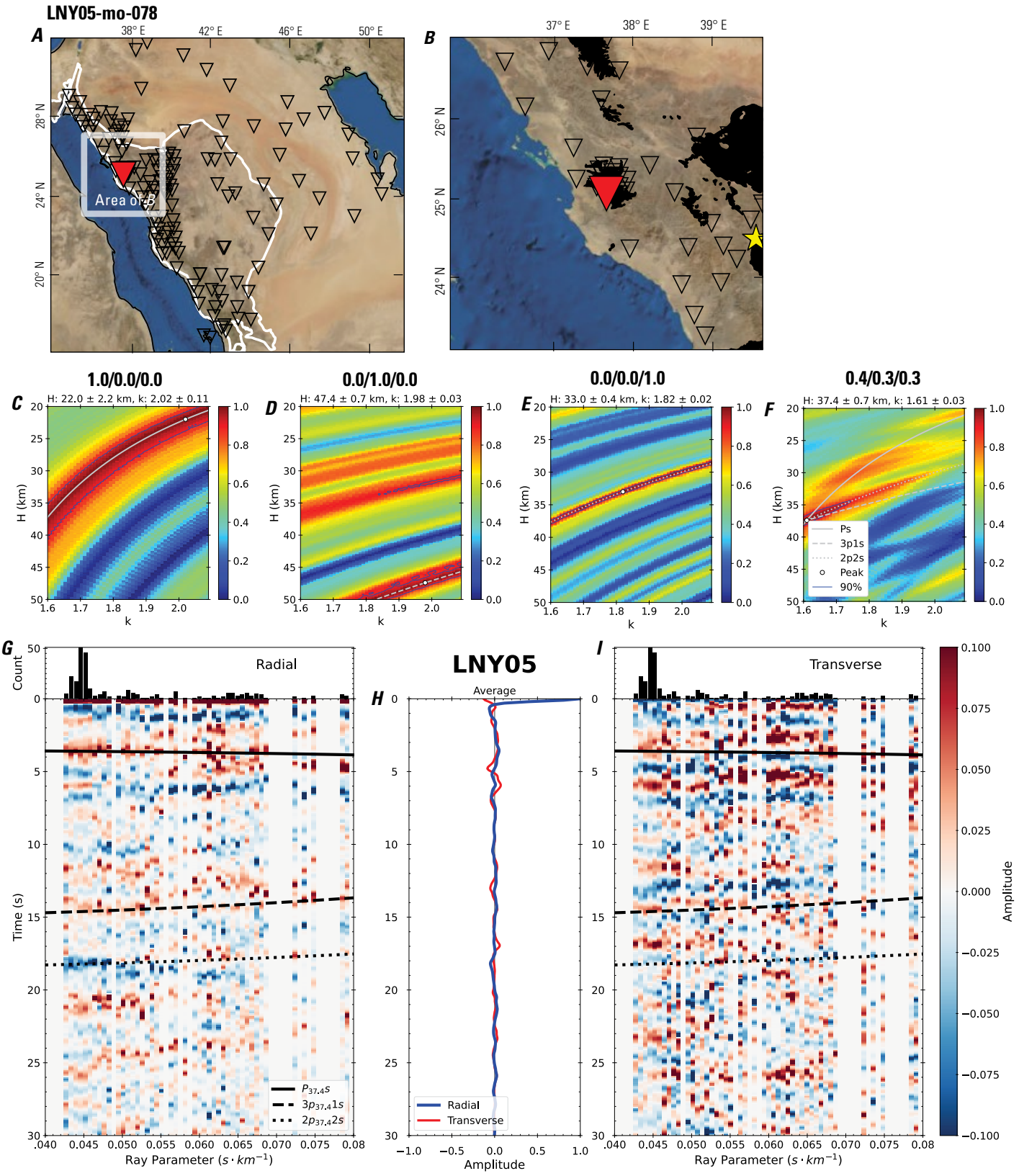
LNY05-mo-078
A
38° E
42° E
46° E
50° E
28° N
24° N
20° N
Area of B
B
37° E
38° E
39° E
26° N
25° N
24° N
1.0/0.0/0.0
0.0/1.0/0.0
0.0/0.0/1.0
0.4/0.3/0.3
C
H: 22.0 ± 2.2 km, k: 2.02 ± 0.11
D
H: 47.4 ± 0.7 km, k: 1.98 ± 0.03
E
H: 33.0 ± 0.4 km, k: 1.82 ± 0.02
F
H: 37.4 ± 0.7 km, k: 1.61 ± 0.03
H (km)
k
Ps
3p1s
2p2s
Peak
90%
G
Radial
Count
Time (s)
Ray Parameter (s · km⁻¹)
P37.4s
3p37.41s
2p37.42s
LNY05
H
Average
Radial
Transverse
Amplitude
I
Transverse
Amplitude

Figure 160 (page 166). Receiver-function analysis for station LNY05. *A*, Regional map of Saudi Arabia showing the entire array (as inverted triangles), the location of station LNY05 (red inverted triangle), the shield-platform boundary (white line), and the bounds of the map in *B* (white box). *B*, Local map of station LNY05. Harrats are shown in black. *C*, Standard, single-layer *H-k* stack with stacking weights 0.4/0.3/0.3. This *H-k* stack ignores sedimentary effects on the receiver functions. *D*, Standard, single-layer *H-k* stack with stacking weights 0.5/0.5/0.0. This *H-k* stack also ignores sedimentary effects on the receiver functions. *E*, Optimized sub-sedimentary *H-k* stack with stacking weights 0.4/0.3/0.3, following the method of Yu and others (2015). *F*, Optimized sedimentary *H-k* stack with stacking weights 0.05/0.70/0.25, following the method of Yu and others (2015). *G*, Radial component P-wave receiver functions (PRFs) plotted against ray parameter. Individual PRFs have had the resonance-removal filter of Yu and others (2015) applied to them and are normalized to the maximum amplitude within the time window shown, binned, and normalized by the number of traces per bin. *H*, Average of every individual normalized radial receiver function with the application of the resonance-removal filter (blue) and average of every individual normalized raw radial receiver function (red). *I*, Radial component of raw PRFs (that is, PRFs with no resonance-removal filter applied) plotted against ray parameter, normalized as in *G*.

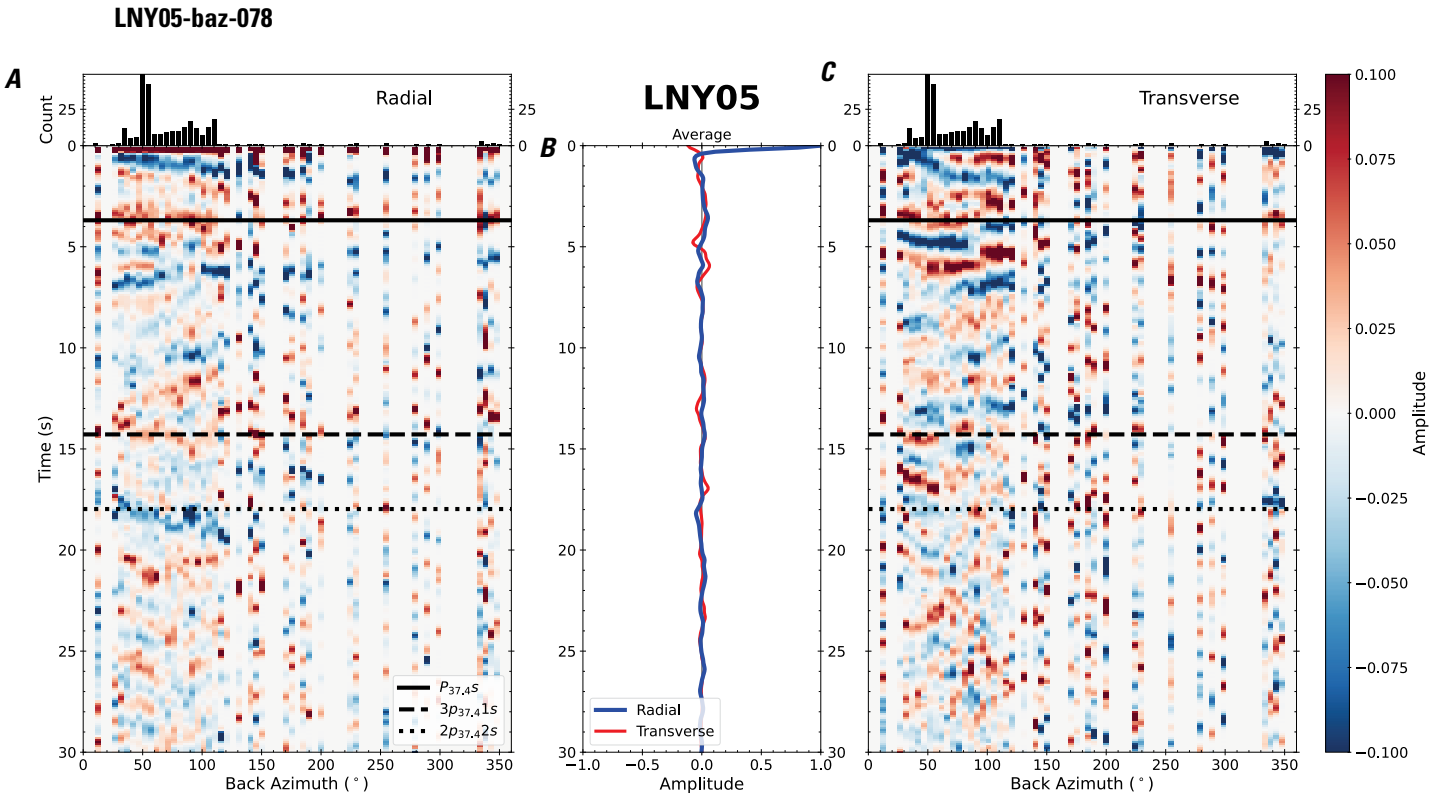

Figure 161. Receiver functions plotted against back azimuth for station LNY05. *A*, Radial component of P-wave receiver functions (PRFs) plotted against back azimuth. Individual PRFs have had the resonance-removal filter of Yu and others (2015) applied to them, are normalized to the maximum amplitude within the time window shown, binned, and normalized by the number of traces per bin. *B*, Average of every individual normalized radial receiver function with the application of the resonance-removal filter (blue) and average of every individual normalized raw radial receiver function (red). *C*, Radial component of raw PRFs, plotted against back azimuth, normalized as in *A*. Ps, 3p1s, and 2p2s arrival times predicted for the preferred Moho depth are shown, assuming a ray parameter of 0.06 s/km.

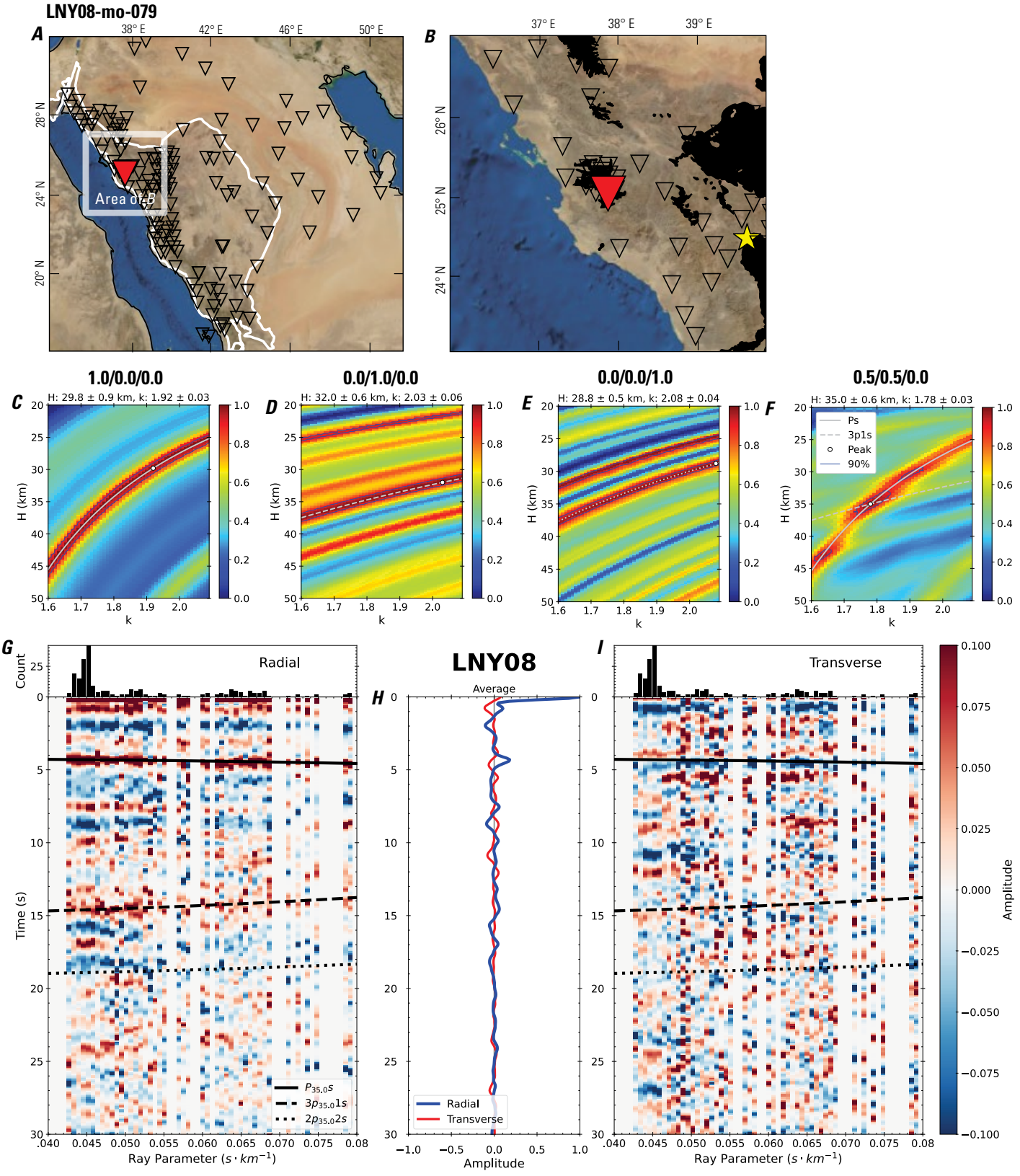
LNY08-mo-079
A
B
Area of B
1.0/0.0/0.0
0.0/1.0/0.0
0.0/0.0/1.0
0.5/0.5/0.0
C
D
E
F
H: 29.8 ± 0.9 km, k: 1.92 ± 0.03
H: 32.0 ± 0.6 km, k: 2.03 ± 0.06
H: 28.8 ± 0.5 km, k: 2.08 ± 0.04
H: 35.0 ± 0.6 km, k: 1.78 ± 0.03
H (km)
k
Ps
3p1s
Peak
90%
G
H
I
LNY08
Radial
Transverse
Average
Count
Time (s)
Ray Parameter (s · km⁻¹)
Amplitude
$P_{35.0}s$
$3p_{35.0}1s$
$2p_{35.0}2s$

Figure 162 (page 168). Receiver-function analysis for station LNY08. *A*, Regional map of Saudi Arabia showing the entire array (as inverted triangles), the location of station LNY08 (red inverted triangle), the shield-platform boundary (white line), and the bounds of the map in *B* (white box). *B*, Local map of station LNY08. Harrats are shown in black. *C*, Standard, single-layer *H-k* stack with stacking weights 0.4/0.3/0.3. This *H-k* stack ignores sedimentary effects on the receiver functions. *D*, Standard, single-layer *H-k* stack with stacking weights 0.5/0.5/0.0. This *H-k* stack also ignores sedimentary effects on the receiver functions. *E*, Optimized sub-sedimentary *H-k* stack with stacking weights 0.4/0.3/0.3, following the method of Yu and others (2015). *F*, Optimized sedimentary *H-k* stack with stacking weights 0.05/0.70/0.25, following the method of Yu and others (2015). *G*, Radial component P-wave receiver functions (PRFs) plotted against ray parameter. Individual PRFs have had the resonance-removal filter of Yu and others (2015) applied to them and are normalized to the maximum amplitude within the time window shown, binned, and normalized by the number of traces per bin. *H*, Average of every individual normalized radial receiver function with the application of the resonance-removal filter (blue) and average of every individual normalized raw radial receiver function (red). *I*, Radial component of raw PRFs (that is, PRFs with no resonance-removal filter applied) plotted against ray parameter, normalized as in *G*.

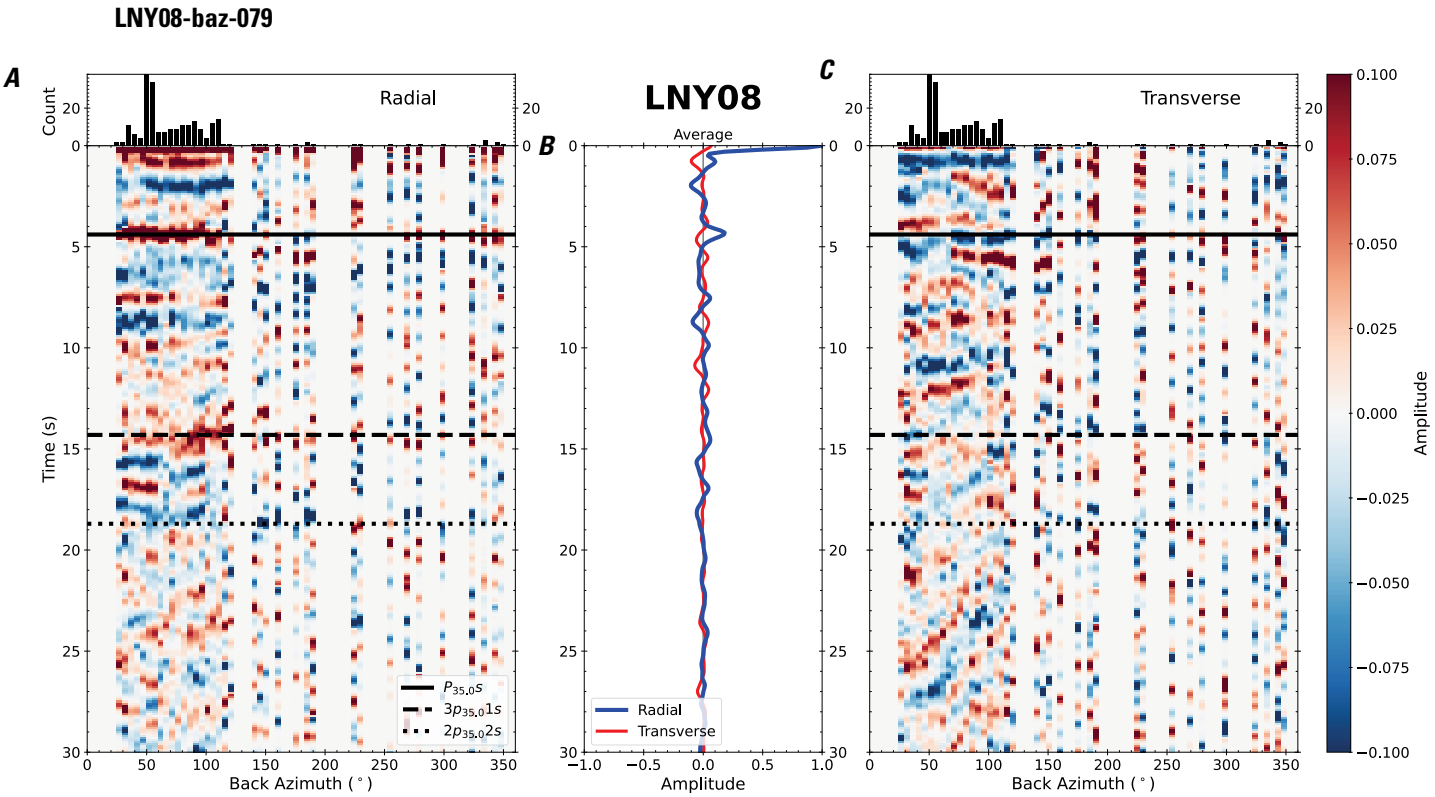

Figure 163. Receiver functions plotted against back azimuth for station LNY08. *A*, Radial component of P-wave receiver functions (PRFs) plotted against back azimuth. Individual PRFs have had the resonance-removal filter of Yu and others (2015) applied to them, are normalized to the maximum amplitude within the time window shown, binned, and normalized by the number of traces per bin. *B*, Average of every individual normalized radial receiver function with the application of the resonance-removal filter (blue) and average of every individual normalized raw radial receiver function (red). *C*, Radial component of raw PRFs, plotted against back azimuth, normalized as in *A*. Ps, 3p1s, and 2p2s arrival times predicted for the preferred Moho depth are shown, assuming a ray parameter of 0.06 s/km.

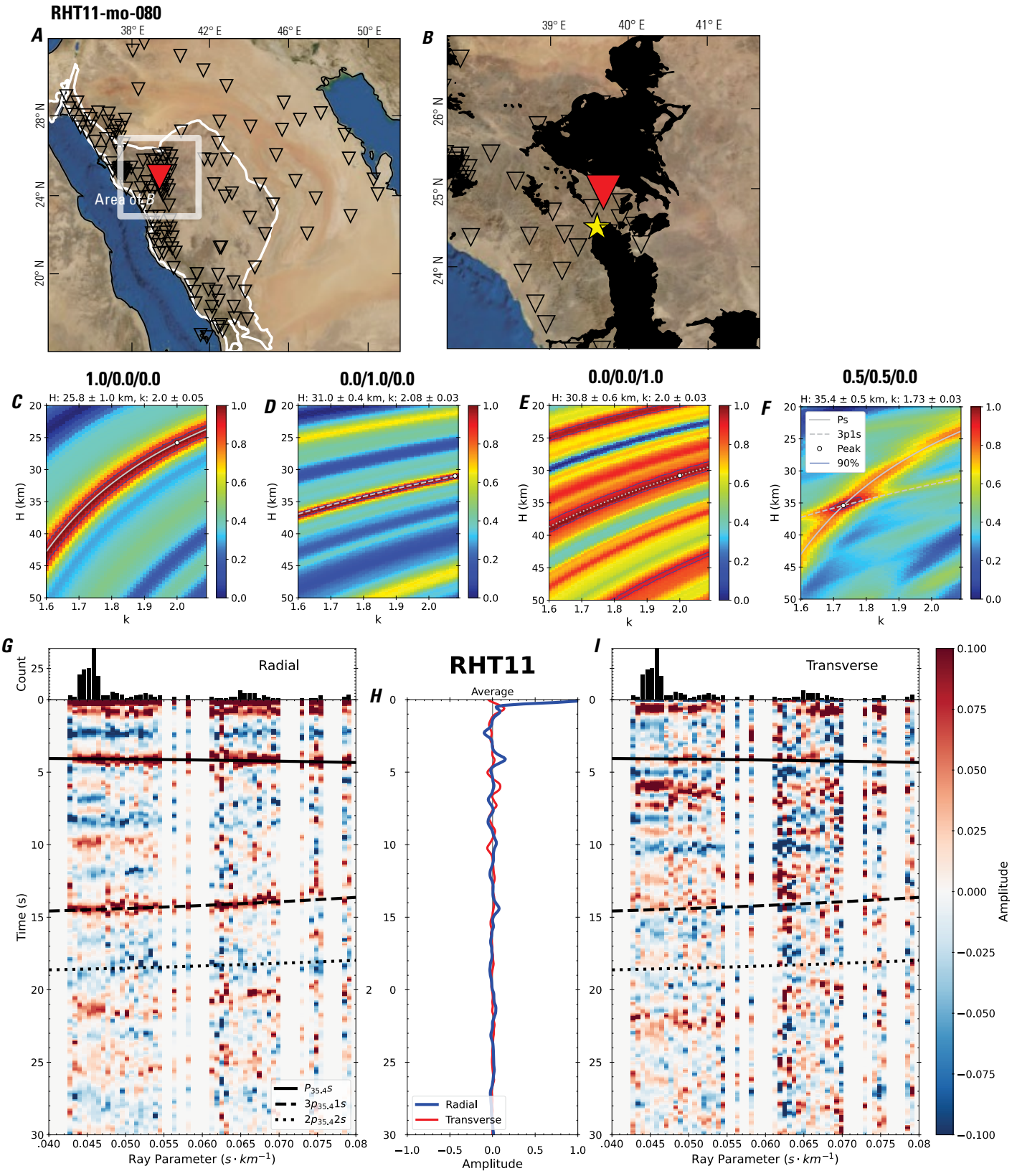
RHT11-mo-080
A
38° E
42° E
46° E
50° E
28° N
24° N
20° N
Area of B
B
39° E
40° E
41° E
26° N
25° N
24° N
1.0/0.0/0.0
0.0/1.0/0.0
0.0/0.0/1.0
0.5/0.5/0.0
C
H: 25.8 ± 1.0 km, k: 2.0 ± 0.05
D
H: 31.0 ± 0.4 km, k: 2.08 ± 0.03
E
H: 30.8 ± 0.6 km, k: 2.0 ± 0.03
F
H: 35.4 ± 0.5 km, k: 1.73 ± 0.03
Ps
3p1s
Peak
90%
H (km)
k
G
Radial
Count
Time (s)
$P_{35.4}s$
$3p_{35.4}1s$
$2p_{35.4}2s$
Ray Parameter ($s \cdot km^{-1}$)
RHT11
H
Average
Radial
Transverse
Amplitude
I
Transverse
Amplitude

Figure 164 (page 170). Receiver-function analysis for station RHT11. *A*, Regional map of Saudi Arabia showing the entire array (as inverted triangles), the location of station RHT11 (red inverted triangle), the shield-platform boundary (white line), and the bounds of the map in *B* (white box). *B*, Local map of station RHT11. Harrats are shown in black. *C*, Standard, single-layer *H-k* stack with stacking weights 0.4/0.3/0.3. This *H-k* stack ignores sedimentary effects on the receiver functions. *D*, Standard, single-layer *H-k* stack with stacking weights 0.5/0.5/0.0. This *H-k* stack also ignores sedimentary effects on the receiver functions. *E*, Optimized sub-sedimentary *H-k* stack with stacking weights 0.4/0.3/0.3, following the method of Yu and others (2015). *F*, Optimized sedimentary *H-k* stack with stacking weights 0.05/0.70/0.25, following the method of Yu and others (2015). *G*, Radial component P-wave receiver functions (PRFs) plotted against ray parameter. Individual PRFs have had the resonance-removal filter of Yu and others (2015) applied to them and are normalized to the maximum amplitude within the time window shown, binned, and normalized by the number of traces per bin. *H*, Average of every individual normalized radial receiver function with the application of the resonance-removal filter (blue) and average of every individual normalized raw radial receiver function (red). *I*, Radial component of raw PRFs (that is, PRFs with no resonance-removal filter applied) plotted against ray parameter, normalized as in *G*.

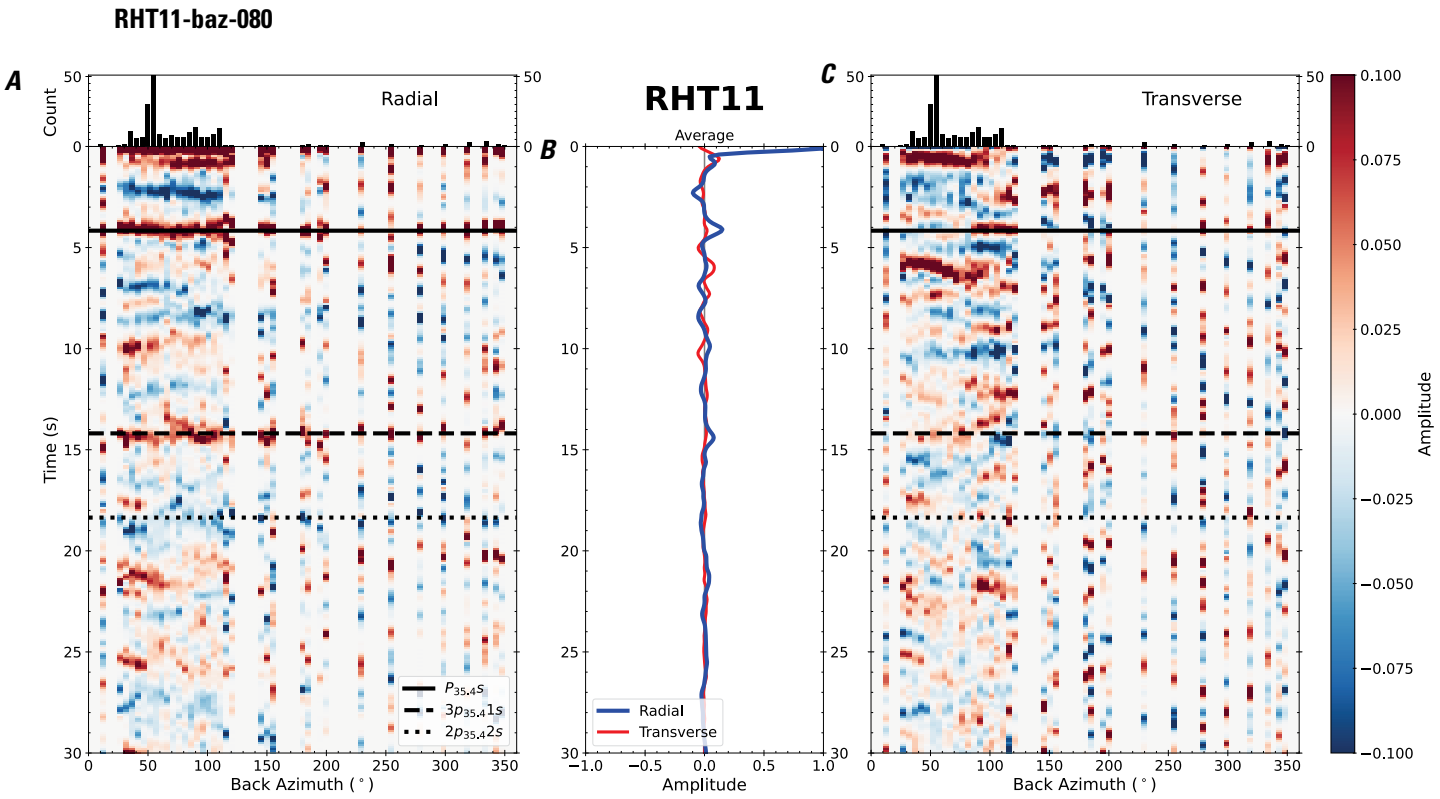

Figure 165. Receiver functions plotted against back azimuth for station RHT11. *A*, Radial component of P-wave receiver functions (PRFs) plotted against back azimuth. Individual PRFs have had the resonance-removal filter of Yu and others (2015) applied to them, are normalized to the maximum amplitude within the time window shown, binned, and normalized by the number of traces per bin. *B*, Average of every individual normalized radial receiver function with the application of the resonance-removal filter (blue) and average of every individual normalized raw radial receiver function (red). *C*, Radial component of raw PRFs, plotted against back azimuth, normalized as in *A*. Ps, 3p1s, and 2p2s arrival times predicted for the preferred Moho depth are shown, assuming a ray parameter of 0.06 s/km.

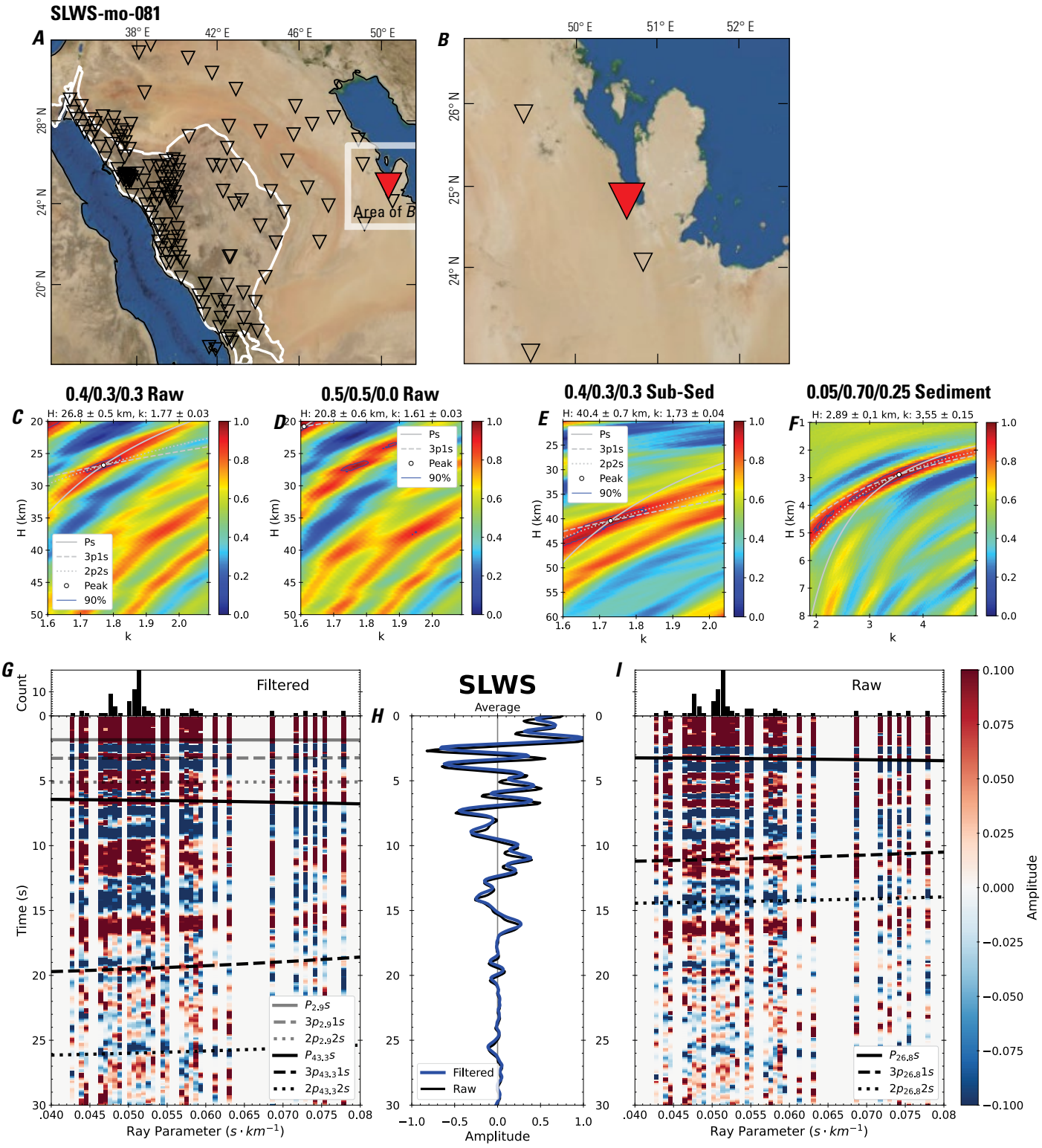
SLWS-mo-081
A
38° E
42° E
46° E
50° E
28° N
24° N
20° N
Area of B
B
50° E
51° E
52° E
26° N
25° N
24° N
0.4/0.3/0.3 Raw
C
H: 26.8 ± 0.5 km, k: 1.77 ± 0.03
0.5/0.5/0.0 Raw
D
H: 20.8 ± 0.6 km, k: 1.61 ± 0.03
0.4/0.3/0.3 Sub-Sed
E
H: 40.4 ± 0.7 km, k: 1.73 ± 0.04
0.05/0.70/0.25 Sediment
F
H: 2.89 ± 0.1 km, k: 3.55 ± 0.15
Ps
3p1s
2p2s
Peak
90%
H (km)
k
G
Filtered
Count
Time (s)
$P_{2.9}s$
$3p_{2.9}1s$
$2p_{2.9}2s$
$P_{43.3}s$
$3p_{43.3}1s$
$2p_{43.3}2s$
Ray Parameter ($s \cdot km^{-1}$)
H
SLWS
Average
Filtered
Raw
Amplitude
I
Raw
$P_{26.8}s$
$3p_{26.8}1s$
$2p_{26.8}2s$
Amplitude

FIgure 166 (page 172). Receiver-function analysis for station SLWS. *A*, Regional map of Saudi Arabia showing the entire array (as inverted triangles), the location of station SLWS (red inverted triangle), the shield-platform boundary (white line), and the bounds of the map in *B* (white box). *B*, Local map of station SLWS. Harrats are shown in black. *C*, Standard, single-layer *H-k* stack with stacking weights 0.4/0.3/0.3. This *H-k* stack ignores sedimentary effects on the receiver functions. *D*, Standard, single-layer *H-k* stack with stacking weights 0.5/0.5/0.0. This *H-k* stack also ignores sedimentary effects on the receiver functions. *E*, Optimized sub-sedimentary *H-k* stack with stacking weights 0.4/0.3/0.3, following the method of Yu and others (2015). *F*, Optimized sedimentary *H-k* stack with stacking weights 0.05/0.70/0.25, following the method of Yu and others (2015). *G*, Radial component P-wave receiver functions (PRFs) plotted against ray parameter. Individual PRFs have had the resonance-removal filter of Yu and others (2015) applied to them and are normalized to the maximum amplitude within the time window shown, binned, and normalized by the number of traces per bin. *H*, Average of every individual normalized radial receiver function with the application of the resonance-removal filter (blue) and average of every individual normalized raw radial receiver function (red). *I*, Radial component of raw PRFs (that is, PRFs with no resonance-removal filter applied) plotted against ray parameter, normalized as in *G*.

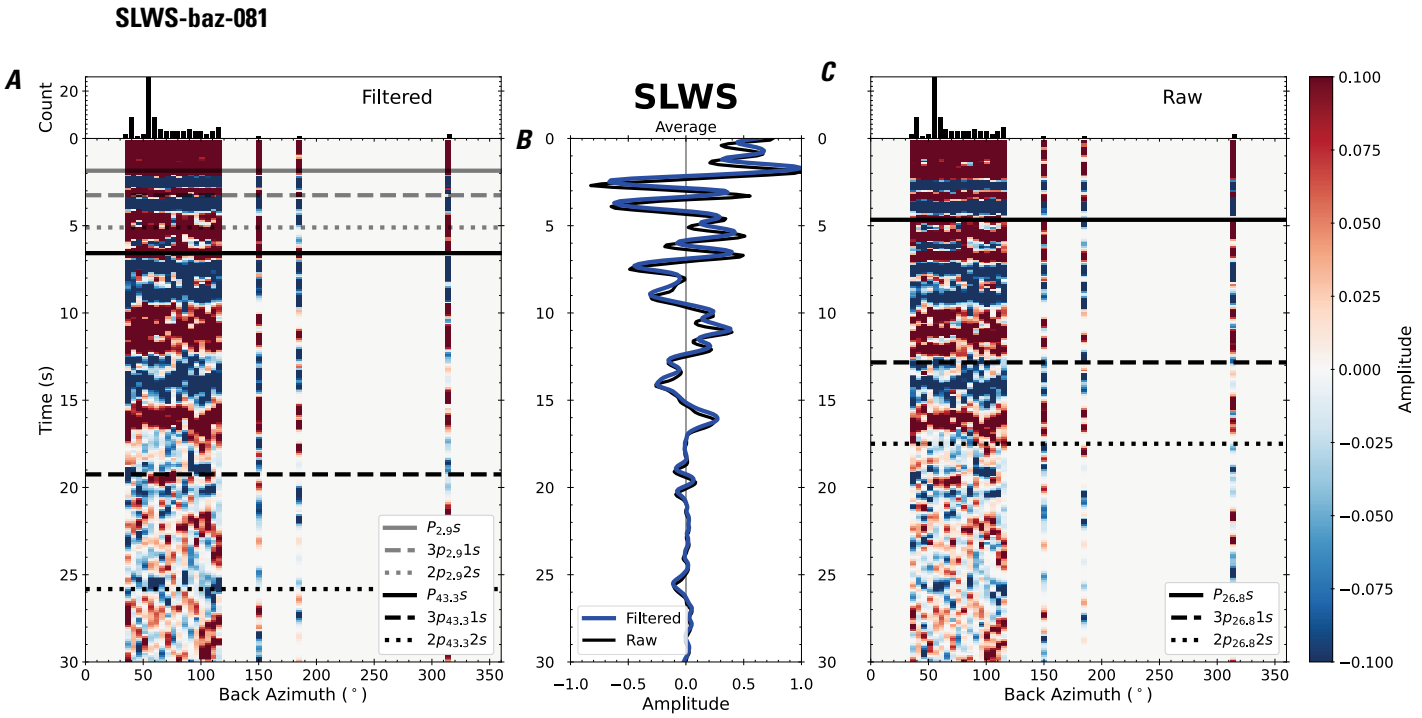

Figure 167. Receiver functions plotted against back azimuth for station SLWS. *A*, Radial component of P-wave receiver functions (PRFs) plotted against back azimuth. Individual PRFs have had the resonance-removal filter of Yu and others (2015) applied to them, are normalized to the maximum amplitude within the time window shown, binned, and normalized by the number of traces per bin. *B*, Average of every individual normalized radial receiver function with the application of the resonance-removal filter (blue) and average of every individual normalized raw radial receiver function (red). *C*, Radial component of raw PRFs, plotted against back azimuth, normalized as in *A*. Ps, 3p1s, and 2p2s arrival times predicted for the preferred Moho depth are shown, assuming a ray parameter of 0.06 s/km.

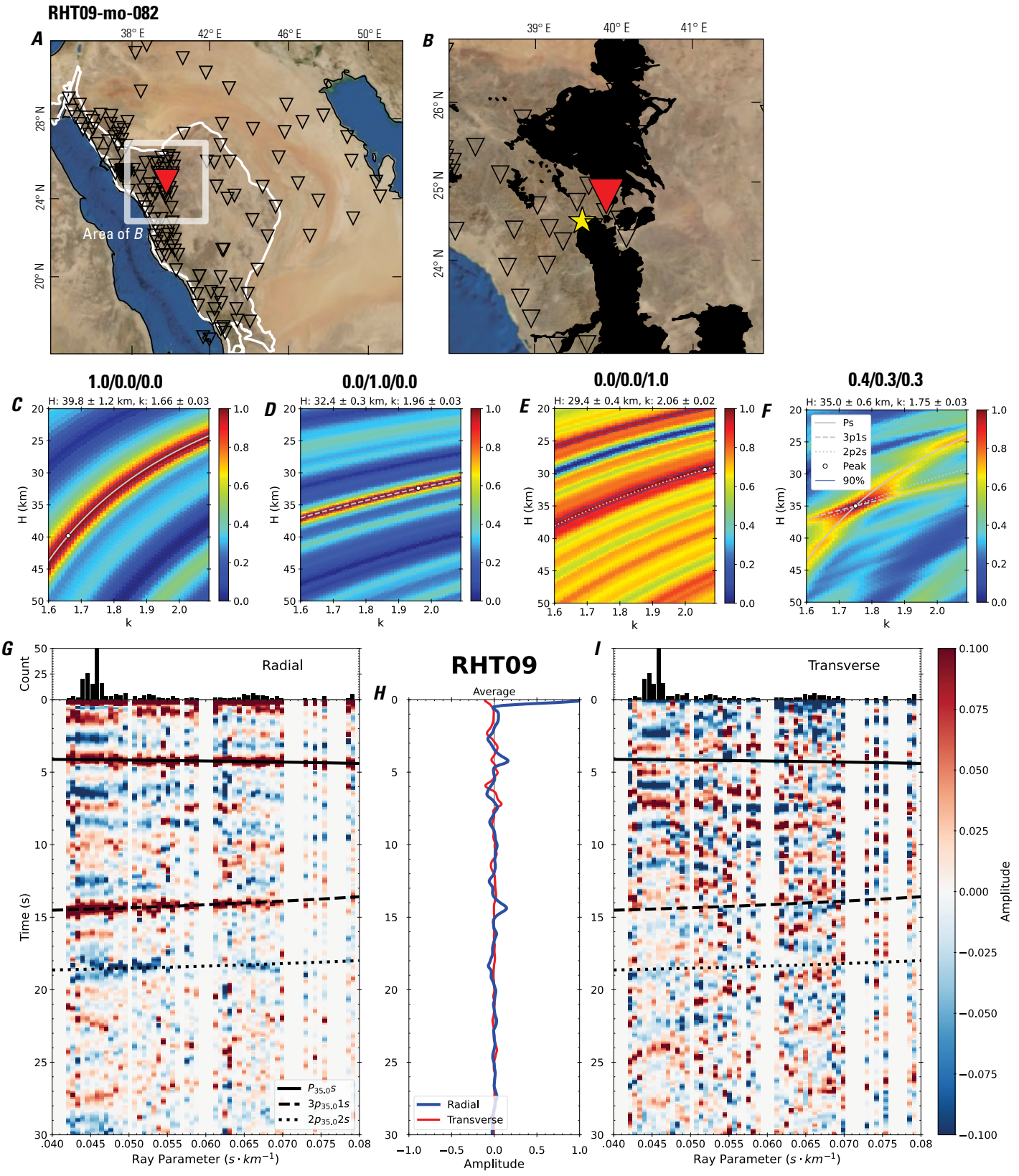
RHT09-mo-082
A
38° E
42° E
46° E
50° E
28° N
24° N
20° N
Area of B
B
39° E
40° E
41° E
26° N
25° N
24° N
1.0/0.0/0.0
0.0/1.0/0.0
0.0/0.0/1.0
0.4/0.3/0.3
C
H: 39.8 ± 1.2 km, k: 1.66 ± 0.03
D
H: 32.4 ± 0.3 km, k: 1.96 ± 0.03
E
H: 29.4 ± 0.4 km, k: 2.06 ± 0.02
F
H: 35.0 ± 0.6 km, k: 1.75 ± 0.03
Ps
3p1s
2p2s
Peak
90%
H (km)
k
G
Radial
Count
Time (s)
$P_{35.0}s$
$3p_{35.0}1s$
$2p_{35.0}2s$
Ray Parameter ($s \cdot km^{-1}$)
RHT09
H
Average
Radial
Transverse
Amplitude
I
Transverse
Amplitude

Figure 168 (page 174). Receiver-function analysis for station RHT09. *A*, Regional map of Saudi Arabia showing the entire array (as inverted triangles), the location of station RHT09 (red inverted triangle), the shield-platform boundary (white line), and the bounds of the map in *B* (white box). *B*, Local map of station RHT09. Harrats are shown in black. *C*, Standard, single-layer *H-k* stack with stacking weights 0.4/0.3/0.3. This *H-k* stack ignores sedimentary effects on the receiver functions. *D*, Standard, single-layer *H-k* stack with stacking weights 0.5/0.5/0.0. This *H-k* stack also ignores sedimentary effects on the receiver functions. *E*, Optimized sub-sedimentary *H-k* stack with stacking weights 0.4/0.3/0.3, following the method of Yu and others (2015). *F*, Optimized sedimentary *H-k* stack with stacking weights 0.05/0.70/0.25, following the method of Yu and others (2015). *G*, Radial component P-wave receiver functions (PRFs) plotted against ray parameter. Individual PRFs have had the resonance-removal filter of Yu and others (2015) applied to them and are normalized to the maximum amplitude within the time window shown, binned, and normalized by the number of traces per bin. *H*, Average of every individual normalized radial receiver function with the application of the resonance-removal filter (blue) and average of every individual normalized raw radial receiver function (red). *I*, Radial component of raw PRFs (that is, PRFs with no resonance-removal filter applied) plotted against ray parameter, normalized as in *G*.

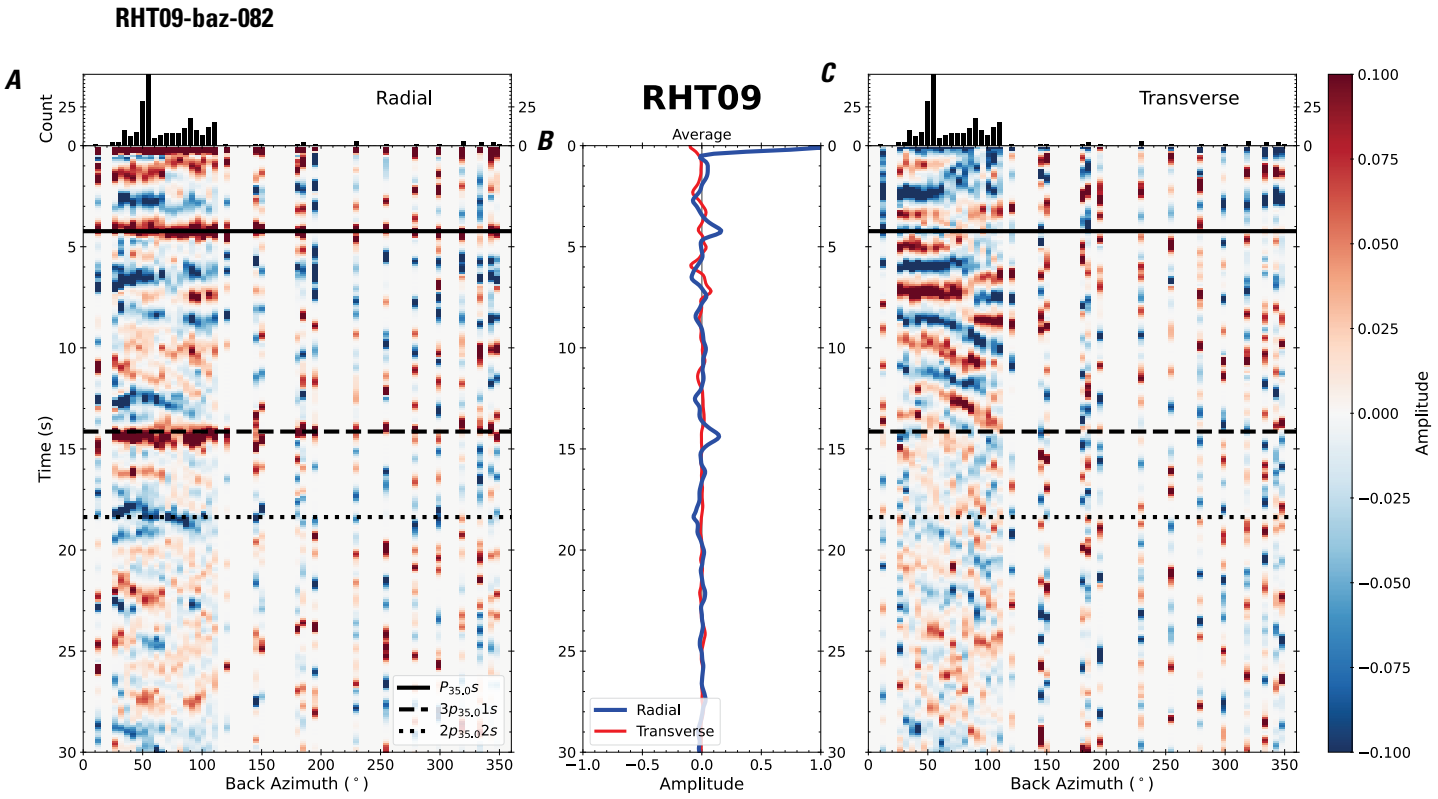

Figure 169. Receiver functions plotted against back azimuth for station RHT09. *A*, Radial component of P-wave receiver functions (PRFs) plotted against back azimuth. Individual PRFs have had the resonance-removal filter of Yu and others (2015) applied to them, are normalized to the maximum amplitude within the time window shown, binned, and normalized by the number of traces per bin. *B*, Average of every individual normalized radial receiver function with the application of the resonance-removal filter (blue) and average of every individual normalized raw radial receiver function (red). *C*, Radial component of raw PRFs, plotted against back azimuth, normalized as in *A*. Ps, 3p1s, and 2p2s arrival times predicted for the preferred Moho depth are shown, assuming a ray parameter of 0.06 s/km.

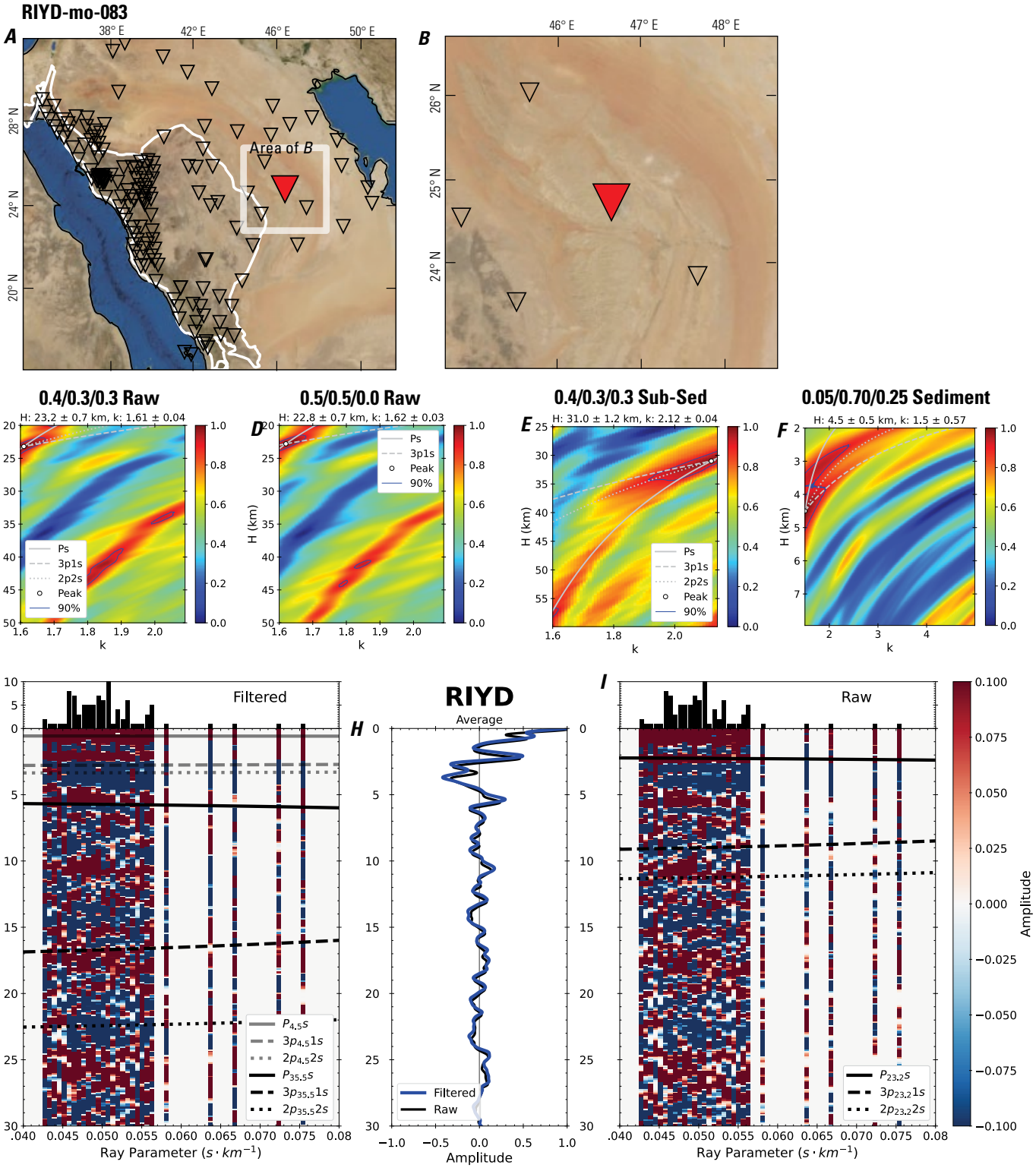
RIYD-mo-083
A
38° E
42° E
46° E
50° E
28° N
24° N
20° N
Area of B
B
46° E
47° E
48° E
26° N
25° N
24° N
0.4/0.3/0.3 Raw
0.5/0.5/0.0 Raw
0.4/0.3/0.3 Sub-Sed
0.05/0.70/0.25 Sediment
C
H: 23.2 ± 0.7 km, k: 1.61 ± 0.04
D
H: 22.8 ± 0.7 km, k: 1.62 ± 0.03
E
H: 31.0 ± 1.2 km, k: 2.12 ± 0.04
F
H: 4.5 ± 0.5 km, k: 1.5 ± 0.57
H (km)
k
Ps
3p1s
2p2s
Peak
90%
G
Filtered
Count
Time (s)
Ray Parameter (s · km⁻¹)
$P_{4.5}s$
$3p_{4.5}1s$
$2p_{4.5}2s$
$P_{35.5}s$
$3p_{35.5}1s$
$2p_{35.5}2s$
H
RIYD
Average
Filtered
Raw
Amplitude
I
Raw
$P_{23.2}s$
$3p_{23.2}1s$
$2p_{23.2}2s$
Amplitude

Figure 170 (page 176). Receiver-function analysis for station RIYD. *A*, Regional map of Saudi Arabia showing the entire array (as inverted triangles), the location of station RIYD (red inverted triangle), the shield-platform boundary (white line), and the bounds of the map in *B* (white box). *B*, Local map of station RIYD. Harrats are shown in black. *C*, Standard, single-layer *H-k* stack with stacking weights 0.4/0.3/0.3. This *H-k* stack ignores sedimentary effects on the receiver functions. *D*, Standard, single-layer *H-k* stack with stacking weights 0.5/0.5/0.0. This *H-k* stack also ignores sedimentary effects on the receiver functions. *E*, Optimized sub-sedimentary *H-k* stack with stacking weights 0.4/0.3/0.3, following the method of Yu and others (2015). *F*, Optimized sedimentary *H-k* stack with stacking weights 0.05/0.70/0.25, following the method of Yu and others (2015). *G*, Radial component P-wave receiver functions (PRFs) plotted against ray parameter. Individual PRFs have had the resonance-removal filter of Yu and others (2015) applied to them and are normalized to the maximum amplitude within the time window shown, binned, and normalized by the number of traces per bin. *H*, Average of every individual normalized radial receiver function with the application of the resonance-removal filter (blue) and average of every individual normalized raw radial receiver function (red). *I*, Radial component of raw PRFs (that is, PRFs with no resonance-removal filter applied) plotted against ray parameter, normalized as in *G*.

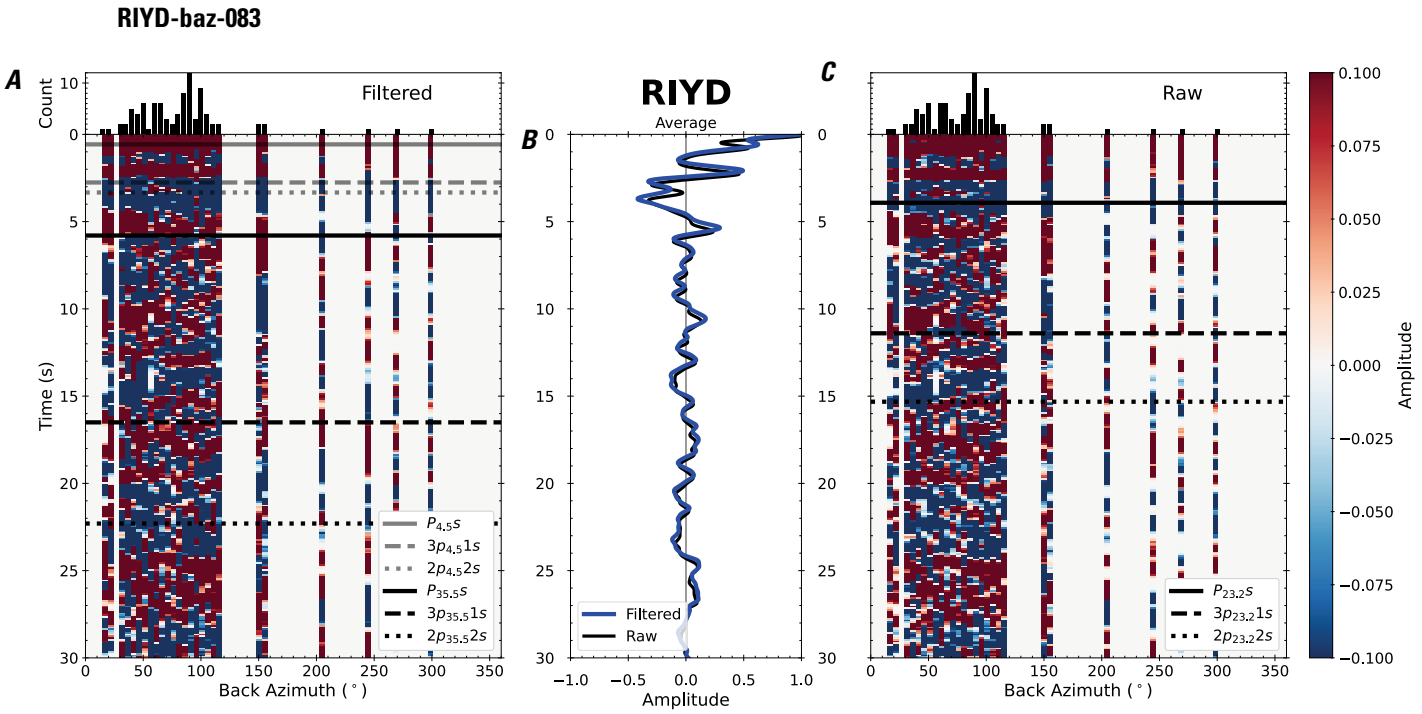

Figure 171. Receiver functions plotted against back azimuth for station RIYD. *A*, Radial component of P-wave receiver functions (PRFs) plotted against back azimuth. Individual PRFs have had the resonance-removal filter of Yu and others (2015) applied to them, are normalized to the maximum amplitude within the time window shown, binned, and normalized by the number of traces per bin. *B*, Average of every individual normalized radial receiver function with the application of the resonance-removal filter (blue) and average of every individual normalized raw radial receiver function (red). *C*, Radial component of raw PRFs, plotted against back azimuth, normalized as in *A*. Ps, 3p1s, and 2p2s arrival times predicted for the preferred Moho depth are shown, assuming a ray parameter of 0.06 s/km.

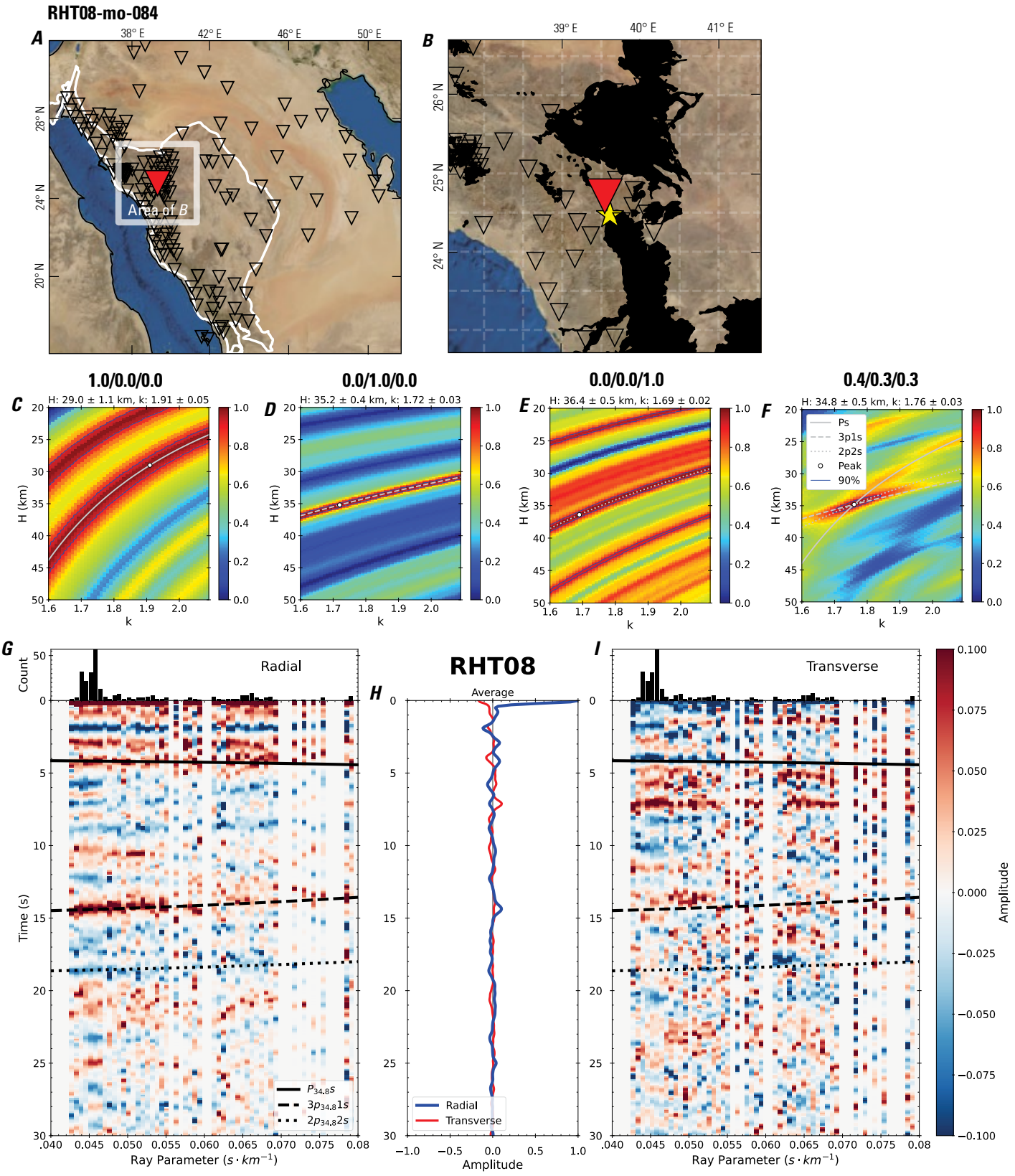
RHT08-mo-084
A
38° E
42° E
46° E
50° E
28° N
24° N
20° N
Area of B
B
39° E
40° E
41° E
26° N
25° N
24° N
1.0/0.0/0.0
0.0/1.0/0.0
0.0/0.0/1.0
0.4/0.3/0.3
C
H: 29.0 ± 1.1 km, k: 1.91 ± 0.05
D
H: 35.2 ± 0.4 km, k: 1.72 ± 0.03
E
H: 36.4 ± 0.5 km, k: 1.69 ± 0.02
F
H: 34.8 ± 0.5 km, k: 1.76 ± 0.03
Ps
3p1s
2p2s
Peak
90%
H (km)
k
G
Radial
Count
Time (s)
$P_{34.8}s$
$3p_{34.8}1s$
$2p_{34.8}2s$
Ray Parameter ($s \cdot km^{-1}$)
RHT08
H
Average
Radial
Transverse
Amplitude
I
Transverse
Amplitude

Figure 172 (page 178). Receiver-function analysis for station RHT08. *A*, Regional map of Saudi Arabia showing the entire array (as inverted triangles), the location of station RHT08 (red inverted triangle), the shield-platform boundary (white line), and the bounds of the map in *B* (white box). *B*, Local map of station RHT08. Harrats are shown in black. *C*, Standard, single-layer *H-k* stack with stacking weights 0.4/0.3/0.3. This *H-k* stack ignores sedimentary effects on the receiver functions. *D*, Standard, single-layer *H-k* stack with stacking weights 0.5/0.5/0.0. This *H-k* stack also ignores sedimentary effects on the receiver functions. *E*, Optimized sub-sedimentary *H-k* stack with stacking weights 0.4/0.3/0.3, following the method of Yu and others (2015). *F*, Optimized sedimentary *H-k* stack with stacking weights 0.05/0.70/0.25, following the method of Yu and others (2015). *G*, Radial component P-wave receiver functions (PRFs) plotted against ray parameter. Individual PRFs have had the resonance-removal filter of Yu and others (2015) applied to them and are normalized to the maximum amplitude within the time window shown, binned, and normalized by the number of traces per bin. *H*, Average of every individual normalized radial receiver function with the application of the resonance-removal filter (blue) and average of every individual normalized raw radial receiver function (red). *I*, Radial component of raw PRFs (that is, PRFs with no resonance-removal filter applied) plotted against ray parameter, normalized as in *G*.

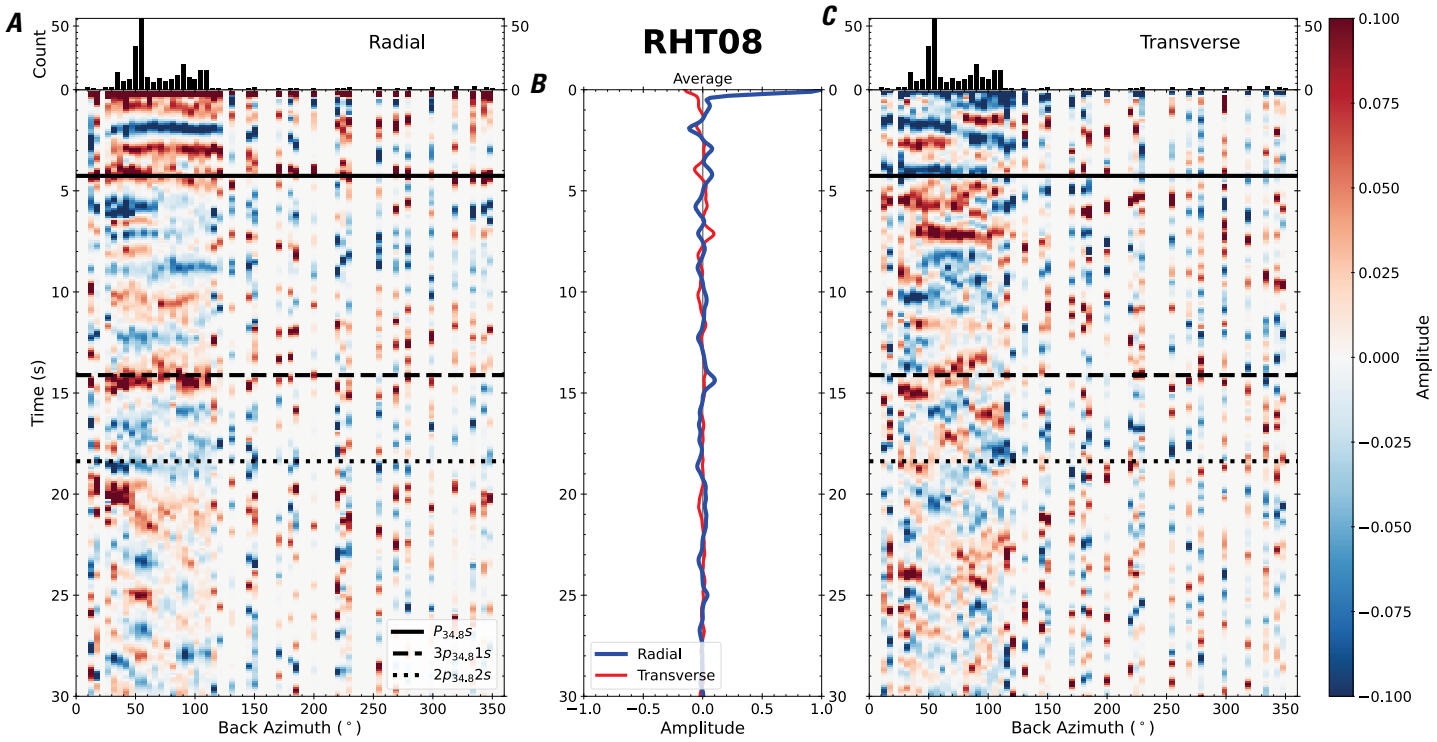

Figure 173. Receiver functions plotted against back azimuth for station RHT08. *A*, Radial component of P-wave receiver functions (PRFs) plotted against back azimuth. Individual PRFs have had the resonance-removal filter of Yu and others (2015) applied to them, are normalized to the maximum amplitude within the time window shown, binned, and normalized by the number of traces per bin. *B*, Average of every individual normalized radial receiver function with the application of the resonance-removal filter (blue) and average of every individual normalized raw radial receiver function (red). *C*, Radial component of raw PRFs, plotted against back azimuth, normalized as in *A*. Ps, 3p1s, and 2p2s arrival times predicted for the preferred Moho depth are shown, assuming a ray parameter of 0.06 s/km.

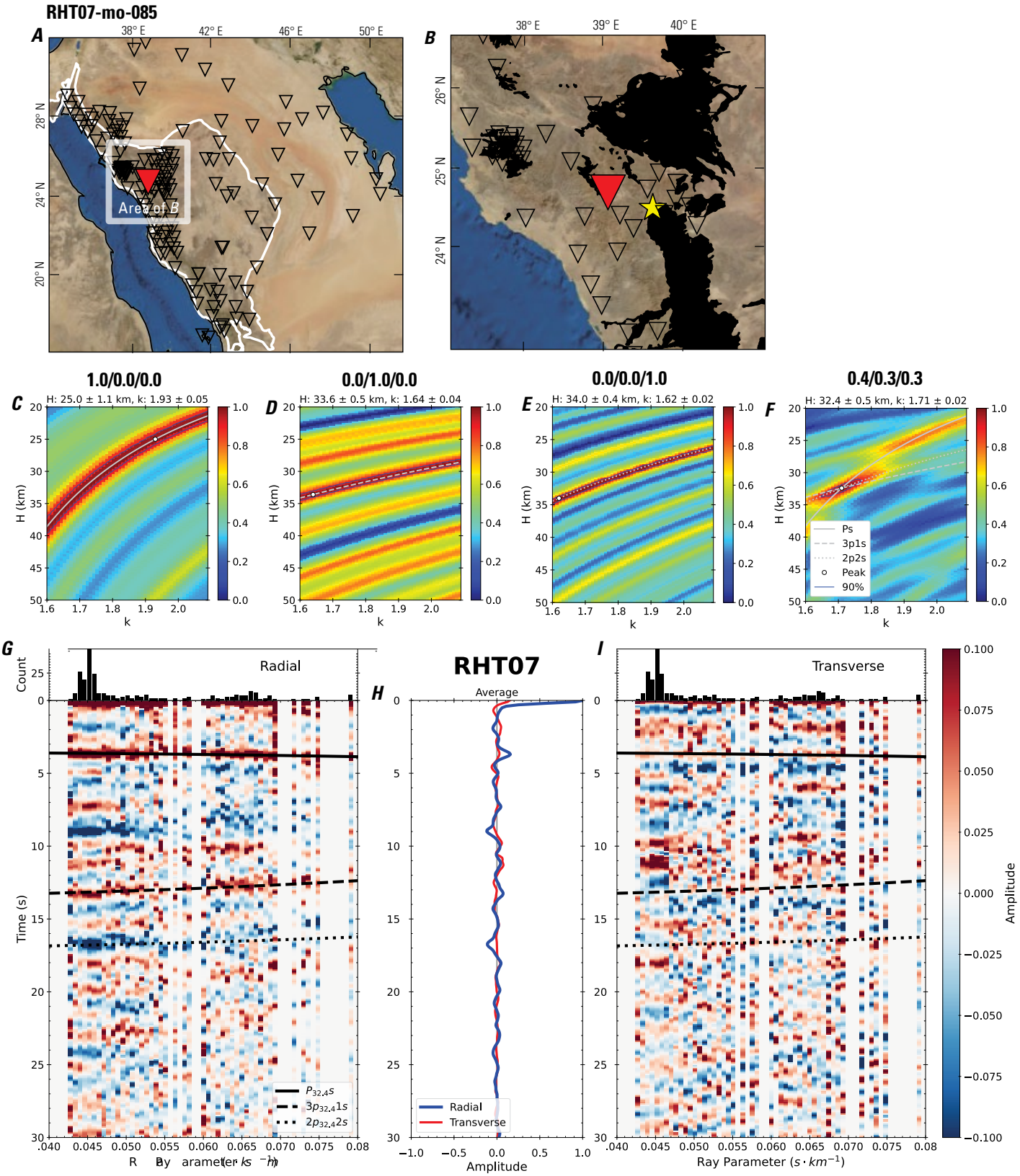
RHT07-mo-085
A
B
Area of B
1.0/0.0/0.0
0.0/1.0/0.0
0.0/0.0/1.0
0.4/0.3/0.3
C
D
E
F
H: 25.0 ± 1.1 km, k: 1.93 ± 0.05
H: 33.6 ± 0.5 km, k: 1.64 ± 0.04
H: 34.0 ± 0.4 km, k: 1.62 ± 0.02
H: 32.4 ± 0.5 km, k: 1.71 ± 0.02
H (km)
k
Ps
3p1s
2p2s
Peak
90%
G
H
I
RHT07
Radial
Transverse
Average
Count
Time (s)
Ray Parameter (s · km⁻¹)
Amplitude
$P_{32.4}s$
$3p_{32.4}1s$
$2p_{32.4}2s$

Figure 174 (page 180). Receiver-function analysis for station RHT07. *A*, Regional map of Saudi Arabia showing the entire array (as inverted triangles), the location of station RHT07 (red inverted triangle), the shield-platform boundary (white line), and the bounds of the map in *B* (white box). *B*, Local map of station RHT07. Harrats are shown in black. *C*, Standard, single-layer *H-k* stack with stacking weights 0.4/0.3/0.3. This *H-k* stack ignores sedimentary effects on the receiver functions. *D*, Standard, single-layer *H-k* stack with stacking weights 0.5/0.5/0.0. This *H-k* stack also ignores sedimentary effects on the receiver functions. *E*, Optimized sub-sedimentary *H-k* stack with stacking weights 0.4/0.3/0.3, following the method of Yu and others (2015). *F*, Optimized sedimentary *H-k* stack with stacking weights 0.05/0.70/0.25, following the method of Yu and others (2015). *G*, Radial component P-wave receiver functions (PRFs) plotted against ray parameter. Individual PRFs have had the resonance-removal filter of Yu and others (2015) applied to them and are normalized to the maximum amplitude within the time window shown, binned, and normalized by the number of traces per bin. *H*, Average of every individual normalized radial receiver function with the application of the resonance-removal filter (blue) and average of every individual normalized raw radial receiver function (red). *I*, Radial component of raw PRFs (that is, PRFs with no resonance-removal filter applied) plotted against ray parameter, normalized as in *G*.

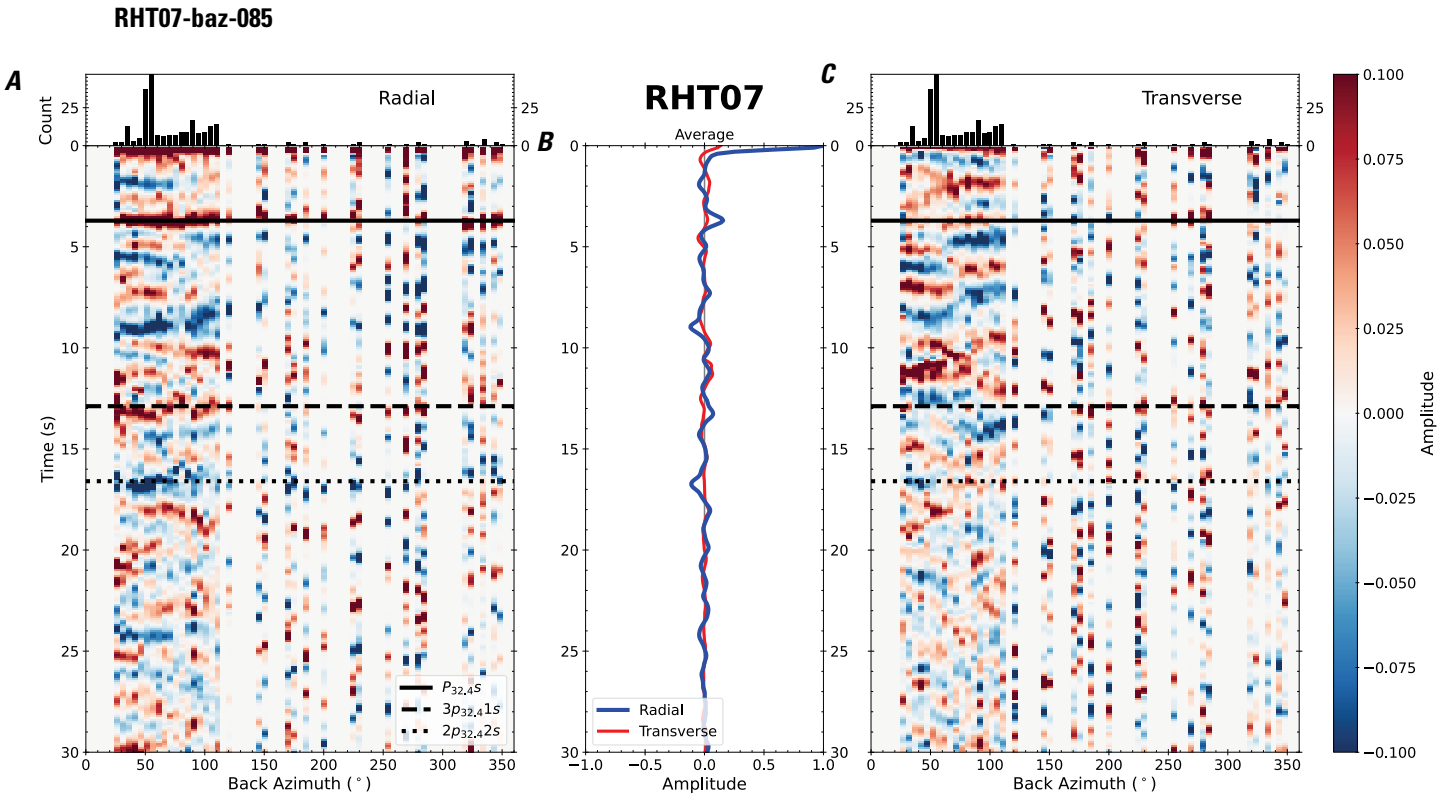

Figure 175. Receiver functions plotted against back azimuth for station RHT07. *A*, Radial component of P-wave receiver functions (PRFs) plotted against back azimuth. Individual PRFs have had the resonance-removal filter of Yu and others (2015) applied to them, are normalized to the maximum amplitude within the time window shown, binned, and normalized by the number of traces per bin. *B*, Average of every individual normalized radial receiver function with the application of the resonance-removal filter (blue) and average of every individual normalized raw radial receiver function (red). *C*, Radial component of raw PRFs, plotted against back azimuth, normalized as in *A*. Ps, 3p1s, and 2p2s arrival times predicted for the preferred Moho depth are shown, assuming a ray parameter of 0.06 s/km.

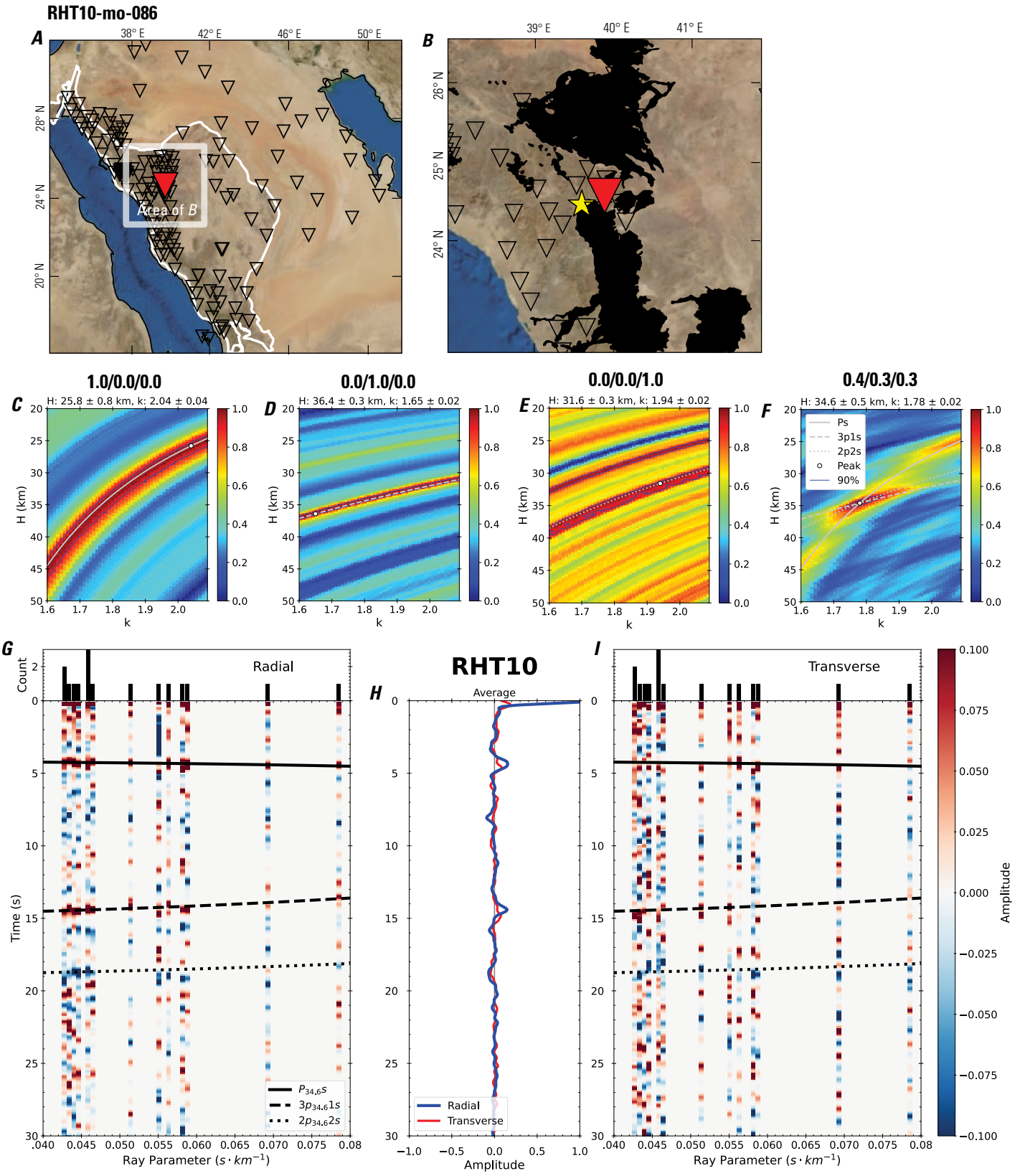
RHT10-mo-086
A
38° E
42° E
46° E
50° E
28° N
24° N
20° N
Area of B
B
39° E
40° E
41° E
26° N
25° N
24° N
1.0/0.0/0.0
0.0/1.0/0.0
0.0/0.0/1.0
0.4/0.3/0.3
C
H: 25.8 ± 0.8 km, k: 2.04 ± 0.04
D
H: 36.4 ± 0.3 km, k: 1.65 ± 0.02
E
H: 31.6 ± 0.3 km, k: 1.94 ± 0.02
F
H: 34.6 ± 0.5 km, k: 1.78 ± 0.02
H (km)
k
Ps
3p1s
2p2s
Peak
90%
G
Radial
Count
Time (s)
Ray Parameter (s · km⁻¹)
$P_{34.6}s$
$3p_{34.6}1s$
$2p_{34.6}2s$
RHT10
H
Average
Amplitude
Radial
Transverse
I
Transverse
Amplitude

Figure 176 (page 182). Receiver-function analysis for station RHT10. *A*, Regional map of Saudi Arabia showing the entire array (as inverted triangles), the location of station RHT10 (red inverted triangle), the shield-platform boundary (white line), and the bounds of the map in *B* (white box). *B*, Local map of station RHT10. Harrats are shown in black. *C*, Standard, single-layer *H-k* stack with stacking weights 0.4/0.3/0.3. This *H-k* stack ignores sedimentary effects on the receiver functions. *D*, Standard, single-layer *H-k* stack with stacking weights 0.5/0.5/0.0. This *H-k* stack also ignores sedimentary effects on the receiver functions. *E*, Optimized sub-sedimentary *H-k* stack with stacking weights 0.4/0.3/0.3, following the method of Yu and others (2015). *F*, Optimized sedimentary *H-k* stack with stacking weights 0.05/0.70/0.25, following the method of Yu and others (2015). *G*, Radial component P-wave receiver functions (PRFs) plotted against ray parameter. Individual PRFs have had the resonance-removal filter of Yu and others (2015) applied to them and are normalized to the maximum amplitude within the time window shown, binned, and normalized by the number of traces per bin. *H*, Average of every individual normalized radial receiver function with the application of the resonance-removal filter (blue) and average of every individual normalized raw radial receiver function (red). *I*, Radial component of raw PRFs (that is, PRFs with no resonance-removal filter applied) plotted against ray parameter, normalized as in *G*.

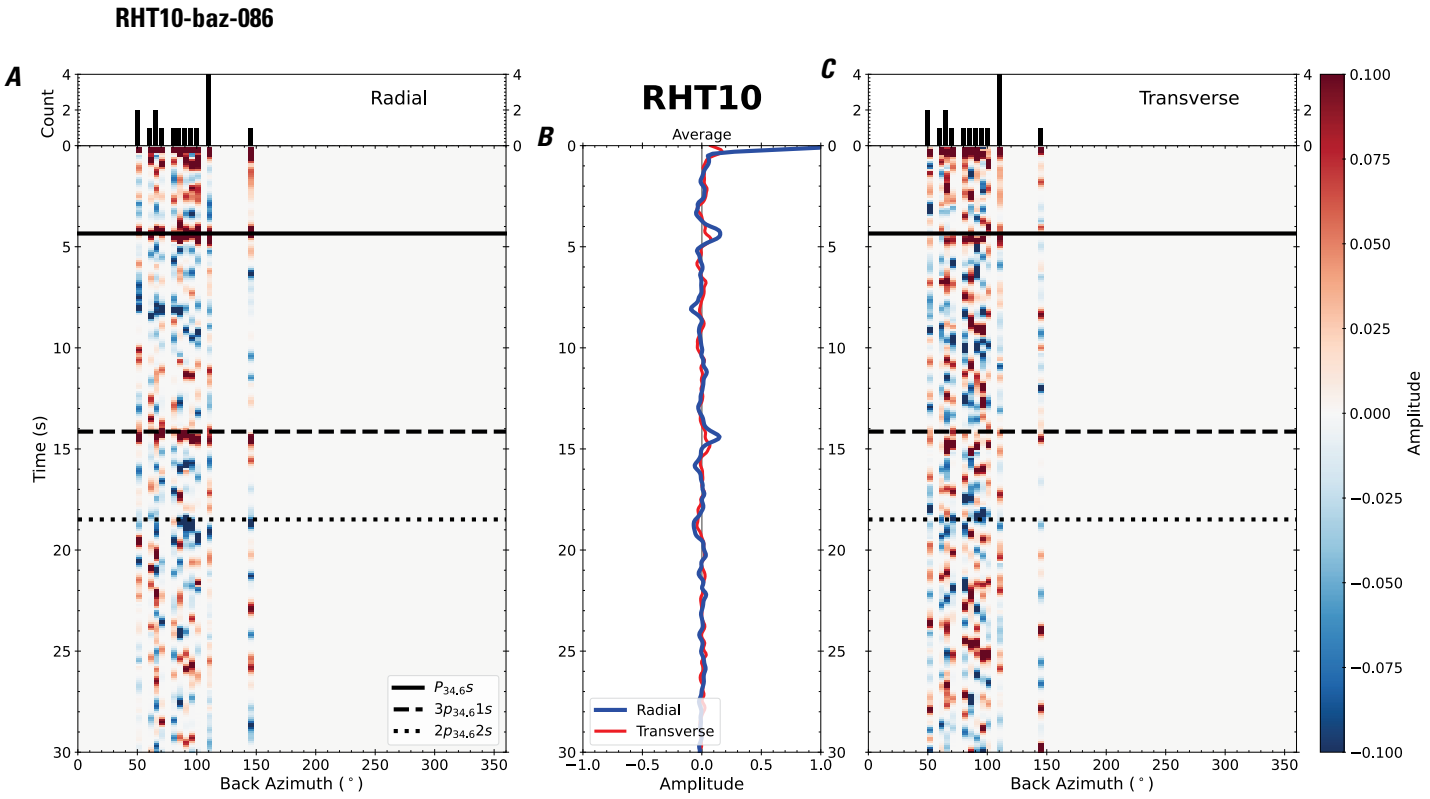

Figure 177. Receiver functions plotted against back azimuth for station RHT10. *A*, Radial component of P-wave receiver functions (PRFs) plotted against back azimuth. Individual PRFs have had the resonance-removal filter of Yu and others (2015) applied to them, are normalized to the maximum amplitude within the time window shown, binned, and normalized by the number of traces per bin. *B*, Average of every individual normalized radial receiver function with the application of the resonance-removal filter (blue) and average of every individual normalized raw radial receiver function (red). *C*, Radial component of raw PRFs, plotted against back azimuth, normalized as in *A*. Ps, 3p1s, and 2p2s arrival times predicted for the preferred Moho depth are shown, assuming a ray parameter of 0.06 s/km.

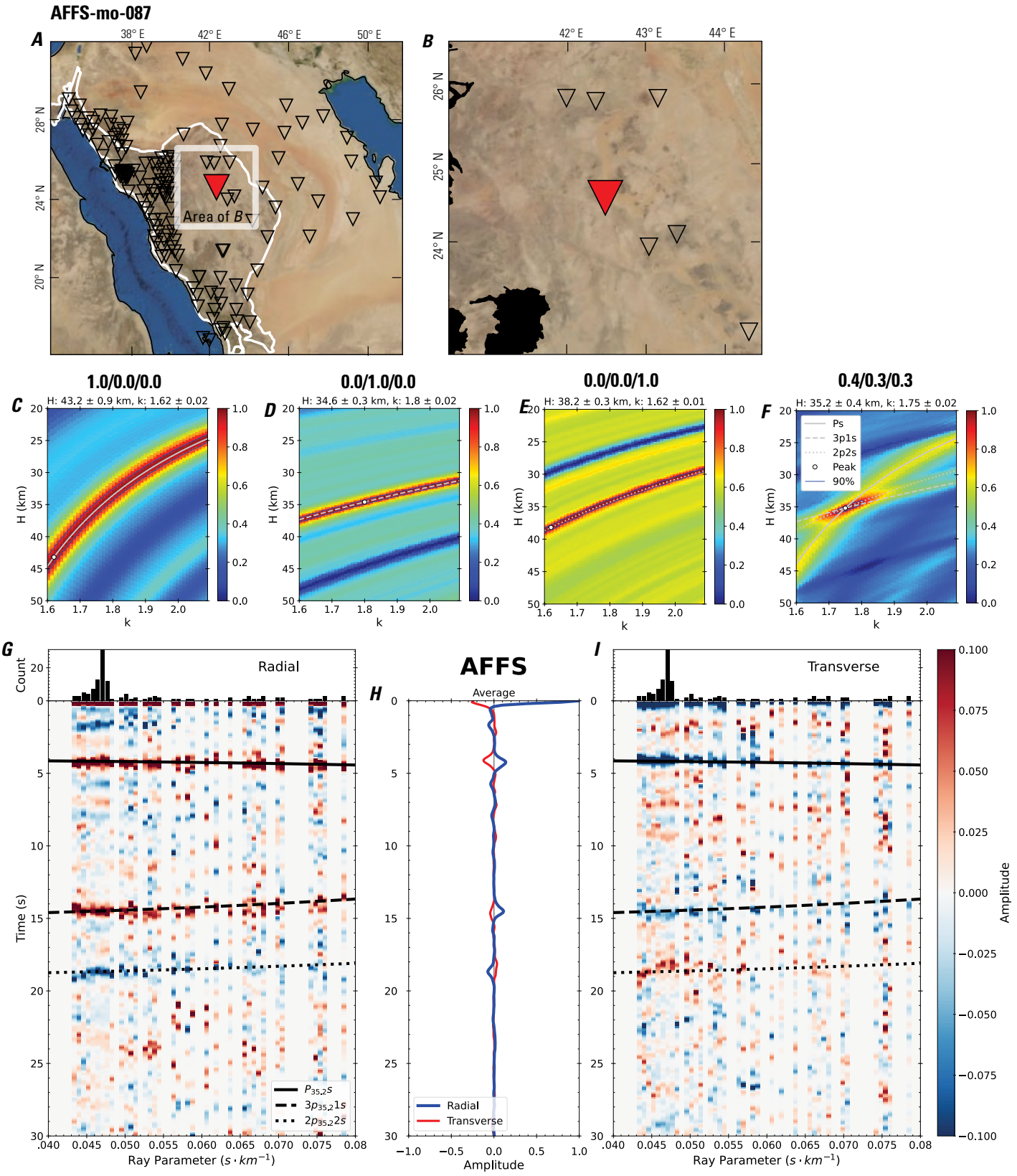
AFFS-mo-087
A
38° E
42° E
46° E
50° E
28° N
24° N
20° N
Area of B
B
42° E
43° E
44° E
26° N
25° N
24° N
1.0/0.0/0.0
0.0/1.0/0.0
0.0/0.0/1.0
0.4/0.3/0.3
C
H: 43.2 ± 0.9 km, k: 1.62 ± 0.02
D
H: 34.6 ± 0.3 km, k: 1.8 ± 0.02
E
H: 38.2 ± 0.3 km, k: 1.62 ± 0.01
F
H: 35.2 ± 0.4 km, k: 1.75 ± 0.02
Ps
3p1s
2p2s
Peak
90%
H (km)
k
G
Radial
Count
Time (s)
$P_{35,2}s$
$3p_{35,2}1s$
$2p_{35,2}2s$
Ray Parameter ($s \cdot km^{-1}$)
H
AFFS
Average
Radial
Transverse
Amplitude
I
Transverse
Ray Parameter ($s \cdot km^{-1}$)
Amplitude

Figure 178 (page 184). Receiver-function analysis for station AFFS. *A*, Regional map of Saudi Arabia showing the entire array (as inverted triangles), the location of station AFFS (red inverted triangle), the shield-platform boundary (white line), and the bounds of the map in *B* (white box). *B*, Local map of station AFFS. Harrats are shown in black. *C*, Standard, single-layer *H-k* stack with stacking weights 0.4/0.3/0.3. This *H-k* stack ignores sedimentary effects on the receiver functions. *D*, Standard, single-layer *H-k* stack with stacking weights 0.5/0.5/0.0. This *H-k* stack also ignores sedimentary effects on the receiver functions. *E*, Optimized sub-sedimentary *H-k* stack with stacking weights 0.4/0.3/0.3, following the method of Yu and others (2015). *F*, Optimized sedimentary *H-k* stack with stacking weights 0.05/0.70/0.25, following the method of Yu and others (2015). *G*, Radial component P-wave receiver functions (PRFs) plotted against ray parameter. Individual PRFs have had the resonance-removal filter of Yu and others (2015) applied to them and are normalized to the maximum amplitude within the time window shown, binned, and normalized by the number of traces per bin. *H*, Average of every individual normalized radial receiver function with the application of the resonance-removal filter (blue) and average of every individual normalized raw radial receiver function (red). *I*, Radial component of raw PRFs (that is, PRFs with no resonance-removal filter applied) plotted against ray parameter, normalized as in *G*.

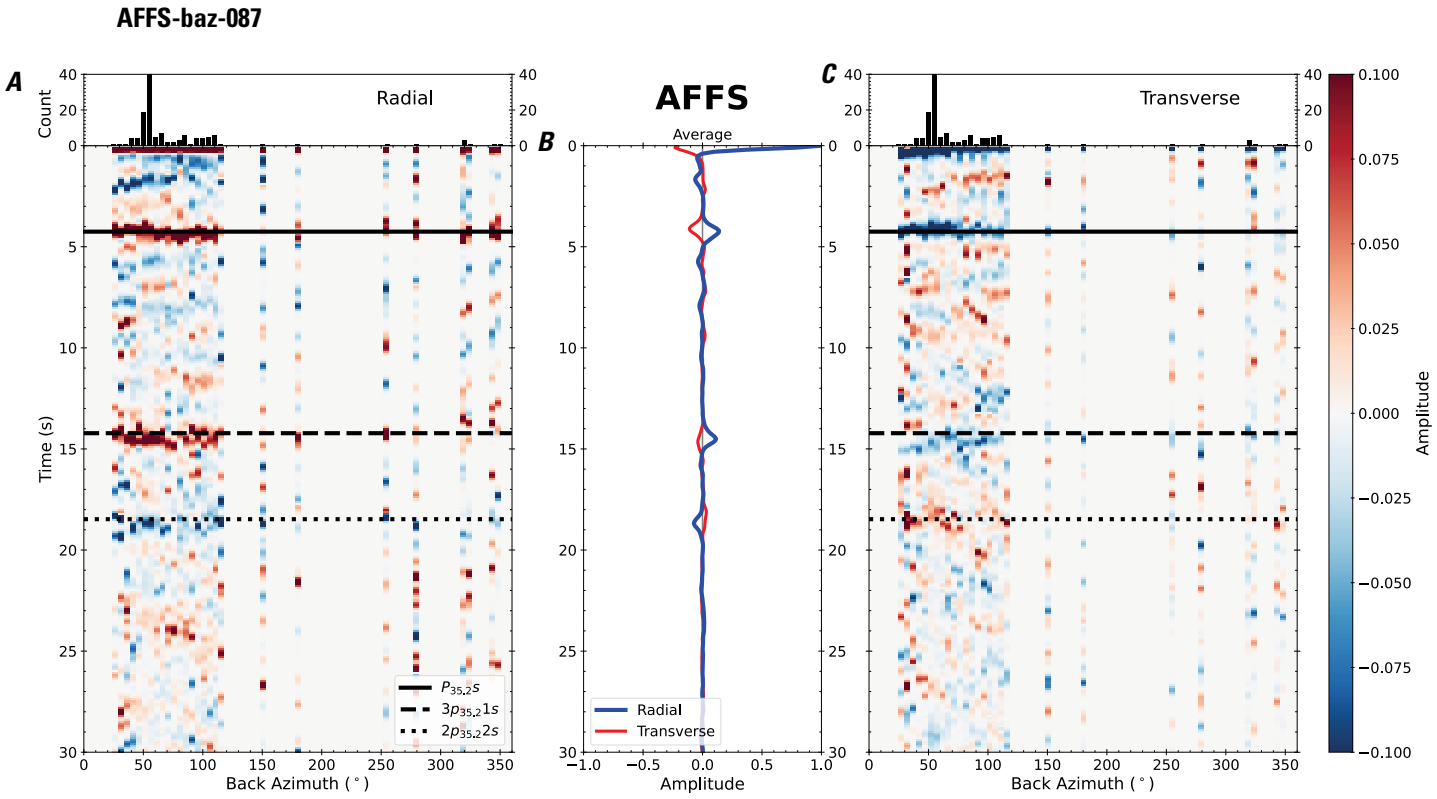

Figure 179. Receiver functions plotted against back azimuth for station AFFS. *A*, Radial component of P-wave receiver functions (PRFs) plotted against back azimuth. Individual PRFs have had the resonance-removal filter of Yu and others (2015) applied to them, are normalized to the maximum amplitude within the time window shown, binned, and normalized by the number of traces per bin. *B*, Average of every individual normalized radial receiver function with the application of the resonance-removal filter (blue) and average of every individual normalized raw radial receiver function (red). *C*, Radial component of raw PRFs, plotted against back azimuth, normalized as in *A*. Ps, 3p1s, and 2p2s arrival times predicted for the preferred Moho depth are shown, assuming a ray parameter of 0.06 s/km.

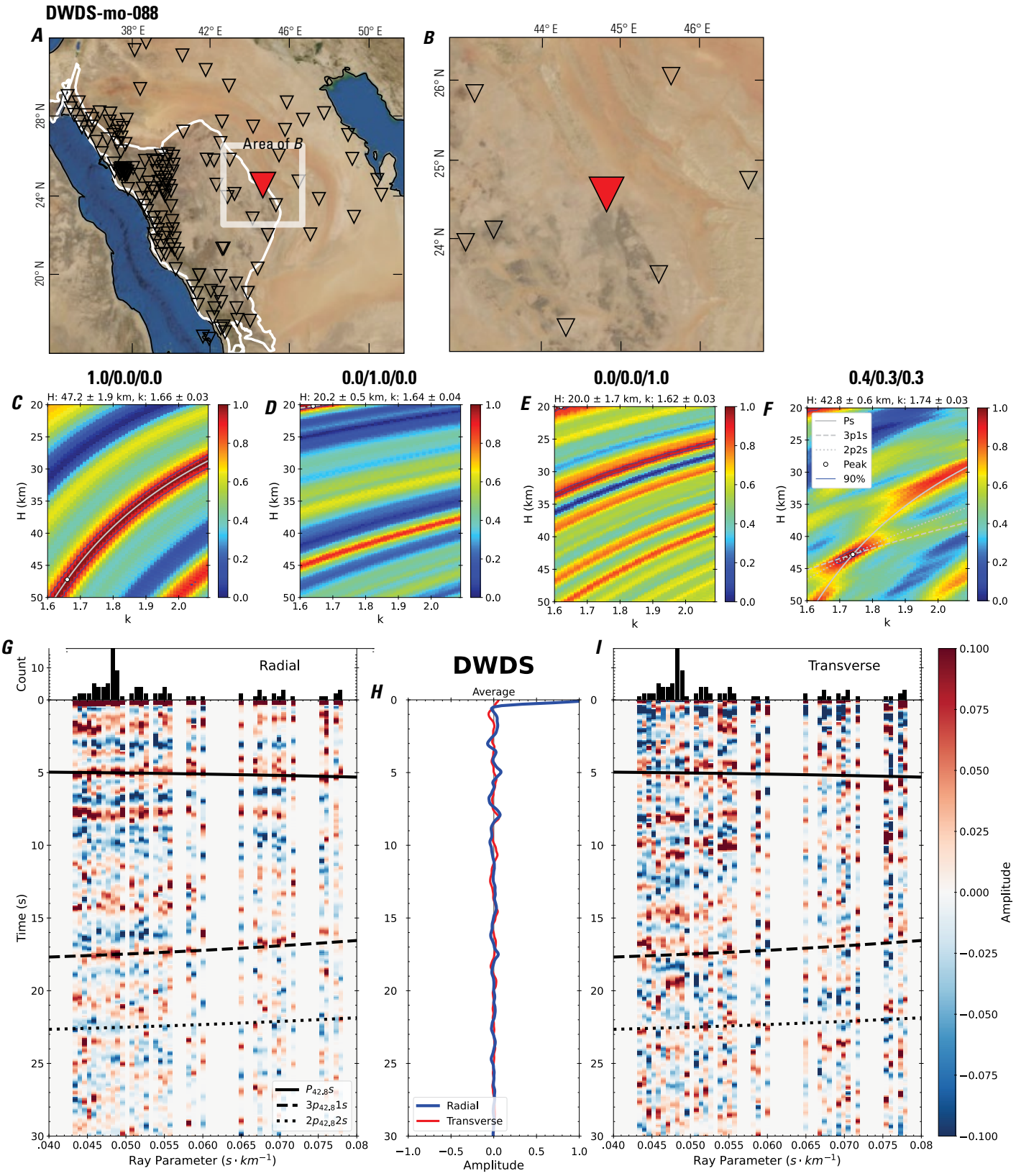
DWDS-mo-088
A
38° E
42° E
46° E
50° E
28° N
24° N
20° N
Area of B
B
44° E
45° E
46° E
26° N
25° N
24° N
1.0/0.0/0.0
0.0/1.0/0.0
0.0/0.0/1.0
0.4/0.3/0.3
C
H: 47.2 ± 1.9 km, k: 1.66 ± 0.03
D
H: 20.2 ± 0.5 km, k: 1.64 ± 0.04
E
H: 20.0 ± 1.7 km, k: 1.62 ± 0.03
F
H: 42.8 ± 0.6 km, k: 1.74 ± 0.03
Ps
3p1s
2p2s
Peak
90%
H (km)
k
G
Radial
Count
Time (s)
$P_{42.8}s$
$3p_{42.8}1s$
$2p_{42.8}2s$
Ray Parameter ($s \cdot km^{-1}$)
H
DWDS
Average
Radial
Transverse
Amplitude
I
Transverse
Ray Parameter ($s \cdot km^{-1}$)
Amplitude

Figure 180 (page 186). Receiver-function analysis for station DWDS. *A*, Regional map of Saudi Arabia showing the entire array (as inverted triangles), the location of station DWDS (red inverted triangle), the shield-platform boundary (white line), and the bounds of the map in *B* (white box). *B*, Local map of station DWDS. Harrats are shown in black. *C*, Standard, single-layer *H-k* stack with stacking weights 0.4/0.3/0.3. This *H-k* stack ignores sedimentary effects on the receiver functions. *D*, Standard, single-layer *H-k* stack with stacking weights 0.5/0.5/0.0. This *H-k* stack also ignores sedimentary effects on the receiver functions. *E*, Optimized sub-sedimentary *H-k* stack with stacking weights 0.4/0.3/0.3, following the method of Yu and others (2015). *F*, Optimized sedimentary *H-k* stack with stacking weights 0.05/0.70/0.25, following the method of Yu and others (2015). *G*, Radial component P-wave receiver functions (PRFs) plotted against ray parameter. Individual PRFs have had the resonance-removal filter of Yu and others (2015) applied to them and are normalized to the maximum amplitude within the time window shown, binned, and normalized by the number of traces per bin. *H*, Average of every individual normalized radial receiver function with the application of the resonance-removal filter (blue) and average of every individual normalized raw radial receiver function (red). *I*, Radial component of raw PRFs (that is, PRFs with no resonance-removal filter applied) plotted against ray parameter, normalized as in *G*.

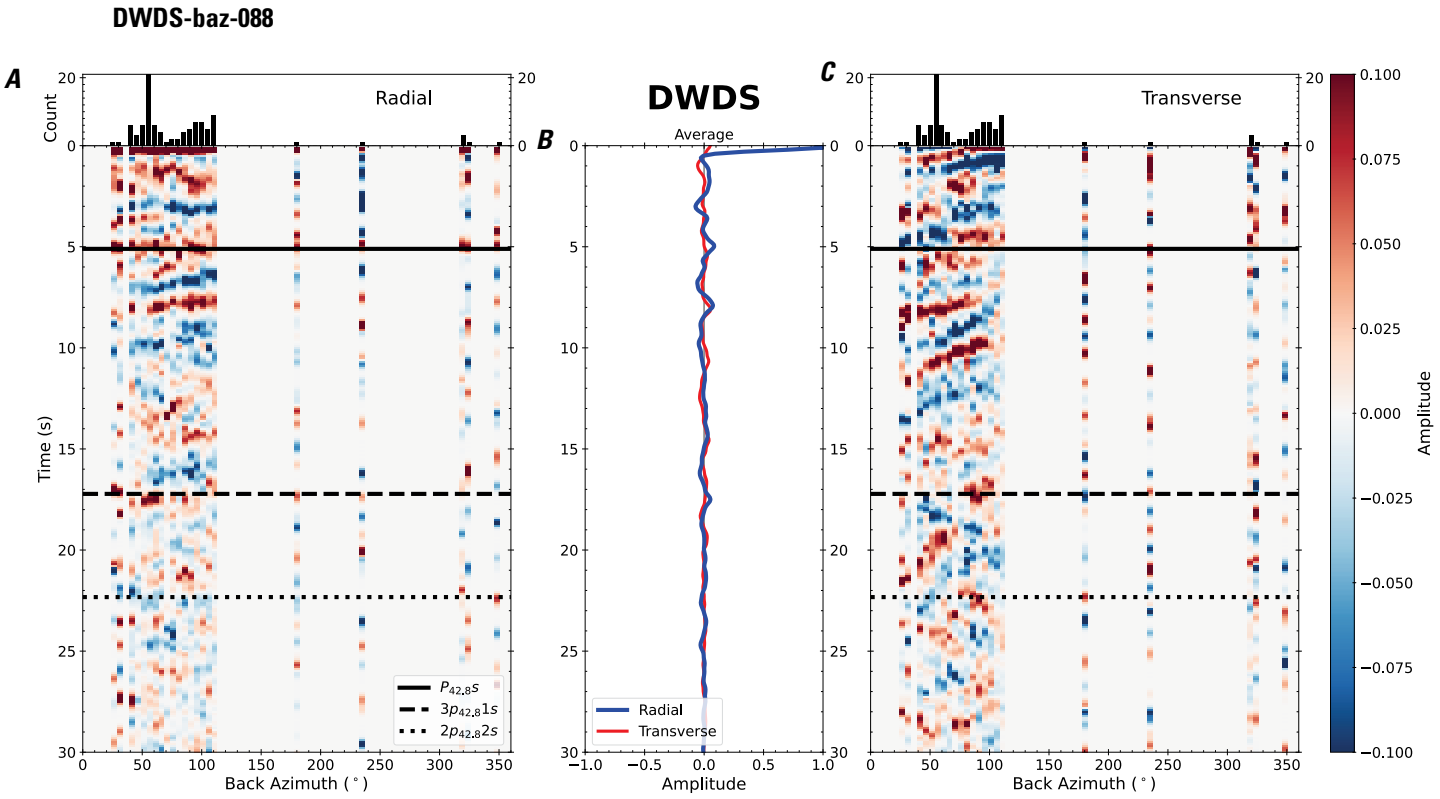

Figure 181. Receiver functions plotted against back azimuth for station DWDS. *A*, Radial component of P-wave receiver functions (PRFs) plotted against back azimuth. Individual PRFs have had the resonance-removal filter of Yu and others (2015) applied to them, are normalized to the maximum amplitude within the time window shown, binned, and normalized by the number of traces per bin. *B*, Average of every individual normalized radial receiver function with the application of the resonance-removal filter (blue) and average of every individual normalized raw radial receiver function (red). *C*, Radial component of raw PRFs, plotted against back azimuth, normalized as in *A*. Ps, 3p1s, and 2p2s arrival times predicted for the preferred Moho depth are shown, assuming a ray parameter of 0.06 s/km.

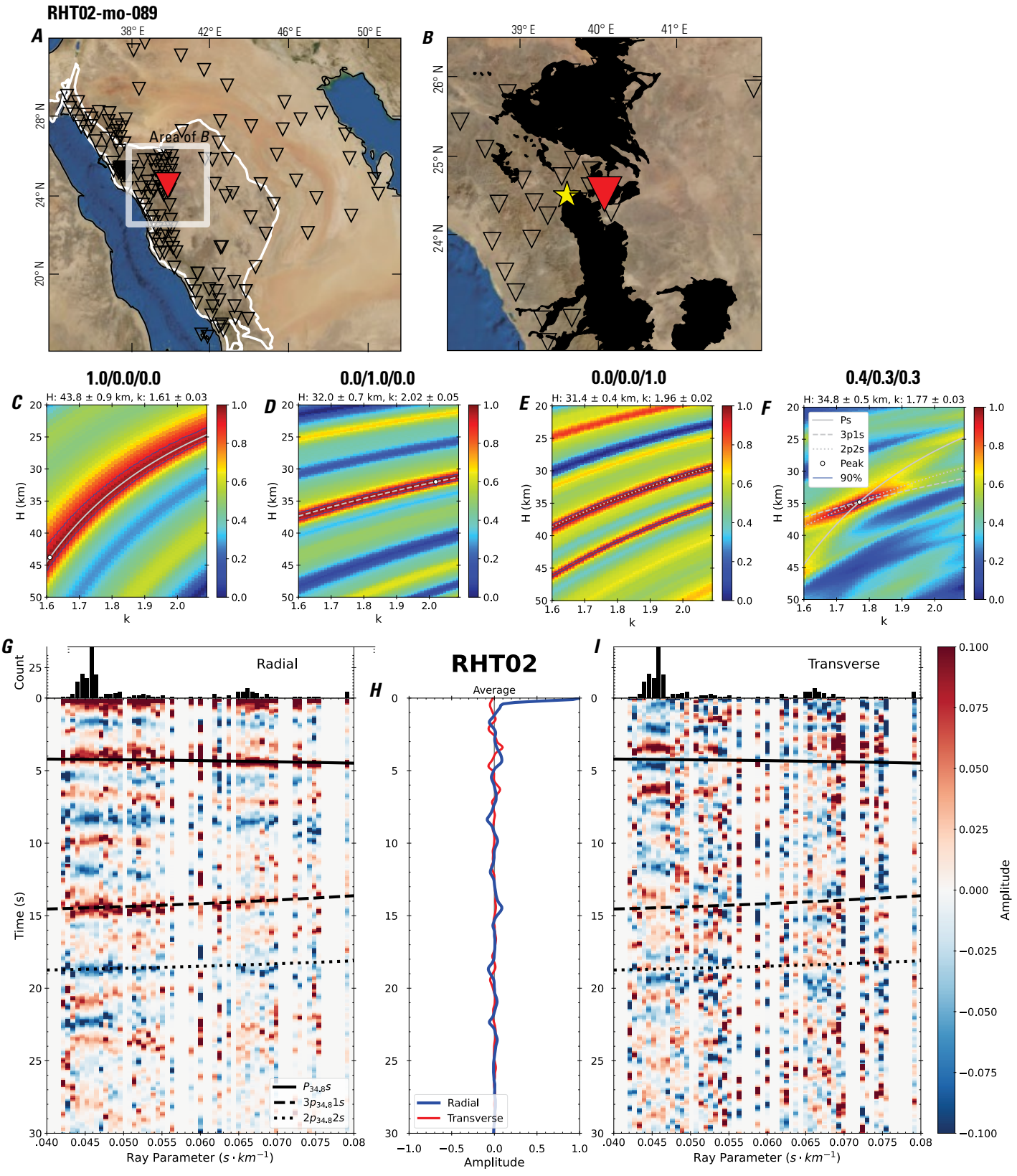
RHT02-mo-089
A
B
Area of B
1.0/0.0/0.0
0.0/1.0/0.0
0.0/0.0/1.0
0.4/0.3/0.3
C
D
E
F
H: 43.8 ± 0.9 km, k: 1.61 ± 0.03
H: 32.0 ± 0.7 km, k: 2.02 ± 0.05
H: 31.4 ± 0.4 km, k: 1.96 ± 0.02
H: 34.8 ± 0.5 km, k: 1.77 ± 0.03
H (km)
k
Ps
3p1s
2p2s
Peak
90%
G
H
I
RHT02
Radial
Transverse
Average
Count
Time (s)
Ray Parameter (s · km⁻¹)
Amplitude
$P_{34.8}s$
$3p_{34.8}1s$
$2p_{34.8}2s$

Figure 182 (page 188). Receiver-function analysis for station RHT02. *A*, Regional map of Saudi Arabia showing the entire array (as inverted triangles), the location of station RHT02 (red inverted triangle), the shield-platform boundary (white line), and the bounds of the map in *B* (white box). *B*, Local map of station RHT02. Harrats are shown in black. *C*, Standard, single-layer *H-k* stack with stacking weights 0.4/0.3/0.3. This *H-k* stack ignores sedimentary effects on the receiver functions. *D*, Standard, single-layer *H-k* stack with stacking weights 0.5/0.5/0.0. This *H-k* stack also ignores sedimentary effects on the receiver functions. *E*, Optimized sub-sedimentary *H-k* stack with stacking weights 0.4/0.3/0.3, following the method of Yu and others (2015). *F*, Optimized sedimentary *H-k* stack with stacking weights 0.05/0.70/0.25, following the method of Yu and others (2015). *G*, Radial component P-wave receiver functions (PRFs) plotted against ray parameter. Individual PRFs have had the resonance-removal filter of Yu and others (2015) applied to them and are normalized to the maximum amplitude within the time window shown, binned, and normalized by the number of traces per bin. *H*, Average of every individual normalized radial receiver function with the application of the resonance-removal filter (blue) and average of every individual normalized raw radial receiver function (red). *I*, Radial component of raw PRFs (that is, PRFs with no resonance-removal filter applied) plotted against ray parameter, normalized as in *G*.

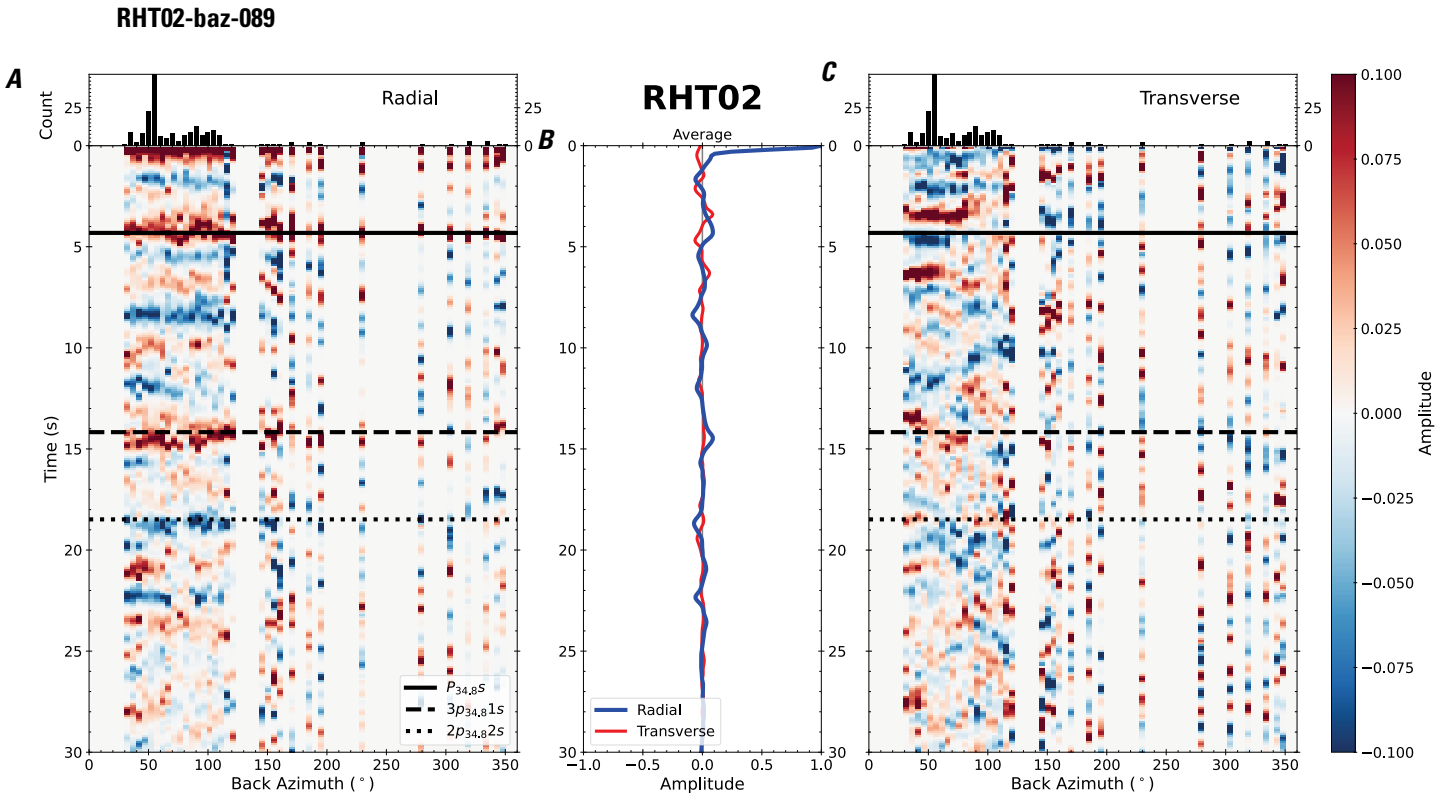

Figure 183. Receiver functions plotted against back azimuth for station RHT02. *A*, Radial component of P-wave receiver functions (PRFs) plotted against back azimuth. Individual PRFs have had the resonance-removal filter of Yu and others (2015) applied to them, are normalized to the maximum amplitude within the time window shown, binned, and normalized by the number of traces per bin. *B*, Average of every individual normalized radial receiver function with the application of the resonance-removal filter (blue) and average of every individual normalized raw radial receiver function (red). *C*, Radial component of raw PRFs, plotted against back azimuth, normalized as in *A*. Ps, 3p1s, and 2p2s arrival times predicted for the preferred Moho depth are shown, assuming a ray parameter of 0.06 s/km.

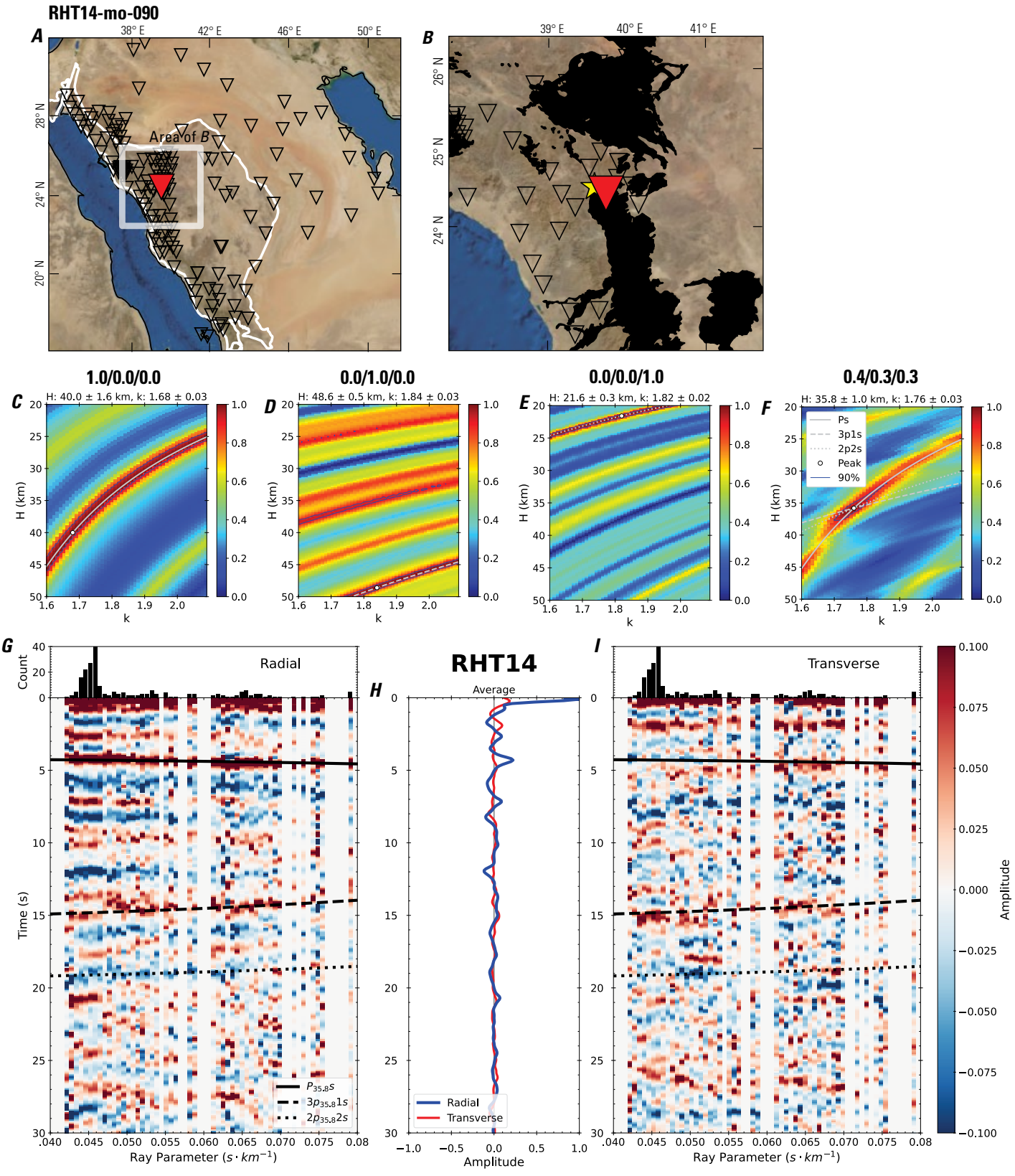
RHT14-mo-090
A
B
Area of B
1.0/0.0/0.0
0.0/1.0/0.0
0.0/0.0/1.0
0.4/0.3/0.3
C
D
E
F
H: 40.0 ± 1.6 km, k: 1.68 ± 0.03
H: 48.6 ± 0.5 km, k: 1.84 ± 0.03
H: 21.6 ± 0.3 km, k: 1.82 ± 0.02
H: 35.8 ± 1.0 km, k: 1.76 ± 0.03
Ps
3p1s
2p2s
Peak
90%
H (km)
k
G
H
I
RHT14
Radial
Transverse
Average
Count
Time (s)
Ray Parameter (s · km⁻¹)
Amplitude
$P_{35.8}s$
$3p_{35.8}1s$
$2p_{35.8}2s$

Figure 184 (page 190). Receiver-function analysis for station RHT14. *A*, Regional map of Saudi Arabia showing the entire array (as inverted triangles), the location of station RHT14 (red inverted triangle), the shield-platform boundary (white line), and the bounds of the map in *B* (white box). *B*, Local map of station RHT14. Harrats are shown in black. *C*, Standard, single-layer *H-k* stack with stacking weights 0.4/0.3/0.3. This *H-k* stack ignores sedimentary effects on the receiver functions. *D*, Standard, single-layer *H-k* stack with stacking weights 0.5/0.5/0.0. This *H-k* stack also ignores sedimentary effects on the receiver functions. *E*, Optimized sub-sedimentary *H-k* stack with stacking weights 0.4/0.3/0.3, following the method of Yu and others (2015). *F*, Optimized sedimentary *H-k* stack with stacking weights 0.05/0.70/0.25, following the method of Yu and others (2015). *G*, Radial component P-wave receiver functions (PRFs) plotted against ray parameter. Individual PRFs have had the resonance-removal filter of Yu and others (2015) applied to them and are normalized to the maximum amplitude within the time window shown, binned, and normalized by the number of traces per bin. *H*, Average of every individual normalized radial receiver function with the application of the resonance-removal filter (blue) and average of every individual normalized raw radial receiver function (red). *I*, Radial component of raw PRFs (that is, PRFs with no resonance-removal filter applied) plotted against ray parameter, normalized as in *G*.

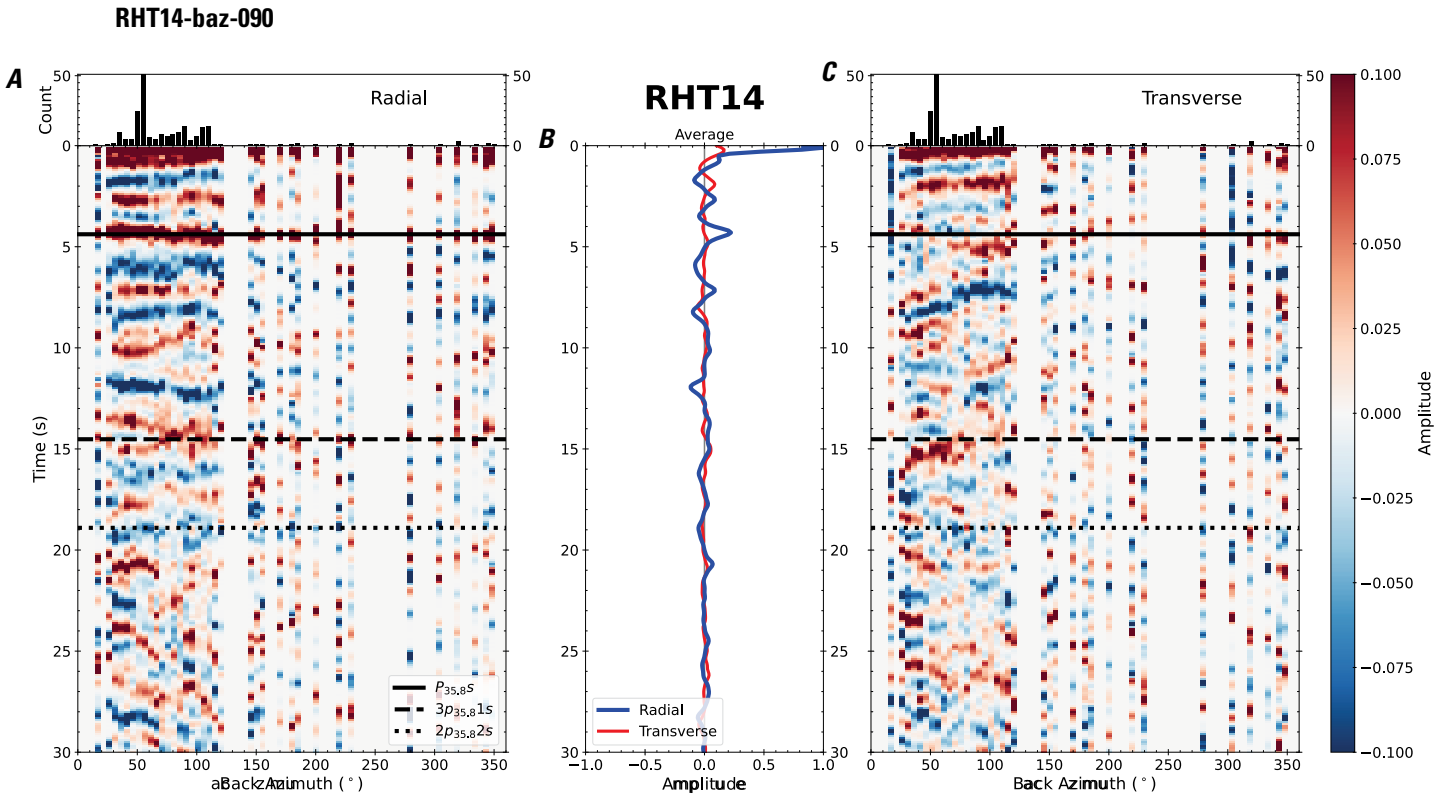

Figure185. Receiver functions plotted against back azimuth for station RHT14. *A*, Radial component of P-wave receiver functions (PRFs) plotted against back azimuth. Individual PRFs have had the resonance-removal filter of Yu and others (2015) applied to them, are normalized to the maximum amplitude within the time window shown, binned, and normalized by the number of traces per bin. *B*, Average of every individual normalized radial receiver function with the application of the resonance-removal filter (blue) and average of every individual normalized raw radial receiver function (red). *C*, Radial component of raw PRFs, plotted against back azimuth, normalized as in *A*. Ps, 3p1s, and 2p2s arrival times predicted for the preferred Moho depth are shown, assuming a ray parameter of 0.06 s/km.

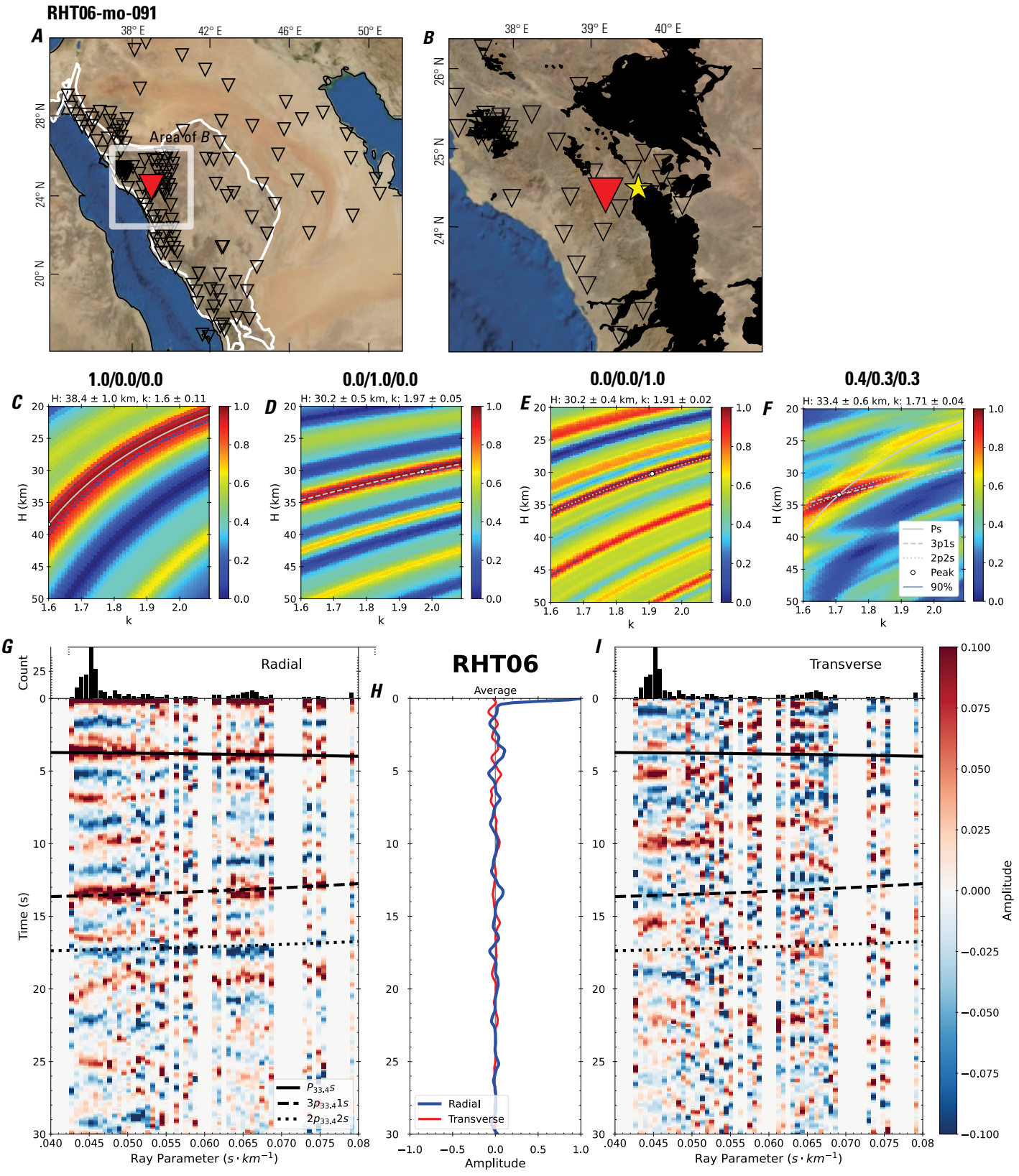
RHT06-mo-091
A
38° E
42° E
46° E
50° E
28° N
24° N
20° N
Area of B
B
38° E
39° E
40° E
26° N
25° N
24° N
1.0/0.0/0.0
0.0/1.0/0.0
0.0/0.0/1.0
0.4/0.3/0.3
C
H: 38.4 ± 1.0 km, k: 1.6 ± 0.11
D
H: 30.2 ± 0.5 km, k: 1.97 ± 0.05
E
H: 30.2 ± 0.4 km, k: 1.91 ± 0.02
F
H: 33.4 ± 0.6 km, k: 1.71 ± 0.04
H (km)
k
Ps
3p1s
2p2s
Peak
90%
G
Radial
Count
Time (s)
Ray Parameter (s · km⁻¹)
$P_{33.4}s$
$3p_{33.4}1s$
$2p_{33.4}2s$
RHT06
H
Average
Radial
Transverse
Amplitude
I
Transverse
Amplitude

Figure 186 (page 192). Receiver-function analysis for station RHT06. *A*, Regional map of Saudi Arabia showing the entire array (as inverted triangles), the location of station RHT06 (red inverted triangle), the shield-platform boundary (white line), and the bounds of the map in *B* (white box). *B*, Local map of station RHT06. Harrats are shown in black. *C*, Standard, single-layer *H-k* stack with stacking weights 0.4/0.3/0.3. This *H-k* stack ignores sedimentary effects on the receiver functions. *D*, Standard, single-layer *H-k* stack with stacking weights 0.5/0.5/0.0. This *H-k* stack also ignores sedimentary effects on the receiver functions. *E*, Optimized sub-sedimentary *H-k* stack with stacking weights 0.4/0.3/0.3, following the method of Yu and others (2015). *F*, Optimized sedimentary *H-k* stack with stacking weights 0.05/0.70/0.25, following the method of Yu and others (2015). *G*, Radial component P-wave receiver functions (PRFs) plotted against ray parameter. Individual PRFs have had the resonance-removal filter of Yu and others (2015) applied to them and are normalized to the maximum amplitude within the time window shown, binned, and normalized by the number of traces per bin. *H*, Average of every individual normalized radial receiver function with the application of the resonance-removal filter (blue) and average of every individual normalized raw radial receiver function (red). *I*, Radial component of raw PRFs (that is, PRFs with no resonance-removal filter applied) plotted against ray parameter, normalized as in *G*.

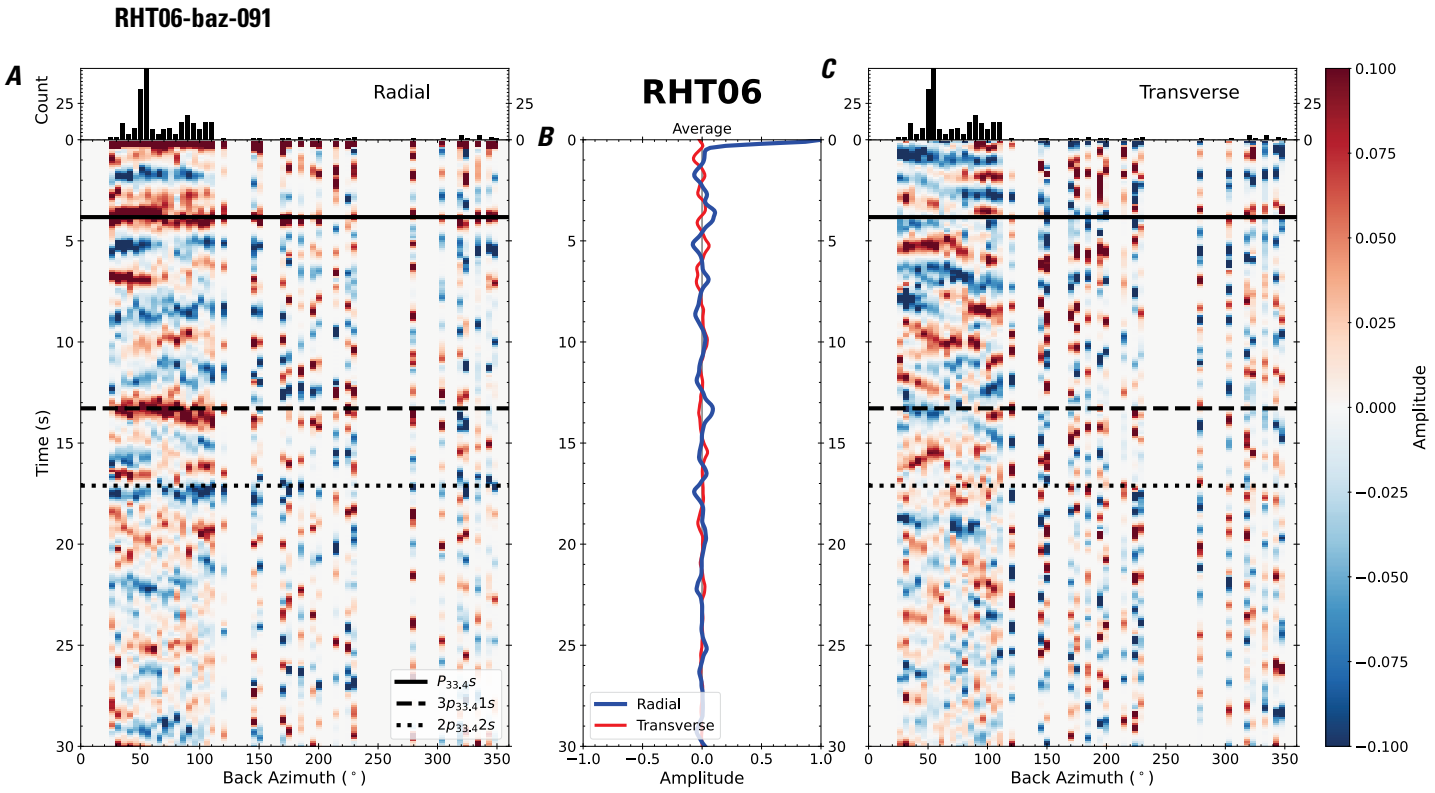

Figure 187. Receiver functions plotted against back azimuth for station RHT06. *A*, Radial component of P-wave receiver functions (PRFs) plotted against back azimuth. Individual PRFs have had the resonance-removal filter of Yu and others (2015) applied to them, are normalized to the maximum amplitude within the time window shown, binned, and normalized by the number of traces per bin. *B*, Average of every individual normalized radial receiver function with the application of the resonance-removal filter (blue) and average of every individual normalized raw radial receiver function (red). *C*, Radial component of raw PRFs, plotted against back azimuth, normalized as in *A*. Ps, 3p1s, and 2p2s arrival times predicted for the preferred Moho depth are shown, assuming a ray parameter of 0.06 s/km.

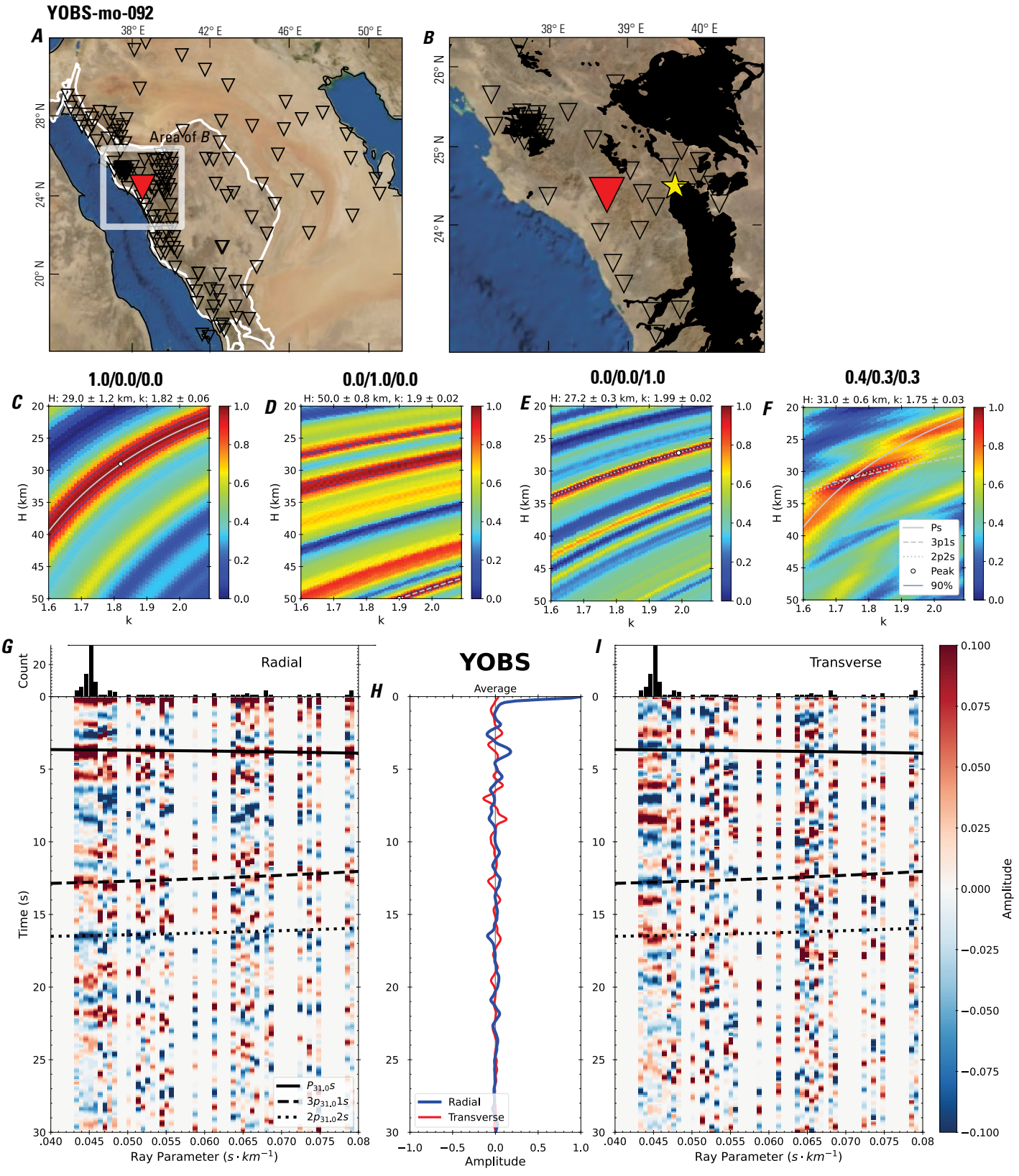
YOBS-mo-092
A
38° E
42° E
46° E
50° E
28° N
24° N
20° N
Area of B
B
38° E
39° E
40° E
26° N
25° N
24° N
1.0/0.0/0.0
0.0/1.0/0.0
0.0/0.0/1.0
0.4/0.3/0.3
C
H: 29.0 ± 1.2 km, k: 1.82 ± 0.06
D
H: 50.0 ± 0.8 km, k: 1.9 ± 0.02
E
H: 27.2 ± 0.3 km, k: 1.99 ± 0.02
F
H: 31.0 ± 0.6 km, k: 1.75 ± 0.03
H (km)
k
Ps
3p1s
2p2s
Peak
90%
G
Radial
Count
Time (s)
$P_{31.0}s$
$3p_{31.0}1s$
$2p_{31.0}2s$
Ray Parameter ($s \cdot km^{-1}$)
YOBS
H
Average
Radial
Transverse
Amplitude
I
Transverse
Amplitude

Figure 188 (page 198). Receiver-function analysis for station YOBS. *A*, Regional map of Saudi Arabia showing the entire array (as inverted triangles), the location of station YOBS (red inverted triangle), the shield-platform boundary (white line), and the bounds of the map in *B* (white box). *B*, Local map of station YOBS. Harrats are shown in black. *C*, Standard, single-layer *H-k* stack with stacking weights 0.4/0.3/0.3. This *H-k* stack ignores sedimentary effects on the receiver functions. *D*, Standard, single-layer *H-k* stack with stacking weights 0.5/0.5/0.0. This *H-k* stack also ignores sedimentary effects on the receiver functions. *E*, Optimized sub-sedimentary *H-k* stack with stacking weights 0.4/0.3/0.3, following the method of Yu and others (2015). *F*, Optimized sedimentary *H-k* stack with stacking weights 0.05/0.70/0.25, following the method of Yu and others (2015). *G*, Radial component P-wave receiver functions (PRFs) plotted against ray parameter. Individual PRFs have had the resonance-removal filter of Yu and others (2015) applied to them and are normalized to the maximum amplitude within the time window shown, binned, and normalized by the number of traces per bin. *H*, Average of every individual normalized radial receiver function with the application of the resonance-removal filter (blue) and average of every individual normalized raw radial receiver function (red). *I*, Radial component of raw PRFs (that is, PRFs with no resonance-removal filter applied) plotted against ray parameter, normalized as in *G*.

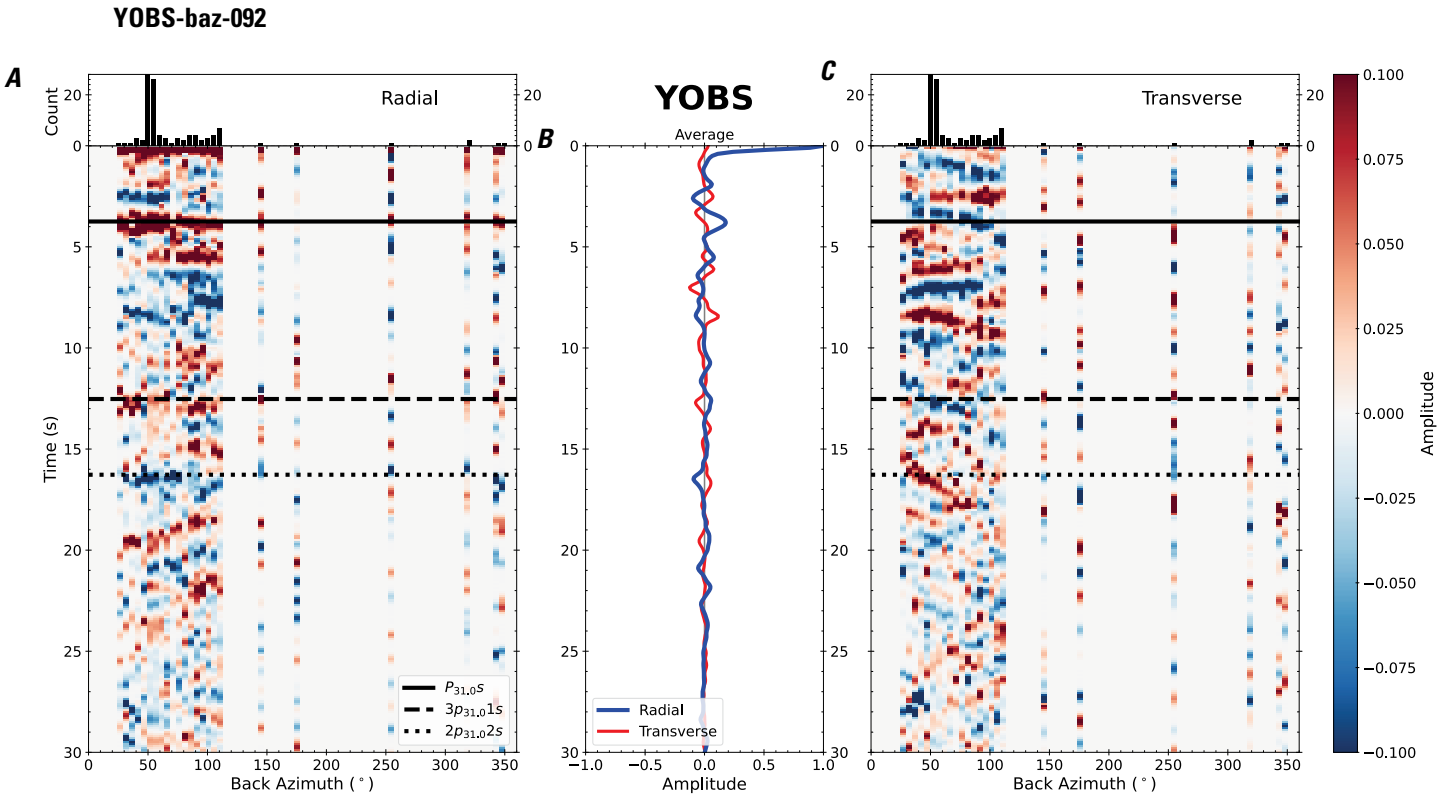

Figure 189. Receiver functions plotted against back azimuth for station YOBS. *A*, Radial component of P-wave receiver functions (PRFs) plotted against back azimuth. Individual PRFs have had the resonance-removal filter of Yu and others (2015) applied to them, are normalized to the maximum amplitude within the time window shown, binned, and normalized by the number of traces per bin. *B*, Average of every individual normalized radial receiver function with the application of the resonance-removal filter (blue) and average of every individual normalized raw radial receiver function (red). *C*, Radial component of raw PRFs, plotted against back azimuth, normalized as in *A*. Ps, 3p1s, and 2p2s arrival times predicted for the preferred Moho depth are shown, assuming a ray parameter of 0.06 s/km.

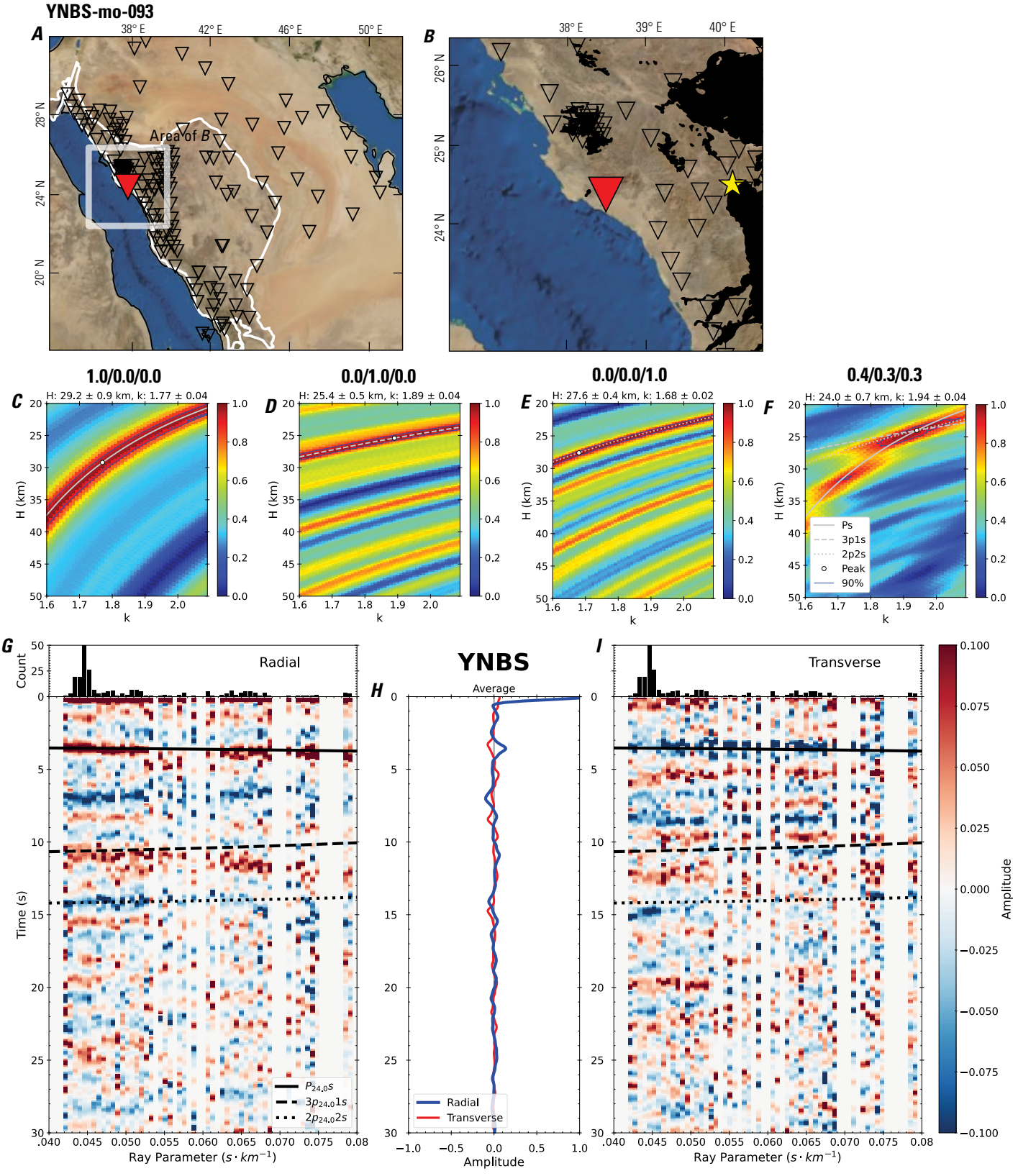
YNBS-mo-093
A
B
Area of B
1.0/0.0/0.0
0.0/1.0/0.0
0.0/0.0/1.0
0.4/0.3/0.3
C
D
E
F
H: 29.2 ± 0.9 km, k: 1.77 ± 0.04
H: 25.4 ± 0.5 km, k: 1.89 ± 0.04
H: 27.6 ± 0.4 km, k: 1.68 ± 0.02
H: 24.0 ± 0.7 km, k: 1.94 ± 0.04
H (km)
k
Ps
3p1s
2p2s
Peak
90%
G
H
I
YNBS
Radial
Transverse
Average
Count
Time (s)
Ray Parameter (s · km⁻¹)
Amplitude
$P_{24.0}s$
$3p_{24.0}1s$
$2p_{24.0}2s$

Figure 190 (page 196). Receiver-function analysis for station YNBS. *A*, Regional map of Saudi Arabia showing the entire array (as inverted triangles), the location of station YNBS (red inverted triangle), the shield-platform boundary (white line), and the bounds of the map in *B* (white box). *B*, Local map of station YNBS. Harrats are shown in black. *C*, Standard, single-layer *H-k* stack with stacking weights 0.4/0.3/0.3. This *H-k* stack ignores sedimentary effects on the receiver functions. *D*, Standard, single-layer *H-k* stack with stacking weights 0.5/0.5/0.0. This *H-k* stack also ignores sedimentary effects on the receiver functions. *E*, Optimized sub-sedimentary *H-k* stack with stacking weights 0.4/0.3/0.3, following the method of Yu and others (2015). *F*, Optimized sedimentary *H-k* stack with stacking weights 0.05/0.70/0.25, following the method of Yu and others (2015). *G*, Radial component P-wave receiver functions (PRFs) plotted against ray parameter. Individual PRFs have had the resonance-removal filter of Yu and others (2015) applied to them and are normalized to the maximum amplitude within the time window shown, binned, and normalized by the number of traces per bin. *H*, Average of every individual normalized radial receiver function with the application of the resonance-removal filter (blue) and average of every individual normalized raw radial receiver function (red). *I*, Radial component of raw PRFs (that is, PRFs with no resonance-removal filter applied) plotted against ray parameter, normalized as in *G*.

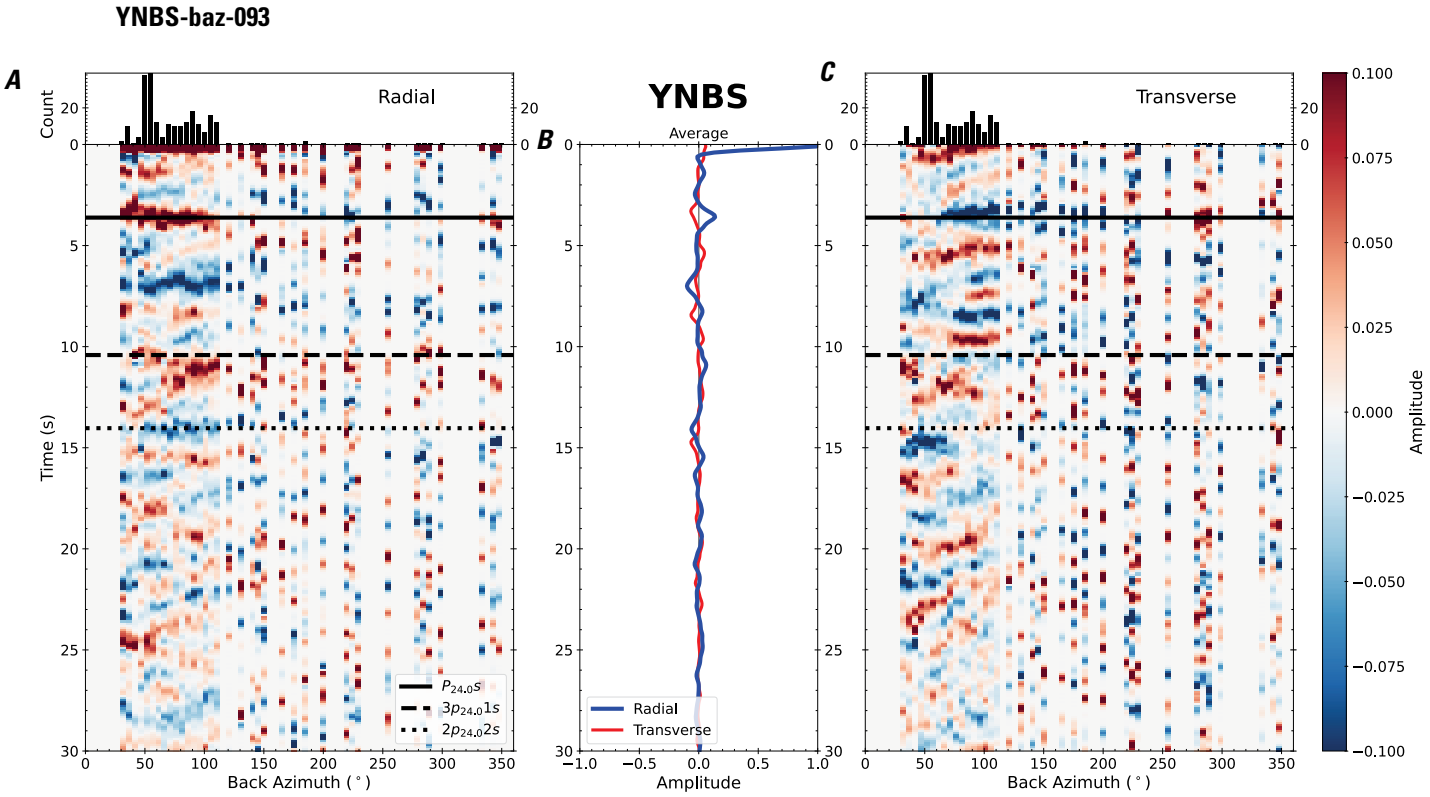

Figure 191. Receiver functions plotted against back azimuth for station YNBS. *A*, Radial component of P-wave receiver functions (PRFs) plotted against back azimuth. Individual PRFs have had the resonance-removal filter of Yu and others (2015) applied to them, are normalized to the maximum amplitude within the time window shown, binned, and normalized by the number of traces per bin. *B*, Average of every individual normalized radial receiver function with the application of the resonance-removal filter (blue) and average of every individual normalized raw radial receiver function (red). *C*, Radial component of raw PRFs, plotted against back azimuth, normalized as in *A*. Ps, 3p1s, and 2p2s arrival times predicted for the preferred Moho depth are shown, assuming a ray parameter of 0.06 s/km.

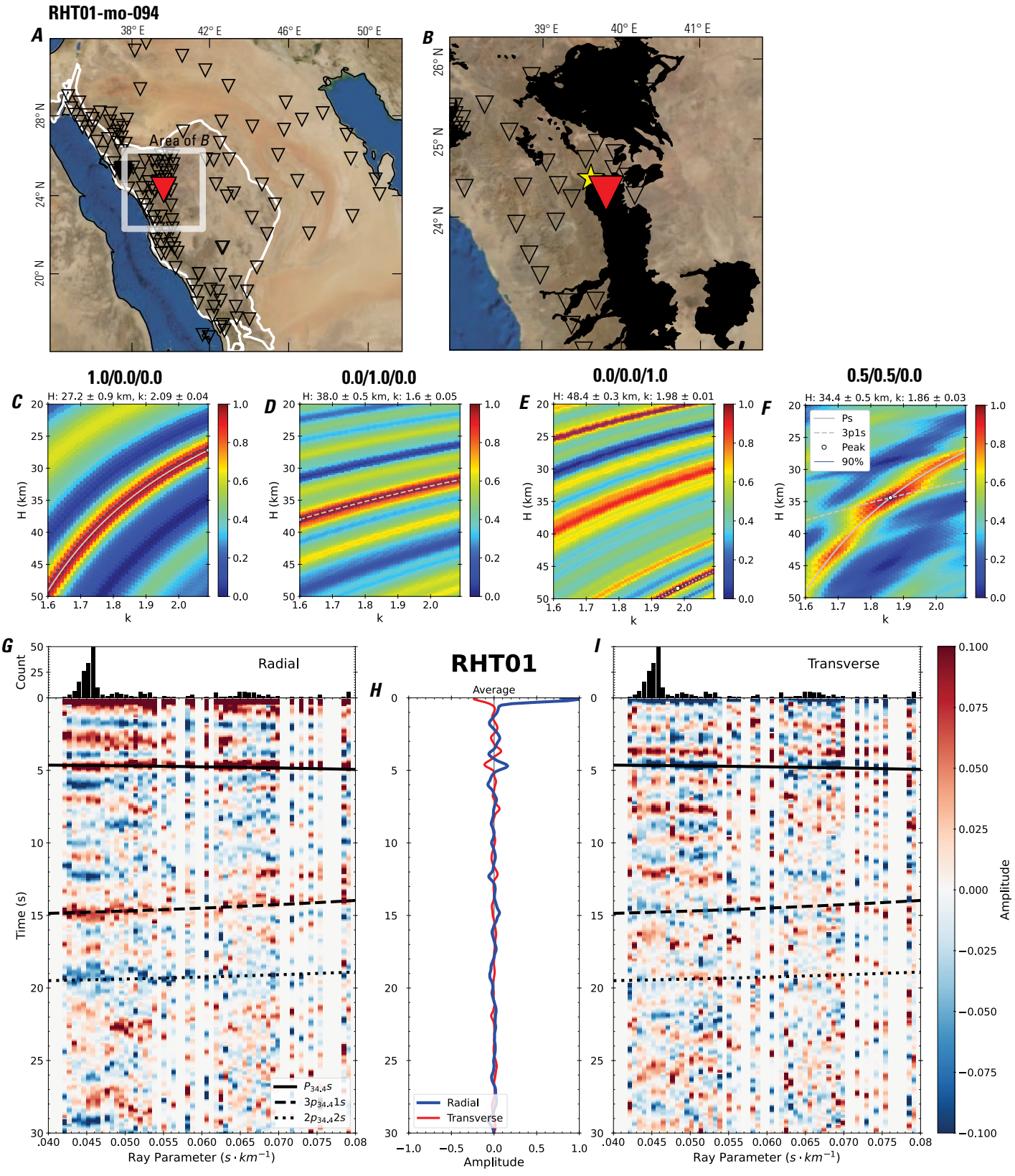
RHT01-mo-094
A
38° E
42° E
46° E
50° E
28° N
24° N
20° N
Area of B
B
39° E
40° E
41° E
26° N
25° N
24° N
1.0/0.0/0.0
0.0/1.0/0.0
0.0/0.0/1.0
0.5/0.5/0.0
C
H: 27.2 ± 0.9 km, k: 2.09 ± 0.04
D
H: 38.0 ± 0.5 km, k: 1.6 ± 0.05
E
H: 48.4 ± 0.3 km, k: 1.98 ± 0.01
F
H: 34.4 ± 0.5 km, k: 1.86 ± 0.03
Ps
3p1s
Peak
90%
H (km)
k
G
Radial
Count
Time (s)
$P_{34.4}s$
$3p_{34.4}1s$
$2p_{34.4}2s$
Ray Parameter ($s \cdot km^{-1}$)
H
RHT01
Average
Radial
Transverse
Amplitude
I
Transverse
Amplitude

Figure 192 (page 198). Receiver-function analysis for station RHT01. *A*, Regional map of Saudi Arabia showing the entire array (as inverted triangles), the location of station RHT01 (red inverted triangle), the shield-platform boundary (white line), and the bounds of the map in *B* (white box). *B*, Local map of station RHT01. Harrats are shown in black. *C*, Standard, single-layer *H-k* stack with stacking weights 0.4/0.3/0.3. This *H-k* stack ignores sedimentary effects on the receiver functions. *D*, Standard, single-layer *H-k* stack with stacking weights 0.5/0.5/0.0. This *H-k* stack also ignores sedimentary effects on the receiver functions. *E*, Optimized sub-sedimentary *H-k* stack with stacking weights 0.4/0.3/0.3, following the method of Yu and others (2015). *F*, Optimized sedimentary *H-k* stack with stacking weights 0.05/0.70/0.25, following the method of Yu and others (2015). *G*, Radial component P-wave receiver functions (PRFs) plotted against ray parameter. Individual PRFs have had the resonance-removal filter of Yu and others (2015) applied to them and are normalized to the maximum amplitude within the time window shown, binned, and normalized by the number of traces per bin. *H*, Average of every individual normalized radial receiver function with the application of the resonance-removal filter (blue) and average of every individual normalized raw radial receiver function (red). *I*, Radial component of raw PRFs (that is, PRFs with no resonance-removal filter applied) plotted against ray parameter, normalized as in *G*.

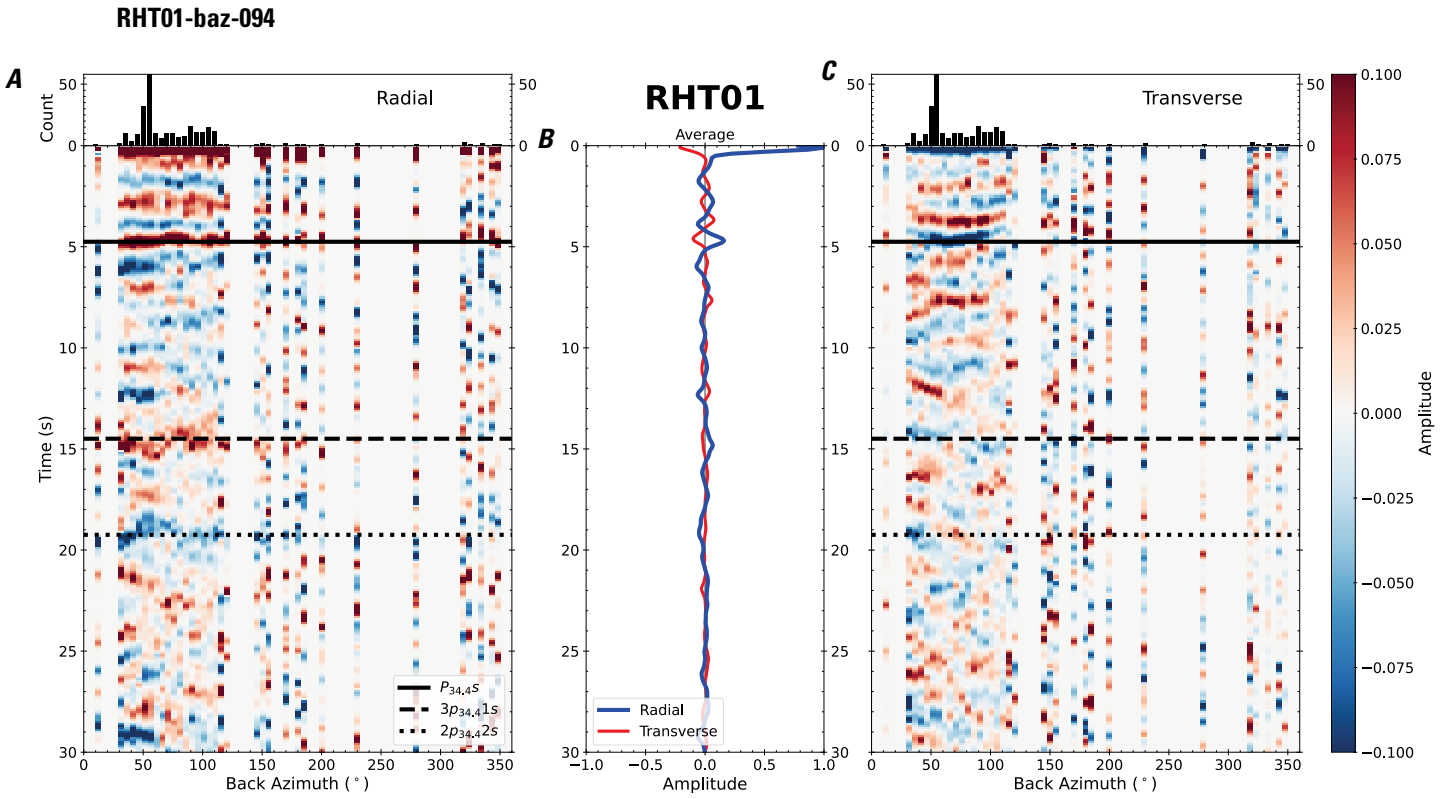

Figure 193. Receiver functions plotted against back azimuth for station RHT01. *A*, Radial component of P-wave receiver functions (PRFs) plotted against back azimuth. Individual PRFs have had the resonance-removal filter of Yu and others (2015) applied to them, are normalized to the maximum amplitude within the time window shown, binned, and normalized by the number of traces per bin. *B*, Average of every individual normalized radial receiver function with the application of the resonance-removal filter (blue) and average of every individual normalized raw radial receiver function (red). *C*, Radial component of raw PRFs, plotted against back azimuth, normalized as in *A*. Ps, 3p1s, and 2p2s arrival times predicted for the preferred Moho depth are shown, assuming a ray parameter of 0.06 s/km.

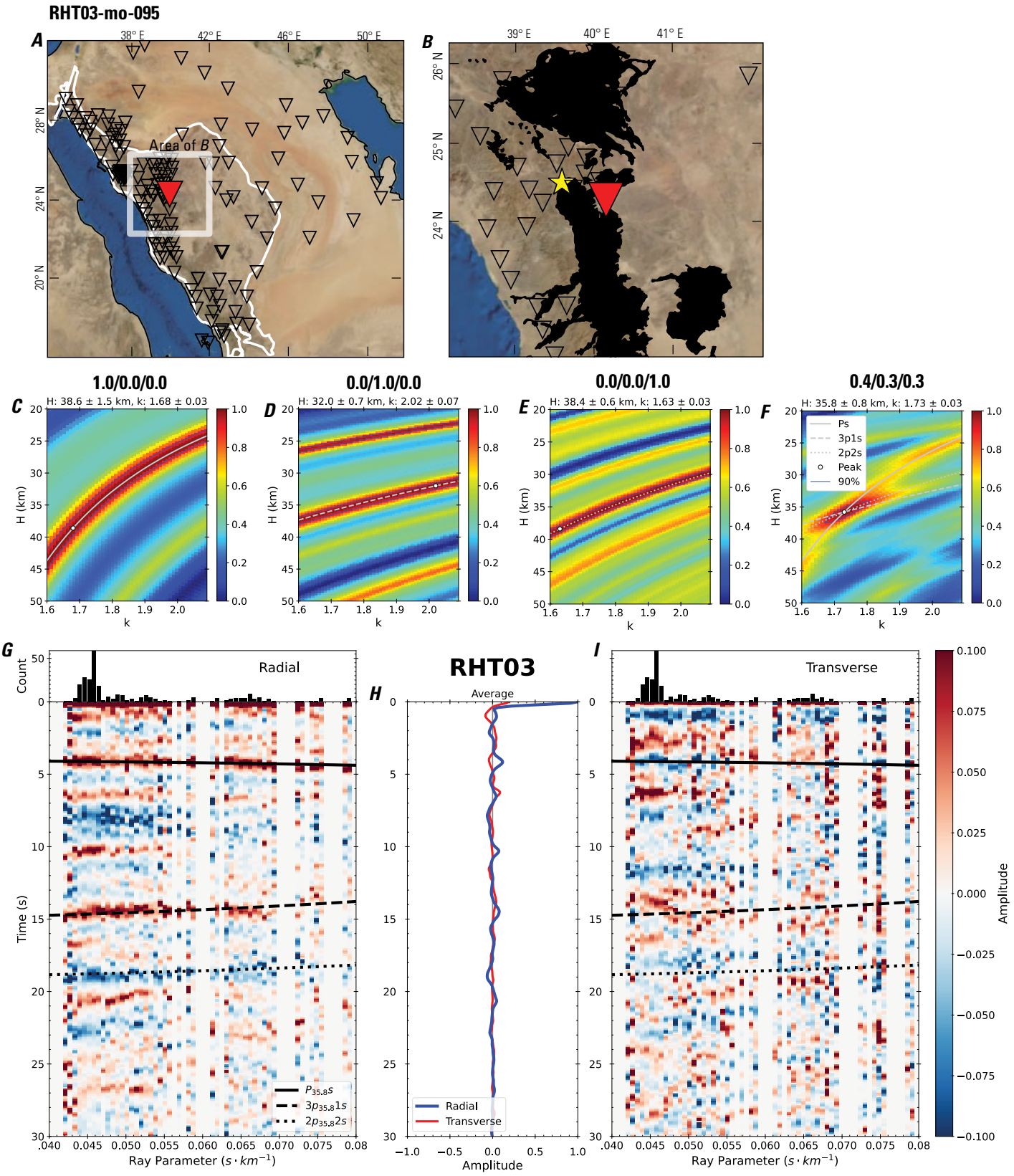
RHT03-mo-095
A
38° E
42° E
46° E
50° E
28° N
24° N
20° N
Area of B
B
39° E
40° E
41° E
26° N
25° N
24° N
1.0/0.0/0.0
0.0/1.0/0.0
0.0/0.0/1.0
0.4/0.3/0.3
C
H: 38.6 ± 1.5 km, k: 1.68 ± 0.03
D
H: 32.0 ± 0.7 km, k: 2.02 ± 0.07
E
H: 38.4 ± 0.6 km, k: 1.63 ± 0.03
F
H: 35.8 ± 0.8 km, k: 1.73 ± 0.03
Ps
3p1s
2p2s
Peak
90%
H (km)
k
G
Radial
Count
Time (s)
$P_{35.8}s$
$3p_{35.8}1s$
$2p_{35.8}2s$
Ray Parameter ($s \cdot km^{-1}$)
H
RHT03
Average
Radial
Transverse
Amplitude
I
Transverse
Amplitude

Figure 194 (page 200). Receiver-function analysis for station RHT03. *A*, Regional map of Saudi Arabia showing the entire array (as inverted triangles), the location of station RHT03 (red inverted triangle), the shield-platform boundary (white line), and the bounds of the map in *B* (white box). *B*, Local map of station RHT03. Harrats are shown in black. *C*, Standard, single-layer *H-k* stack with stacking weights 0.4/0.3/0.3. This *H-k* stack ignores sedimentary effects on the receiver functions. *D*, Standard, single-layer *H-k* stack with stacking weights 0.5/0.5/0.0. This *H-k* stack also ignores sedimentary effects on the receiver functions. *E*, Optimized sub-sedimentary *H-k* stack with stacking weights 0.4/0.3/0.3, following the method of Yu and others (2015). *F*, Optimized sedimentary *H-k* stack with stacking weights 0.05/0.70/0.25, following the method of Yu and others (2015). *G*, Radial component P-wave receiver functions (PRFs) plotted against ray parameter. Individual PRFs have had the resonance-removal filter of Yu and others (2015) applied to them and are normalized to the maximum amplitude within the time window shown, binned, and normalized by the number of traces per bin. *H*, Average of every individual normalized radial receiver function with the application of the resonance-removal filter (blue) and average of every individual normalized raw radial receiver function (red). *I*, Radial component of raw PRFs (that is, PRFs with no resonance-removal filter applied) plotted against ray parameter, normalized as in *G*.

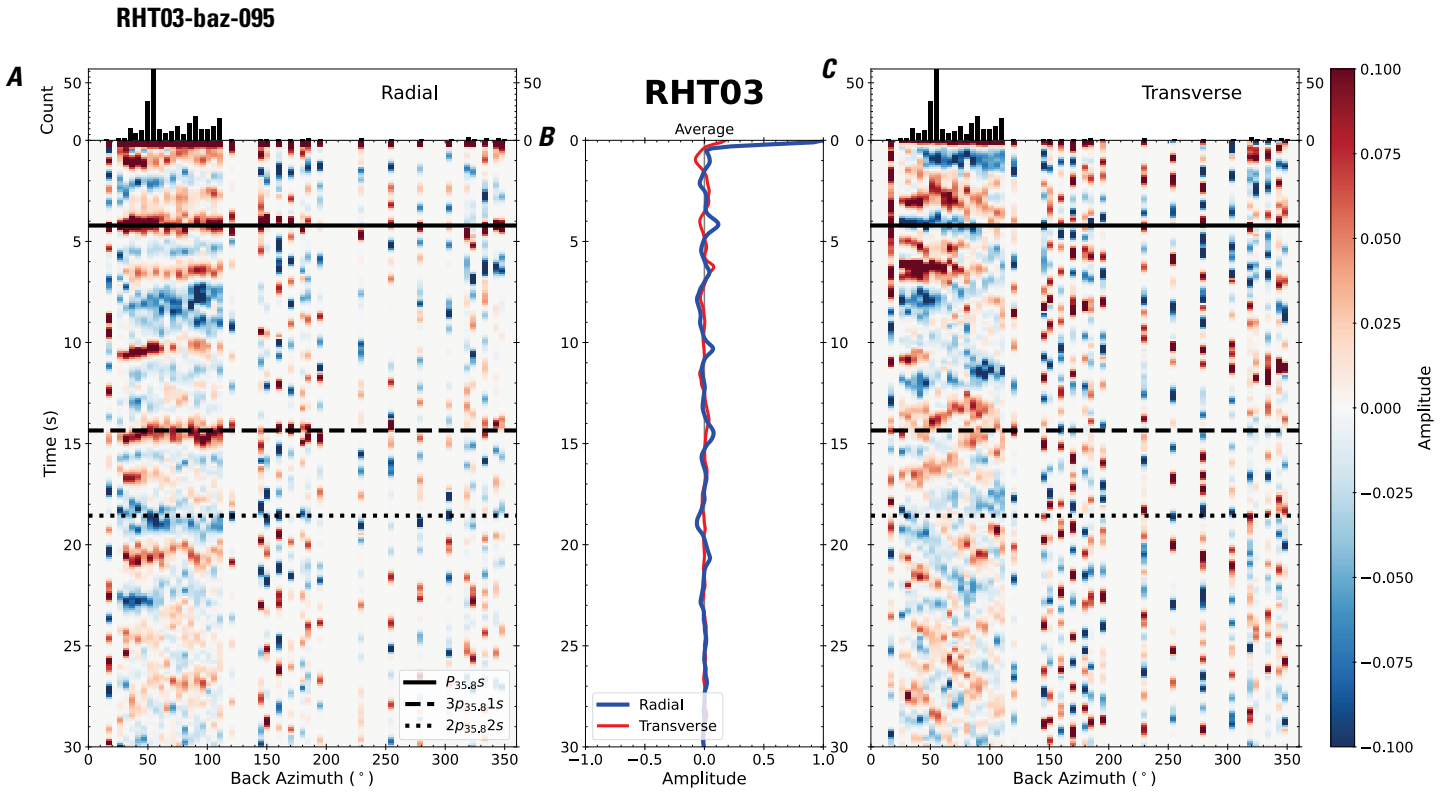

Figure 195. Receiver functions plotted against back azimuth for station RHT03. *A*, Radial component of P-wave receiver functions (PRFs) plotted against back azimuth. Individual PRFs have had the resonance-removal filter of Yu and others (2015) applied to them, are normalized to the maximum amplitude within the time window shown, binned, and normalized by the number of traces per bin. *B*, Average of every individual normalized radial receiver function with the application of the resonance-removal filter (blue) and average of every individual normalized raw radial receiver function (red). *C*, Radial component of raw PRFs, plotted against back azimuth, normalized as in *A*. Ps, 3p1s, and 2p2s arrival times predicted for the preferred Moho depth are shown, assuming a ray parameter of 0.06 s/km.

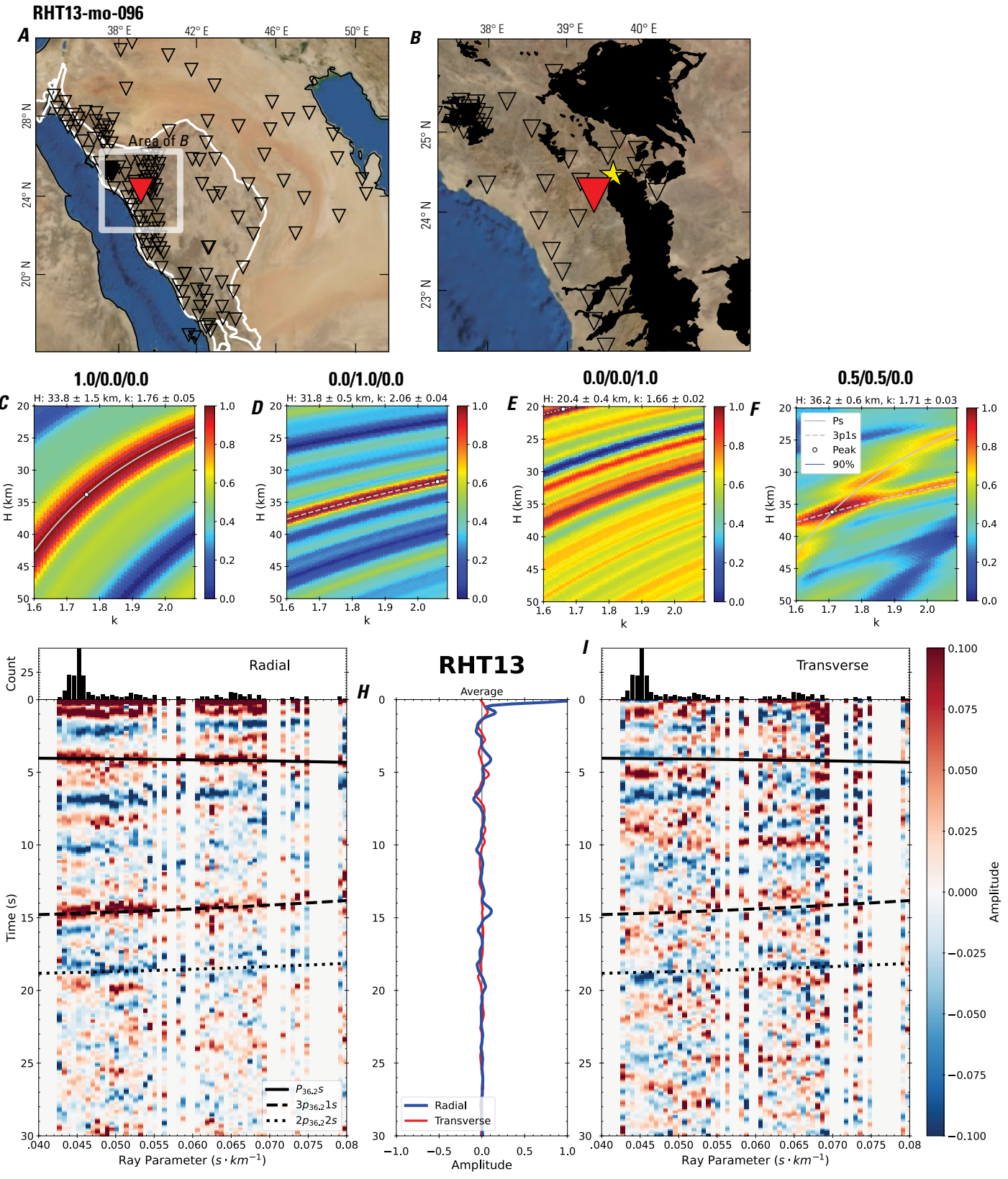
RHT13-mo-096
A
38° E
42° E
46° E
50° E
28° N
24° N
20° N
Area of B
B
38° E
39° E
40° E
25° N
24° N
23° N
1.0/0.0/0.0
C
H: 33.8 ± 1.5 km, k: 1.76 ± 0.05
0.0/1.0/0.0
D
H: 31.8 ± 0.5 km, k: 2.06 ± 0.04
0.0/0.0/1.0
E
H: 20.4 ± 0.4 km, k: 1.66 ± 0.02
0.5/0.5/0.0
F
H: 36.2 ± 0.6 km, k: 1.71 ± 0.03
Ps
3p1s
Peak
90%
H (km)
k
G
Radial
Count
Time (s)
$P_{36.2}s$
$3p_{36.2}1s$
$2p_{36.2}2s$
Ray Parameter ($s \cdot km^{-1}$)
RHT13
H
Average
Radial
Transverse
Amplitude
I
Transverse
Ray Parameter ($s \cdot km^{-1}$)
Amplitude

Figure 196 (page 202). Receiver-function analysis for station RHT13. *A*, Regional map of Saudi Arabia showing the entire array (as inverted triangles), the location of station RHT13 (red inverted triangle), the shield-platform boundary (white line), and the bounds of the map in *B* (white box). *B*, Local map of station RHT13. Harrats are shown in black. *C*, Standard, single-layer *H-k* stack with stacking weights 0.4/0.3/0.3. This *H-k* stack ignores sedimentary effects on the receiver functions. *D*, Standard, single-layer *H-k* stack with stacking weights 0.5/0.5/0.0. This *H-k* stack also ignores sedimentary effects on the receiver functions. *E*, Optimized sub-sedimentary *H-k* stack with stacking weights 0.4/0.3/0.3, following the method of Yu and others (2015). *F*, Optimized sedimentary *H-k* stack with stacking weights 0.05/0.70/0.25, following the method of Yu and others (2015). *G*, Radial component P-wave receiver functions (PRFs) plotted against ray parameter. Individual PRFs have had the resonance-removal filter of Yu and others (2015) applied to them and are normalized to the maximum amplitude within the time window shown, binned, and normalized by the number of traces per bin. *H*, Average of every individual normalized radial receiver function with the application of the resonance-removal filter (blue) and average of every individual normalized raw radial receiver function (red). *I*, Radial component of raw PRFs (that is, PRFs with no resonance-removal filter applied) plotted against ray parameter, normalized as in *G*.

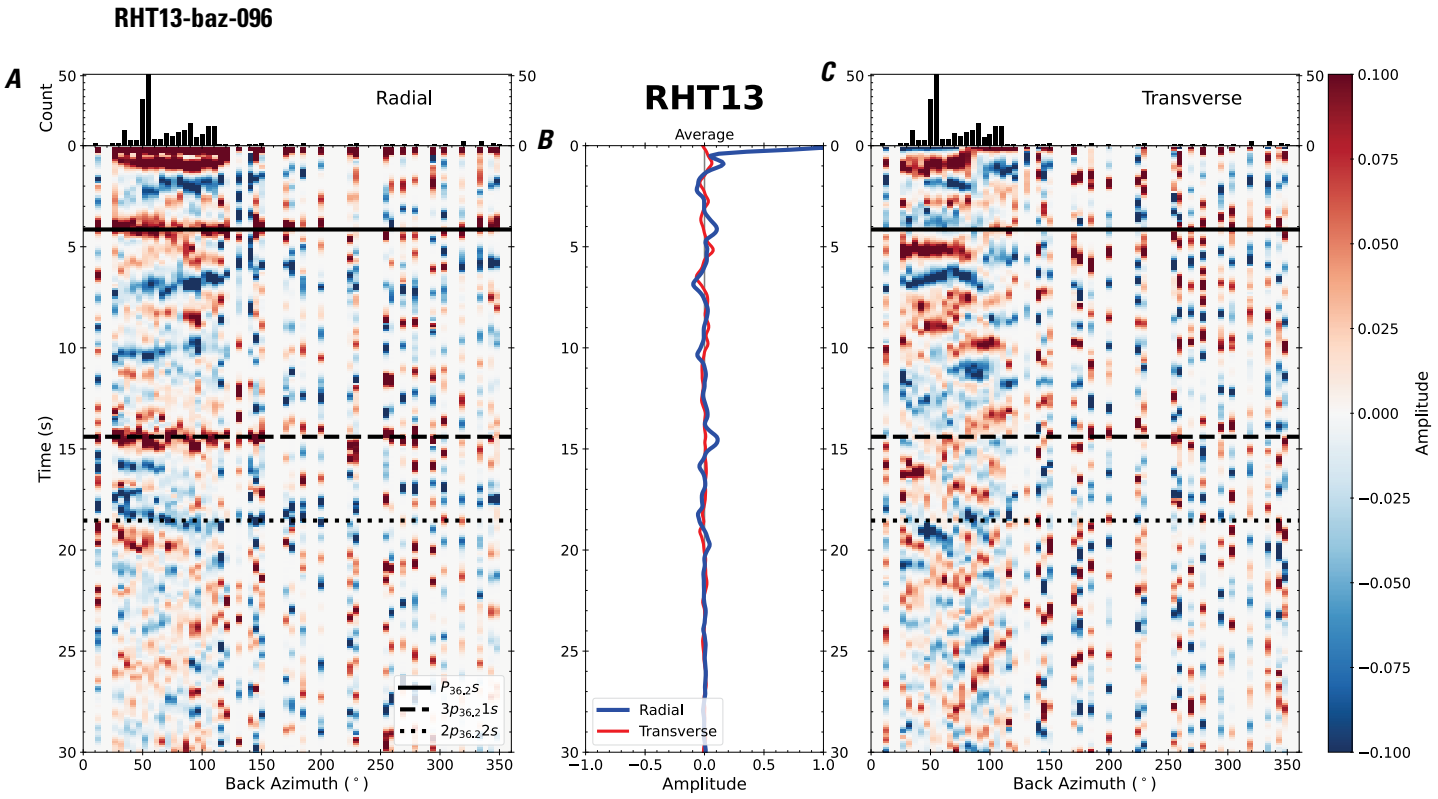

Figure 197. Receiver functions plotted against back azimuth for station RHT13. *A*, Radial component of P-wave receiver functions (PRFs) plotted against back azimuth. Individual PRFs have had the resonance-removal filter of Yu and others (2015) applied to them, are normalized to the maximum amplitude within the time window shown, binned, and normalized by the number of traces per bin. *B*, Average of every individual normalized radial receiver function with the application of the resonance-removal filter (blue) and average of every individual normalized raw radial receiver function (red). *C*, Radial component of raw PRFs, plotted against back azimuth, normalized as in *A*. Ps, 3p1s, and 2p2s arrival times predicted for the preferred Moho depth are shown, assuming a ray parameter of 0.06 s/km.

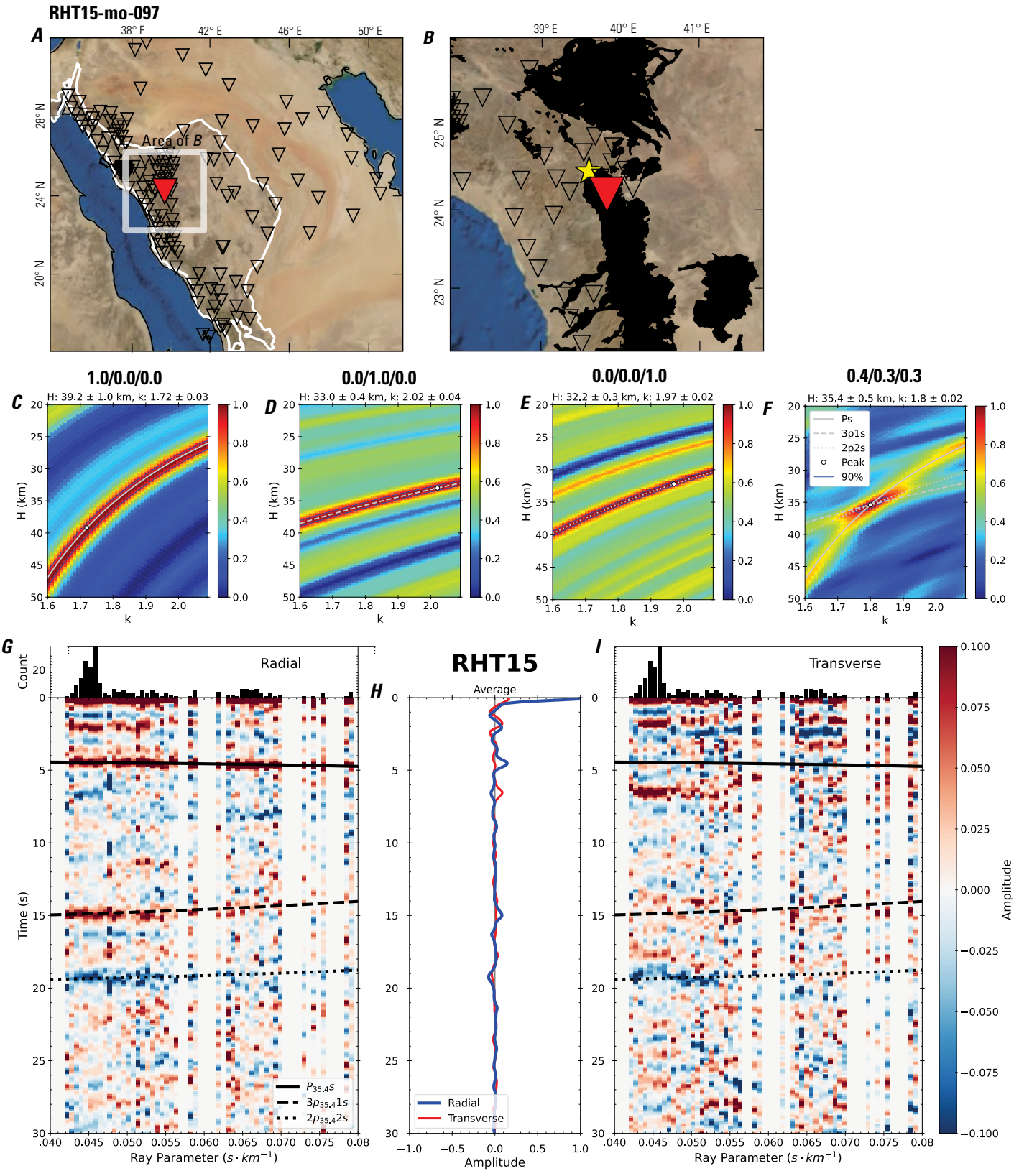
RHT15-mo-097
A
B
Area of B
1.0/0.0/0.0
0.0/1.0/0.0
0.0/0.0/1.0
0.4/0.3/0.3
C
D
E
F
H: 39.2 ± 1.0 km, k: 1.72 ± 0.03
H: 33.0 ± 0.4 km, k: 2.02 ± 0.04
H: 32.2 ± 0.3 km, k: 1.97 ± 0.02
H: 35.4 ± 0.5 km, k: 1.8 ± 0.02
H (km)
k
Ps
3p1s
2p2s
Peak
90%
G
H
I
RHT15
Radial
Transverse
Average
Count
Time (s)
Ray Parameter (s · km⁻¹)
Amplitude
P35.4s
3p35.41s
2p35.42s

Figure 198 (page 204). Receiver-function analysis for station RHT15. *A*, Regional map of Saudi Arabia showing the entire array (as inverted triangles), the location of station RHT15 (red inverted triangle), the shield-platform boundary (white line), and the bounds of the map in *B* (white box). *B*, Local map of station RHT15. Harrats are shown in black. *C*, Standard, single-layer *H-k* stack with stacking weights 0.4/0.3/0.3. This *H-k* stack ignores sedimentary effects on the receiver functions. *D*, Standard, single-layer *H-k* stack with stacking weights 0.5/0.5/0.0. This *H-k* stack also ignores sedimentary effects on the receiver functions. *E*, Optimized sub-sedimentary *H-k* stack with stacking weights 0.4/0.3/0.3, following the method of Yu and others (2015). *F*, Optimized sedimentary *H-k* stack with stacking weights 0.05/0.70/0.25, following the method of Yu and others (2015). *G*, Radial component P-wave receiver functions (PRFs) plotted against ray parameter. Individual PRFs have had the resonance-removal filter of Yu and others (2015) applied to them and are normalized to the maximum amplitude within the time window shown, binned, and normalized by the number of traces per bin. *H*, Average of every individual normalized radial receiver function with the application of the resonance-removal filter (blue) and average of every individual normalized raw radial receiver function (red). *I*, Radial component of raw PRFs (that is, PRFs with no resonance-removal filter applied) plotted against ray parameter, normalized as in *G*.

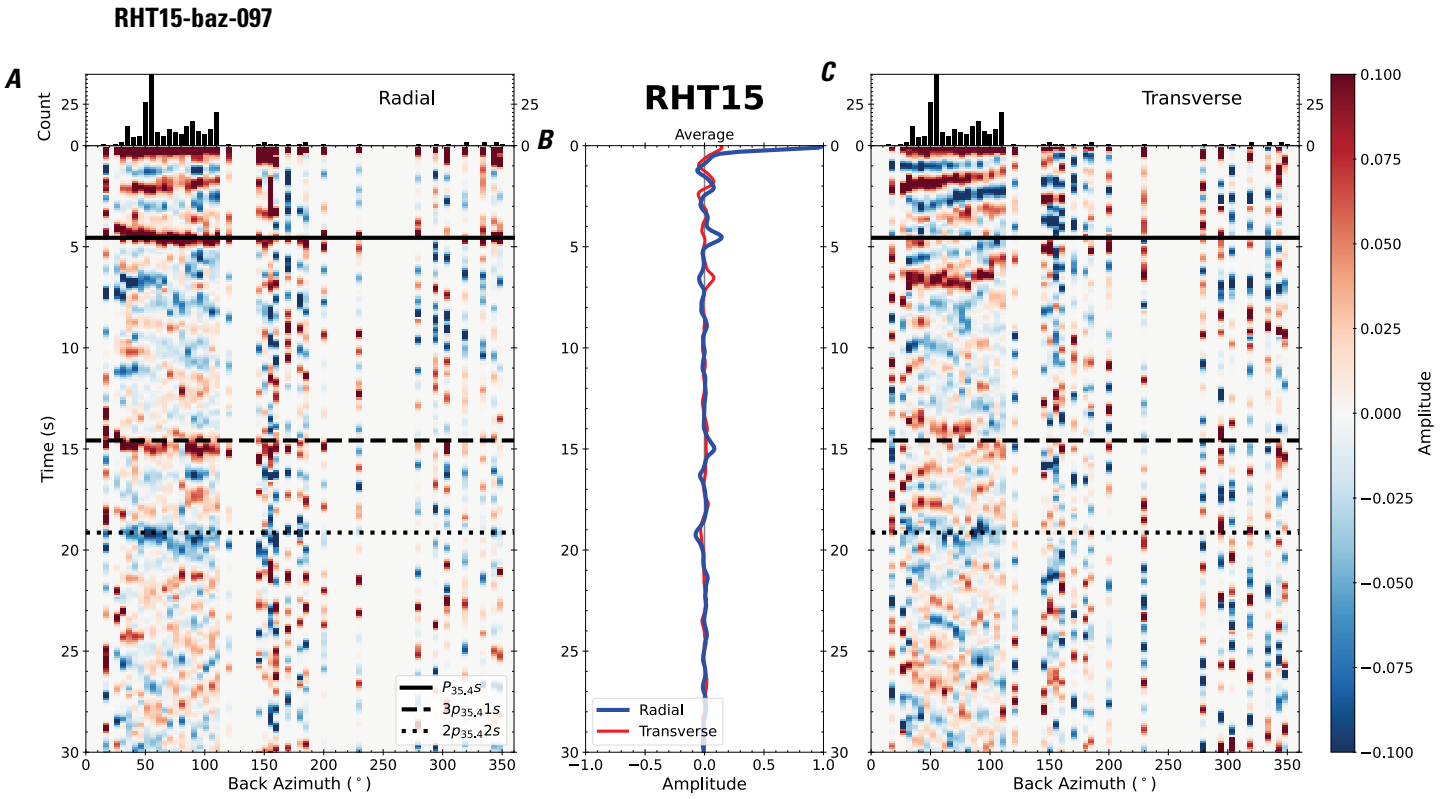

Figure 199. Receiver functions plotted against back azimuth for station RHT15. *A*, Radial component of P-wave receiver functions (PRFs) plotted against back azimuth. Individual PRFs have had the resonance-removal filter of Yu and others (2015) applied to them, are normalized to the maximum amplitude within the time window shown, binned, and normalized by the number of traces per bin. *B*, Average of every individual normalized radial receiver function with the application of the resonance-removal filter (blue) and average of every individual normalized raw radial receiver function (red). *C*, Radial component of raw PRFs, plotted against back azimuth, normalized as in *A*. Ps, 3p1s, and 2p2s arrival times predicted for the preferred Moho depth are shown, assuming a ray parameter of 0.06 s/km.

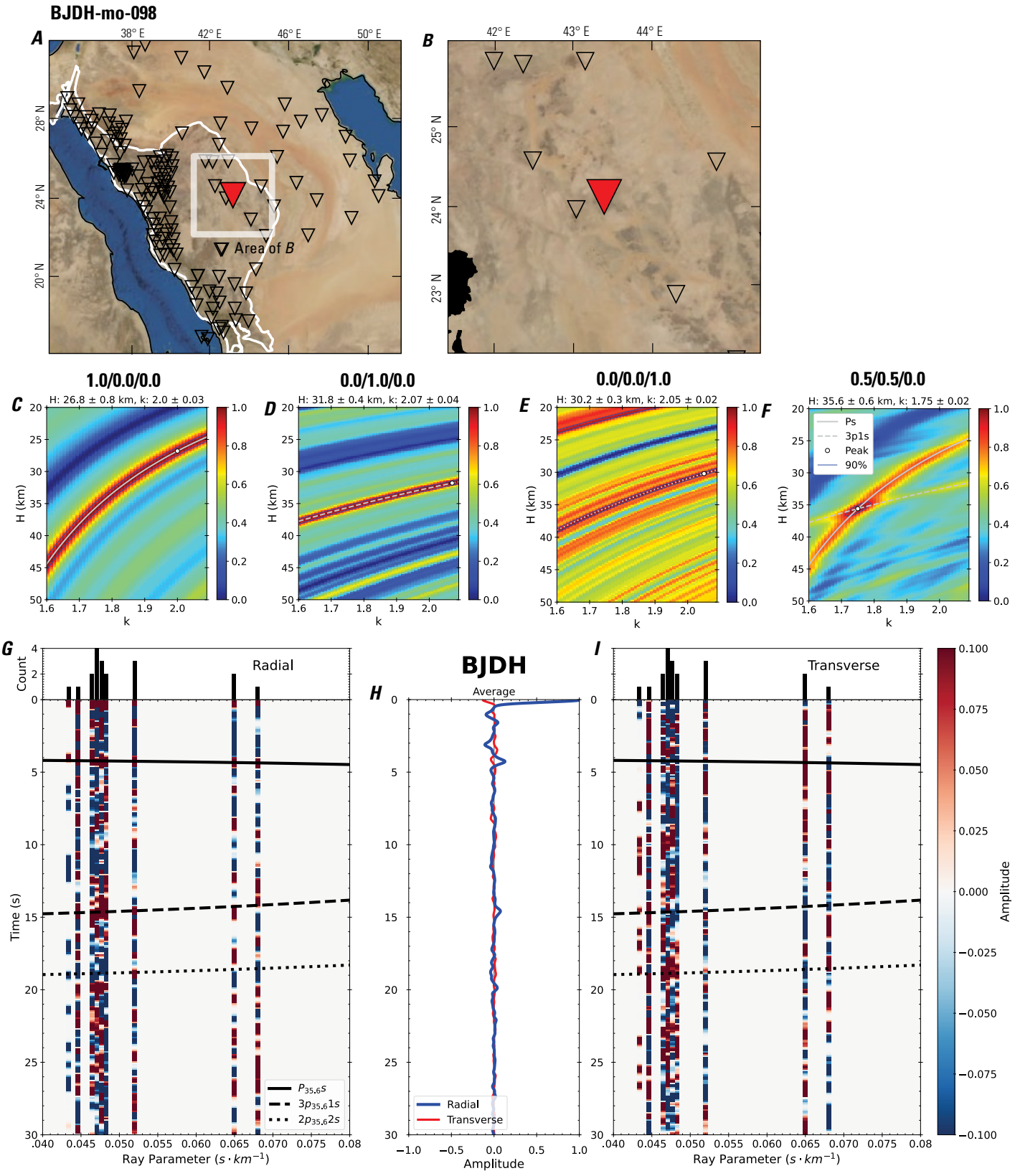
BJDH-mo-098
A
38° E
42° E
46° E
50° E
28° N
24° N
20° N
Area of B
B
42° E
43° E
44° E
25° N
24° N
23° N
1.0/0.0/0.0
0.0/1.0/0.0
0.0/0.0/1.0
0.5/0.5/0.0
C
H: 26.8 ± 0.8 km, k: 2.0 ± 0.03
D
H: 31.8 ± 0.4 km, k: 2.07 ± 0.04
E
H: 30.2 ± 0.3 km, k: 2.05 ± 0.02
F
H: 35.6 ± 0.6 km, k: 1.75 ± 0.02
Ps
3p1s
Peak
90%
H (km)
k
G
Radial
Count
Time (s)
$P_{35.6}s$
$3p_{35.6}1s$
$2p_{35.6}2s$
Ray Parameter ($s \cdot km^{-1}$)
BJDH
H
Average
Radial
Transverse
Amplitude
I
Transverse
Amplitude

Figure 200 (page 206). Receiver-function analysis for station BJDH. *A*, Regional map of Saudi Arabia showing the entire array (as inverted triangles), the location of station BJDH (red inverted triangle), the shield-platform boundary (white line), and the bounds of the map in *B* (white box). *B*, Local map of station BJDH. Harrats are shown in black. *C*, Standard, single-layer *H-k* stack with stacking weights 0.4/0.3/0.3. This *H-k* stack ignores sedimentary effects on the receiver functions. *D*, Standard, single-layer *H-k* stack with stacking weights 0.5/0.5/0.0. This *H-k* stack also ignores sedimentary effects on the receiver functions. *E*, Optimized sub-sedimentary *H-k* stack with stacking weights 0.4/0.3/0.3, following the method of Yu and others (2015). *F*, Optimized sedimentary *H-k* stack with stacking weights 0.05/0.70/0.25, following the method of Yu and others (2015). *G*, Radial component P-wave receiver functions (PRFs) plotted against ray parameter. Individual PRFs have had the resonance-removal filter of Yu and others (2015) applied to them and are normalized to the maximum amplitude within the time window shown, binned, and normalized by the number of traces per bin. *H*, Average of every individual normalized radial receiver function with the application of the resonance-removal filter (blue) and average of every individual normalized raw radial receiver function (red). *I*, Radial component of raw PRFs (that is, PRFs with no resonance-removal filter applied) plotted against ray parameter, normalized as in *G*.

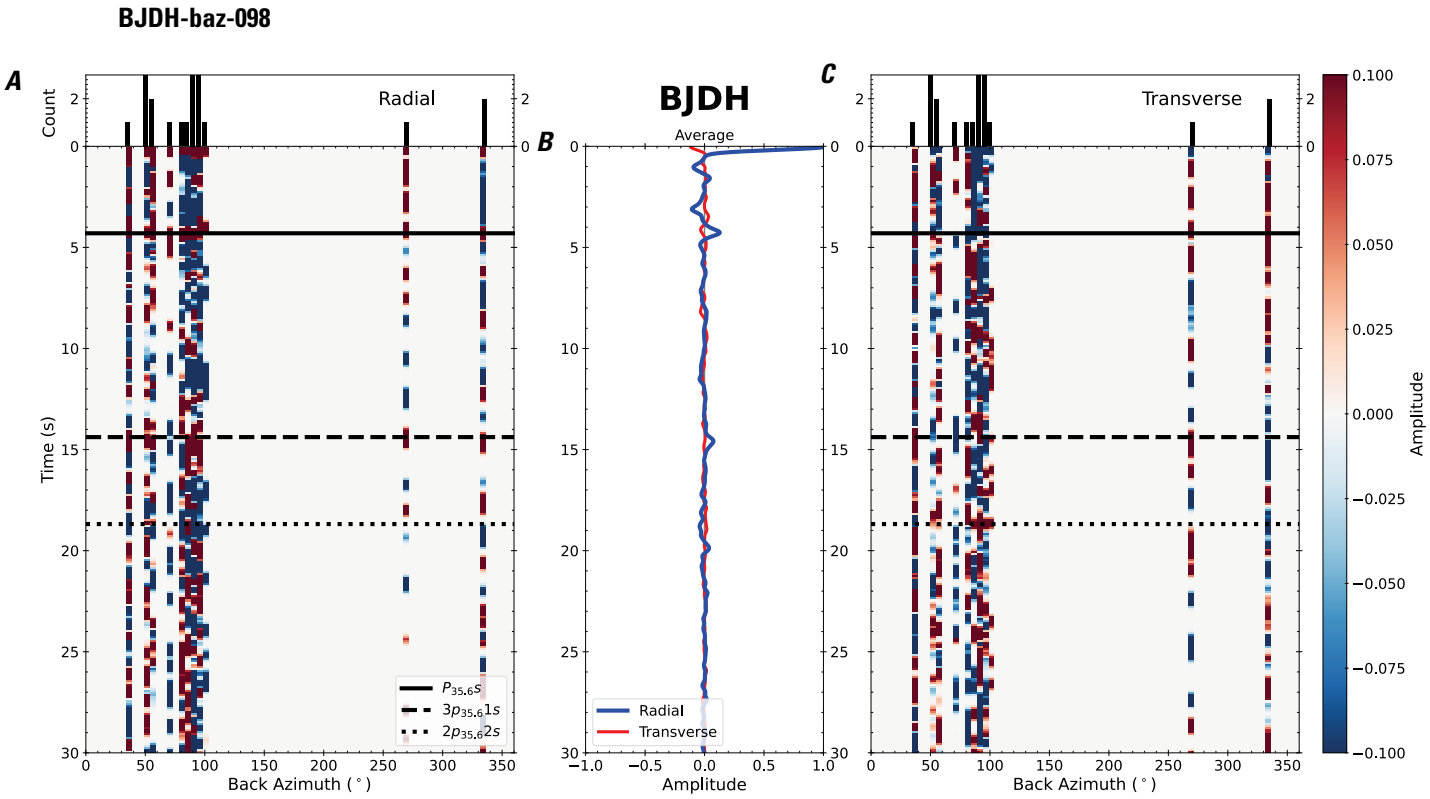

Figure 201. Receiver functions plotted against back azimuth for station BJDH. *A*, Radial component of P-wave receiver functions (PRFs) plotted against back azimuth. Individual PRFs have had the resonance-removal filter of Yu and others (2015) applied to them, are normalized to the maximum amplitude within the time window shown, binned, and normalized by the number of traces per bin. *B*, Average of every individual normalized radial receiver function with the application of the resonance-removal filter (blue) and average of every individual normalized raw radial receiver function (red). *C*, Radial component of raw PRFs, plotted against back azimuth, normalized as in *A*. Ps, 3p1s, and 2p2s arrival times predicted for the preferred Moho depth are shown, assuming a ray parameter of 0.06 s/km.

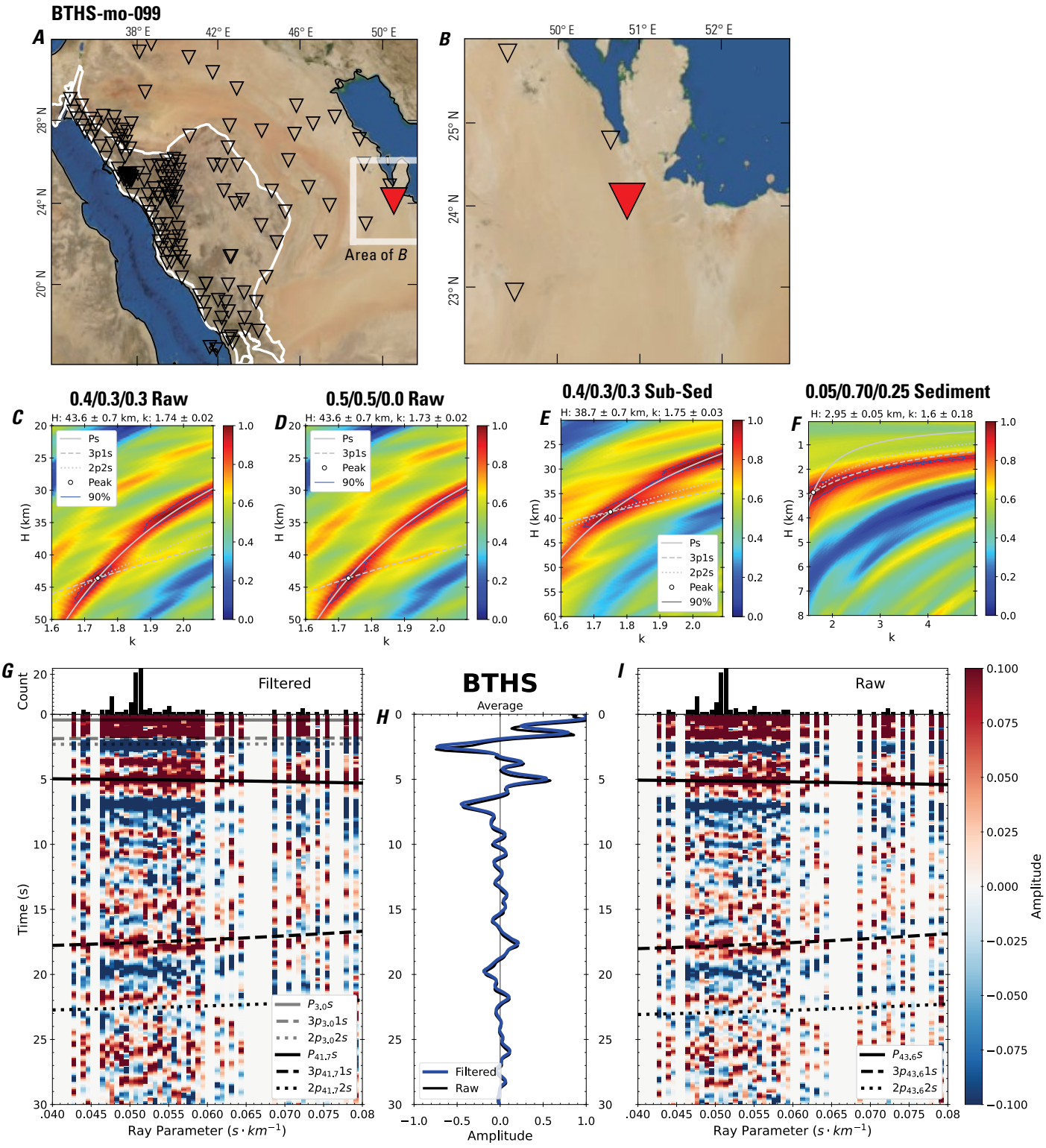
BTHS-mo-099
A
38° E
42° E
46° E
50° E
28° N
24° N
20° N
Area of B
B
50° E
51° E
52° E
25° N
24° N
23° N
0.4/0.3/0.3 Raw
C
H: 43.6 ± 0.7 km, k: 1.74 ± 0.02
0.5/0.5/0.0 Raw
D
H: 43.6 ± 0.7 km, k: 1.73 ± 0.02
0.4/0.3/0.3 Sub-Sed
E
H: 38.7 ± 0.7 km, k: 1.75 ± 0.03
0.05/0.70/0.25 Sediment
F
H: 2.95 ± 0.05 km, k: 1.6 ± 0.18
Ps
3p1s
2p2s
Peak
90%
H (km)
k
G
Filtered
Count
Time (s)
$P_{3.0}s$
$3p_{3.0}1s$
$2p_{3.0}2s$
$P_{41.7}s$
$3p_{41.7}1s$
$2p_{41.7}2s$
Ray Parameter ($s \cdot km^{-1}$)
BTHS
H
Average
Filtered
Raw
Amplitude
I
Raw
$P_{43.6}s$
$3p_{43.6}1s$
$2p_{43.6}2s$
Amplitude

Figure 202 (page 208). Receiver-function analysis for station BTHS. *A*, Regional map of Saudi Arabia showing the entire array (as inverted triangles), the location of station BTHS (red inverted triangle), the shield-platform boundary (white line), and the bounds of the map in *B* (white box). *B*, Local map of station BTHS. Harrats are shown in black. *C*, Standard, single-layer *H-k* stack with stacking weights 0.4/0.3/0.3. This *H-k* stack ignores sedimentary effects on the receiver functions. *D*, Standard, single-layer *H-k* stack with stacking weights 0.5/0.5/0.0. This *H-k* stack also ignores sedimentary effects on the receiver functions. *E*, Optimized sub-sedimentary *H-k* stack with stacking weights 0.4/0.3/0.3, following the method of Yu and others (2015). *F*, Optimized sedimentary *H-k* stack with stacking weights 0.05/0.70/0.25, following the method of Yu and others (2015). *G*, Radial component P-wave receiver functions (PRFs) plotted against ray parameter. Individual PRFs have had the resonance-removal filter of Yu and others (2015) applied to them and are normalized to the maximum amplitude within the time window shown, binned, and normalized by the number of traces per bin. *H*, Average of every individual normalized radial receiver function with the application of the resonance-removal filter (blue) and average of every individual normalized raw radial receiver function (red). *I*, Radial component of raw PRFs (that is, PRFs with no resonance-removal filter applied) plotted against ray parameter, normalized as in *G*.

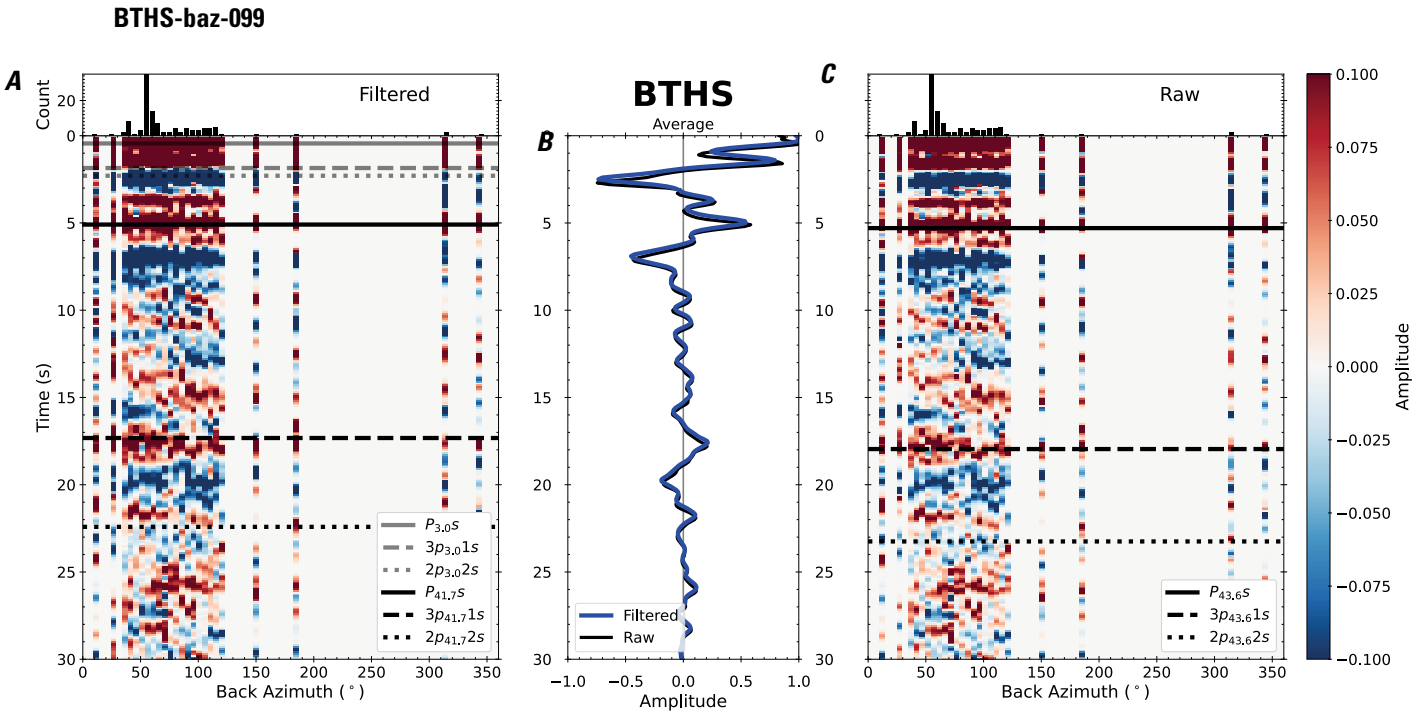

Figure 203. Receiver functions plotted against back azimuth for station BTHS. *A*, Radial component of P-wave receiver functions (PRFs) plotted against back azimuth. Individual PRFs have had the resonance-removal filter of Yu and others (2015) applied to them, are normalized to the maximum amplitude within the time window shown, binned, and normalized by the number of traces per bin. *B*, Average of every individual normalized radial receiver function with the application of the resonance-removal filter (blue) and average of every individual normalized raw radial receiver function (red). *C*, Radial component of raw PRFs, plotted against back azimuth, normalized as in *A*. Ps, 3p1s, and 2p2s arrival times predicted for the preferred Moho depth are shown, assuming a ray parameter of 0.06 s/km.

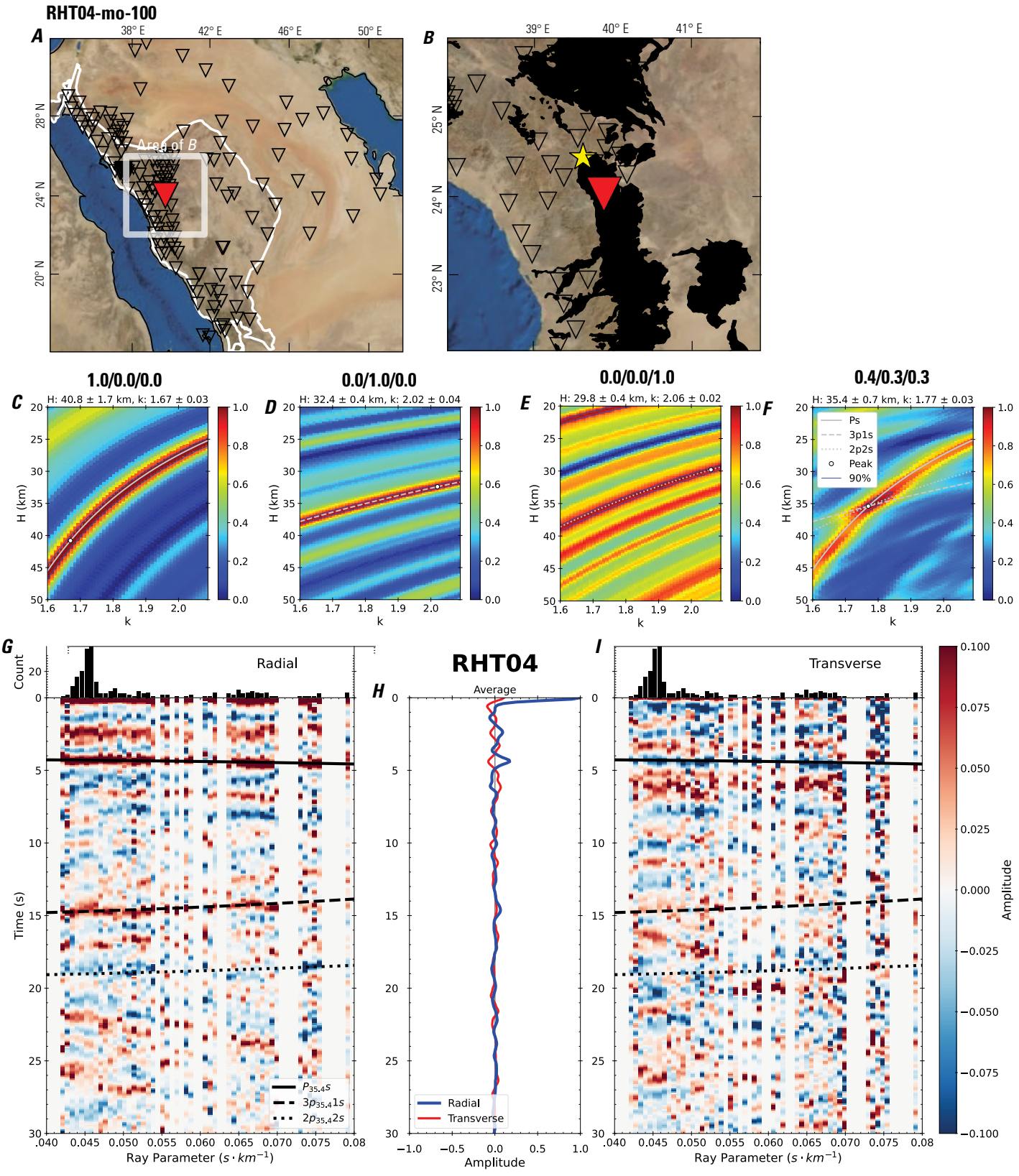
RHT04-mo-100
A
38° E
42° E
46° E
50° E
28° N
24° N
20° N
Area of B
B
39° E
40° E
41° E
25° N
24° N
23° N
1.0/0.0/0.0
0.0/1.0/0.0
0.0/0.0/1.0
0.4/0.3/0.3
C
H: 40.8 ± 1.7 km, k: 1.67 ± 0.03
D
H: 32.4 ± 0.4 km, k: 2.02 ± 0.04
E
H: 29.8 ± 0.4 km, k: 2.06 ± 0.02
F
H: 35.4 ± 0.7 km, k: 1.77 ± 0.03
Ps
3p1s
2p2s
Peak
90%
H (km)
k
G
Radial
Count
Time (s)
$P_{35.4}s$
$3p_{35.4}1s$
$2p_{35.4}2s$
Ray Parameter ($s \cdot km^{-1}$)
RHT04
H
Average
Radial
Transverse
Amplitude
I
Transverse
Amplitude

Figure 204 (page 210). Receiver-function analysis for station RHT04. *A*, Regional map of Saudi Arabia showing the entire array (as inverted triangles), the location of station RHT04 (red inverted triangle), the shield-platform boundary (white line), and the bounds of the map in *B* (white box). *B*, Local map of station RHT04. Harrats are shown in black. *C*, Standard, single-layer *H-k* stack with stacking weights 0.4/0.3/0.3. This *H-k* stack ignores sedimentary effects on the receiver functions. *D*, Standard, single-layer *H-k* stack with stacking weights 0.5/0.5/0.0. This *H-k* stack also ignores sedimentary effects on the receiver functions. *E*, Optimized sub-sedimentary *H-k* stack with stacking weights 0.4/0.3/0.3, following the method of Yu and others (2015). *F*, Optimized sedimentary *H-k* stack with stacking weights 0.05/0.70/0.25, following the method of Yu and others (2015). *G*, Radial component P-wave receiver functions (PRFs) plotted against ray parameter. Individual PRFs have had the resonance-removal filter of Yu and others (2015) applied to them and are normalized to the maximum amplitude within the time window shown, binned, and normalized by the number of traces per bin. *H*, Average of every individual normalized radial receiver function with the application of the resonance-removal filter (blue) and average of every individual normalized raw radial receiver function (red). *I*, Radial component of raw PRFs (that is, PRFs with no resonance-removal filter applied) plotted against ray parameter, normalized as in *G*.

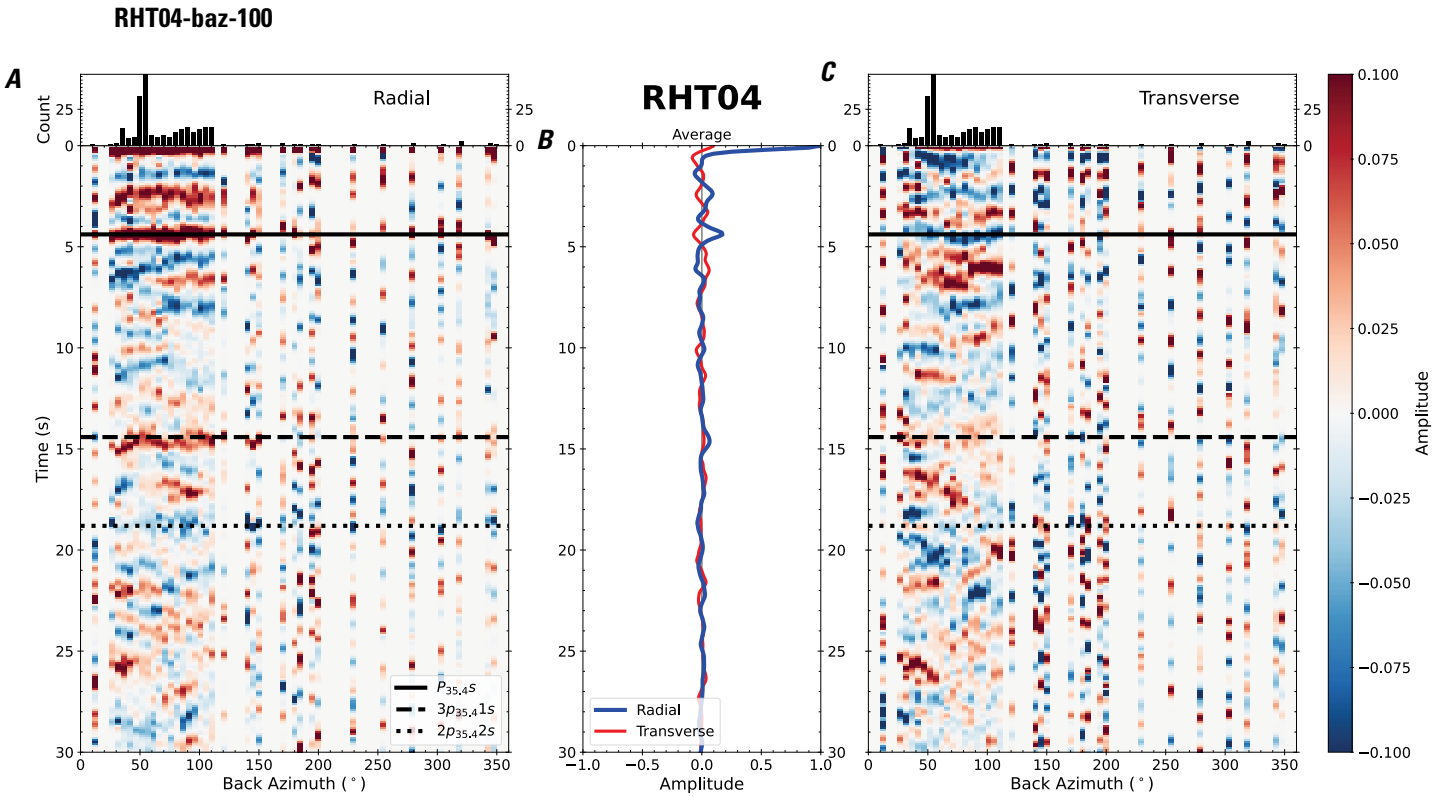

Figure 205. Receiver functions plotted against back azimuth for station RHT04. *A*, Radial component of P-wave receiver functions (PRFs) plotted against back azimuth. Individual PRFs have had the resonance-removal filter of Yu and others (2015) applied to them, are normalized to the maximum amplitude within the time window shown, binned, and normalized by the number of traces per bin. *B*, Average of every individual normalized radial receiver function with the application of the resonance-removal filter (blue) and average of every individual normalized raw radial receiver function (red). *C*, Radial component of raw PRFs, plotted against back azimuth, normalized as in *A*. Ps, 3p1s, and 2p2s arrival times predicted for the preferred Moho depth are shown, assuming a ray parameter of 0.06 s/km.

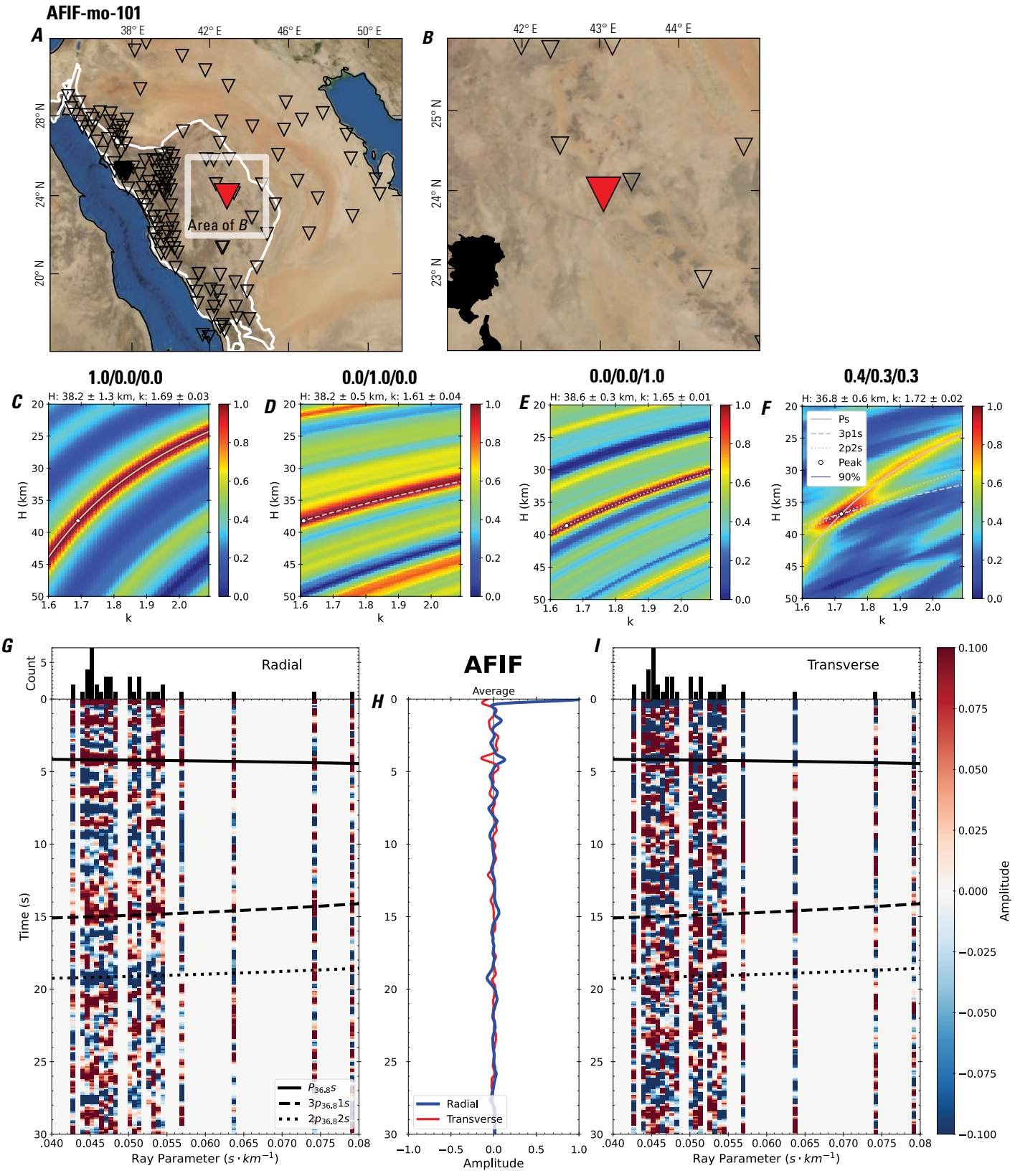
AFIF-mo-101
A
38° E
42° E
46° E
50° E
28° N
24° N
20° N
Area of B
B
42° E
43° E
44° E
25° N
24° N
23° N
1.0/0.0/0.0
C
H: 38.2 ± 1.3 km, k: 1.69 ± 0.03
0.0/1.0/0.0
D
H: 38.2 ± 0.5 km, k: 1.61 ± 0.04
0.0/0.0/1.0
E
H: 38.6 ± 0.3 km, k: 1.65 ± 0.01
0.4/0.3/0.3
F
H: 36.8 ± 0.6 km, k: 1.72 ± 0.02
Ps
3p1s
2p2s
Peak
90%
H (km)
k
G
Radial
Count
Time (s)
$P_{36.8}s$
$3p_{36.8}1s$
$2p_{36.8}2s$
Ray Parameter ($s \cdot km^{-1}$)
AFIF
Average
H
Radial
Transverse
Amplitude
I
Transverse
Amplitude

Figure 206 (page 212). Receiver-function analysis for station AFIF. *A*, Regional map of Saudi Arabia showing the entire array (as inverted triangles), the location of station AFIF (red inverted triangle), the shield-platform boundary (white line), and the bounds of the map in *B* (white box). *B*, Local map of station AFIF. Harrats are shown in black. *C*, Standard, single-layer *H-k* stack with stacking weights 0.4/0.3/0.3. This *H-k* stack ignores sedimentary effects on the receiver functions. *D*, Standard, single-layer *H-k* stack with stacking weights 0.5/0.5/0.0. This *H-k* stack also ignores sedimentary effects on the receiver functions. *E*, Optimized sub-sedimentary *H-k* stack with stacking weights 0.4/0.3/0.3, following the method of Yu and others (2015). *F*, Optimized sedimentary *H-k* stack with stacking weights 0.05/0.70/0.25, following the method of Yu and others (2015). *G*, Radial component P-wave receiver functions (PRFs) plotted against ray parameter. Individual PRFs have had the resonance-removal filter of Yu and others (2015) applied to them and are normalized to the maximum amplitude within the time window shown, binned, and normalized by the number of traces per bin. *H*, Average of every individual normalized radial receiver function with the application of the resonance-removal filter (blue) and average of every individual normalized raw radial receiver function (red). *I*, Radial component of raw PRFs (that is, PRFs with no resonance-removal filter applied) plotted against ray parameter, normalized as in *G*.

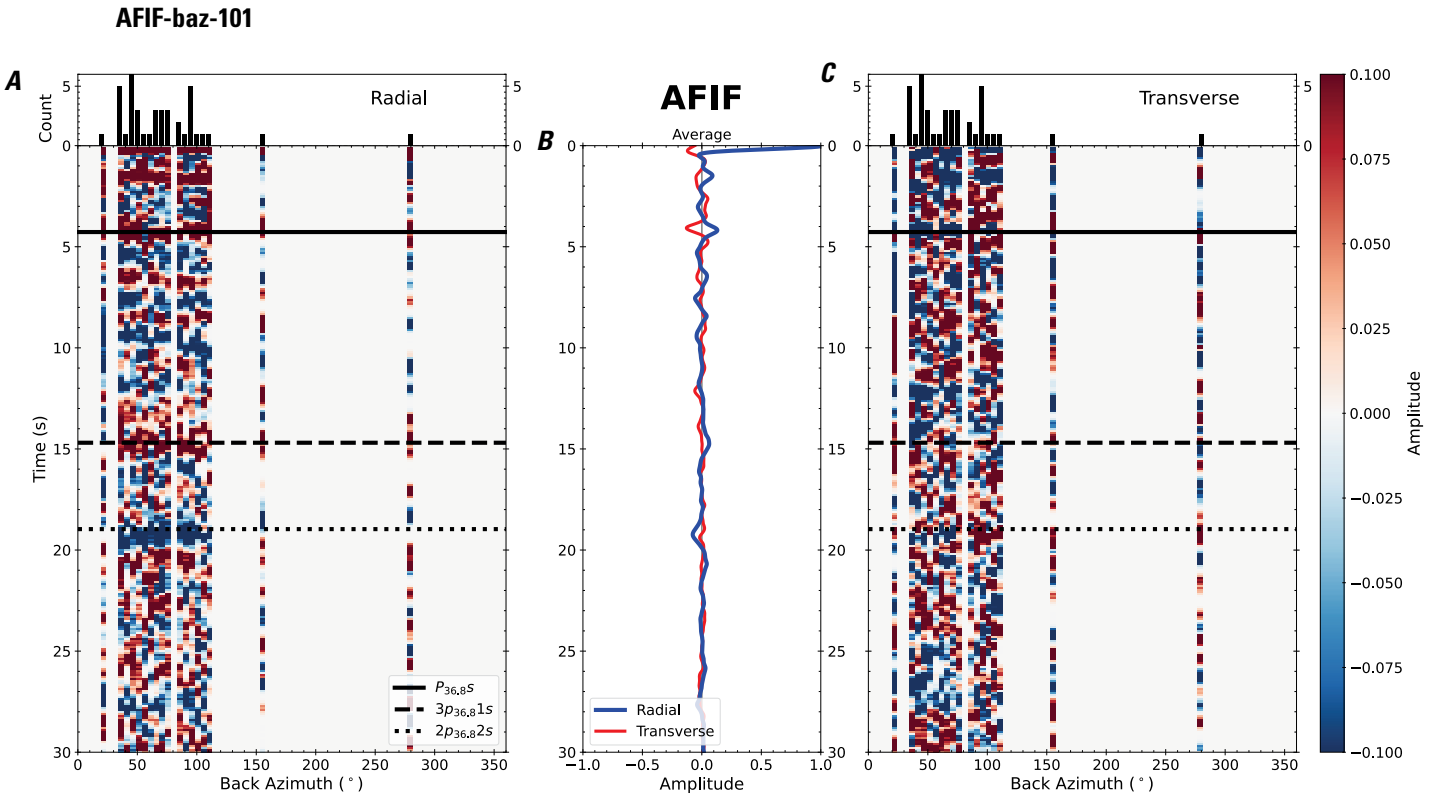

Figure 207. Receiver functions plotted against back azimuth for station AFIF. *A*, Radial component of P-wave receiver functions (PRFs) plotted against back azimuth. Individual PRFs have had the resonance-removal filter of Yu and others (2015) applied to them, are normalized to the maximum amplitude within the time window shown, binned, and normalized by the number of traces per bin. *B*, Average of every individual normalized radial receiver function with the application of the resonance-removal filter (blue) and average of every individual normalized raw radial receiver function (red). *C*, Radial component of raw PRFs, plotted against back azimuth, normalized as in *A*. Ps, 3p1s, and 2p2s arrival times predicted for the preferred Moho depth are shown, assuming a ray parameter of 0.06 s/km.

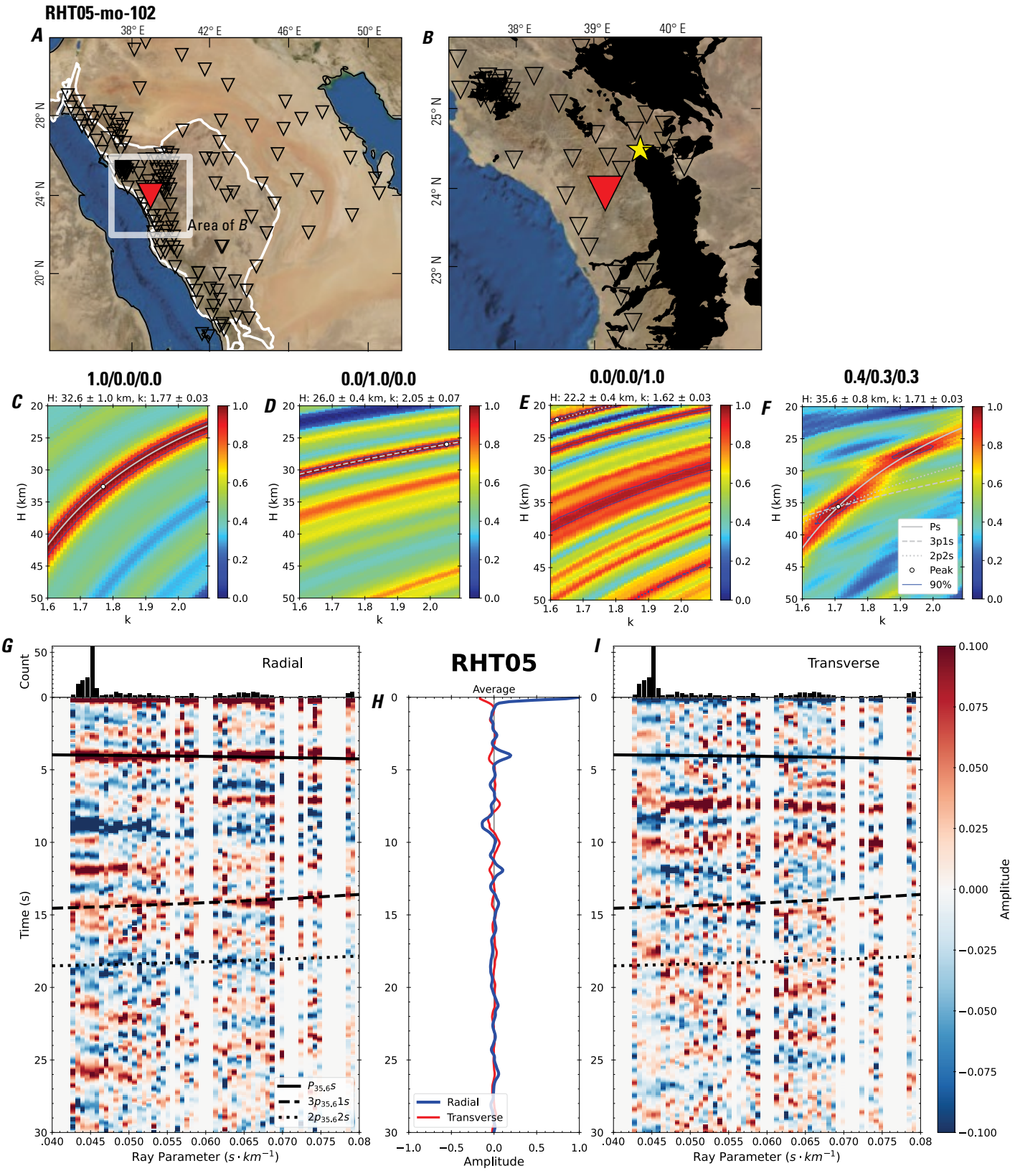
RHT05-mo-102
A
38° E
42° E
46° E
50° E
28° N
24° N
20° N
Area of B
B
38° E
39° E
40° E
25° N
24° N
23° N
1.0/0.0/0.0
0.0/1.0/0.0
0.0/0.0/1.0
0.4/0.3/0.3
C
H: 32.6 ± 1.0 km, k: 1.77 ± 0.03
D
H: 26.0 ± 0.4 km, k: 2.05 ± 0.07
E
H: 22.2 ± 0.4 km, k: 1.62 ± 0.03
F
H: 35.6 ± 0.8 km, k: 1.71 ± 0.03
H (km)
k
Ps
3p1s
2p2s
Peak
90%
G
Radial
Count
Time (s)
$P_{35.6}s$
$3p_{35.6}1s$
$2p_{35.6}2s$
Ray Parameter ($s \cdot km^{-1}$)
RHT05
H
Average
Radial
Transverse
Amplitude
I
Transverse
Ray Parameter ($s \cdot km^{-1}$)
Amplitude

Figure 208 (page 214). Receiver-function analysis for station RHT05. *A*, Regional map of Saudi Arabia showing the entire array (as inverted triangles), the location of station RHT05 (red inverted triangle), the shield-platform boundary (white line), and the bounds of the map in *B* (white box). *B*, Local map of station RHT05. Harrats are shown in black. *C*, Standard, single-layer *H-k* stack with stacking weights 0.4/0.3/0.3. This *H-k* stack ignores sedimentary effects on the receiver functions. *D*, Standard, single-layer *H-k* stack with stacking weights 0.5/0.5/0.0. This *H-k* stack also ignores sedimentary effects on the receiver functions. *E*, Optimized sub-sedimentary *H-k* stack with stacking weights 0.4/0.3/0.3, following the method of Yu and others (2015). *F*, Optimized sedimentary *H-k* stack with stacking weights 0.05/0.70/0.25, following the method of Yu and others (2015). *G*, Radial component P-wave receiver functions (PRFs) plotted against ray parameter. Individual PRFs have had the resonance-removal filter of Yu and others (2015) applied to them and are normalized to the maximum amplitude within the time window shown, binned, and normalized by the number of traces per bin. *H*, Average of every individual normalized radial receiver function with the application of the resonance-removal filter (blue) and average of every individual normalized raw radial receiver function (red). *I*, Radial component of raw PRFs (that is, PRFs with no resonance-removal filter applied) plotted against ray parameter, normalized as in *G*.

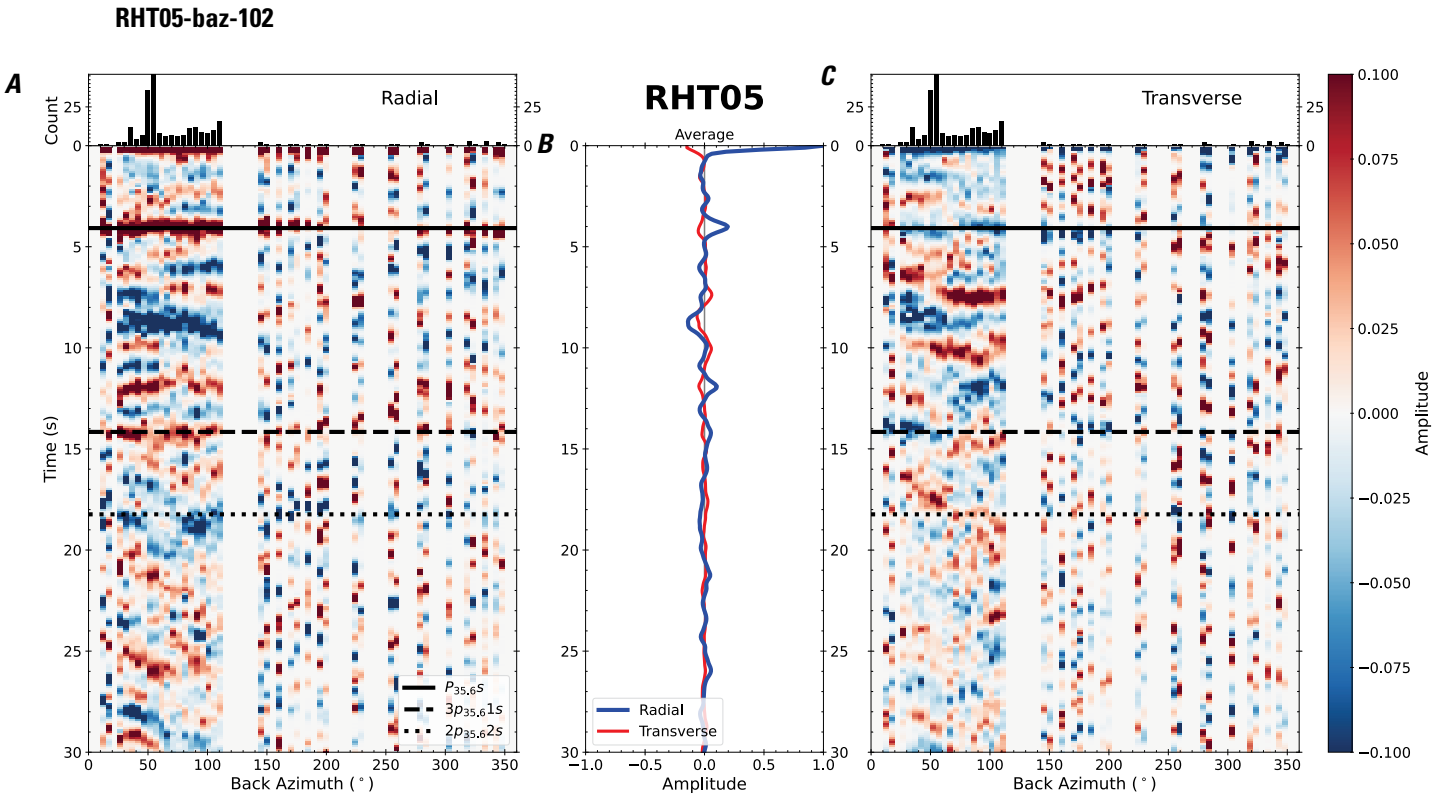

Figure 209. Receiver functions plotted against back azimuth for station RHT05. *A*, Radial component of P-wave receiver functions (PRFs) plotted against back azimuth. Individual PRFs have had the resonance-removal filter of Yu and others (2015) applied to them, are normalized to the maximum amplitude within the time window shown, binned, and normalized by the number of traces per bin. *B*, Average of every individual normalized radial receiver function with the application of the resonance-removal filter (blue) and average of every individual normalized raw radial receiver function (red). *C*, Radial component of raw PRFs, plotted against back azimuth, normalized as in *A*. Ps, 3p1s, and 2p2s arrival times predicted for the preferred Moho depth are shown, assuming a ray parameter of 0.06 s/km.

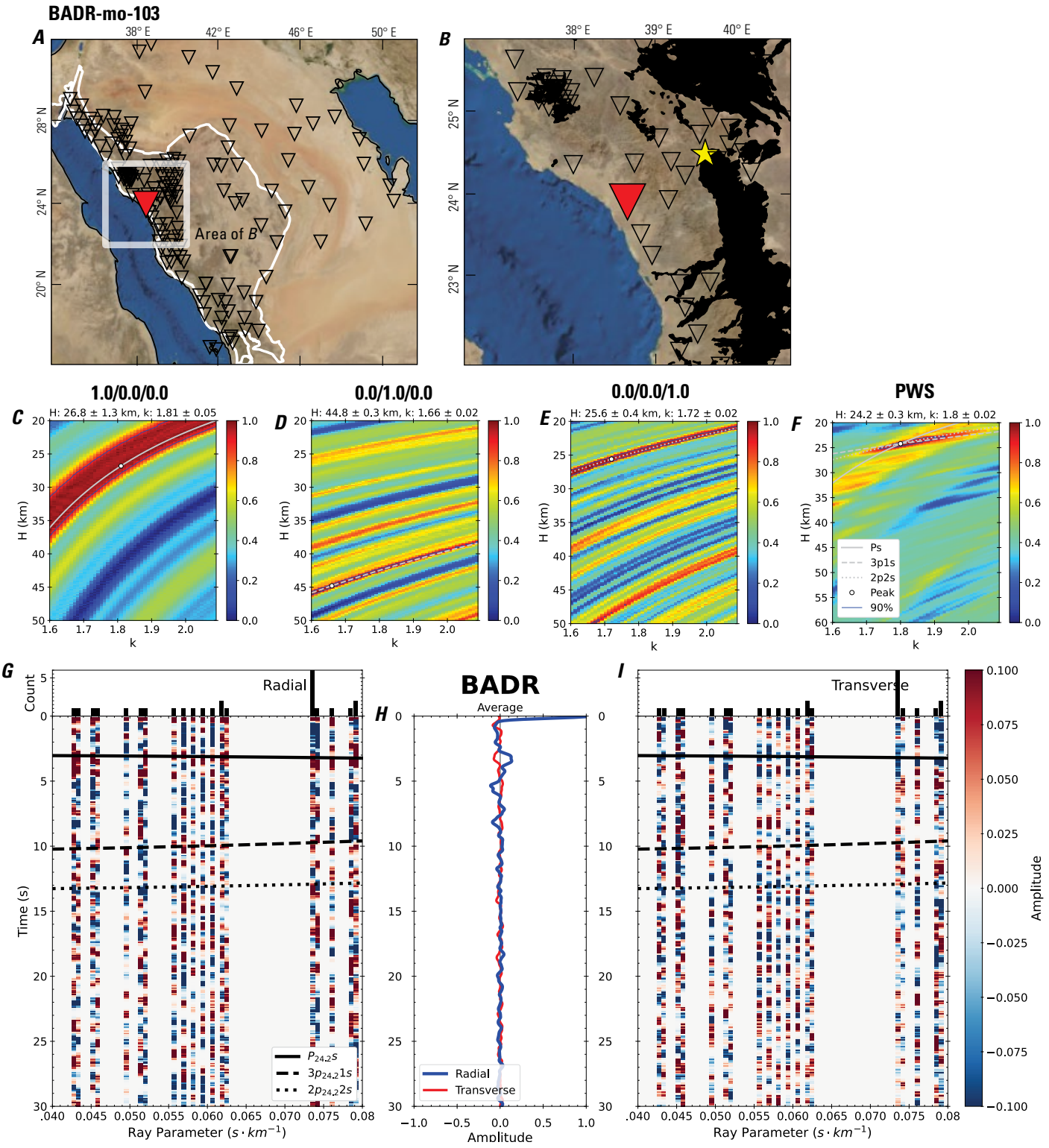
BADR-mo-103
A
38° E
42° E
46° E
50° E
28° N
24° N
20° N
Area of B
B
38° E
39° E
40° E
25° N
24° N
23° N
1.0/0.0/0.0
C
H: 26.8 ± 1.3 km, k: 1.81 ± 0.05
0.0/1.0/0.0
D
H: 44.8 ± 0.3 km, k: 1.66 ± 0.02
0.0/0.0/1.0
E
H: 25.6 ± 0.4 km, k: 1.72 ± 0.02
PWS
F
H: 24.2 ± 0.3 km, k: 1.8 ± 0.02
H (km)
k
Ps
3p1s
2p2s
Peak
90%
G
Radial
Count
Time (s)
Ray Parameter (s · km⁻¹)
$P_{24,2}s$
$3p_{24,2}1s$
$2p_{24,2}2s$
BADR
Average
H
Radial
Transverse
Amplitude
I
Transverse
Amplitude

Figure 210 (page 216). Receiver-function analysis for station BADR. *A*, Regional map of Saudi Arabia showing the entire array (as inverted triangles), the location of station BADR (red inverted triangle), the shield-platform boundary (white line), and the bounds of the map in *B* (white box). *B*, Local map of station BADR. Harrats are shown in black. *C*, Standard, single-layer *H-k* stack with stacking weights 0.4/0.3/0.3. This *H-k* stack ignores sedimentary effects on the receiver functions. *D*, Standard, single-layer *H-k* stack with stacking weights 0.5/0.5/0.0. This *H-k* stack also ignores sedimentary effects on the receiver functions. *E*, Optimized sub-sedimentary *H-k* stack with stacking weights 0.4/0.3/0.3, following the method of Yu and others (2015). *F*, Optimized sedimentary *H-k* stack with stacking weights 0.05/0.70/0.25, following the method of Yu and others (2015). *G*, Radial component P-wave receiver functions (PRFs) plotted against ray parameter. Individual PRFs have had the resonance-removal filter of Yu and others (2015) applied to them and are normalized to the maximum amplitude within the time window shown, binned, and normalized by the number of traces per bin. *H*, Average of every individual normalized radial receiver function with the application of the resonance-removal filter (blue) and average of every individual normalized raw radial receiver function (red). *I*, Radial component of raw PRFs (that is, PRFs with no resonance-removal filter applied) plotted against ray parameter, normalized as in *G*.

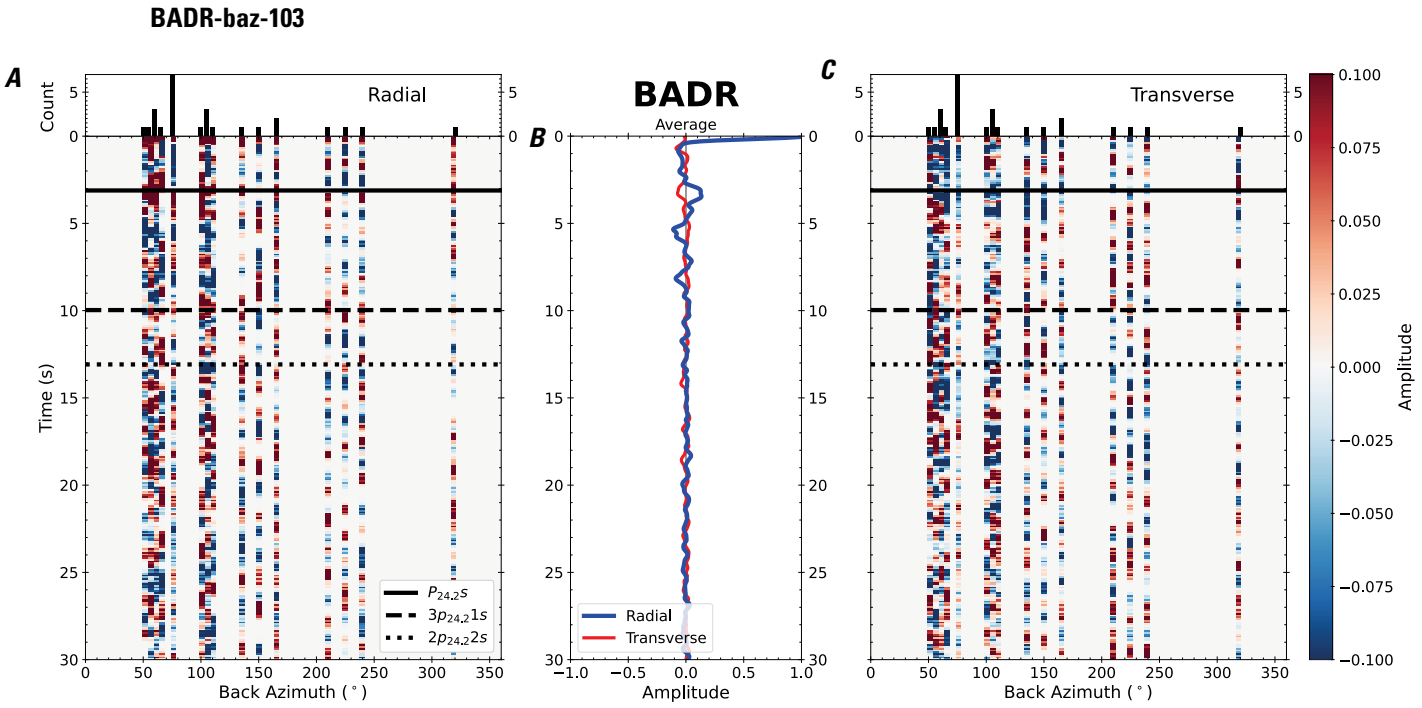

Figure 211. Receiver functions plotted against back azimuth for station BADR. *A*, Radial component of P-wave receiver functions (PRFs) plotted against back azimuth. Individual PRFs have had the resonance-removal filter of Yu and others (2015) applied to them, are normalized to the maximum amplitude within the time window shown, binned, and normalized by the number of traces per bin. *B*, Average of every individual normalized radial receiver function with the application of the resonance-removal filter (blue) and average of every individual normalized raw radial receiver function (red). *C*, Radial component of raw PRFs, plotted against back azimuth, normalized as in *A*. Ps, 3p1s, and 2p2s arrival times predicted for the preferred Moho depth are shown, assuming a ray parameter of 0.06 s/km.

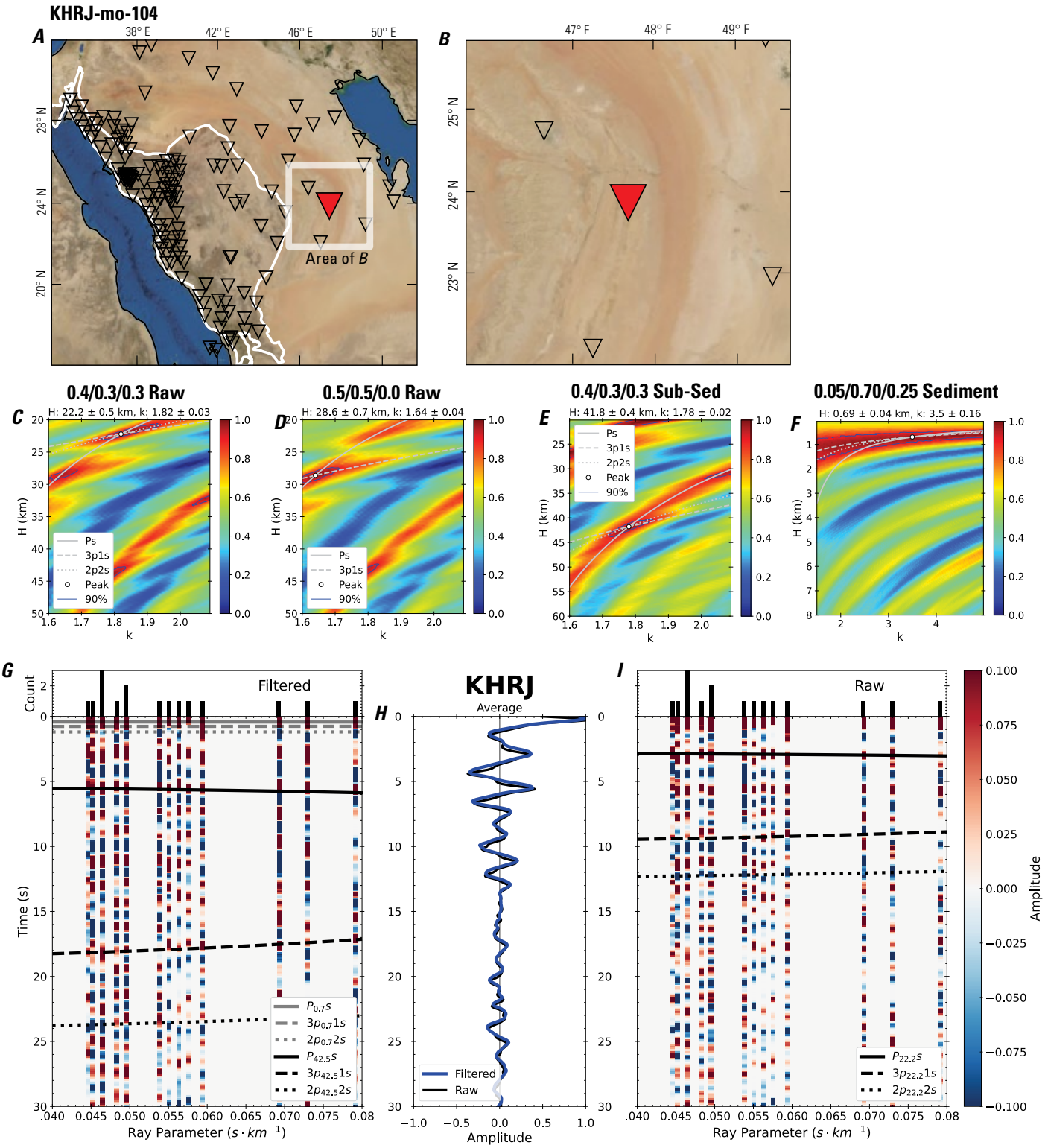
KHRJ-mo-104
A
38° E
42° E
46° E
50° E
28° N
24° N
20° N
Area of B
B
47° E
48° E
49° E
25° N
24° N
23° N
0.4/0.3/0.3 Raw
C
H: 22.2 ± 0.5 km, k: 1.82 ± 0.03
0.5/0.5/0.0 Raw
D
H: 28.6 ± 0.7 km, k: 1.64 ± 0.04
0.4/0.3/0.3 Sub-Sed
E
H: 41.8 ± 0.4 km, k: 1.78 ± 0.02
0.05/0.70/0.25 Sediment
F
H: 0.69 ± 0.04 km, k: 3.5 ± 0.16
H (km)
k
Ps
3p1s
2p2s
Peak
90%
G
Filtered
Count
Time (s)
Ray Parameter (s · km⁻¹)
$P_{0.7}s$
$3p_{0.7}1s$
$2p_{0.7}2s$
$P_{42.5}s$
$3p_{42.5}1s$
$2p_{42.5}2s$
H
KHRJ
Average
Filtered
Raw
Amplitude
I
Raw
$P_{22.2}s$
$3p_{22.2}1s$
$2p_{22.2}2s$
Amplitude

Figure 212 (page 218). Receiver-function analysis for station KHRJ. *A*, Regional map of Saudi Arabia showing the entire array (as inverted triangles), the location of station KHRJ (red inverted triangle), the shield-platform boundary (white line), and the bounds of the map in *B* (white box). *B*, Local map of station KHRJ. Harrats are shown in black. *C*, Standard, single-layer *H-k* stack with stacking weights 0.4/0.3/0.3. This *H-k* stack ignores sedimentary effects on the receiver functions. *D*, Standard, single-layer *H-k* stack with stacking weights 0.5/0.5/0.0. This *H-k* stack also ignores sedimentary effects on the receiver functions. *E*, Optimized sub-sedimentary *H-k* stack with stacking weights 0.4/0.3/0.3, following the method of Yu and others (2015). *F*, Optimized sedimentary *H-k* stack with stacking weights 0.05/0.70/0.25, following the method of Yu and others (2015). *G*, Radial component P-wave receiver functions (PRFs) plotted against ray parameter. Individual PRFs have had the resonance-removal filter of Yu and others (2015) applied to them and are normalized to the maximum amplitude within the time window shown, binned, and normalized by the number of traces per bin. *H*, Average of every individual normalized radial receiver function with the application of the resonance-removal filter (blue) and average of every individual normalized raw radial receiver function (red). *I*, Radial component of raw PRFs (that is, PRFs with no resonance-removal filter applied) plotted against ray parameter, normalized as in *G*.

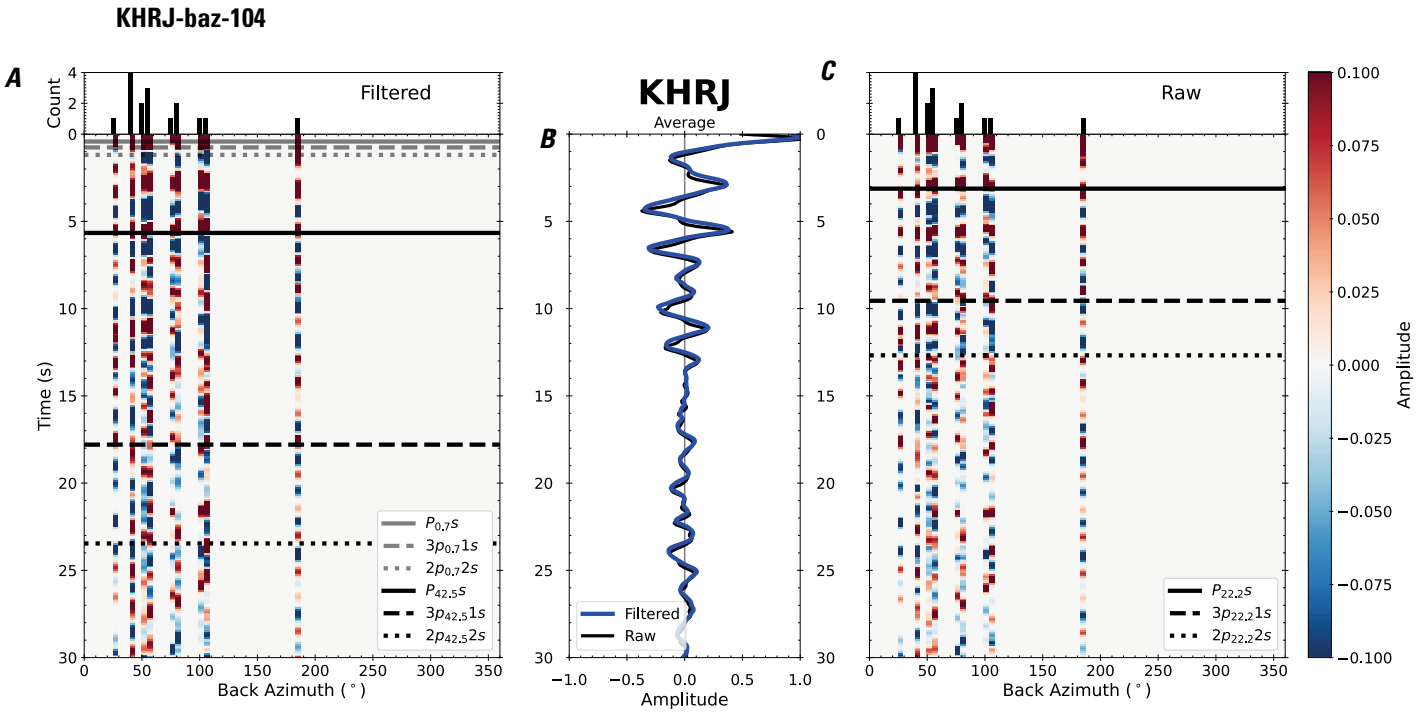

Figure 213. Receiver functions plotted against back azimuth for station KHRJ. *A*, Radial component of P-wave receiver functions (PRFs) plotted against back azimuth. Individual PRFs have had the resonance-removal filter of Yu and others (2015) applied to them, are normalized to the maximum amplitude within the time window shown, binned, and normalized by the number of traces per bin. *B*, Average of every individual normalized radial receiver function with the application of the resonance-removal filter (blue) and average of every individual normalized raw radial receiver function (red). *C*, Radial component of raw PRFs, plotted against back azimuth, normalized as in *A*. Ps, 3p1s, and 2p2s arrival times predicted for the preferred Moho depth are shown, assuming a ray parameter of 0.06 s/km.

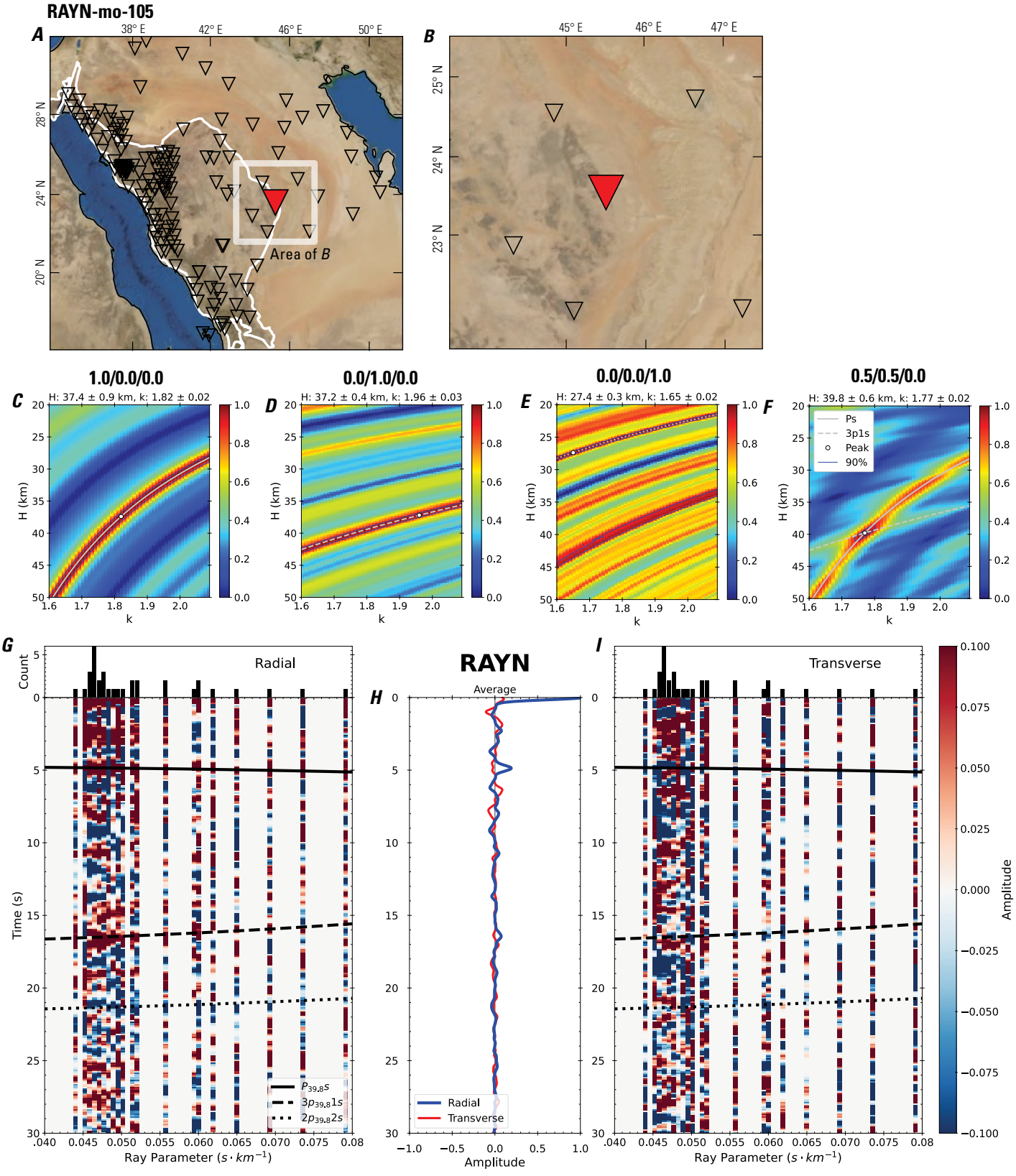
RAYN-mo-105
A
38° E
42° E
46° E
50° E
28° N
24° N
20° N
Area of B
B
45° E
46° E
47° E
25° N
24° N
23° N
1.0/0.0/0.0
C
H: 37.4 ± 0.9 km, k: 1.82 ± 0.02
0.0/1.0/0.0
D
H: 37.2 ± 0.4 km, k: 1.96 ± 0.03
0.0/0.0/1.0
E
H: 27.4 ± 0.3 km, k: 1.65 ± 0.02
0.5/0.5/0.0
F
H: 39.8 ± 0.6 km, k: 1.77 ± 0.02
Ps
3p1s
Peak
90%
H (km)
k
G
Radial
Count
Time (s)
Ray Parameter (s · km⁻¹)
$P_{39.8}s$
$3p_{39.8}1s$
$2p_{39.8}2s$
RAYN
H
Average
Radial
Transverse
Amplitude
I
Transverse
Amplitude

Figure 214 (page 220). Receiver-function analysis for station RAYN. *A*, Regional map of Saudi Arabia showing the entire array (as inverted triangles), the location of station RAYN (red inverted triangle), the shield-platform boundary (white line), and the bounds of the map in *B* (white box). *B*, Local map of station RAYN. Harrats are shown in black. *C*, Standard, single-layer *H-k* stack with stacking weights 0.4/0.3/0.3. This *H-k* stack ignores sedimentary effects on the receiver functions. *D*, Standard, single-layer *H-k* stack with stacking weights 0.5/0.5/0.0. This *H-k* stack also ignores sedimentary effects on the receiver functions. *E*, Optimized sub-sedimentary *H-k* stack with stacking weights 0.4/0.3/0.3, following the method of Yu and others (2015). *F*, Optimized sedimentary *H-k* stack with stacking weights 0.05/0.70/0.25, following the method of Yu and others (2015). *G*, Radial component P-wave receiver functions (PRFs) plotted against ray parameter. Individual PRFs have had the resonance-removal filter of Yu and others (2015) applied to them and are normalized to the maximum amplitude within the time window shown, binned, and normalized by the number of traces per bin. *H*, Average of every individual normalized radial receiver function with the application of the resonance-removal filter (blue) and average of every individual normalized raw radial receiver function (red). *I*, Radial component of raw PRFs (that is, PRFs with no resonance-removal filter applied) plotted against ray parameter, normalized as in *G*.

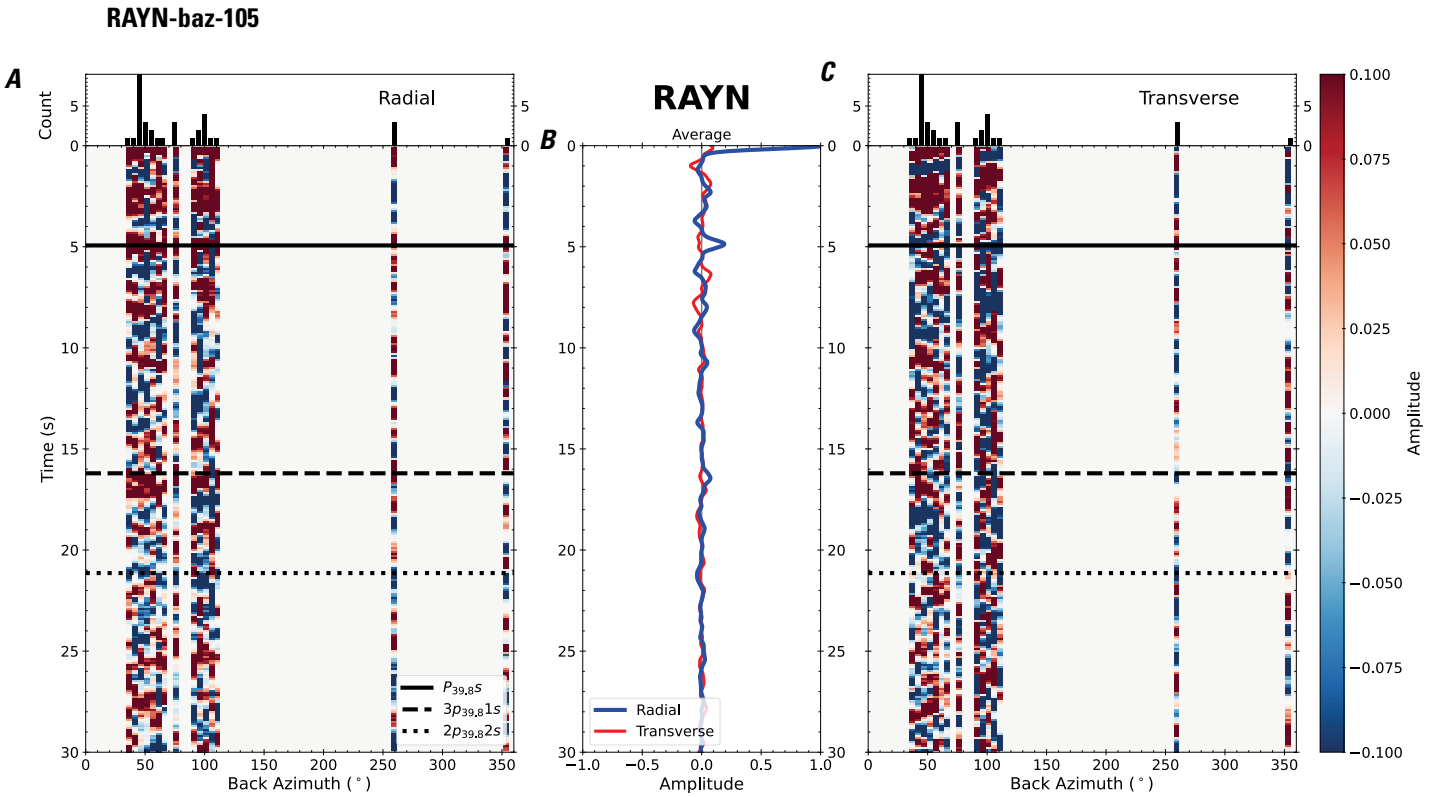

Figure 215. Receiver functions plotted against back azimuth for station RAYN. *A*, Radial component of P-wave receiver functions (PRFs) plotted against back azimuth. Individual PRFs have had the resonance-removal filter of Yu and others (2015) applied to them, are normalized to the maximum amplitude within the time window shown, binned, and normalized by the number of traces per bin. *B*, Average of every individual normalized radial receiver function with the application of the resonance-removal filter (blue) and average of every individual normalized raw radial receiver function (red). *C*, Radial component of raw PRFs, plotted against back azimuth, normalized as in *A*. Ps, 3p1s, and 2p2s arrival times predicted for the preferred Moho depth are shown, assuming a ray parameter of 0.06 s/km.

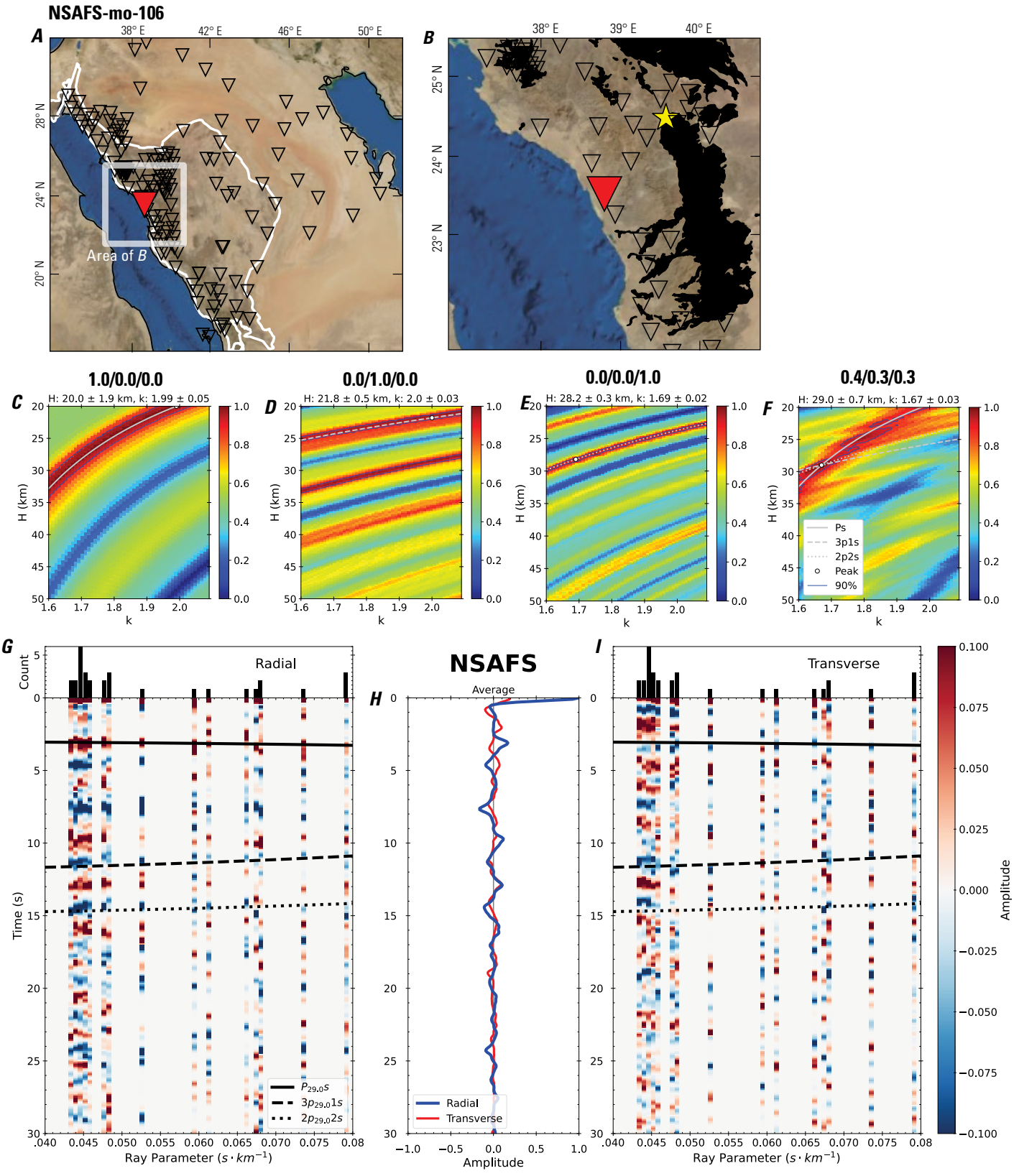
NSAFS-mo-106
A
38° E
42° E
46° E
50° E
28° N
24° N
20° N
Area of B
B
38° E
39° E
40° E
25° N
24° N
23° N
1.0/0.0/0.0
0.0/1.0/0.0
0.0/0.0/1.0
0.4/0.3/0.3
C
H: 20.0 ± 1.9 km, k: 1.99 ± 0.05
D
H: 21.8 ± 0.5 km, k: 2.0 ± 0.03
E
H: 28.2 ± 0.3 km, k: 1.69 ± 0.02
F
H: 29.0 ± 0.7 km, k: 1.67 ± 0.03
H (km)
k
Ps
3p1s
2p2s
Peak
90%
G
Radial
Count
Time (s)
Ray Parameter (s · km⁻¹)
P29.0s
3p29.0 1s
2p29.0 2s
H
NSAFS
Average
Radial
Transverse
Amplitude
I
Transverse
Amplitude

Figure 216 (page 222). Receiver-function analysis for station NSAFS. *A*, Regional map of Saudi Arabia showing the entire array (as inverted triangles), the location of station NSAFS (red inverted triangle), the shield-platform boundary (white line), and the bounds of the map in *B* (white box). *B*, Local map of station NSAFS. Harrats are shown in black. *C*, Standard, single-layer *H-k* stack with stacking weights 0.4/0.3/0.3. This *H-k* stack ignores sedimentary effects on the receiver functions. *D*, Standard, single-layer *H-k* stack with stacking weights 0.5/0.5/0.0. This *H-k* stack also ignores sedimentary effects on the receiver functions. *E*, Optimized sub-sedimentary *H-k* stack with stacking weights 0.4/0.3/0.3, following the method of Yu and others (2015). *F*, Optimized sedimentary *H-k* stack with stacking weights 0.05/0.70/0.25, following the method of Yu and others (2015). *G*, Radial component P-wave receiver functions (PRFs) plotted against ray parameter. Individual PRFs have had the resonance-removal filter of Yu and others (2015) applied to them and are normalized to the maximum amplitude within the time window shown, binned, and normalized by the number of traces per bin. *H*, Average of every individual normalized radial receiver function with the application of the resonance-removal filter (blue) and average of every individual normalized raw radial receiver function (red). *I*, Radial component of raw PRFs (that is, PRFs with no resonance-removal filter applied) plotted against ray parameter, normalized as in *G*.

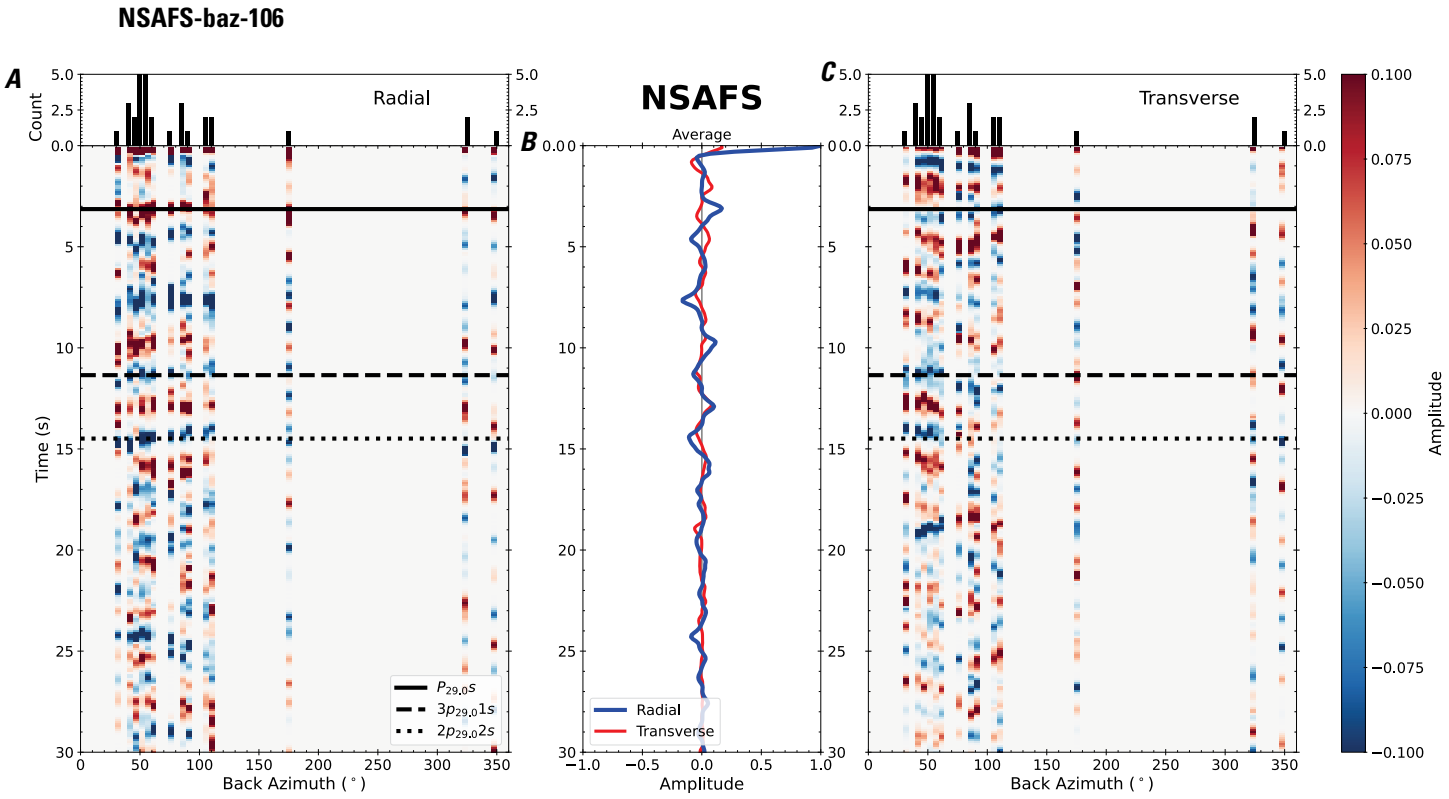

Figure 217. Receiver functions plotted against back azimuth for station NSAFS. *A*, Radial component of P-wave receiver functions (PRFs) plotted against back azimuth. Individual PRFs have had the resonance-removal filter of Yu and others (2015) applied to them, are normalized to the maximum amplitude within the time window shown, binned, and normalized by the number of traces per bin. *B*, Average of every individual normalized radial receiver function with the application of the resonance-removal filter (blue) and average of every individual normalized raw radial receiver function (red). *C*, Radial component of raw PRFs, plotted against back azimuth, normalized as in *A*. Ps, 3p1s, and 2p2s arrival times predicted for the preferred Moho depth are shown, assuming a ray parameter of 0.06 s/km.

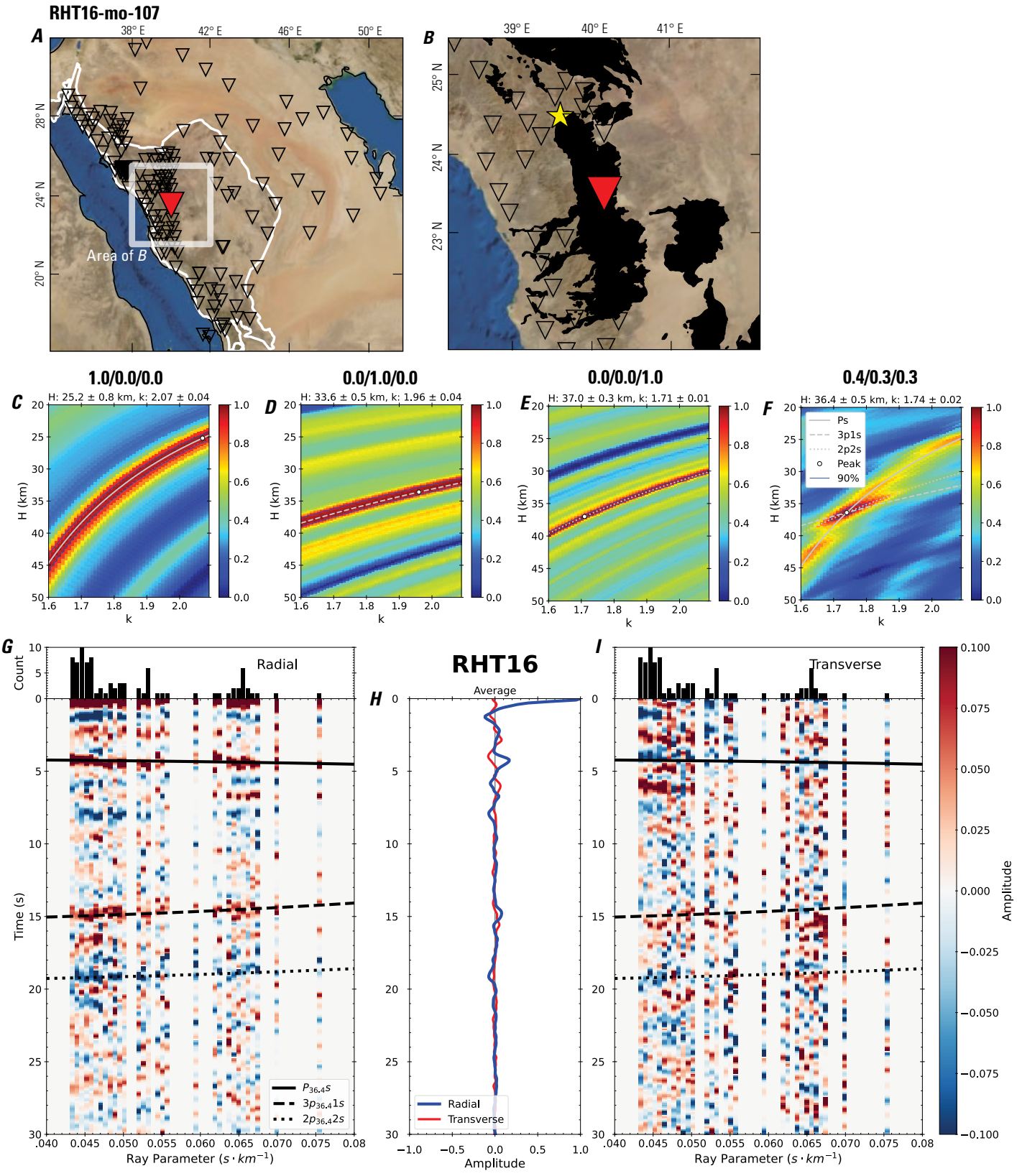
RHT16-mo-107
A
38° E
42° E
46° E
50° E
28° N
24° N
20° N
Area of B
B
39° E
40° E
41° E
25° N
24° N
23° N
1.0/0.0/0.0
0.0/1.0/0.0
0.0/0.0/1.0
0.4/0.3/0.3
C
H: 25.2 ± 0.8 km, k: 2.07 ± 0.04
D
H: 33.6 ± 0.5 km, k: 1.96 ± 0.04
E
H: 37.0 ± 0.3 km, k: 1.71 ± 0.01
F
H: 36.4 ± 0.5 km, k: 1.74 ± 0.02
H (km)
k
Ps
3p1s
2p2s
Peak
90%
G
Radial
Count
Time (s)
Ray Parameter (s · km⁻¹)
P36.4s
3p36.41s
2p36.42s
H
RHT16
Average
Radial
Transverse
Amplitude
I
Transverse
Amplitude

Figure 218 (page 224). Receiver-function analysis for station RHT16. *A*, Regional map of Saudi Arabia showing the entire array (as inverted triangles), the location of station RHT16 (red inverted triangle), the shield-platform boundary (white line), and the bounds of the map in *B* (white box). *B*, Local map of station RHT16. Harrats are shown in black. *C*, Standard, single-layer *H-k* stack with stacking weights 0.4/0.3/0.3. This *H-k* stack ignores sedimentary effects on the receiver functions. *D*, Standard, single-layer *H-k* stack with stacking weights 0.5/0.5/0.0. This *H-k* stack also ignores sedimentary effects on the receiver functions. *E*, Optimized sub-sedimentary *H-k* stack with stacking weights 0.4/0.3/0.3, following the method of Yu and others (2015). *F*, Optimized sedimentary *H-k* stack with stacking weights 0.05/0.70/0.25, following the method of Yu and others (2015). *G*, Radial component P-wave receiver functions (PRFs) plotted against ray parameter. Individual PRFs have had the resonance-removal filter of Yu and others (2015) applied to them and are normalized to the maximum amplitude within the time window shown, binned, and normalized by the number of traces per bin. *H*, Average of every individual normalized radial receiver function with the application of the resonance-removal filter (blue) and average of every individual normalized raw radial receiver function (red). *I*, Radial component of raw PRFs (that is, PRFs with no resonance-removal filter applied) plotted against ray parameter, normalized as in *G*.

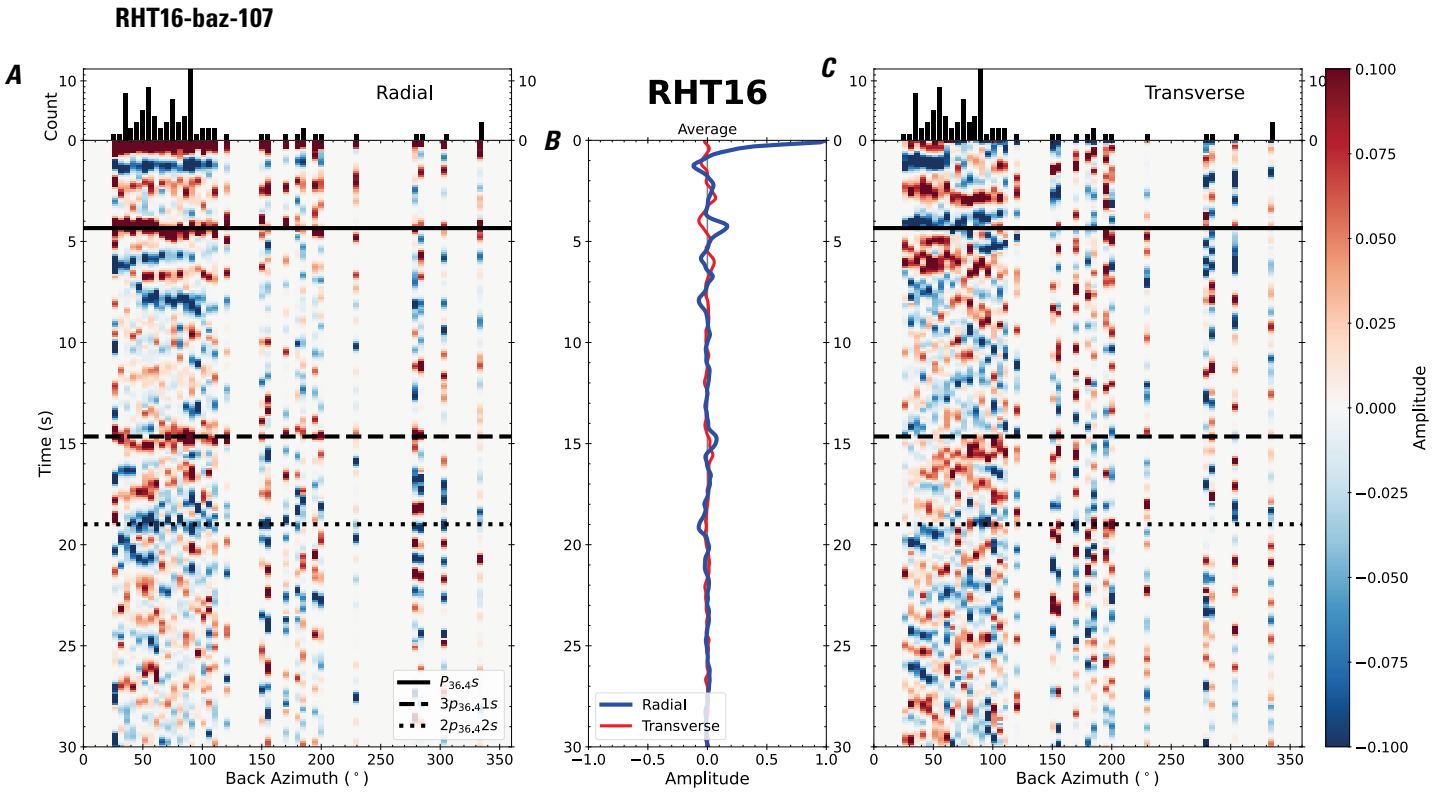

Figure 219. Receiver functions plotted against back azimuth for station RHT16. *A*, Radial component of P-wave receiver functions (PRFs) plotted against back azimuth. Individual PRFs have had the resonance-removal filter of Yu and others (2015) applied to them, are normalized to the maximum amplitude within the time window shown, binned, and normalized by the number of traces per bin. *B*, Average of every individual normalized radial receiver function with the application of the resonance-removal filter (blue) and average of every individual normalized raw radial receiver function (red). *C*, Radial component of raw PRFs, plotted against back azimuth, normalized as in *A*. Ps, 3p1s, and 2p2s arrival times predicted for the preferred Moho depth are shown, assuming a ray parameter of 0.06 s/km.

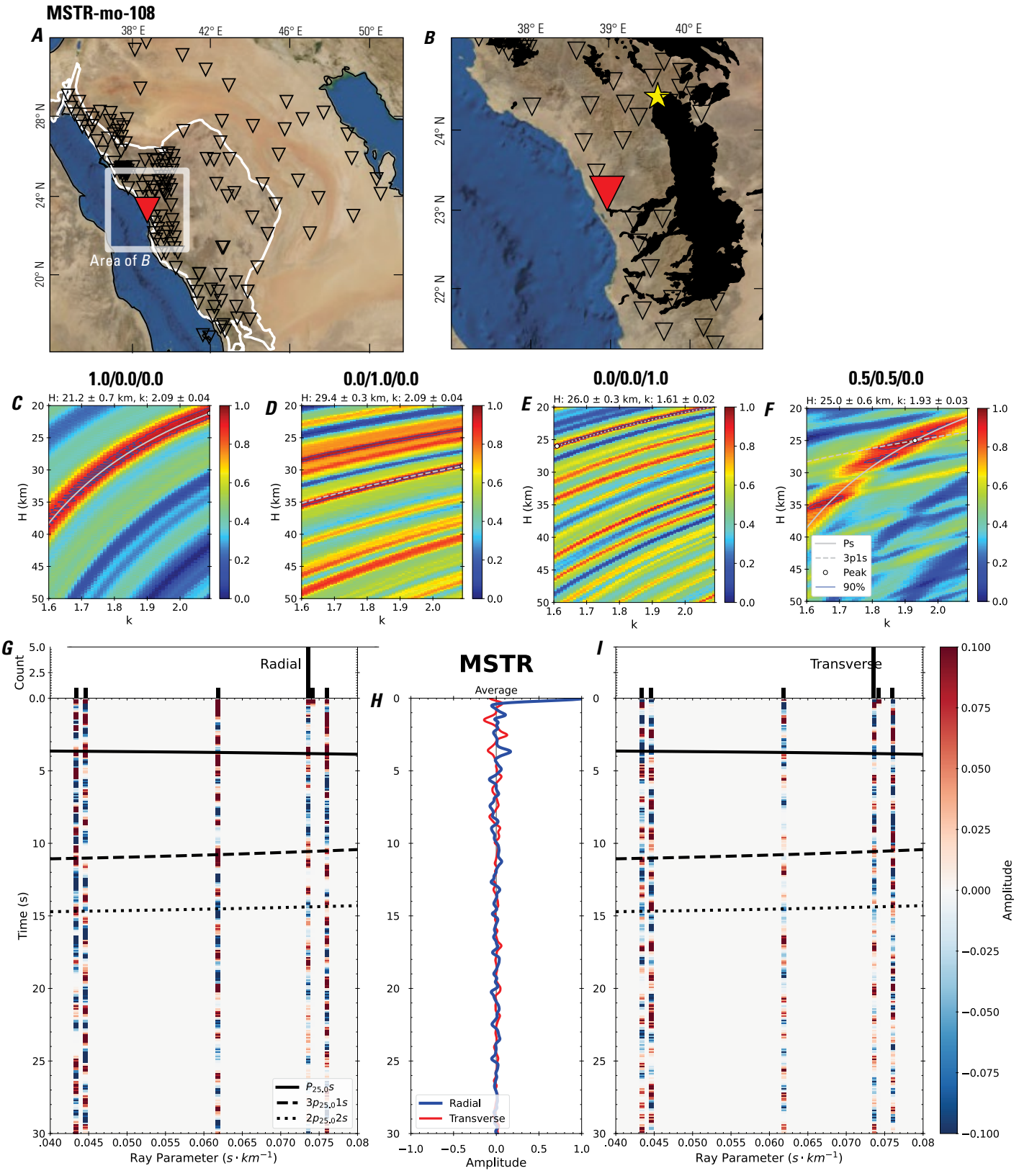
MSTR-mo-108
A
38° E
42° E
46° E
50° E
28° N
24° N
20° N
Area of B
B
38° E
39° E
40° E
24° N
23° N
22° N
1.0/0.0/0.0
0.0/1.0/0.0
0.0/0.0/1.0
0.5/0.5/0.0
C
D
E
F
H: 21.2 ± 0.7 km, k: 2.09 ± 0.04
H: 29.4 ± 0.3 km, k: 2.09 ± 0.04
H: 26.0 ± 0.3 km, k: 1.61 ± 0.02
H: 25.0 ± 0.6 km, k: 1.93 ± 0.03
H (km)
k
Ps
3p1s
Peak
90%
G
H
I
MSTR
Radial
Transverse
Average
Count
Time (s)
Ray Parameter (s · km⁻¹)
Amplitude
$P_{25.0}s$
$3p_{25.0}1s$
$2p_{25.0}2s$
Radial
Transverse

Figure 220 (page 226). Receiver-function analysis for station MSTR. *A*, Regional map of Saudi Arabia showing the entire array (as inverted triangles), the location of station MSTR (red inverted triangle), the shield-platform boundary (white line), and the bounds of the map in *B* (white box). *B*, Local map of station MSTR. Harrats are shown in black. *C*, Standard, single-layer *H-k* stack with stacking weights 0.4/0.3/0.3. This *H-k* stack ignores sedimentary effects on the receiver functions. *D*, Standard, single-layer *H-k* stack with stacking weights 0.5/0.5/0.0. This *H-k* stack also ignores sedimentary effects on the receiver functions. *E*, Optimized sub-sedimentary *H-k* stack with stacking weights 0.4/0.3/0.3, following the method of Yu and others (2015). *F*, Optimized sedimentary *H-k* stack with stacking weights 0.05/0.70/0.25, following the method of Yu and others (2015). *G*, Radial component P-wave receiver functions (PRFs) plotted against ray parameter. Individual PRFs have had the resonance-removal filter of Yu and others (2015) applied to them and are normalized to the maximum amplitude within the time window shown, binned, and normalized by the number of traces per bin. *H*, Average of every individual normalized radial receiver function with the application of the resonance-removal filter (blue) and average of every individual normalized raw radial receiver function (red). *I*, Radial component of raw PRFs (that is, PRFs with no resonance-removal filter applied) plotted against ray parameter, normalized as in *G*.

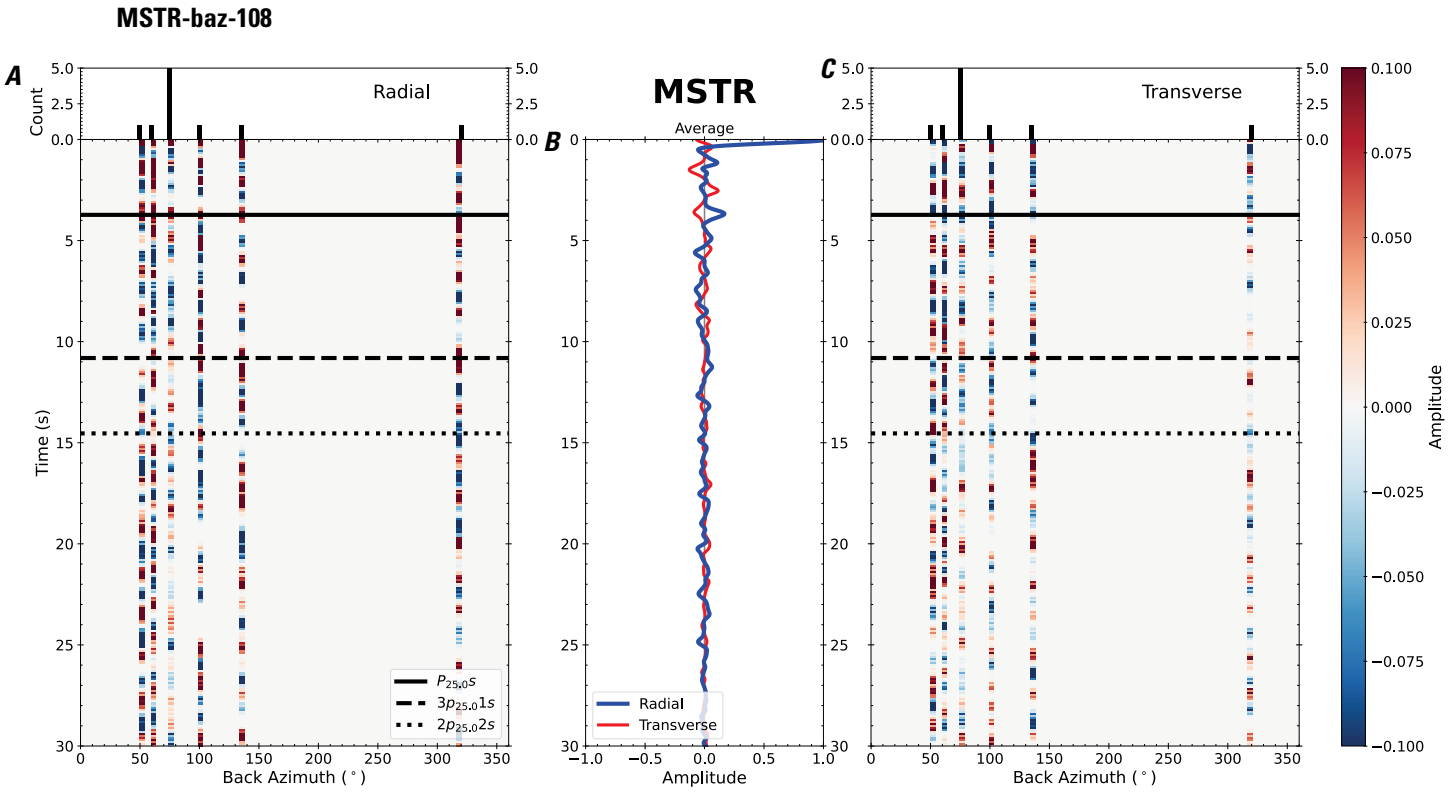

Figure 221. Receiver functions plotted against back azimuth for station MSTR. *A*, Radial component of P-wave receiver functions (PRFs) plotted against back azimuth. Individual PRFs have had the resonance-removal filter of Yu and others (2015) applied to them, are normalized to the maximum amplitude within the time window shown, binned, and normalized by the number of traces per bin. *B*, Average of every individual normalized radial receiver function with the application of the resonance-removal filter (blue) and average of every individual normalized raw radial receiver function (red). *C*, Radial component of raw PRFs, plotted against back azimuth, normalized as in *A*. Ps, 3p1s, and 2p2s arrival times predicted for the preferred Moho depth are shown, assuming a ray parameter of 0.06 s/km.

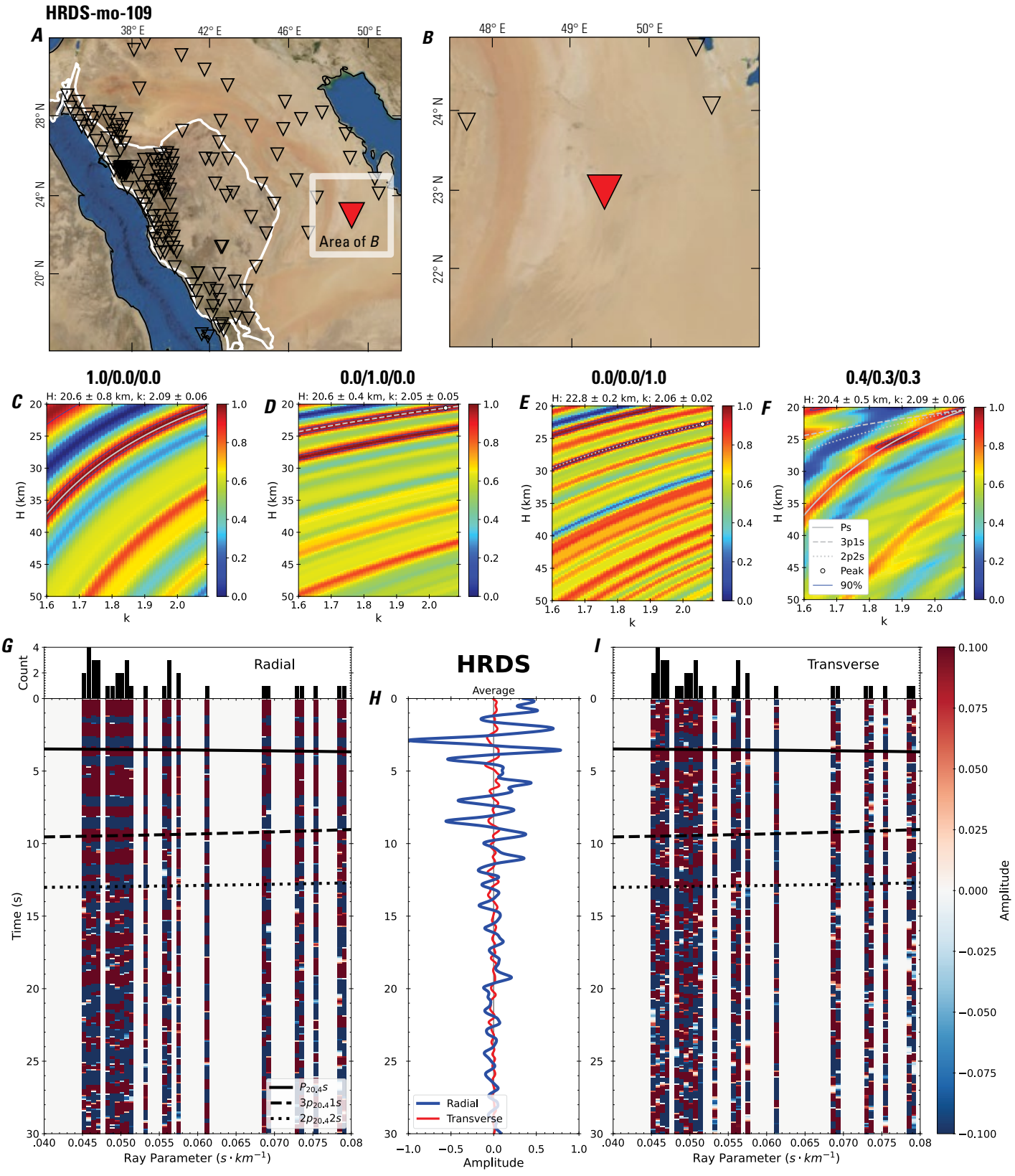
HRDS-mo-109
A
38° E
42° E
46° E
50° E
28° N
24° N
20° N
Area of B
B
48° E
49° E
50° E
24° N
23° N
22° N
1.0/0.0/0.0
0.0/1.0/0.0
0.0/0.0/1.0
0.4/0.3/0.3
C
H: 20.6 ± 0.8 km, k: 2.09 ± 0.06
D
H: 20.6 ± 0.4 km, k: 2.05 ± 0.05
E
H: 22.8 ± 0.2 km, k: 2.06 ± 0.02
F
H: 20.4 ± 0.5 km, k: 2.09 ± 0.06
H (km)
k
Ps
3p1s
2p2s
Peak
90%
G
Radial
Count
Time (s)
Ray Parameter (s · km⁻¹)
P20,4s
3p20,41s
2p20,42s
HRDS
H
Average
Radial
Transverse
Amplitude
I
Transverse
Amplitude

FIgure 222 (page 228). Receiver-function analysis for station HRDS. *A*, Regional map of Saudi Arabia showing the entire array (as inverted triangles), the location of station HRDS (red inverted triangle), the shield-platform boundary (white line), and the bounds of the map in *B* (white box). *B*, Local map of station HRDS. Harrats are shown in black. *C*, Standard, single-layer *H-k* stack with stacking weights 0.4/0.3/0.3. This *H-k* stack ignores sedimentary effects on the receiver functions. *D*, Standard, single-layer *H-k* stack with stacking weights 0.5/0.5/0.0. This *H-k* stack also ignores sedimentary effects on the receiver functions. *E*, Optimized sub-sedimentary *H-k* stack with stacking weights 0.4/0.3/0.3, following the method of Yu and others (2015). *F*, Optimized sedimentary *H-k* stack with stacking weights 0.05/0.70/0.25, following the method of Yu and others (2015). *G*, Radial component P-wave receiver functions (PRFs) plotted against ray parameter. Individual PRFs have had the resonance-removal filter of Yu and others (2015) applied to them and are normalized to the maximum amplitude within the time window shown, binned, and normalized by the number of traces per bin. *H*, Average of every individual normalized radial receiver function with the application of the resonance-removal filter (blue) and average of every individual normalized raw radial receiver function (red). *I*, Radial component of raw PRFs (that is, PRFs with no resonance-removal filter applied) plotted against ray parameter, normalized as in *G*.

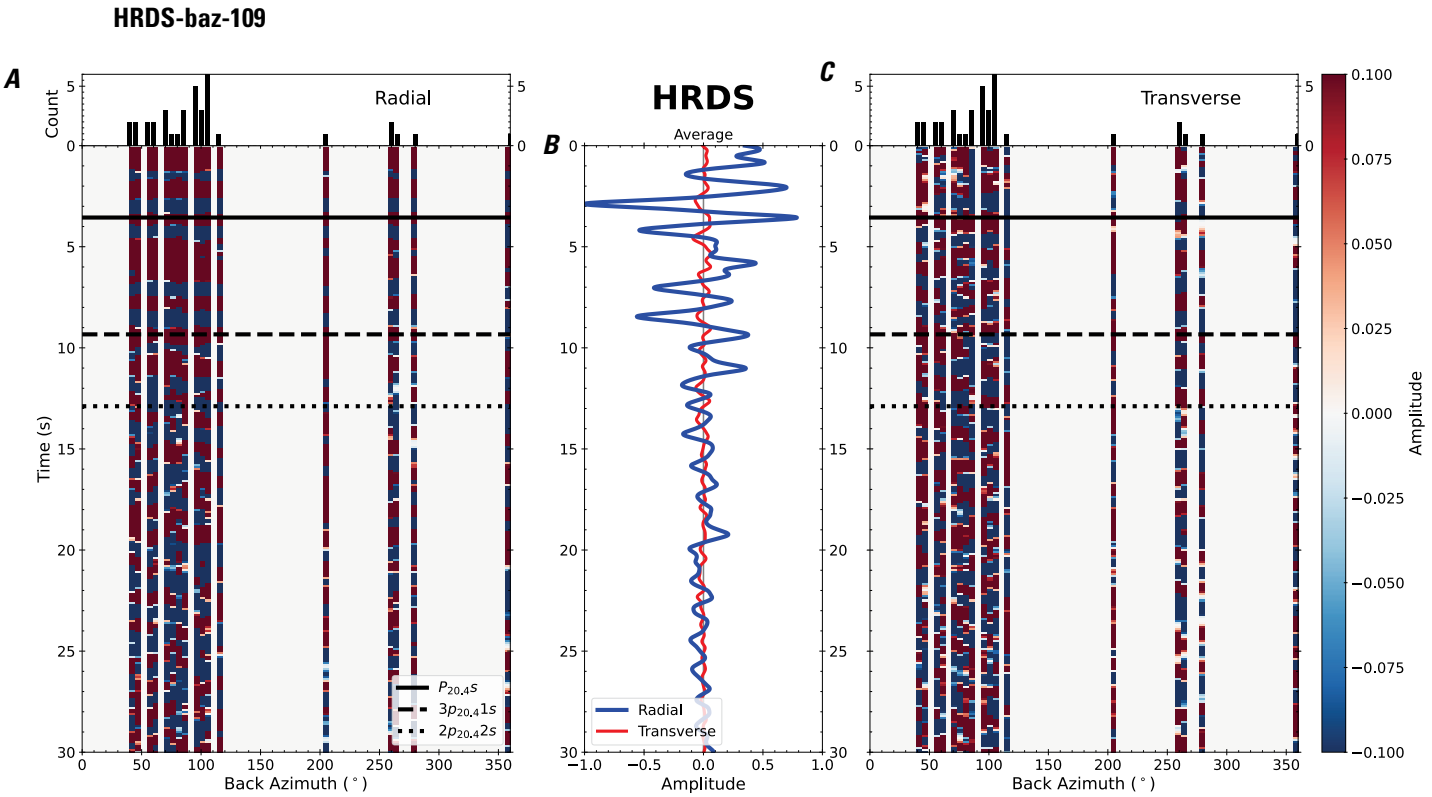

Figure 223. Receiver functions plotted against back azimuth for station HRDS. *A*, Radial component of P-wave receiver functions (PRFs) plotted against back azimuth. Individual PRFs have had the resonance-removal filter of Yu and others (2015) applied to them, are normalized to the maximum amplitude within the time window shown, binned, and normalized by the number of traces per bin. *B*, Average of every individual normalized radial receiver function with the application of the resonance-removal filter (blue) and average of every individual normalized raw radial receiver function (red). *C*, Radial component of raw PRFs, plotted against back azimuth, normalized as in *A*. Ps, 3p1s, and 2p2s arrival times predicted for the preferred Moho depth are shown, assuming a ray parameter of 0.06 s/km.

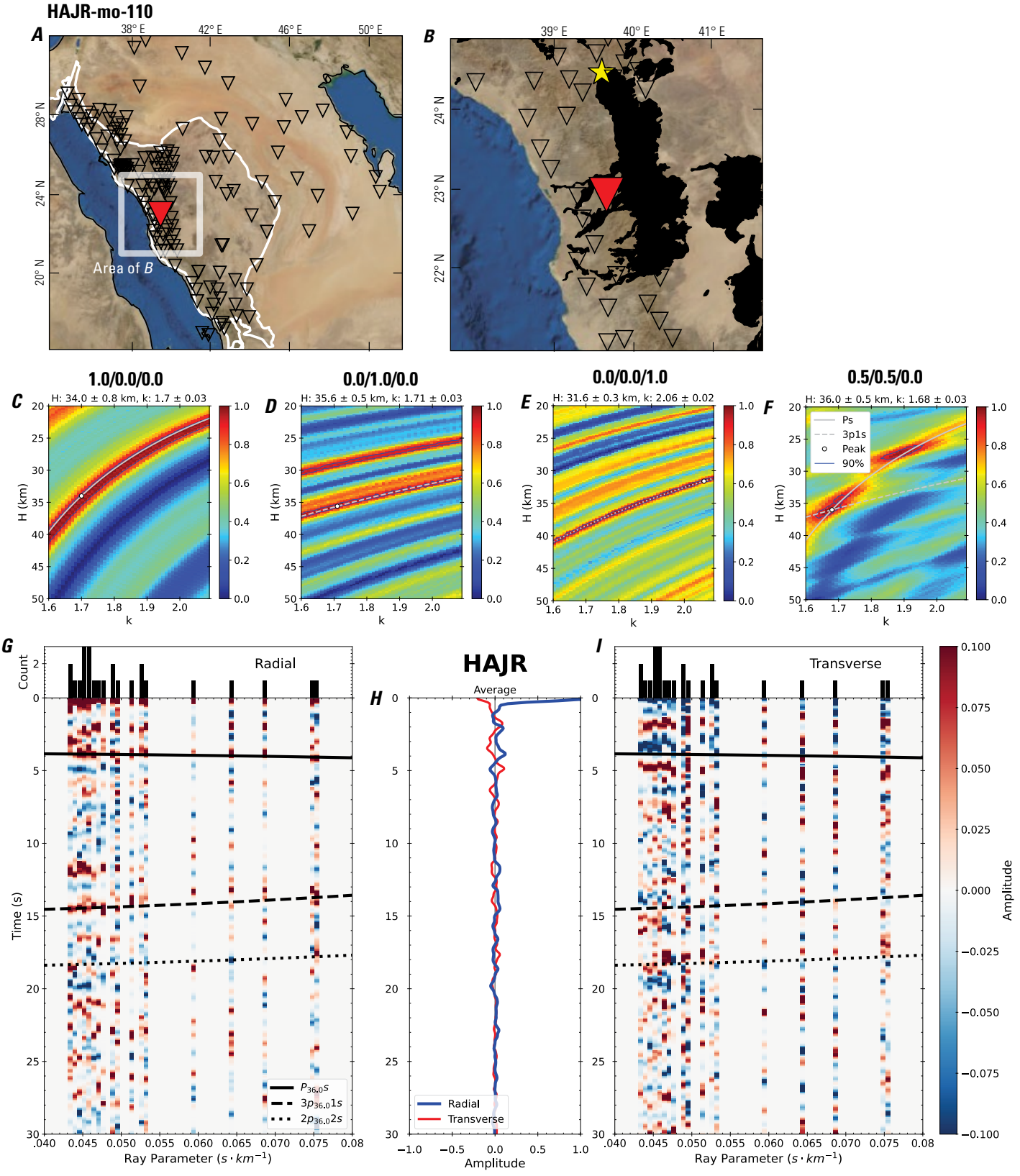
HAJR-mo-110
A
38° E
42° E
46° E
50° E
28° N
24° N
20° N
Area of B
B
39° E
40° E
41° E
24° N
23° N
22° N
1.0/0.0/0.0
C
H: 34.0 ± 0.8 km, k: 1.7 ± 0.03
0.0/1.0/0.0
D
H: 35.6 ± 0.5 km, k: 1.71 ± 0.03
0.0/0.0/1.0
E
H: 31.6 ± 0.3 km, k: 2.06 ± 0.02
0.5/0.5/0.0
F
H: 36.0 ± 0.5 km, k: 1.68 ± 0.03
Ps
3p1s
Peak
90%
H (km)
k
G
Radial
Count
Time (s)
$P_{36.0}s$
$3p_{36.0}1s$
$2p_{36.0}2s$
Ray Parameter ($s \cdot km^{-1}$)
HAJR
H
Average
Radial
Transverse
Amplitude
I
Transverse
Amplitude

Figure 224 (page 230). Receiver-function analysis for station HAJR. *A*, Regional map of Saudi Arabia showing the entire array (as inverted triangles), the location of station HAJR (red inverted triangle), the shield-platform boundary (white line), and the bounds of the map in *B* (white box). *B*, Local map of station HAJR. Harrats are shown in black. *C*, Standard, single-layer *H-k* stack with stacking weights 0.4/0.3/0.3. This *H-k* stack ignores sedimentary effects on the receiver functions. *D*, Standard, single-layer *H-k* stack with stacking weights 0.5/0.5/0.0. This *H-k* stack also ignores sedimentary effects on the receiver functions. *E*, Optimized sub-sedimentary *H-k* stack with stacking weights 0.4/0.3/0.3, following the method of Yu and others (2015). *F*, Optimized sedimentary *H-k* stack with stacking weights 0.05/0.70/0.25, following the method of Yu and others (2015). *G*, Radial component P-wave receiver functions (PRFs) plotted against ray parameter. Individual PRFs have had the resonance-removal filter of Yu and others (2015) applied to them and are normalized to the maximum amplitude within the time window shown, binned, and normalized by the number of traces per bin. *H*, Average of every individual normalized radial receiver function with the application of the resonance-removal filter (blue) and average of every individual normalized raw radial receiver function (red). *I*, Radial component of raw PRFs (that is, PRFs with no resonance-removal filter applied) plotted against ray parameter, normalized as in *G*.

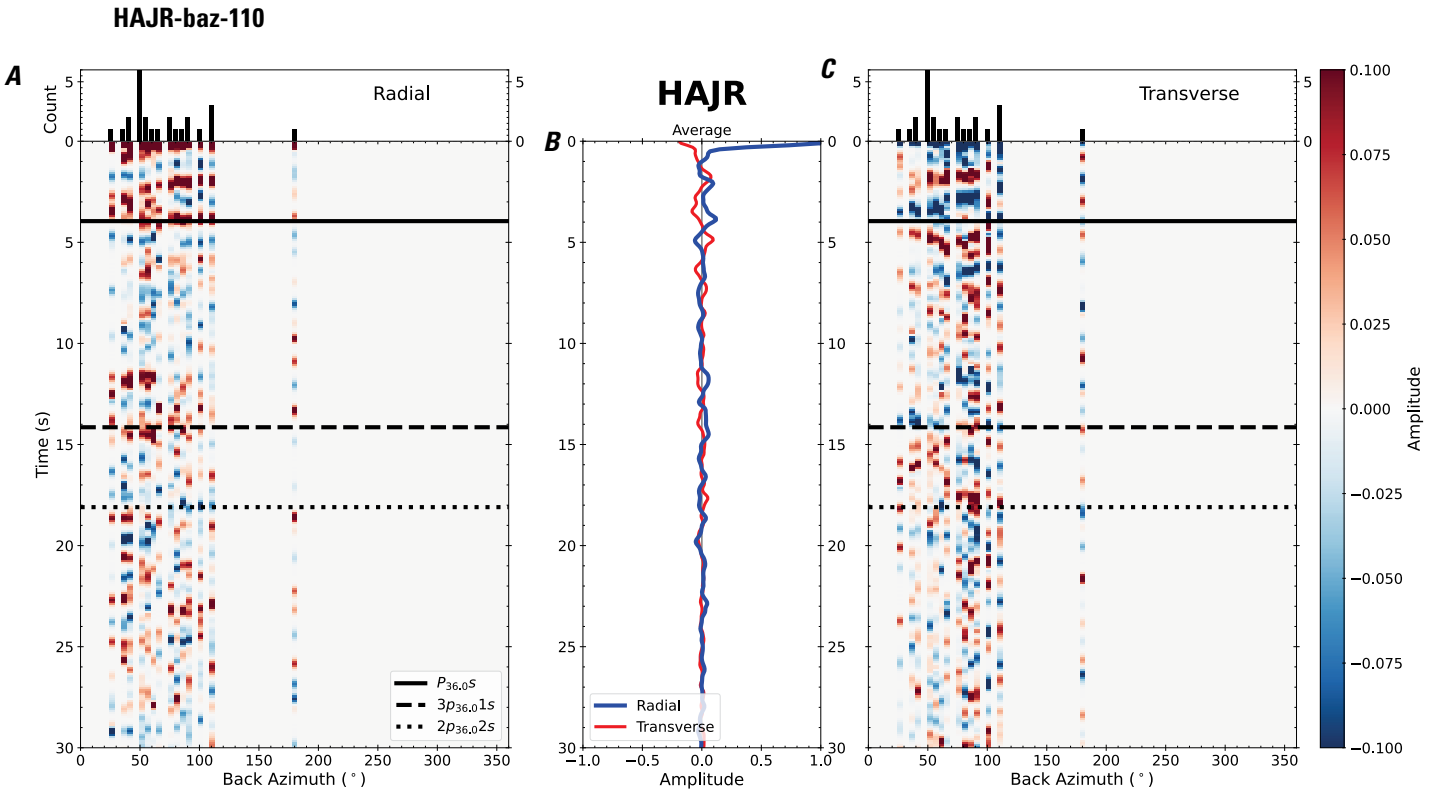

Figure 225. Receiver functions plotted against back azimuth for station HAJR. *A*, Radial component of P-wave receiver functions (PRFs) plotted against back azimuth. Individual PRFs have had the resonance-removal filter of Yu and others (2015) applied to them, are normalized to the maximum amplitude within the time window shown, binned, and normalized by the number of traces per bin. *B*, Average of every individual normalized radial receiver function with the application of the resonance-removal filter (blue) and average of every individual normalized raw radial receiver function (red). *C*, Radial component of raw PRFs, plotted against back azimuth, normalized as in *A*. Ps, 3p1s, and 2p2s arrival times predicted for the preferred Moho depth are shown, assuming a ray parameter of 0.06 s/km.

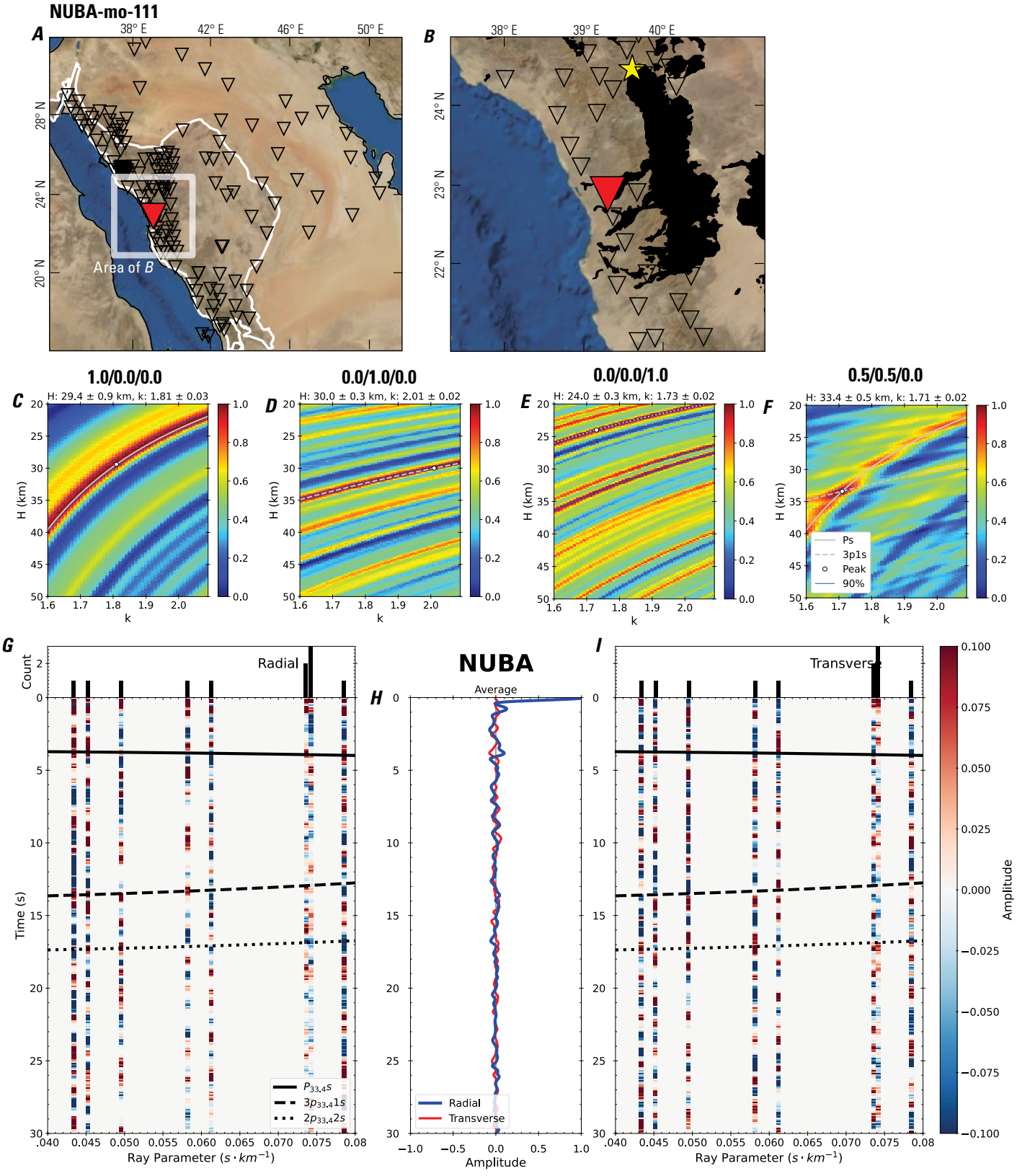
NUBA-mo-111
A
38° E
42° E
46° E
50° E
28° N
24° N
20° N
Area of B
B
38° E
39° E
40° E
24° N
23° N
22° N
1.0/0.0/0.0
0.0/1.0/0.0
0.0/0.0/1.0
0.5/0.5/0.0
C
H: 29.4 ± 0.9 km, k: 1.81 ± 0.03
D
H: 30.0 ± 0.3 km, k: 2.01 ± 0.02
E
H: 24.0 ± 0.3 km, k: 1.73 ± 0.02
F
H: 33.4 ± 0.5 km, k: 1.71 ± 0.02
H (km)
k
Ps
3p1s
Peak
90%
G
Radial
Count
Time (s)
Ray Parameter (s · km⁻¹)
P33,4s
3p33,41s
2p33,42s
H
NUBA
Average
Radial
Transverse
Amplitude
I
Transverse
Amplitude

Figure 226 (page 232). Receiver-function analysis for station NUBA. *A*, Regional map of Saudi Arabia showing the entire array (as inverted triangles), the location of station NUBA (red inverted triangle), the shield-platform boundary (white line), and the bounds of the map in *B* (white box). *B*, Local map of station NUBA. Harrats are shown in black. *C*, Standard, single-layer *H-k* stack with stacking weights 0.4/0.3/0.3. This *H-k* stack ignores sedimentary effects on the receiver functions. *D*, Standard, single-layer *H-k* stack with stacking weights 0.5/0.5/0.0. This *H-k* stack also ignores sedimentary effects on the receiver functions. *E*, Optimized sub-sedimentary *H-k* stack with stacking weights 0.4/0.3/0.3, following the method of Yu and others (2015). *F*, Optimized sedimentary *H-k* stack with stacking weights 0.05/0.70/0.25, following the method of Yu and others (2015). *G*, Radial component P-wave receiver functions (PRFs) plotted against ray parameter. Individual PRFs have had the resonance-removal filter of Yu and others (2015) applied to them and are normalized to the maximum amplitude within the time window shown, binned, and normalized by the number of traces per bin. *H*, Average of every individual normalized radial receiver function with the application of the resonance-removal filter (blue) and average of every individual normalized raw radial receiver function (red). *I*, Radial component of raw PRFs (that is, PRFs with no resonance-removal filter applied) plotted against ray parameter, normalized as in *G*.

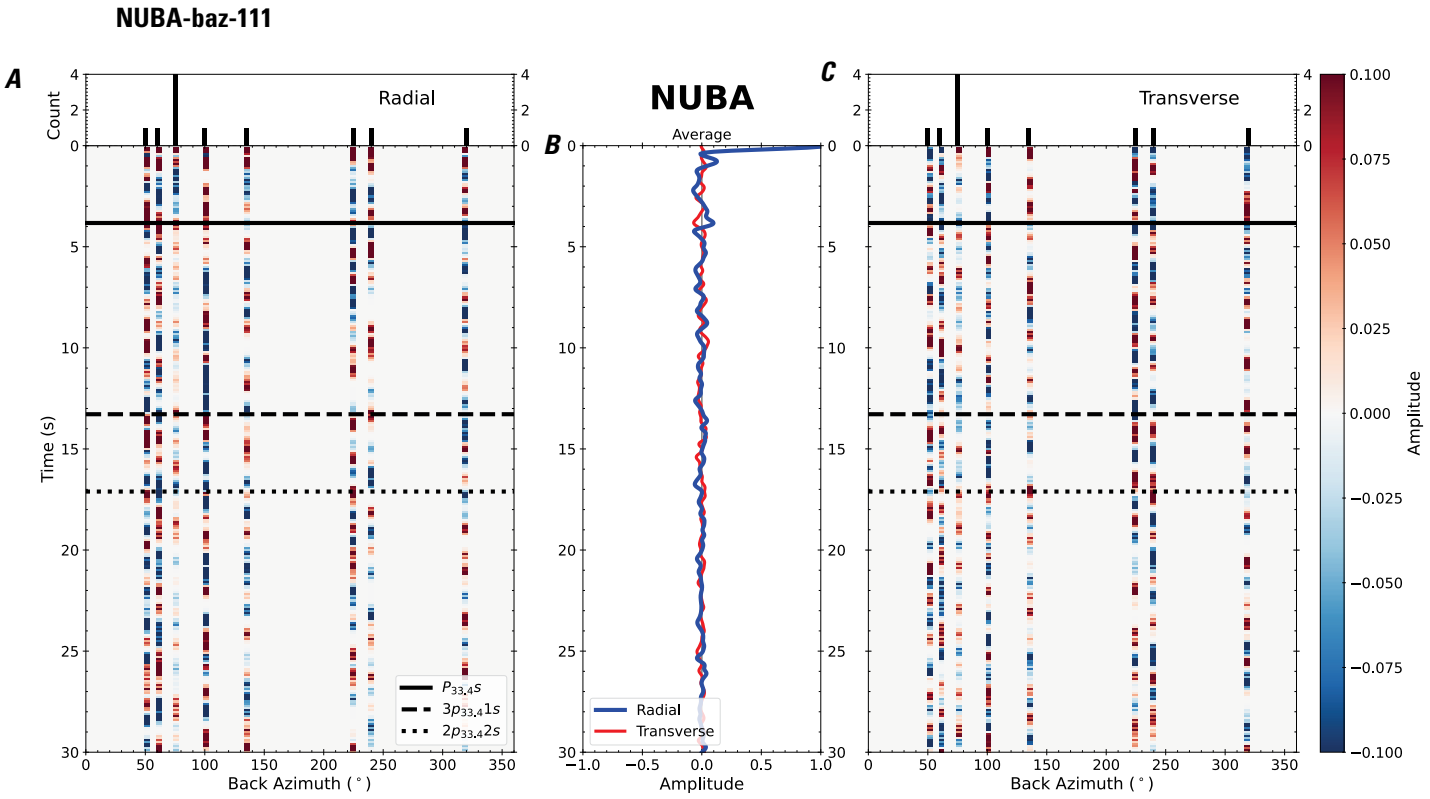

Figure 227. Receiver functions plotted against back azimuth for station NUBA. *A*, Radial component of P-wave receiver functions (PRFs) plotted against back azimuth. Individual PRFs have had the resonance-removal filter of Yu and others (2015) applied to them, are normalized to the maximum amplitude within the time window shown, binned, and normalized by the number of traces per bin. *B*, Average of every individual normalized radial receiver function with the application of the resonance-removal filter (blue) and average of every individual normalized raw radial receiver function (red). *C*, Radial component of raw PRFs, plotted against back azimuth, normalized as in *A*. Ps, 3p1s, and 2p2s arrival times predicted for the preferred Moho depth are shown, assuming a ray parameter of 0.06 s/km.

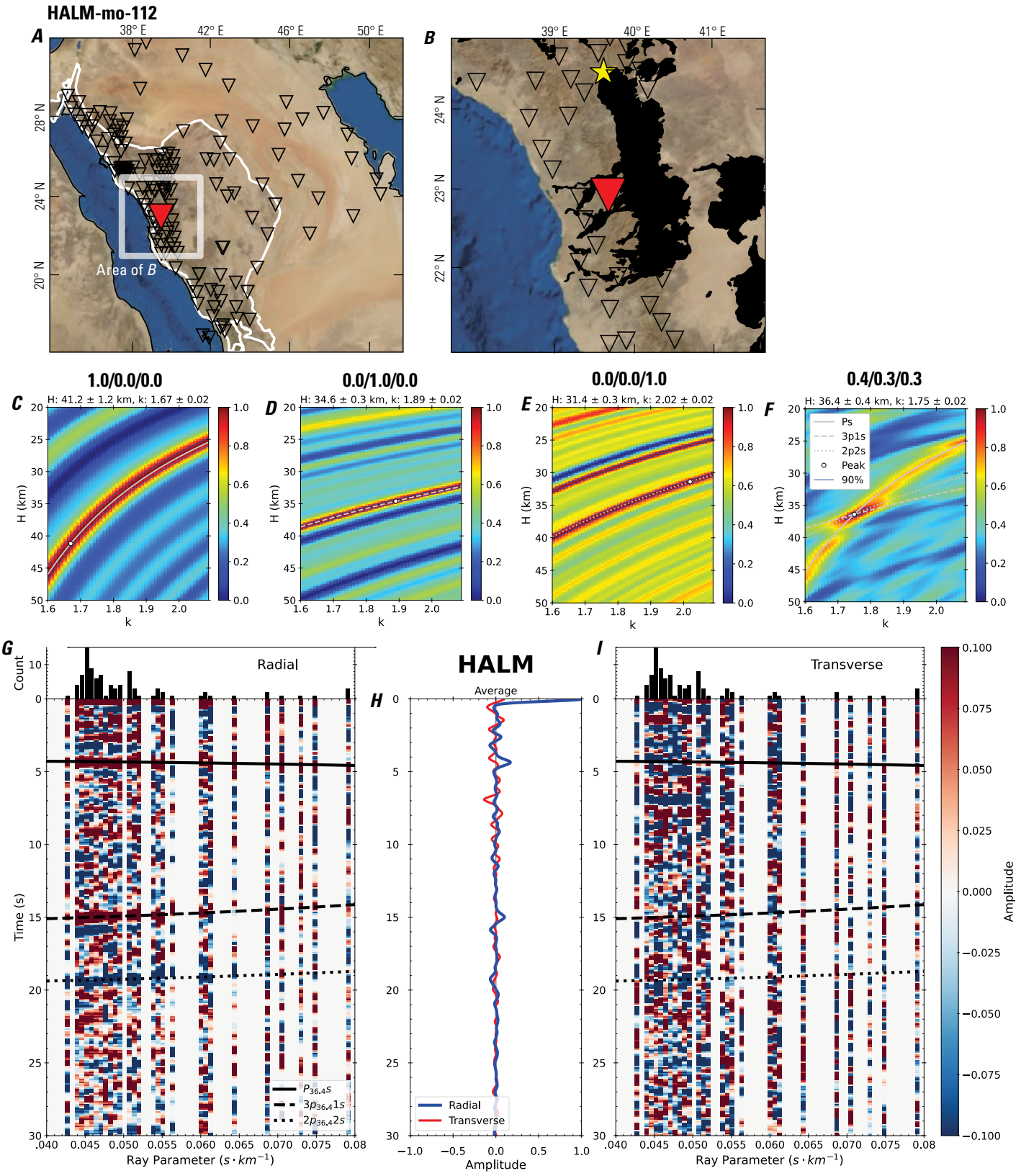
HALM-mo-112
A
38° E
42° E
46° E
50° E
28° N
24° N
20° N
Area of B
B
39° E
40° E
41° E
24° N
23° N
22° N
1.0/0.0/0.0
C
H: 41.2 ± 1.2 km, k: 1.67 ± 0.02
0.0/1.0/0.0
D
H: 34.6 ± 0.3 km, k: 1.89 ± 0.02
0.0/0.0/1.0
E
H: 31.4 ± 0.3 km, k: 2.02 ± 0.02
0.4/0.3/0.3
F
H: 36.4 ± 0.4 km, k: 1.75 ± 0.02
Ps
3p1s
2p2s
Peak
90%
H (km)
k
G
Radial
Count
Time (s)
$P_{36.4}s$
$3p_{36.4}1s$
$2p_{36.4}2s$
Ray Parameter ($s \cdot km^{-1}$)
HALM
H
Average
Radial
Transverse
Amplitude
I
Transverse
Amplitude

Figure 228 (page 234). Receiver-function analysis for station HALM. *A*, Regional map of Saudi Arabia showing the entire array (as inverted triangles), the location of station HALM (red inverted triangle), the shield-platform boundary (white line), and the bounds of the map in *B* (white box). *B*, Local map of station HALM. Harrats are shown in black. *C*, Standard, single-layer *H-k* stack with stacking weights 0.4/0.3/0.3. This *H-k* stack ignores sedimentary effects on the receiver functions. *D*, Standard, single-layer *H-k* stack with stacking weights 0.5/0.5/0.0. This *H-k* stack also ignores sedimentary effects on the receiver functions. *E*, Optimized sub-sedimentary *H-k* stack with stacking weights 0.4/0.3/0.3, following the method of Yu and others (2015). *F*, Optimized sedimentary *H-k* stack with stacking weights 0.05/0.70/0.25, following the method of Yu and others (2015). *G*, Radial component P-wave receiver functions (PRFs) plotted against ray parameter. Individual PRFs have had the resonance-removal filter of Yu and others (2015) applied to them and are normalized to the maximum amplitude within the time window shown, binned, and normalized by the number of traces per bin. *H*, Average of every individual normalized radial receiver function with the application of the resonance-removal filter (blue) and average of every individual normalized raw radial receiver function (red). *I*, Radial component of raw PRFs (that is, PRFs with no resonance-removal filter applied) plotted against ray parameter, normalized as in *G*.

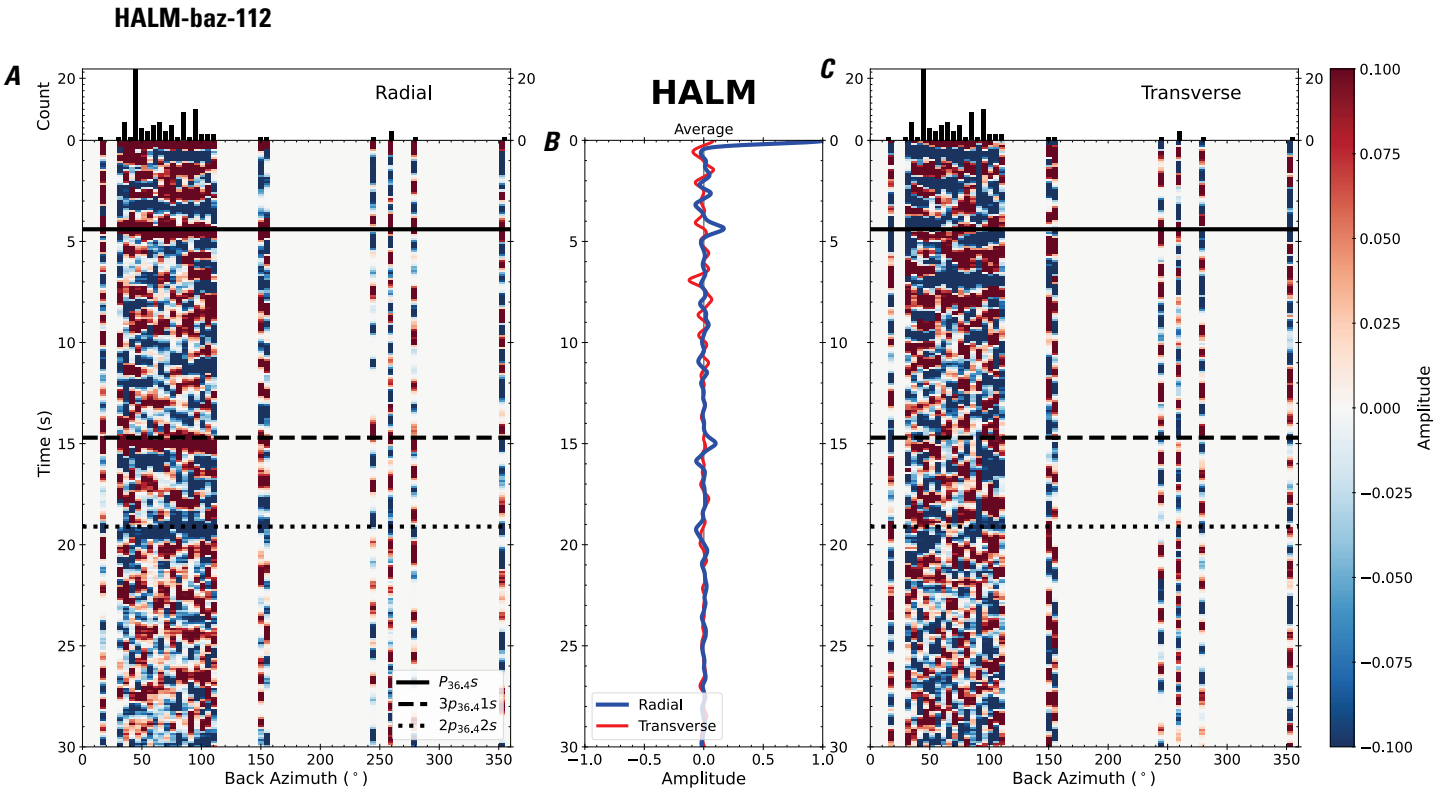

Figure 229. Receiver functions plotted against back azimuth for station HALM. *A*, Radial component of P-wave receiver functions (PRFs) plotted against back azimuth. Individual PRFs have had the resonance-removal filter of Yu and others (2015) applied to them, are normalized to the maximum amplitude within the time window shown, binned, and normalized by the number of traces per bin. *B*, Average of every individual normalized radial receiver function with the application of the resonance-removal filter (blue) and average of every individual normalized raw radial receiver function (red). *C*, Radial component of raw PRFs, plotted against back azimuth, normalized as in *A*. Ps, 3p1s, and 2p2s arrival times predicted for the preferred Moho depth are shown, assuming a ray parameter of 0.06 s/km.

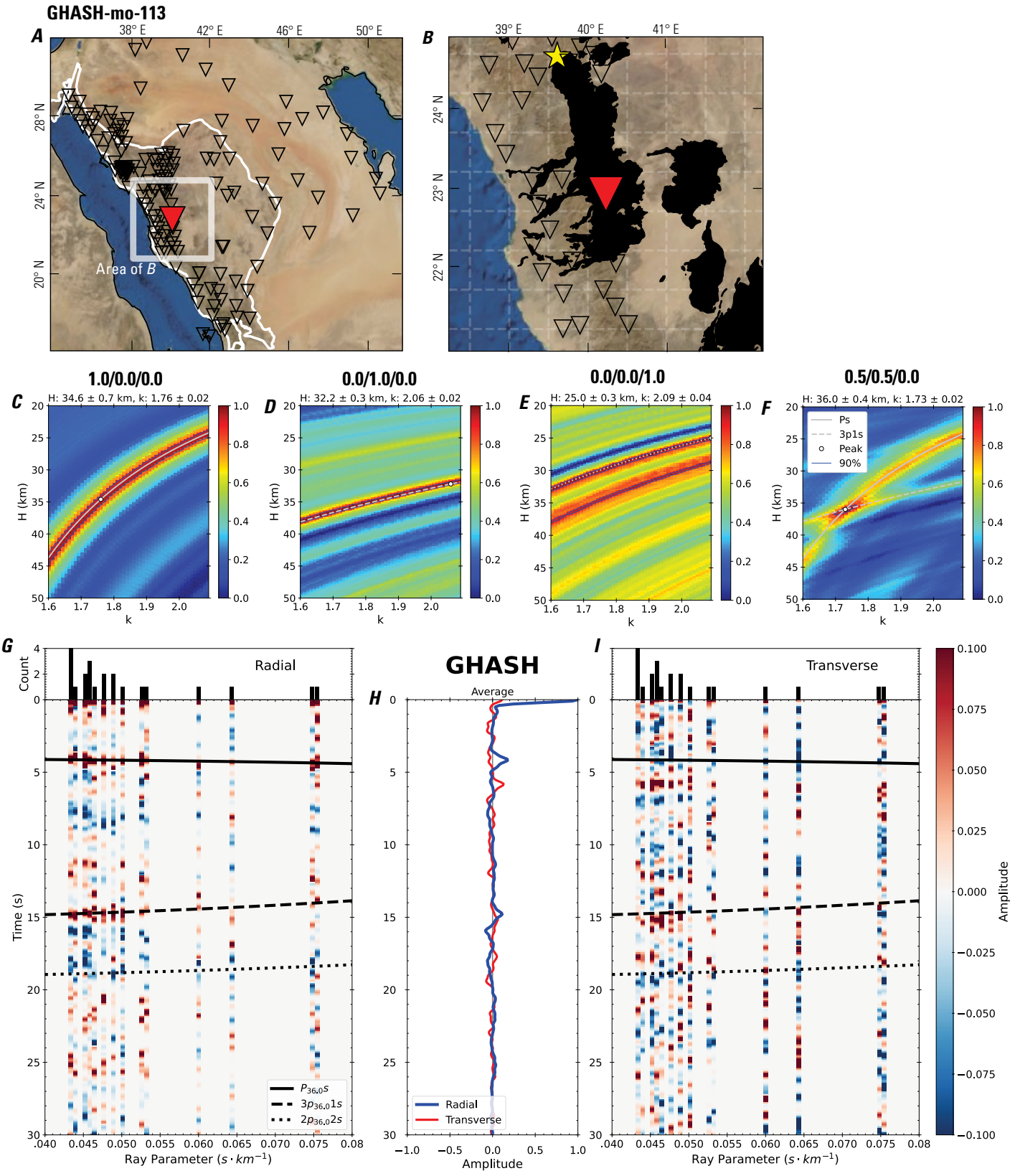
GHASH-mo-113
A
38° E
42° E
46° E
50° E
28° N
24° N
20° N
Area of B
B
39° E
40° E
41° E
24° N
23° N
22° N
1.0/0.0/0.0
C
H: 34.6 ± 0.7 km, k: 1.76 ± 0.02
0.0/1.0/0.0
D
H: 32.2 ± 0.3 km, k: 2.06 ± 0.02
0.0/0.0/1.0
E
H: 25.0 ± 0.3 km, k: 2.09 ± 0.04
0.5/0.5/0.0
F
H: 36.0 ± 0.4 km, k: 1.73 ± 0.02
Ps
3p1s
Peak
90%
H (km)
k
G
Radial
Count
Time (s)
$P_{36.0}s$
$3p_{36.0}1s$
$2p_{36.0}2s$
Ray Parameter ($s \cdot km^{-1}$)
GHASH
H
Average
Radial
Transverse
Amplitude
I
Transverse
Amplitude

Figure 230 (page 236). Receiver-function analysis for station GHASH. *A*, Regional map of Saudi Arabia showing the entire array (as inverted triangles), the location of station GHASH (red inverted triangle), the shield-platform boundary (white line), and the bounds of the map in *B* (white box). *B*, Local map of station GHASH. Harrats are shown in black. *C*, Standard, single-layer *H-k* stack with stacking weights 0.4/0.3/0.3. This *H-k* stack ignores sedimentary effects on the receiver functions. *D*, Standard, single-layer *H-k* stack with stacking weights 0.5/0.5/0.0. This *H-k* stack also ignores sedimentary effects on the receiver functions. *E*, Optimized sub-sedimentary *H-k* stack with stacking weights 0.4/0.3/0.3, following the method of Yu and others (2015). *F*, Optimized sedimentary *H-k* stack with stacking weights 0.05/0.70/0.25, following the method of Yu and others (2015). *G*, Radial component P-wave receiver functions (PRFs) plotted against ray parameter. Individual PRFs have had the resonance-removal filter of Yu and others (2015) applied to them and are normalized to the maximum amplitude within the time window shown, binned, and normalized by the number of traces per bin. *H*, Average of every individual normalized radial receiver function with the application of the resonance-removal filter (blue) and average of every individual normalized raw radial receiver function (red). *I*, Radial component of raw PRFs (that is, PRFs with no resonance-removal filter applied) plotted against ray parameter, normalized as in *G*.

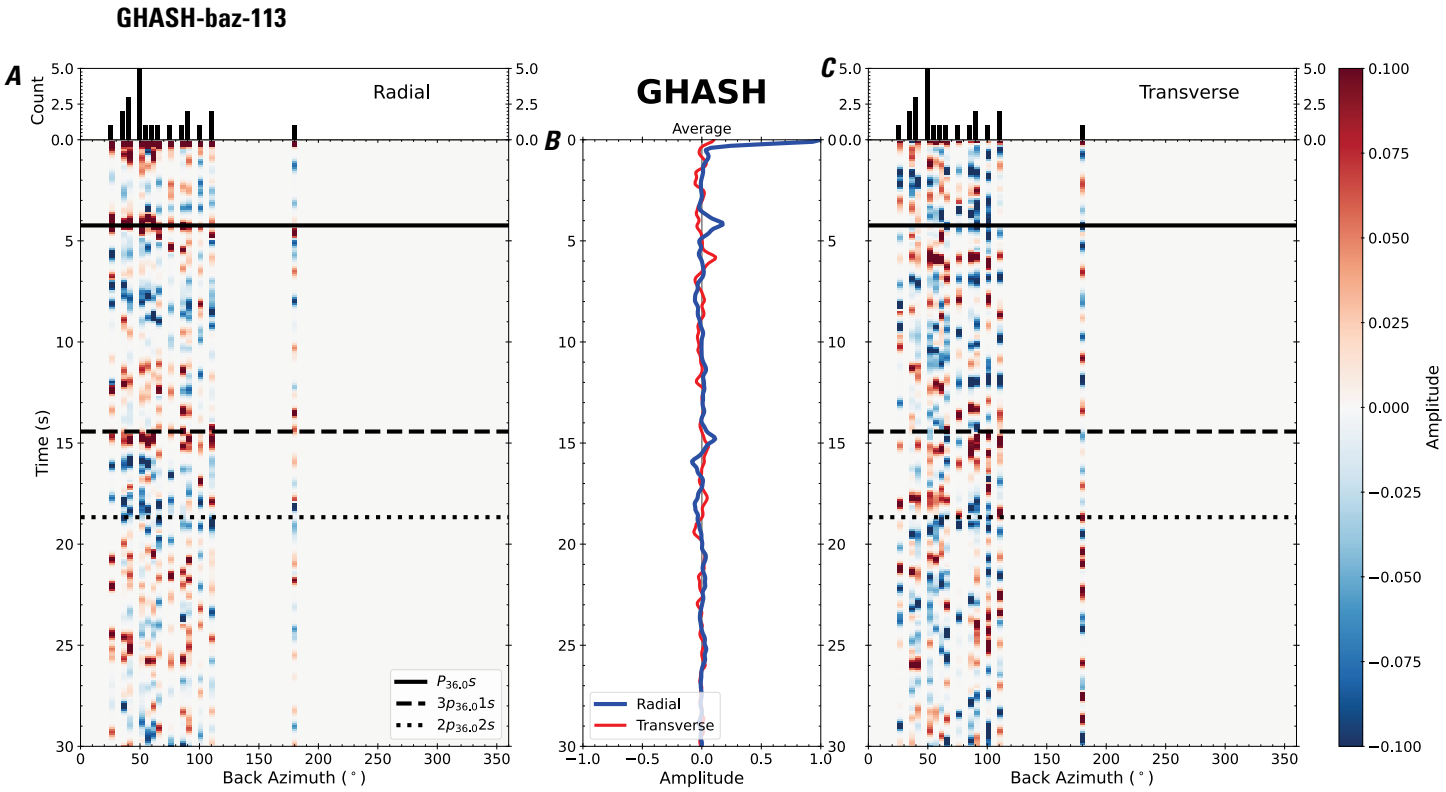

Figure 231. Receiver functions plotted against back azimuth for station GHASH. *A*, Radial component of P-wave receiver functions (PRFs) plotted against back azimuth. Individual PRFs have had the resonance-removal filter of Yu and others (2015) applied to them, are normalized to the maximum amplitude within the time window shown, binned, and normalized by the number of traces per bin. *B*, Average of every individual normalized radial receiver function with the application of the resonance-removal filter (blue) and average of every individual normalized raw radial receiver function (red). *C*, Radial component of raw PRFs, plotted against back azimuth, normalized as in *A*. Ps, 3p1s, and 2p2s arrival times predicted for the preferred Moho depth are shown, assuming a ray parameter of 0.06 s/km.

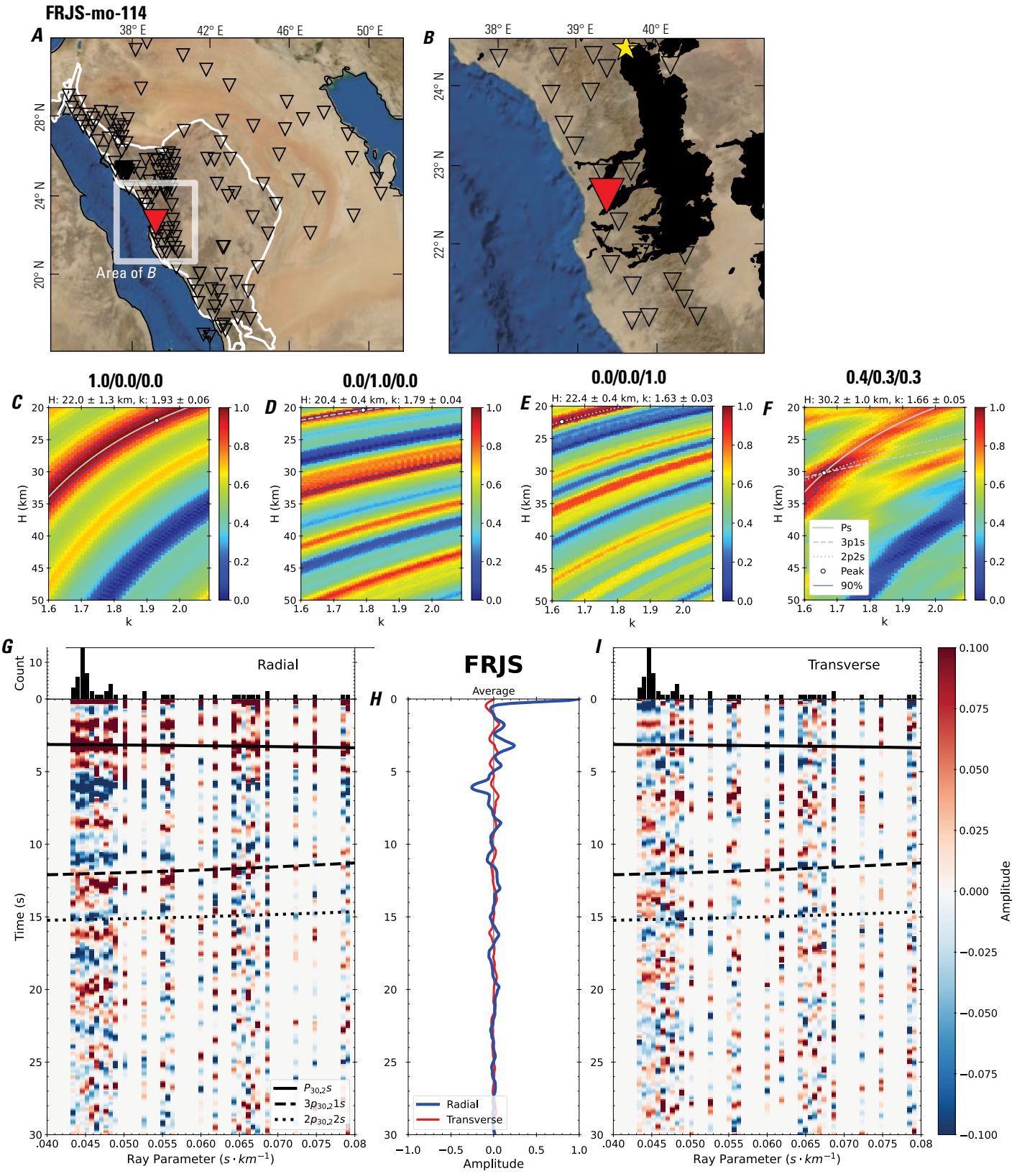
FRJS-mo-114
A
38° E
42° E
46° E
50° E
28° N
24° N
20° N
Area of B
B
38° E
39° E
40° E
24° N
23° N
22° N
1.0/0.0/0.0
0.0/1.0/0.0
0.0/0.0/1.0
0.4/0.3/0.3
C
H: 22.0 ± 1.3 km, k: 1.93 ± 0.06
D
H: 20.4 ± 0.4 km, k: 1.79 ± 0.04
E
H: 22.4 ± 0.4 km, k: 1.63 ± 0.03
F
H: 30.2 ± 1.0 km, k: 1.66 ± 0.05
H (km)
k
Ps
3p1s
2p2s
Peak
90%
G
Radial
Count
Time (s)
$P_{30.2}s$
$3p_{30.2}1s$
$2p_{30.2}2s$
Ray Parameter ($s \cdot km^{-1}$)
FRJS
Average
H
Radial
Transverse
Amplitude
I
Transverse
Ray Parameter ($s \cdot km^{-1}$)
Amplitude

Figure 232 (page 238). Receiver-function analysis for station FRJS. *A*, Regional map of Saudi Arabia showing the entire array (as inverted triangles), the location of station FRJS (red inverted triangle), the shield-platform boundary (white line), and the bounds of the map in *B* (white box). *B*, Local map of station FRJS. Harrats are shown in black. *C*, Standard, single-layer *H-k* stack with stacking weights 0.4/0.3/0.3. This *H-k* stack ignores sedimentary effects on the receiver functions. *D*, Standard, single-layer *H-k* stack with stacking weights 0.5/0.5/0.0. This *H-k* stack also ignores sedimentary effects on the receiver functions. *E*, Optimized sub-sedimentary *H-k* stack with stacking weights 0.4/0.3/0.3, following the method of Yu and others (2015). *F*, Optimized sedimentary *H-k* stack with stacking weights 0.05/0.70/0.25, following the method of Yu and others (2015). *G*, Radial component P-wave receiver functions (PRFs) plotted against ray parameter. Individual PRFs have had the resonance-removal filter of Yu and others (2015) applied to them and are normalized to the maximum amplitude within the time window shown, binned, and normalized by the number of traces per bin. *H*, Average of every individual normalized radial receiver function with the application of the resonance-removal filter (blue) and average of every individual normalized raw radial receiver function (red). *I*, Radial component of raw PRFs (that is, PRFs with no resonance-removal filter applied) plotted against ray parameter, normalized as in *G*.

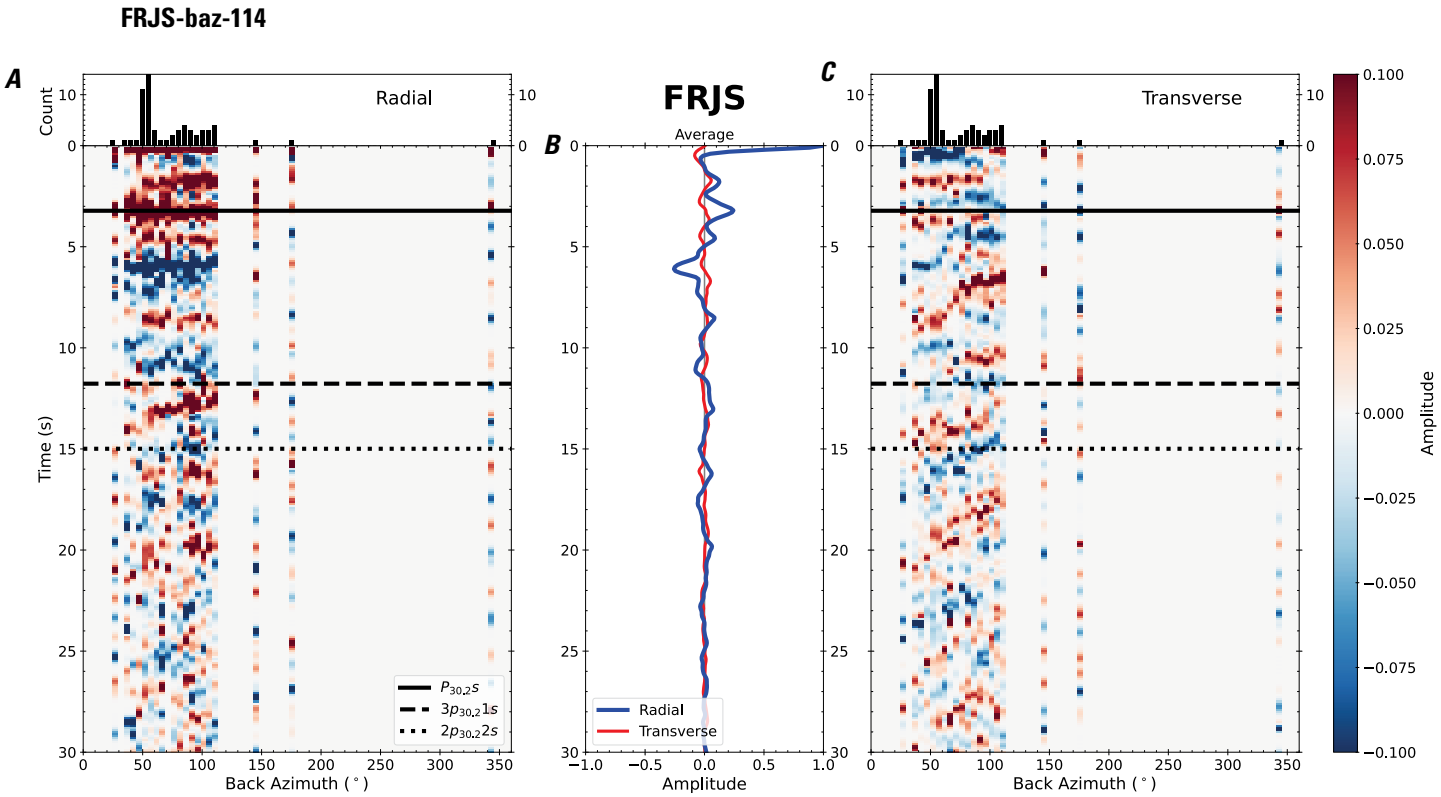

Figure 233. Receiver functions plotted against back azimuth for station FRJS. *A*, Radial component of P-wave receiver functions (PRFs) plotted against back azimuth. Individual PRFs have had the resonance-removal filter of Yu and others (2015) applied to them, are normalized to the maximum amplitude within the time window shown, binned, and normalized by the number of traces per bin. *B*, Average of every individual normalized radial receiver function with the application of the resonance-removal filter (blue) and average of every individual normalized raw radial receiver function (red). *C*, Radial component of raw PRFs, plotted against back azimuth, normalized as in *A*. Ps, 3p1s, and 2p2s arrival times predicted for the preferred Moho depth are shown, assuming a ray parameter of 0.06 s/km.

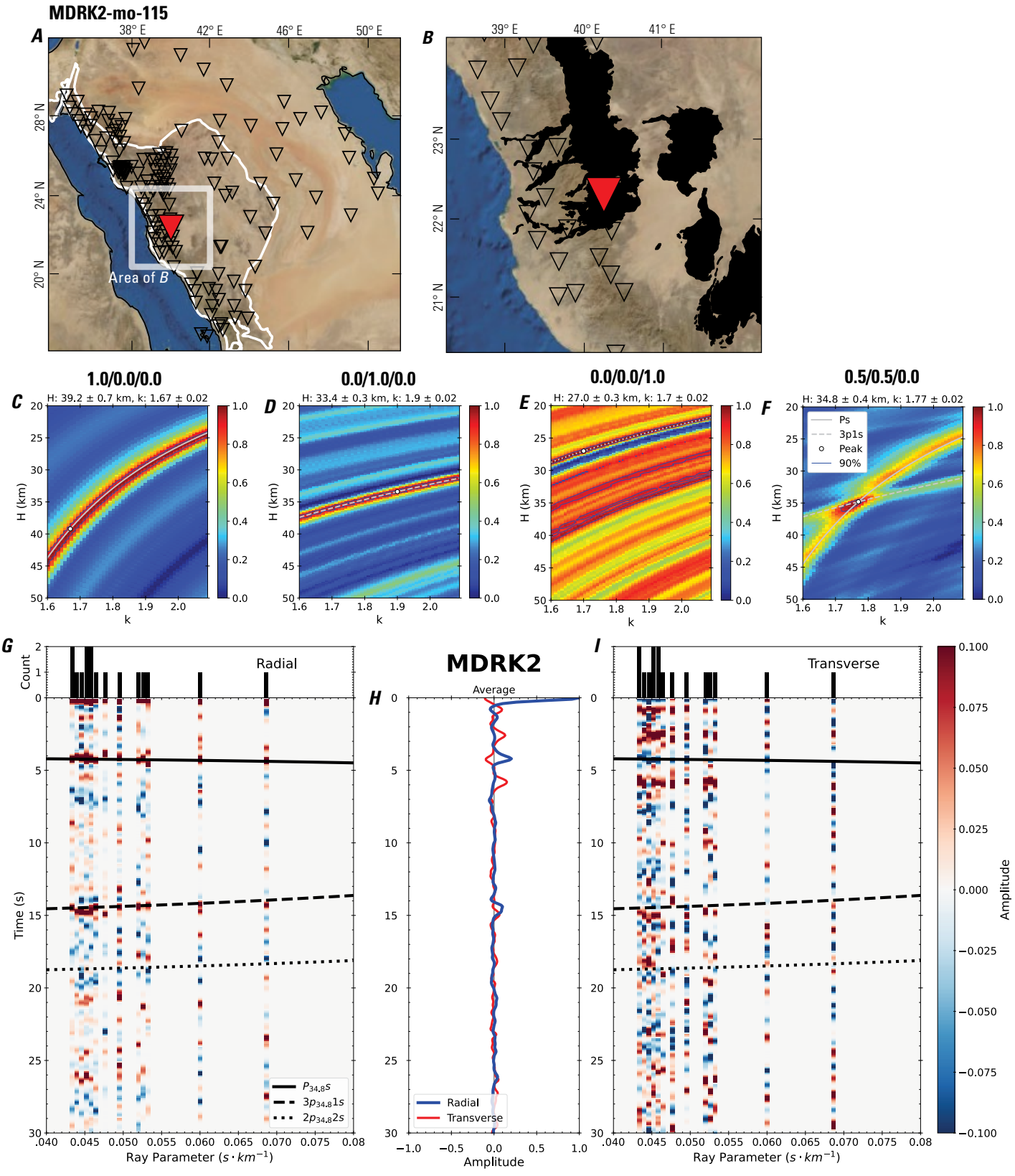
MDRK2-mo-115
A
38° E
42° E
46° E
50° E
28° N
24° N
20° N
Area of B
B
39° E
40° E
41° E
23° N
22° N
21° N
1.0/0.0/0.0
C
H: 39.2 ± 0.7 km, k: 1.67 ± 0.02
0.0/1.0/0.0
D
H: 33.4 ± 0.3 km, k: 1.9 ± 0.02
0.0/0.0/1.0
E
H: 27.0 ± 0.3 km, k: 1.7 ± 0.02
0.5/0.5/0.0
F
H: 34.8 ± 0.4 km, k: 1.77 ± 0.02
Ps
3p1s
Peak
90%
H (km)
k
G
Radial
Count
Time (s)
$P_{34.8}s$
$3p_{34.8}1s$
$2p_{34.8}2s$
Ray Parameter ($s \cdot km^{-1}$)
MDRK2
H
Average
Radial
Transverse
Amplitude
I
Transverse
Amplitude

Figure 234 (page 240). Receiver-function analysis for station MDRK2. *A*, Regional map of Saudi Arabia showing the entire array (as inverted triangles), the location of station MDRK2 (red inverted triangle), the shield-platform boundary (white line), and the bounds of the map in *B* (white box). *B*, Local map of station MDRK2. Harrats are shown in black. *C*, Standard, single-layer *H-k* stack with stacking weights 0.4/0.3/0.3. This *H-k* stack ignores sedimentary effects on the receiver functions. *D*, Standard, single-layer *H-k* stack with stacking weights 0.5/0.5/0.0. This *H-k* stack also ignores sedimentary effects on the receiver functions. *E*, Optimized sub-sedimentary *H-k* stack with stacking weights 0.4/0.3/0.3, following the method of Yu and others (2015). *F*, Optimized sedimentary *H-k* stack with stacking weights 0.05/0.70/0.25, following the method of Yu and others (2015). *G*, Radial component P-wave receiver functions (PRFs) plotted against ray parameter. Individual PRFs have had the resonance-removal filter of Yu and others (2015) applied to them and are normalized to the maximum amplitude within the time window shown, binned, and normalized by the number of traces per bin. *H*, Average of every individual normalized radial receiver function with the application of the resonance-removal filter (blue) and average of every individual normalized raw radial receiver function (red). *I*, Radial component of raw PRFs (that is, PRFs with no resonance-removal filter applied) plotted against ray parameter, normalized as in *G*.

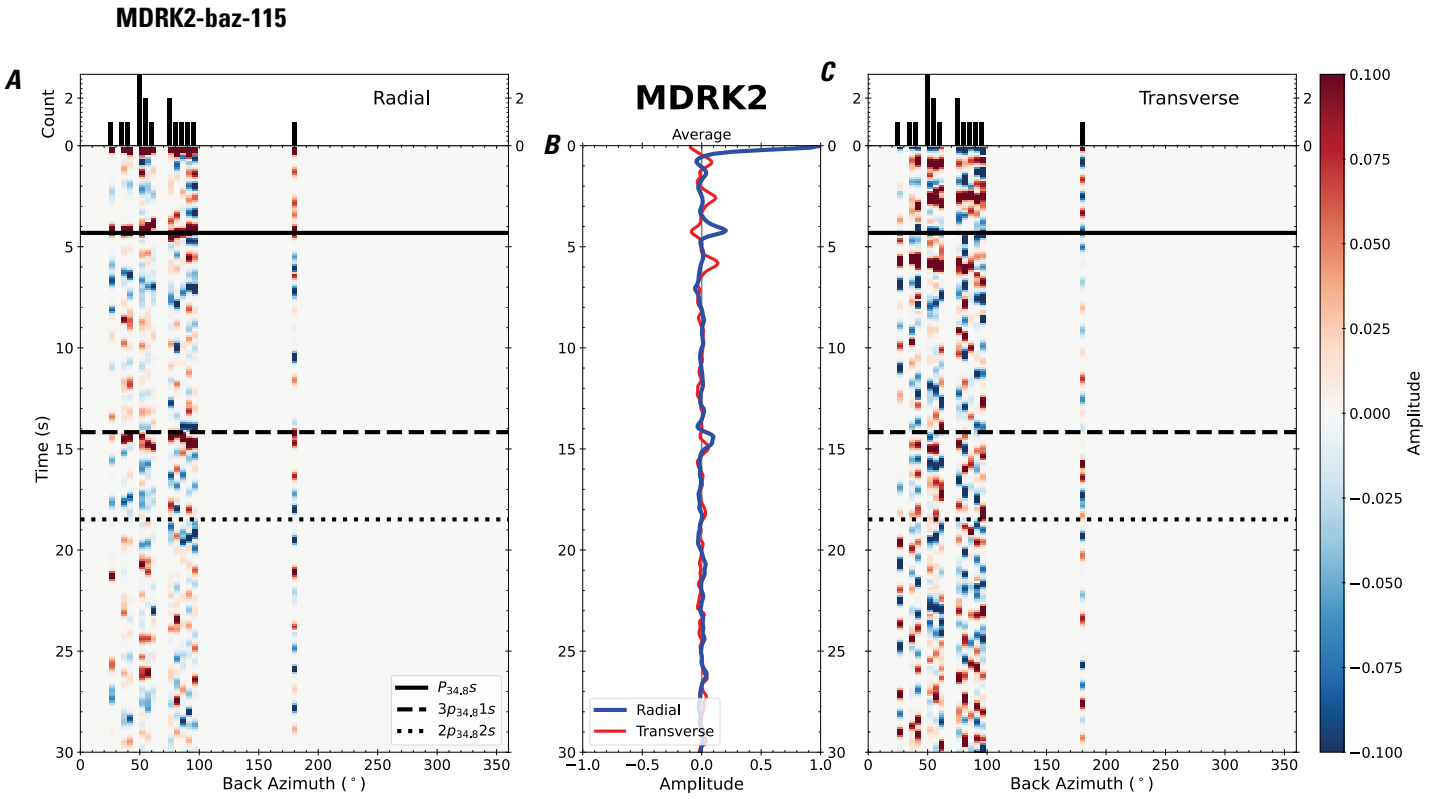

Figure 235. Receiver functions plotted against back azimuth for station MDRK2. *A*, Radial component of P-wave receiver functions (PRFs) plotted against back azimuth. Individual PRFs have had the resonance-removal filter of Yu and others (2015) applied to them, are normalized to the maximum amplitude within the time window shown, binned, and normalized by the number of traces per bin. *B*, Average of every individual normalized radial receiver function with the application of the resonance-removal filter (blue) and average of every individual normalized raw radial receiver function (red). *C*, Radial component of raw PRFs, plotted against back azimuth, normalized as in *A*. Ps, 3p1s, and 2p2s arrival times predicted for the preferred Moho depth are shown, assuming a ray parameter of 0.06 s/km.

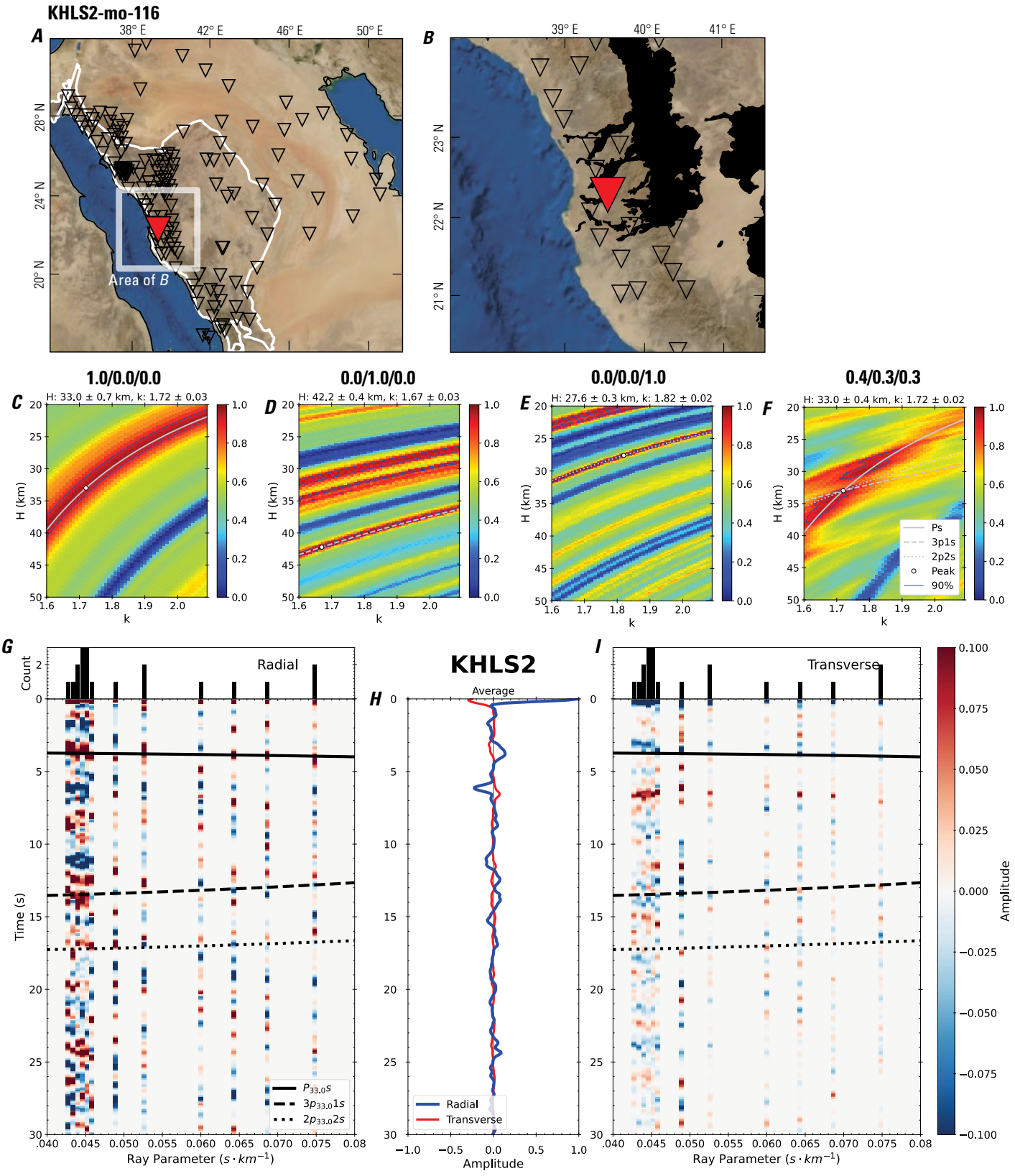
KHLS2-mo-116
A
38° E
42° E
46° E
50° E
28° N
24° N
20° N
Area of B
B
39° E
40° E
41° E
23° N
22° N
21° N
1.0/0.0/0.0
C
H: 33.0 ± 0.7 km, k: 1.72 ± 0.03
0.0/1.0/0.0
D
H: 42.2 ± 0.4 km, k: 1.67 ± 0.03
0.0/0.0/1.0
E
H: 27.6 ± 0.3 km, k: 1.82 ± 0.02
0.4/0.3/0.3
F
H: 33.0 ± 0.4 km, k: 1.72 ± 0.02
H (km)
k
Ps
3p1s
2p2s
Peak
90%
G
Radial
Count
Time (s)
$P_{33.0}s$
$3p_{33.0}1s$
$2p_{33.0}2s$
Ray Parameter ($s \cdot km^{-1}$)
KHLS2
Average
H
Radial
Transverse
Amplitude
I
Transverse
Amplitude

Figure 236 (page 242). Receiver-function analysis for station KHLS2. *A*, Regional map of Saudi Arabia showing the entire array (as inverted triangles), the location of station KHLS2 (red inverted triangle), the shield-platform boundary (white line), and the bounds of the map in *B* (white box). *B*, Local map of station KHLS2. Harrats are shown in black. *C*, Standard, single-layer *H-k* stack with stacking weights 0.4/0.3/0.3. This *H-k* stack ignores sedimentary effects on the receiver functions. *D*, Standard, single-layer *H-k* stack with stacking weights 0.5/0.5/0.0. This *H-k* stack also ignores sedimentary effects on the receiver functions. *E*, Optimized sub-sedimentary *H-k* stack with stacking weights 0.4/0.3/0.3, following the method of Yu and others (2015). *F*, Optimized sedimentary *H-k* stack with stacking weights 0.05/0.70/0.25, following the method of Yu and others (2015). *G*, Radial component P-wave receiver functions (PRFs) plotted against ray parameter. Individual PRFs have had the resonance-removal filter of Yu and others (2015) applied to them and are normalized to the maximum amplitude within the time window shown, binned, and normalized by the number of traces per bin. *H*, Average of every individual normalized radial receiver function with the application of the resonance-removal filter (blue) and average of every individual normalized raw radial receiver function (red). *I*, Radial component of raw PRFs (that is, PRFs with no resonance-removal filter applied) plotted against ray parameter, normalized as in *G*.

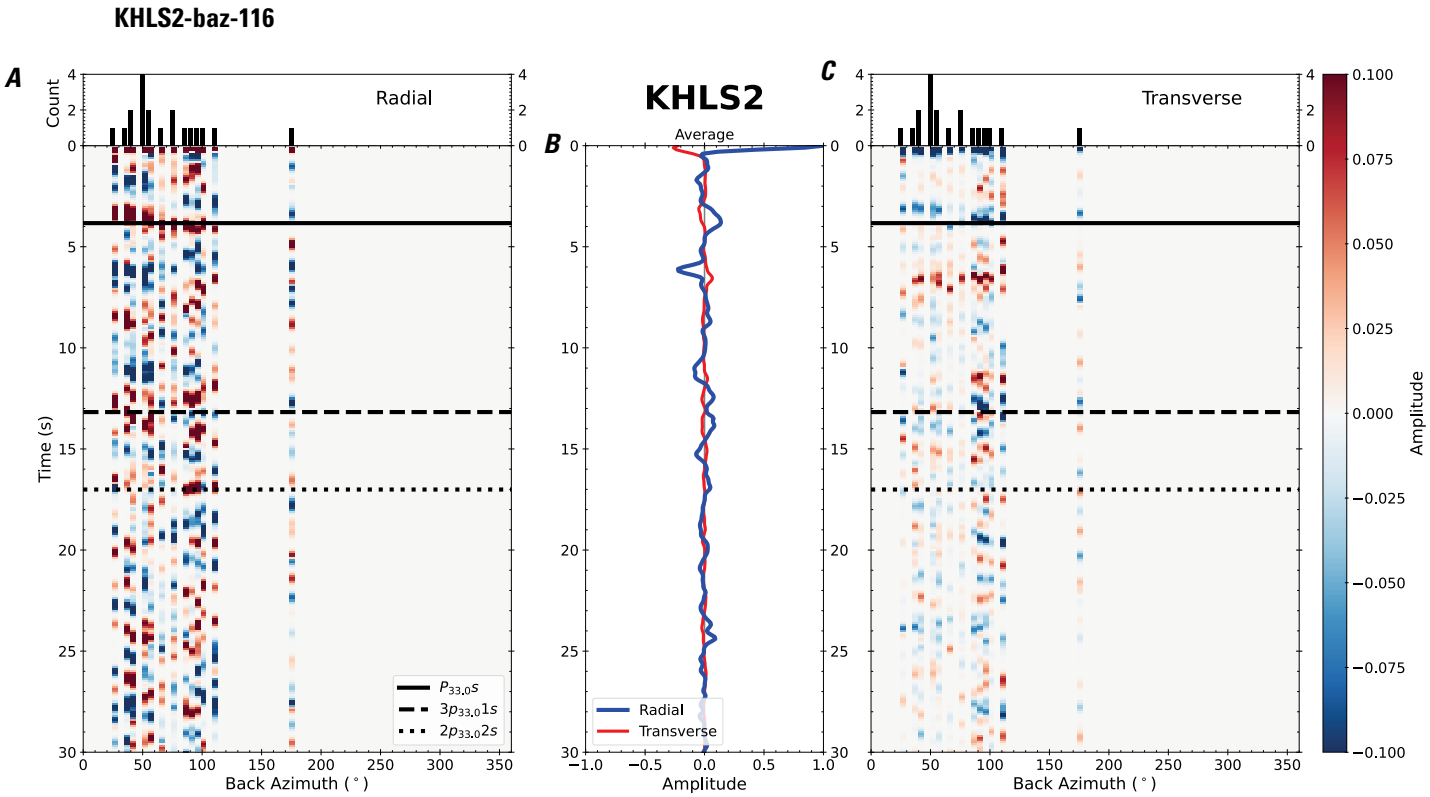

Figure 237. Receiver functions plotted against back azimuth for station KHLS2. *A*, Radial component of P-wave receiver functions (PRFs) plotted against back azimuth. Individual PRFs have had the resonance-removal filter of Yu and others (2015) applied to them, are normalized to the maximum amplitude within the time window shown, binned, and normalized by the number of traces per bin. *B*, Average of every individual normalized radial receiver function with the application of the resonance-removal filter (blue) and average of every individual normalized raw radial receiver function (red). *C*, Radial component of raw PRFs, plotted against back azimuth, normalized as in *A*. Ps, 3p1s, and 2p2s arrival times predicted for the preferred Moho depth are shown, assuming a ray parameter of 0.06 s/km.

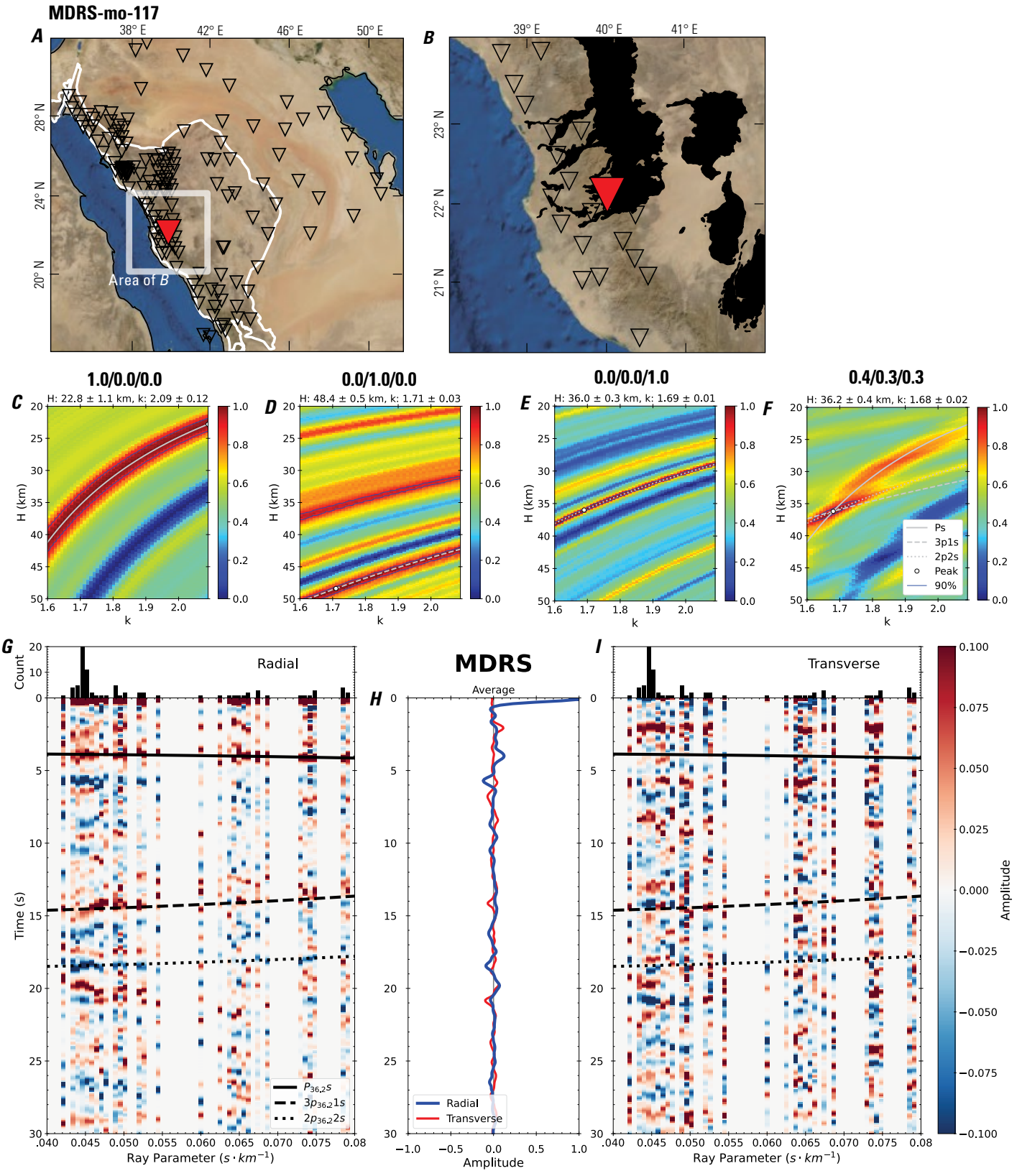
MDRS-mo-117
A
38° E
42° E
46° E
50° E
28° N
24° N
20° N
Area of B
B
39° E
40° E
41° E
23° N
22° N
21° N
1.0/0.0/0.0
C
H: 22.8 ± 1.1 km, k: 2.09 ± 0.12
0.0/1.0/0.0
D
H: 48.4 ± 0.5 km, k: 1.71 ± 0.03
0.0/0.0/1.0
E
H: 36.0 ± 0.3 km, k: 1.69 ± 0.01
0.4/0.3/0.3
F
H: 36.2 ± 0.4 km, k: 1.68 ± 0.02
H (km)
k
Ps
3p1s
2p2s
Peak
90%
G
Radial
Count
Time (s)
$P_{36.2}s$
$3p_{36.2}1s$
$2p_{36.2}2s$
Ray Parameter ($s \cdot km^{-1}$)
MDRS
H
Average
Radial
Transverse
Amplitude
I
Transverse
Amplitude

Figure 238 (page 244). Receiver-function analysis for station MDRS. *A*, Regional map of Saudi Arabia showing the entire array (as inverted triangles), the location of station MDRS (red inverted triangle), the shield-platform boundary (white line), and the bounds of the map in *B* (white box). *B*, Local map of station MDRS. Harrats are shown in black. *C*, Standard, single-layer *H-k* stack with stacking weights 0.4/0.3/0.3. This *H-k* stack ignores sedimentary effects on the receiver functions. *D*, Standard, single-layer *H-k* stack with stacking weights 0.5/0.5/0.0. This *H-k* stack also ignores sedimentary effects on the receiver functions. *E*, Optimized sub-sedimentary *H-k* stack with stacking weights 0.4/0.3/0.3, following the method of Yu and others (2015). *F*, Optimized sedimentary *H-k* stack with stacking weights 0.05/0.70/0.25, following the method of Yu and others (2015). *G*, Radial component P-wave receiver functions (PRFs) plotted against ray parameter. Individual PRFs have had the resonance-removal filter of Yu and others (2015) applied to them and are normalized to the maximum amplitude within the time window shown, binned, and normalized by the number of traces per bin. *H*, Average of every individual normalized radial receiver function with the application of the resonance-removal filter (blue) and average of every individual normalized raw radial receiver function (red). *I*, Radial component of raw PRFs (that is, PRFs with no resonance-removal filter applied) plotted against ray parameter, normalized as in *G*.

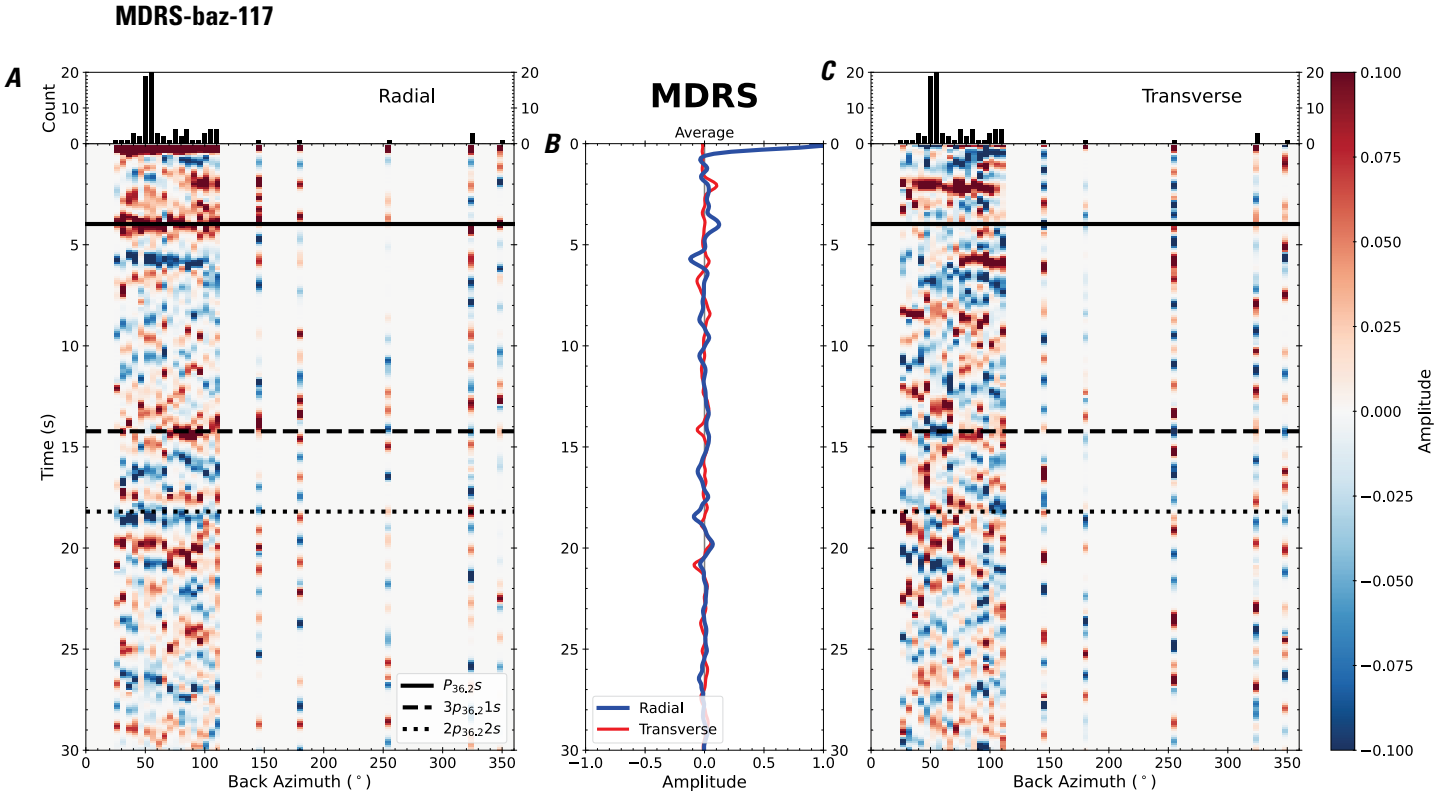

Figure 239. Receiver functions plotted against back azimuth for station MDRS. *A*, Radial component of P-wave receiver functions (PRFs) plotted against back azimuth. Individual PRFs have had the resonance-removal filter of Yu and others (2015) applied to them, are normalized to the maximum amplitude within the time window shown, binned, and normalized by the number of traces per bin. *B*, Average of every individual normalized radial receiver function with the application of the resonance-removal filter (blue) and average of every individual normalized raw radial receiver function (red). *C*, Radial component of raw PRFs, plotted against back azimuth, normalized as in *A*. Ps, 3p1s, and 2p2s arrival times predicted for the preferred Moho depth are shown, assuming a ray parameter of 0.06 s/km.

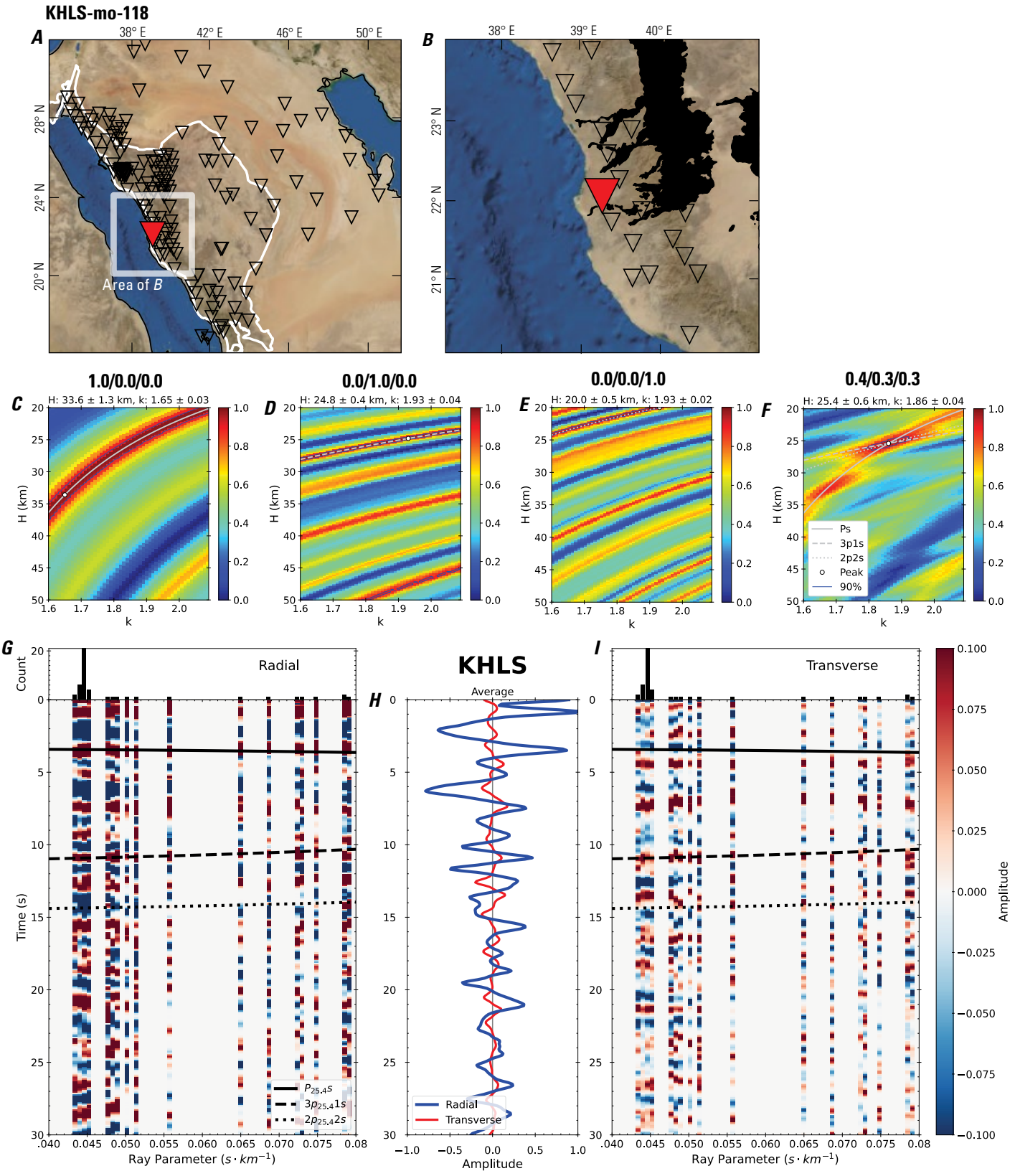
KHLS-mo-118
A
38° E
42° E
46° E
50° E
28° N
24° N
20° N
Area of B
B
38° E
39° E
40° E
23° N
22° N
21° N
1.0/0.0/0.0
0.0/1.0/0.0
0.0/0.0/1.0
0.4/0.3/0.3
C
H: 33.6 ± 1.3 km, k: 1.65 ± 0.03
D
H: 24.8 ± 0.4 km, k: 1.93 ± 0.04
E
H: 20.0 ± 0.5 km, k: 1.93 ± 0.02
F
H: 25.4 ± 0.6 km, k: 1.86 ± 0.04
H (km)
k
Ps
3p1s
2p2s
Peak
90%
G
Radial
Count
Time (s)
$P_{25.4}s$
$3p_{25.4}1s$
$2p_{25.4}2s$
Ray Parameter ($s \cdot km^{-1}$)
KHLS
Average
H
Radial
Transverse
Amplitude
I
Transverse
Amplitude

Figure 240 (page 246). Receiver-function analysis for station KHLS. *A*, Regional map of Saudi Arabia showing the entire array (as inverted triangles), the location of station KHLS (red inverted triangle), the shield-platform boundary (white line), and the bounds of the map in *B* (white box). *B*, Local map of station KHLS. Harrats are shown in black. *C*, Standard, single-layer *H-k* stack with stacking weights 0.4/0.3/0.3. This *H-k* stack ignores sedimentary effects on the receiver functions. *D*, Standard, single-layer *H-k* stack with stacking weights 0.5/0.5/0.0. This *H-k* stack also ignores sedimentary effects on the receiver functions. *E*, Optimized sub-sedimentary *H-k* stack with stacking weights 0.4/0.3/0.3, following the method of Yu and others (2015). *F*, Optimized sedimentary *H-k* stack with stacking weights 0.05/0.70/0.25, following the method of Yu and others (2015). *G*, Radial component P-wave receiver functions (PRFs) plotted against ray parameter. Individual PRFs have had the resonance-removal filter of Yu and others (2015) applied to them and are normalized to the maximum amplitude within the time window shown, binned, and normalized by the number of traces per bin. *H*, Average of every individual normalized radial receiver function with the application of the resonance-removal filter (blue) and average of every individual normalized raw radial receiver function (red). *I*, Radial component of raw PRFs (that is, PRFs with no resonance-removal filter applied) plotted against ray parameter, normalized as in *G*.

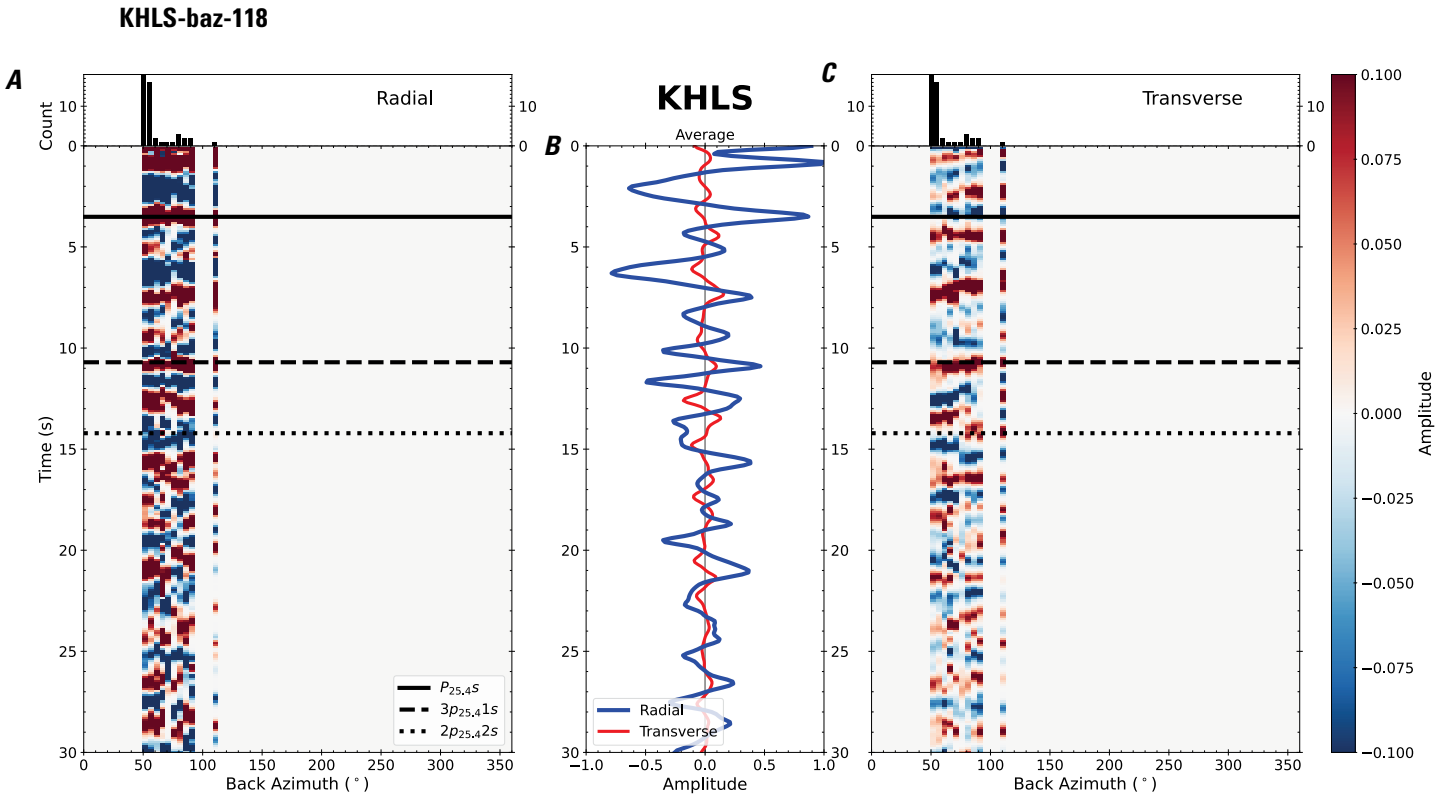

Figure 241. Receiver functions plotted against back azimuth for station KHLS. *A*, Radial component of P-wave receiver functions (PRFs) plotted against back azimuth. Individual PRFs have had the resonance-removal filter of Yu and others (2015) applied to them, are normalized to the maximum amplitude within the time window shown, binned, and normalized by the number of traces per bin. *B*, Average of every individual normalized radial receiver function with the application of the resonance-removal filter (blue) and average of every individual normalized raw radial receiver function (red). *C*, Radial component of raw PRFs, plotted against back azimuth, normalized as in *A*. Ps, 3p1s, and 2p2s arrival times predicted for the preferred Moho depth are shown, assuming a ray parameter of 0.06 s/km.

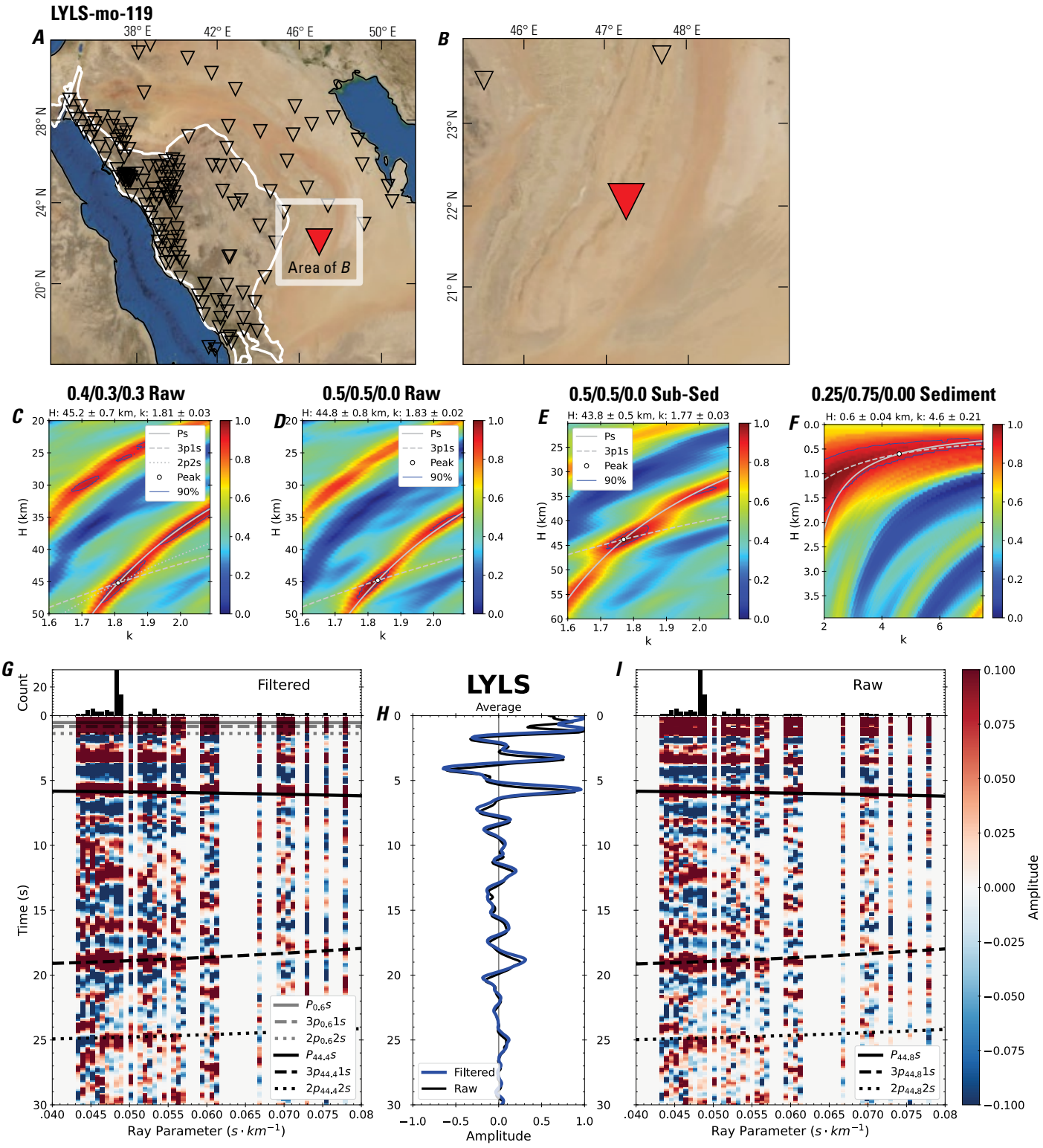
LYLS-mo-119
A
38° E
42° E
46° E
50° E
28° N
24° N
20° N
Area of B
B
46° E
47° E
48° E
23° N
22° N
21° N
0.4/0.3/0.3 Raw
C
H: 45.2 ± 0.7 km, k: 1.81 ± 0.03
0.5/0.5/0.0 Raw
D
H: 44.8 ± 0.8 km, k: 1.83 ± 0.02
0.5/0.5/0.0 Sub-Sed
E
H: 43.8 ± 0.5 km, k: 1.77 ± 0.03
0.25/0.75/0.00 Sediment
F
H: 0.6 ± 0.04 km, k: 4.6 ± 0.21
Ps
3p1s
2p2s
Peak
90%
H (km)
k
G
Filtered
Count
Time (s)
$P_{0.6}s$
$3p_{0.6}1s$
$2p_{0.6}2s$
$P_{44.4}s$
$3p_{44.4}1s$
$2p_{44.4}2s$
Ray Parameter ($s \cdot km^{-1}$)
LYLS
Average
H
Filtered
Raw
Amplitude
I
Raw
$P_{44.8}s$
$3p_{44.8}1s$
$2p_{44.8}2s$
Amplitude

Figure 242 (page 248). Receiver-function analysis for station LYLS. *A*, Regional map of Saudi Arabia showing the entire array (as inverted triangles), the location of station LYLS (red inverted triangle), the shield-platform boundary (white line), and the bounds of the map in *B* (white box). *B*, Local map of station LYLS. Harrats are shown in black. *C*, Standard, single-layer *H-k* stack with stacking weights 0.4/0.3/0.3. This *H-k* stack ignores sedimentary effects on the receiver functions. *D*, Standard, single-layer *H-k* stack with stacking weights 0.5/0.5/0.0. This *H-k* stack also ignores sedimentary effects on the receiver functions. *E*, Optimized sub-sedimentary *H-k* stack with stacking weights 0.4/0.3/0.3, following the method of Yu and others (2015). *F*, Optimized sedimentary *H-k* stack with stacking weights 0.05/0.70/0.25, following the method of Yu and others (2015). *G*, Radial component P-wave receiver functions (PRFs) plotted against ray parameter. Individual PRFs have had the resonance-removal filter of Yu and others (2015) applied to them and are normalized to the maximum amplitude within the time window shown, binned, and normalized by the number of traces per bin. *H*, Average of every individual normalized radial receiver function with the application of the resonance-removal filter (blue) and average of every individual normalized raw radial receiver function (red). *I*, Radial component of raw PRFs (that is, PRFs with no resonance-removal filter applied) plotted against ray parameter, normalized as in *G*.

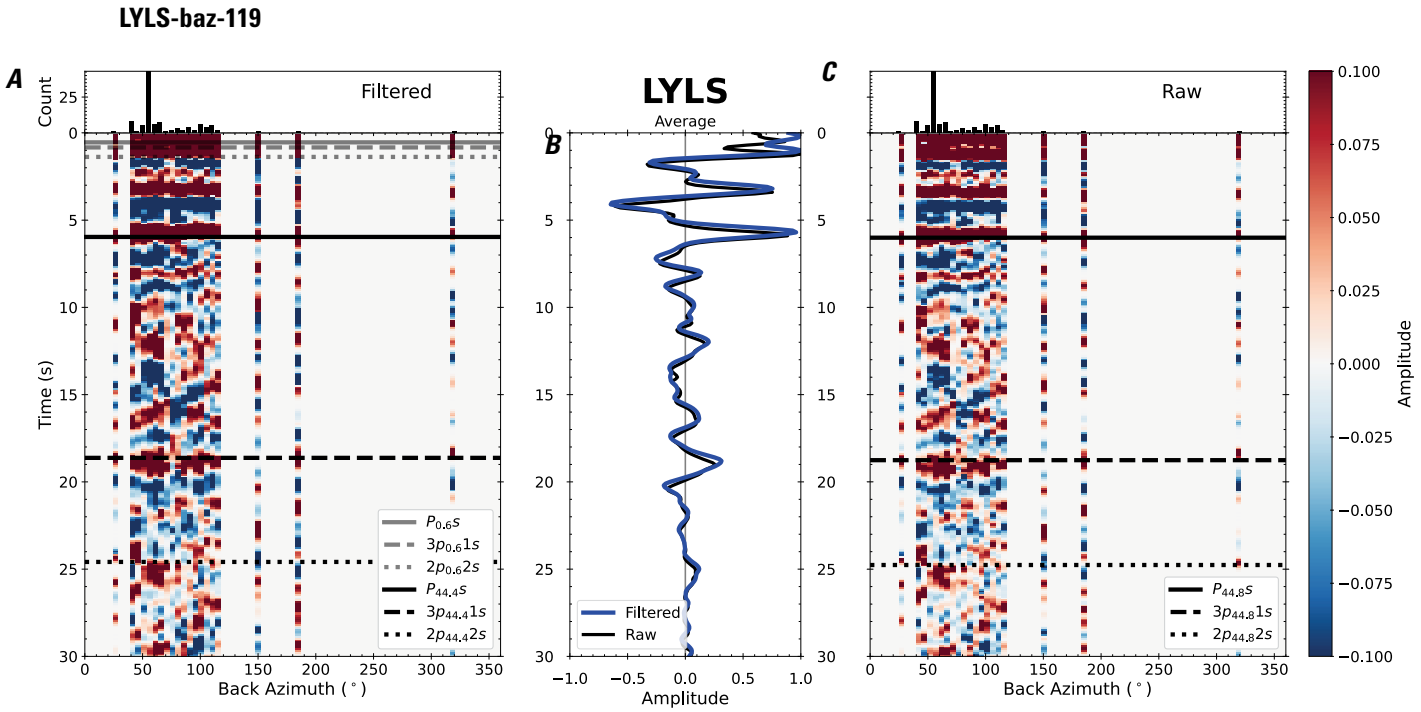

Figure 243. Receiver functions plotted against back azimuth for station LYLS. *A*, Radial component of P-wave receiver functions (PRFs) plotted against back azimuth. Individual PRFs have had the resonance-removal filter of Yu and others (2015) applied to them, are normalized to the maximum amplitude within the time window shown, binned, and normalized by the number of traces per bin. *B*, Average of every individual normalized radial receiver function with the application of the resonance-removal filter (blue) and average of every individual normalized raw radial receiver function (red). *C*, Radial component of raw PRFs, plotted against back azimuth, normalized as in *A*. Ps, 3p1s, and 2p2s arrival times predicted for the preferred Moho depth are shown, assuming a ray parameter of 0.06 s/km.

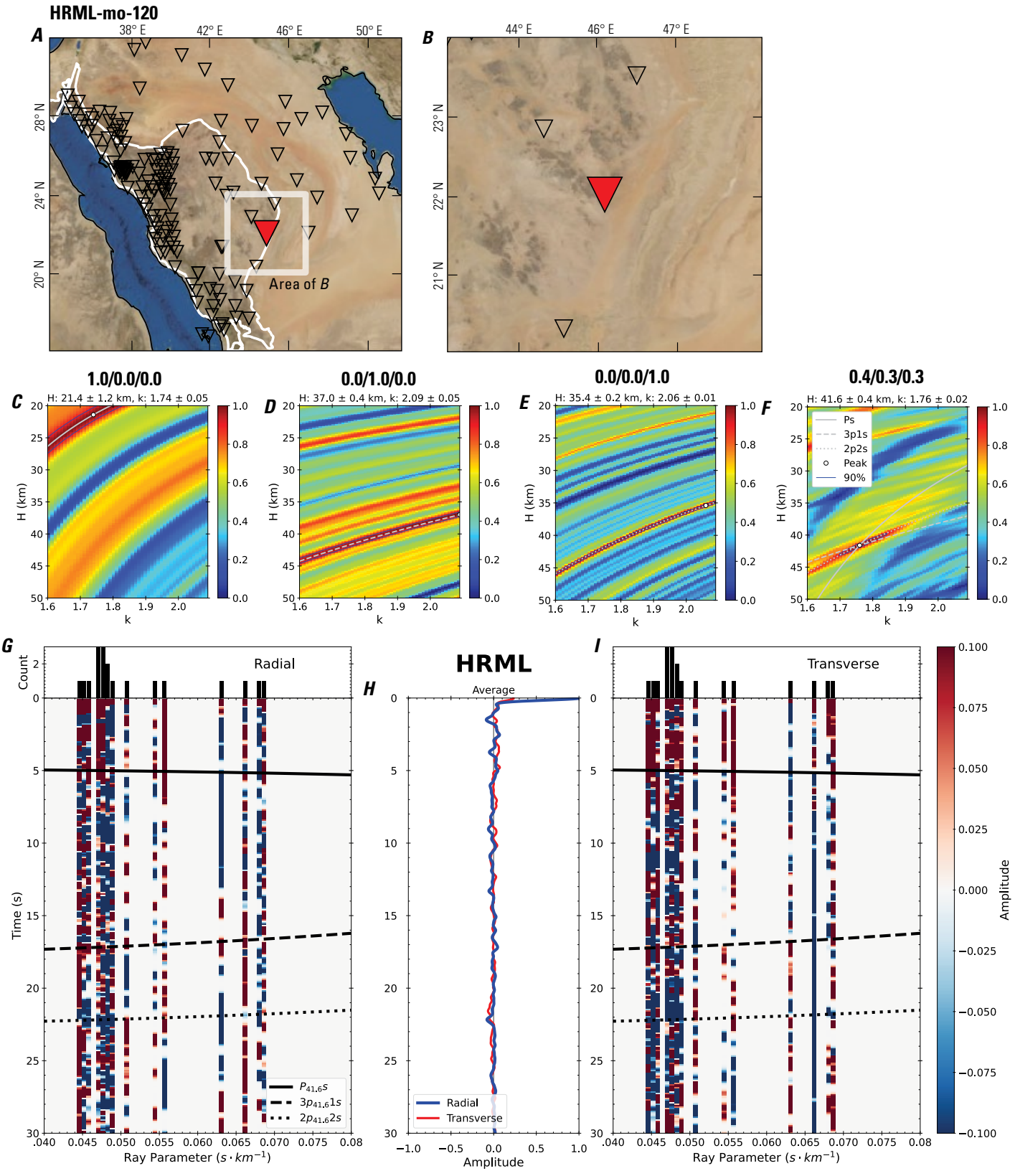
HRML-mo-120
A
38° E
42° E
46° E
50° E
28° N
24° N
20° N
Area of B
B
44° E
46° E
47° E
23° N
22° N
21° N
1.0/0.0/0.0
0.0/1.0/0.0
0.0/0.0/1.0
0.4/0.3/0.3
C
H: 21.4 ± 1.2 km, k: 1.74 ± 0.05
D
H: 37.0 ± 0.4 km, k: 2.09 ± 0.05
E
H: 35.4 ± 0.2 km, k: 2.06 ± 0.01
F
H: 41.6 ± 0.4 km, k: 1.76 ± 0.02
H (km)
k
Ps
3p1s
2p2s
Peak
90%
G
Radial
Count
Time (s)
Ray Parameter (s · km⁻¹)
$P_{41.6}s$
$3p_{41.6}1s$
$2p_{41.6}2s$
H
HRML
Average
Radial
Transverse
Amplitude
I
Transverse
Amplitude

Figure 244 (page 250). Receiver-function analysis for station HRML. *A*, Regional map of Saudi Arabia showing the entire array (as inverted triangles), the location of station HRML (red inverted triangle), the shield-platform boundary (white line), and the bounds of the map in *B* (white box). *B*, Local map of station HRML. Harrats are shown in black. *C*, Standard, single-layer *H-k* stack with stacking weights 0.4/0.3/0.3. This *H-k* stack ignores sedimentary effects on the receiver functions. *D*, Standard, single-layer *H-k* stack with stacking weights 0.5/0.5/0.0. This *H-k* stack also ignores sedimentary effects on the receiver functions. *E*, Optimized sub-sedimentary *H-k* stack with stacking weights 0.4/0.3/0.3, following the method of Yu and others (2015). *F*, Optimized sedimentary *H-k* stack with stacking weights 0.05/0.70/0.25, following the method of Yu and others (2015). *G*, Radial component P-wave receiver functions (PRFs) plotted against ray parameter. Individual PRFs have had the resonance-removal filter of Yu and others (2015) applied to them and are normalized to the maximum amplitude within the time window shown, binned, and normalized by the number of traces per bin. *H*, Average of every individual normalized radial receiver function with the application of the resonance-removal filter (blue) and average of every individual normalized raw radial receiver function (red). *I*, Radial component of raw PRFs (that is, PRFs with no resonance-removal filter applied) plotted against ray parameter, normalized as in *G*.

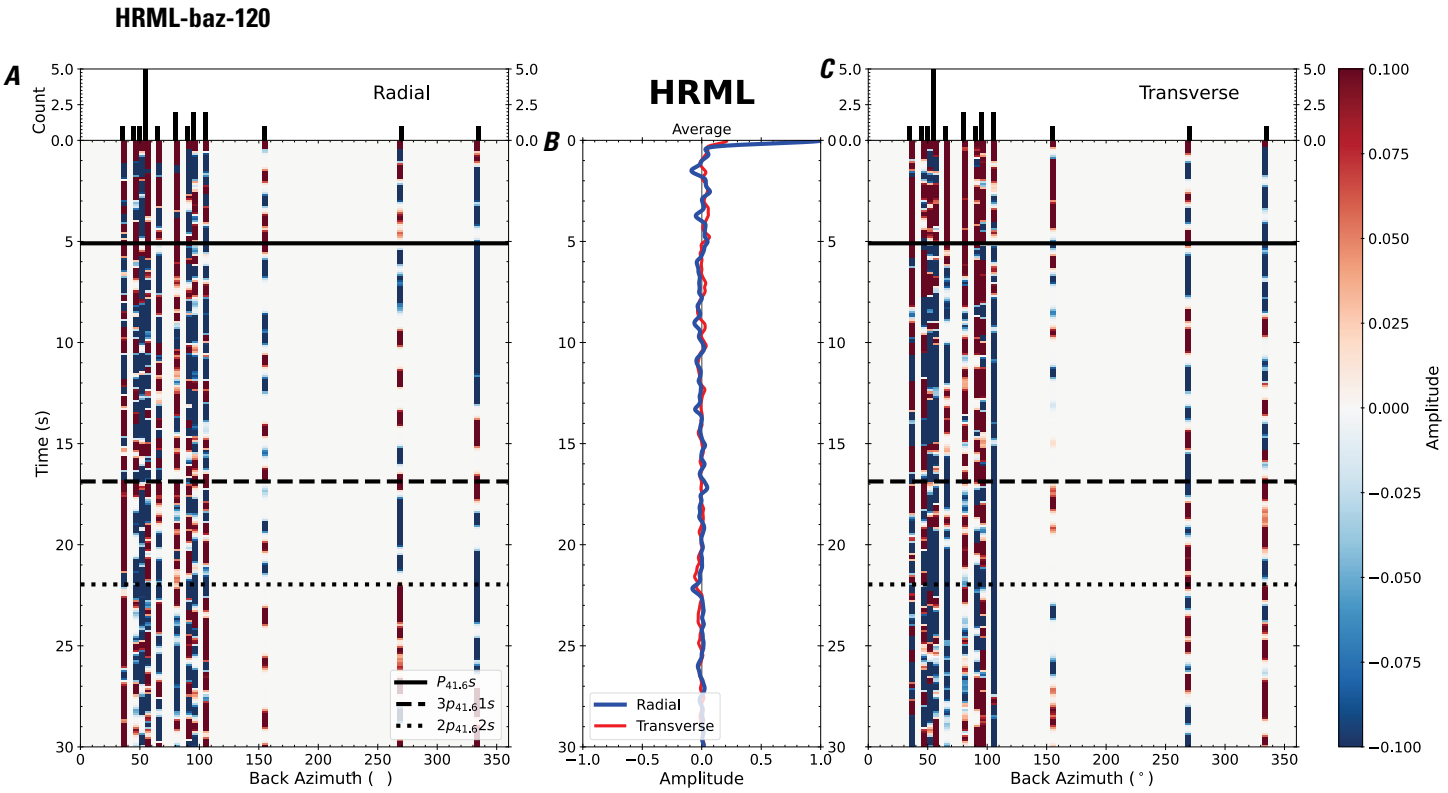

Figure 245. Receiver functions plotted against back azimuth for station HRML. *A*, Radial component of P-wave receiver functions (PRFs) plotted against back azimuth. Individual PRFs have had the resonance-removal filter of Yu and others (2015) applied to them, are normalized to the maximum amplitude within the time window shown, binned, and normalized by the number of traces per bin. *B*, Average of every individual normalized radial receiver function with the application of the resonance-removal filter (blue) and average of every individual normalized raw radial receiver function (red). *C*, Radial component of raw PRFs, plotted against back azimuth, normalized as in *A*. Ps, 3p1s, and 2p2s arrival times predicted for the preferred Moho depth are shown, assuming a ray parameter of 0.06 s/km.

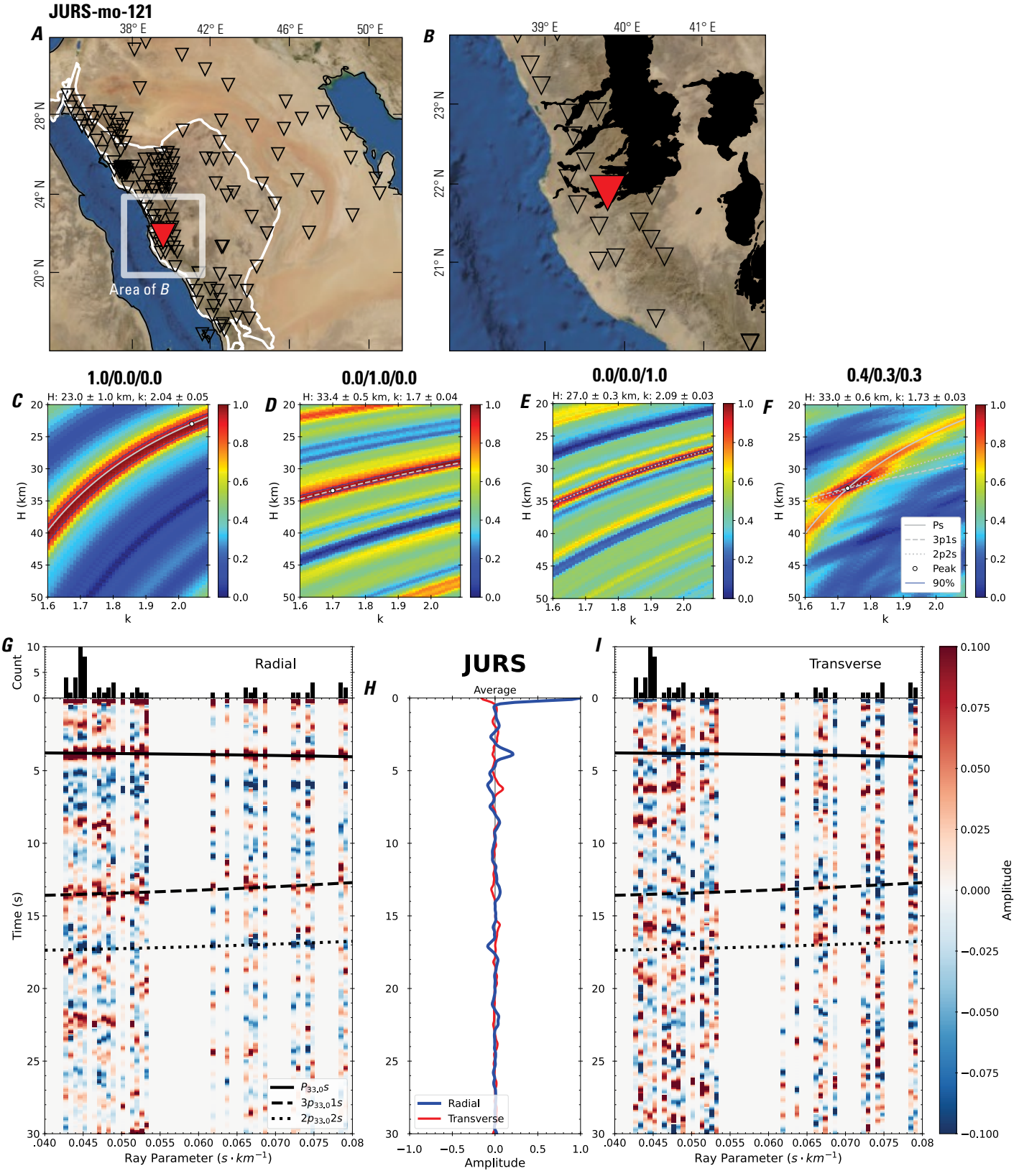
JURS-mo-121
A
38° E
42° E
46° E
50° E
28° N
24° N
20° N
Area of B
B
39° E
40° E
41° E
23° N
22° N
21° N
1.0/0.0/0.0
C
H: 23.0 ± 1.0 km, k: 2.04 ± 0.05
0.0/1.0/0.0
D
H: 33.4 ± 0.5 km, k: 1.7 ± 0.04
0.0/0.0/1.0
E
H: 27.0 ± 0.3 km, k: 2.09 ± 0.03
0.4/0.3/0.3
F
H: 33.0 ± 0.6 km, k: 1.73 ± 0.03
H (km)
k
Ps
3p1s
2p2s
Peak
90%
G
Radial
Count
Time (s)
$P_{33,0}s$
$3p_{33,0}1s$
$2p_{33,0}2s$
Ray Parameter ($s \cdot km^{-1}$)
H
JURS
Average
Radial
Transverse
Amplitude
I
Transverse
Amplitude

Figure 246 (page 252). Receiver-function analysis for station JURS. *A*, Regional map of Saudi Arabia showing the entire array (as inverted triangles), the location of station JURS (red inverted triangle), the shield-platform boundary (white line), and the bounds of the map in *B* (white box). *B*, Local map of station JURS. Harrats are shown in black. *C*, Standard, single-layer *H-k* stack with stacking weights 0.4/0.3/0.3. This *H-k* stack ignores sedimentary effects on the receiver functions. *D*, Standard, single-layer *H-k* stack with stacking weights 0.5/0.5/0.0. This *H-k* stack also ignores sedimentary effects on the receiver functions. *E*, Optimized sub-sedimentary *H-k* stack with stacking weights 0.4/0.3/0.3, following the method of Yu and others (2015). *F*, Optimized sedimentary *H-k* stack with stacking weights 0.05/0.70/0.25, following the method of Yu and others (2015). *G*, Radial component P-wave receiver functions (PRFs) plotted against ray parameter. Individual PRFs have had the resonance-removal filter of Yu and others (2015) applied to them and are normalized to the maximum amplitude within the time window shown, binned, and normalized by the number of traces per bin. *H*, Average of every individual normalized radial receiver function with the application of the resonance-removal filter (blue) and average of every individual normalized raw radial receiver function (red). *I*, Radial component of raw PRFs (that is, PRFs with no resonance-removal filter applied) plotted against ray parameter, normalized as in *G*.

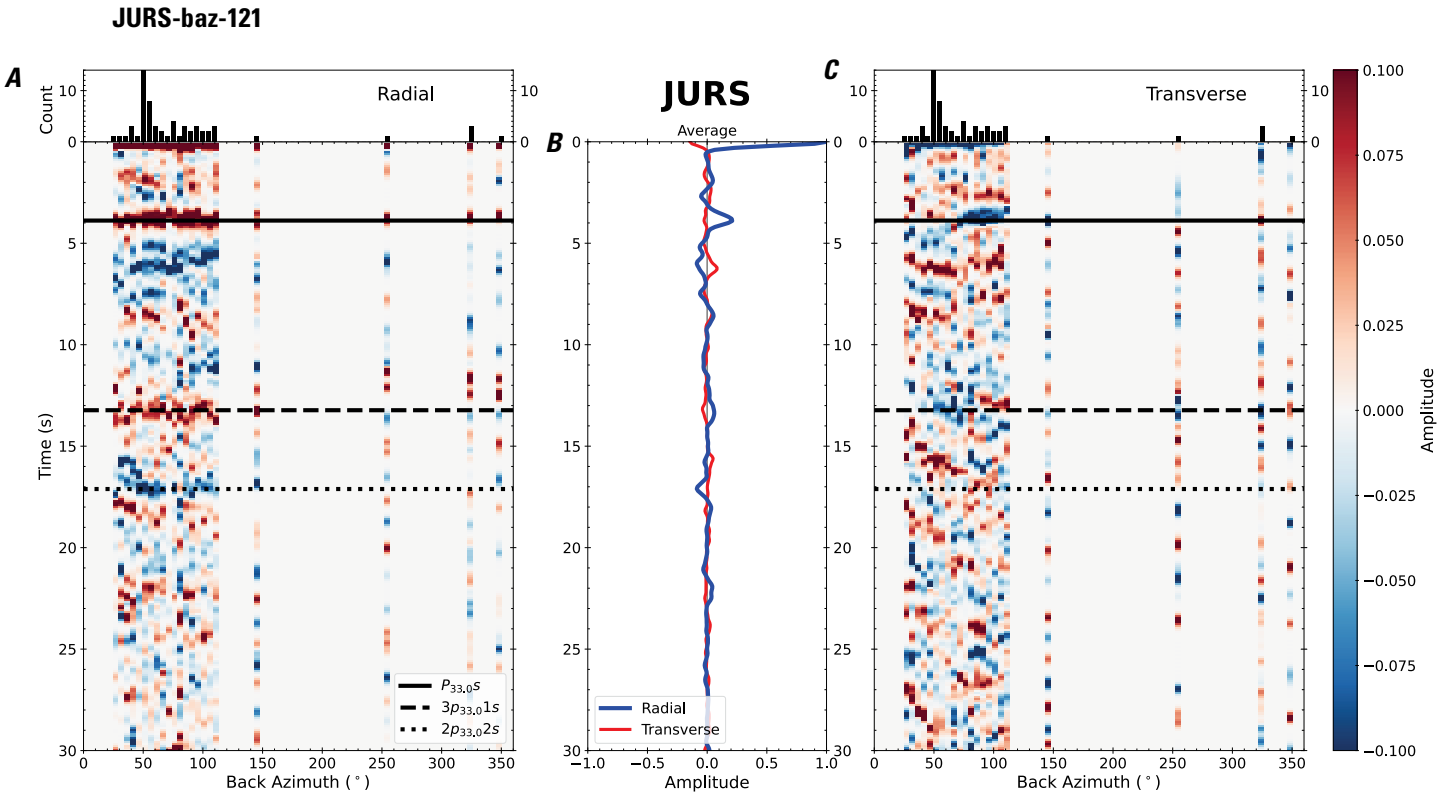

Figure 247. Receiver functions plotted against back azimuth for station JURS. *A*, Radial component of P-wave receiver functions (PRFs) plotted against back azimuth. Individual PRFs have had the resonance-removal filter of Yu and others (2015) applied to them, are normalized to the maximum amplitude within the time window shown, binned, and normalized by the number of traces per bin. *B*, Average of every individual normalized radial receiver function with the application of the resonance-removal filter (blue) and average of every individual normalized raw radial receiver function (red). *C*, Radial component of raw PRFs, plotted against back azimuth, normalized as in *A*. Ps, 3p1s, and 2p2s arrival times predicted for the preferred Moho depth are shown, assuming a ray parameter of 0.06 s/km.

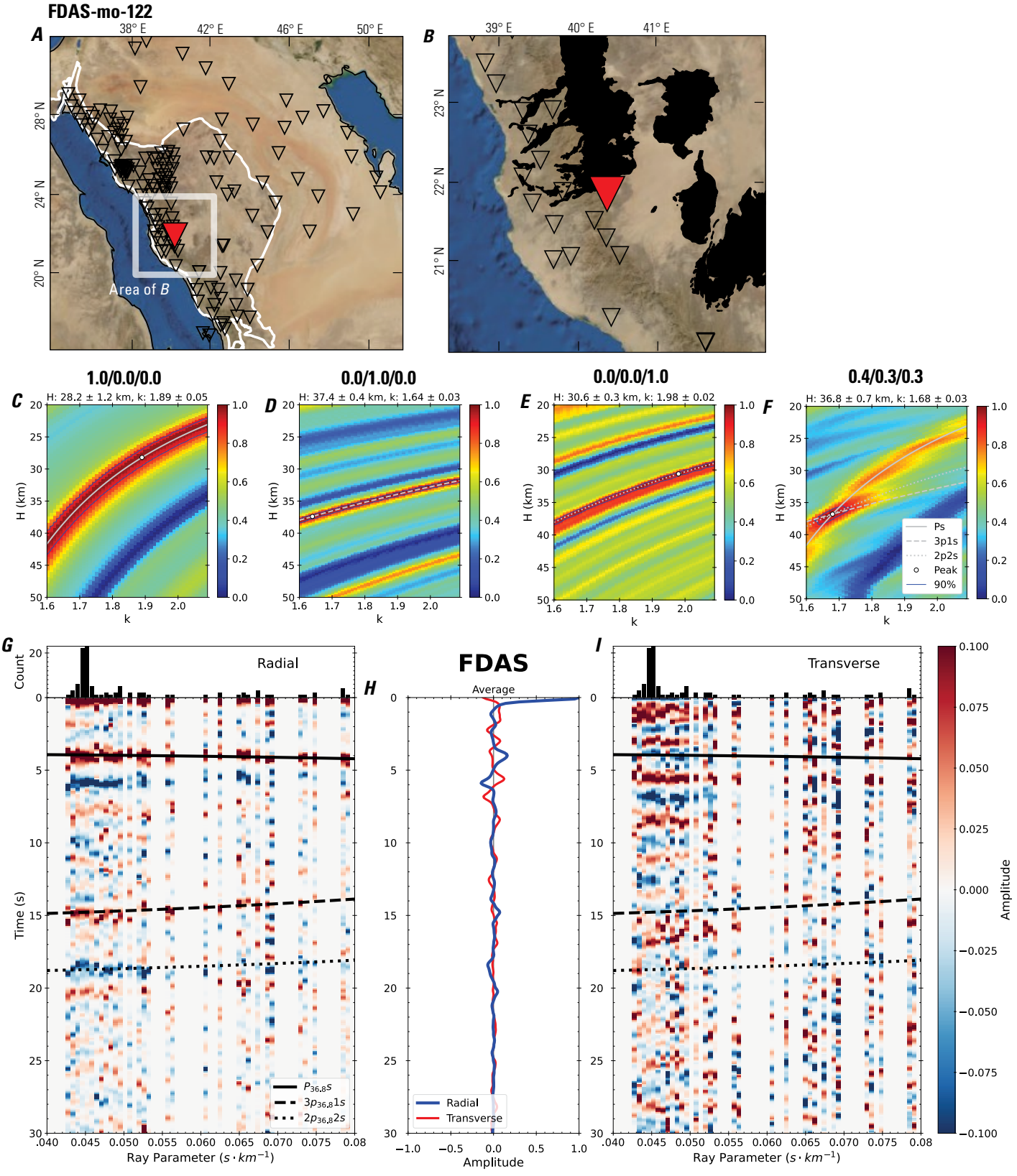
FDAS-mo-122
A
38° E
42° E
46° E
50° E
28° N
24° N
20° N
Area of B
B
39° E
40° E
41° E
23° N
22° N
21° N
1.0/0.0/0.0
C
H: 28.2 ± 1.2 km, k: 1.89 ± 0.05
0.0/1.0/0.0
D
H: 37.4 ± 0.4 km, k: 1.64 ± 0.03
0.0/0.0/1.0
E
H: 30.6 ± 0.3 km, k: 1.98 ± 0.02
0.4/0.3/0.3
F
H: 36.8 ± 0.7 km, k: 1.68 ± 0.03
H (km)
k
Ps
3p1s
2p2s
Peak
90%
G
Radial
Count
Time (s)
$P_{36.8}s$
$3p_{36.8}1s$
$2p_{36.8}2s$
Ray Parameter ($s \cdot km^{-1}$)
FDAS
H
Average
Radial
Transverse
Amplitude
I
Transverse
Amplitude

Figure 248 (page 254). Receiver-function analysis for station FDAS. *A*, Regional map of Saudi Arabia showing the entire array (as inverted triangles), the location of station FDAS (red inverted triangle), the shield-platform boundary (white line), and the bounds of the map in *B* (white box). *B*, Local map of station FDAS. Harrats are shown in black. *C*, Standard, single-layer *H-k* stack with stacking weights 0.4/0.3/0.3. This *H-k* stack ignores sedimentary effects on the receiver functions. *D*, Standard, single-layer *H-k* stack with stacking weights 0.5/0.5/0.0. This *H-k* stack also ignores sedimentary effects on the receiver functions. *E*, Optimized sub-sedimentary *H-k* stack with stacking weights 0.4/0.3/0.3, following the method of Yu and others (2015). *F*, Optimized sedimentary *H-k* stack with stacking weights 0.05/0.70/0.25, following the method of Yu and others (2015). *G*, Radial component P-wave receiver functions (PRFs) plotted against ray parameter. Individual PRFs have had the resonance-removal filter of Yu and others (2015) applied to them and are normalized to the maximum amplitude within the time window shown, binned, and normalized by the number of traces per bin. *H*, Average of every individual normalized radial receiver function with the application of the resonance-removal filter (blue) and average of every individual normalized raw radial receiver function (red). *I*, Radial component of raw PRFs (that is, PRFs with no resonance-removal filter applied) plotted against ray parameter, normalized as in *G*.

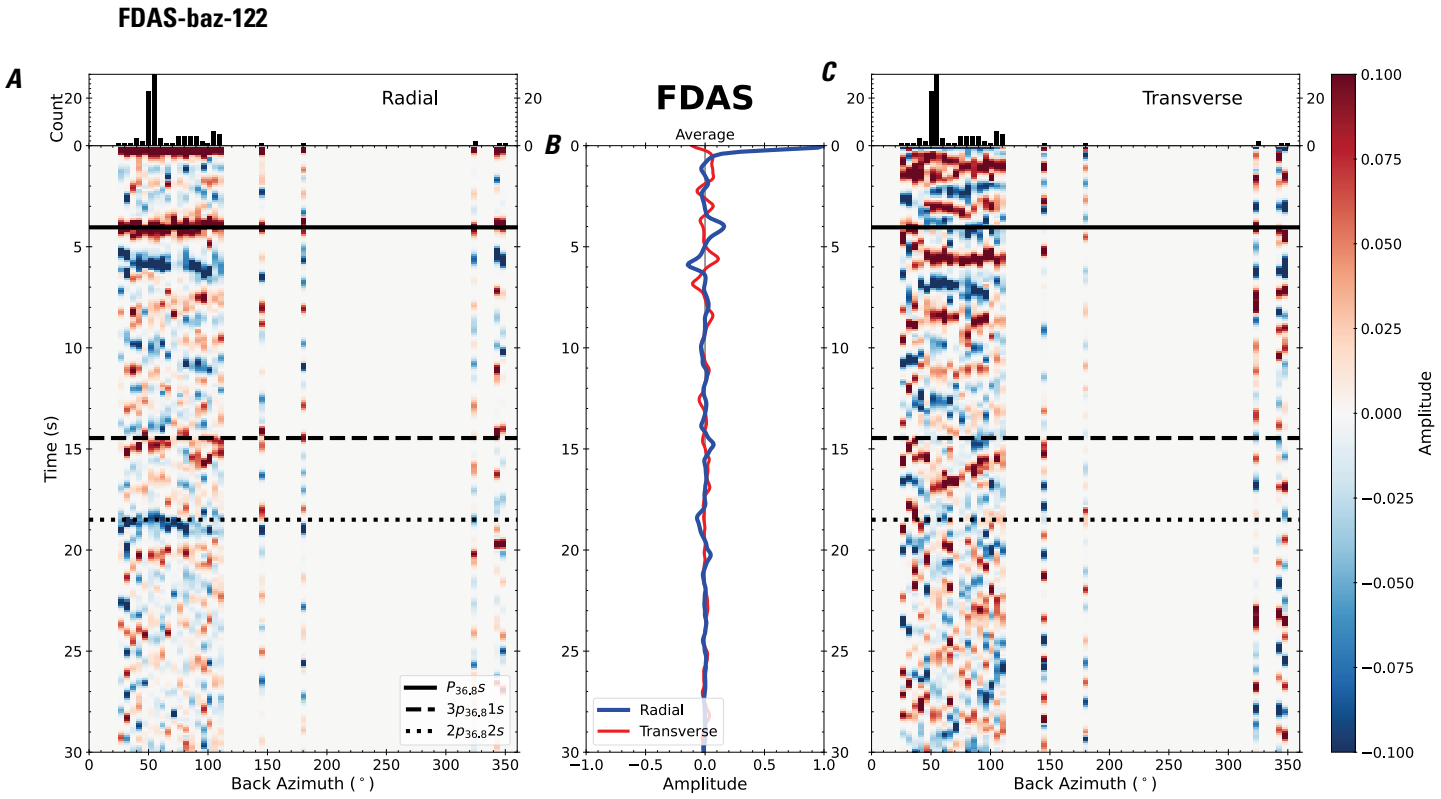

Figure 249. Receiver functions plotted against back azimuth for station FDAS. *A*, Radial component of P-wave receiver functions (PRFs) plotted against back azimuth. Individual PRFs have had the resonance-removal filter of Yu and others (2015) applied to them, are normalized to the maximum amplitude within the time window shown, binned, and normalized by the number of traces per bin. *B*, Average of every individual normalized radial receiver function with the application of the resonance-removal filter (blue) and average of every individual normalized raw radial receiver function (red). *C*, Radial component of raw PRFs, plotted against back azimuth, normalized as in *A*. Ps, 3p1s, and 2p2s arrival times predicted for the preferred Moho depth are shown, assuming a ray parameter of 0.06 s/km.

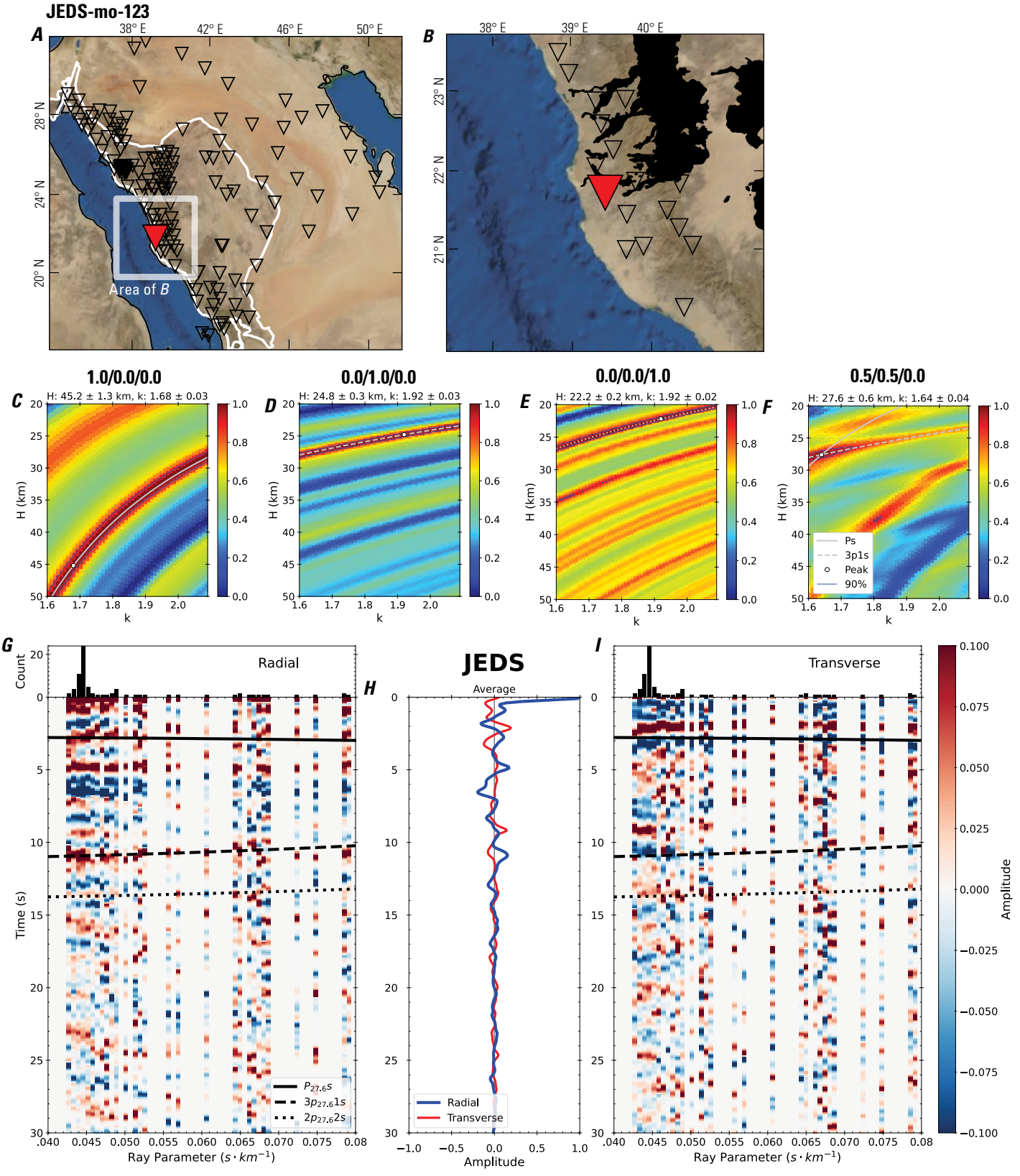
JEDS-mo-123
A
38° E
42° E
46° E
50° E
28° N
24° N
20° N
Area of B
B
38° E
39° E
40° E
23° N
22° N
21° N
1.0/0.0/0.0
C
H: 45.2 ± 1.3 km, k: 1.68 ± 0.03
0.0/1.0/0.0
D
H: 24.8 ± 0.3 km, k: 1.92 ± 0.03
0.0/0.0/1.0
E
H: 22.2 ± 0.2 km, k: 1.92 ± 0.02
0.5/0.5/0.0
F
H: 27.6 ± 0.6 km, k: 1.64 ± 0.04
H (km)
k
Ps
3p1s
Peak
90%
G
Radial
Count
Time (s)
Ray Parameter (s · km⁻¹)
P27.6s
3p27.61s
2p27.62s
JEDS
H
Average
Radial
Transverse
Amplitude
I
Transverse
Amplitude

Figure 250 (page 256). Receiver-function analysis for station JEDS. *A*, Regional map of Saudi Arabia showing the entire array (as inverted triangles), the location of station JEDS (red inverted triangle), the shield-platform boundary (white line), and the bounds of the map in *B* (white box). *B*, Local map of station JEDS. Harrats are shown in black. *C*, Standard, single-layer *H-k* stack with stacking weights 0.4/0.3/0.3. This *H-k* stack ignores sedimentary effects on the receiver functions. *D*, Standard, single-layer *H-k* stack with stacking weights 0.5/0.5/0.0. This *H-k* stack also ignores sedimentary effects on the receiver functions. *E*, Optimized sub-sedimentary *H-k* stack with stacking weights 0.4/0.3/0.3, following the method of Yu and others (2015). *F*, Optimized sedimentary *H-k* stack with stacking weights 0.05/0.70/0.25, following the method of Yu and others (2015). *G*, Radial component P-wave receiver functions (PRFs) plotted against ray parameter. Individual PRFs have had the resonance-removal filter of Yu and others (2015) applied to them and are normalized to the maximum amplitude within the time window shown, binned, and normalized by the number of traces per bin. *H*, Average of every individual normalized radial receiver function with the application of the resonance-removal filter (blue) and average of every individual normalized raw radial receiver function (red). *I*, Radial component of raw PRFs (that is, PRFs with no resonance-removal filter applied) plotted against ray parameter, normalized as in *G*.

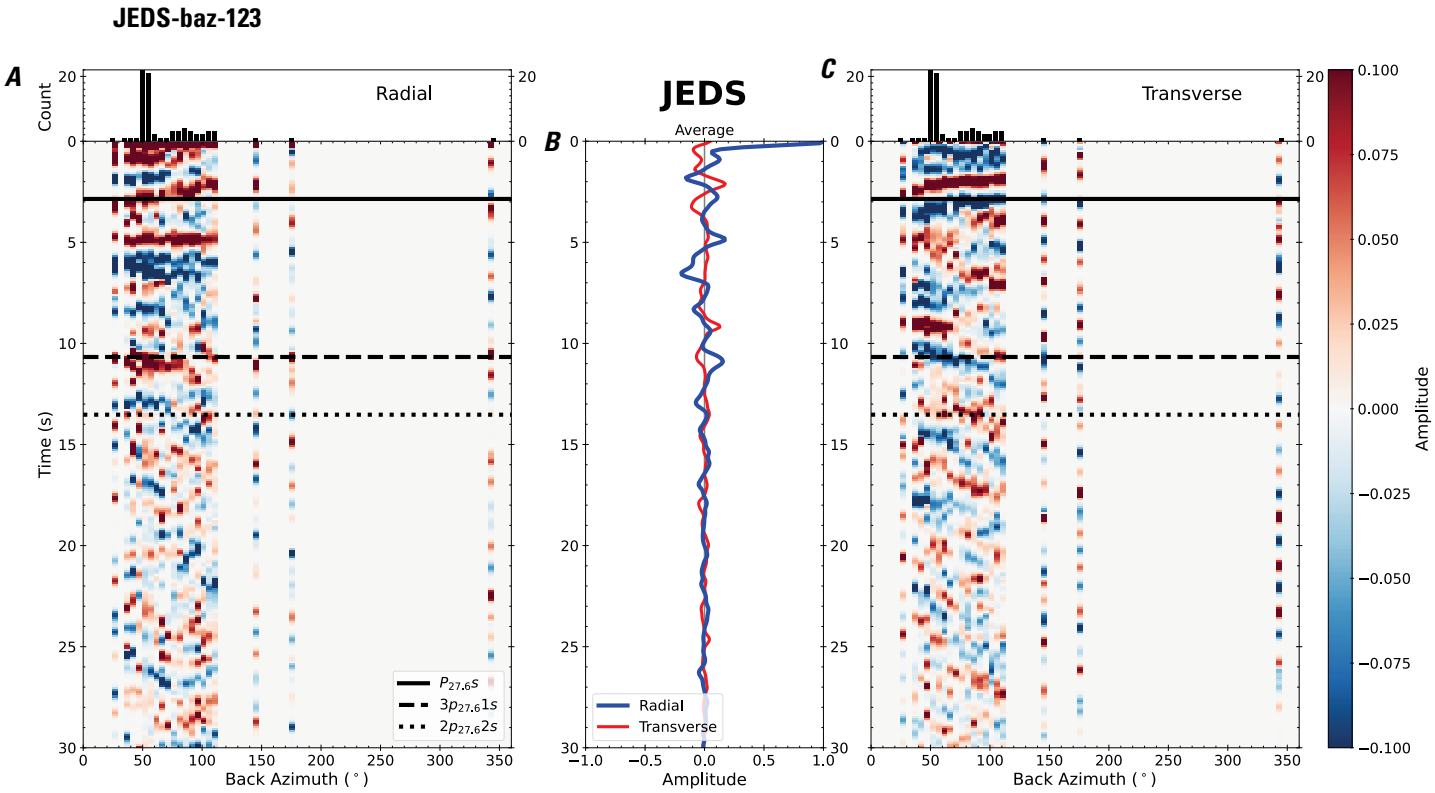

Figure 251. Receiver functions plotted against back azimuth for station JEDS. *A*, Radial component of P-wave receiver functions (PRFs) plotted against back azimuth. Individual PRFs have had the resonance-removal filter of Yu and others (2015) applied to them, are normalized to the maximum amplitude within the time window shown, binned, and normalized by the number of traces per bin. *B*, Average of every individual normalized radial receiver function with the application of the resonance-removal filter (blue) and average of every individual normalized raw radial receiver function (red). *C*, Radial component of raw PRFs, plotted against back azimuth, normalized as in *A*. Ps, 3p1s, and 2p2s arrival times predicted for the preferred Moho depth are shown, assuming a ray parameter of 0.06 s/km.

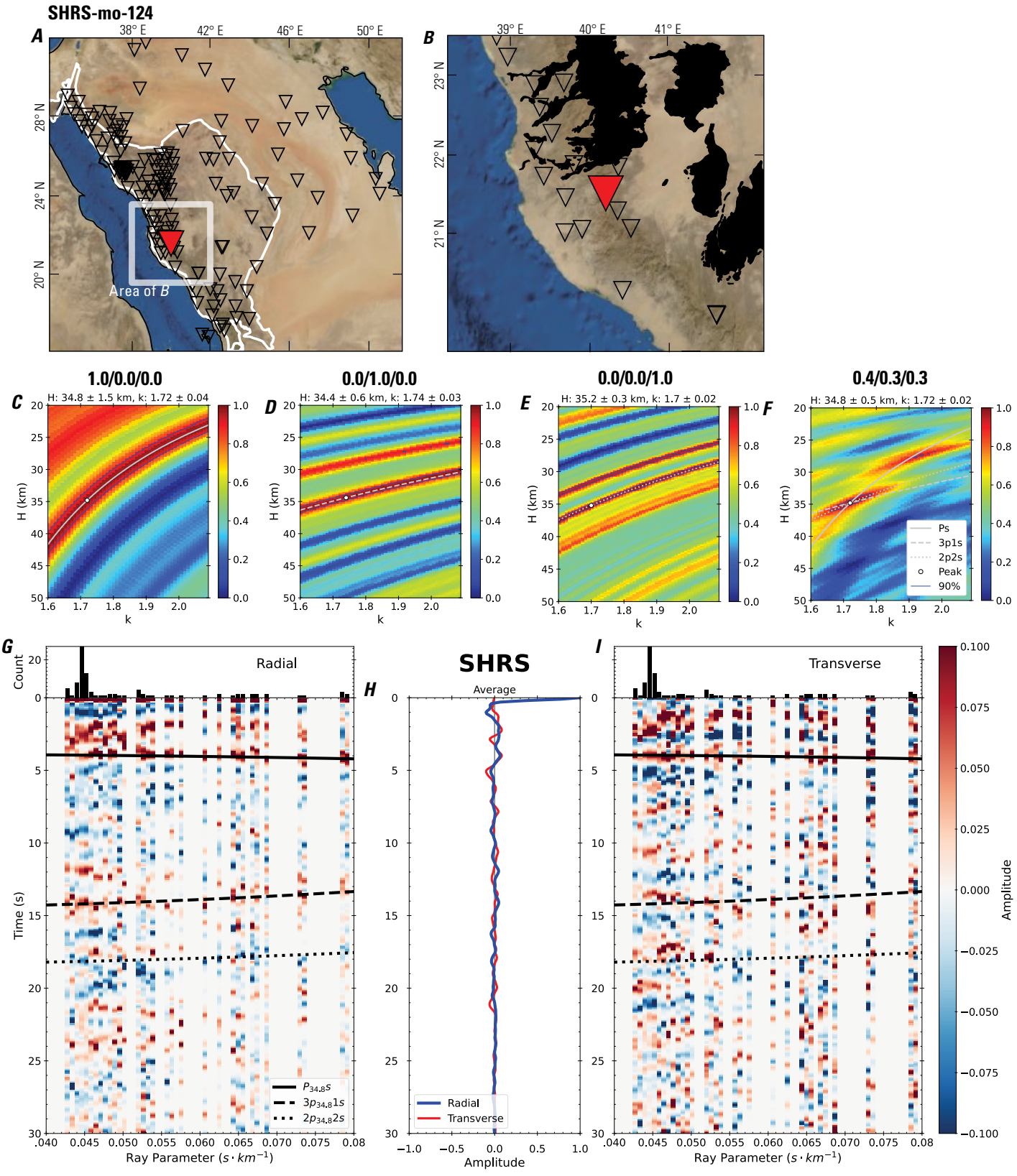
SHRS-mo-124
A
38° E
42° E
46° E
50° E
28° N
24° N
20° N
Area of B
B
39° E
40° E
41° E
23° N
22° N
21° N
1.0/0.0/0.0
0.0/1.0/0.0
0.0/0.0/1.0
0.4/0.3/0.3
C
H: 34.8 ± 1.5 km, k: 1.72 ± 0.04
D
H: 34.4 ± 0.6 km, k: 1.74 ± 0.03
E
H: 35.2 ± 0.3 km, k: 1.7 ± 0.02
F
H: 34.8 ± 0.5 km, k: 1.72 ± 0.02
H (km)
k
Ps
3p1s
2p2s
Peak
90%
G
Radial
Count
Time (s)
$P_{34.8}s$
$3p_{34.8}1s$
$2p_{34.8}2s$
Ray Parameter ($s \cdot km^{-1}$)
H
SHRS
Average
Radial
Transverse
Amplitude
I
Transverse
Amplitude

Figure 252 (page 258). Receiver-function analysis for station SHRS. *A*, Regional map of Saudi Arabia showing the entire array (as inverted triangles), the location of station SHRS (red inverted triangle), the shield-platform boundary (white line), and the bounds of the map in *B* (white box). *B*, Local map of station SHRS. Harrats are shown in black. *C*, Standard, single-layer *H-k* stack with stacking weights 0.4/0.3/0.3. This *H-k* stack ignores sedimentary effects on the receiver functions. *D*, Standard, single-layer *H-k* stack with stacking weights 0.5/0.5/0.0. This *H-k* stack also ignores sedimentary effects on the receiver functions. *E*, Optimized sub-sedimentary *H-k* stack with stacking weights 0.4/0.3/0.3, following the method of Yu and others (2015). *F*, Optimized sedimentary *H-k* stack with stacking weights 0.05/0.70/0.25, following the method of Yu and others (2015). *G*, Radial component P-wave receiver functions (PRFs) plotted against ray parameter. Individual PRFs have had the resonance-removal filter of Yu and others (2015) applied to them and are normalized to the maximum amplitude within the time window shown, binned, and normalized by the number of traces per bin. *H*, Average of every individual normalized radial receiver function with the application of the resonance-removal filter (blue) and average of every individual normalized raw radial receiver function (red). *I*, Radial component of raw PRFs (that is, PRFs with no resonance-removal filter applied) plotted against ray parameter, normalized as in *G*.

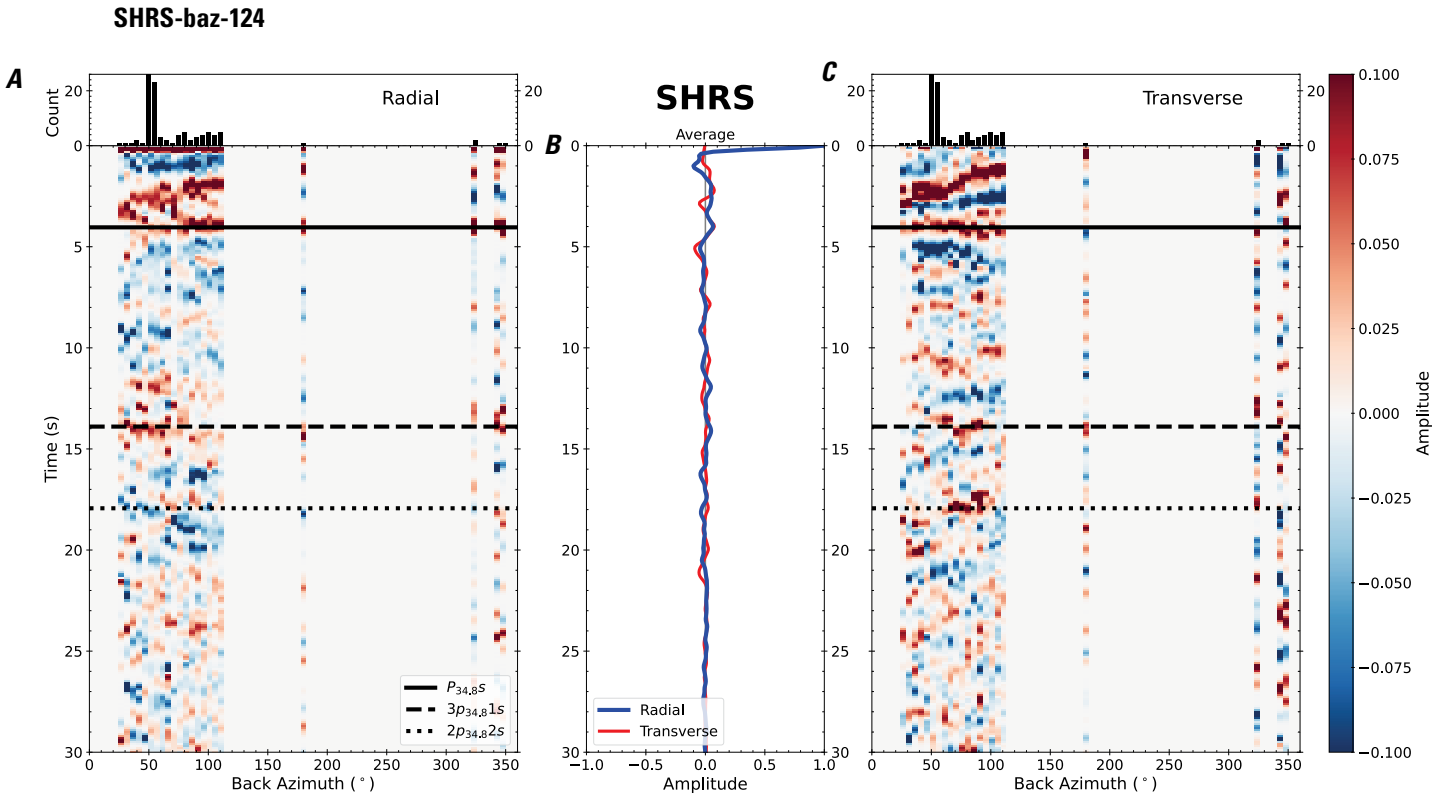

Figure 253. Receiver functions plotted against back azimuth for station SHRS. *A*, Radial component of P-wave receiver functions (PRFs) plotted against back azimuth. Individual PRFs have had the resonance-removal filter of Yu and others (2015) applied to them, are normalized to the maximum amplitude within the time window shown, binned, and normalized by the number of traces per bin. *B*, Average of every individual normalized radial receiver function with the application of the resonance-removal filter (blue) and average of every individual normalized raw radial receiver function (red). *C*, Radial component of raw PRFs, plotted against back azimuth, normalized as in *A*. Ps, 3p1s, and 2p2s arrival times predicted for the preferred Moho depth are shown, assuming a ray parameter of 0.06 s/km.

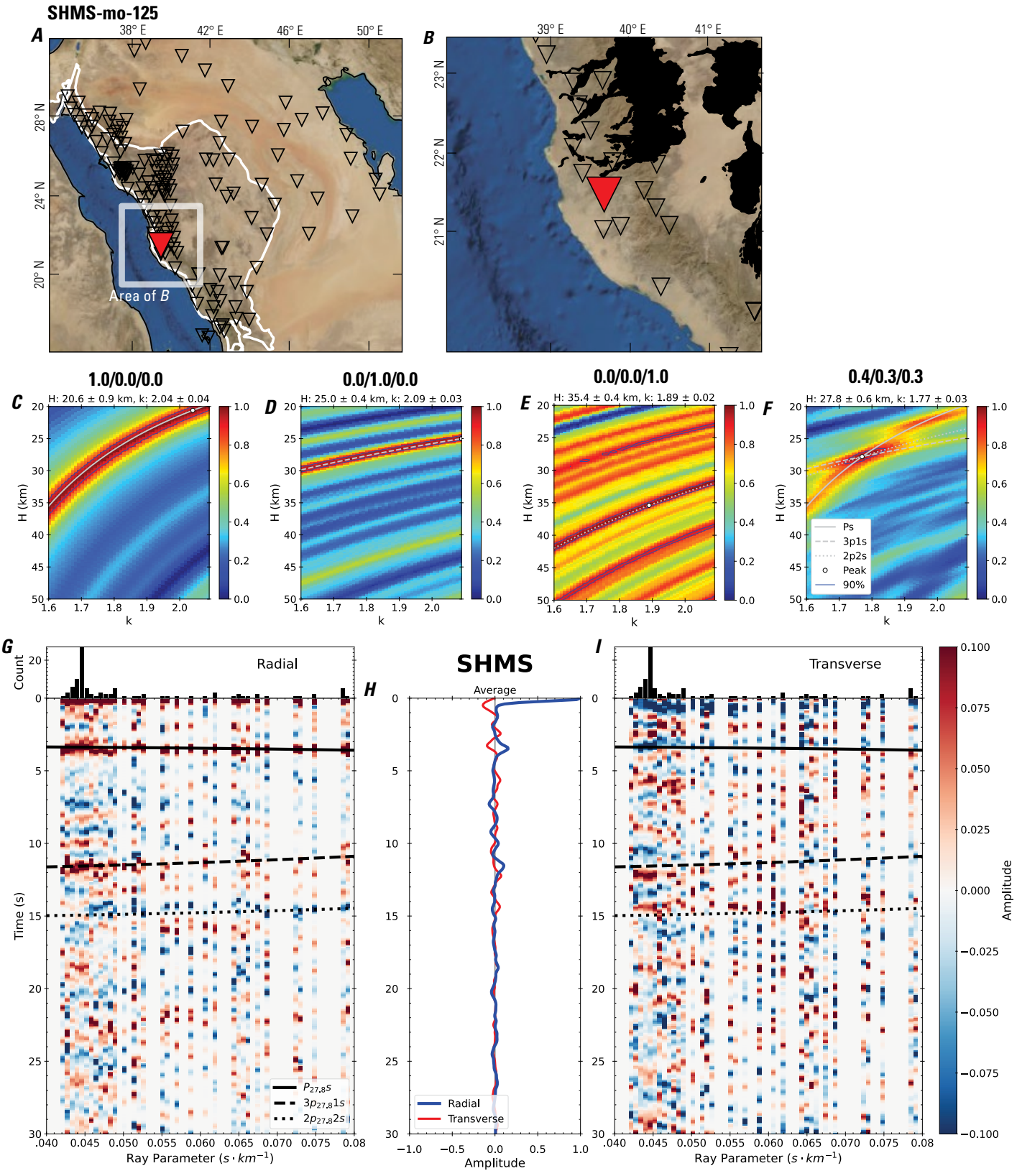
SHMS-mo-125
A
38° E
42° E
46° E
50° E
28° N
24° N
20° N
Area of B
B
39° E
40° E
41° E
23° N
22° N
21° N
1.0/0.0/0.0
0.0/1.0/0.0
0.0/0.0/1.0
0.4/0.3/0.3
C
H: 20.6 ± 0.9 km, k: 2.04 ± 0.04
D
H: 25.0 ± 0.4 km, k: 2.09 ± 0.03
E
H: 35.4 ± 0.4 km, k: 1.89 ± 0.02
F
H: 27.8 ± 0.6 km, k: 1.77 ± 0.03
H (km)
k
Ps
3p1s
2p2s
Peak
90%
G
Radial
Count
Time (s)
$P_{27.8}s$
$3p_{27.8}1s$
$2p_{27.8}2s$
Ray Parameter ($s \cdot km^{-1}$)
H
SHMS
Average
Radial
Transverse
Amplitude
I
Transverse
Amplitude

Figure 254 (page 260). Receiver-function analysis for station SHMS. *A*, Regional map of Saudi Arabia showing the entire array (as inverted triangles), the location of station SHMS (red inverted triangle), the shield-platform boundary (white line), and the bounds of the map in *B* (white box). *B*, Local map of station SHMS. Harrats are shown in black. *C*, Standard, single-layer *H-k* stack with stacking weights 0.4/0.3/0.3. This *H-k* stack ignores sedimentary effects on the receiver functions. *D*, Standard, single-layer *H-k* stack with stacking weights 0.5/0.5/0.0. This *H-k* stack also ignores sedimentary effects on the receiver functions. *E*, Optimized sub-sedimentary *H-k* stack with stacking weights 0.4/0.3/0.3, following the method of Yu and others (2015). *F*, Optimized sedimentary *H-k* stack with stacking weights 0.05/0.70/0.25, following the method of Yu and others (2015). *G*, Radial component P-wave receiver functions (PRFs) plotted against ray parameter. Individual PRFs have had the resonance-removal filter of Yu and others (2015) applied to them and are normalized to the maximum amplitude within the time window shown, binned, and normalized by the number of traces per bin. *H*, Average of every individual normalized radial receiver function with the application of the resonance-removal filter (blue) and average of every individual normalized raw radial receiver function (red). *I*, Radial component of raw PRFs (that is, PRFs with no resonance-removal filter applied) plotted against ray parameter, normalized as in *G*.

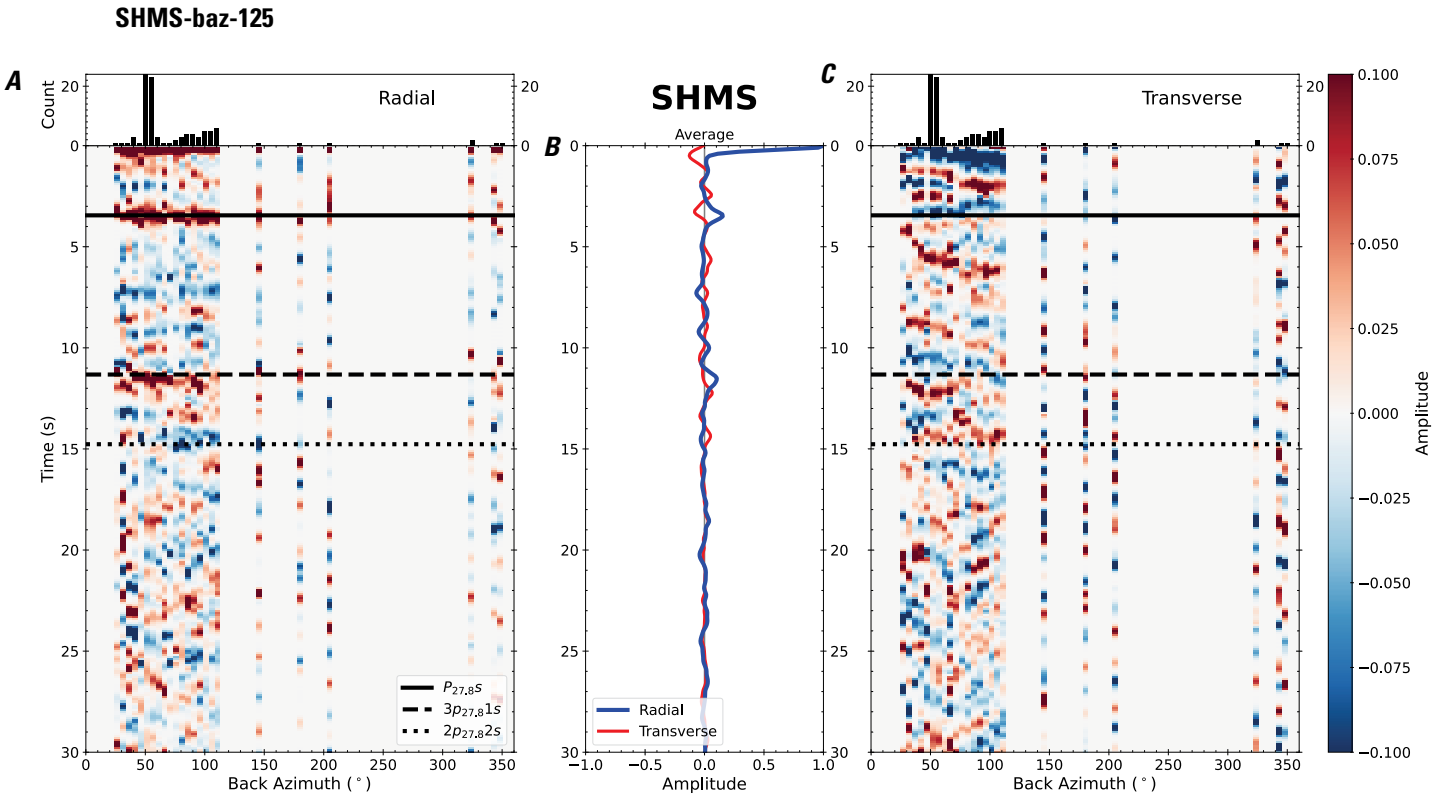

Figure 255. Receiver functions plotted against back azimuth for station SHMS. *A*, Radial component of P-wave receiver functions (PRFs) plotted against back azimuth. Individual PRFs have had the resonance-removal filter of Yu and others (2015) applied to them, are normalized to the maximum amplitude within the time window shown, binned, and normalized by the number of traces per bin. *B*, Average of every individual normalized radial receiver function with the application of the resonance-removal filter (blue) and average of every individual normalized raw radial receiver function (red). *C*, Radial component of raw PRFs, plotted against back azimuth, normalized as in *A*. Ps, 3p1s, and 2p2s arrival times predicted for the preferred Moho depth are shown, assuming a ray parameter of 0.06 s/km.

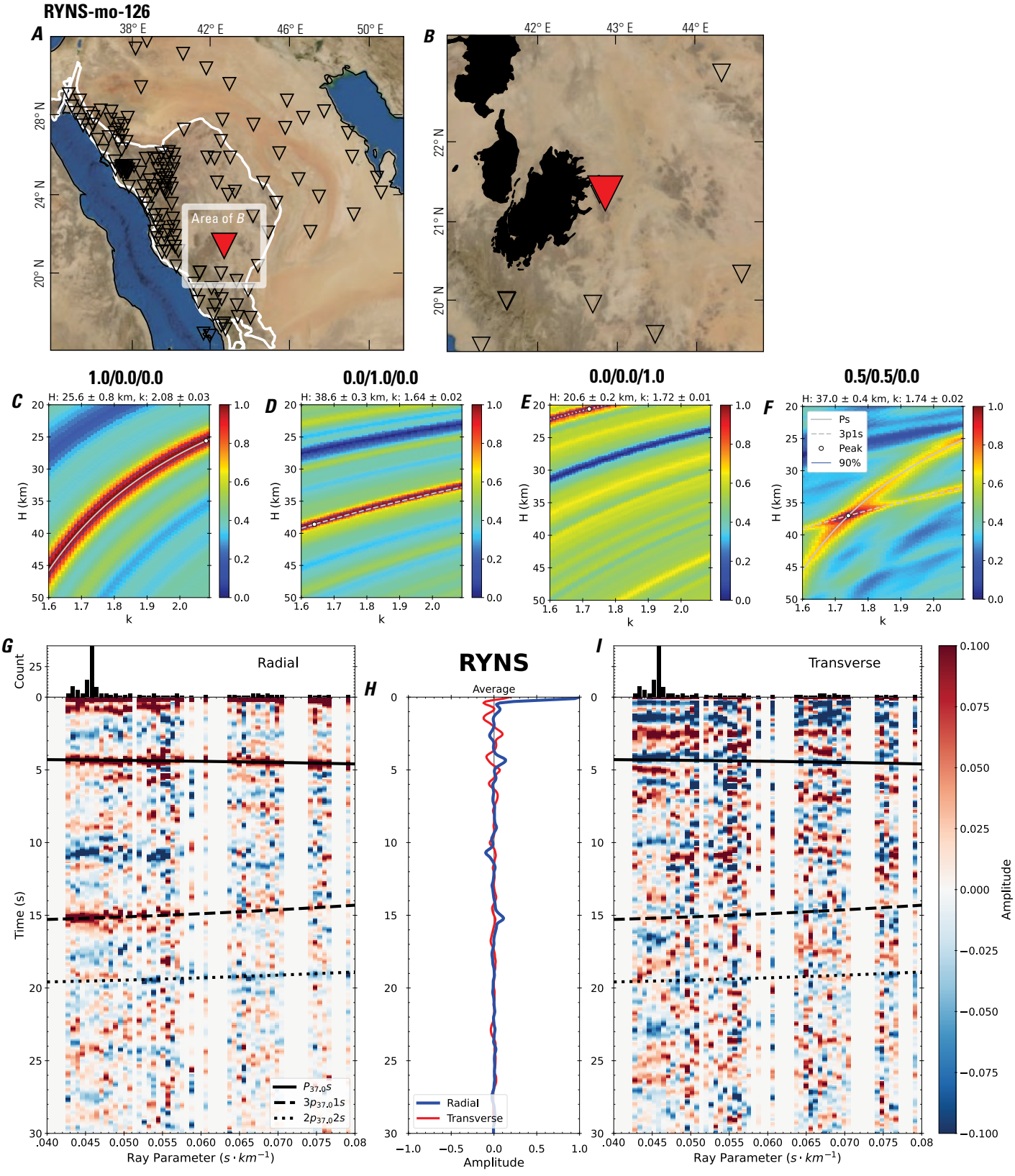
RYNS-mo-126
A
38° E
42° E
46° E
50° E
28° N
24° N
20° N
Area of B
B
42° E
43° E
44° E
22° N
21° N
20° N
1.0/0.0/0.0
C
H: 25.6 ± 0.8 km, k: 2.08 ± 0.03
0.0/1.0/0.0
D
H: 38.6 ± 0.3 km, k: 1.64 ± 0.02
0.0/0.0/1.0
E
H: 20.6 ± 0.2 km, k: 1.72 ± 0.01
0.5/0.5/0.0
F
H: 37.0 ± 0.4 km, k: 1.74 ± 0.02
Ps
3p1s
Peak
90%
H (km)
k
G
Radial
Count
Time (s)
$P_{37.0}s$
$3p_{37.0}1s$
$2p_{37.0}2s$
Ray Parameter ($s \cdot km^{-1}$)
RYNS
H
Average
Radial
Transverse
Amplitude
I
Transverse
Amplitude

Figure 256 (page 262). Receiver-function analysis for station RYNS. *A*, Regional map of Saudi Arabia showing the entire array (as inverted triangles), the location of station RYNS (red inverted triangle), the shield-platform boundary (white line), and the bounds of the map in *B* (white box). *B*, Local map of station RYNS. Harrats are shown in black. *C*, Standard, single-layer *H-k* stack with stacking weights 0.4/0.3/0.3. This *H-k* stack ignores sedimentary effects on the receiver functions. *D*, Standard, single-layer *H-k* stack with stacking weights 0.5/0.5/0.0. This *H-k* stack also ignores sedimentary effects on the receiver functions. *E*, Optimized sub-sedimentary *H-k* stack with stacking weights 0.4/0.3/0.3, following the method of Yu and others (2015). *F*, Optimized sedimentary *H-k* stack with stacking weights 0.05/0.70/0.25, following the method of Yu and others (2015). *G*, Radial component P-wave receiver functions (PRFs) plotted against ray parameter. Individual PRFs have had the resonance-removal filter of Yu and others (2015) applied to them and are normalized to the maximum amplitude within the time window shown, binned, and normalized by the number of traces per bin. *H*, Average of every individual normalized radial receiver function with the application of the resonance-removal filter (blue) and average of every individual normalized raw radial receiver function (red). *I*, Radial component of raw PRFs (that is, PRFs with no resonance-removal filter applied) plotted against ray parameter, normalized as in *G*.

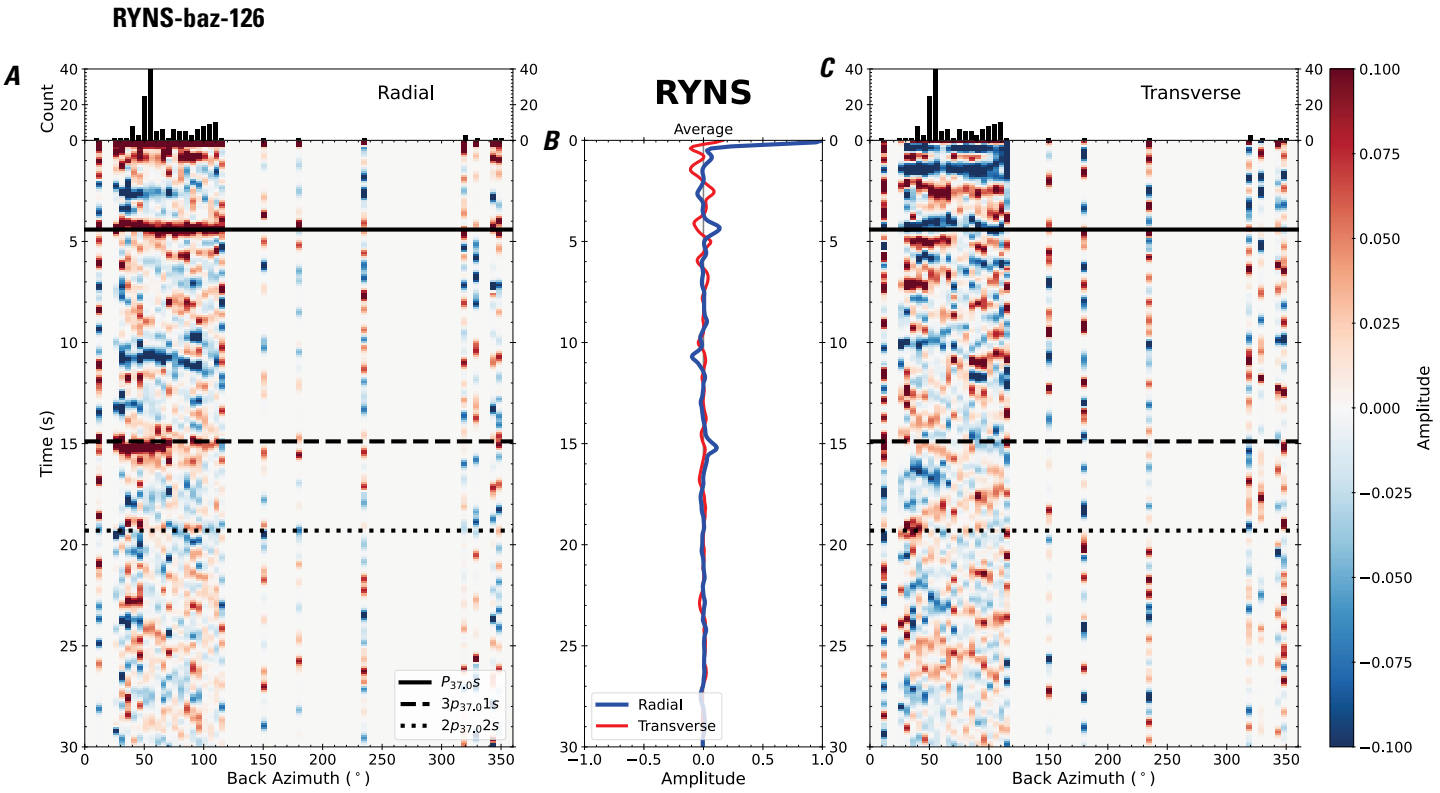

Figure 257. Receiver functions plotted against back azimuth for station RYNS. *A*, Radial component of P-wave receiver functions (PRFs) plotted against back azimuth. Individual PRFs have had the resonance-removal filter of Yu and others (2015) applied to them, are normalized to the maximum amplitude within the time window shown, binned, and normalized by the number of traces per bin. *B*, Average of every individual normalized radial receiver function with the application of the resonance-removal filter (blue) and average of every individual normalized raw radial receiver function (red). *C*, Radial component of raw PRFs, plotted against back azimuth, normalized as in *A*. Ps, 3p1s, and 2p2s arrival times predicted for the preferred Moho depth are shown, assuming a ray parameter of 0.06 s/km.

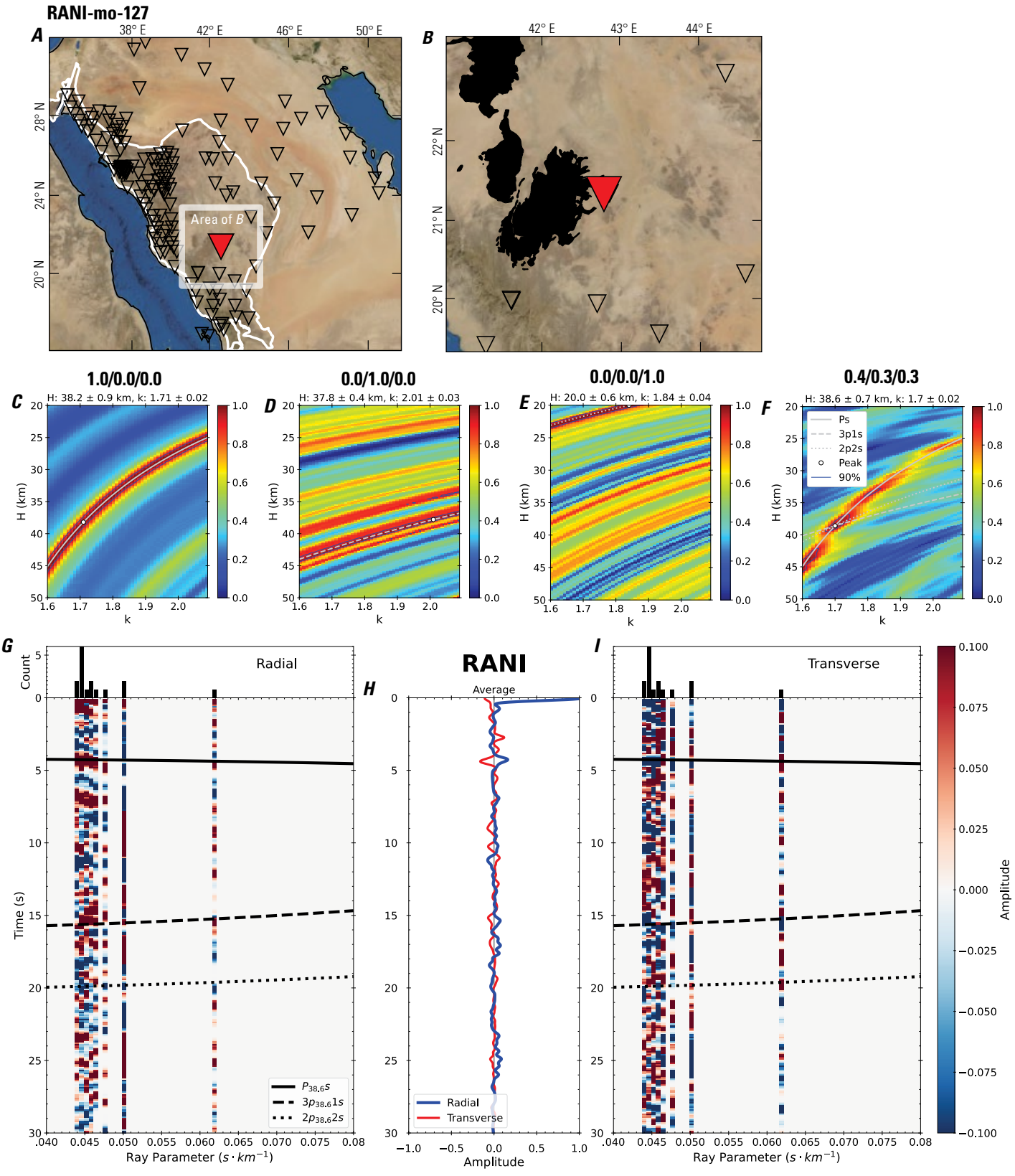
RANI-mo-127
A
38° E
42° E
46° E
50° E
28° N
24° N
20° N
Area of B
B
42° E
43° E
44° E
22° N
21° N
20° N
1.0/0.0/0.0
C
H: 38.2 ± 0.9 km, k: 1.71 ± 0.02
0.0/1.0/0.0
D
H: 37.8 ± 0.4 km, k: 2.01 ± 0.03
0.0/0.0/1.0
E
H: 20.0 ± 0.6 km, k: 1.84 ± 0.04
0.4/0.3/0.3
F
H: 38.6 ± 0.7 km, k: 1.7 ± 0.02
H (km)
k
Ps
3p1s
2p2s
Peak
90%
G
Radial
Count
Time (s)
Ray Parameter (s · km⁻¹)
$P_{38.6}s$
$3p_{38.6}1s$
$2p_{38.6}2s$
RANI
H
Average
Radial
Transverse
Amplitude
I
Transverse
Amplitude

Figure 258 (page 264). Receiver-function analysis for station RANI. *A*, Regional map of Saudi Arabia showing the entire array (as inverted triangles), the location of station RANI (red inverted triangle), the shield-platform boundary (white line), and the bounds of the map in *B* (white box). *B*, Local map of station RANI. Harrats are shown in black. *C*, Standard, single-layer *H-k* stack with stacking weights 0.4/0.3/0.3. This *H-k* stack ignores sedimentary effects on the receiver functions. *D*, Standard, single-layer *H-k* stack with stacking weights 0.5/0.5/0.0. This *H-k* stack also ignores sedimentary effects on the receiver functions. *E*, Optimized sub-sedimentary *H-k* stack with stacking weights 0.4/0.3/0.3, following the method of Yu and others (2015). *F*, Optimized sedimentary *H-k* stack with stacking weights 0.05/0.70/0.25, following the method of Yu and others (2015). *G*, Radial component P-wave receiver functions (PRFs) plotted against ray parameter. Individual PRFs have had the resonance-removal filter of Yu and others (2015) applied to them and are normalized to the maximum amplitude within the time window shown, binned, and normalized by the number of traces per bin. *H*, Average of every individual normalized radial receiver function with the application of the resonance-removal filter (blue) and average of every individual normalized raw radial receiver function (red). *I*, Radial component of raw PRFs (that is, PRFs with no resonance-removal filter applied) plotted against ray parameter, normalized as in *G*.

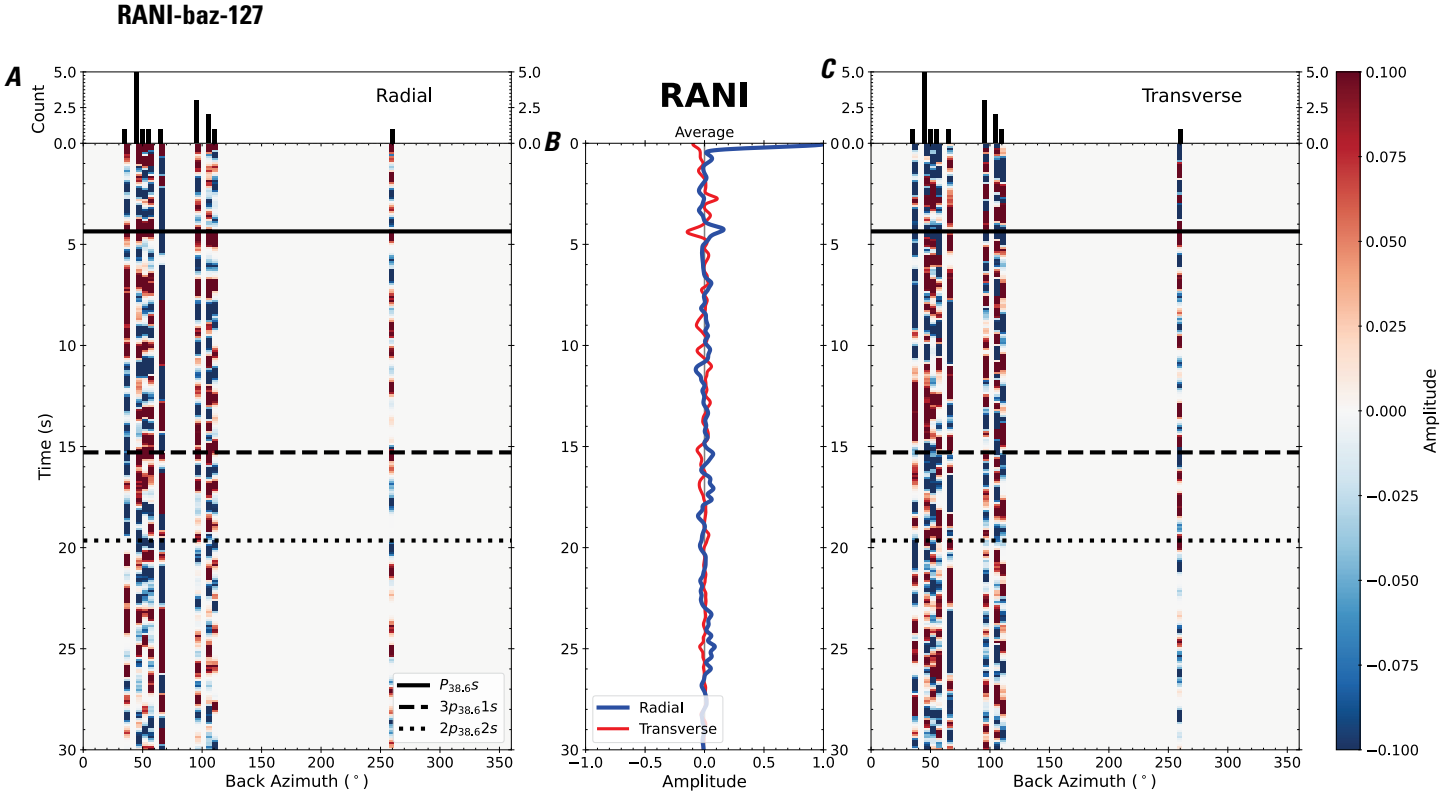

Figure 259. Receiver functions plotted against back azimuth for station RANI. *A*, Radial component of P-wave receiver functions (PRFs) plotted against back azimuth. Individual PRFs have had the resonance-removal filter of Yu and others (2015) applied to them, are normalized to the maximum amplitude within the time window shown, binned, and normalized by the number of traces per bin. *B*, Average of every individual normalized radial receiver function with the application of the resonance-removal filter (blue) and average of every individual normalized raw radial receiver function (red). *C*, Radial component of raw PRFs, plotted against back azimuth, normalized as in *A*. Ps, 3p1s, and 2p2s arrival times predicted for the preferred Moho depth are shown, assuming a ray parameter of 0.06 s/km.

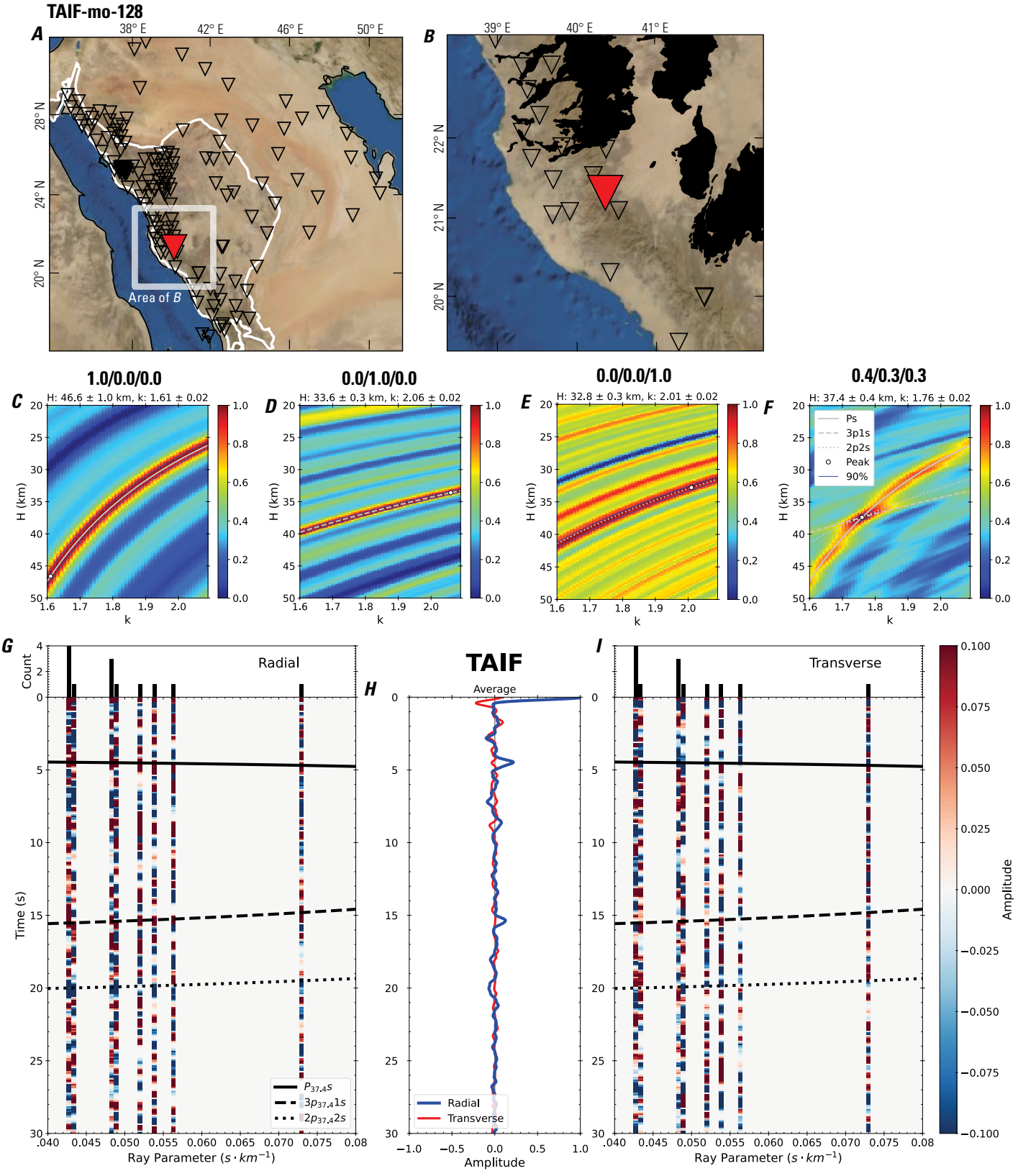
TAIF-mo-128
A
38° E
42° E
46° E
50° E
28° N
24° N
20° N
Area of B
B
39° E
40° E
41° E
22° N
21° N
20° N
1.0/0.0/0.0
0.0/1.0/0.0
0.0/0.0/1.0
0.4/0.3/0.3
C
H: 46.6 ± 1.0 km, k: 1.61 ± 0.02
D
H: 33.6 ± 0.3 km, k: 2.06 ± 0.02
E
H: 32.8 ± 0.3 km, k: 2.01 ± 0.02
F
H: 37.4 ± 0.4 km, k: 1.76 ± 0.02
Ps
3p1s
2p2s
Peak
90%
H (km)
k
G
Radial
Count
Time (s)
$P_{37.4}s$
$3p_{37.4}1s$
$2p_{37.4}2s$
Ray Parameter ($s \cdot km^{-1}$)
H
TAIF
Average
Radial
Transverse
Amplitude
I
Transverse
Amplitude

Figure 260 (page 260). Receiver-function analysis for station TAIF. *A*, Regional map of Saudi Arabia showing the entire array (as inverted triangles), the location of station TAIF (red inverted triangle), the shield-platform boundary (white line), and the bounds of the map in *B* (white box). *B*, Local map of station TAIF. Harrats are shown in black. *C*, Standard, single-layer *H-k* stack with stacking weights 0.4/0.3/0.3. This *H-k* stack ignores sedimentary effects on the receiver functions. *D*, Standard, single-layer *H-k* stack with stacking weights 0.5/0.5/0.0. This *H-k* stack also ignores sedimentary effects on the receiver functions. *E*, Optimized sub-sedimentary *H-k* stack with stacking weights 0.4/0.3/0.3, following the method of Yu and others (2015). *F*, Optimized sedimentary *H-k* stack with stacking weights 0.05/0.70/0.25, following the method of Yu and others (2015). *G*, Radial component P-wave receiver functions (PRFs) plotted against ray parameter. Individual PRFs have had the resonance-removal filter of Yu and others (2015) applied to them and are normalized to the maximum amplitude within the time window shown, binned, and normalized by the number of traces per bin. *H*, Average of every individual normalized radial receiver function with the application of the resonance-removal filter (blue) and average of every individual normalized raw radial receiver function (red). *I*, Radial component of raw PRFs (that is, PRFs with no resonance-removal filter applied) plotted against ray parameter, normalized as in *G*.

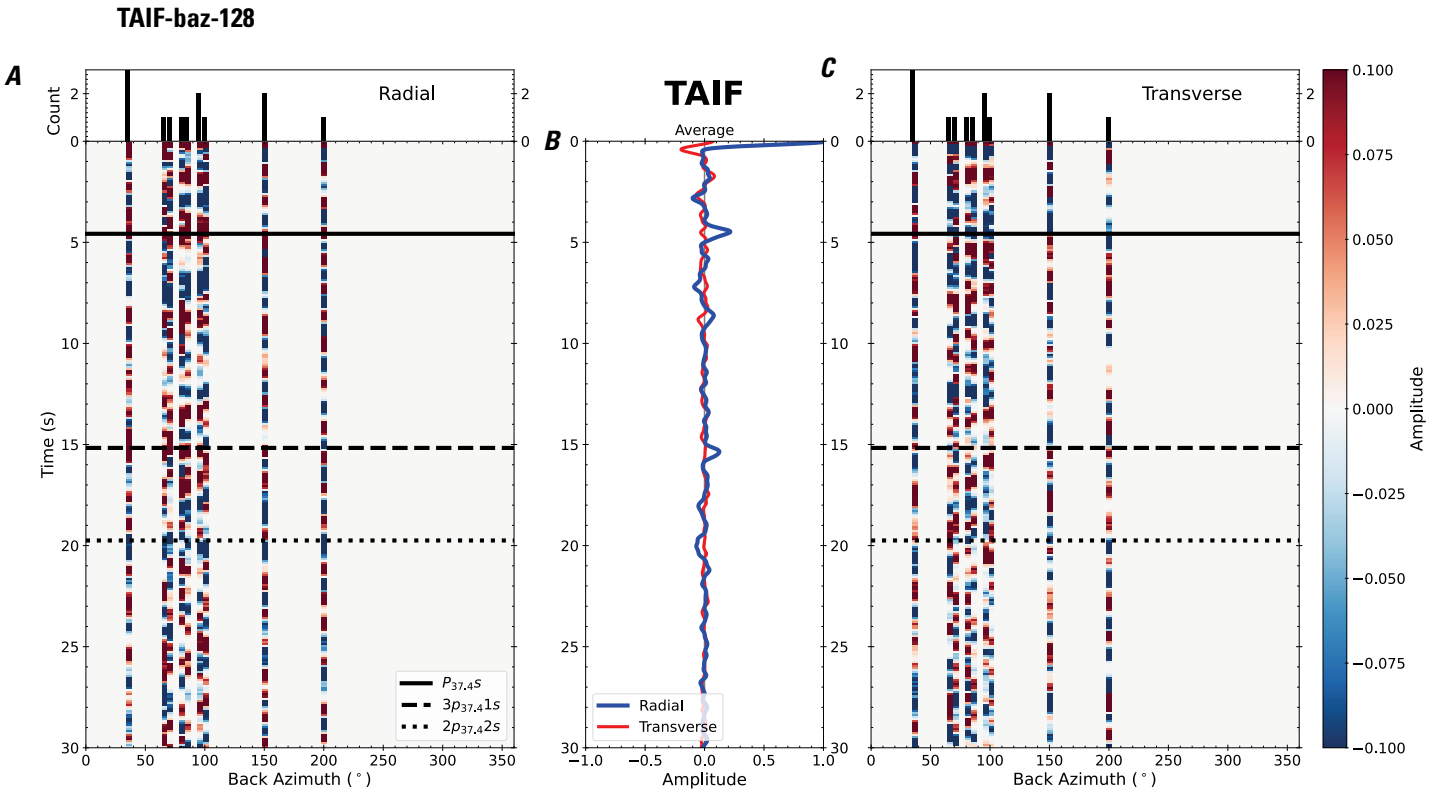

Figure 261. Receiver functions plotted against back azimuth for station TAIF. *A*, Radial component of P-wave receiver functions (PRFs) plotted against back azimuth. Individual PRFs have had the resonance-removal filter of Yu and others (2015) applied to them, are normalized to the maximum amplitude within the time window shown, binned, and normalized by the number of traces per bin. *B*, Average of every individual normalized radial receiver function with the application of the resonance-removal filter (blue) and average of every individual normalized raw radial receiver function (red). *C*, Radial component of raw PRFs, plotted against back azimuth, normalized as in *A*. Ps, 3p1s, and 2p2s arrival times predicted for the preferred Moho depth are shown, assuming a ray parameter of 0.06 s/km.

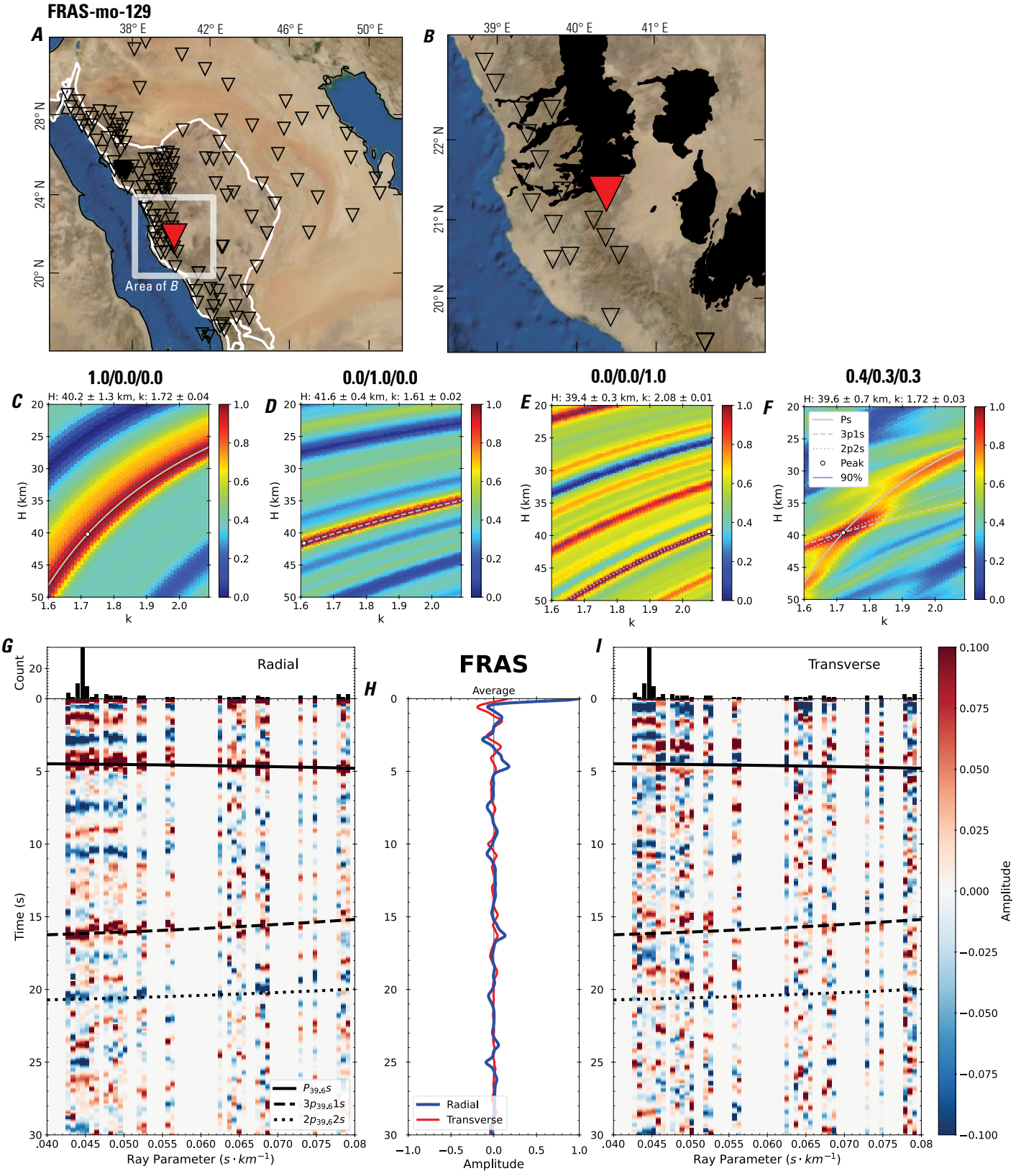
FRAS-mo-129
A
38° E
42° E
46° E
50° E
28° N
24° N
20° N
Area of B
B
39° E
40° E
41° E
22° N
21° N
20° N
1.0/0.0/0.0
C
H: 40.2 ± 1.3 km, k: 1.72 ± 0.04
0.0/1.0/0.0
D
H: 41.6 ± 0.4 km, k: 1.61 ± 0.02
0.0/0.0/1.0
E
H: 39.4 ± 0.3 km, k: 2.08 ± 0.01
0.4/0.3/0.3
F
H: 39.6 ± 0.7 km, k: 1.72 ± 0.03
H (km)
k
Ps
3p1s
2p2s
Peak
90%
G
Radial
Count
Time (s)
Ray Parameter (s · km⁻¹)
$P_{39.6}s$
$3p_{39.6}1s$
$2p_{39.6}2s$
H
FRAS
Average
Radial
Transverse
Amplitude
I
Transverse
Amplitude

Figure 262 (page 268). Receiver-function analysis for station FRAS. *A*, Regional map of Saudi Arabia showing the entire array (as inverted triangles), the location of station FRAS (red inverted triangle), the shield-platform boundary (white line), and the bounds of the map in *B* (white box). *B*, Local map of station FRAS. Harrats are shown in black. *C*, Standard, single-layer *H-k* stack with stacking weights 0.4/0.3/0.3. This *H-k* stack ignores sedimentary effects on the receiver functions. *D*, Standard, single-layer *H-k* stack with stacking weights 0.5/0.5/0.0. This *H-k* stack also ignores sedimentary effects on the receiver functions. *E*, Optimized sub-sedimentary *H-k* stack with stacking weights 0.4/0.3/0.3, following the method of Yu and others (2015). *F*, Optimized sedimentary *H-k* stack with stacking weights 0.05/0.70/0.25, following the method of Yu and others (2015). *G*, Radial component P-wave receiver functions (PRFs) plotted against ray parameter. Individual PRFs have had the resonance-removal filter of Yu and others (2015) applied to them and are normalized to the maximum amplitude within the time window shown, binned, and normalized by the number of traces per bin. *H*, Average of every individual normalized radial receiver function with the application of the resonance-removal filter (blue) and average of every individual normalized raw radial receiver function (red). *I*, Radial component of raw PRFs (that is, PRFs with no resonance-removal filter applied) plotted against ray parameter, normalized as in *G*.

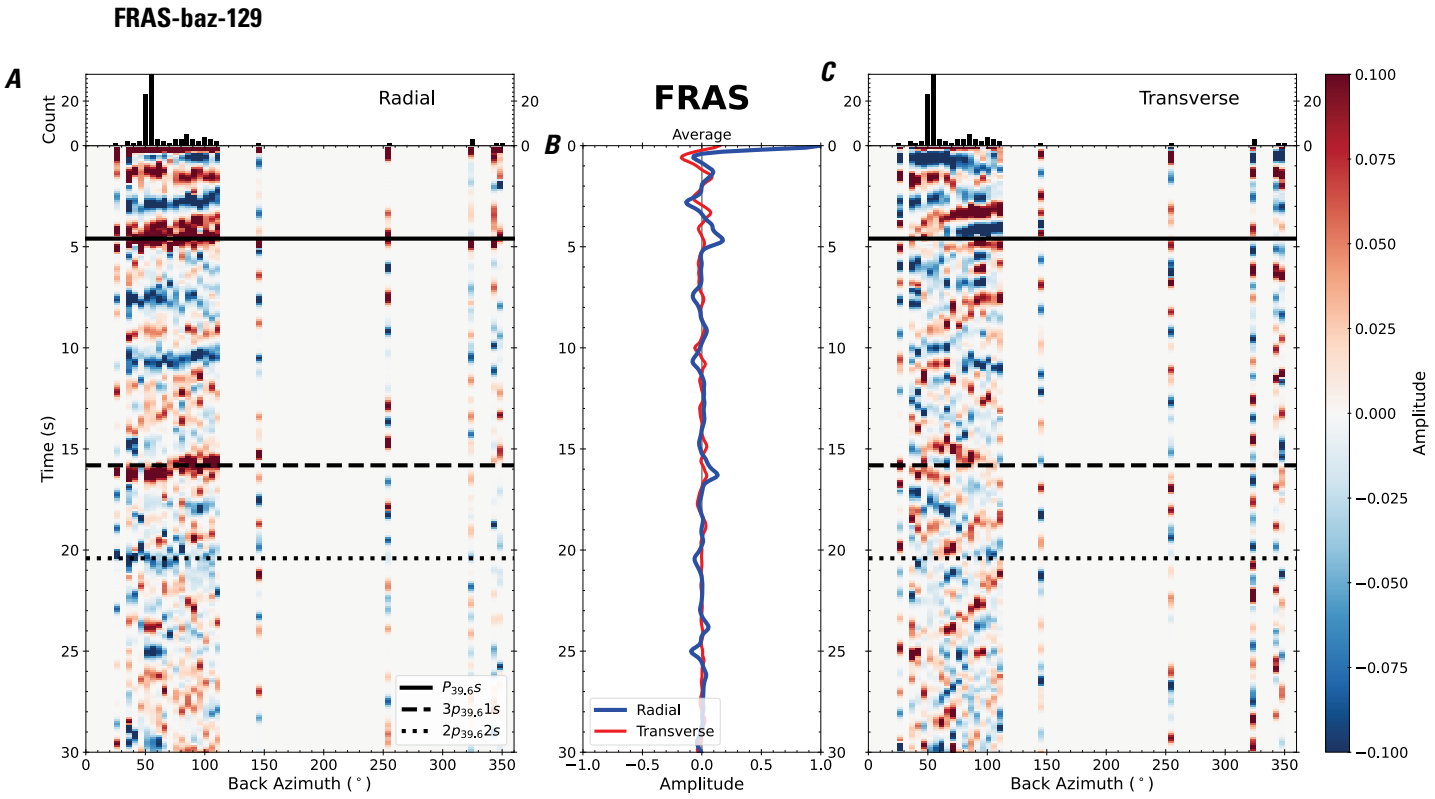

Figure 263. Receiver functions plotted against back azimuth for station FRAS. *A*, Radial component of P-wave receiver functions (PRFs) plotted against back azimuth. Individual PRFs have had the resonance-removal filter of Yu and others (2015) applied to them, are normalized to the maximum amplitude within the time window shown, binned, and normalized by the number of traces per bin. *B*, Average of every individual normalized radial receiver function with the application of the resonance-removal filter (blue) and average of every individual normalized raw radial receiver function (red). *C*, Radial component of raw PRFs, plotted against back azimuth, normalized as in *A*. Ps, 3p1s, and 2p2s arrival times predicted for the preferred Moho depth are shown, assuming a ray parameter of 0.06 s/km.

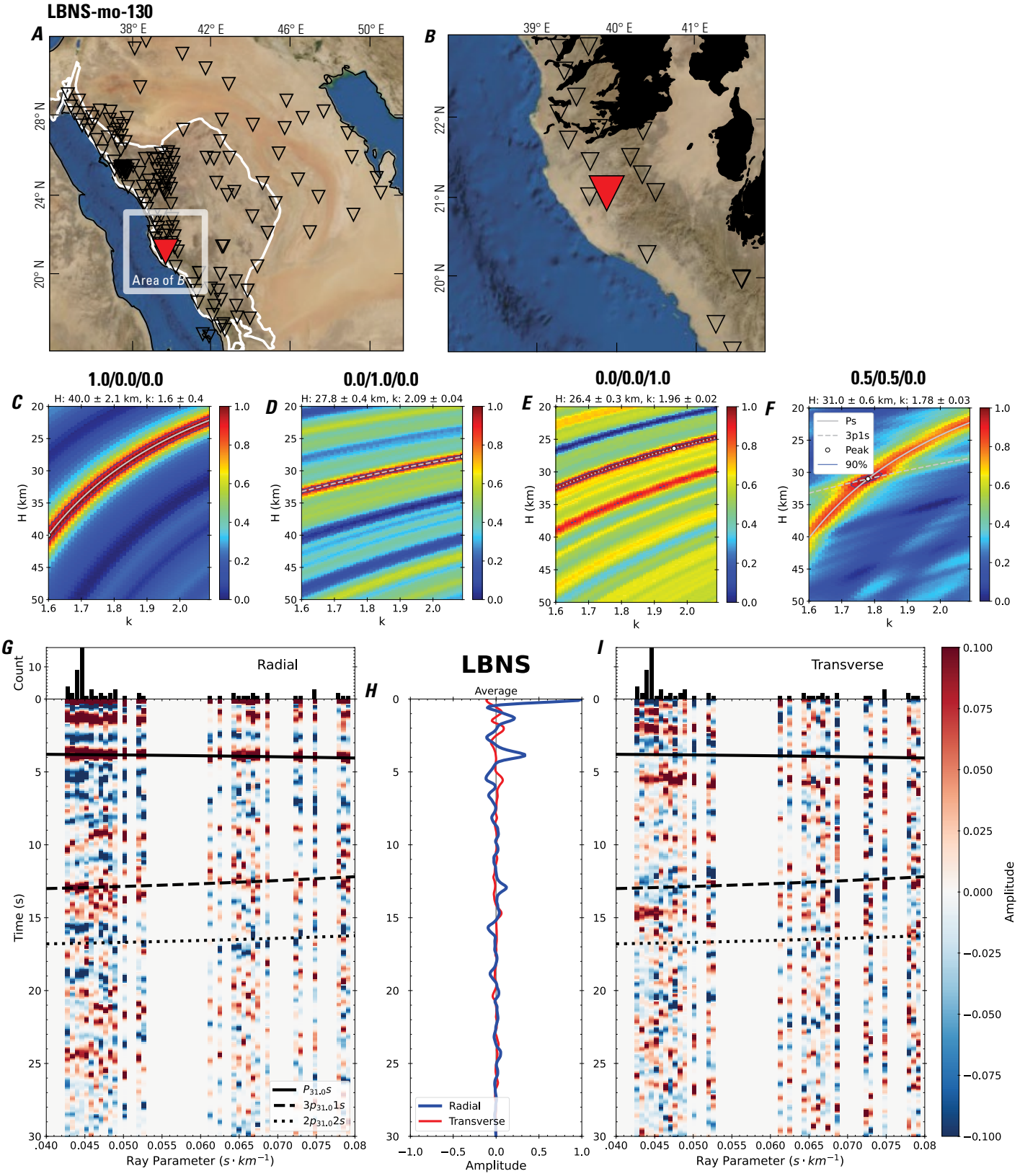
LBNS-mo-130
A
38° E
42° E
46° E
50° E
28° N
24° N
20° N
Area of B
B
39° E
40° E
41° E
22° N
21° N
20° N
1.0/0.0/0.0
C
H: 40.0 ± 2.1 km, k: 1.6 ± 0.4
0.0/1.0/0.0
D
H: 27.8 ± 0.4 km, k: 2.09 ± 0.04
0.0/0.0/1.0
E
H: 26.4 ± 0.3 km, k: 1.96 ± 0.02
0.5/0.5/0.0
F
H: 31.0 ± 0.6 km, k: 1.78 ± 0.03
Ps
3p1s
Peak
90%
H (km)
k
G
Radial
Count
Time (s)
$P_{31.0}s$
$3p_{31.0}1s$
$2p_{31.0}2s$
Ray Parameter ($s \cdot km^{-1}$)
LBNS
H
Average
Radial
Transverse
Amplitude
I
Transverse
Amplitude

Figure 264 (page 270). Receiver-function analysis for station LBNS. *A*, Regional map of Saudi Arabia showing the entire array (as inverted triangles), the location of station LBNS (red inverted triangle), the shield-platform boundary (white line), and the bounds of the map in *B* (white box). *B*, Local map of station LBNS. Harrats are shown in black. *C*, Standard, single-layer *H-k* stack with stacking weights 0.4/0.3/0.3. This *H-k* stack ignores sedimentary effects on the receiver functions. *D*, Standard, single-layer *H-k* stack with stacking weights 0.5/0.5/0.0. This *H-k* stack also ignores sedimentary effects on the receiver functions. *E*, Optimized sub-sedimentary *H-k* stack with stacking weights 0.4/0.3/0.3, following the method of Yu and others (2015). *F*, Optimized sedimentary *H-k* stack with stacking weights 0.05/0.70/0.25, following the method of Yu and others (2015). *G*, Radial component P-wave receiver functions (PRFs) plotted against ray parameter. Individual PRFs have had the resonance-removal filter of Yu and others (2015) applied to them and are normalized to the maximum amplitude within the time window shown, binned, and normalized by the number of traces per bin. *H*, Average of every individual normalized radial receiver function with the application of the resonance-removal filter (blue) and average of every individual normalized raw radial receiver function (red). *I*, Radial component of raw PRFs (that is, PRFs with no resonance-removal filter applied) plotted against ray parameter, normalized as in *G*.

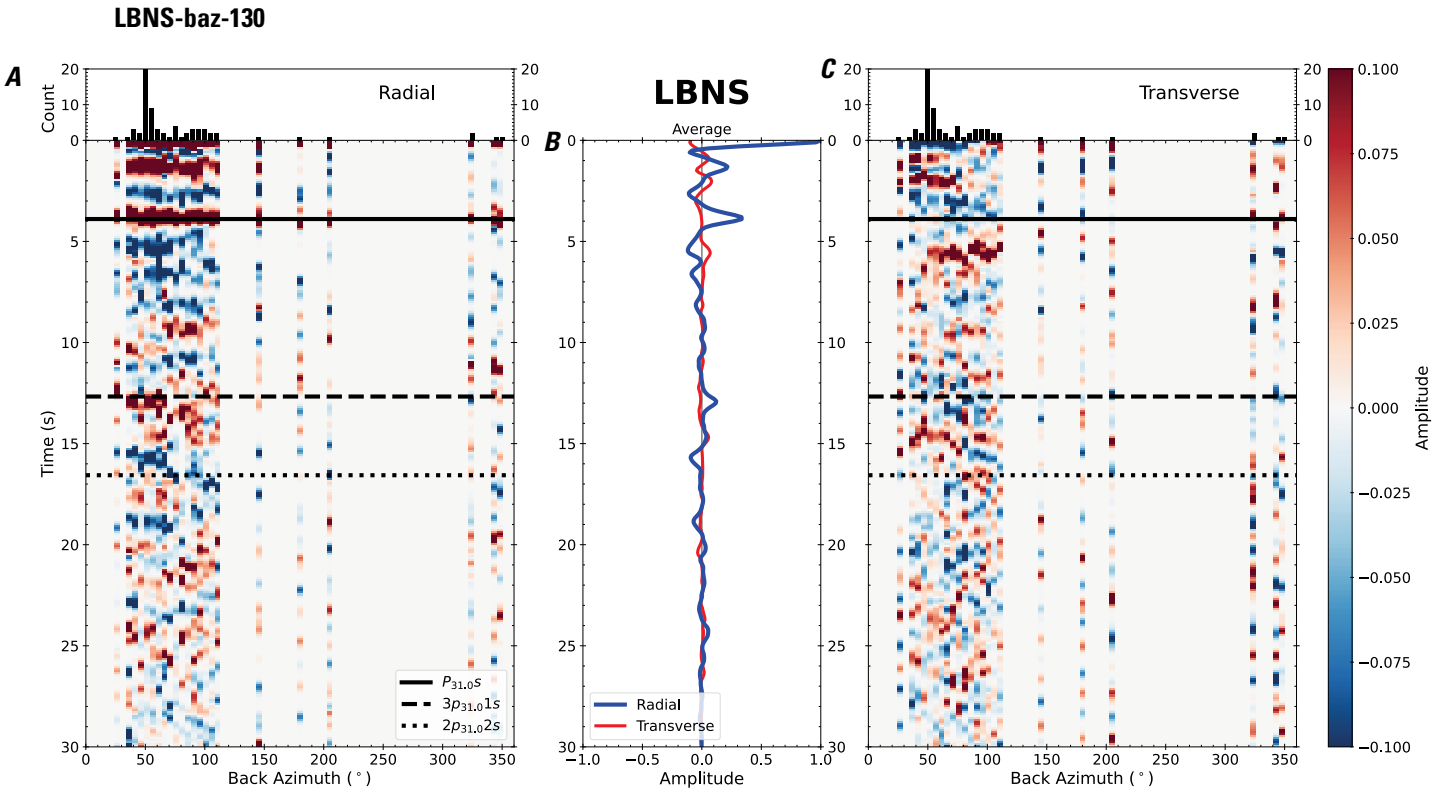

Figure 265. Receiver functions plotted against back azimuth for station LBNS. *A*, Radial component of P-wave receiver functions (PRFs) plotted against back azimuth. Individual PRFs have had the resonance-removal filter of Yu and others (2015) applied to them, are normalized to the maximum amplitude within the time window shown, binned, and normalized by the number of traces per bin. *B*, Average of every individual normalized radial receiver function with the application of the resonance-removal filter (blue) and average of every individual normalized raw radial receiver function (red). *C*, Radial component of raw PRFs, plotted against back azimuth, normalized as in *A*. Ps, 3p1s, and 2p2s arrival times predicted for the preferred Moho depth are shown, assuming a ray parameter of 0.06 s/km.

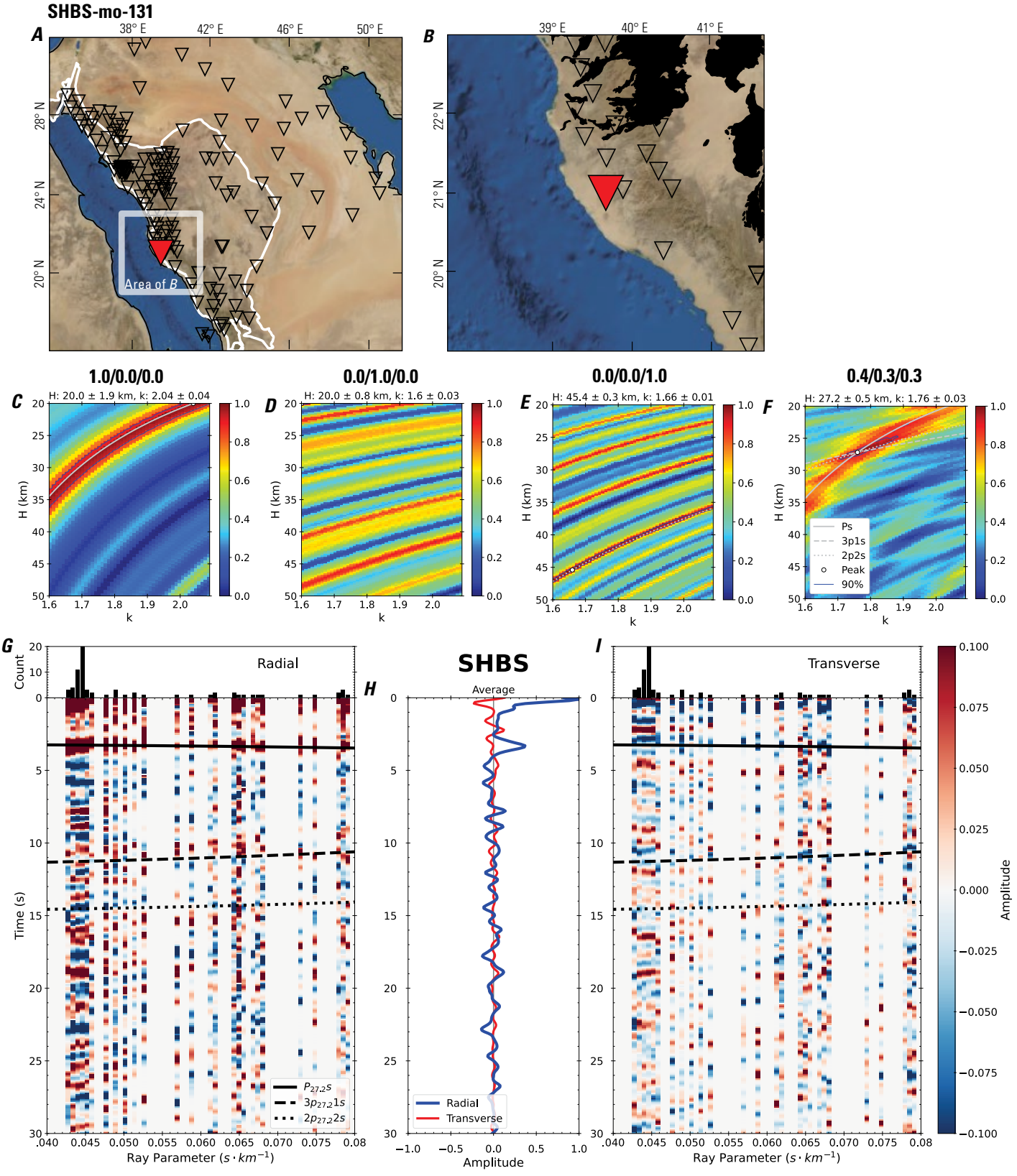
SHBS-mo-131
A
38° E
42° E
46° E
50° E
28° N
24° N
20° N
Area of B
B
39° E
40° E
41° E
22° N
21° N
20° N
1.0/0.0/0.0
0.0/1.0/0.0
0.0/0.0/1.0
0.4/0.3/0.3
C
H: 20.0 ± 1.9 km, k: 2.04 ± 0.04
D
H: 20.0 ± 0.8 km, k: 1.6 ± 0.03
E
H: 45.4 ± 0.3 km, k: 1.66 ± 0.01
F
H: 27.2 ± 0.5 km, k: 1.76 ± 0.03
H (km)
k
Ps
3p1s
2p2s
Peak
90%
G
Radial
Count
Time (s)
Ray Parameter (s · km⁻¹)
P27.2s
3p27.2 1s
2p27.2 2s
H
SHBS
Average
Radial
Transverse
Amplitude
I
Transverse
Amplitude

Figure 266 (page 272). Receiver-function analysis for station SHBS. *A*, Regional map of Saudi Arabia showing the entire array (as inverted triangles), the location of station SHBS (red inverted triangle), the shield-platform boundary (white line), and the bounds of the map in *B* (white box). *B*, Local map of station SHBS. Harrats are shown in black. *C*, Standard, single-layer *H-k* stack with stacking weights 0.4/0.3/0.3. This *H-k* stack ignores sedimentary effects on the receiver functions. *D*, Standard, single-layer *H-k* stack with stacking weights 0.5/0.5/0.0. This *H-k* stack also ignores sedimentary effects on the receiver functions. *E*, Optimized sub-sedimentary *H-k* stack with stacking weights 0.4/0.3/0.3, following the method of Yu and others (2015). *F*, Optimized sedimentary *H-k* stack with stacking weights 0.05/0.70/0.25, following the method of Yu and others (2015). *G*, Radial component P-wave receiver functions (PRFs) plotted against ray parameter. Individual PRFs have had the resonance-removal filter of Yu and others (2015) applied to them and are normalized to the maximum amplitude within the time window shown, binned, and normalized by the number of traces per bin. *H*, Average of every individual normalized radial receiver function with the application of the resonance-removal filter (blue) and average of every individual normalized raw radial receiver function (red). *I*, Radial component of raw PRFs (that is, PRFs with no resonance-removal filter applied) plotted against ray parameter, normalized as in *G*.

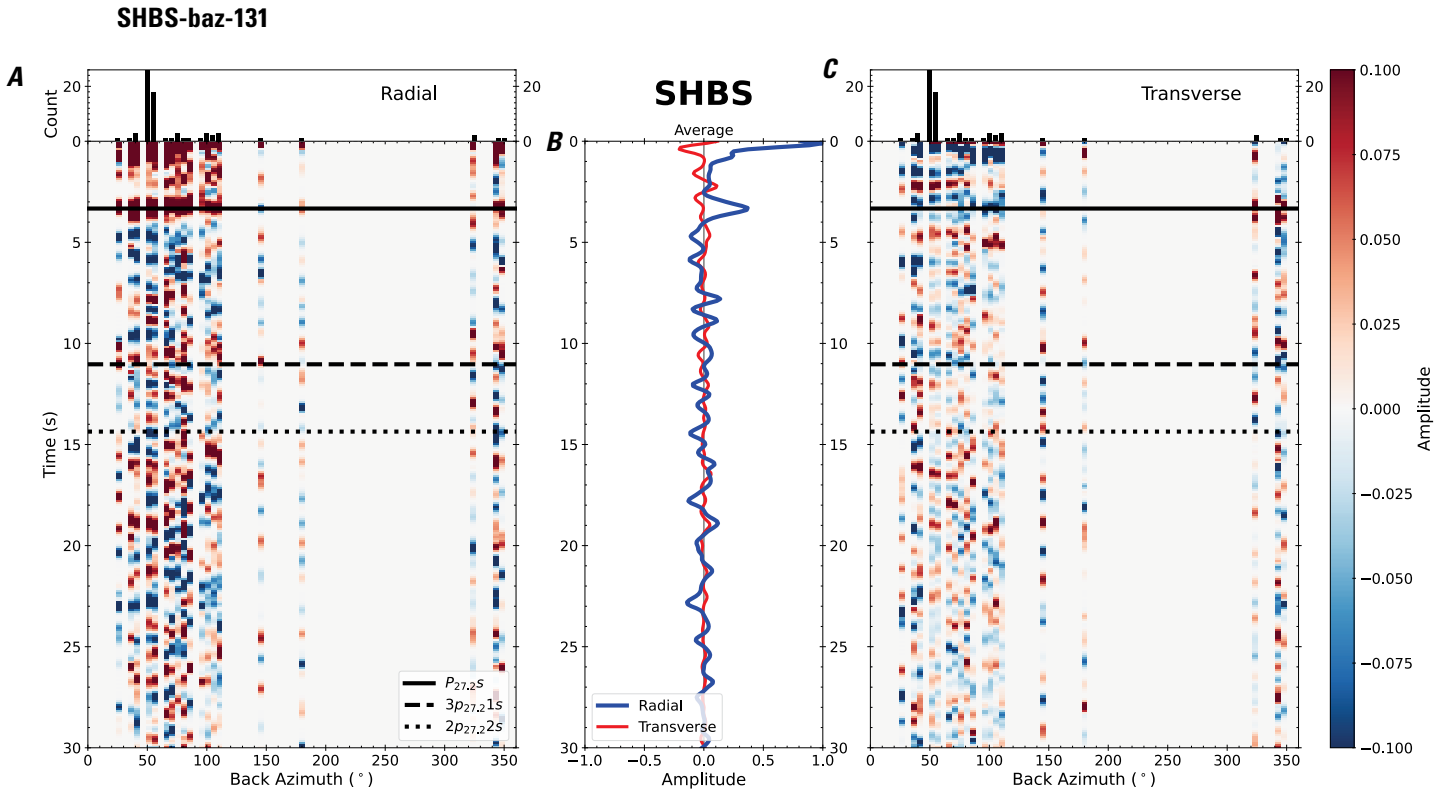

Figure 267. Receiver functions plotted against back azimuth for station SHBS. *A*, Radial component of P-wave receiver functions (PRFs) plotted against back azimuth. Individual PRFs have had the resonance-removal filter of Yu and others (2015) applied to them, are normalized to the maximum amplitude within the time window shown, binned, and normalized by the number of traces per bin. *B*, Average of every individual normalized radial receiver function with the application of the resonance-removal filter (blue) and average of every individual normalized raw radial receiver function (red). *C*, Radial component of raw PRFs, plotted against back azimuth, normalized as in *A*. Ps, 3p1s, and 2p2s arrival times predicted for the preferred Moho depth are shown, assuming a ray parameter of 0.06 s/km.

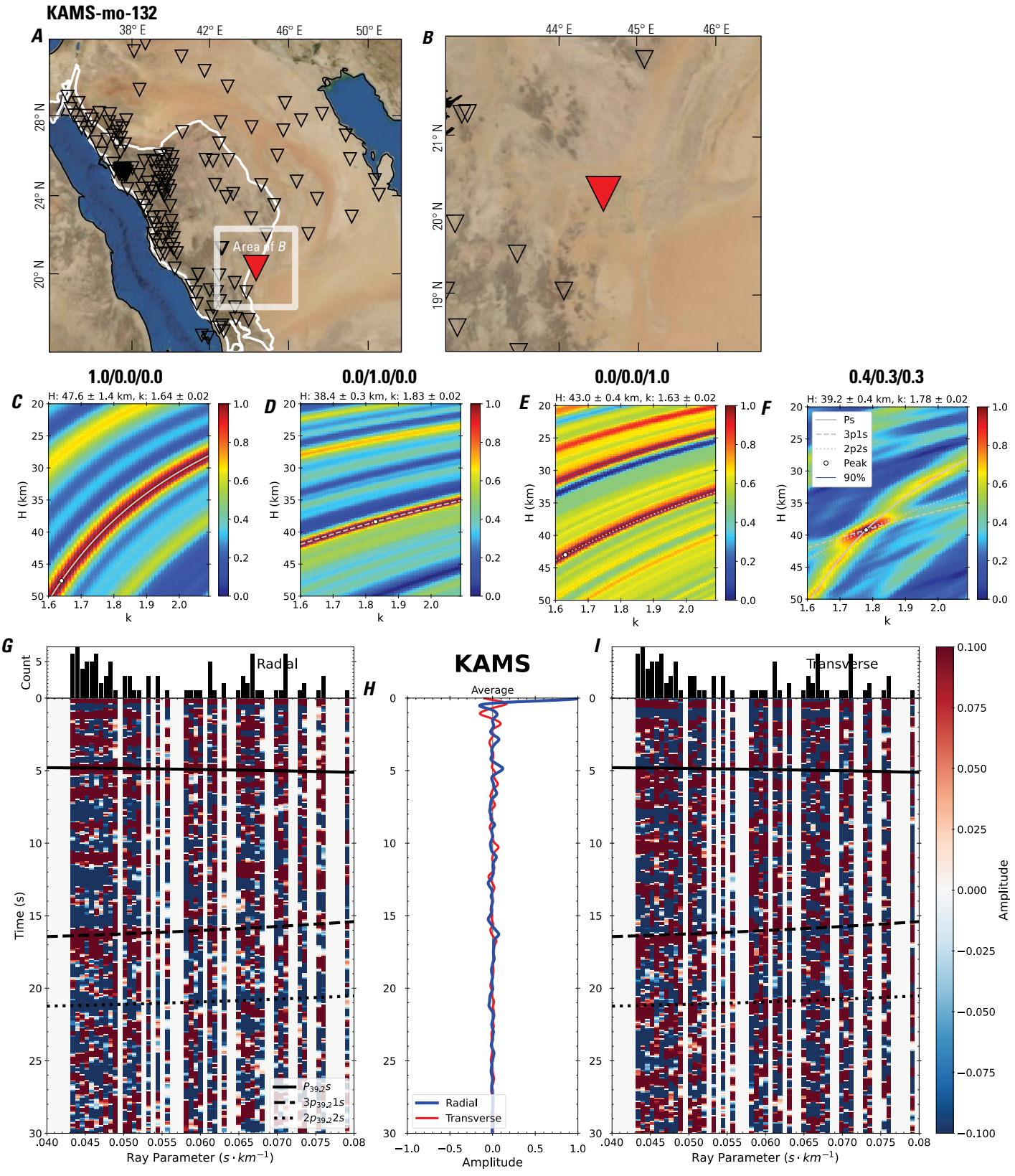
KAMS-mo-132
A
38° E
42° E
46° E
50° E
28° N
24° N
20° N
Area of B
B
44° E
45° E
46° E
21° N
20° N
19° N
1.0/0.0/0.0
0.0/1.0/0.0
0.0/0.0/1.0
0.4/0.3/0.3
C
H: 47.6 ± 1.4 km, k: 1.64 ± 0.02
D
H: 38.4 ± 0.3 km, k: 1.83 ± 0.02
E
H: 43.0 ± 0.4 km, k: 1.63 ± 0.02
F
H: 39.2 ± 0.4 km, k: 1.78 ± 0.02
Ps
3p1s
2p2s
Peak
90%
H (km)
k
G
Radial
Count
Time (s)
Ray Parameter (s · km⁻¹)
$P_{39.2}s$
$3p_{39.2}1s$
$2p_{39.2}2s$
H
KAMS
Average
Radial
Transverse
Amplitude
I
Transverse
Amplitude

Figure 268 (page 274). Receiver-function analysis for station KAMS. *A*, Regional map of Saudi Arabia showing the entire array (as inverted triangles), the location of station KAMS (red inverted triangle), the shield-platform boundary (white line), and the bounds of the map in *B* (white box). *B*, Local map of station KAMS. Harrats are shown in black. *C*, Standard, single-layer *H-k* stack with stacking weights 0.4/0.3/0.3. This *H-k* stack ignores sedimentary effects on the receiver functions. *D*, Standard, single-layer *H-k* stack with stacking weights 0.5/0.5/0.0. This *H-k* stack also ignores sedimentary effects on the receiver functions. *E*, Optimized sub-sedimentary *H-k* stack with stacking weights 0.4/0.3/0.3, following the method of Yu and others (2015). *F*, Optimized sedimentary *H-k* stack with stacking weights 0.05/0.70/0.25, following the method of Yu and others (2015). *G*, Radial component P-wave receiver functions (PRFs) plotted against ray parameter. Individual PRFs have had the resonance-removal filter of Yu and others (2015) applied to them and are normalized to the maximum amplitude within the time window shown, binned, and normalized by the number of traces per bin. *H*, Average of every individual normalized radial receiver function with the application of the resonance-removal filter (blue) and average of every individual normalized raw radial receiver function (red). *I*, Radial component of raw PRFs (that is, PRFs with no resonance-removal filter applied) plotted against ray parameter, normalized as in *G*.

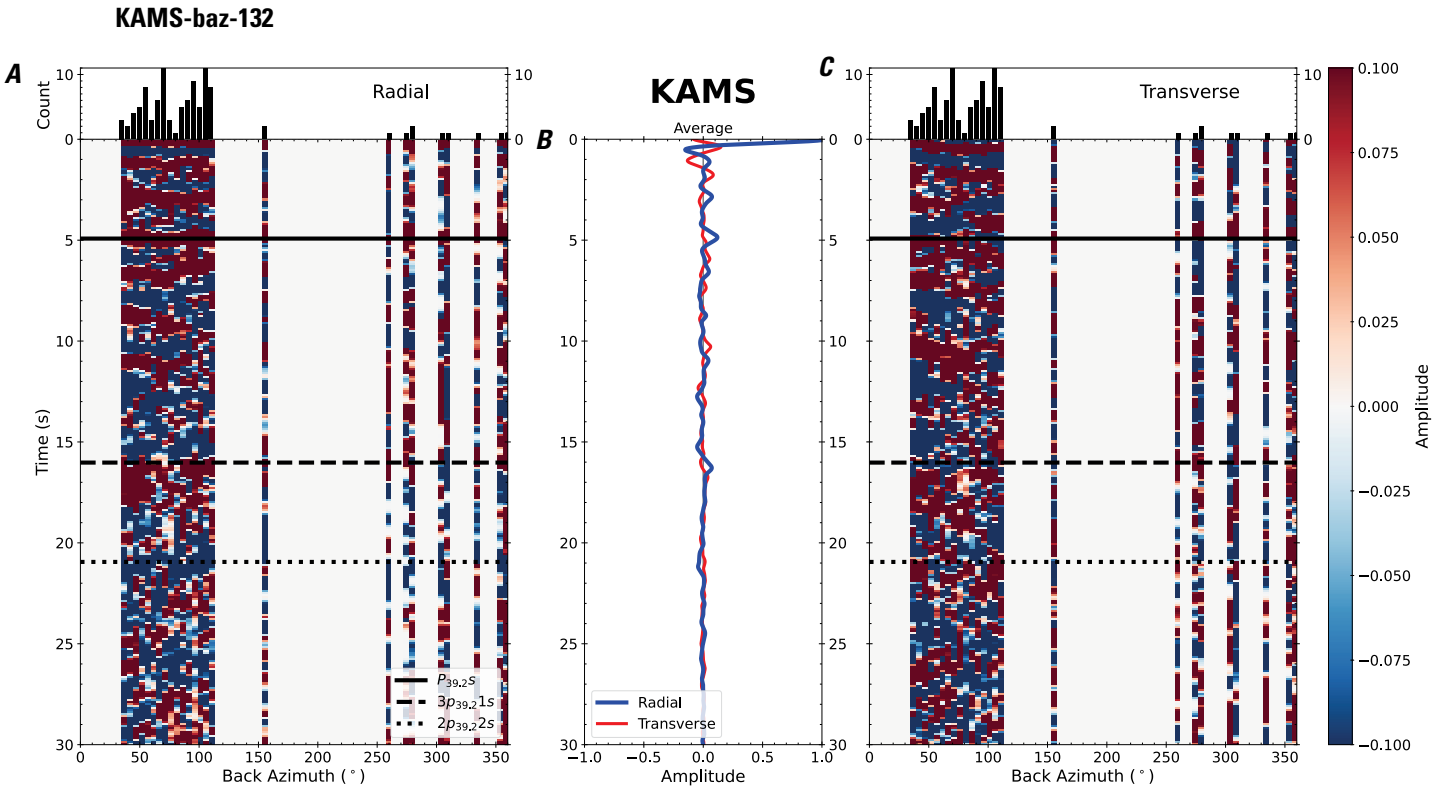

Figure 269. Receiver functions plotted against back azimuth for station KAMS. *A*, Radial component of P-wave receiver functions (PRFs) plotted against back azimuth. Individual PRFs have had the resonance-removal filter of Yu and others (2015) applied to them, are normalized to the maximum amplitude within the time window shown, binned, and normalized by the number of traces per bin. *B*, Average of every individual normalized radial receiver function with the application of the resonance-removal filter (blue) and average of every individual normalized raw radial receiver function (red). *C*, Radial component of raw PRFs, plotted against back azimuth, normalized as in *A*. Ps, 3p1s, and 2p2s arrival times predicted for the preferred Moho depth are shown, assuming a ray parameter of 0.06 s/km.

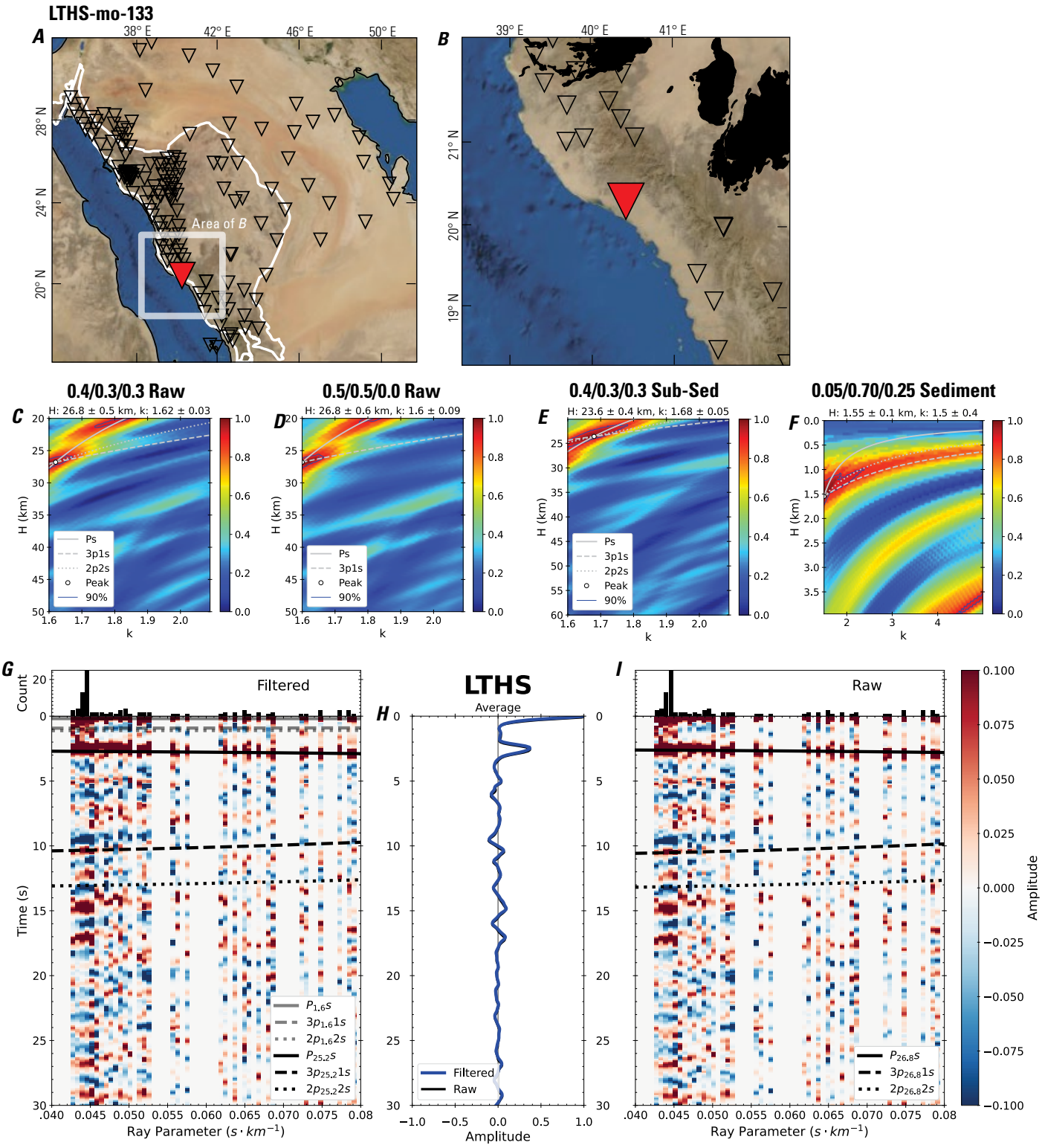
LTHS-mo-133
A
38° E
42° E
46° E
50° E
28° N
24° N
20° N
Area of B
B
39° E
40° E
41° E
21° N
20° N
19° N
0.4/0.3/0.3 Raw
0.5/0.5/0.0 Raw
0.4/0.3/0.3 Sub-Sed
0.05/0.70/0.25 Sediment
C
H: 26.8 ± 0.5 km, k: 1.62 ± 0.03
D
H: 26.8 ± 0.6 km, k: 1.6 ± 0.09
E
H: 23.6 ± 0.4 km, k: 1.68 ± 0.05
F
H: 1.55 ± 0.1 km, k: 1.5 ± 0.4
H (km)
k
Ps
3p1s
2p2s
Peak
90%
G
Filtered
Count
Time (s)
$P_{1.6}s$
$3p_{1.6}1s$
$2p_{1.6}2s$
$P_{25.2}s$
$3p_{25.2}1s$
$2p_{25.2}2s$
Ray Parameter ($s \cdot km^{-1}$)
H
LTHS
Average
Filtered
Raw
Amplitude
I
Raw
$P_{26.8}s$
$3p_{26.8}1s$
$2p_{26.8}2s$
Ray Parameter ($s \cdot km^{-1}$)
Amplitude

Figure 270 (page 276). Receiver-function analysis for station LTHS. *A*, Regional map of Saudi Arabia showing the entire array (as inverted triangles), the location of station LTHS (red inverted triangle), the shield-platform boundary (white line), and the bounds of the map in *B* (white box). *B*, Local map of station LTHS. Harrats are shown in black. *C*, Standard, single-layer *H-k* stack with stacking weights 0.4/0.3/0.3. This *H-k* stack ignores sedimentary effects on the receiver functions. *D*, Standard, single-layer *H-k* stack with stacking weights 0.5/0.5/0.0. This *H-k* stack also ignores sedimentary effects on the receiver functions. *E*, Optimized sub-sedimentary *H-k* stack with stacking weights 0.4/0.3/0.3, following the method of Yu and others (2015). *F*, Optimized sedimentary *H-k* stack with stacking weights 0.05/0.70/0.25, following the method of Yu and others (2015). *G*, Radial component P-wave receiver functions (PRFs) plotted against ray parameter. Individual PRFs have had the resonance-removal filter of Yu and others (2015) applied to them and are normalized to the maximum amplitude within the time window shown, binned, and normalized by the number of traces per bin. *H*, Average of every individual normalized radial receiver function with the application of the resonance-removal filter (blue) and average of every individual normalized raw radial receiver function (red). *I*, Radial component of raw PRFs (that is, PRFs with no resonance-removal filter applied) plotted against ray parameter, normalized as in *G*.

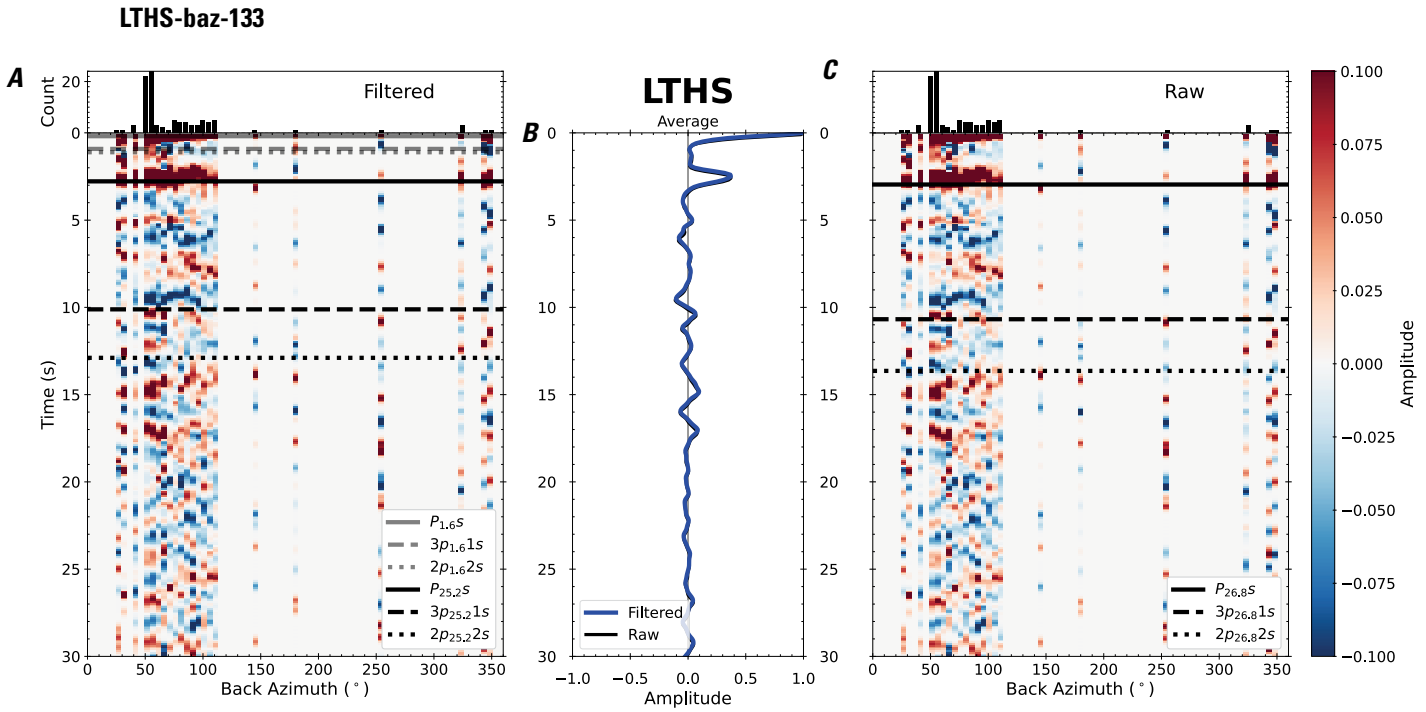

Figure 271. Receiver functions plotted against back azimuth for station LTHS. *A*, Radial component of P-wave receiver functions (PRFs) plotted against back azimuth. Individual PRFs have had the resonance-removal filter of Yu and others (2015) applied to them, are normalized to the maximum amplitude within the time window shown, binned, and normalized by the number of traces per bin. *B*, Average of every individual normalized radial receiver function with the application of the resonance-removal filter (blue) and average of every individual normalized raw radial receiver function (red). *C*, Radial component of raw PRFs, plotted against back azimuth, normalized as in *A*. Ps, 3p1s, and 2p2s arrival times predicted for the preferred Moho depth are shown, assuming a ray parameter of 0.06 s/km.

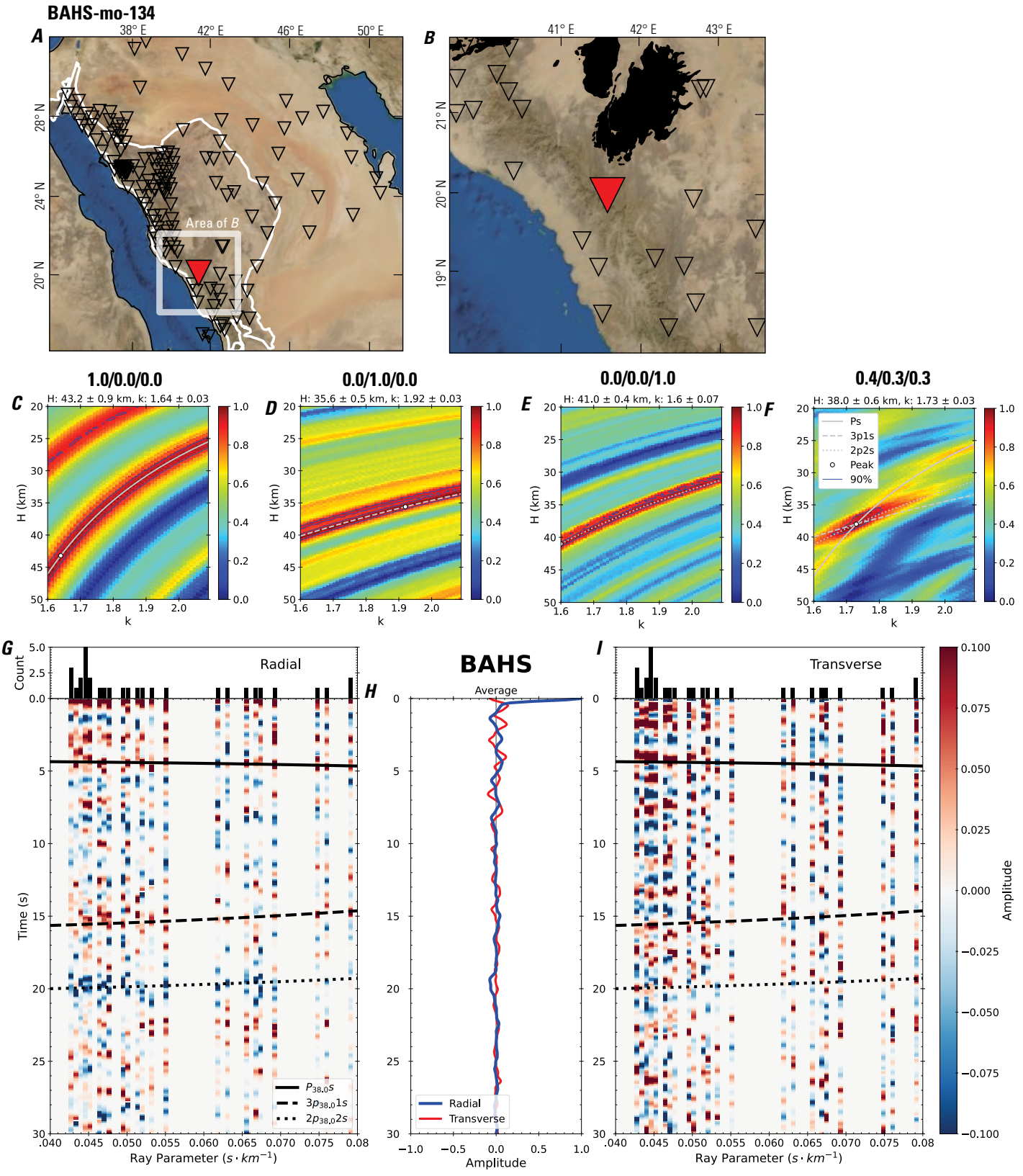
BAHS-mo-134
A
38° E
42° E
46° E
50° E
28° N
24° N
20° N
Area of B
B
41° E
42° E
43° E
21° N
20° N
19° N
1.0/0.0/0.0
0.0/1.0/0.0
0.0/0.0/1.0
0.4/0.3/0.3
C
H: 43.2 ± 0.9 km, k: 1.64 ± 0.03
D
H: 35.6 ± 0.5 km, k: 1.92 ± 0.03
E
H: 41.0 ± 0.4 km, k: 1.6 ± 0.07
F
H: 38.0 ± 0.6 km, k: 1.73 ± 0.03
Ps
3p1s
2p2s
Peak
90%
H (km)
k
G
Radial
Count
Time (s)
$P_{38.0}s$
$3p_{38.0}1s$
$2p_{38.0}2s$
Ray Parameter ($s \cdot km^{-1}$)
H
BAHS
Average
Radial
Transverse
Amplitude
I
Transverse
Amplitude

Figure 272 (page 278). Receiver-function analysis for station BAHS. *A*, Regional map of Saudi Arabia showing the entire array (as inverted triangles), the location of station BAHS (red inverted triangle), the shield-platform boundary (white line), and the bounds of the map in *B* (white box). *B*, Local map of station BAHS. Harrats are shown in black. *C*, Standard, single-layer *H-k* stack with stacking weights 0.4/0.3/0.3. This *H-k* stack ignores sedimentary effects on the receiver functions. *D*, Standard, single-layer *H-k* stack with stacking weights 0.5/0.5/0.0. This *H-k* stack also ignores sedimentary effects on the receiver functions. *E*, Optimized sub-sedimentary *H-k* stack with stacking weights 0.4/0.3/0.3, following the method of Yu and others (2015). *F*, Optimized sedimentary *H-k* stack with stacking weights 0.05/0.70/0.25, following the method of Yu and others (2015). *G*, Radial component P-wave receiver functions (PRFs) plotted against ray parameter. Individual PRFs have had the resonance-removal filter of Yu and others (2015) applied to them and are normalized to the maximum amplitude within the time window shown, binned, and normalized by the number of traces per bin. *H*, Average of every individual normalized radial receiver function with the application of the resonance-removal filter (blue) and average of every individual normalized raw radial receiver function (red). *I*, Radial component of raw PRFs (that is, PRFs with no resonance-removal filter applied) plotted against ray parameter, normalized as in *G*.

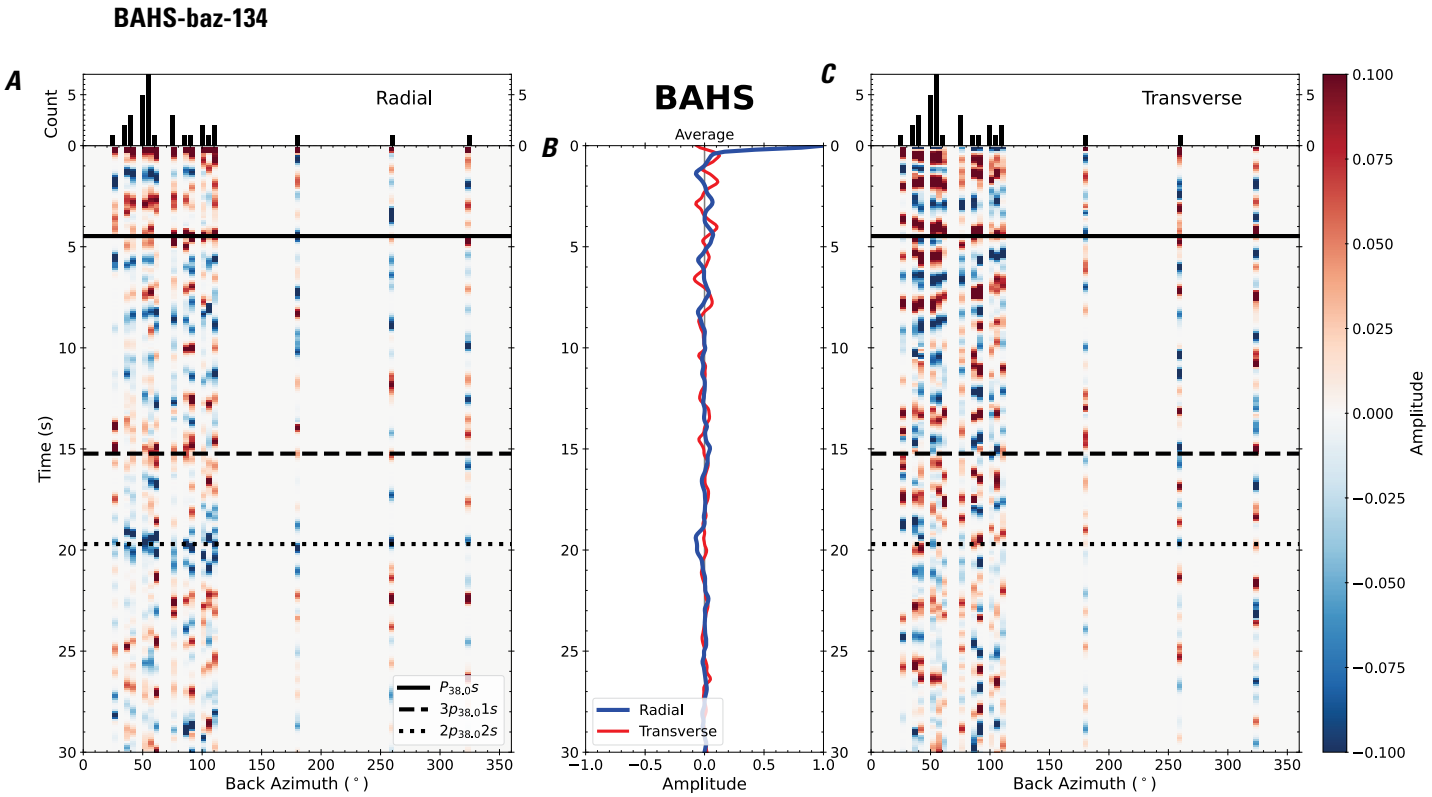

Figure 273. Receiver functions plotted against back azimuth for station BAHS. *A*, Radial component of P-wave receiver functions (PRFs) plotted against back azimuth. Individual PRFs have had the resonance-removal filter of Yu and others (2015) applied to them, are normalized to the maximum amplitude within the time window shown, binned, and normalized by the number of traces per bin. *B*, Average of every individual normalized radial receiver function with the application of the resonance-removal filter (blue) and average of every individual normalized raw radial receiver function (red). *C*, Radial component of raw PRFs, plotted against back azimuth, normalized as in *A*. Ps, 3p1s, and 2p2s arrival times predicted for the preferred Moho depth are shown, assuming a ray parameter of 0.06 s/km.

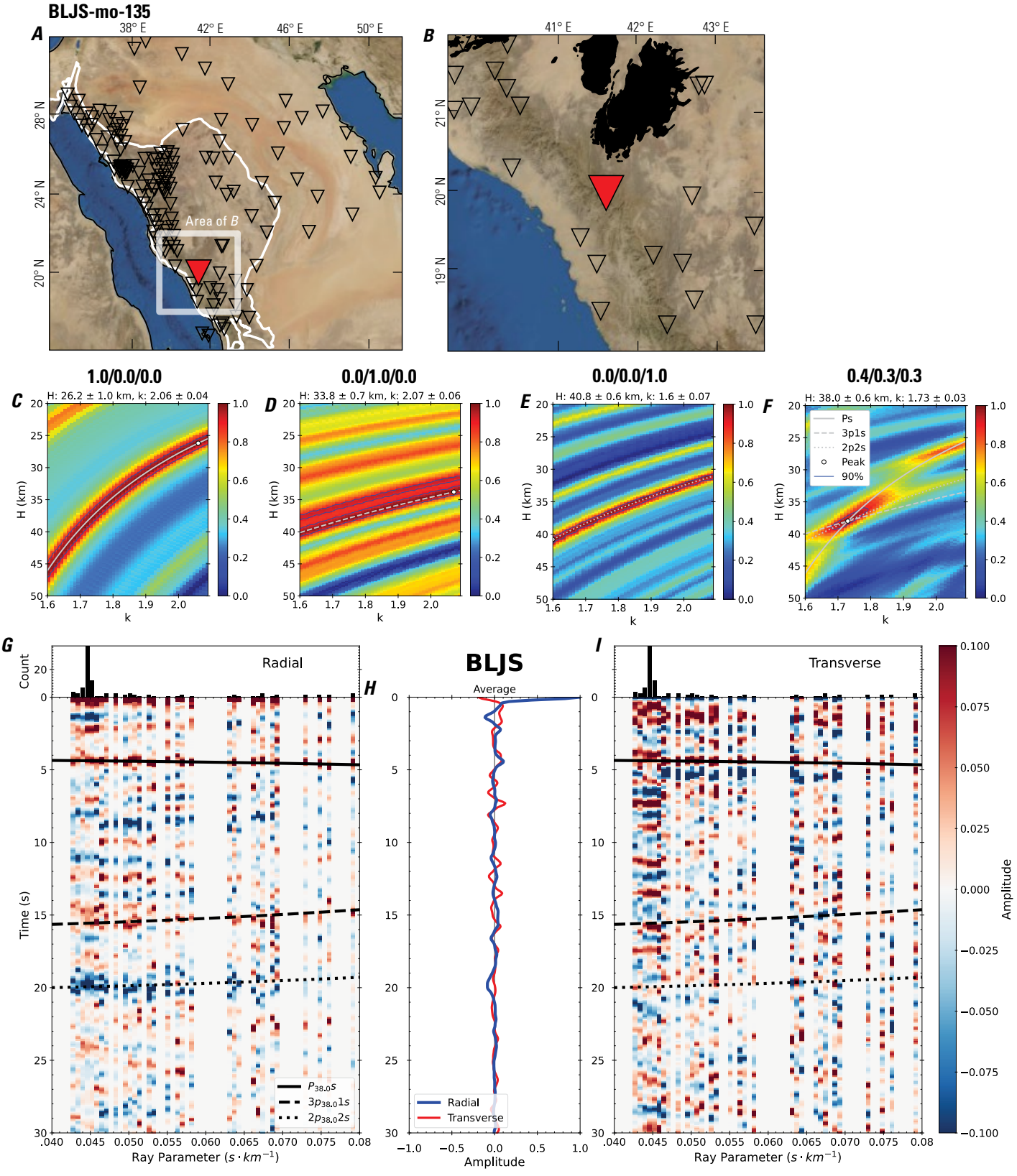
BLJS-mo-135
A
38° E
42° E
46° E
50° E
28° N
24° N
20° N
Area of B
B
41° E
42° E
43° E
21° N
20° N
19° N
1.0/0.0/0.0
0.0/1.0/0.0
0.0/0.0/1.0
0.4/0.3/0.3
C
H: 26.2 ± 1.0 km, k: 2.06 ± 0.04
D
H: 33.8 ± 0.7 km, k: 2.07 ± 0.06
E
H: 40.8 ± 0.6 km, k: 1.6 ± 0.07
F
H: 38.0 ± 0.6 km, k: 1.73 ± 0.03
Ps
3p1s
2p2s
Peak
90%
H (km)
k
G
Radial
Count
Time (s)
$P_{38.0}s$
$3p_{38.0}1s$
$2p_{38.0}2s$
Ray Parameter ($s \cdot km^{-1}$)
H
BLJS
Average
Radial
Transverse
Amplitude
I
Transverse
Amplitude

Figure 274 (page 280). Receiver-function analysis for station BLJS. *A*, Regional map of Saudi Arabia showing the entire array (as inverted triangles), the location of station BLJS (red inverted triangle), the shield-platform boundary (white line), and the bounds of the map in *B* (white box). *B*, Local map of station BLJS. Harrats are shown in black. *C*, Standard, single-layer *H-k* stack with stacking weights 0.4/0.3/0.3. This *H-k* stack ignores sedimentary effects on the receiver functions. *D*, Standard, single-layer *H-k* stack with stacking weights 0.5/0.5/0.0. This *H-k* stack also ignores sedimentary effects on the receiver functions. *E*, Optimized sub-sedimentary *H-k* stack with stacking weights 0.4/0.3/0.3, following the method of Yu and others (2015). *F*, Optimized sedimentary *H-k* stack with stacking weights 0.05/0.70/0.25, following the method of Yu and others (2015). *G*, Radial component P-wave receiver functions (PRFs) plotted against ray parameter. Individual PRFs have had the resonance-removal filter of Yu and others (2015) applied to them and are normalized to the maximum amplitude within the time window shown, binned, and normalized by the number of traces per bin. *H*, Average of every individual normalized radial receiver function with the application of the resonance-removal filter (blue) and average of every individual normalized raw radial receiver function (red). *I*, Radial component of raw PRFs (that is, PRFs with no resonance-removal filter applied) plotted against ray parameter, normalized as in *G*.

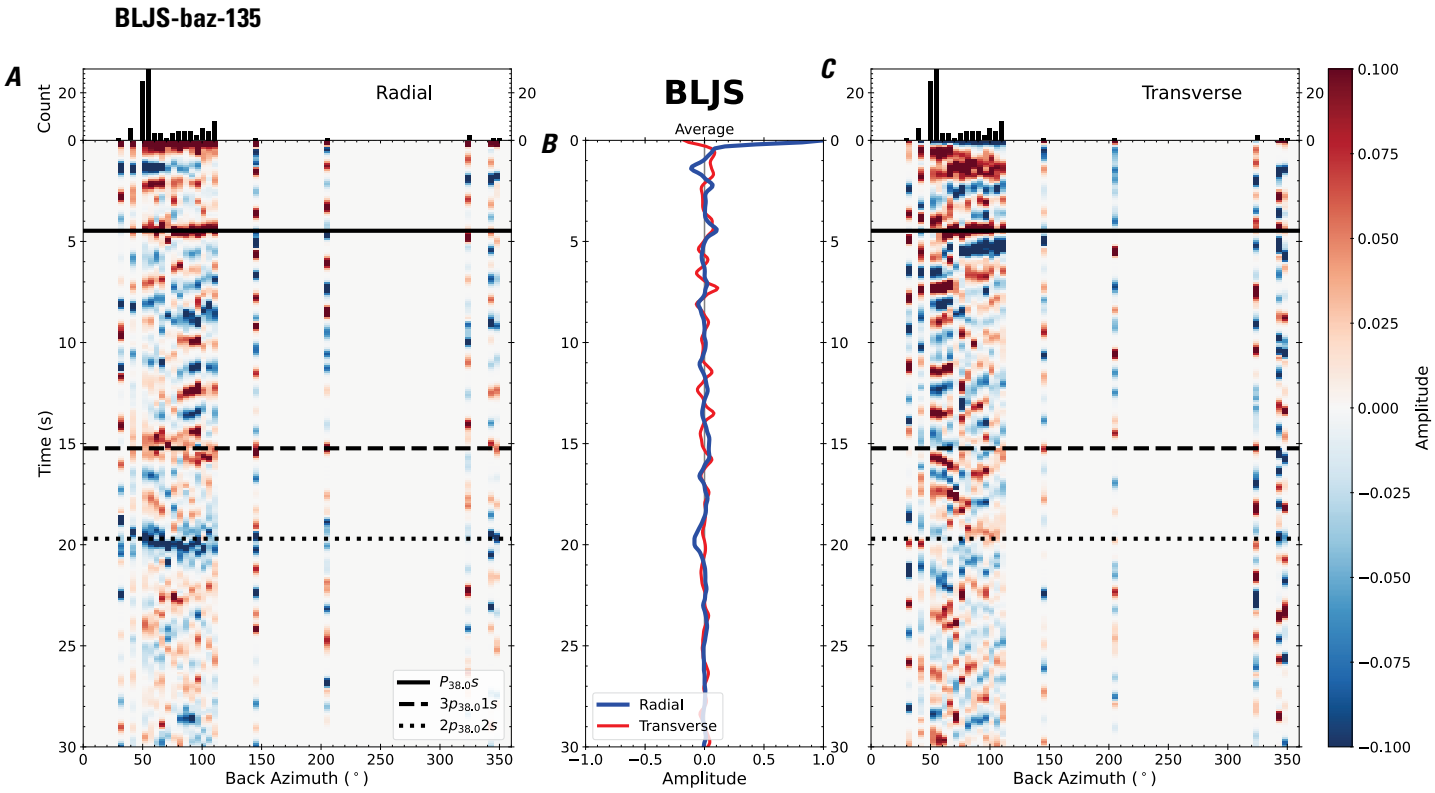

Figure 275. Receiver functions plotted against back azimuth for station BLJS. *A*, Radial component of P-wave receiver functions (PRFs) plotted against back azimuth. Individual PRFs have had the resonance-removal filter of Yu and others (2015) applied to them, are normalized to the maximum amplitude within the time window shown, binned, and normalized by the number of traces per bin. *B*, Average of every individual normalized radial receiver function with the application of the resonance-removal filter (blue) and average of every individual normalized raw radial receiver function (red). *C*, Radial component of raw PRFs, plotted against back azimuth, normalized as in *A*. Ps, 3p1s, and 2p2s arrival times predicted for the preferred Moho depth are shown, assuming a ray parameter of 0.06 s/km.

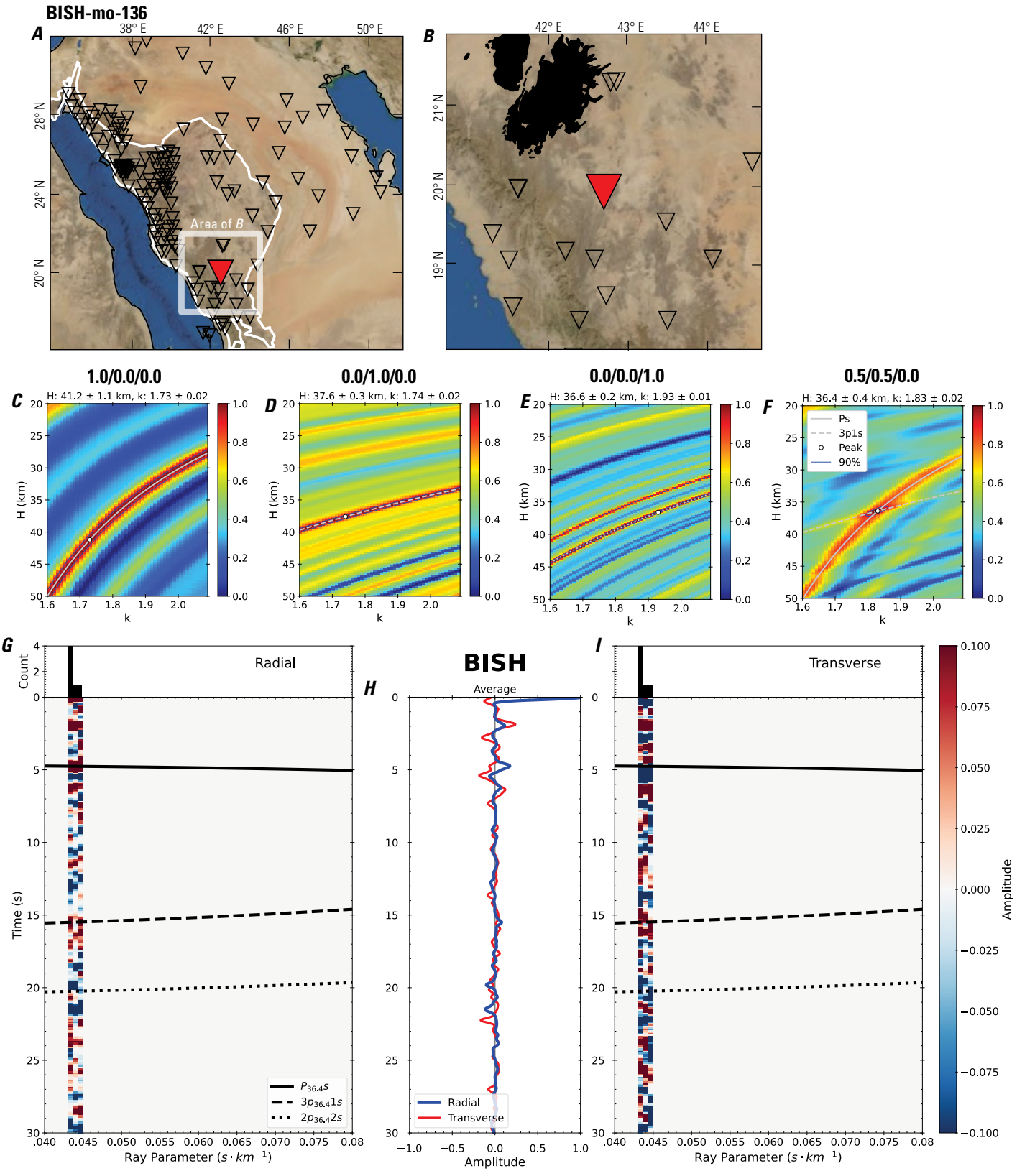
BISH-mo-136
A
B
Area of B
1.0/0.0/0.0
0.0/1.0/0.0
0.0/0.0/1.0
0.5/0.5/0.0
C
D
E
F
H: 41.2 ± 1.1 km, k: 1.73 ± 0.02
H: 37.6 ± 0.3 km, k: 1.74 ± 0.02
H: 36.6 ± 0.2 km, k: 1.93 ± 0.01
H: 36.4 ± 0.4 km, k: 1.83 ± 0.02
Ps
3p1s
Peak
90%
H (km)
k
G
H
I
Radial
Transverse
BISH
Average
Count
Time (s)
Ray Parameter (s · km⁻¹)
Amplitude
P36.4s
3p36.41s
2p36.42s

Figure 276 (page 282). Receiver-function analysis for station BISH. *A*, Regional map of Saudi Arabia showing the entire array (as inverted triangles), the location of station BISH (red inverted triangle), the shield-platform boundary (white line), and the bounds of the map in *B* (white box). *B*, Local map of station BISH. Harrats are shown in black. *C*, Standard, single-layer *H-k* stack with stacking weights 0.4/0.3/0.3. This *H-k* stack ignores sedimentary effects on the receiver functions. *D*, Standard, single-layer *H-k* stack with stacking weights 0.5/0.5/0.0. This *H-k* stack also ignores sedimentary effects on the receiver functions. *E*, Optimized sub-sedimentary *H-k* stack with stacking weights 0.4/0.3/0.3, following the method of Yu and others (2015). *F*, Optimized sedimentary *H-k* stack with stacking weights 0.05/0.70/0.25, following the method of Yu and others (2015). *G*, Radial component P-wave receiver functions (PRFs) plotted against ray parameter. Individual PRFs have had the resonance-removal filter of Yu and others (2015) applied to them and are normalized to the maximum amplitude within the time window shown, binned, and normalized by the number of traces per bin. *H*, Average of every individual normalized radial receiver function with the application of the resonance-removal filter (blue) and average of every individual normalized raw radial receiver function (red). *I*, Radial component of raw PRFs (that is, PRFs with no resonance-removal filter applied) plotted against ray parameter, normalized as in *G*.

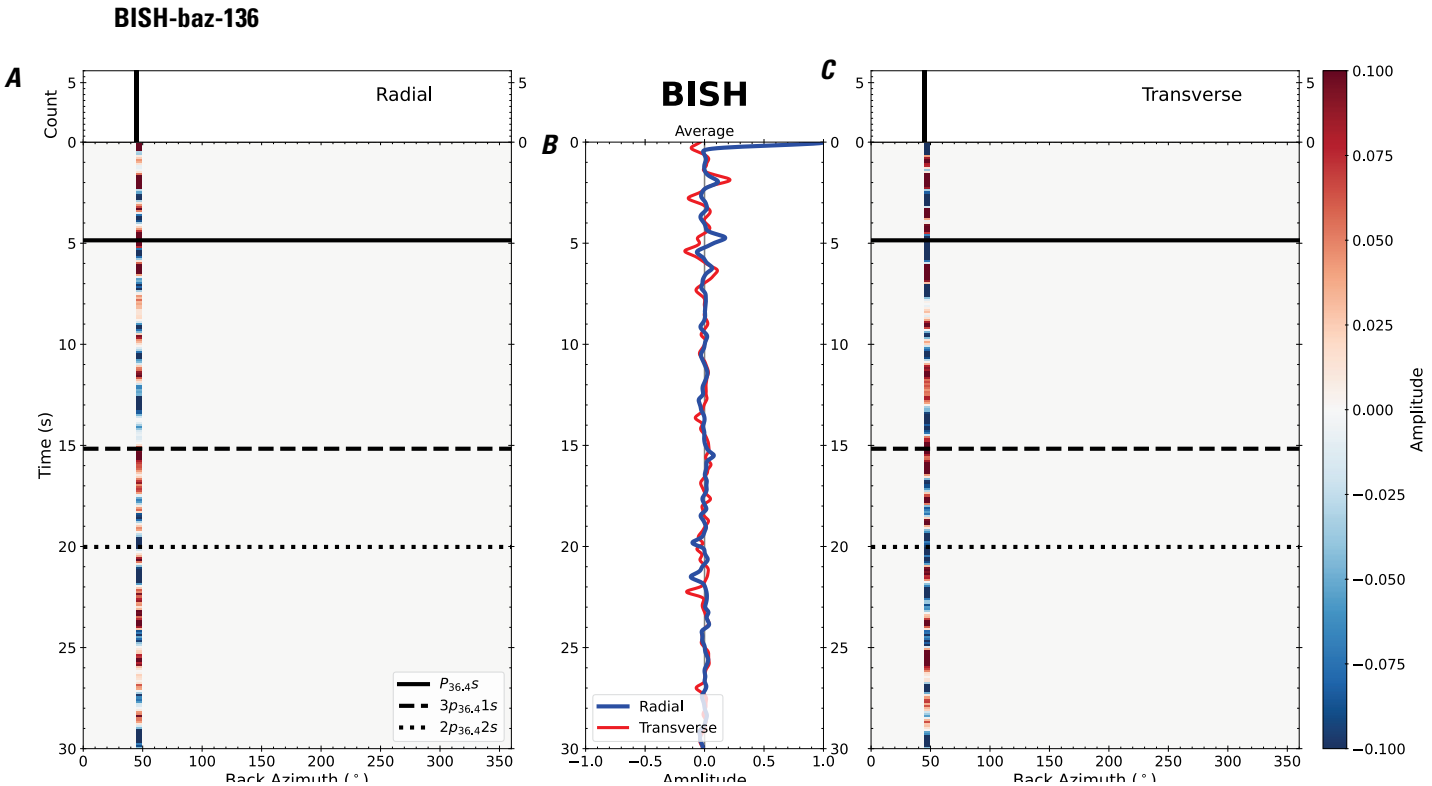

Figure 277. Receiver functions plotted against back azimuth for station BISH. *A*, Radial component of P-wave receiver functions (PRFs) plotted against back azimuth. Individual PRFs have had the resonance-removal filter of Yu and others (2015) applied to them, are normalized to the maximum amplitude within the time window shown, binned, and normalized by the number of traces per bin. *B*, Average of every individual normalized radial receiver function with the application of the resonance-removal filter (blue) and average of every individual normalized raw radial receiver function (red). *C*, Radial component of raw PRFs, plotted against back azimuth, normalized as in *A*. Ps, 3p1s, and 2p2s arrival times predicted for the preferred Moho depth are shown, assuming a ray parameter of 0.06 s/km.

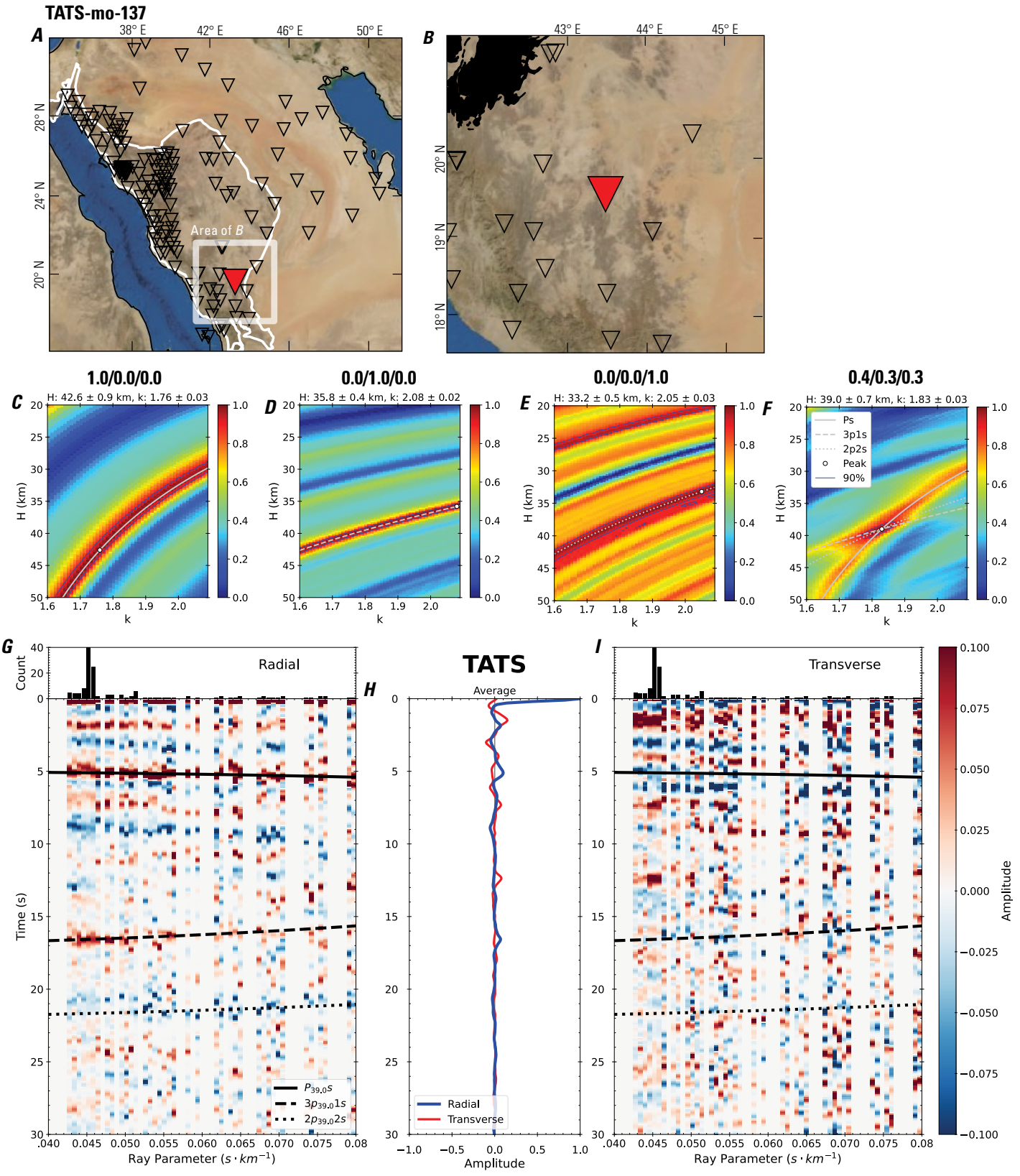
TATS-mo-137
A
38° E
42° E
46° E
50° E
28° N
24° N
20° N
Area of B
B
43° E
44° E
45° E
20° N
19° N
18° N
1.0/0.0/0.0
0.0/1.0/0.0
0.0/0.0/1.0
0.4/0.3/0.3
C
H: 42.6 ± 0.9 km, k: 1.76 ± 0.03
D
H: 35.8 ± 0.4 km, k: 2.08 ± 0.02
E
H: 33.2 ± 0.5 km, k: 2.05 ± 0.03
F
H: 39.0 ± 0.7 km, k: 1.83 ± 0.03
Ps
3p1s
2p2s
Peak
90%
H (km)
k
G
Radial
Count
Time (s)
$P_{39.0}s$
$3p_{39.0}1s$
$2p_{39.0}2s$
Ray Parameter ($s \cdot km^{-1}$)
H
TATS
Average
Radial
Transverse
Amplitude
I
Transverse
Amplitude

Figure 278 (page 284). Receiver-function analysis for station TATS. *A*, Regional map of Saudi Arabia showing the entire array (as inverted triangles), the location of station TATS (red inverted triangle), the shield-platform boundary (white line), and the bounds of the map in *B* (white box). *B*, Local map of station TATS. Harrats are shown in black. *C*, Standard, single-layer *H-k* stack with stacking weights 0.4/0.3/0.3. This *H-k* stack ignores sedimentary effects on the receiver functions. *D*, Standard, single-layer *H-k* stack with stacking weights 0.5/0.5/0.0. This *H-k* stack also ignores sedimentary effects on the receiver functions. *E*, Optimized sub-sedimentary *H-k* stack with stacking weights 0.4/0.3/0.3, following the method of Yu and others (2015). *F*, Optimized sedimentary *H-k* stack with stacking weights 0.05/0.70/0.25, following the method of Yu and others (2015). *G*, Radial component P-wave receiver functions (PRFs) plotted against ray parameter. Individual PRFs have had the resonance-removal filter of Yu and others (2015) applied to them and are normalized to the maximum amplitude within the time window shown, binned, and normalized by the number of traces per bin. *H*, Average of every individual normalized radial receiver function with the application of the resonance-removal filter (blue) and average of every individual normalized raw radial receiver function (red). *I*, Radial component of raw PRFs (that is, PRFs with no resonance-removal filter applied) plotted against ray parameter, normalized as in *G*.

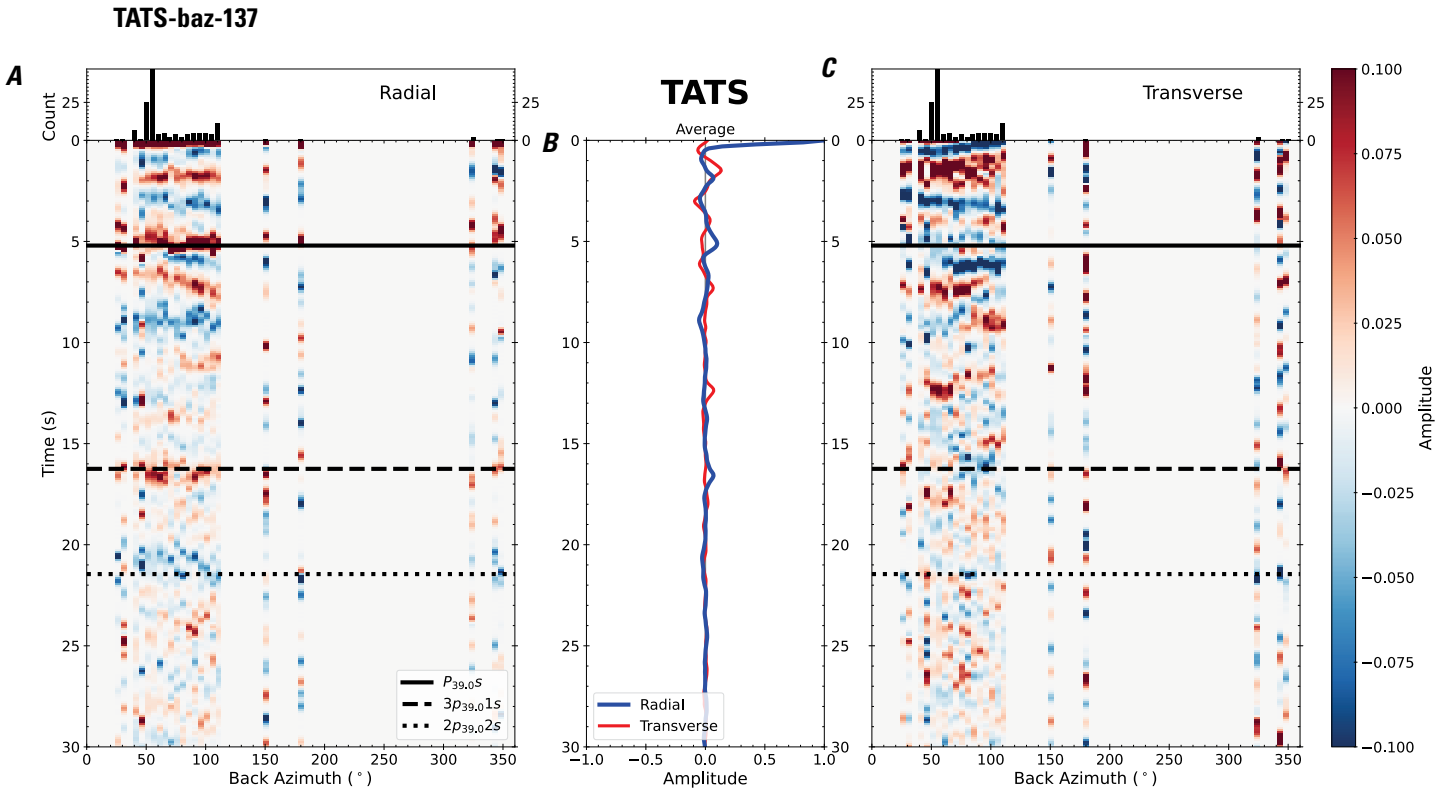

Figure 279. Receiver functions plotted against back azimuth for station TATS. *A*, Radial component of P-wave receiver functions (PRFs) plotted against back azimuth. Individual PRFs have had the resonance-removal filter of Yu and others (2015) applied to them, are normalized to the maximum amplitude within the time window shown, binned, and normalized by the number of traces per bin. *B*, Average of every individual normalized radial receiver function with the application of the resonance-removal filter (blue) and average of every individual normalized raw radial receiver function (red). *C*, Radial component of raw PRFs, plotted against back azimuth, normalized as in *A*. Ps, 3p1s, and 2p2s arrival times predicted for the preferred Moho depth are shown, assuming a ray parameter of 0.06 s/km.

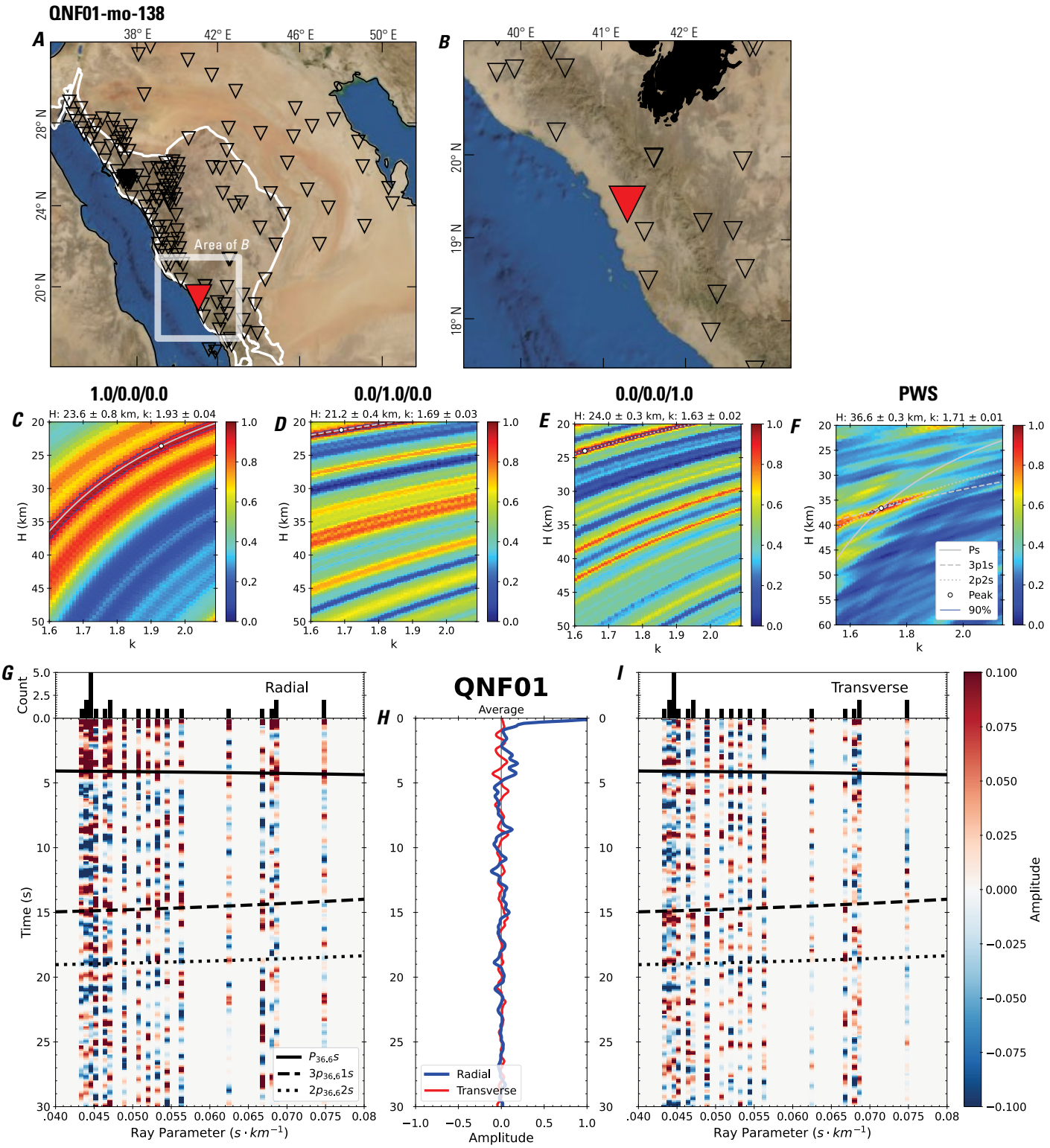
QNF01-mo-138
A
38° E
42° E
46° E
50° E
28° N
24° N
20° N
Area of B
B
40° E
41° E
42° E
20° N
19° N
18° N
1.0/0.0/0.0
0.0/1.0/0.0
0.0/0.0/1.0
PWS
C
H: 23.6 ± 0.8 km, k: 1.93 ± 0.04
D
H: 21.2 ± 0.4 km, k: 1.69 ± 0.03
E
H: 24.0 ± 0.3 km, k: 1.63 ± 0.02
F
H: 36.6 ± 0.3 km, k: 1.71 ± 0.01
H (km)
k
Ps
3p1s
2p2s
Peak
90%
G
Radial
Count
Time (s)
$P_{36.6}s$
$3p_{36.6}1s$
$2p_{36.6}2s$
Ray Parameter ($s \cdot km^{-1}$)
QNF01
Average
H
Radial
Transverse
Amplitude
I
Transverse
Amplitude

Figure 280 (page 286). Receiver-function analysis for station QNF01. *A*, Regional map of Saudi Arabia showing the entire array (as inverted triangles), the location of station QNF01 (red inverted triangle), the shield-platform boundary (white line), and the bounds of the map in *B* (white box). *B*, Local map of station QNF01. Harrats are shown in black. *C*, Standard, single-layer *H-k* stack with stacking weights 0.4/0.3/0.3. This *H-k* stack ignores sedimentary effects on the receiver functions. *D*, Standard, single-layer *H-k* stack with stacking weights 0.5/0.5/0.0. This *H-k* stack also ignores sedimentary effects on the receiver functions. *E*, Optimized sub-sedimentary *H-k* stack with stacking weights 0.4/0.3/0.3, following the method of Yu and others (2015). *F*, Optimized sedimentary *H-k* stack with stacking weights 0.05/0.70/0.25, following the method of Yu and others (2015). *G*, Radial component P-wave receiver functions (PRFs) plotted against ray parameter. Individual PRFs have had the resonance-removal filter of Yu and others (2015) applied to them and are normalized to the maximum amplitude within the time window shown, binned, and normalized by the number of traces per bin. *H*, Average of every individual normalized radial receiver function with the application of the resonance-removal filter (blue) and average of every individual normalized raw radial receiver function (red). *I*, Radial component of raw PRFs (that is, PRFs with no resonance-removal filter applied) plotted against ray parameter, normalized as in *G*.

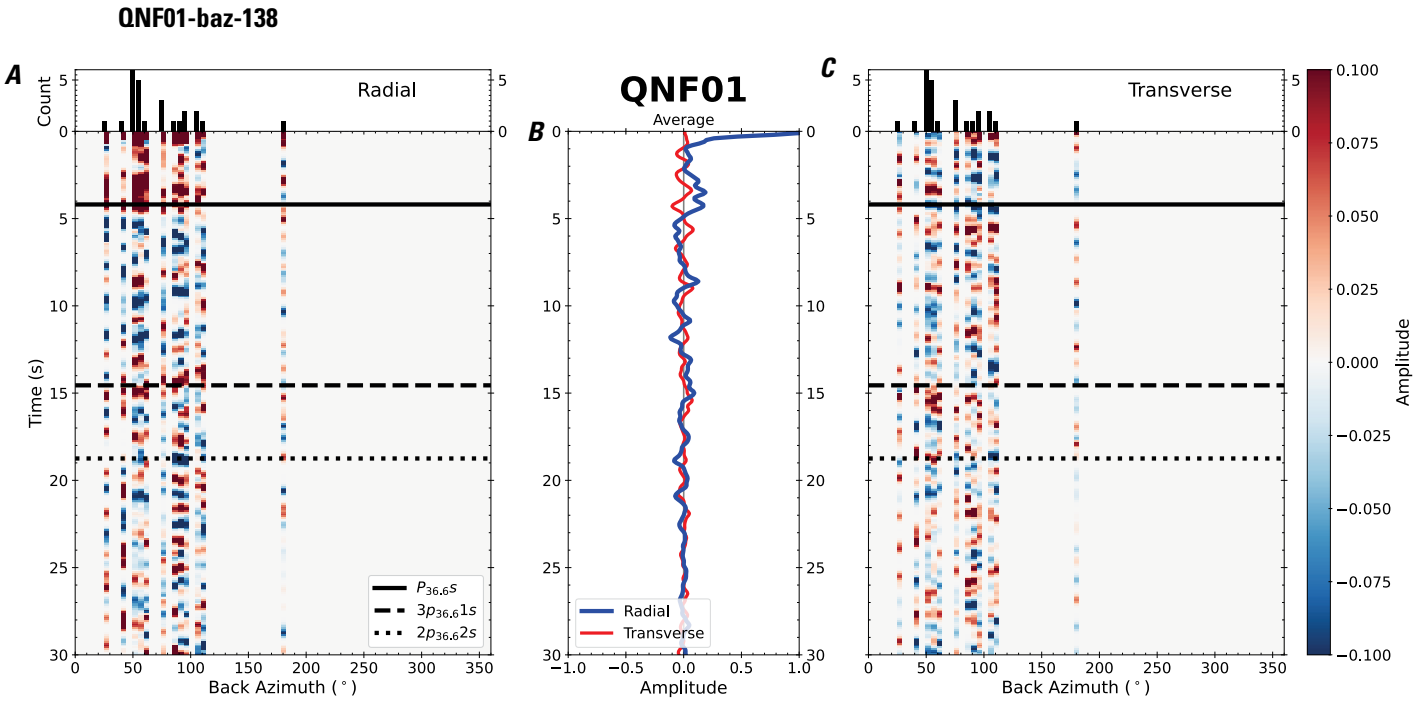

Figure 281. Receiver functions plotted against back azimuth for station QNF01. *A*, Radial component of P-wave receiver functions (PRFs) plotted against back azimuth. Individual PRFs have had the resonance-removal filter of Yu and others (2015) applied to them, are normalized to the maximum amplitude within the time window shown, binned, and normalized by the number of traces per bin. *B*, Average of every individual normalized radial receiver function with the application of the resonance-removal filter (blue) and average of every individual normalized raw radial receiver function (red). *C*, Radial component of raw PRFs, plotted against back azimuth, normalized as in *A*. Ps, 3p1s, and 2p2s arrival times predicted for the preferred Moho depth are shown, assuming a ray parameter of 0.06 s/km.

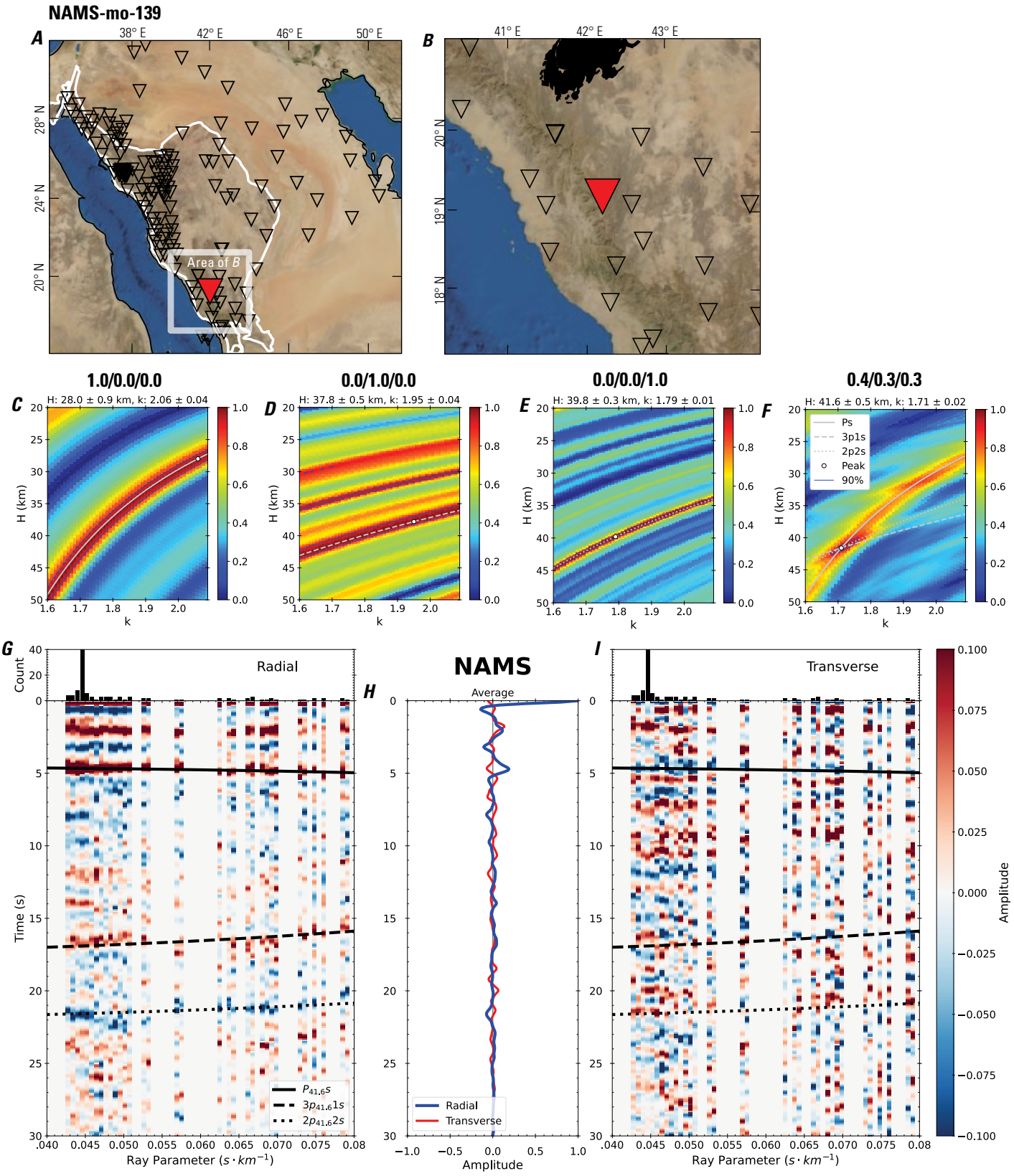
NAMS-mo-139
A
38° E
42° E
46° E
50° E
28° N
24° N
20° N
Area of B
B
41° E
42° E
43° E
20° N
19° N
18° N
1.0/0.0/0.0
0.0/1.0/0.0
0.0/0.0/1.0
0.4/0.3/0.3
C
H: 28.0 ± 0.9 km, k: 2.06 ± 0.04
D
H: 37.8 ± 0.5 km, k: 1.95 ± 0.04
E
H: 39.8 ± 0.3 km, k: 1.79 ± 0.01
F
H: 41.6 ± 0.5 km, k: 1.71 ± 0.02
H (km)
k
Ps
3p1s
2p2s
Peak
90%
G
Radial
Count
Time (s)
Ray Parameter (s · km⁻¹)
$P_{41.6}s$
$3p_{41.6}1s$
$2p_{41.6}2s$
H
NAMS
Average
Radial
Transverse
Amplitude
I
Transverse
Amplitude

Figure 282 (page 288). Receiver-function analysis for station NAMS. *A*, Regional map of Saudi Arabia showing the entire array (as inverted triangles), the location of station NAMS (red inverted triangle), the shield-platform boundary (white line), and the bounds of the map in *B* (white box). *B*, Local map of station NAMS. Harrats are shown in black. *C*, Standard, single-layer *H-k* stack with stacking weights 0.4/0.3/0.3. This *H-k* stack ignores sedimentary effects on the receiver functions. *D*, Standard, single-layer *H-k* stack with stacking weights 0.5/0.5/0.0. This *H-k* stack also ignores sedimentary effects on the receiver functions. *E*, Optimized sub-sedimentary *H-k* stack with stacking weights 0.4/0.3/0.3, following the method of Yu and others (2015). *F*, Optimized sedimentary *H-k* stack with stacking weights 0.05/0.70/0.25, following the method of Yu and others (2015). *G*, Radial component P-wave receiver functions (PRFs) plotted against ray parameter. Individual PRFs have had the resonance-removal filter of Yu and others (2015) applied to them and are normalized to the maximum amplitude within the time window shown, binned, and normalized by the number of traces per bin. *H*, Average of every individual normalized radial receiver function with the application of the resonance-removal filter (blue) and average of every individual normalized raw radial receiver function (red). *I*, Radial component of raw PRFs (that is, PRFs with no resonance-removal filter applied) plotted against ray parameter, normalized as in *G*.

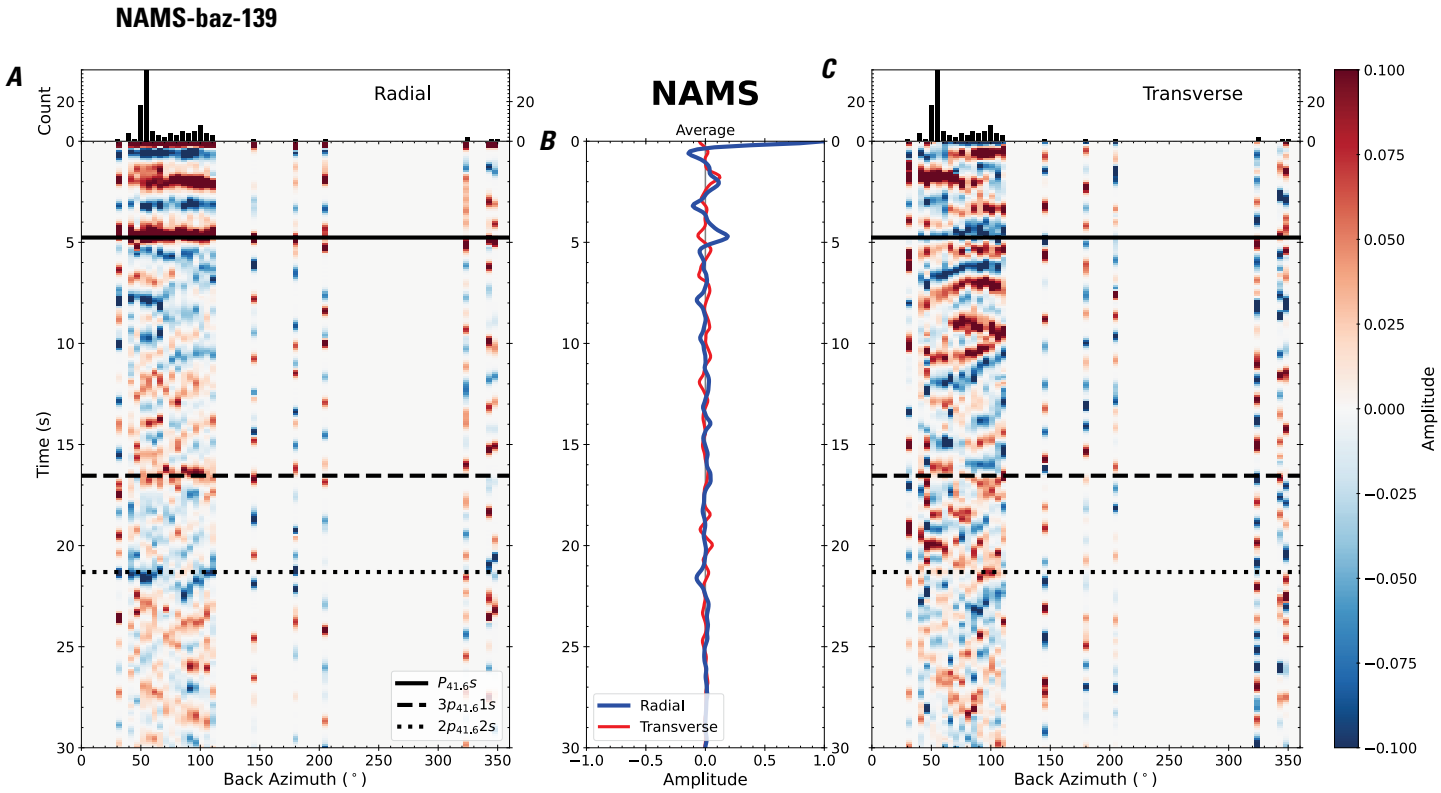

Figure 283. Receiver functions plotted against back azimuth for station NAMS. *A*, Radial component of P-wave receiver functions (PRFs) plotted against back azimuth. Individual PRFs have had the resonance-removal filter of Yu and others (2015) applied to them, are normalized to the maximum amplitude within the time window shown, binned, and normalized by the number of traces per bin. *B*, Average of every individual normalized radial receiver function with the application of the resonance-removal filter (blue) and average of every individual normalized raw radial receiver function (red). *C*, Radial component of raw PRFs, plotted against back azimuth, normalized as in *A*. Ps, 3p1s, and 2p2s arrival times predicted for the preferred Moho depth are shown, assuming a ray parameter of 0.06 s/km.

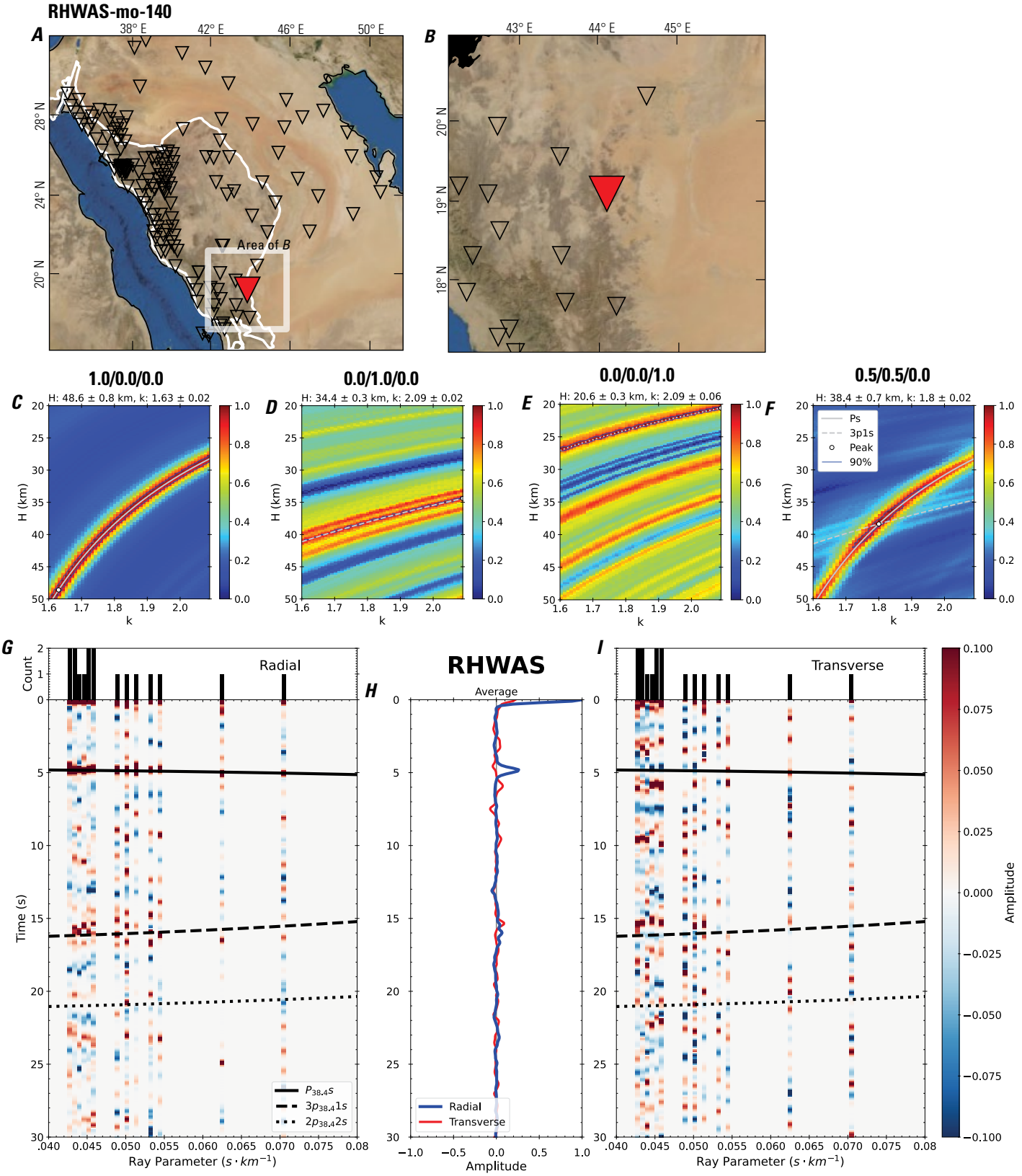
RHWAS-mo-140
A
38° E
42° E
46° E
50° E
28° N
24° N
20° N
Area of B
B
43° E
44° E
45° E
20° N
19° N
18° N
1.0/0.0/0.0
C
H: 48.6 ± 0.8 km, k: 1.63 ± 0.02
0.0/1.0/0.0
D
H: 34.4 ± 0.3 km, k: 2.09 ± 0.02
0.0/0.0/1.0
E
H: 20.6 ± 0.3 km, k: 2.09 ± 0.06
0.5/0.5/0.0
F
H: 38.4 ± 0.7 km, k: 1.8 ± 0.02
Ps
3p1s
Peak
90%
H (km)
k
G
Radial
Count
Time (s)
$P_{38.4}s$
$3p_{38.4}1s$
$2p_{38.4}2s$
Ray Parameter ($s \cdot km^{-1}$)
RHWAS
H
Average
Radial
Transverse
Amplitude
I
Transverse
Amplitude

Figure 284 (page 290). Receiver-function analysis for station RHWAS. *A*, Regional map of Saudi Arabia showing the entire array (as inverted triangles), the location of station RHWAS (red inverted triangle), the shield-platform boundary (white line), and the bounds of the map in *B* (white box). *B*, Local map of station RHWAS. Harrats are shown in black. *C*, Standard, single-layer *H-k* stack with stacking weights 0.4/0.3/0.3. This *H-k* stack ignores sedimentary effects on the receiver functions. *D*, Standard, single-layer *H-k* stack with stacking weights 0.5/0.5/0.0. This *H-k* stack also ignores sedimentary effects on the receiver functions. *E*, Optimized sub-sedimentary *H-k* stack with stacking weights 0.4/0.3/0.3, following the method of Yu and others (2015). *F*, Optimized sedimentary *H-k* stack with stacking weights 0.05/0.70/0.25, following the method of Yu and others (2015). *G*, Radial component P-wave receiver functions (PRFs) plotted against ray parameter. Individual PRFs have had the resonance-removal filter of Yu and others (2015) applied to them and are normalized to the maximum amplitude within the time window shown, binned, and normalized by the number of traces per bin. *H*, Average of every individual normalized radial receiver function with the application of the resonance-removal filter (blue) and average of every individual normalized raw radial receiver function (red). *I*, Radial component of raw PRFs (that is, PRFs with no resonance-removal filter applied) plotted against ray parameter, normalized as in *G*.

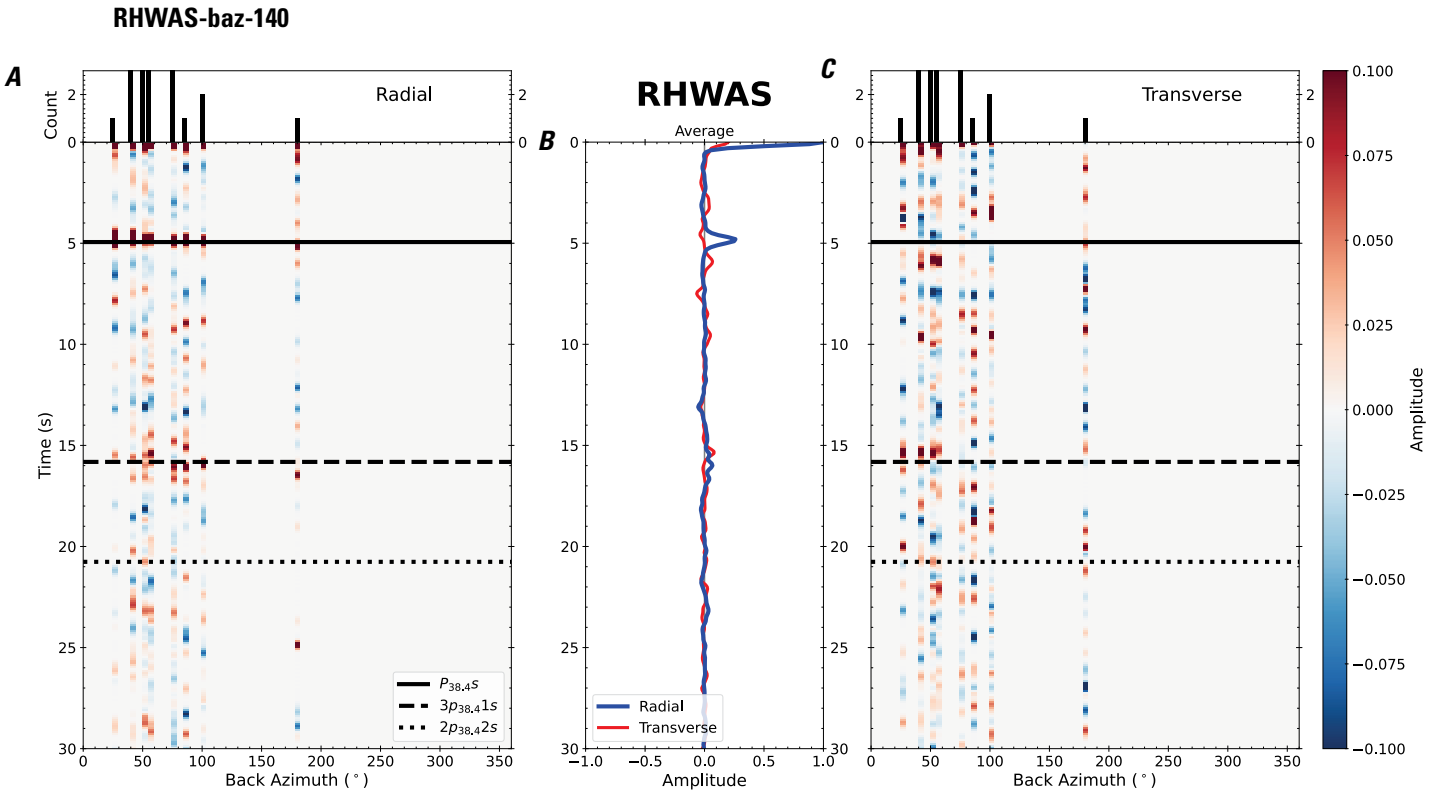

Figure 285. Receiver functions plotted against back azimuth for station RHWAS. *A*, Radial component of P-wave receiver functions (PRFs) plotted against back azimuth. Individual PRFs have had the resonance-removal filter of Yu and others (2015) applied to them, are normalized to the maximum amplitude within the time window shown, binned, and normalized by the number of traces per bin. *B*, Average of every individual normalized radial receiver function with the application of the resonance-removal filter (blue) and average of every individual normalized raw radial receiver function (red). *C*, Radial component of raw PRFs, plotted against back azimuth, normalized as in *A*. Ps, 3p1s, and 2p2s arrival times predicted for the preferred Moho depth are shown, assuming a ray parameter of 0.06 s/km.

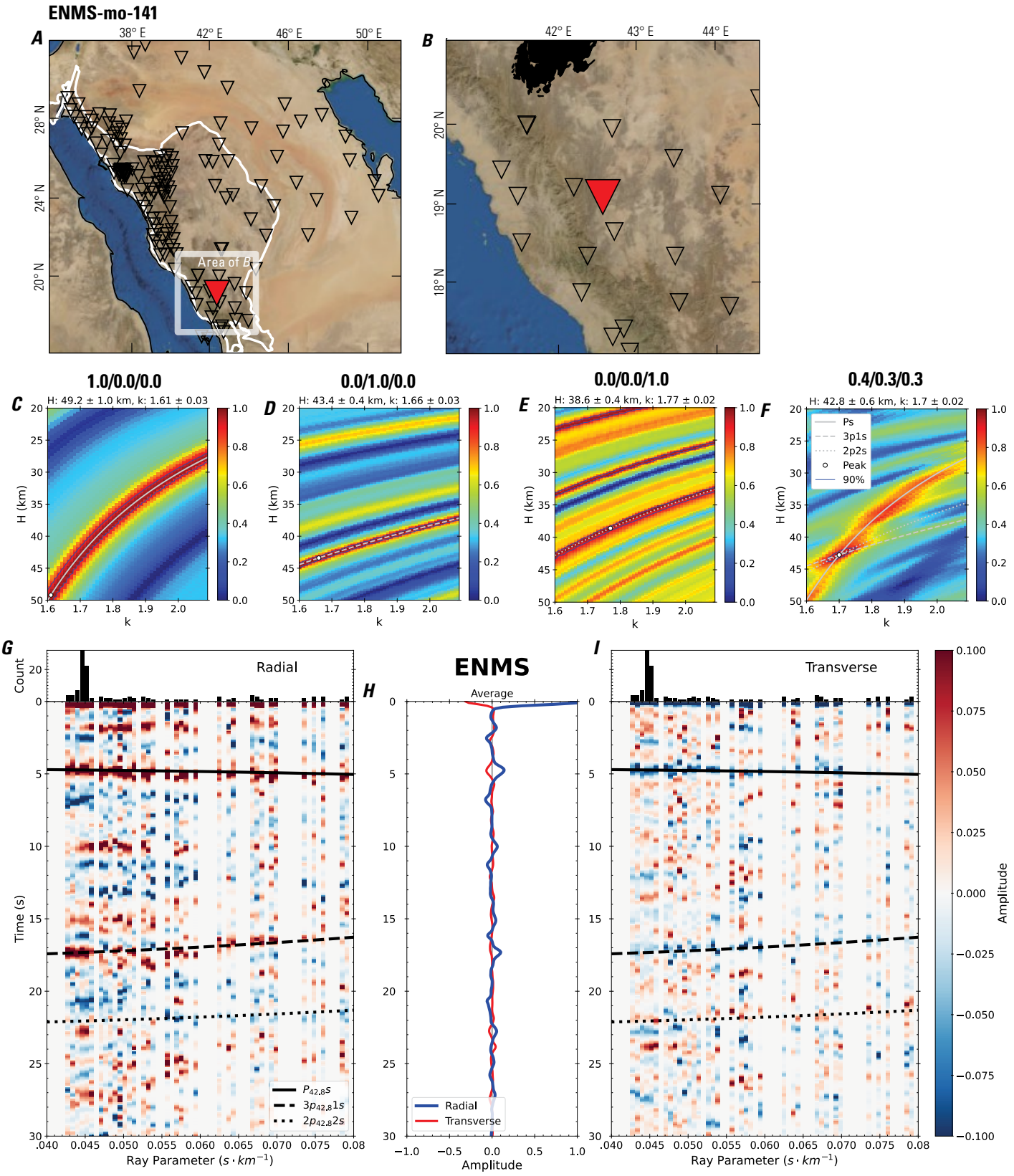
ENMS-mo-141
A
B
Area of B
1.0/0.0/0.0
0.0/1.0/0.0
0.0/0.0/1.0
0.4/0.3/0.3
C
D
E
F
H: 49.2 ± 1.0 km, k: 1.61 ± 0.03
H: 43.4 ± 0.4 km, k: 1.66 ± 0.03
H: 38.6 ± 0.4 km, k: 1.77 ± 0.02
H: 42.8 ± 0.6 km, k: 1.7 ± 0.02
H (km)
k
Ps
3p1s
2p2s
Peak
90%
G
H
I
Radial
Transverse
ENMS
Average
Count
Time (s)
Ray Parameter (s · km⁻¹)
Amplitude
$P_{42.8}s$
$3p_{42.8}1s$
$2p_{42.8}2s$

Figure 286 (page 292). Receiver-function analysis for station ENMS. *A*, Regional map of Saudi Arabia showing the entire array (as inverted triangles), the location of station ENMS (red inverted triangle), the shield-platform boundary (white line), and the bounds of the map in *B* (white box). *B*, Local map of station ENMS. Harrats are shown in black. *C*, Standard, single-layer *H-k* stack with stacking weights 0.4/0.3/0.3. This *H-k* stack ignores sedimentary effects on the receiver functions. *D*, Standard, single-layer *H-k* stack with stacking weights 0.5/0.5/0.0. This *H-k* stack also ignores sedimentary effects on the receiver functions. *E*, Optimized sub-sedimentary *H-k* stack with stacking weights 0.4/0.3/0.3, following the method of Yu and others (2015). *F*, Optimized sedimentary *H-k* stack with stacking weights 0.05/0.70/0.25, following the method of Yu and others (2015). *G*, Radial component P-wave receiver functions (PRFs) plotted against ray parameter. Individual PRFs have had the resonance-removal filter of Yu and others (2015) applied to them and are normalized to the maximum amplitude within the time window shown, binned, and normalized by the number of traces per bin. *H*, Average of every individual normalized radial receiver function with the application of the resonance-removal filter (blue) and average of every individual normalized raw radial receiver function (red). *I*, Radial component of raw PRFs (that is, PRFs with no resonance-removal filter applied) plotted against ray parameter, normalized as in *G*.

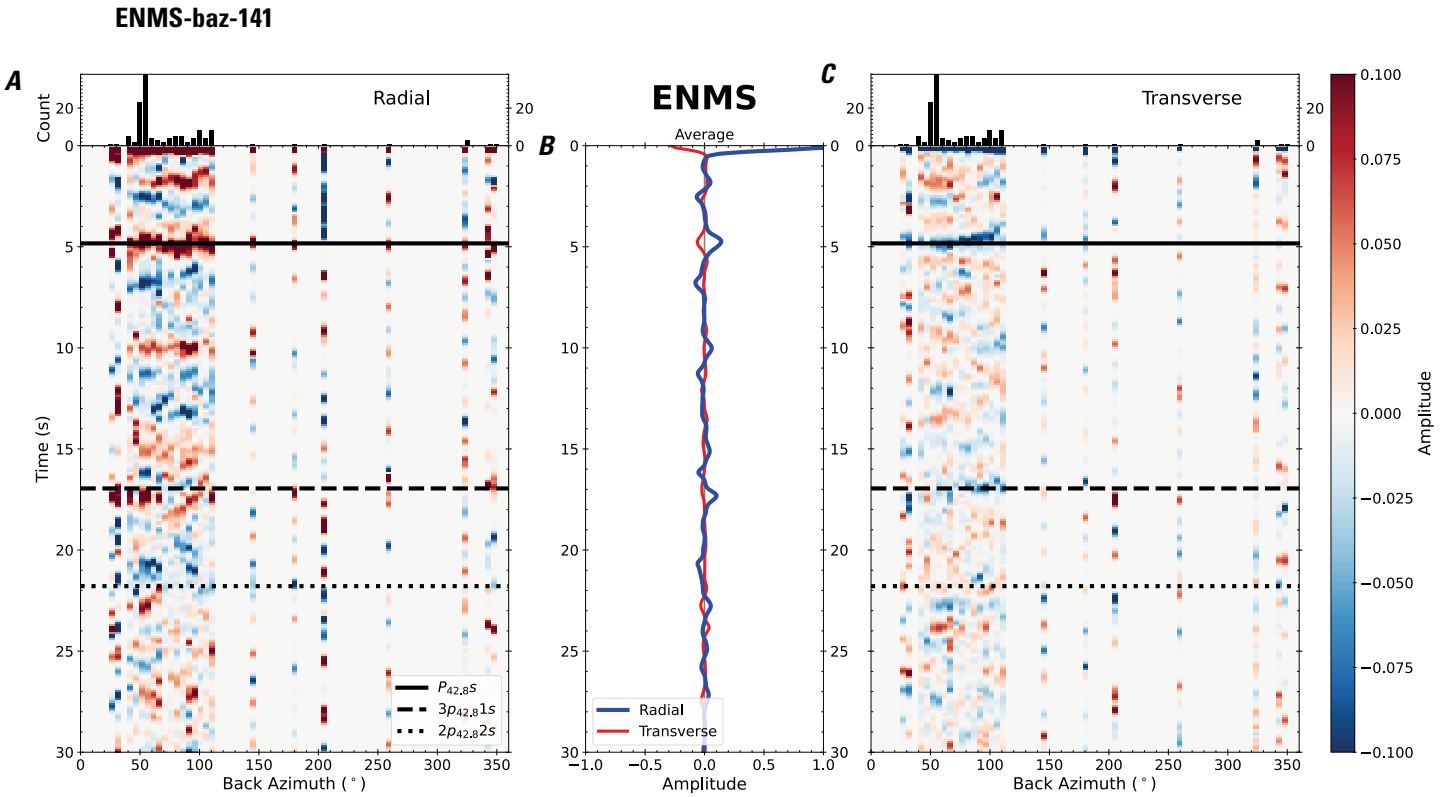

Figure 287. Receiver functions plotted against back azimuth for station ENMS. *A*, Radial component of P-wave receiver functions (PRFs) plotted against back azimuth. Individual PRFs have had the resonance-removal filter of Yu and others (2015) applied to them, are normalized to the maximum amplitude within the time window shown, binned, and normalized by the number of traces per bin. *B*, Average of every individual normalized radial receiver function with the application of the resonance-removal filter (blue) and average of every individual normalized raw radial receiver function (red). *C*, Radial component of raw PRFs, plotted against back azimuth, normalized as in *A*. Ps, 3p1s, and 2p2s arrival times predicted for the preferred Moho depth are shown, assuming a ray parameter of 0.06 s/km.

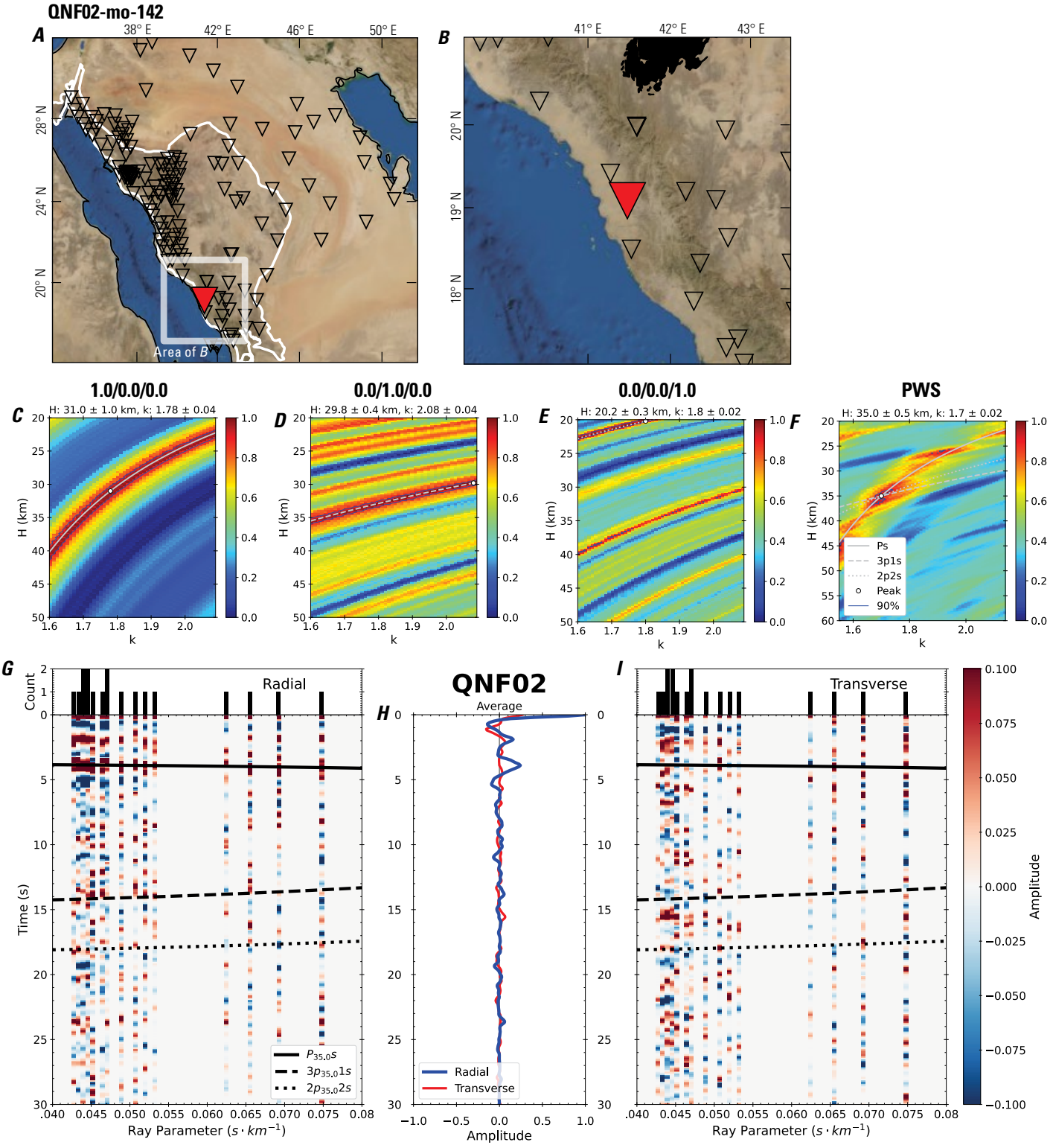
QNF02-mo-142
A
38° E
42° E
46° E
50° E
28° N
24° N
20° N
Area of B
B
41° E
42° E
43° E
20° N
19° N
18° N
1.0/0.0/0.0
0.0/1.0/0.0
0.0/0.0/1.0
PWS
C
H: 31.0 ± 1.0 km, k: 1.78 ± 0.04
D
H: 29.8 ± 0.4 km, k: 2.08 ± 0.04
E
H: 20.2 ± 0.3 km, k: 1.8 ± 0.02
F
H: 35.0 ± 0.5 km, k: 1.7 ± 0.02
H (km)
k
Ps
3p1s
2p2s
Peak
90%
G
Radial
Count
Time (s)
Ray Parameter (s · km⁻¹)
$P_{35.0}s$
$3p_{35.0}1s$
$2p_{35.0}2s$
QNF02
Average
H
Radial
Transverse
Amplitude
I
Transverse
Amplitude

Figure 288 (page 294). Receiver-function analysis for station QNF02. *A*, Regional map of Saudi Arabia showing the entire array (as inverted triangles), the location of station QNF02 (red inverted triangle), the shield-platform boundary (white line), and the bounds of the map in *B* (white box). *B*, Local map of station QNF02. Harrats are shown in black. *C*, Standard, single-layer *H-k* stack with stacking weights 0.4/0.3/0.3. This *H-k* stack ignores sedimentary effects on the receiver functions. *D*, Standard, single-layer *H-k* stack with stacking weights 0.5/0.5/0.0. This *H-k* stack also ignores sedimentary effects on the receiver functions. *E*, Optimized sub-sedimentary *H-k* stack with stacking weights 0.4/0.3/0.3, following the method of Yu and others (2015). *F*, Optimized sedimentary *H-k* stack with stacking weights 0.05/0.70/0.25, following the method of Yu and others (2015). *G*, Radial component P-wave receiver functions (PRFs) plotted against ray parameter. Individual PRFs have had the resonance-removal filter of Yu and others (2015) applied to them and are normalized to the maximum amplitude within the time window shown, binned, and normalized by the number of traces per bin. *H*, Average of every individual normalized radial receiver function with the application of the resonance-removal filter (blue) and average of every individual normalized raw radial receiver function (red). *I*, Radial component of raw PRFs (that is, PRFs with no resonance-removal filter applied) plotted against ray parameter, normalized as in *G*.

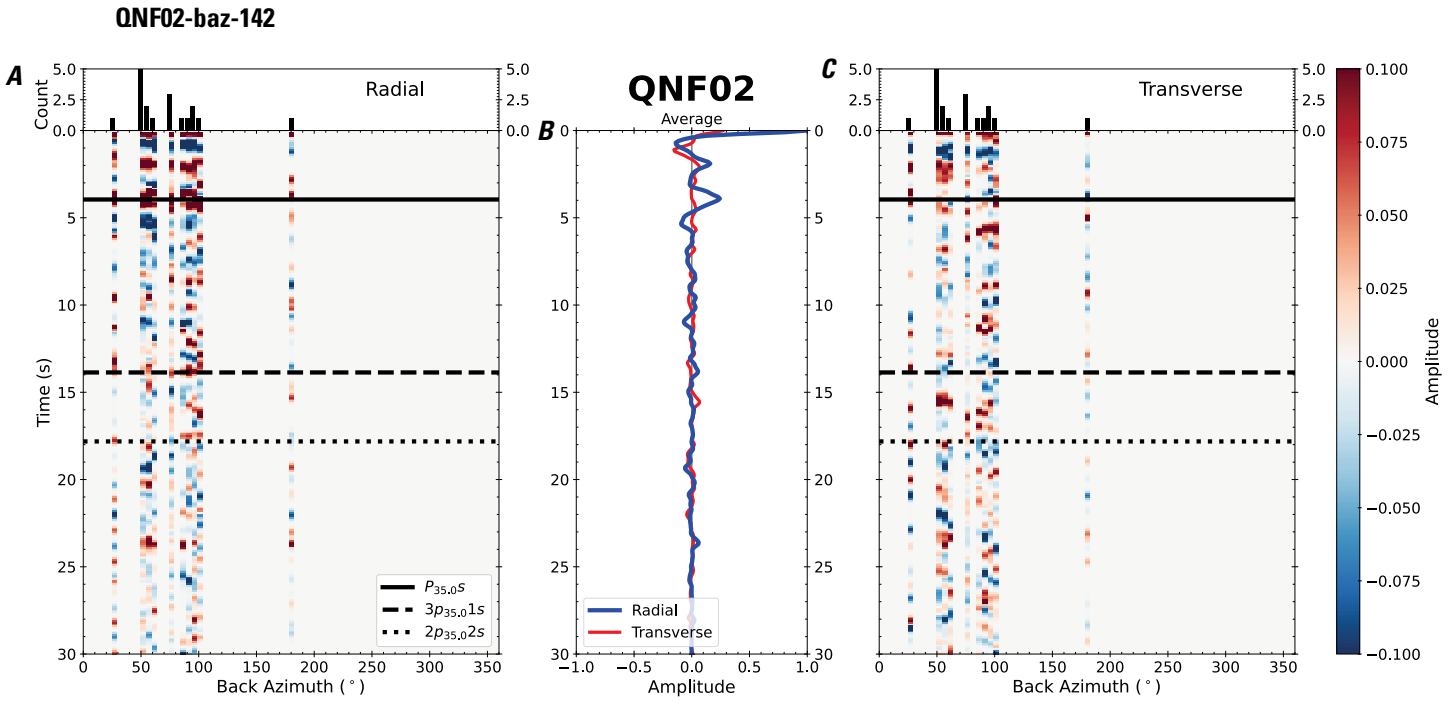

Figure 289. Receiver functions plotted against back azimuth for station QNF02. *A*, Radial component of P-wave receiver functions (PRFs) plotted against back azimuth. Individual PRFs have had the resonance-removal filter of Yu and others (2015) applied to them, are normalized to the maximum amplitude within the time window shown, binned, and normalized by the number of traces per bin. *B*, Average of every individual normalized radial receiver function with the application of the resonance-removal filter (blue) and average of every individual normalized raw radial receiver function (red). *C*, Radial component of raw PRFs, plotted against back azimuth, normalized as in *A*. Ps, 3p1s, and 2p2s arrival times predicted for the preferred Moho depth are shown, assuming a ray parameter of 0.06 s/km.

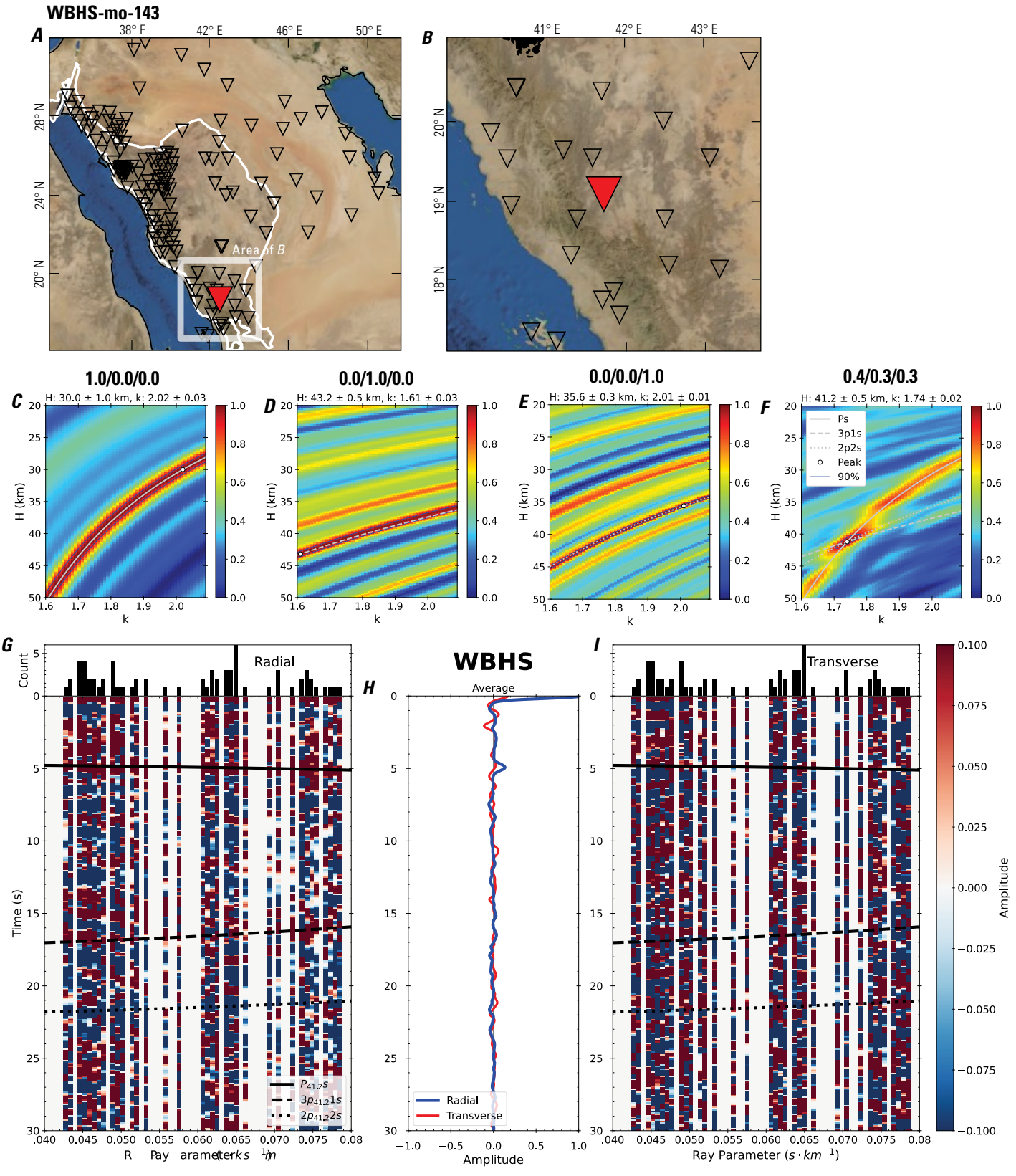
WBHS-mo-143
A
38° E
42° E
46° E
50° E
28° N
24° N
20° N
Area of B
B
41° E
42° E
43° E
20° N
19° N
18° N
1.0/0.0/0.0
C
H: 30.0 ± 1.0 km, k: 2.02 ± 0.03
0.0/1.0/0.0
D
H: 43.2 ± 0.5 km, k: 1.61 ± 0.03
0.0/0.0/1.0
E
H: 35.6 ± 0.3 km, k: 2.01 ± 0.01
0.4/0.3/0.3
F
H: 41.2 ± 0.5 km, k: 1.74 ± 0.02
Ps
3p1s
2p2s
Peak
90%
H (km)
k
G
Radial
Count
Time (s)
$P_{41,2}s$
$3p_{41,2}1s$
$2p_{41,2}2s$
Ray Parameter ($s \cdot km^{-1}$)
H
WBHS
Average
Radial
Transverse
Amplitude
I
Transverse
Ray Parameter ($s \cdot km^{-1}$)
Amplitude

Figure 290 (page 296). Receiver-function analysis for station WBHS. *A*, Regional map of Saudi Arabia showing the entire array (as inverted triangles), the location of station WBHS (red inverted triangle), the shield-platform boundary (white line), and the bounds of the map in *B* (white box). *B*, Local map of station WBHS. Harrats are shown in black. *C*, Standard, single-layer *H-k* stack with stacking weights 0.4/0.3/0.3. This *H-k* stack ignores sedimentary effects on the receiver functions. *D*, Standard, single-layer *H-k* stack with stacking weights 0.5/0.5/0.0. This *H-k* stack also ignores sedimentary effects on the receiver functions. *E*, Optimized sub-sedimentary *H-k* stack with stacking weights 0.4/0.3/0.3, following the method of Yu and others (2015). *F*, Optimized sedimentary *H-k* stack with stacking weights 0.05/0.70/0.25, following the method of Yu and others (2015). *G*, Radial component P-wave receiver functions (PRFs) plotted against ray parameter. Individual PRFs have had the resonance-removal filter of Yu and others (2015) applied to them and are normalized to the maximum amplitude within the time window shown, binned, and normalized by the number of traces per bin. *H*, Average of every individual normalized radial receiver function with the application of the resonance-removal filter (blue) and average of every individual normalized raw radial receiver function (red). *I*, Radial component of raw PRFs (that is, PRFs with no resonance-removal filter applied) plotted against ray parameter, normalized as in *G*.

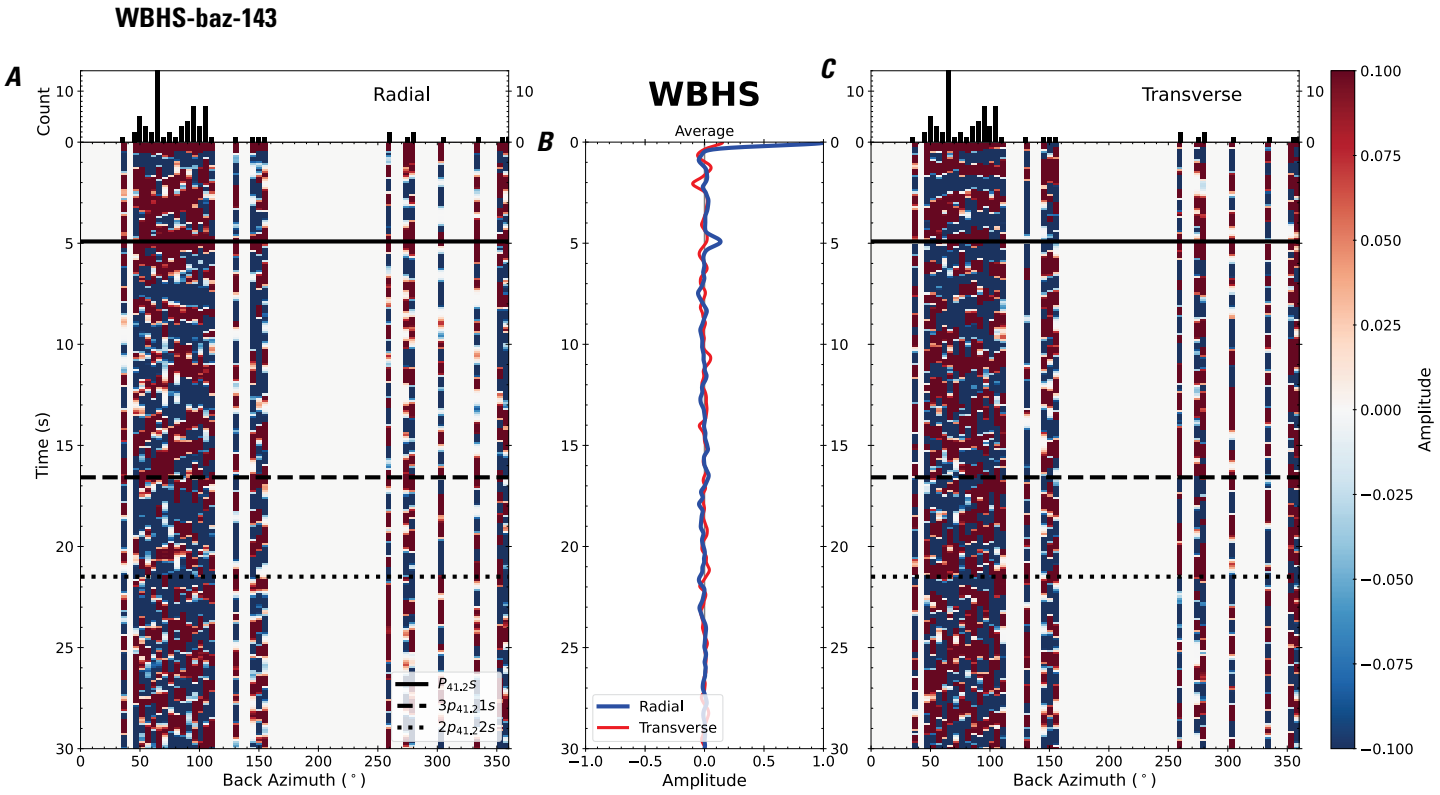

Figure 291. Receiver functions plotted against back azimuth for station WBHS. *A*, Radial component of P-wave receiver functions (PRFs) plotted against back azimuth. Individual PRFs have had the resonance-removal filter of Yu and others (2015) applied to them, are normalized to the maximum amplitude within the time window shown, binned, and normalized by the number of traces per bin. *B*, Average of every individual normalized radial receiver function with the application of the resonance-removal filter (blue) and average of every individual normalized raw radial receiver function (red). *C*, Radial component of raw PRFs, plotted against back azimuth, normalized as in *A*. Ps, 3p1s, and 2p2s arrival times predicted for the preferred Moho depth are shown, assuming a ray parameter of 0.06 s/km.

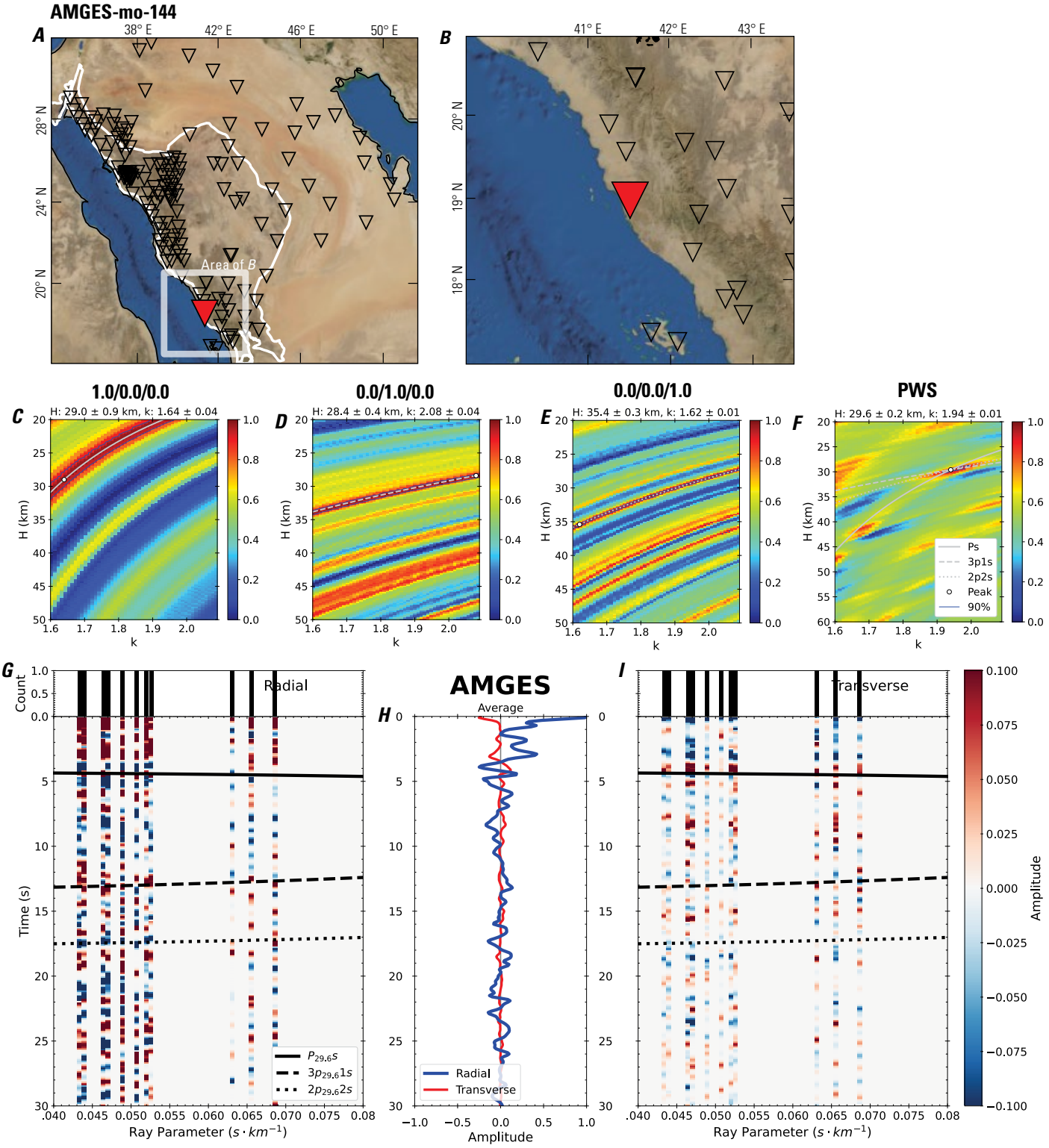
AMGES-mo-144
A
38° E
42° E
46° E
50° E
28° N
24° N
20° N
Area of B
B
41° E
42° E
43° E
20° N
19° N
18° N
1.0/0.0/0.0
0.0/1.0/0.0
0.0/0.0/1.0
PWS
C
H: 29.0 ± 0.9 km, k: 1.64 ± 0.04
D
H: 28.4 ± 0.4 km, k: 2.08 ± 0.04
E
H: 35.4 ± 0.3 km, k: 1.62 ± 0.01
F
H: 29.6 ± 0.2 km, k: 1.94 ± 0.01
H (km)
k
Ps
3p1s
2p2s
Peak
90%
G
Radial
Count
Time (s)
$P_{29.6}s$
$3p_{29.6}1s$
$2p_{29.6}2s$
Ray Parameter ($s \cdot km^{-1}$)
AMGES
Average
H
Radial
Transverse
Amplitude
I
Transverse
Amplitude

Figure 292 (page 298). Receiver-function analysis for station AMGES. *A*, Regional map of Saudi Arabia showing the entire array (as inverted triangles), the location of station AMGES (red inverted triangle), the shield-platform boundary (white line), and the bounds of the map in *B* (white box). *B*, Local map of station AMGES. Harrats are shown in black. *C*, Standard, single-layer *H-k* stack with stacking weights 0.4/0.3/0.3. This *H-k* stack ignores sedimentary effects on the receiver functions. *D*, Standard, single-layer *H-k* stack with stacking weights 0.5/0.5/0.0. This *H-k* stack also ignores sedimentary effects on the receiver functions. *E*, Optimized sub-sedimentary *H-k* stack with stacking weights 0.4/0.3/0.3, following the method of Yu and others (2015). *F*, Optimized sedimentary *H-k* stack with stacking weights 0.05/0.70/0.25, following the method of Yu and others (2015). *G*, Radial component P-wave receiver functions (PRFs) plotted against ray parameter. Individual PRFs have had the resonance-removal filter of Yu and others (2015) applied to them and are normalized to the maximum amplitude within the time window shown, binned, and normalized by the number of traces per bin. *H*, Average of every individual normalized radial receiver function with the application of the resonance-removal filter (blue) and average of every individual normalized raw radial receiver function (red). *I*, Radial component of raw PRFs (that is, PRFs with no resonance-removal filter applied) plotted against ray parameter, normalized as in *G*.

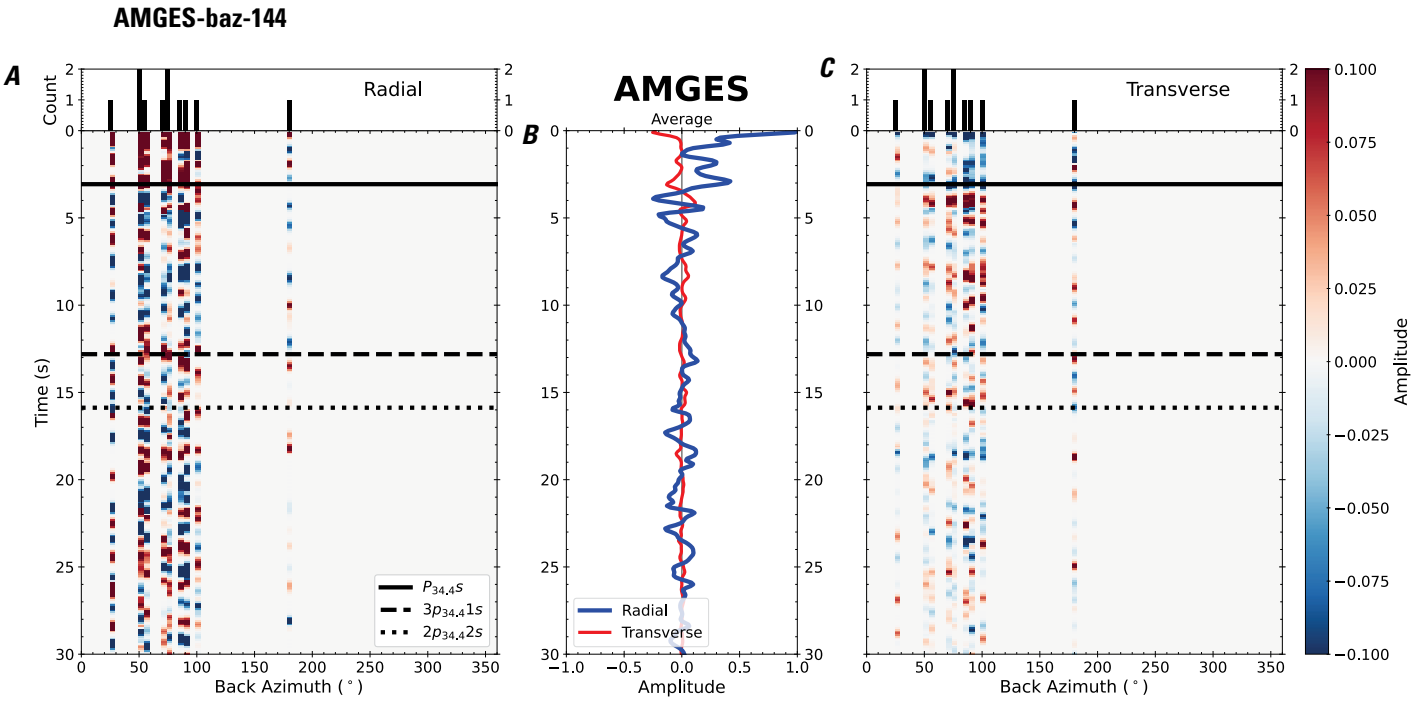

Figure 293. Receiver functions plotted against back azimuth for station AMGES. *A*, Radial component of P-wave receiver functions (PRFs) plotted against back azimuth. Individual PRFs have had the resonance-removal filter of Yu and others (2015) applied to them, are normalized to the maximum amplitude within the time window shown, binned, and normalized by the number of traces per bin. *B*, Average of every individual normalized radial receiver function with the application of the resonance-removal filter (blue) and average of every individual normalized raw radial receiver function (red). *C*, Radial component of raw PRFs, plotted against back azimuth, normalized as in *A*. Ps, 3p1s, and 2p2s arrival times predicted for the preferred Moho depth are shown, assuming a ray parameter of 0.06 s/km.

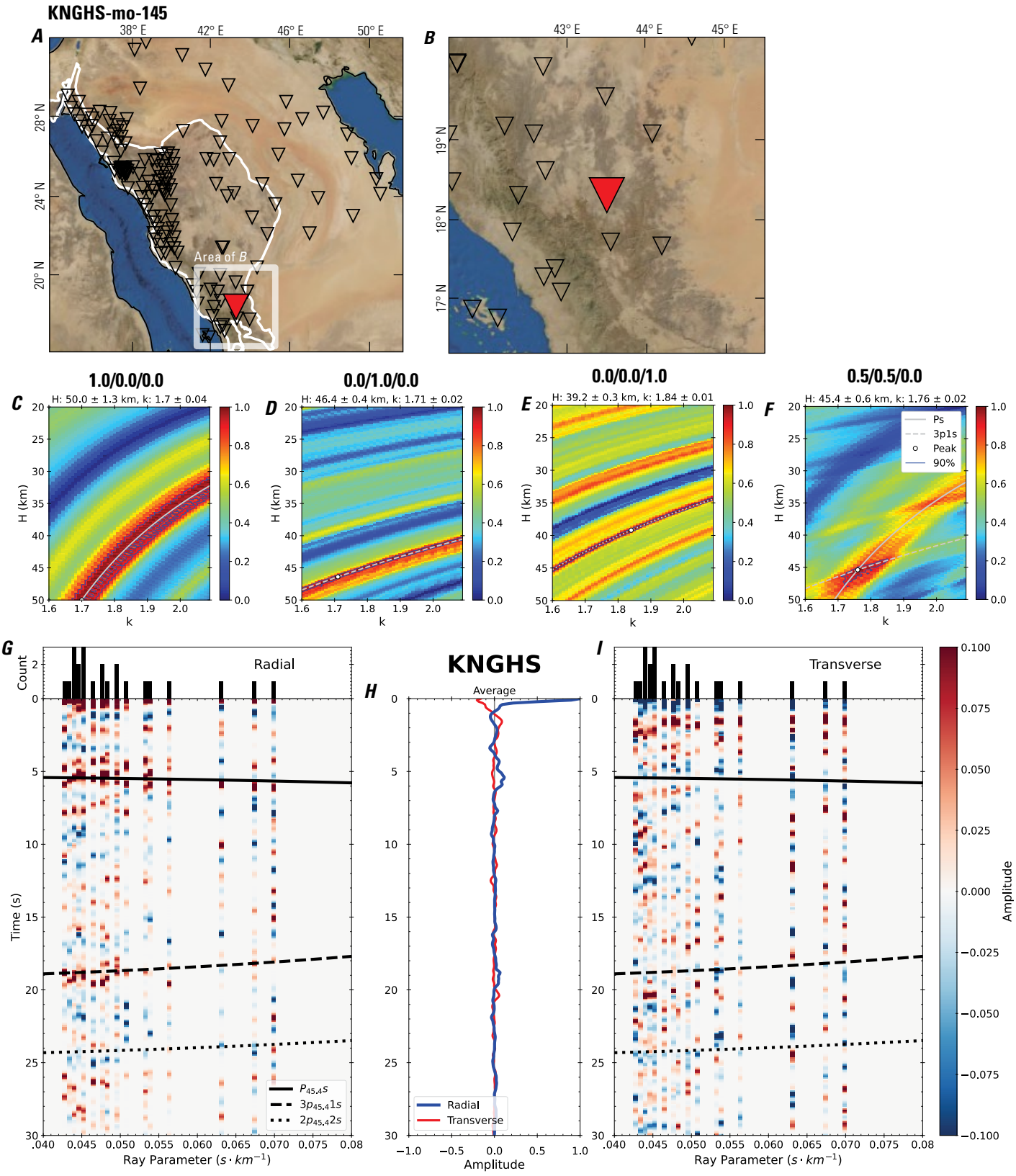
KNGHS-mo-145
A
38° E
42° E
46° E
50° E
28° N
24° N
20° N
Area of B
B
43° E
44° E
45° E
19° N
18° N
17° N
1.0/0.0/0.0
C
H: 50.0 ± 1.3 km, k: 1.7 ± 0.04
0.0/1.0/0.0
D
H: 46.4 ± 0.4 km, k: 1.71 ± 0.02
0.0/0.0/1.0
E
H: 39.2 ± 0.3 km, k: 1.84 ± 0.01
0.5/0.5/0.0
F
H: 45.4 ± 0.6 km, k: 1.76 ± 0.02
H (km)
k
Ps
3p1s
Peak
90%
G
Radial
Count
Time (s)
$P_{45.4}s$
$3p_{45.4}1s$
$2p_{45.4}2s$
Ray Parameter ($s \cdot km^{-1}$)
KNGHS
H
Average
Radial
Transverse
Amplitude
I
Transverse
Amplitude

Figure 294 (page 300). Receiver-function analysis for station KNGHS. *A*, Regional map of Saudi Arabia showing the entire array (as inverted triangles), the location of station KNGHS (red inverted triangle), the shield-platform boundary (white line), and the bounds of the map in *B* (white box). *B*, Local map of station KNGHS. Harrats are shown in black. *C*, Standard, single-layer *H-k* stack with stacking weights 0.4/0.3/0.3. This *H-k* stack ignores sedimentary effects on the receiver functions. *D*, Standard, single-layer *H-k* stack with stacking weights 0.5/0.5/0.0. This *H-k* stack also ignores sedimentary effects on the receiver functions. *E*, Optimized sub-sedimentary *H-k* stack with stacking weights 0.4/0.3/0.3, following the method of Yu and others (2015). *F*, Optimized sedimentary *H-k* stack with stacking weights 0.05/0.70/0.25, following the method of Yu and others (2015). *G*, Radial component P-wave receiver functions (PRFs) plotted against ray parameter. Individual PRFs have had the resonance-removal filter of Yu and others (2015) applied to them and are normalized to the maximum amplitude within the time window shown, binned, and normalized by the number of traces per bin. *H*, Average of every individual normalized radial receiver function with the application of the resonance-removal filter (blue) and average of every individual normalized raw radial receiver function (red). *I*, Radial component of raw PRFs (that is, PRFs with no resonance-removal filter applied) plotted against ray parameter, normalized as in *G*.

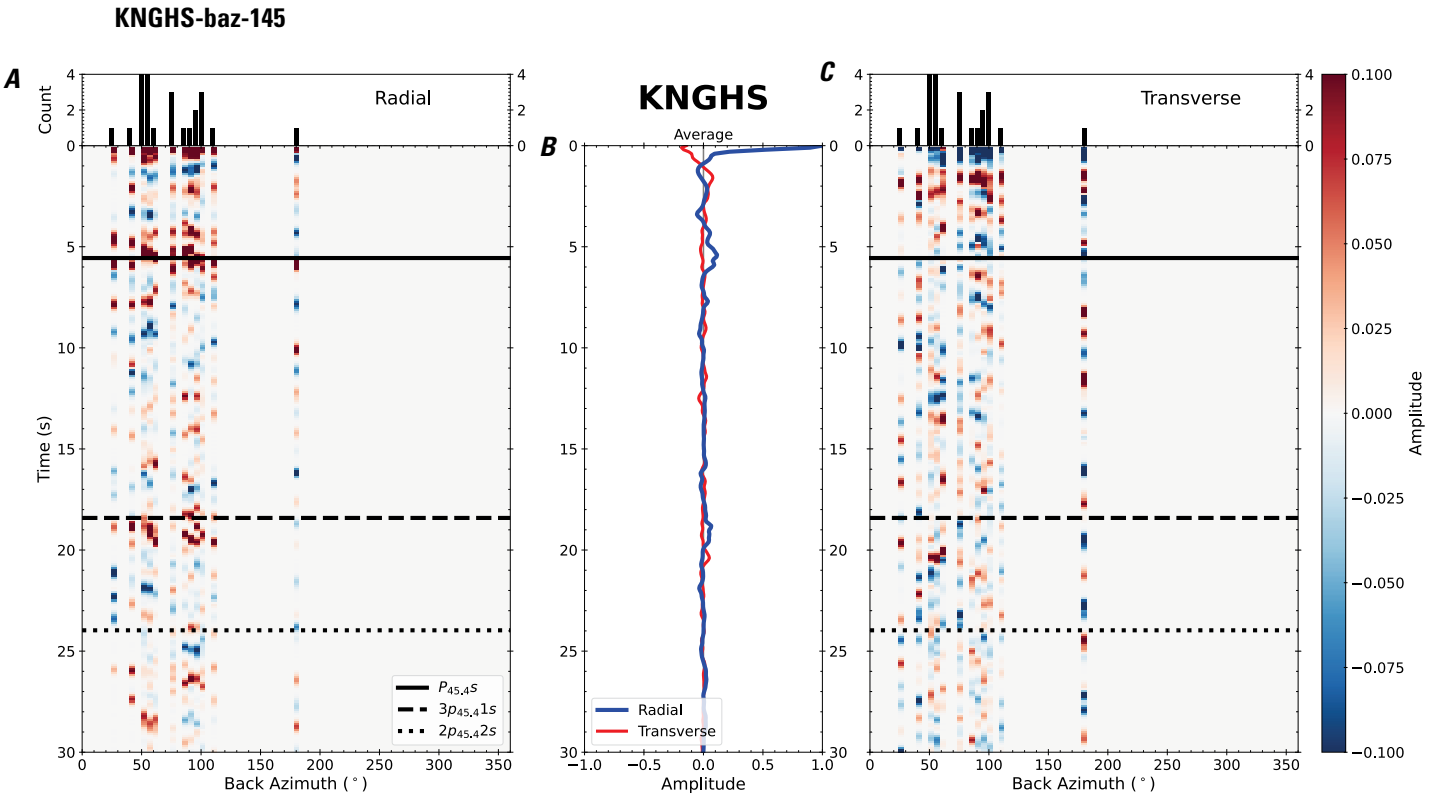

Figure 295. Receiver functions plotted against back azimuth for station KNGHS. *A*, Radial component of P-wave receiver functions (PRFs) plotted against back azimuth. Individual PRFs have had the resonance-removal filter of Yu and others (2015) applied to them, are normalized to the maximum amplitude within the time window shown, binned, and normalized by the number of traces per bin. *B*, Average of every individual normalized radial receiver function with the application of the resonance-removal filter (blue) and average of every individual normalized raw radial receiver function (red). *C*, Radial component of raw PRFs, plotted against back azimuth, normalized as in *A*. Ps, 3p1s, and 2p2s arrival times predicted for the preferred Moho depth are shown, assuming a ray parameter of 0.06 s/km.

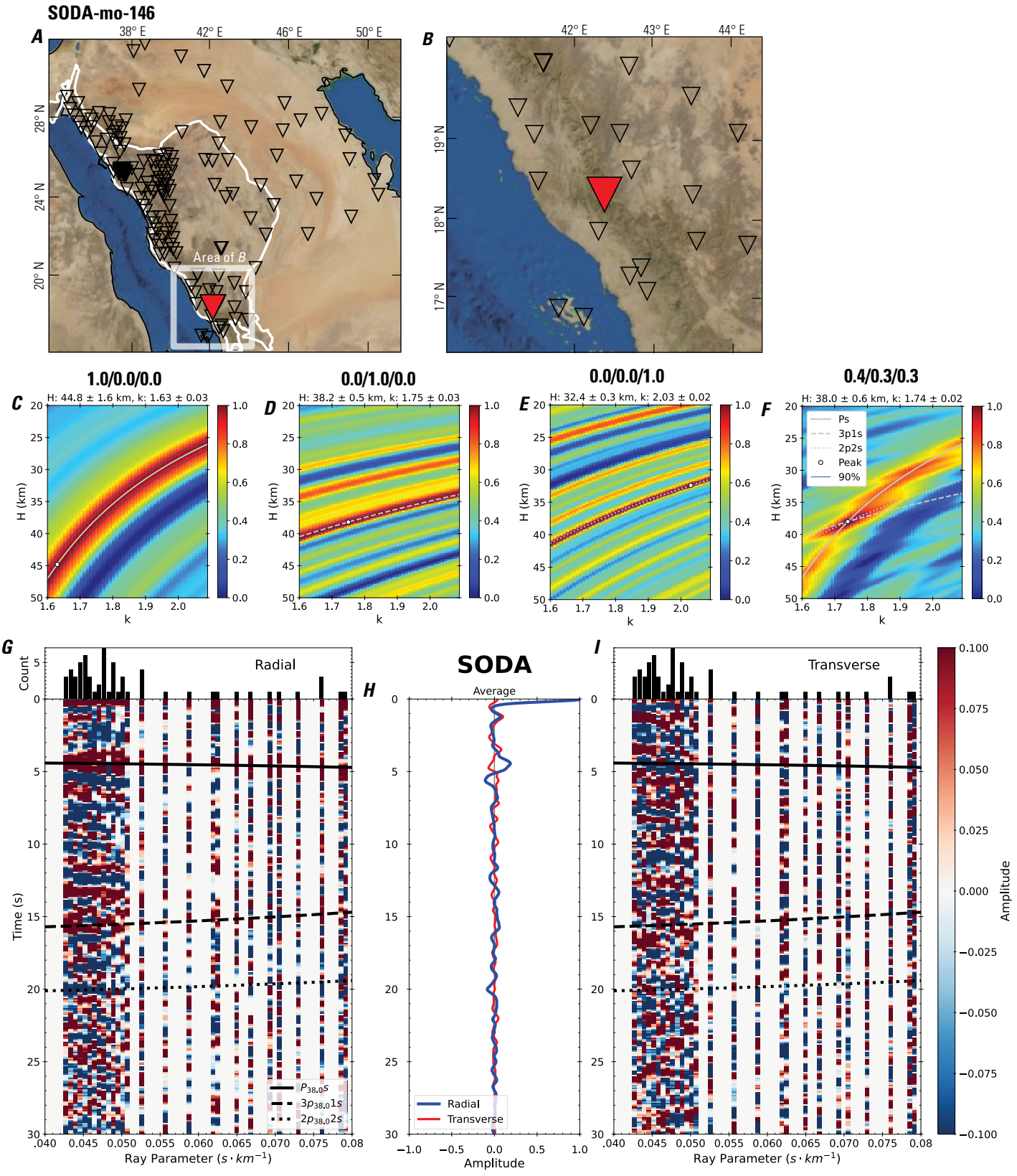
SODA-mo-146
A
38° E
42° E
46° E
50° E
28° N
24° N
20° N
Area of B
B
42° E
43° E
44° E
19° N
18° N
17° N
1.0/0.0/0.0
C
H: 44.8 ± 1.6 km, k: 1.63 ± 0.03
0.0/1.0/0.0
D
H: 38.2 ± 0.5 km, k: 1.75 ± 0.03
0.0/0.0/1.0
E
H: 32.4 ± 0.3 km, k: 2.03 ± 0.02
0.4/0.3/0.3
F
H: 38.0 ± 0.6 km, k: 1.74 ± 0.02
Ps
3p1s
2p2s
Peak
90%
H (km)
k
G
Radial
Count
Time (s)
Ray Parameter (s · km⁻¹)
$P_{38.0}s$
$3p_{38.0}1s$
$2p_{38.0}2s$
H
SODA
Average
Radial
Transverse
Amplitude
I
Transverse
Amplitude

Figure 296 (page 302). Receiver-function analysis for station SODA. *A*, Regional map of Saudi Arabia showing the entire array (as inverted triangles), the location of station SODA (red inverted triangle), the shield-platform boundary (white line), and the bounds of the map in *B* (white box). *B*, Local map of station SODA. Harrats are shown in black. *C*, Standard, single-layer *H-k* stack with stacking weights 0.4/0.3/0.3. This *H-k* stack ignores sedimentary effects on the receiver functions. *D*, Standard, single-layer *H-k* stack with stacking weights 0.5/0.5/0.0. This *H-k* stack also ignores sedimentary effects on the receiver functions. *E*, Optimized sub-sedimentary *H-k* stack with stacking weights 0.4/0.3/0.3, following the method of Yu and others (2015). *F*, Optimized sedimentary *H-k* stack with stacking weights 0.05/0.70/0.25, following the method of Yu and others (2015). *G*, Radial component P-wave receiver functions (PRFs) plotted against ray parameter. Individual PRFs have had the resonance-removal filter of Yu and others (2015) applied to them and are normalized to the maximum amplitude within the time window shown, binned, and normalized by the number of traces per bin. *H*, Average of every individual normalized radial receiver function with the application of the resonance-removal filter (blue) and average of every individual normalized raw radial receiver function (red). *I*, Radial component of raw PRFs (that is, PRFs with no resonance-removal filter applied) plotted against ray parameter, normalized as in *G*.

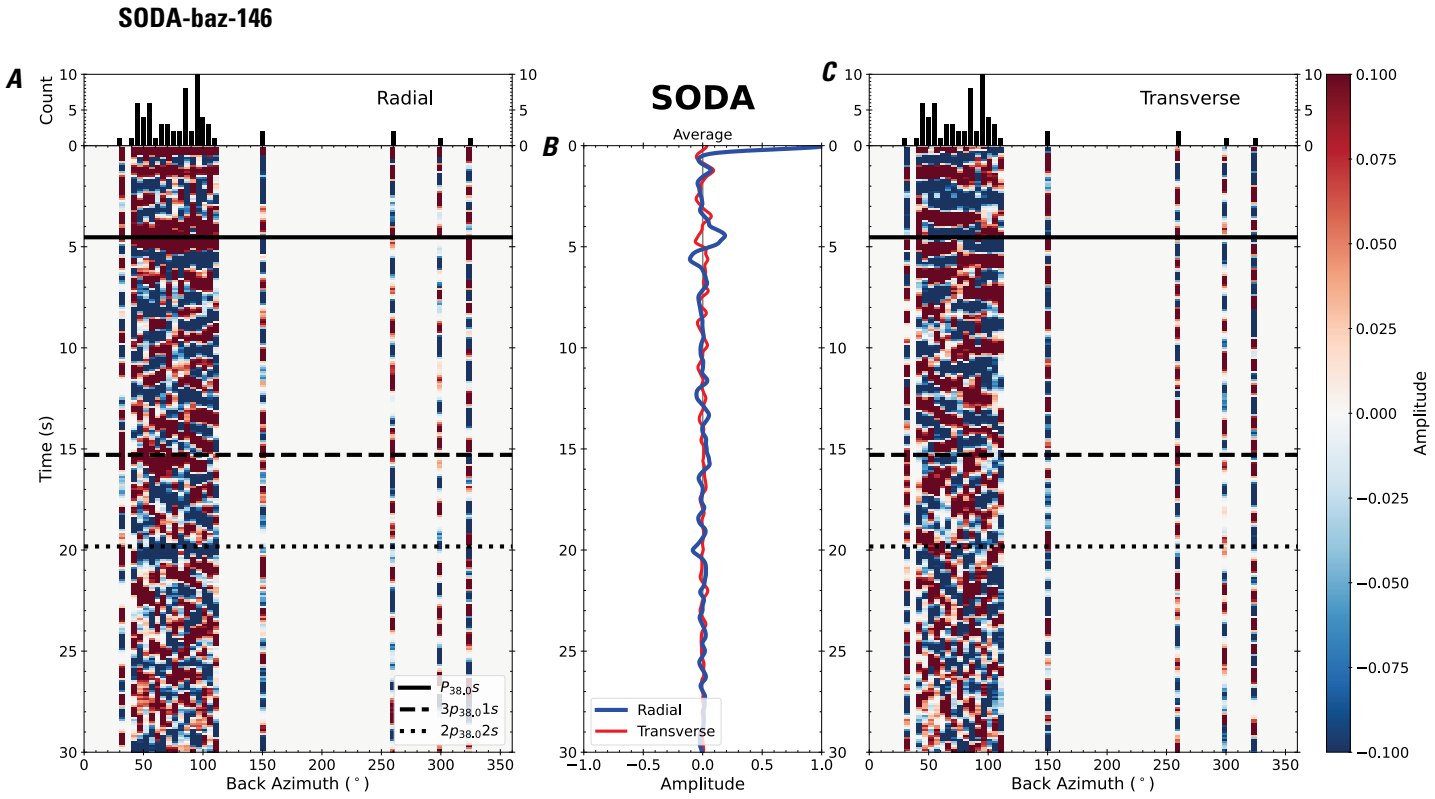

Figure 297. Receiver functions plotted against back azimuth for station SODA. *A*, Radial component of P-wave receiver functions (PRFs) plotted against back azimuth. Individual PRFs have had the resonance-removal filter of Yu and others (2015) applied to them, are normalized to the maximum amplitude within the time window shown, binned, and normalized by the number of traces per bin. *B*, Average of every individual normalized radial receiver function with the application of the resonance-removal filter (blue) and average of every individual normalized raw radial receiver function (red). *C*, Radial component of raw PRFs, plotted against back azimuth, normalized as in *A*. Ps, 3p1s, and 2p2s arrival times predicted for the preferred Moho depth are shown, assuming a ray parameter of 0.06 s/km.

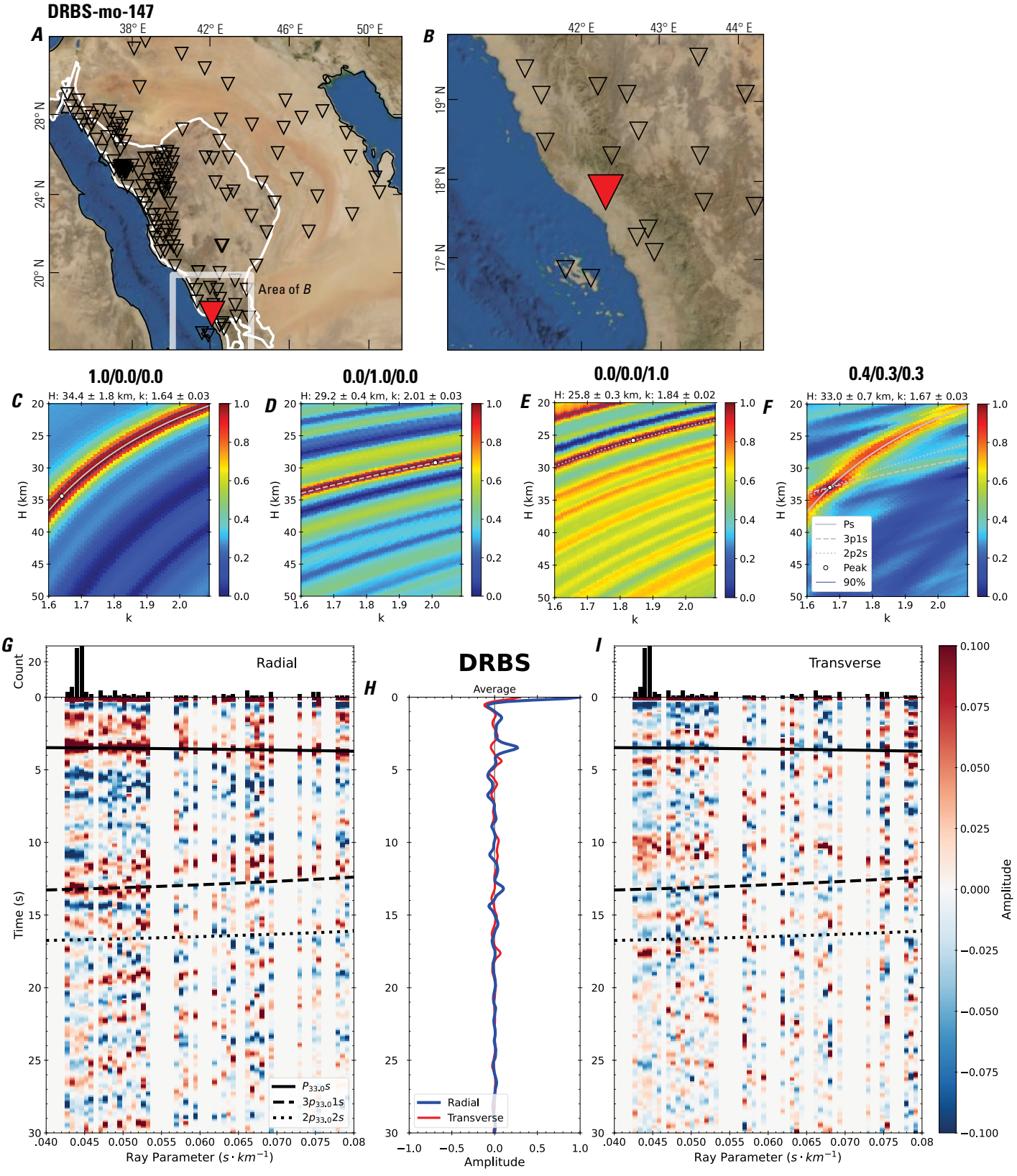
DRBS-mo-147
A
38° E
42° E
46° E
50° E
28° N
24° N
20° N
Area of B
B
42° E
43° E
44° E
19° N
18° N
17° N
1.0/0.0/0.0
C
H: 34.4 ± 1.8 km, k: 1.64 ± 0.03
0.0/1.0/0.0
D
H: 29.2 ± 0.4 km, k: 2.01 ± 0.03
0.0/0.0/1.0
E
H: 25.8 ± 0.3 km, k: 1.84 ± 0.02
0.4/0.3/0.3
F
H: 33.0 ± 0.7 km, k: 1.67 ± 0.03
H (km)
k
Ps
3p1s
2p2s
Peak
90%
G
Radial
Count
Time (s)
$P_{33.0}s$
$3p_{33.0}1s$
$2p_{33.0}2s$
Ray Parameter ($s \cdot km^{-1}$)
DRBS
H
Average
Radial
Transverse
Amplitude
I
Transverse
Amplitude

Figure 298 (page 304). Receiver-function analysis for station DRBS. *A*, Regional map of Saudi Arabia showing the entire array (as inverted triangles), the location of station DRBS (red inverted triangle), the shield-platform boundary (white line), and the bounds of the map in *B* (white box). *B*, Local map of station DRBS. Harrats are shown in black. *C*, Standard, single-layer *H-k* stack with stacking weights 0.4/0.3/0.3. This *H-k* stack ignores sedimentary effects on the receiver functions. *D*, Standard, single-layer *H-k* stack with stacking weights 0.5/0.5/0.0. This *H-k* stack also ignores sedimentary effects on the receiver functions. *E*, Optimized sub-sedimentary *H-k* stack with stacking weights 0.4/0.3/0.3, following the method of Yu and others (2015). *F*, Optimized sedimentary *H-k* stack with stacking weights 0.05/0.70/0.25, following the method of Yu and others (2015). *G*, Radial component P-wave receiver functions (PRFs) plotted against ray parameter. Individual PRFs have had the resonance-removal filter of Yu and others (2015) applied to them and are normalized to the maximum amplitude within the time window shown, binned, and normalized by the number of traces per bin. *H*, Average of every individual normalized radial receiver function with the application of the resonance-removal filter (blue) and average of every individual normalized raw radial receiver function (red). *I*, Radial component of raw PRFs (that is, PRFs with no resonance-removal filter applied) plotted against ray parameter, normalized as in *G*.

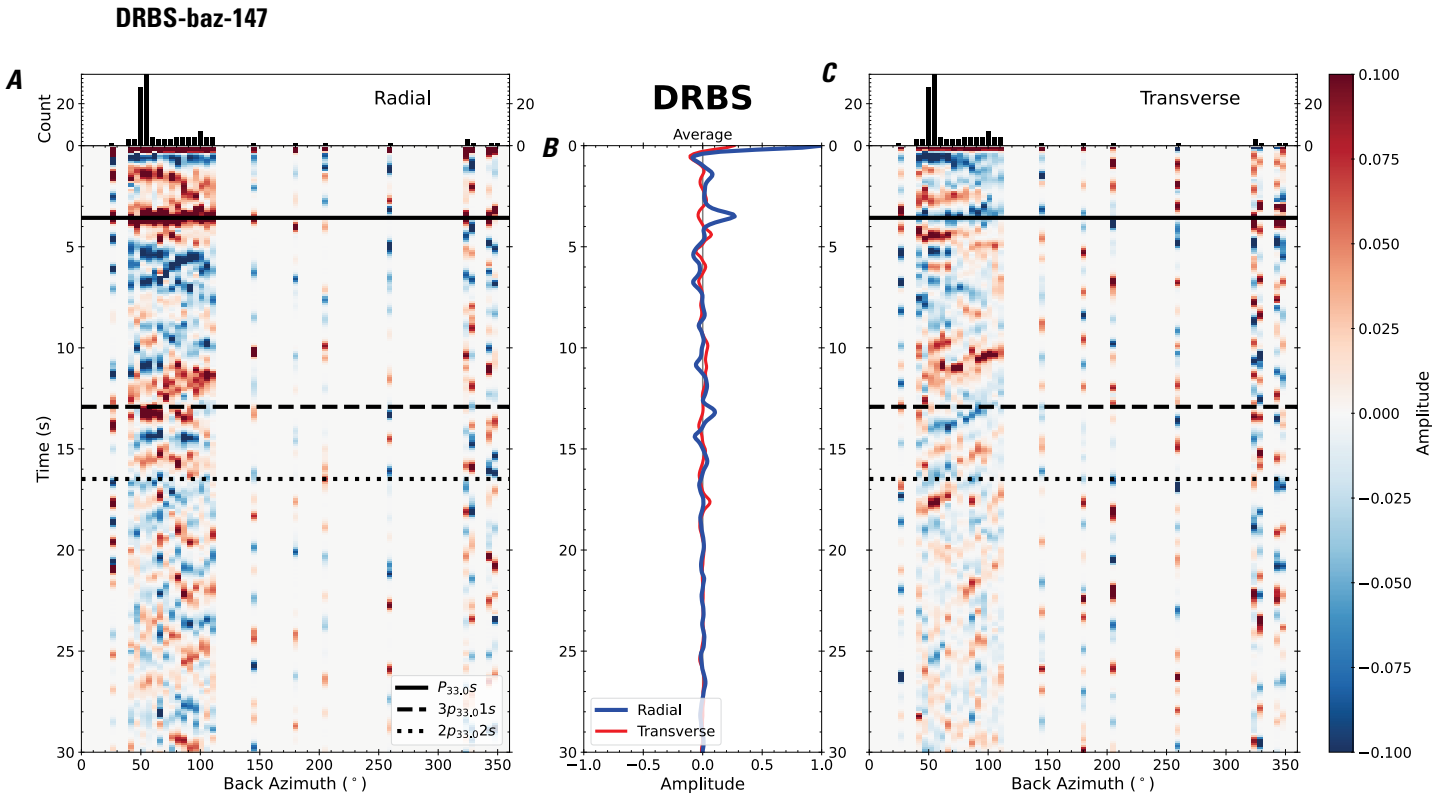

Figure 299. Receiver functions plotted against back azimuth for station DRBS. *A*, Radial component of P-wave receiver functions (PRFs) plotted against back azimuth. Individual PRFs have had the resonance-removal filter of Yu and others (2015) applied to them, are normalized to the maximum amplitude within the time window shown, binned, and normalized by the number of traces per bin. *B*, Average of every individual normalized radial receiver function with the application of the resonance-removal filter (blue) and average of every individual normalized raw radial receiver function (red). *C*, Radial component of raw PRFs, plotted against back azimuth, normalized as in *A*. Ps, 3p1s, and 2p2s arrival times predicted for the preferred Moho depth are shown, assuming a ray parameter of 0.06 s/km.

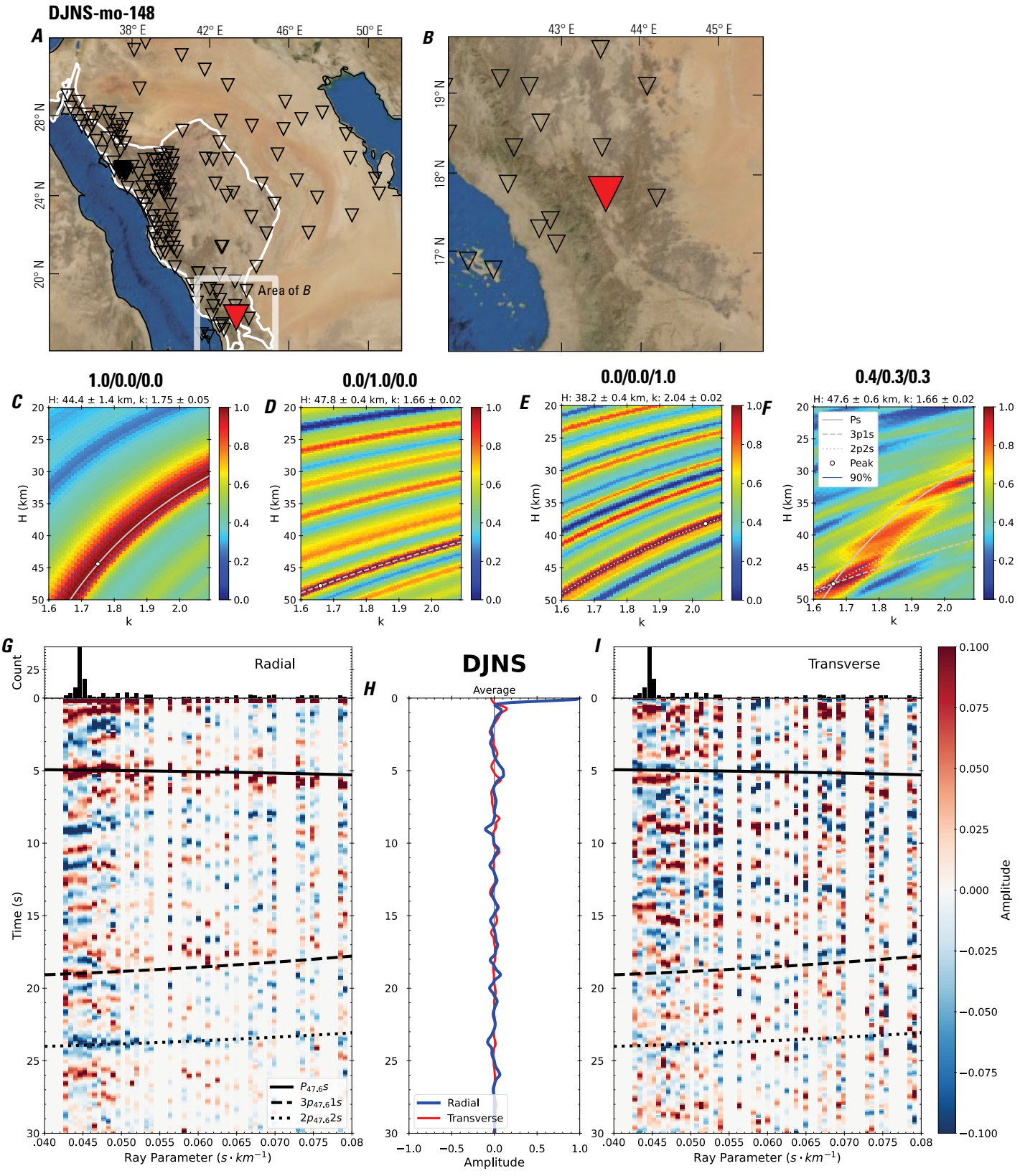
DJNS-mo-148
A
38° E
42° E
46° E
50° E
28° N
24° N
20° N
Area of B
B
43° E
44° E
45° E
19° N
18° N
17° N
1.0/0.0/0.0
C
H: 44.4 ± 1.4 km, k: 1.75 ± 0.05
0.0/1.0/0.0
D
H: 47.8 ± 0.4 km, k: 1.66 ± 0.02
0.0/0.0/1.0
E
H: 38.2 ± 0.4 km, k: 2.04 ± 0.02
0.4/0.3/0.3
F
H: 47.6 ± 0.6 km, k: 1.66 ± 0.02
Ps
3p1s
2p2s
Peak
90%
H (km)
k
G
Radial
Count
Time (s)
$P_{47.6}s$
$3p_{47.6}1s$
$2p_{47.6}2s$
Ray Parameter ($s \cdot km^{-1}$)
H
DJNS
Average
Radial
Transverse
Amplitude
I
Transverse
Amplitude

Figure 300 (page 306). Receiver-function analysis for station DJNS. *A*, Regional map of Saudi Arabia showing the entire array (as inverted triangles), the location of station DJNS (red inverted triangle), the shield-platform boundary (white line), and the bounds of the map in *B* (white box). *B*, Local map of station DJNS. Harrats are shown in black. *C*, Standard, single-layer *H-k* stack with stacking weights 0.4/0.3/0.3. This *H-k* stack ignores sedimentary effects on the receiver functions. *D*, Standard, single-layer *H-k* stack with stacking weights 0.5/0.5/0.0. This *H-k* stack also ignores sedimentary effects on the receiver functions. *E*, Optimized sub-sedimentary *H-k* stack with stacking weights 0.4/0.3/0.3, following the method of Yu and others (2015). *F*, Optimized sedimentary *H-k* stack with stacking weights 0.05/0.70/0.25, following the method of Yu and others (2015). *G*, Radial component P-wave receiver functions (PRFs) plotted against ray parameter. Individual PRFs have had the resonance-removal filter of Yu and others (2015) applied to them and are normalized to the maximum amplitude within the time window shown, binned, and normalized by the number of traces per bin. *H*, Average of every individual normalized radial receiver function with the application of the resonance-removal filter (blue) and average of every individual normalized raw radial receiver function (red). *I*, Radial component of raw PRFs (that is, PRFs with no resonance-removal filter applied) plotted against ray parameter, normalized as in *G*.

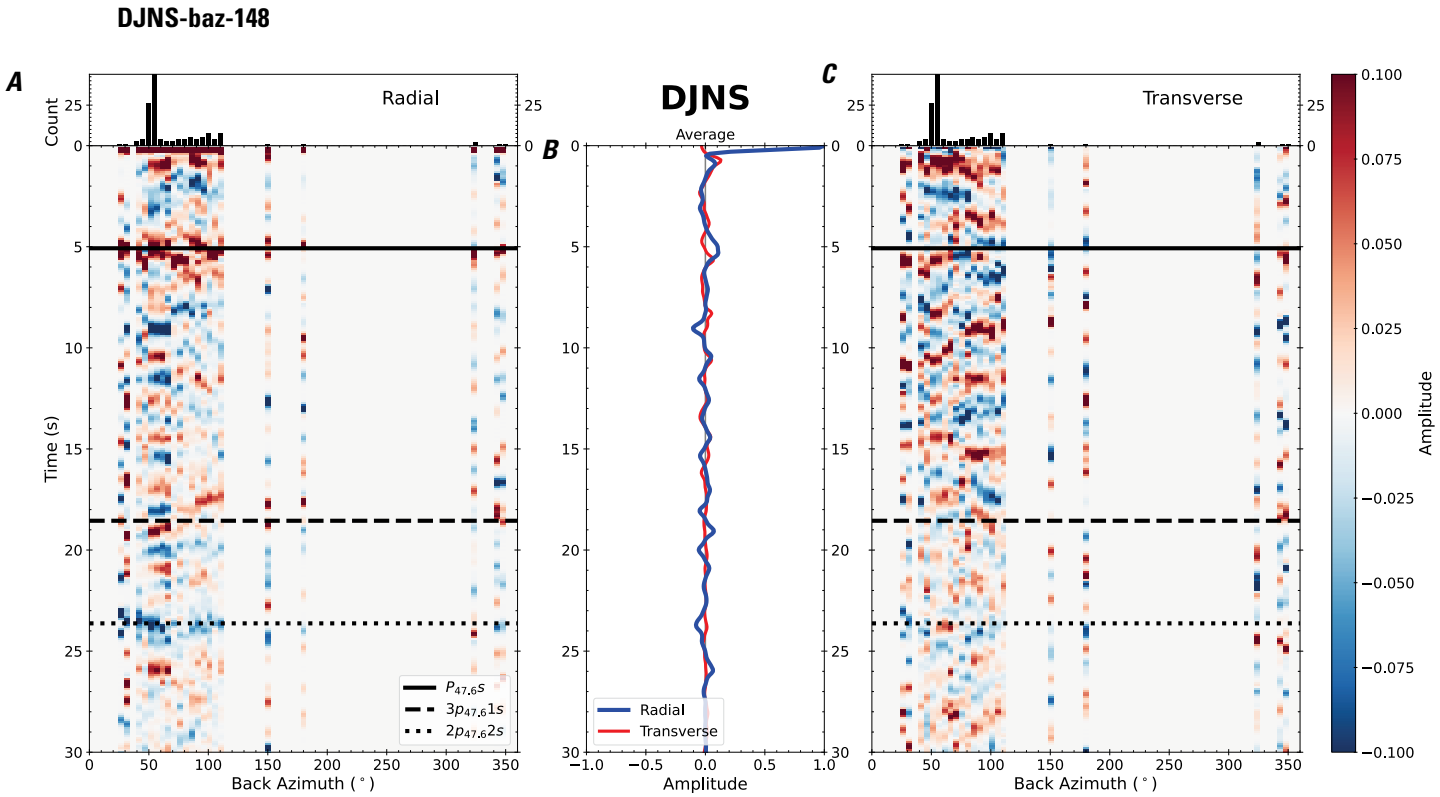

Figure 301. Receiver functions plotted against back azimuth for station DJNS. *A*, Radial component of P-wave receiver functions (PRFs) plotted against back azimuth. Individual PRFs have had the resonance-removal filter of Yu and others (2015) applied to them, are normalized to the maximum amplitude within the time window shown, binned, and normalized by the number of traces per bin. *B*, Average of every individual normalized radial receiver function with the application of the resonance-removal filter (blue) and average of every individual normalized raw radial receiver function (red). *C*, Radial component of raw PRFs, plotted against back azimuth, normalized as in *A*. Ps, 3p1s, and 2p2s arrival times predicted for the preferred Moho depth are shown, assuming a ray parameter of 0.06 s/km.

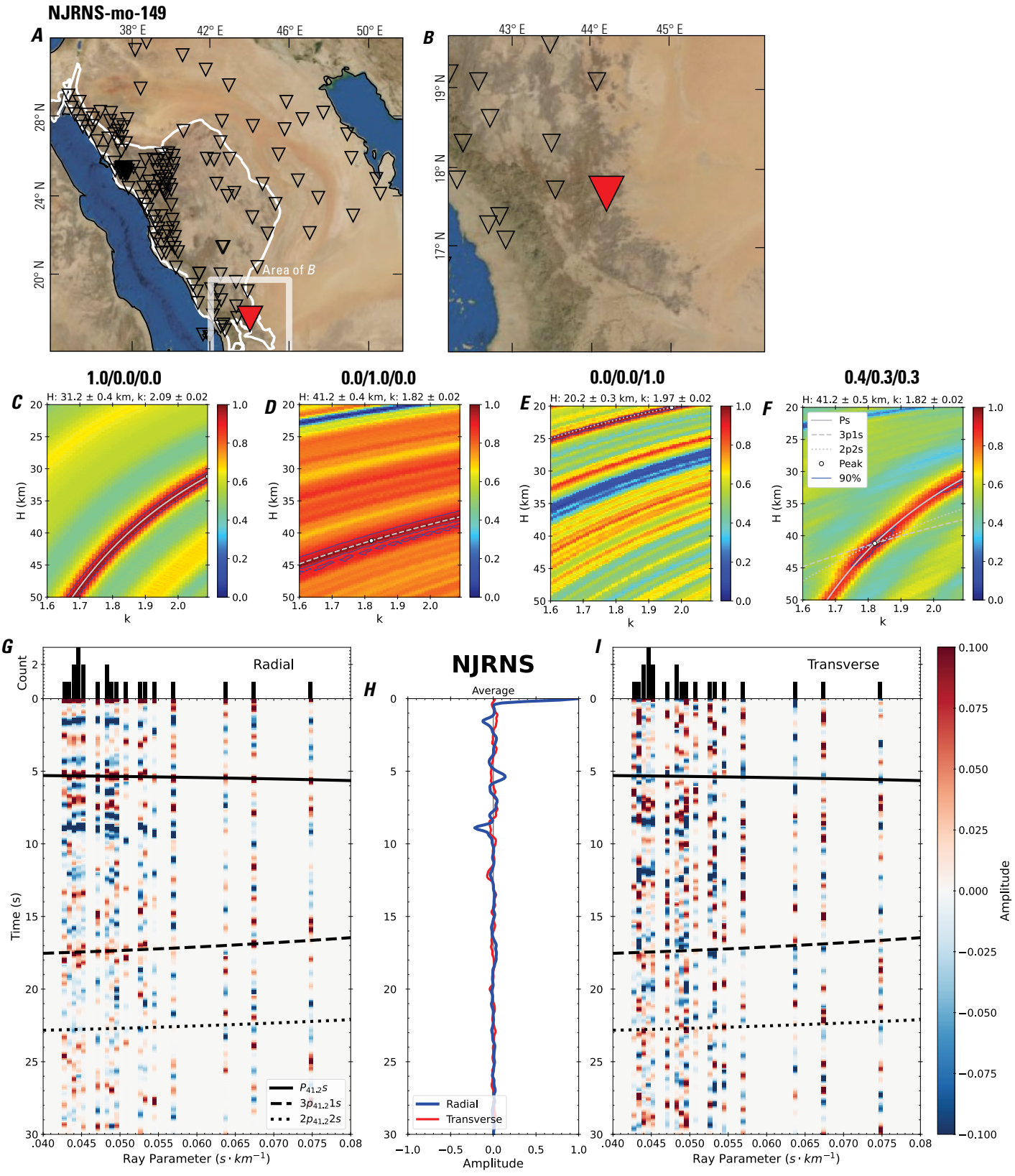
NJRNS-mo-149
A
38° E
42° E
46° E
50° E
28° N
24° N
20° N
Area of B
B
43° E
44° E
45° E
19° N
18° N
17° N
1.0/0.0/0.0
0.0/1.0/0.0
0.0/0.0/1.0
0.4/0.3/0.3
C
H: 31.2 ± 0.4 km, k: 2.09 ± 0.02
D
H: 41.2 ± 0.4 km, k: 1.82 ± 0.02
E
H: 20.2 ± 0.3 km, k: 1.97 ± 0.02
F
H: 41.2 ± 0.5 km, k: 1.82 ± 0.02
Ps
3p1s
2p2s
Peak
90%
H (km)
k
G
Radial
Count
Time (s)
Ray Parameter (s · km⁻¹)
$P_{41.2}s$
$3p_{41.2}1s$
$2p_{41.2}2s$
H
NJRNS
Average
Radial
Transverse
Amplitude
I
Transverse
Amplitude

Figure 302 (page 308). Receiver-function analysis for station NJRNS. *A*, Regional map of Saudi Arabia showing the entire array (as inverted triangles), the location of station NJRNS (red inverted triangle), the shield-platform boundary (white line), and the bounds of the map in *B* (white box). *B*, Local map of station NJRNS. Harrats are shown in black. *C*, Standard, single-layer *H-k* stack with stacking weights 0.4/0.3/0.3. This *H-k* stack ignores sedimentary effects on the receiver functions. *D*, Standard, single-layer *H-k* stack with stacking weights 0.5/0.5/0.0. This *H-k* stack also ignores sedimentary effects on the receiver functions. *E*, Optimized sub-sedimentary *H-k* stack with stacking weights 0.4/0.3/0.3, following the method of Yu and others (2015). *F*, Optimized sedimentary *H-k* stack with stacking weights 0.05/0.70/0.25, following the method of Yu and others (2015). *G*, Radial component P-wave receiver functions (PRFs) plotted against ray parameter. Individual PRFs have had the resonance-removal filter of Yu and others (2015) applied to them and are normalized to the maximum amplitude within the time window shown, binned, and normalized by the number of traces per bin. *H*, Average of every individual normalized radial receiver function with the application of the resonance-removal filter (blue) and average of every individual normalized raw radial receiver function (red). *I*, Radial component of raw PRFs (that is, PRFs with no resonance-removal filter applied) plotted against ray parameter, normalized as in *G*.

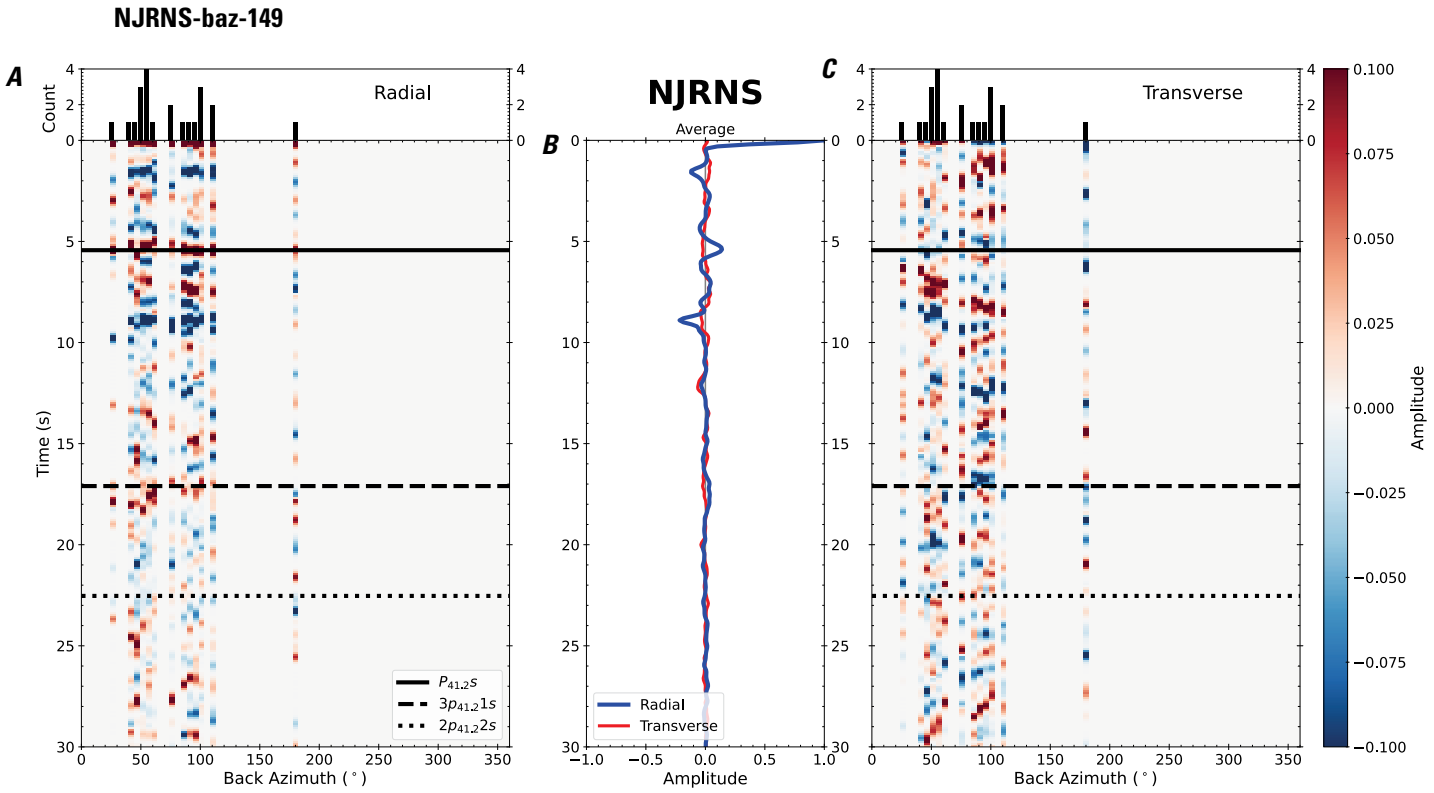

Figure 303. Receiver functions plotted against back azimuth for station NJRNS. *A*, Radial component of P-wave receiver functions (PRFs) plotted against back azimuth. Individual PRFs have had the resonance-removal filter of Yu and others (2015) applied to them, are normalized to the maximum amplitude within the time window shown, binned, and normalized by the number of traces per bin. *B*, Average of every individual normalized radial receiver function with the application of the resonance-removal filter (blue) and average of every individual normalized raw radial receiver function (red). *C*, Radial component of raw PRFs, plotted against back azimuth, normalized as in *A*. Ps, 3p1s, and 2p2s arrival times predicted for the preferred Moho depth are shown, assuming a ray parameter of 0.06 s/km.

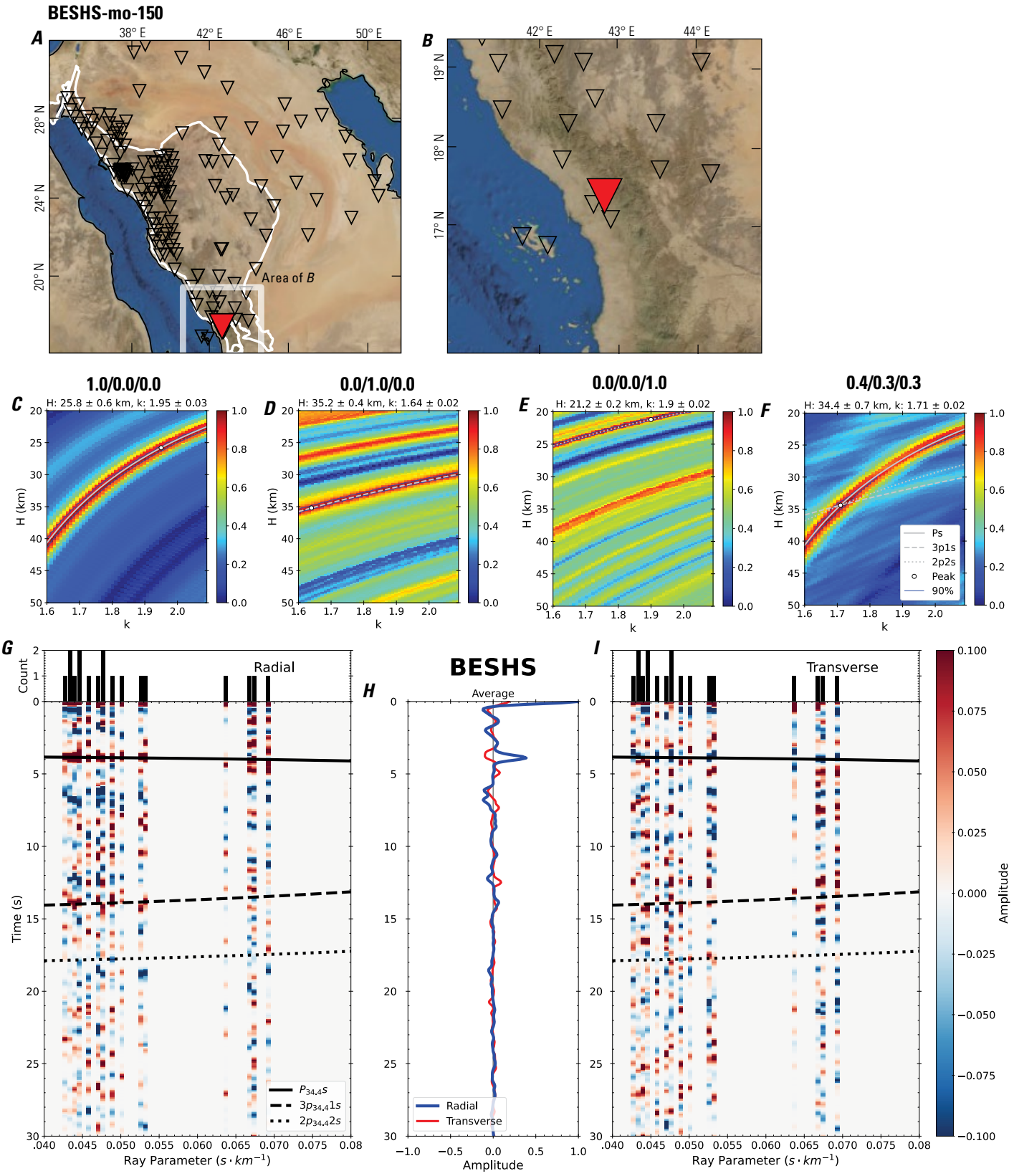
BESHS-mo-150
A
38° E
42° E
46° E
50° E
28° N
24° N
20° N
Area of B
B
42° E
43° E
44° E
19° N
18° N
17° N
1.0/0.0/0.0
C
H: 25.8 ± 0.6 km, k: 1.95 ± 0.03
0.0/1.0/0.0
D
H: 35.2 ± 0.4 km, k: 1.64 ± 0.02
0.0/0.0/1.0
E
H: 21.2 ± 0.2 km, k: 1.9 ± 0.02
0.4/0.3/0.3
F
H: 34.4 ± 0.7 km, k: 1.71 ± 0.02
H (km)
k
Ps
3p1s
2p2s
Peak
90%
G
Radial
Count
Time (s)
Ray Parameter (s · km⁻¹)
$P_{34,4}s$
$3p_{34,4}1s$
$2p_{34,4}2s$
H
BESHS
Average
Radial
Transverse
Amplitude
I
Transverse
Amplitude

Figure 304 (page 310). Receiver-function analysis for station BESHS. *A*, Regional map of Saudi Arabia showing the entire array (as inverted triangles), the location of station BESHS (red inverted triangle), the shield-platform boundary (white line), and the bounds of the map in *B* (white box). *B*, Local map of station BESHS. Harrats are shown in black. *C*, Standard, single-layer *H-k* stack with stacking weights 0.4/0.3/0.3. This *H-k* stack ignores sedimentary effects on the receiver functions. *D*, Standard, single-layer *H-k* stack with stacking weights 0.5/0.5/0.0. This *H-k* stack also ignores sedimentary effects on the receiver functions. *E*, Optimized sub-sedimentary *H-k* stack with stacking weights 0.4/0.3/0.3, following the method of Yu and others (2015). *F*, Optimized sedimentary *H-k* stack with stacking weights 0.05/0.70/0.25, following the method of Yu and others (2015). *G*, Radial component P-wave receiver functions (PRFs) plotted against ray parameter. Individual PRFs have had the resonance-removal filter of Yu and others (2015) applied to them and are normalized to the maximum amplitude within the time window shown, binned, and normalized by the number of traces per bin. *H*, Average of every individual normalized radial receiver function with the application of the resonance-removal filter (blue) and average of every individual normalized raw radial receiver function (red). *I*, Radial component of raw PRFs (that is, PRFs with no resonance-removal filter applied) plotted against ray parameter, normalized as in *G*.

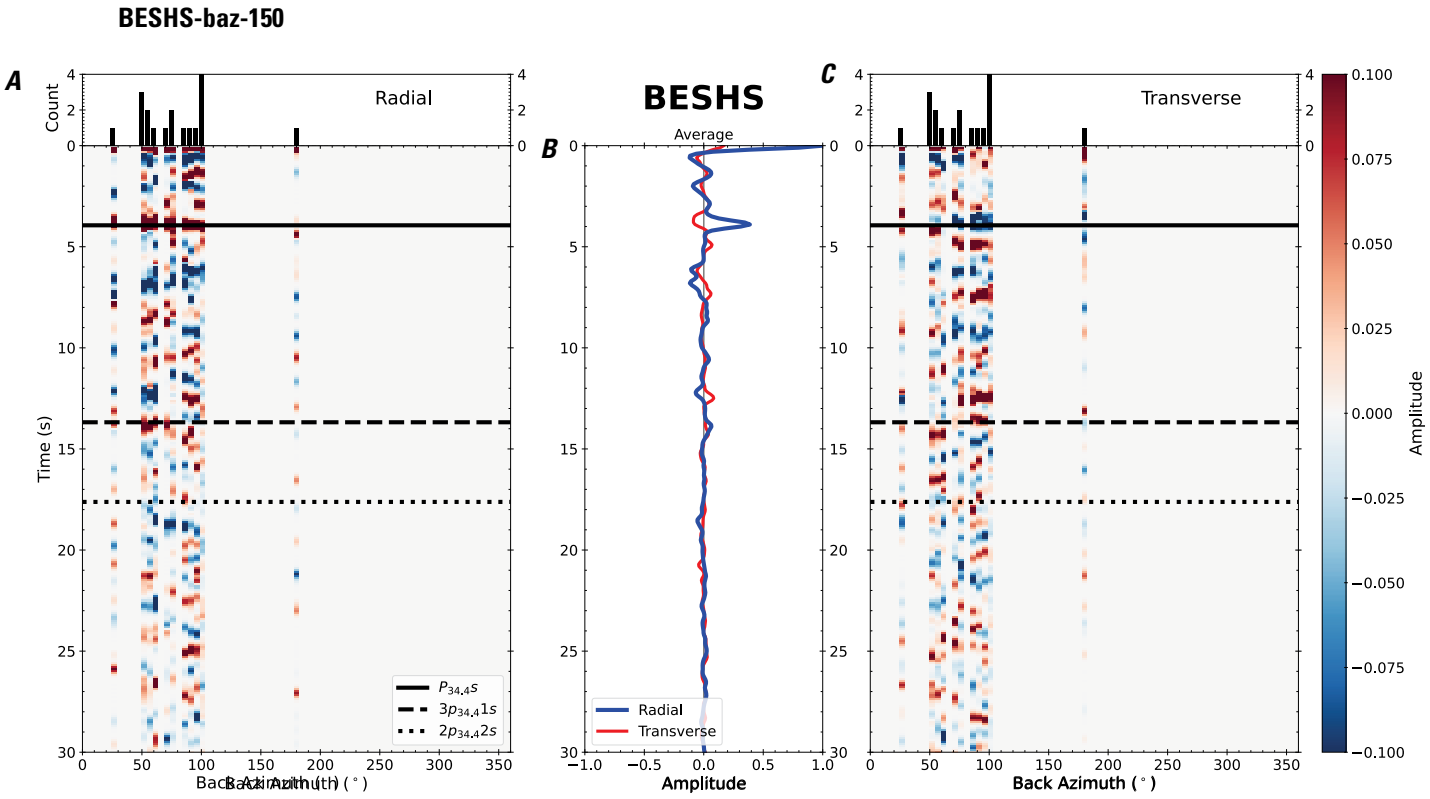

Figure 305. Receiver functions plotted against back azimuth for station BESHS. *A*, Radial component of P-wave receiver functions (PRFs) plotted against back azimuth. Individual PRFs have had the resonance-removal filter of Yu and others (2015) applied to them, are normalized to the maximum amplitude within the time window shown, binned, and normalized by the number of traces per bin. *B*, Average of every individual normalized radial receiver function with the application of the resonance-removal filter (blue) and average of every individual normalized raw radial receiver function (red). *C*, Radial component of raw PRFs, plotted against back azimuth, normalized as in *A*. Ps, 3p1s, and 2p2s arrival times predicted for the preferred Moho depth are shown, assuming a ray parameter of 0.06 s/km.

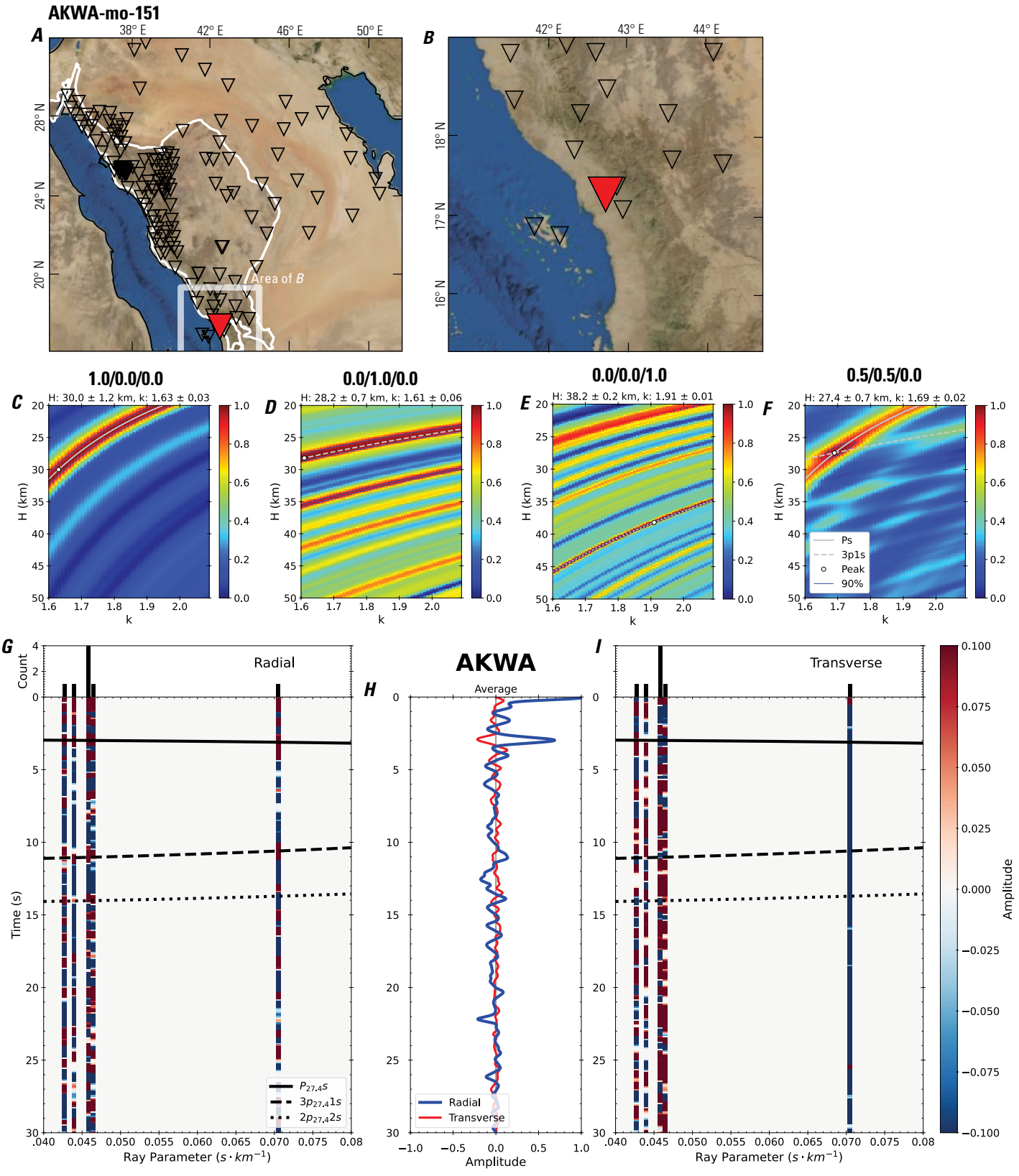
AKWA-mo-151
A
38° E
42° E
46° E
50° E
28° N
24° N
20° N
Area of B
B
42° E
43° E
44° E
18° N
17° N
16° N
1.0/0.0/0.0
C
H: 30.0 ± 1.2 km, k: 1.63 ± 0.03
0.0/1.0/0.0
D
H: 28.2 ± 0.7 km, k: 1.61 ± 0.06
0.0/0.0/1.0
E
H: 38.2 ± 0.2 km, k: 1.91 ± 0.01
0.5/0.5/0.0
F
H: 27.4 ± 0.7 km, k: 1.69 ± 0.02
H (km)
k
Ps
3p1s
Peak
90%
G
Radial
Count
Time (s)
$P_{27.4}s$
$3p_{27.4}1s$
$2p_{27.4}2s$
Ray Parameter ($s \cdot km^{-1}$)
AKWA
H
Average
Radial
Transverse
Amplitude
I
Transverse
Amplitude

Figure 306 (page 312). Receiver-function analysis for station AKWA. *A*, Regional map of Saudi Arabia showing the entire array (as inverted triangles), the location of station AKWA (red inverted triangle), the shield-platform boundary (white line), and the bounds of the map in *B* (white box). *B*, Local map of station AKWA. Harrats are shown in black. *C*, Standard, single-layer *H-k* stack with stacking weights 0.4/0.3/0.3. This *H-k* stack ignores sedimentary effects on the receiver functions. *D*, Standard, single-layer *H-k* stack with stacking weights 0.5/0.5/0.0. This *H-k* stack also ignores sedimentary effects on the receiver functions. *E*, Optimized sub-sedimentary *H-k* stack with stacking weights 0.4/0.3/0.3, following the method of Yu and others (2015). *F*, Optimized sedimentary *H-k* stack with stacking weights 0.05/0.70/0.25, following the method of Yu and others (2015). *G*, Radial component P-wave receiver functions (PRFs) plotted against ray parameter. Individual PRFs have had the resonance-removal filter of Yu and others (2015) applied to them and are normalized to the maximum amplitude within the time window shown, binned, and normalized by the number of traces per bin. *H*, Average of every individual normalized radial receiver function with the application of the resonance-removal filter (blue) and average of every individual normalized raw radial receiver function (red). *I*, Radial component of raw PRFs (that is, PRFs with no resonance-removal filter applied) plotted against ray parameter, normalized as in *G*.

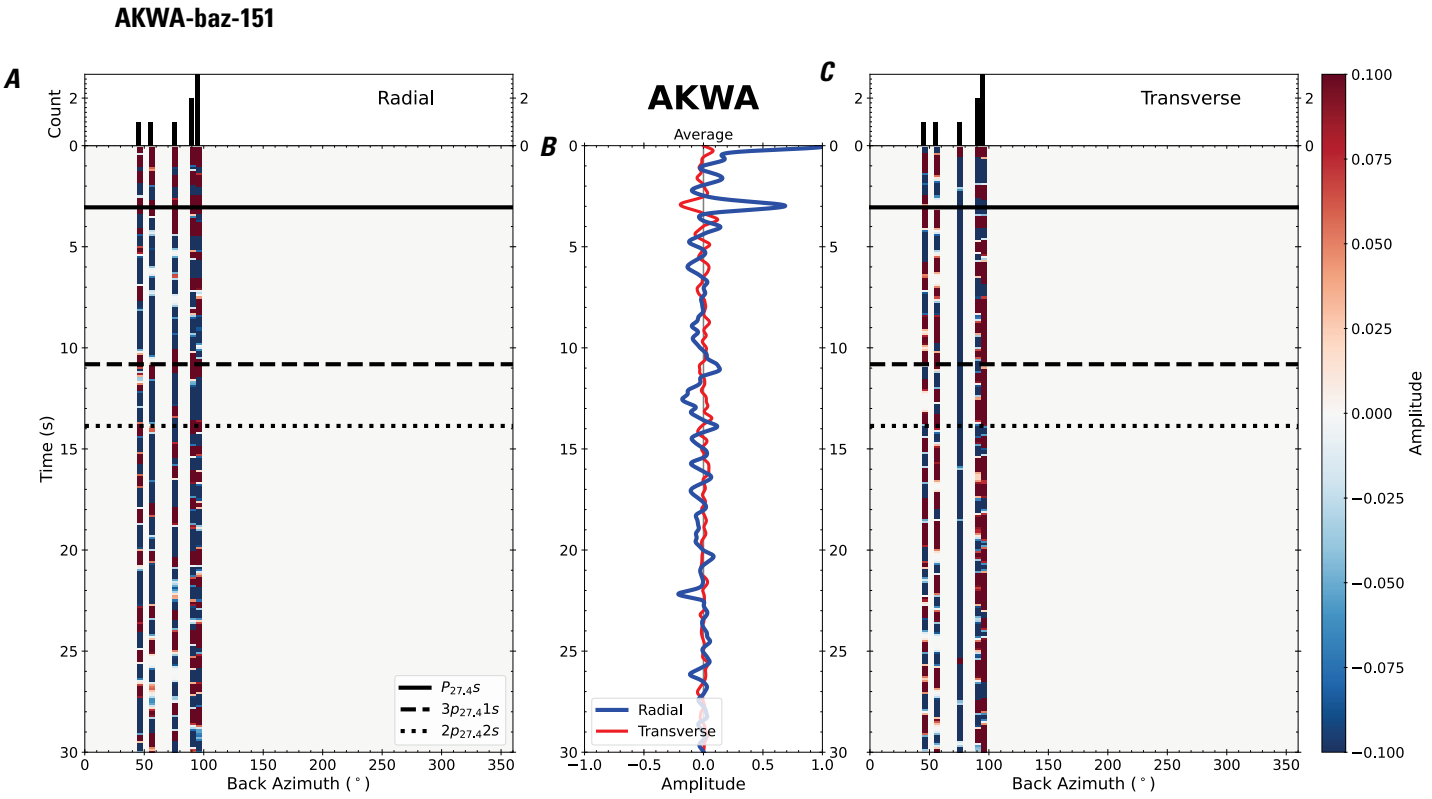

Figure 307. Receiver functions plotted against back azimuth for station AKWA. *A*, Radial component of P-wave receiver functions (PRFs) plotted against back azimuth. Individual PRFs have had the resonance-removal filter of Yu and others (2015) applied to them, are normalized to the maximum amplitude within the time window shown, binned, and normalized by the number of traces per bin. *B*, Average of every individual normalized radial receiver function with the application of the resonance-removal filter (blue) and average of every individual normalized raw radial receiver function (red). *C*, Radial component of raw PRFs, plotted against back azimuth, normalized as in *A*. Ps, 3p1s, and 2p2s arrival times predicted for the preferred Moho depth are shown, assuming a ray parameter of 0.06 s/km.

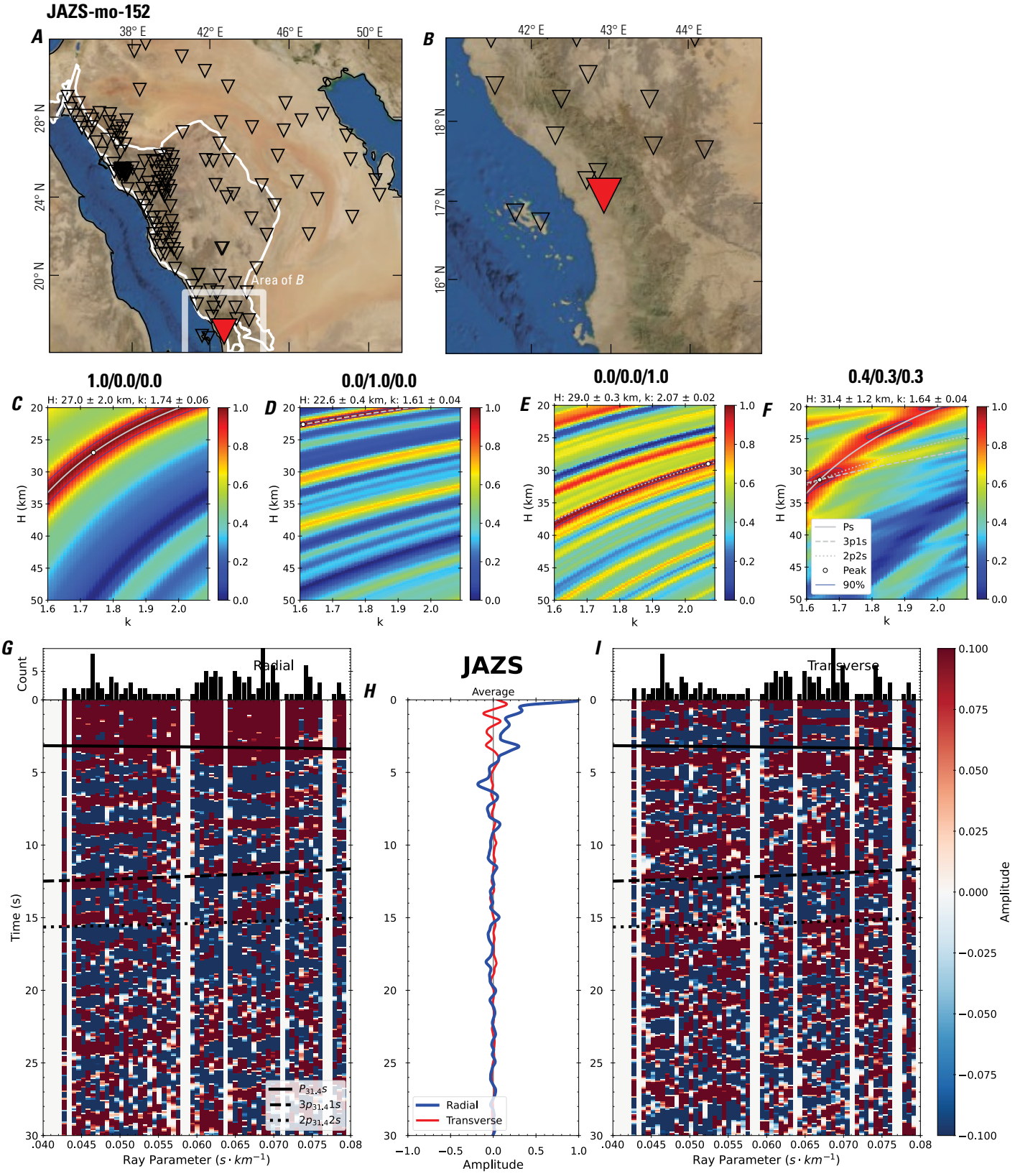
JAZS-mo-152
A
38° E
42° E
46° E
50° E
28° N
24° N
20° N
Area of B
B
42° E
43° E
44° E
18° N
17° N
16° N
1.0/0.0/0.0
0.0/1.0/0.0
0.0/0.0/1.0
0.4/0.3/0.3
C
H: 27.0 ± 2.0 km, k: 1.74 ± 0.06
D
H: 22.6 ± 0.4 km, k: 1.61 ± 0.04
E
H: 29.0 ± 0.3 km, k: 2.07 ± 0.02
F
H: 31.4 ± 1.2 km, k: 1.64 ± 0.04
H (km)
k
Ps
3p1s
2p2s
Peak
90%
G
Radial
Count
Time (s)
Ray Parameter (s · km⁻¹)
P31,4s
3p31,41s
2p31,42s
H
JAZS
Average
Radial
Transverse
Amplitude
I
Transverse
Amplitude

Figure 308 (page 314). Receiver-function analysis for station JAZS. *A*, Regional map of Saudi Arabia showing the entire array (as inverted triangles), the location of station JAZS (red inverted triangle), the shield-platform boundary (white line), and the bounds of the map in *B* (white box). *B*, Local map of station JAZS. Harrats are shown in black. *C*, Standard, single-layer *H-k* stack with stacking weights 0.4/0.3/0.3. This *H-k* stack ignores sedimentary effects on the receiver functions. *D*, Standard, single-layer *H-k* stack with stacking weights 0.5/0.5/0.0. This *H-k* stack also ignores sedimentary effects on the receiver functions. *E*, Optimized sub-sedimentary *H-k* stack with stacking weights 0.4/0.3/0.3, following the method of Yu and others (2015). *F*, Optimized sedimentary *H-k* stack with stacking weights 0.05/0.70/0.25, following the method of Yu and others (2015). *G*, Radial component P-wave receiver functions (PRFs) plotted against ray parameter. Individual PRFs have had the resonance-removal filter of Yu and others (2015) applied to them and are normalized to the maximum amplitude within the time window shown, binned, and normalized by the number of traces per bin. *H*, Average of every individual normalized radial receiver function with the application of the resonance-removal filter (blue) and average of every individual normalized raw radial receiver function (red). *I*, Radial component of raw PRFs (that is, PRFs with no resonance-removal filter applied) plotted against ray parameter, normalized as in *G*.

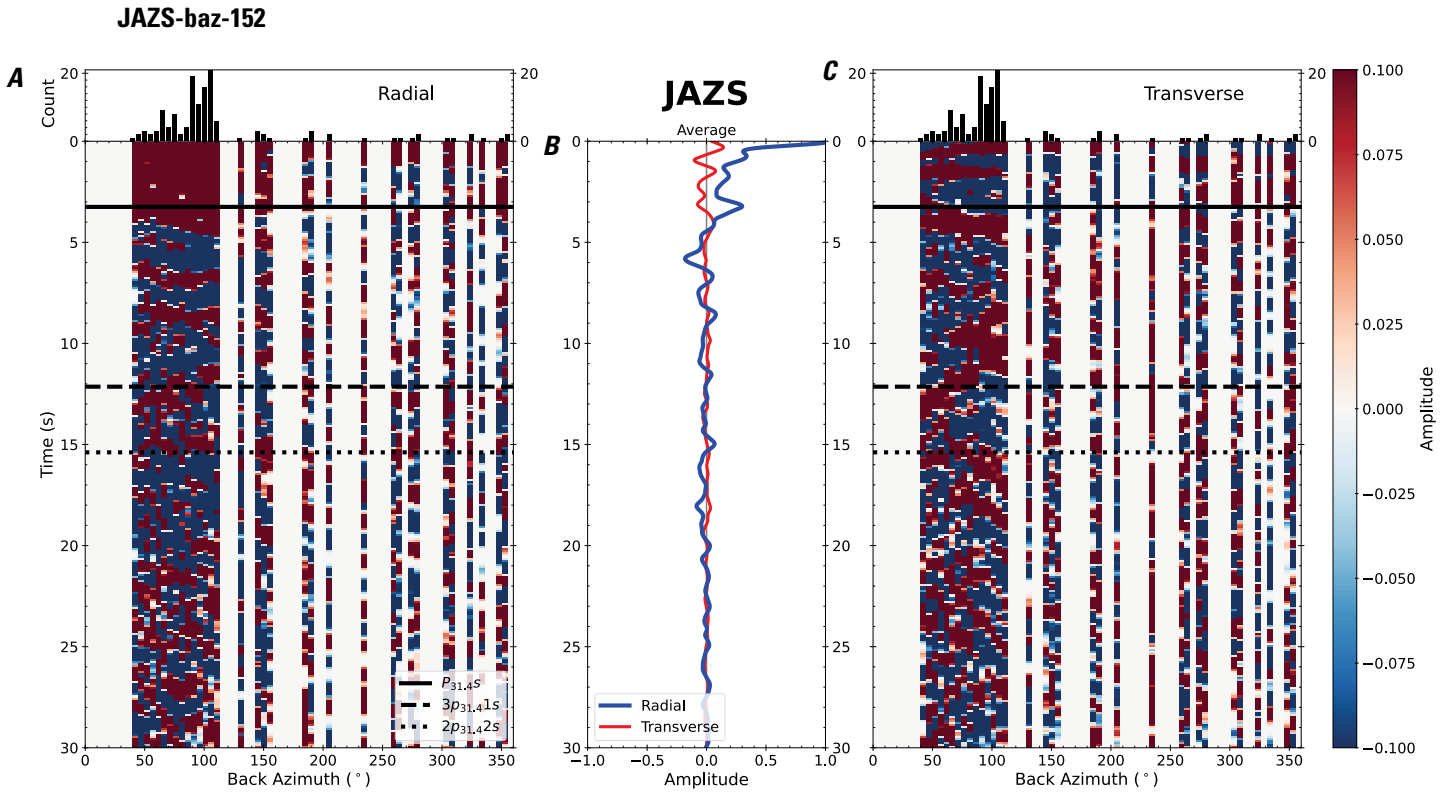

Figure 309. Receiver functions plotted against back azimuth for station JAZS. *A*, Radial component of P-wave receiver functions (PRFs) plotted against back azimuth. Individual PRFs have had the resonance-removal filter of Yu and others (2015) applied to them, are normalized to the maximum amplitude within the time window shown, binned, and normalized by the number of traces per bin. *B*, Average of every individual normalized radial receiver function with the application of the resonance-removal filter (blue) and average of every individual normalized raw radial receiver function (red). *C*, Radial component of raw PRFs, plotted against back azimuth, normalized as in *A*. Ps, 3p1s, and 2p2s arrival times predicted for the preferred Moho depth are shown, assuming a ray parameter of 0.06 s/km.

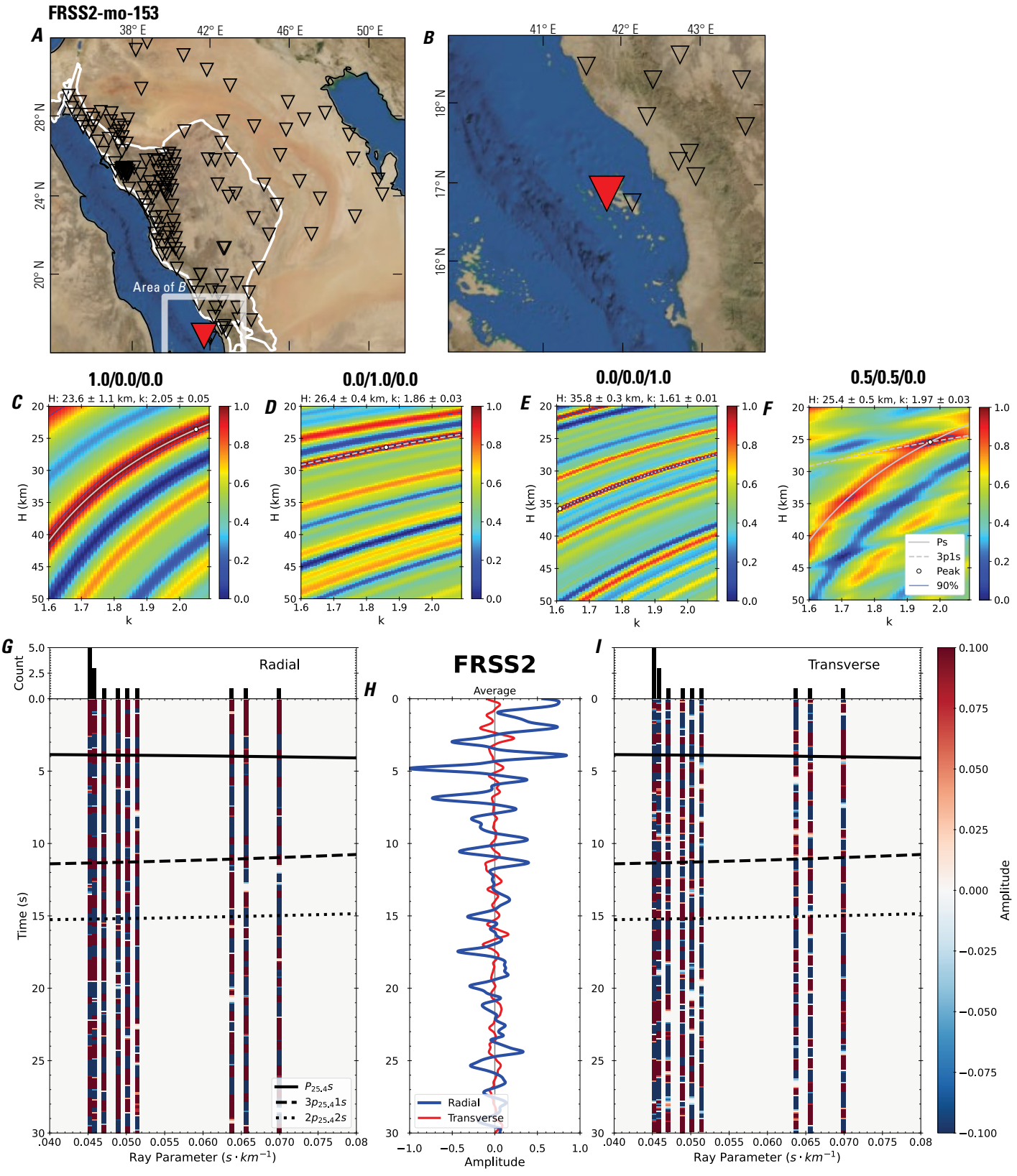
FRSS2-mo-153
A
38° E
42° E
46° E
50° E
28° N
24° N
20° N
Area of B
B
41° E
42° E
43° E
18° N
17° N
16° N
1.0/0.0/0.0
0.0/1.0/0.0
0.0/0.0/1.0
0.5/0.5/0.0
C
H: 23.6 ± 1.1 km, k: 2.05 ± 0.05
D
H: 26.4 ± 0.4 km, k: 1.86 ± 0.03
E
H: 35.8 ± 0.3 km, k: 1.61 ± 0.01
F
H: 25.4 ± 0.5 km, k: 1.97 ± 0.03
H (km)
k
Ps
3p1s
Peak
90%
G
Radial
Count
Time (s)
$P_{25.4}s$
$3p_{25.4}1s$
$2p_{25.4}2s$
Ray Parameter ($s \cdot km^{-1}$)
H
FRSS2
Average
Radial
Transverse
Amplitude
I
Transverse
Amplitude

Figure 310 (page 316). Receiver-function analysis for station FRSS2. *A*, Regional map of Saudi Arabia showing the entire array (as inverted triangles), the location of station FRSS2 (red inverted triangle), the shield-platform boundary (white line), and the bounds of the map in *B* (white box). *B*, Local map of station FRSS2. Harrats are shown in black. *C*, Standard, single-layer *H-k* stack with stacking weights 0.4/0.3/0.3. This *H-k* stack ignores sedimentary effects on the receiver functions. *D*, Standard, single-layer *H-k* stack with stacking weights 0.5/0.5/0.0. This *H-k* stack also ignores sedimentary effects on the receiver functions. *E*, Optimized sub-sedimentary *H-k* stack with stacking weights 0.4/0.3/0.3, following the method of Yu and others (2015). *F*, Optimized sedimentary *H-k* stack with stacking weights 0.05/0.70/0.25, following the method of Yu and others (2015). *G*, Radial component P-wave receiver functions (PRFs) plotted against ray parameter. Individual PRFs have had the resonance-removal filter of Yu and others (2015) applied to them and are normalized to the maximum amplitude within the time window shown, binned, and normalized by the number of traces per bin. *H*, Average of every individual normalized radial receiver function with the application of the resonance-removal filter (blue) and average of every individual normalized raw radial receiver function (red). *I*, Radial component of raw PRFs (that is, PRFs with no resonance-removal filter applied) plotted against ray parameter, normalized as in *G*.

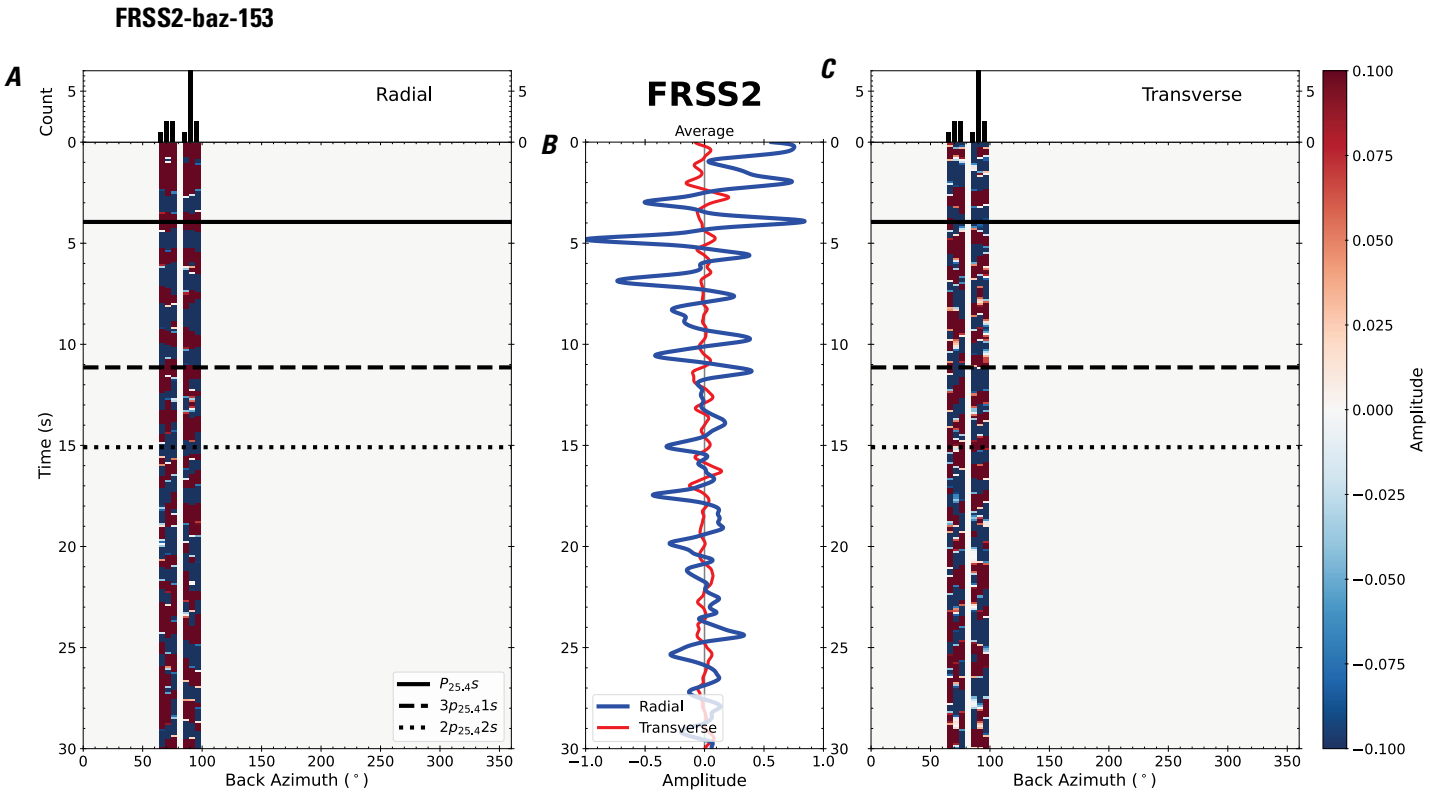

Figure 311. Receiver functions plotted against back azimuth for station FRSS2. *A*, Radial component of P-wave receiver functions (PRFs) plotted against back azimuth. Individual PRFs have had the resonance-removal filter of Yu and others (2015) applied to them, are normalized to the maximum amplitude within the time window shown, binned, and normalized by the number of traces per bin. *B*, Average of every individual normalized radial receiver function with the application of the resonance-removal filter (blue) and average of every individual normalized raw radial receiver function (red). *C*, Radial component of raw PRFs, plotted against back azimuth, normalized as in *A*. Ps, 3p1s, and 2p2s arrival times predicted for the preferred Moho depth are shown, assuming a ray parameter of 0.06 s/km.

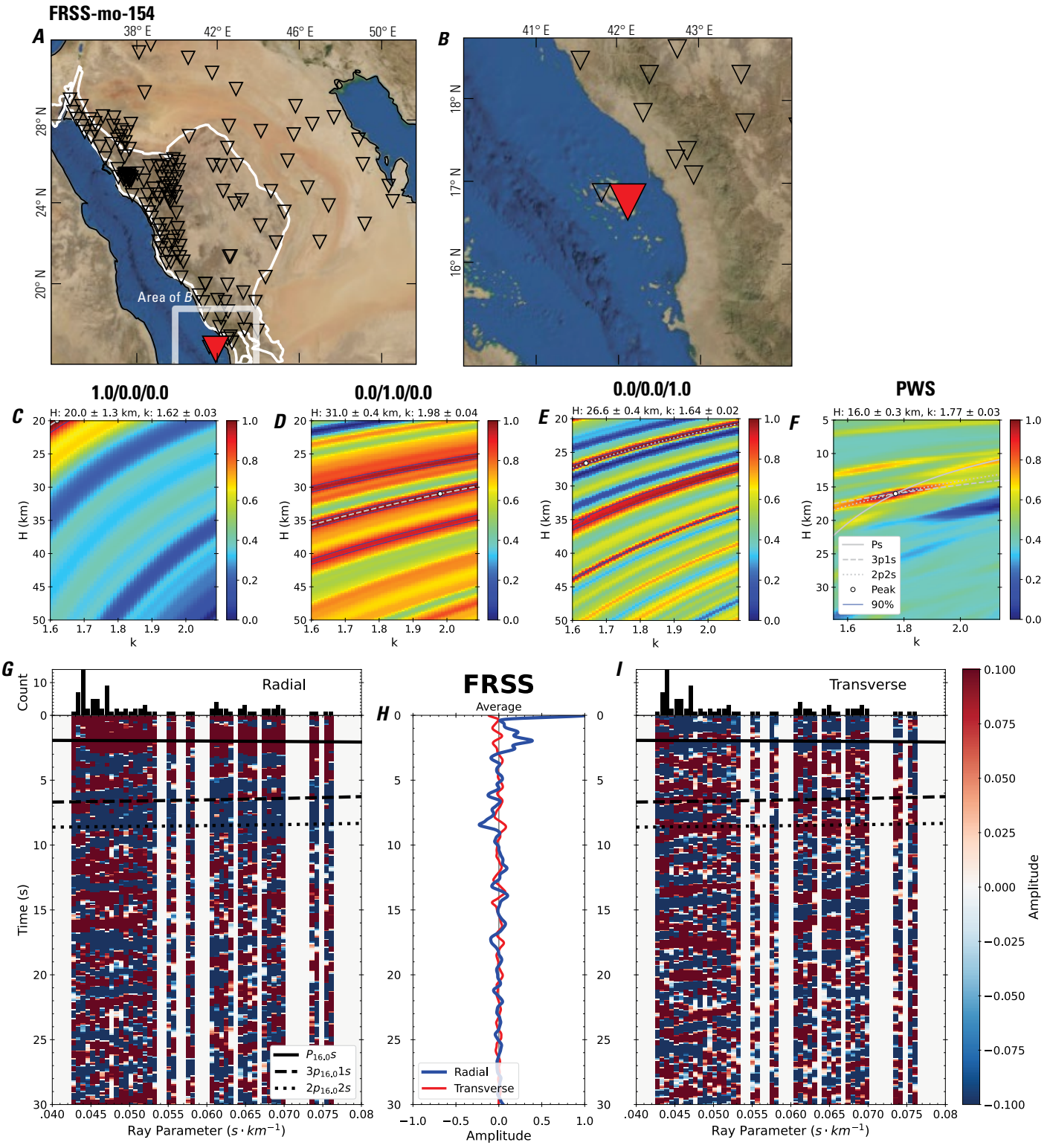
FRSS-mo-154
A
38° E
42° E
46° E
50° E
28° N
24° N
20° N
Area of B
B
41° E
42° E
43° E
18° N
17° N
16° N
1.0/0.0/0.0
0.0/1.0/0.0
0.0/0.0/1.0
PWS
C
D
E
F
H: 20.0 ± 1.3 km, k: 1.62 ± 0.03
H: 31.0 ± 0.4 km, k: 1.98 ± 0.04
H: 26.6 ± 0.4 km, k: 1.64 ± 0.02
H: 16.0 ± 0.3 km, k: 1.77 ± 0.03
H (km)
k
Ps
3p1s
2p2s
Peak
90%
G
H
I
Radial
Transverse
FRSS
Average
Count
Time (s)
Ray Parameter ($s \cdot km^{-1}$)
Amplitude
$P_{16.0}s$
$3p_{16.0}1s$
$2p_{16.0}2s$
Radial
Transverse

Figure 312 (page 318). Receiver-function analysis for station FRSS. *A*, Regional map of Saudi Arabia showing the entire array (as inverted triangles), the location of station FRSS (red inverted triangle), the shield-platform boundary (white line), and the bounds of the map in *B* (white box). *B*, Local map of station FRSS. Harrats are shown in black. *C*, Standard, single-layer *H-k* stack with stacking weights 0.4/0.3/0.3. This *H-k* stack ignores sedimentary effects on the receiver functions. *D*, Standard, single-layer *H-k* stack with stacking weights 0.5/0.5/0.0. This *H-k* stack also ignores sedimentary effects on the receiver functions. *E*, Optimized sub-sedimentary *H-k* stack with stacking weights 0.4/0.3/0.3, following the method of Yu and others (2015). *F*, Optimized sedimentary *H-k* stack with stacking weights 0.05/0.70/0.25, following the method of Yu and others (2015). *G*, Radial component P-wave receiver functions (PRFs) plotted against ray parameter. Individual PRFs have had the resonance-removal filter of Yu and others (2015) applied to them and are normalized to the maximum amplitude within the time window shown, binned, and normalized by the number of traces per bin. *H*, Average of every individual normalized radial receiver function with the application of the resonance-removal filter (blue) and average of every individual normalized raw radial receiver function (red). *I*, Radial component of raw PRFs (that is, PRFs with no resonance-removal filter applied) plotted against ray parameter, normalized as in *G*.

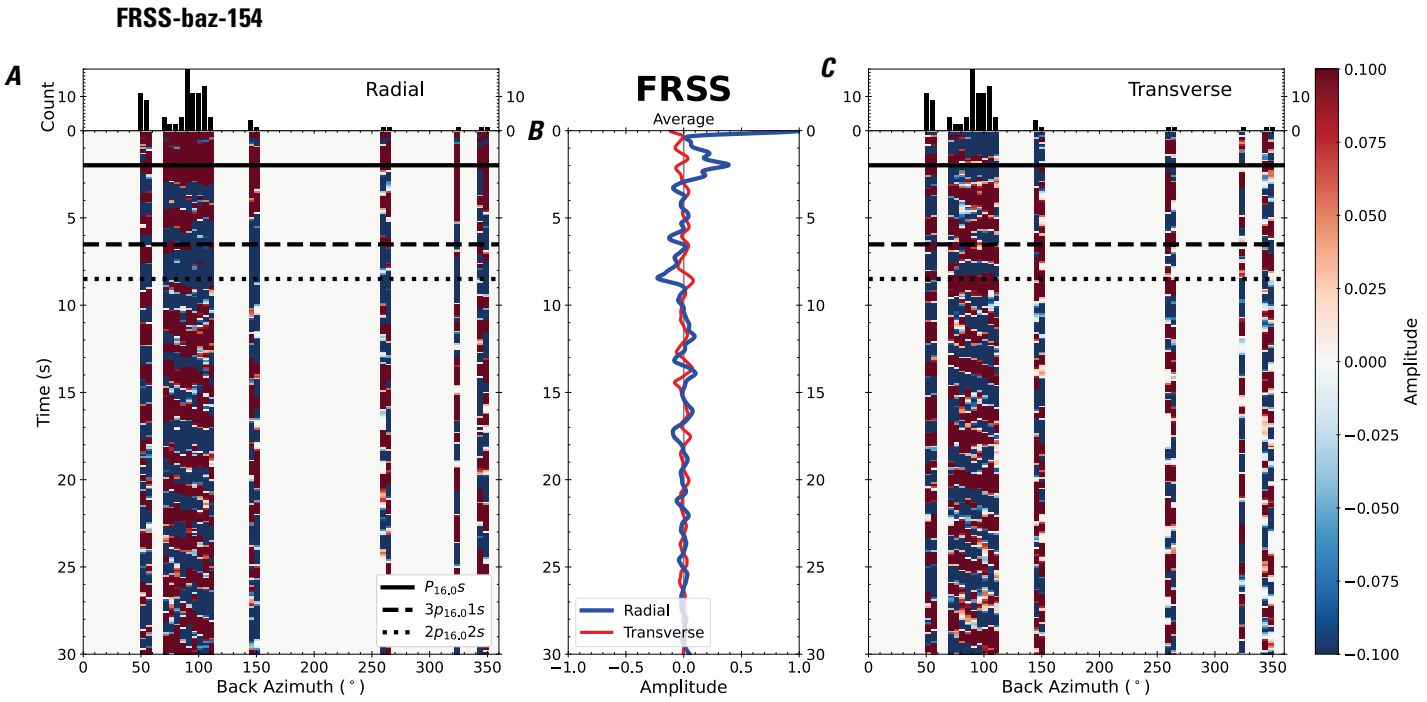

Figure 313. Receiver functions plotted against back azimuth for station FRSS. *A*, Radial component of P-wave receiver functions (PRFs) plotted against back azimuth. Individual PRFs have had the resonance-removal filter of Yu and others (2015) applied to them, are normalized to the maximum amplitude within the time window shown, binned, and normalized by the number of traces per bin. *B*, Average of every individual normalized radial receiver function with the application of the resonance-removal filter (blue) and average of every individual normalized raw radial receiver function (red). *C*, Radial component of raw PRFs, plotted against back azimuth, normalized as in *A*. Ps, 3p1s, and 2p2s arrival times predicted for the preferred Moho depth are shown, assuming a ray parameter of 0.06 s/km.

References Cited

Al-Damegh, K., Sandvol, E., and Barazangi, M., 2005, Crustal structure of the Arabian plate—New constraints from the analysis of teleseismic receiver functions: Earth and Planetary Science Letters, v. 231, nos. 3–4, p. 177–196, https://doi.org/10.1016/j.epsl.2004.12.020.

Blanchette, A.R., Klemperer, S.L., Mooney, W.D., and Zahran, H.M., [in press], Thickness of the Saudi Arabian crust, chap. M *of* Sisson, T.W., Calvert, A.T., and Mooney, W.D., eds., Active volcanism on the Arabian Shield—Geology, volcanology, and geophysics of northern Harrat Rahat and vicinity, Kingdom of Saudi Arabia: U.S. Geological Survey Professional Paper 1862 [also released as Saudi Geological Survey Special Report SGS–SP–2021–1], 49 p., https://doi.org/10.3133/pp1862M.

Bosworth, W., 2015, Geological evolution of the Red Sea—Historical background, review and synthesis, *in* Rasul, N.M., and Stewart, I.C.F., eds., The Red Sea: Berlin, Springer-Verlag, p. 45–78.

Bosworth, W., Huchon, P., and McClay, K., 2005, The Red Sea and Gulf of Aden Basins, *in* Catuneanu, O., Guiraud, R., Eriksson, P., Thomas, B., Shone, R., and Key, R., eds., Phanerozoic evolution of Africa: Journal of African Earth Sciences, v. 43, p. 334–378.

Brew, G.E., Litak, R.K., Seber, D., Barazangi, M., Al-Imam, A., and Sawaf, T., 1997, Basement depth and sedimentary velocity structure in the northern Arabian platform, eastern Syria: Geophysical Journal International, v. 128, no. 3, p. 617–631, https://doi.org/10.1111/j.1365-246X.1997.tb05323.x.

Brocher, T.M., 2005, Empirical relations between elastic wavespeeds and density in the Earth's crust: Bulletin of the Seismological Society of America, v. 95, no. 6, p. 2081–2092, https://doi.org/10.1785/0120050077.

Camp, V.E., Roobol, M.J., and Hooper, P.R., 1991, The Arabian continental alkali basalt province—Part II—Evolution of Harrats Khaybar, Ithnayn, and Kura, Kingdom of Saudi Arabia: Geological Society of America Bulletin, v. 103, no. 3, p. 363–391, https://doi.org/10.1130/0016-7606(1991)103%3C0363:TACABP%3E2.3.CO;2.

Camp, V.E., and Roobol, M.J., 1992, Upwelling asthenosphere beneath western Arabia and its regional implications: Journal of Geophysical Research—Solid Earth, v. 97, no. B11, p. 15255–15271, https://doi.org/10.1029/92JB00943.

Champion, D.E., Downs, D.T., Stelten, M.E., Robinson, J.E., Sisson, T.W., Shawali, J., Hassan, K., and Zahran, H., [in press], Paleomagnetism of the northern Harrat Rahat volcanic field, Kingdom of Saudi Arabia—Geologic correlations and geomagnetic cryptochron identifications, chap. H *of* Sisson, T.W., Calvert, A.T., and Mooney, W.D., eds., Active volcanism on the Arabian Shield—Geology, volcanology, and geophysics of northern Harrat Rahat and vicinity, Kingdom of Saudi Arabia: U.S. Geological Survey Professional Paper 1862 [also released as Saudi Geological Survey Special Report SGS–SP–2021–1], 31 p., https://doi.org/10.3133/pp1862H.

Coleman, R.G., 1993, Geologic evolution of the Red Sea: Oxford Monographs on Geology and Geophysics, v. 24, 186 p.

Crotwell, H.P., 2007, High data volume seismology—Surviving the avalanche: Columbia, S.C., University of South Carolina, Ph.D. dissertation, 86 p.

Earle, P.S., and Shearer, P.M., 1994, Characterization of global seismograms using an automatic-picking algorithm: Bulletin of the Seismological Society of America, v. 84, no. 2, p. 366–376, https://doi.org/10.1785/BSSA0840020366.

Endo, E., Zahran, H., Nofal, H., and Hadidy, S., 2007, The Saudi National Seismic Network: Seismological Research Letters, v. 78, no. 4, p. 439–445, https://doi.org/10.1785/gssrl.78.4.439.

Healy, J.H., Mooney, W.D., Blank, H.R., Gettings, M.E., Kohler, W.M., Lamson, R.J., and Leone, L.E., 1983, Saudi Arabian seismic deep-refraction profiles; final project report (no. 83-390): U.S. Geological Survey Open-File Report 83-390, https://doi.org/10.3133/ofr83390.

Julià, J., Ammon, C.J., and Herrmann, R.B., 2003, Lithospheric structure of the Arabian Shield from the joint inversion of receiver functions and surface-wave group velocities: Tectonophysics, v. 371, nos. 1–4, p. 1–21, https://doi.org/10.1016/S0040-1951(03)00196-3.

Karplus, M.S., Klemperer, S.L., Zhao, W., Kind, R., Wu, Z., Mechie, J., Shi, D., Brown, L.D., Chen, C., Su, H., Xue, G., Sandvol, E., Ni, J., Tilmann, F.J., Chen, Y.J., 2019, Receiver-function imaging of the lithosphere at the Kunlun-Qaidam boundary, Northeast Tibet: Tectonophysics, v. 759, p. 30–43, https://doi.org/10.1016/j.tecto.2019.03.015.

Konert, G., Afifi, A.M., Al-Harjri, S.A., and Droste, H.J., 2001, Paleozoic stratigraphic and hydrocarbon habitat of the Arabian Plate: GeoArabia, v. 6, no. 3, p. 407–442.

Langston, C.A., 1979, Structure under Mount Rainier, Washington, inferred from teleseismic body waves: Journal of Geophysical Research—Solid Earth, v. 84, no. B9, p. 4749–4762, https://doi.org/10.1029/JB084iB09p04749.

Langston, C.A., 2011, Wave-field continuation and decomposition for passive seismic imaging under deep unconsolidated sediments: Bulletin of the Seismological Society of America, v. 101, no. 5, p. 2176–2190, https://doi.org/10.1785/0120100299.

Ligorría, J.P., and Ammon, C.J., 1999, Iterative deconvolution and receiver-function estimation: Bulletin of the Seismological Society of America, v. 89, no. 5, p. 1395–1400, https://doi.org/10.1785/BSSA0890051395.

Miller, M.S., O'Driscoll, L.J., Porritt, R.W., and Roeske, S.M., 2018, Multiscale crustal architecture of Alaska inferred from P receiver functions: Lithosphere, v. 10, no. 2, p. 267–278, https://doi.org/10.1130/L701.1.

Mooney, W.D., 1984, A traveltime interpretation of the 1978 seismic refraction profile in the Kingdom of Saudi Arabia, *in* Mooney, W.D., and Prodehl, C., eds., Proceedings of the 1980 workshop of the International Association of Seismology and Physics of the Earth's Interior on the seismic modeling of laterally varying structures—Contributions based on data from the 1978 Saudi Arabian refraction profile: U.S. Geological Survey Circular 937, p. 49–79, https://doi.org/10.3133/cir937.

Mooney, W.D., Gettings, M.E., Blank, H.R., and Healy, J.H., 1985, Saudi Arabian seismic-refraction profile—A traveltime interpretation of crustal and upper mantle structure: Tectonophysics, v. 111, nos. 3–4, p. 173–197, 201–202, 205–206, 209–210, 213–215, 223–224, 227–246, https://doi.org/10.1016/0040-1951(85)90287-2.

Neumann van Padang, M., 1963, Arabia and the Indian Ocean—Catalogue of the active volcanoes and solfatara fields: Rome, International Association of Volcanology, v. 16, 64 p.

Ogden, C.S., Bastow, I.D., Gilligan, A., and Rondenay, S., 2019, A reappraisal of the H–κ stacking technique—Implications for global crustal structure: Geophysical Journal International, v. 219, no. 3, p. 1491–1513, https://doi.org/10.1093/gji/ggz364.

Pallister, J.S., McCausland, W.A., Jónsson, S., Lu, Z., Zahran, H.M., El Hadidy, S., Aburukbah, A., Stewart, I.C.F., Lundgren, P.R., White, R.A., and Moufti, M.R.H., 2010, Broad accommodation of rift-related extension recorded by dyke intrusion in Saudi Arabia: Nature Geoscience, v. 3, p. 705–712, https://doi.org/10.1038/ngeo966.

Pollastro, R.M., 1998a, Bedrock geology of the Arabian Peninsula and selected adjacent areas (geo2bg): U.S. Geological Survey data release, accessed October 15, 2018, at https://catalog.data.gov/dataset/bedrock-geology-of-the-arabian-peninsula-and-selected-adjacent-areas-geo2bg.

Pollastro, R.M., 1998b, Geologic Provinces of the Arabian Peninsula and adjacent areas, 2000 (prv2bg): U.S. Geological Survey data release, accessed October 15, 2018, at https://catalog.data.gov/dataset/geologic-provinces-of-the-arabian-peninsula-and-adjacent-areas-2000-prv2bg.

Sandvol, E., Seber, D., Barazangi, M., Vernon, F., Mellors, R., and Al-Amri, A., 1998, Lithospheric seismic velocity discontinuities beneath the Arabian Shield: Geophysical Research Letters, v. 25, no. 15, p. 2873–2876, https://doi.org/10.1029/98GL02214.

Seber, D., Barazangi, M., Chaimov, T.A., Al-Saad, D., Sawaf, T., and Khaddour, M., 1993, Upper crustal velocity structure and basement morphology beneath the intracontinental Palmyride fold-thrust belt and north Arabian platform in Syria: Geophysical Journal International, v. 113, no. 3, p. 752–766, https://doi.org/10.1111/j.1365-246X.1993.tb04666.x.

Stelten, M.E., Downs, D.T., Champion, D.E., Dietterich, H.R., Calvert, A.T., Sisson, T.W., Mahood, G.A., and Zahran, H., [in press], Eruptive history of northern Harrat Rahat—Volume, timing, and composition of volcanism over the past 1.2 million years, chap. D *of* Sisson, T.W., Calvert, A.T., and Mooney, W.D., eds., Active volcanism on the Arabian Shield—Geology, volcanology, and geophysics of northern Harrat Rahat and vicinity, Kingdom of Saudi Arabia: U.S. Geological Survey Professional Paper 1862 [also released as Saudi Geological Survey Special Report SGS–SP–2021–1], 46 p., https://doi.org/10.3133/pp1862D.

Stern, R.J., and Johnson, P., 2010, Continental lithosphere of the Arabian plate—A geologic, petrologic, and geophysical synthesis: Earth-Science Reviews, v. 101, no. 1, p. 29–67, https://doi.org/10.1016/j.earscirev.2010.01.002.

Tang, Z., Julià, J., Zahran, H., and Mai, P.M., 2016, The lithospheric shear-wave velocity structure of Saudi Arabia—Young volcanism in an old shield: Tectonophysics, v. 680, p. 8–27, https://doi.org/10.1016/j.tecto.2016.05.004.

Tang, Z., Mai, P.M., Julià, J., and Zahran, H., 2019, Shear velocity structure beneath Saudi Arabia from the joint inversion of P and S wave receiver functions, and Rayleigh wave group velocity dispersion data: Journal of Geophysical Research—Solid Earth, v. 124, no. 5, p. 4767–4787, https://doi.org/10.1029/2018JB017131.

Thurner, S., Margolis, R., Levander, A., and Niu, F., 2015, PdS receiver function evidence for crustal scale thrusting, relic subduction, and mafic underplating in the Trans-Hudson Orogen and Yavapai province: Earth and Planetary Science Letters, v. 426, p. 13–22, https://doi.org/10.1016/j.epsl.2015.06.007.

Tkalčić, H., Pasyanos, M.E., Rodgers, A.J., Gök, R., Walter, W.R., and Al-Amri, A., 2006, A multistep approach for joint modeling of surface wave dispersion and teleseismic receiver functions—Implications for lithospheric structure of the Arabian Peninsula: Journal of Geophysical Research—Solid Earth, v. 111, no. B11, 25 p., https://doi.org/10.1029/2005JB004130.

Vernon, F., 1995, Broadband seismic characterization of the Arabian Shield: International Federation of Digital Seismograph Networks dataset, accessed July 6, 2022, at https://doi.org/10.7914/SN/XI_1995.

Yu, Y., Song, J., Liu, K.H., and Gao, S.S., 2015, Determining crustal structure beneath seismic stations overlying a low-velocity sedimentary layer using receiver functions: Journal of Geophysical Research—Solid Earth, v. 120, no. 5, p. 3208–3218, https://doi.org/10.1002/2014JB011610.

Zhu, L., and Kanamori, H., 2000, Moho depth variation in southern California from teleseismic receiver functions: Journal of Geophysical Research—Solid Earth, v. 105, no. B2, p. 2969–2980, https://doi.org/10.1029/1999JB900322.

Appendix 1. Quantitative Values Obtained in This Study

Table 1.1 Summary of seismic results by station number (1-154), station letter code, latitude, longitude, weighting factors (equation 4), thickness (H) of crystalline crust, two sigma error, V_P/V_S ratio (k), two sigma error, and weighting factors (equation 4), sediment thickness (H), two sigma error, V_P/V_S ratio (k), two sigma error, final crustal thickness after accounting for sediments, geologic category, data source, maximum frequency of recorded seismic data, number of first figure for each station.

				Crystalline crust										Sedimentary layer								
No.	Station	Latitude	Longitude	w_1	w_2	w_3	H (km)	$2\sigma_H$	k	$2\sigma_k$	w_4	w_5	w_6	H (km)	$2\sigma_H$	k	$2\sigma_k$	H_{final}	Category	Source	Maximum frequency (Hz)	First figure number
1	WELA	31.78	38.91	0.4	0.3	0.3	34.3	0.4	1.6	0.03	0.05	0.7	0.25	2.09	0.1	3.6	0.14	34.1	Platform	SGS	100	6
2	HANO	31.39	38.33	0.5	0.5	0	32.7	0.4	1.73	0.03	0.25	0.75	0	2.38	0.04	2.05	0.14	33.9	Platform	SGS	100	8
3	NARAR	31.12	40.75	0.5	0.5	0	38.5	1	1.7	0.02	0.25	0.75	0	5.4	0.2	4.2	0.19	40.7	Platform	SGS	20	10
4	SARAR	30.38	41.94	0.4	0.3	0.3	34.5	1.2	1.72	0.03	0.05	0.7	0.25	5.3	0.4	1.65	0.17	36.7	Platform	SGS	20	12
5	WRFHA	29.58	43.11	0.4	0.3	0.3	40	0.4	1.87	0.02	0.05	0.7	0.25	0.72	0.2	1.5	0.59	37	Platform	SGS	100	14
6	JOFS	29.41	38.61	0.4	0.3	0.3	40	0.6	1.73	0.03								36.9	Platform	SGS	100	16
7	HAQS	29.06	34.93	0.4	0.3	0.3	28	0.7	1.77	0.03								28	Shield	SGS	100	18
8	JLOS	28.74	35.49	0.4	0.3	0.3	31.4	0.4	1.62	0.02								31.4	Shield	SGS	100	20
9	HBTS	28.73	46.05	0.5	0.5	0	43.6	0.4	1.79	0.02								40.1	Platform	SGS	100	22
10	BDAS	28.43	35.09	0.5	0.5	0	33.6	0.5	1.64	0.03								33.6	Coast	SGS	100	24
11	TBKS	28.23	36.55	0.5	0.5	0	35.4	0.5	1.8	0.04								34.6	Platform	SGS	100	26
12	KFJS	28.19	47.94	0.5	0.5	0	47	0.8	1.83	0.04								41.5	Platform	SGS	100	28
13	URD10	28.17	37.1	0.4	0.3	0.3	34.8	0.7	1.74	0.02								34.5	Platform	SGS	20	30
14	KRABS	28.1	35.26	0.5	0.5	0	31.8	0.6	1.6	0.05								31.8	Coast	SGS	100	32
15	WTBKS	28.08	35.91	0.5	0.5	0	32.4	0.5	1.93	0.03								32.4	Shield	SGS	100	34
16	SHQRE	27.9	36.17	0.5	0.5	0	31.2	0.6	1.83	0.03								31.2	Shield	SGS	20	36
17	QLABS	27.86	37.93	0.4	0.3	0.3	35.8	0.8	1.76	0.03								34.5	Platform	SGS	100	38
18	QYSM	27.85	46.88	0.4	0.3	0.3	44.3	0.3	1.74	0.02	0.05	0.7	0.25	0.95	0.05	1.6	0.16	41.9	Platform	SGS	100	40
19	URD12	27.76	37.06	0.5	0.5	0	34.6	0.9	1.76	0.04								34.6	Platform	SGS	20	42
20	HIL04	27.76	42.76	0.4	0.3	0.3	39	0.6	1.79	0.02								39	Shield	SGS	100	44
21	MWLHS	27.75	35.52	0.5	0.5	0	29.8	0.3	1.71	0.02								29.8	Coast	SGS	100	46
22	URD13	27.54	37.48	0.5	0.5	0	35	0.6	1.77	0.03								35	Platform	SGS	20	48
23	DESA	27.51	36.16	0.3	0.3	0.3	29	0.2	1.9	0.01								29	Shield	SGS	100	50
24	ASYS	27.5	44.34	0.4	0.3	0.3	40.9	0.4	1.78	0.02	0.05	0.7	0.25	3.8	0.1	1.6	0.11	45.4	Platform	SGS	100	52
25	NDEBA	27.47	35.65	0.5	0.5	0	29.4	0.7	1.71	0.03								29.4	Coast	SGS	100	54
26	URD14	27.44	37.74	0.4	0.3	0.3	34.6	0.4	1.74	0.02								34.6	Platform	SGS	20	56
27	RQBS	27.34	45.96	0.4	0.3	0.3	36.9	0.4	1.95	0.03	0.05	0.7	0.25	0.72	0.1	1.6	0.34	35.1	Platform	SGS	100	58
28	HIL03	27.25	40.8	0.4	0.3	0.3	36.2	0.7	1.77	0.02								36.2	Shield	SGS	100	60
29	URD15	27.25	37.45	0.5	0.5	0	38	0.5	1.71	0.02								38.4	Platform	SGS	20	62
30	DBAS	27.21	35.97	0.5	0.5	0	28.4	0.8	1.71	0.03								28.4	Coast	SGS	100	64
31	NRYS	27.08	49.16	0.5	0.5	0	45.8	0.8	1.71	0.02								41	Platform	SGS	100	66
32	URD04	27.08	37.26	0.4	0.3	0.3	36.8	0.6	1.73	0.02								36.8	Shield	SGS	20	68
33	URD01	26.95	37.66	0.4	0.3	0.3	38.2	0.5	1.75	0.02								38.2	Shield	SGS	20	70
34	BIDS	26.87	36.96	0.4	0.3	0.3	35.6	0.6	1.72	0.03								35.6	Shield	SGS	100	72
35	WJHS	26.73	36.39	0.5	0.5	0	27.8	0.9	1.72	0.04								27.8	Coast	SGS	100	74
36	QSMS	26.67	42.69	0.5	0.5	0	36	0.7	1.8	0.02								36	Shield	SGS	100	76

Table 1.1 Summary of seismic results by station number (1-154), station letter code, latitude, longitude, weighting factors (equation 4), thickness (*H*) of crystalline crust, two sigma error, V_P/V_S ratio (*k*), two sigma error, and weighting factors (equation 4), sediment thickness (*H*), two sigma error, V_P/V_S ratio (*k*), two sigma error, final crustal thickness after accounting for sediments, geologic category, data source, maximum frequency of recorded seismic data, number of first figure for each station.—Continued

				Crystalline crust										Sedimentary layer								
No.	Station	Latitude	Longitude	w_1	w_2	w_3	*H* (km)	$2\sigma_H$	*k*	$2\sigma_k$	w_4	w_5	w_6	*H* (km)	$2\sigma_H$	*k*	$2\sigma_k$	H_{final}	Category	Source	Maximum frequency (Hz)	First figure number
37	URD03	26.67	37.45	0.4	0.3	0.3	36.8	0.8	1.74	0.03								36.8	Shield	SGS	20	78
38	URD02	26.62	37.86	0.5	0.5	0	37.8	0.9	1.69	0.03								37.8	Shield	SGS	20	80
39	OLAS	26.25	37.63	0.5	0.5	0	36.2	0.5	1.73	0.03								36.2	Shield	SGS	100	82
40	EWJHS	26.16	36.66	0.4	0.3	0.3	27.4	0.6	1.73	0.03								27.4	Coast	SGS	100	84
41	KBR06	26.11	40.03	0.5	0.5	0	34.6	0.5	1.76	0.03								34.6	HK	SGS	100	86
42	MJMS	26.05	45.66	0.5	0.5	0	45.2	0.5	1.78	0.02								43.3	Platform	SGS	100	88
43	KBR09	26.03	39.67	0.4	0.3	0.3	36.6	0.6	1.7	0.02								36.6	HK	SGS	100	90
44	KBR04	25.98	40.28	0.5	0.5	0	34	0.4	1.77	0.02								34	HK	SGS	100	92
45	BOQS	25.87	49.38	0.5	0.5	0	40.5	1.4	1.73	0.04	0.25	0.75	0	1.6	0.2	4.25	0.34	39.3	Platform	SGS	100	94
46	HIL01	25.83	41.99	0.4	0.3	0.3	36	0.7	1.73	0.02								36	Shield	SGS	100	96
47	ARSS	25.83	43.15	0.4	0.3	0.3	38.8	0.5	1.74	0.02								38.8	Shield	SGS	100	98
48	KBR03	25.82	39.95	0.4	0.3	0.3	36.2	0.5	1.76	0.02								36.2	HK	SGS	100	100
49	UQSK	25.79	42.36	0.4	0.3	0.3	36.8	0.4	1.75	0.02								36.8	Shield	IRIS	40	102
50	KBRS	25.79	39.26	0.4	0.3	0.3	38.2	0.5	1.76	0.02								38.2	HK	SGS	20	104
51	KBR13	25.77	38.85	0.5	0.5	0	34	0.5	1.75	0.02								34	HK	SGS	20	106
52	KBR08	25.72	39.48	0.5	0.5	0	36.4	0.5	1.72	0.02								36.4	HK	SGS	100	108
53	NUMJS	25.63	37.27	0.4	0.3	0.3	24.4	0.4	1.8	0.02								24.4	Shield	SGS	100	110
54	KBR05	25.57	40.31	0.5	0.5	0	34	0.5	1.79	0.04								34	HK	SGS	100	112
55	KBR01	25.46	39.78	0.4	0.3	0.3	36.2	0.7	1.74	0.04								36.2	HK	SGS	100	114
56	MURBA	25.41	38.25	0.5	0.5	0	31.6	0.5	1.73	0.03								31.6	HL	SGS	20	116
57	LNY09	25.4	37.66	0.4	0.3	0.3	37	0.5	1.64	0.02								37	HL	SGS	100	118
58	LNY03	25.38	37.85	0.5	0.5	0	36	0.6	1.68	0.03								36	HL	SGS	100	120
59	LNY16	25.35	37.6	0.4	0.3	0.3	32.6	0.8	1.75	0.04								32.6	HL	SGS	100	122
60	LNY11	25.32	37.77	0.4	0.3	0.3	31.8	0.4	1.97	0.03								31.8	HL	SGS	100	124
61	LNY04	25.27	37.65	0.4	0.3	0.3	32.4	0.7	1.86	0.04								32.4	HL	SGS	100	126
62	LNY12	25.27	37.77	0.5	0.5	0	32.8	0.9	1.75	0.05								32.8	HL	SGS	100	128
63	LNY10	25.27	37.86	0.4	0.3	0.3	33	0.5	1.84	0.03								33	HL	SGS	100	130
64	LNY15	25.26	37.8	0.4	0.3	0.3	33	0.6	1.8	0.03								33	HL	SGS	100	132
65	KBR07	25.26	39.46	0.5	0.5	0	35	0.5	1.75	0.02								35	HK	SGS	100	134
66	LNY14	25.25	37.77	0.4	0.3	0.3	33	0.7	1.82	0.04								33	HL	SGS	100	136
67	LNY17	25.24	37.8	0.5	0.5	0	33.8	0.7	1.79	0.04								33.8	HL	SGS	100	138
68	UMJS	25.23	37.31	0.4	0.3	0.3	25.4	0.5	1.63	0.02								25.4	Coast	SGS	100	140
69	KBR02	25.23	40.24	0.4	0.3	0.3	35.8	0.5	1.78	0.02								35.8	HK	SGS	100	142
70	LNY01	25.22	37.96	0.4	0.3	0.3	32.6	0.6	1.85	0.04								32.6	HL	SGS	100	144
71	LNY06	25.21	37.78	0.5	0.5	0	34.4	0.5	1.81	0.03								34.4	HL	SGS	100	146
72	LNY13	25.17	37.63	0.4	0.3	0.3	31.2	0.5	1.85	0.03								31.2	HL	SGS	100	148
73	LNY02	25.14	37.86	0.5	0.5	0	34	0.6	1.8	0.03								34	HL	SGS	100	150
74	LNY07	25.13	37.57	0.4	0.3	0.3	32.4	0.5	1.77	0.03								32.4	Coast	SGS	100	152
75	KBR10	25.13	39.94	0.5	0.5	0	35	0.7	1.77	0.02								35	HK	SGS	100	154

Table 1.1 Summary of seismic results by station number (1-154), station letter code, latitude, longitude, weighting factors (equation 4), thickness (H) of crystalline crust, two sigma error, V_P/V_S ratio (k), two sigma error, and weighting factors (equation 4), sediment thickness (H), two sigma error, V_P/V_S ratio (k), two sigma error, final crustal thickness after accounting for sediments, geologic category, data source, maximum frequency of recorded seismic data, number of first figure for each station.—Continued

							Crystalline crust							Sedimentary layer								
No.	Station	Latitude	Longitude	w_1	w_2	w_3	H (km)	$2\sigma_H$	k	$2\sigma_k$	w_4	w_5	w_6	H (km)	$2\sigma_H$	k	$2\sigma_k$	H_{final}	Category	Source	Maximum frequency (Hz)	First figure number
76	LNYS	25.08	37.94	0.5	0.5	0	35.2	0.7	1.76	0.04								35.2	HL	SGS	100	156
77	TRAS	25.06	38.57	0.4	0.3	0.3	35	0.7	1.62	0.03								35	HL	SGS	100	158
78	LNY05	25.05	37.7	0.4	0.3	0.3	37.4	0.7	1.61	0.03								37.4	HL	SGS	100	160
79	LNY08	25.03	37.85	0.5	0.5	0	35	0.6	1.78	0.03								35	HL	SGS	100	162
80	RHT11	24.92	39.69	0.5	0.5	0	35.4	0.5	1.73	0.03								35.4	HR	SGS	100	164
81	SLWS	24.8	50.64	0.4	0.3	0.3	40.4	0.7	1.73	0.04	0.05	0.7	0.25	2.89	0.1	3.55	0.15	40.5	Platform	SGS	100	166
82	RHT09	24.78	39.91	0.4	0.3	0.3	35	0.6	1.75	0.03								35	HR	SGS	100	168
83	RIYD	24.72	46.64	0.4	0.3	0.3	31	1.2	2.12	0.04	0.05	0.7	0.25	4.5	0.5	1.5	0.57	36.6	Platform	IRIS	40	170
84	RHT08	24.71	39.54	0.4	0.3	0.3	34.8	0.5	1.76	0.03								34.8	HR	SGS	100	172
85	RHT07	24.67	39.04	0.4	0.3	0.3	32.4	0.6	1.71	0.02								32.4	HR	SGS	100	174
86	RHT10	24.58	39.9	0.4	0.3	0.3	34.6	0.5	1.78	0.02								34.6	HR	SGS	100	176
87	AFFS	24.56	42.48	0.4	0.3	0.3	35.2	0.4	1.75	0.02								35.2	Shield	SGS	100	178
88	DWDS	24.54	44.84	0.4	0.3	0.3	42.8	0.6	1.74	0.03								42.8	Shield	SGS	100	180
89	RHT02	24.48	40.09	0.4	0.3	0.3	34.8	0.5	1.77	0.03								34.8	HR	SGS	100	182
90	RHT14	24.39	39.76	0.4	0.3	0.3	35.8	1	1.76	0.03								35.8	HR	SGS	100	184
91	RHT06	24.38	39.19	0.4	0.3	0.3	33.4	0.6	1.71	0.04								33.4	Shield	SGS	100	186
92	YOBS	24.36	38.74	0.4	0.3	0.3	31	0.6	1.75	0.03								31	Coast	SGS	100	188
93	YNBS	24.34	37.99	0.4	0.3	0.3	24	0.7	1.94	0.04								24	Coast	SGS	100	190
94	RHT01	24.27	39.81	0.5	0.5	0	34.4	0.5	1.86	0.03								34.4	HR	SGS	100	192
95	RHT03	24.25	40.17	0.4	0.3	0.3	35.8	0.8	1.73	0.03								35.8	HR	SGS	100	194
96	RHT13	24.21	39.37	0.5	0.5	0	36.2	0.6	1.71	0.03								36.2	Shield	SGS	100	196
97	RHT15	24.17	39.84	0.4	0.3	0.3	35.4	0.4	1.8	0.02								35.4	HR	SGS	100	198
98	BJDH	24.09	43.4	0.5	0.5	0	35.6	0.6	1.75	0.02								35.6	Shield	SGS	100	200
99	BTHS	24.05	50.85	0.4	0.3	0.3	38.7	0.7	1.75	0.03	0.05	0.7	0.25	2.95	0.05	1.6	0.18	39.3	Platform	SGS	100	202
100	RHT04	23.99	39.88	0.4	0.3	0.3	35.4	0.6	1.77	0.03								35.4	HR	SGS	100	204
101	AFIF	23.93	43.04	0.4	0.3	0.3	36.8	0.6	1.72	0.02								36.8	Shield	IRIS	40	206
102	RHT05	23.91	39.16	0.4	0.3	0.3	35.6	0.8	1.71	0.03								35.6	Shield	SGS	100	208
103	BADR	23.88	38.66	0.3	0.3	0.3	24.2	0.3	1.8	0.02								24.2	Shield	SGS	20	210
104	KHRJ	23.84	47.68	0.4	0.3	0.3	41.8	0.4	1.78	0.02	0.05	0.7	0.25	0.69	0.04	3.5	0.16	40.4	Platform	SGS	100	212
105	RAYN	23.52	45.5	0.5	0.5	0	39.8	0.6	1.77	0.02								39.8	Shield	IRIS	40	214
106	NSAFS	23.49	38.82	0.4	0.3	0.3	29	0.7	1.67	0.03								29	Coast	SGS	100	216
107	RHT16	23.47	40.17	0.4	0.3	0.3	36.4	0.4	1.74	0.02								36.4	HR	SGS	100	218
108	MSTR	23.23	38.96	0.5	0.5	0	25.4	0.4	1.9	0.03								25.4	Shield	SGS	20	220
109	HRDS	22.93	49.46	0.4	0.3	0.3	46.1	0.6	1.79	0.02								42.3	Platform	SGS	100	222
110	HAJR	22.9	39.67	0.5	0.5	0	36	0.5	1.68	0.03								36	HR	SGS	100	224
111	NUBA	22.88	39.3	0.5	0.5	0	33.4	0.5	1.71	0.02								33.4	Shield	SGS	20	226
112	HALM	22.85	44.32	0.4	0.3	0.3	36.4	0.4	1.75	0.02								36.4	Shield	IRIS	40	228
113	GHASH	22.72	40.23	0.5	0.5	0	36	0.4	1.73	0.02								36	HR	SGS	100	230
114	FRJS	22.59	39.36	0.4	0.3	0.3	30.2	1	1.66	0.05								30.2	Coast	SGS	100	232
115	MDRK2	22.29	40.26	0.5	0.5	0	34.8	0.4	1.77	0.02								34.8	HR	SGS	100	234

Table 1.1 Summary of seismic results by station number (1-154), station letter code, latitude, longitude, weighting factors (equation 4), thickness (H) of crystalline crust, two sigma error, V_P/V_S ratio (k), two sigma error, and weighting factors (equation 4), sediment thickness (H), two sigma error, V_P/V_S ratio (k), two sigma error, final crustal thickness after accounting for sediments, geologic category, data source, maximum frequency of recorded seismic data, number of first figure for each station.—Continued

				Crystalline crust										Sedimentary layer								
No.	Station	Latitude	Longitude	w_1	w_2	w_3	H (km)	$2\sigma_H$	k	$2\sigma_k$	w_4	w_5	w_6	H (km)	$2\sigma_H$	k	$2\sigma_k$	H_{final}	Category	Source	Maximum frequency (Hz)	First figure number
116	KHLS2	22.26	39.52	0.4	0.3	0.3	33	0.4	1.72	0.02								33	Coast	SGS	100	236
117	MDRS	22.09	40	0.4	0.3	0.3	36.2	0.4	1.68	0.02								36.2	HR	SGS	100	238
118	KHLS	22.05	39.3	0.4	0.3	0.3	25.4	0.6	1.86	0.04								25.4	Coast	SGS	100	240
119	LYLS	22.04	47.24	0.5	0.5	0	43.8	0.5	1.77	0.03	0.25	0.75	0	0.6	0.04	4.6	0.21	42.1	Platform	SGS	100	242
120	HRML	22.01	45.09	0.4	0.3	0.3	41.6	0.3	1.76	0.01								41.6	Shield	SGS	100	244
121	JURS	21.87	39.8	0.4	0.3	0.3	33	0.6	1.73	0.03								33	HR	SGS	100	246
122	FDAS	21.83	40.36	0.4	0.3	0.3	36.8	0.7	1.68	0.03								36.8	HR	SGS	100	248
123	JEDS	21.72	39.42	0.5	0.5	0	27.6	0.6	1.64	0.04								27.6	Coast	SGS	100	250
124	SHRS	21.5	40.2	0.4	0.3	0.3	34.8	0.4	1.72	0.02								34.8	Shield	SGS	100	252
125	SHMS	21.45	39.69	0.4	0.3	0.3	27.8	0.6	1.77	0.03								27.8	Coast	SGS	100	254
126	RYNS	21.32	42.85	0.5	0.5	0	37	0.4	1.74	0.02								37	Shield	SGS	100	256
127	RANI	21.31	42.78	0.4	0.3	0.3	38.6	0.7	1.7	0.02								38.6	Shield	IRIS	40	258
128	TAIF	21.28	40.35	0.4	0.3	0.3	37.4	0.4	1.76	0.02								37.4	Shield	IRIS	40	260
129	FRAS	21.06	40.52	0.4	0.3	0.3	39.6	0.7	1.72	0.03								39.6	Shield	SGS	100	262
130	LBNS	21.05	39.9	0.5	0.5	0	31	0.6	1.78	0.03								31	Coast	SGS	100	264
131	SHBS	21	39.68	0.4	0.3	0.3	27.2	0.5	1.76	0.03								27.2	Coast	SGS	100	266
132	KAMS	20.3	44.57	0.4	0.3	0.3	39.2	0.4	1.78	0.01								39.2	Shield	SGS	100	268
133	LTHS	20.28	40.41	0.4	0.3	0.3	23.6	0.4	1.68	0.05	0.05	0.7	0.25	1.55	0.1	1.5	0.4	25.2	Coast	SGS	100	270
134	BAHS	19.97	41.6	0.4	0.3	0.3	38	0.6	1.73	0.03								38	Shield	SGS	100	272
135	BLJS	19.96	41.61	0.4	0.3	0.3	38	0.6	1.73	0.02								38	Shield	SGS	100	274
136	BISH	19.92	42.69	0.5	0.5	0	36.4	0.4	1.83	0.02								36.4	Shield	IRIS	40	276
137	TATS	19.54	43.48	0.4	0.3	0.3	39	0.7	1.83	0.03								39	Shield	SGS	100	278
138	QNF01	19.39	41.28	0.3	0.3	0.3	36.6	0.3	1.71	0.01								36	Coast	SGS	100	280
139	NAMS	19.17	42.2	0.4	0.3	0.3	41.6	0.5	1.71	0.02								41.6	Shield	SGS	100	282
140	RHWAS	19.07	44.07	0.5	0.5	0	38.4	0.7	1.8	0.02								38.4	Shield	SGS	100	284
141	ENMS	19.07	42.57	0.4	0.3	0.3	42.8	0.6	1.7	0.02								42.8	Shield	SGS	100	286
142	QNF02	19.06	41.49	0.3	0.3	0.3	35	0.4	1.7	0.01								35	Coast	SGS	100	288
143	WBHS	18.61	42.72	0.4	0.3	0.3	41.2	0.5	1.74	0.02								41.2	Shield	SGS	100	290
144	AMGES	18.46	41.54	0.3	0.3	0.3	29.6	0.2	1.94	0.01								29.6	Coast	SGS	100	292
145	KNGHS	18.29	43.5	0.5	0.5	0	45.4	0.6	1.76	0.02								45.4	Shield	SGS	100	294
146	SODA	18.29	42.38	0.4	0.3	0.3	38	0.6	1.74	0.02								38	Shield	IRIS	40	296
147	DRBS	17.83	42.3	0.4	0.3	0.3	33	0.6	1.67	0.02								33	Coast	SGS	100	298
148	DJNS	17.7	43.54	0.4	0.3	0.3	47.6	0.6	1.66	0.02								47.6	Shield	SGS	100	300
149	NJRNS	17.65	44.19	0.4	0.3	0.3	41.2	0.5	1.82	0.02								41.2	Shield	SGS	100	302
150	BESHS	17.37	42.84	0.4	0.3	0.3	34.4	0.7	1.71	0.02								34.4	Coast	SGS	100	304
151	AKWA	17.26	42.7	0.5	0.5	0	27.4	0.7	1.69	0.03								27.4	Coast	SGS	100	306
152	JAZS	17.07	42.92	0.4	0.3	0.3	31.4	1.2	1.64	0.04								31.4	Coast	SGS	100	308
153	FRSS2	16.85	41.79	0.5	0.5	0	25.4	0.5	1.97	0.03								25	Coast	SGS	100	310
154	FRSS	16.74	42.11	0.3	0.3	0.3	16	0.3	1.77	0.03								15.6	Coast	SGS	100	312

ISSN 2331-1258 (online)
https://doi.org/10.3133/ofr20231042